Tritium and Deuterium Labelling of Bioactive Molecules Catalyzed by Metallic Nanoparticles

Viktor Pfeifer

UNIVERSITÉ PARIS SUD

université PARIS-SACLAY

Tritium and Deuterium Labelling of Bioactive Molecules Catalyzed by Metallic Nanoparticles

Thèse de doctorat de l'Université Paris-Saclay
préparée à l´Université Paris-Sud
au CEA-Saclay

École doctorale n°571, Sciences Chimiques: Molécules, Matériaux, Instrumentation et Biosystèmes (2MIB)
Spécialité de doctorat: Chimie

Thèse présentée et soutenue à Gif-sur-Yvette, le 16 Septembre 2019, par

Viktor Pfeifer

Composition du Jury :

Françoise Colobert Professeure, Université de Strasbourg	Rapporteur
Olivier Baudoin Professeur, Université de Basel	Rapporteur
Emmanuelle Schulz Directeur de Recherche, Université Paris-Sud	Présidente
Thomas Cailly Maître de Conférences, Université de Caen	Examinateur
Grégory Pieters Directeur de Recherche, CEA-Saclay	Directeur de thèse
Sophie Feuillastre Ingénieur de Recherche, CEA-Saclay	Invité
Philippe Lesot Directeur de Recherche, Université Paris-Sud	Invité

To my grandmothers

Table of contents

Acknowledgments

I wholeheartedly thank all jury members for making the defense of this PhD thesis possible. I am grateful to Prof. Françoise Colobert and Prof. Olivier Baudoin for having accepted to survey my work as referees and for their presence at my PhD defense. I'm very thankful to Dr. Emmanuelle Schulz for having accepted to review my work as a member of the University Paris-Sud during the last three years. I was very happy and delighted to lead valuable discussions with Dr. Emmanuelle Schulz and to be provided with constant feed-back from her side. Dr. Emmanuelle Schulz is also thanked for her participation as examiner during my PhD defense. Moreover, I would like to thank Dr. Thomas Cailly for taking part as examiner in my PhD defense and for reviewing my PhD thesis. A special and sincere gratitude goes to my supervisor Dr. Grégory Pieters, who gave me the opportunity to perform this PhD thesis in his working group. Further, I am thankful to Dr. Grégory Pieters for his permanent support and encouragement in many aspects, whether in science or in everyday life. I also thank Dr. Sophie Feuillastre for supervising my work, for furnishing many productive ideas and for her willingness to help with materials and advice whenever needed. Dr. Sophie Feuillastre is also thanked for being part of the jury during my PhD defense. With a special mention to Dr. Philippe Lesot, who followed-up my work with a big curiosity and accepted to be part of the jury. I express another gratitude to Dr. Philippe Lesot for supporting this PhD thesis with his great knowledge of NMR and for all the efforts he made to conduct ^{2}H-NMR analysis for this work. My sincere thanks goes to Dr. Bernard Rousseau for reviewing this work, for his powerful attitude towards science and life and for creating a familiar and enthusiastic atmosphere with his presence. I am very grateful to Dr. Bruno Chaudret and Dr. Simon Tricard for welcoming me in their laboratory during my secondment and for pioneering the modern world of metal nanoparticles. I also thank Dr. Bruno Chaudret and Dr. Simon Tricard for sharing their valuable knowledge with me and my supervisors on this field. I am thankful to Donia Bouzouita for her eagerness to support this work with metal nanoparticles and for being a pleasant laboratory mate during my stay in Toulouse. My sincere gratitude goes to Romuald Poteau, Iker del Rosal, Marie Certiat and Laurent Maron for dedicating a huge amount of time and efforts for the performance and management of the DFT-calculations within this work. Further, I want to express another gratitude to Dr. Volker Derdau for welcoming me in his laboratory during another secondment. I am very thankful to Dr. Volker Derdau for his advice and supply with pharmaceuticals for this work. I am grateful

for the social events Dr. Volker Derdau initiated and organized during my two-month stay in his laboratory. I also would like to thank Mégane Valero for being a pleasant laboratory mate during my secondment time. Another thanks goes to Dr. Jens Atzrodt for his curiosity about my work and for taking part in our group meetings. Dr. Thibault Cantat and Dr. Davide Audisio are thanked for interesting scientific discussion and their promptness to launch new projects in collaboration with me. Furthermore, I am sincerely grateful to Sébastien Garcia-Argote who conducted the tritiation experiments and the analyses of the radiolabelled molecules, which represented an essential part of this PhD thesis. A special thank you also goes to David Buisson, Elodie Marcon, Céline Chollet, Amélie Goudet, Sabrina Lebrequier and Timothée D'anfray who built up the analysis team of our department at CEA in Saclay. I also would like to thank Chantal Faux for managing many administrative issues during the course of my PhD thesis. Sophie Dezard, Christophe Créminon, and Christelle Bisson are thanked for assuring the safety at our department and for spreading a hilarious mood. My sincere gratitude goes to the European Union's Horizon 2020 research and innovation program under the Marie Sklodowska-Curie grant agreement no. 675071 for funding. I express a great thank you to Dr. Karen Hinsinger, Dr. Christophe Dugave and Dr. Emilie Nehlig for their support in managing the ISOTOPICS project. Every other member of the ISOTOPICS consortium is acknowledged for the organization of ISOTOPICS training- and meeting events. Further, I am grateful to Dr. Alaric Desmarchelier who gave valuable advice for the presentation of my work and for laboratory experiments. Additionally, I am thankful to Dr. Eric Doris and Dr. Edmond Gravel for their disposition to help every member of the laboratory with organizational and administrative questions. I also want to thank Florence Pillon for all the cakes and biscuits she baked for us and the friendly and interesting conversations we lead. I would like to give special thanks to Alberto Palazzolo, Antonio Del Vecchio and Gianluca Destro for being pleasant and reliant companions during this life period. My office- and laboratory mates Lucie Jamgotchian, Lucas Frédéric, Jérémy Schild, Timothée Narret, Laurélie Poulard, Minh Duc Hoang, Marielle Tamigney and Marion Daniel-Bertrand deserve another gratitude for helping me a lot with French vocabulary and the deeper comprehension of the French language. Further, I would like to pronounce a general thank you to every member of the SCBM department at CEA in Saclay for their helpful and considerate attitudes, the friendly atmosphere and the organization of unforgettable social events. Last but not least, I thank all my family, with special mention to my parents and my sister for supporting me in every point of view throughout all my life before and during the PhD thesis.

Abbreviations

ADME .....absorption, distribution, metabolism and excretion

API.....Active Pharmaceutical Ingredient

COD..... 1,5-cyclooctadiene

COT 1,3,5-cyclooctatriene

DCM ..... dichloromethane

DFT..... density functional theory

EtOAc ..... ethylacetate

fcc..... face-centered cubic

FDA .....U.S. Food and Drug Administration

FTIR..... Fourier-transform infrared

hcp ..... hexagonal close-packed

HIE.....hydrogen isotope exchange

HPLC ..... high-pressure liquid chromatography

ICP-MS ..... inductively coupled plasma-mass spectrometry

ICy 1,3-dicyclohexylimidazol-2-ylidene

IMes 1,3-dimesitylimidazol-2-ylidene

KO*t*Bu..... potassium *tert*-butoxide

MAS..... magic-angle-spinning

MNp..... metal nanoparticles

NaOMe .....sodium methoxide

NHC..... *N*-heterocyclic carbene

Ni-*ICy* Np .....Nickel nanoparticles stabilized by 1,3- dicyclohexylimidazol-2-ylidene

Ni-*IMes* Np ..... Nickel nanoparticles stabilized by 1,3-dimesitylimidazol-2-ylidene

NMR ..... nuclear magnetic resonance

Np ..... nanoparticles

PBE ..... Perdew-Burke-Ernzerhof

PVP ..... polyvinylpyrolidone

QWBA ..... quantitative whole body audioradiography

RIS ..... relative isotopic abundance

RuNp@PVP ..... ruthenium nanoparticles embedded in a PVP matrix

Ru-*ICy* Np ..... ruthenium nanoparticles stabilized by 1,3-dicyclohexylimidazol-2-ylidene

SILS ..... stable isotopically labelled internal standard

TEM ..... transmission electron microscopy

TGA ..... thermal gravimetric analysis

THF ..... tetrahydrofurane

TON ..... turnover number

WAXS ..... wide-angle X-ray scattering

ZPE ..... zero-point energy

Table of Figures

I. Introduction

1. Hydrogen isotopes in organic molecules

Hydrogen $^{1}_{1}H$ has the highest abundance among all elements in the universe. Deuterium $^{2}_{1}H$ is the nonradioactive and herewith the stable isotope of hydrogen. The deuterium atom $^{2}_{1}H$ is composed of one electron and the nucleus which is called deuteron. The deuteron consists of one proton and one neutron. Natural hydrogen is composed to 0.0145% of deuterium.[1] Tritium $^{3}_{1}H$ is the radioactive isotope of hydrogen. The nucleus of the tritium atom $^{3}_{1}H$ consists of one proton and two neutrons. The tritium atom also has one electron. It is a β-emitter, it has a half-life of 12.346 years and a molar activity of 29.2 Ci/mmol which corresponds to 1080.4 GBq/mmol. Naturally occurring hydrogen atoms consist to 10^{-18}% of tritium atoms. In the following, the interest in incorporating hydrogen isotopes in organic molecules is going to be detailed. Since the two isotopes deuterium and tritium differ in certain properties from hydrogen (different spin, higher mass, radioactivity), numerous applications of deuterium and tritium labelled molecules were developed in many fields of life science such as drug discovery.

1.1 Deuterium: the kinetic isotope effect and its applications

Deuterium has a slightly lower electronegativity and electronic polarizability than hydrogen, but both isotopes are chemically mostly undistinguishable.[2] The electronegativity refers to the ability of an atom to withdraw electrons from neighboring atoms and the electronic polarizability refers to the potential of an atom to keep its own electrons. However, if we assume that hydrogen is replaced by deuterium on a C–H bond, a C–D bond is obtained that manifests higher stability. The stability increase is reasoned in the higher mass of deuterium and the weaker vibration frequency that brings about a lower zero-point energy (ZPE) of the C–D bond in the Morse diagram. Hence, the needed energy $\Delta E^{\ddagger}$ to overcome the barrier for bond breaking is then also higher (**figure 1**). This phenomenon is called the kinetic isotope effect (KIE). The KIEs of hydrogen isotopes are the most developed among every other

kinetic isotope effect, since hydrogen is the lightest element in the periodic table. Thus, the relative mass change from hydrogen to deuterium is much bigger than e.g. from ^{11}C to ^{12}C.

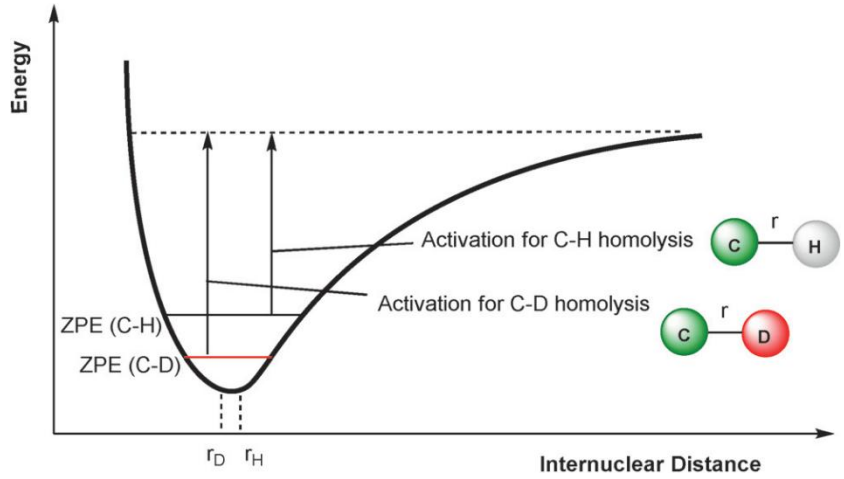

Figure 1. Morse potential of a C–H and a C–D bond illustrating the origin of the KIE. Figure extracted from reference 3.

As mentioned above, deuterium merely appears in low percentages in the natural environment. High amounts of deuterium in living organisms (>20% of the body weight) even revealed to be toxic because it evokes a "solvent isotope effect" and the deuteration of biomolecules, changing kinetics of processes being important for live.[4] However, there are numerous chemical strategies developed with the objective to incorporate hydrogen isotopes in a targeted manner in organic molecules. The most important methods to do so are going to be detailed in chapter **I.***3*. The isotopic enrichment of bioactive molecules and materials by deuterium paves the way to a vast repertory of applications. Some of them benefit from the described KIE and others from the mass shift that is conferred to an organic molecule when its hydrogens are exchanged for deuteriums. Nonetheless, every hereinafter described application benefits from the fact that different isotopes of an element do not significantly differ in terms of chemical and biological properties.

1.1.1 Heavy Drugs

A real therapeutic value of deuterium was demonstrated by the recent commercialization of "Heavy Drugs". In drug development, fluorine was usually used to replace hydrogen in order to stabilize metabolically fragile sites of drug development candidates, such as in the case of pleconaril.[5] However, a major drawback of fluorine is its high electronegativity and the concomitant polarity change of the drug molecule to which it is bound. Thus, compared to

fluorine, deuterium must be a much better bioisosteric substitution of hydrogen. Additionally, a bond stabilization is also achieved through the KIE that appears when hydrogen is exchanged for deuterium. This is evidenced in the recent approval of deutetrabenazine, a deuteroanalogue of tetrabenazine, by the U.S. Food and Drug Administration (FDA) thanks to its advantageous pharmacological and toxicological profile over its protioanalogue (**figure 2**)[6]. By deuterating key metabolism sites, chemists managed to increase the lifetime of the drug and its active metabolites whereas the breakdown of the drug to inactive metabolites could be delayed. This effect reduced the required daily dose and helped to overcome undesired side-effects on patients. Another example for the improvement of a toxicological profile by deuteration is AVP-786, a deutero-analogue of dextromethorphan which is currently under clinical trials (**figure 2**). In certain cases, dextromethorphan had to be applied with the cardiotoxic additive quinidine because dextromethorphan alone is known to be metabolized to rapidly. The development of the deuterated analogue AVP-786 allowed to decrease the amount of required harmful quinidine to a half.[7] Most probably the deuteration of methyl groups like in deutetrabenazine or AVP-786 aims at slowing down the CYP-450 metabolism. The incorporation of deuterium was also performed on a *N*-heterocyclic moiety of the third example to give VX-984, another drug that reached clinical trials. This modification could be potentially useful to slow down the metabolism by the enzyme aldehyde oxidase.[8]

Deutetrabenazine
(SD-809)

Dextromethorphan-d_6
(AVP-786)

VX-984

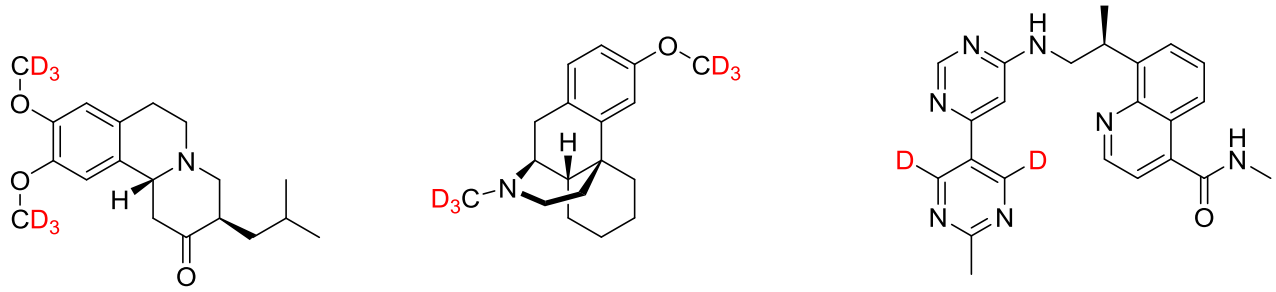

Figure 2. Deuterated tetrabenazine (left, FDA approved), deuterated dextromethorphan (middle, in clinical trials) and VX-984 (right, in clinical trials).

1.1.2 Stable isotopically labelled internal standards (SILSs)

The application of deuterium labelled molecules described herein is based on the fact that the replacement of a hydrogen for a deuterium atom endows an organic molecule with a mass label and generates a shift within its mass spectrum but does not significantly change the chemical properties of the molecule. In this manner, the unlabelled compound and the deuterium labelled compound have the same retention times in liquid- and gas chromatography, but they can be still distinguished through mass-spectrometry (MS) (**figure 3**).

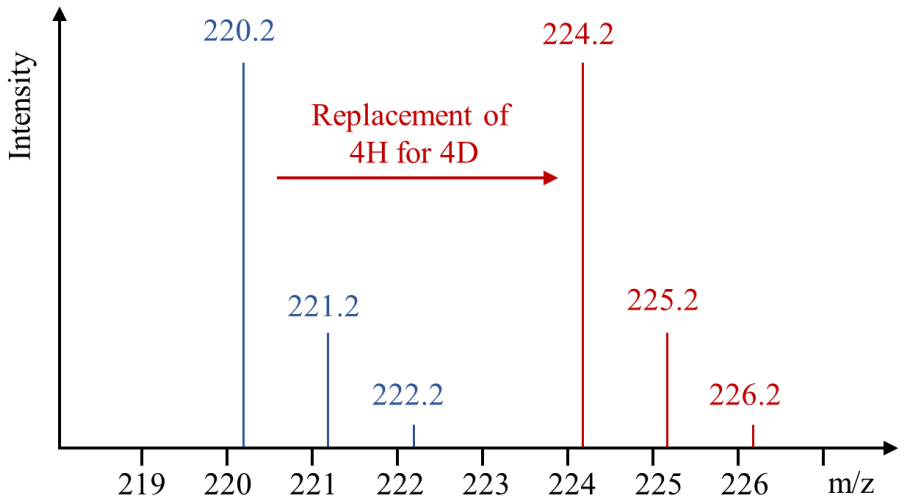

Figure 3. Mass shift achieved when four hydrogen atoms are replaced by four deuterium atoms in a hypothetical organic molecule.

Thus, the deuteration of a molecule of interest can generate an internal standard that paves the way to many analytical tools through liquid chromatography (LC) and gas chromatography (GC) coupled to mass spectrometry (LC-MS/MS, GC-MS/MS). In order to avoid an overlap of the MS pattern of the natural isotopomer and isotopologue distribution of the unlabelled analyte with the MS pattern of the internal MS-standard, in the ideal case, the deuterated internal standard is supposed to accommodate at least three deuterium atoms and to contain less than 0.5% of unlabelled starting material.[9] Isotopologues are mass variants of the same molecule displaying different amounts of isotopes in their chemical structures (**figure 4**, top). Chemical structures of an isotopologue with different isotope substitution patterns and the same molar masses, are called isotopomers (**figure 4**, bottom).

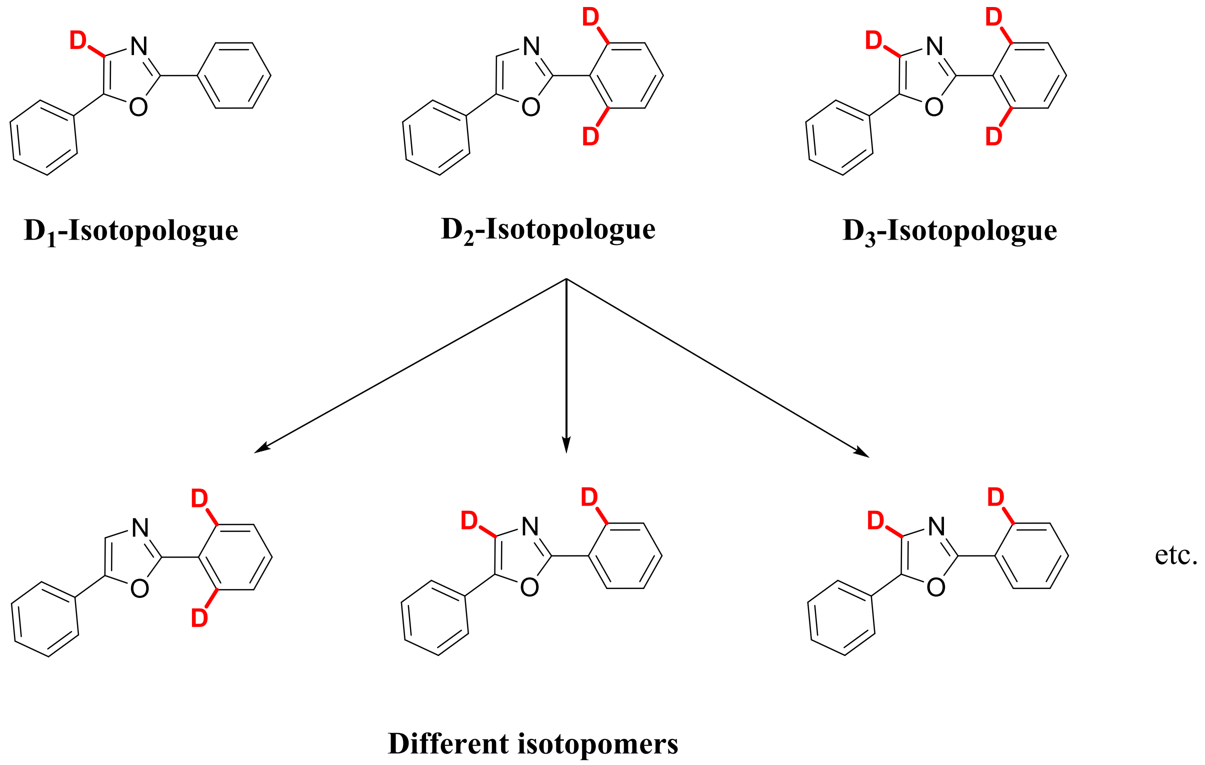

Figure 4. Different isotopologues and isotopomers of 2,5-diphenyloxazole as an example.

A deutero-analogue that is used in this kind of application is referred to as a stable isotopically labelled internal standard (SILS), because deuterium is a stable isotope. The incorporation of other stable isotopes like ^{13}C, ^{15}N and ^{18}O into organic molecules very often proceeds through synthetic pathways and usually not over isotope exchange reactions as for hydrogen isotopes (see chapter **I.***3*). Owing to the availability of more convenient methods for the incorporation of several deuterium atoms per molecule which brings about higher time- and cost efficiency, deuterium can be largely preferred over ^{13}C, ^{15}N and ^{18}O in some of the following applications.

1.1.3 SILSs for metabolism studies of drugs

The first applications of deuterium in metabolism studies are even longer ago than the invention of nuclear magnetic resonance (NMR).[10] Deuterated analogues of drug development candidates are predominantly used by pharmaceutical companies for monitoring the fate of the drug compound issued and its metabolism inside an organism. In the early stages of clinical studies in drug development processes, it is crucial to gain knowledge about the structures, pharmacokinetics and toxicological profiles of every drug metabolite. To this end, usually 1:1 mixtures are prepared from the unlabelled analyte and the deuterated analogue.

After being applied to the body and isolated from a biological liquid (blood plasma, urine etc.) every downstream metabolite stemming from the metabolized drug would show again the characteristic 1:1 pattern in MS-analysis. In this manner, every drug metabolite can be isolated through HPLC and identified, e.g. through additional isotopic labelling (^{13}C labelling for subsequent ^{13}C-NMR analysis).3

1.1.4 SILSs in metabolomics

The term metabolomics defines the study and analysis of the metabolic phenotype of a biological system. The metabolic phenotype refers to the entirety of all metabolites and their quantities in a biological system or sample.[11] Metabolomic studies are subdivided into three main branches. Firstly, the identification and characterization of all metabolites of an organism. Secondly, their quantification and thirdly, the investigation of their pathways inside the organism, in other words, the metabolite flux analysis. The so called untargeted or nonbiased approach in metabolomics is used to determine and to characterize the ensemble of all present metabolites in the sample. The difference between metabolism studies (**I**.*1.1.3*) and untargeted metabolomics is that the latter require the pool of all metabolites which are isotopically labelled, not just the compound of interest. Thus, the internal standard in untargeted metabolomics represents usually a mixture of hundreds of different deuterated metabolites to exclude background ions like sample contaminations which are visible in MS-spectra but do not result from metabolic processes. Such mixtures can be prepared e.g. by supplying [$^{13}C_6$]-glucose to an organism as a feedstock of ^{13}C atoms. However, the determination of the full metabolic phenotype also requires thorough quantifications of every metabolite. This kind of analysis can be disturbed by several factors. On the one hand, highly abundant metabolites could saturate the detector of the mass spectrometer, making the measurement of high metabolite amounts impossible. On the other hand, metabolite concentrations could deviate due to matrix effects of biological probes. Matrix effects occur in mixtures of complex composition and they can affect the stability, binding behavior and other properties of a certain compound which is present in the given mixture. To overcome those effects and to solve these problems, internal standardization through isotopically labelled analogues is effectuated to generate calibration curves for the detector response. For this analytical step, a SILS of the metabolite of interest is needed to be isolated and pure. Hence, it is indispensable to have many alternative methods available for the preparation of

stable isotopically labelled metabolites, also because of the high number of possible metabolites and their structural diversity. The metabolite flux analysis is rather achieved through ^{13}C-labelling. Deuterium plays a minor role in this context, because it is known to have a potential impact on metabolic pathways, as described for "Heavy Drugs" in section **I**.*1.1.1*. Published works using deuterated molecules for this purpose are still known. Metabolic fluxes in potato tubers, for example, could be elucidated by incubating tuber slices with deuterated phenylalanine and subsequent LC-MS analysis.[12]

Apart from drug development, metabolism studies and the investigation of other cellular processes, deuterium is applied in many other disciplines, which cannot be described in detail here. Deuterated analogues are also used in material science[13], for the elucidation of mechanistic pathways in chemical synthesis[14] and different imaging techniques like deuterium metabolic imaging (DMI) by means of magnetic resonance spectroscopic imaging (MRSI).[15] The stability of ^{11}C-labelled radiotracers for positron emission tomography (PET) towards metabolism could be also increased by deuteration.[16]

1.2 Tritium and its applications

The radioactive isotope tritium is produced in nuclear reactors through neutron irradiation of compounds containing high percentages of lithium-6, e.g. lithium fluoride or lithium alloys as Li–Al and Li–Mg. One part is formed as $^{3}H_2$ (T_2) gas and the other part is retained in the solid state which can be recovered chemically. Since tritium is a β-emitter, the maximum penetration depth of the radiation in air is 6mm and in glass or concrete 2µm.[17] For this reason, tritium containing material can be handled in usual glass ware without further risks of irradiation, if all safety rules are respected. The incorporation of tritium into organic molecules is performed in order to obtain tracer molecules and radioligands used in diverse life-science applications. As it could be seen in the precedent sections, light can be already shed on many aspects related to metabolism with deuterium labelled compounds in hand, but the detection of a radioactive compound unambiguously confirms with higher precision that it must be a metabolite of the tritium labelled compound which was applied initially. Radioactive detection also ensures that no relevant compound is missed during analysis of a mixture. Hence, drug metabolism studies are rather carried out through radioactive isotope labelling of the drug candidate. Indeed, when candidates of interest are evaluated within drug development processes, tritiated analogues thereof are constantly demanded for absorption,

distribution, metabolism and excretion (ADME) studies. The general preference of ^{3}H over ^{14}C can be explained in the lower costs and more rapid procedures for the preparation of tritium labelled compounds. However, the common risk of tritium and deuterium labels is that they can be lost more easily then ^{13}C- or ^{14}C labels when attached to a position being sensitive to metabolic degradation. *In vitro*, tritium labelled drug development candidates or reference compounds, i.e. well-characterized benchmark compounds, are mainly used for radio ligand binding assays. Although there is a big variety of strategies using different tags, the general objective is the determination of the affinity of a compound to a biological target, which is very often a protein. In a typical example of an *in vitro* competitive binding assay, a tritium labelled reference ligand [^{3}H]-astemizole, the membrane suspension of a cell that was transfected before with the membrane protein of interest (**figure 5**, vial 1) and the analyte, a small-molecule drug as potential inhibitor of the membrane protein, were incubated together (**figure 5**, vial 2). After filtration and washing of the mixture, the value of the scintillation counter reflected the amount of bound radioligand relative to the amount of bound analyte (**figure 5**, vial 3).[18]

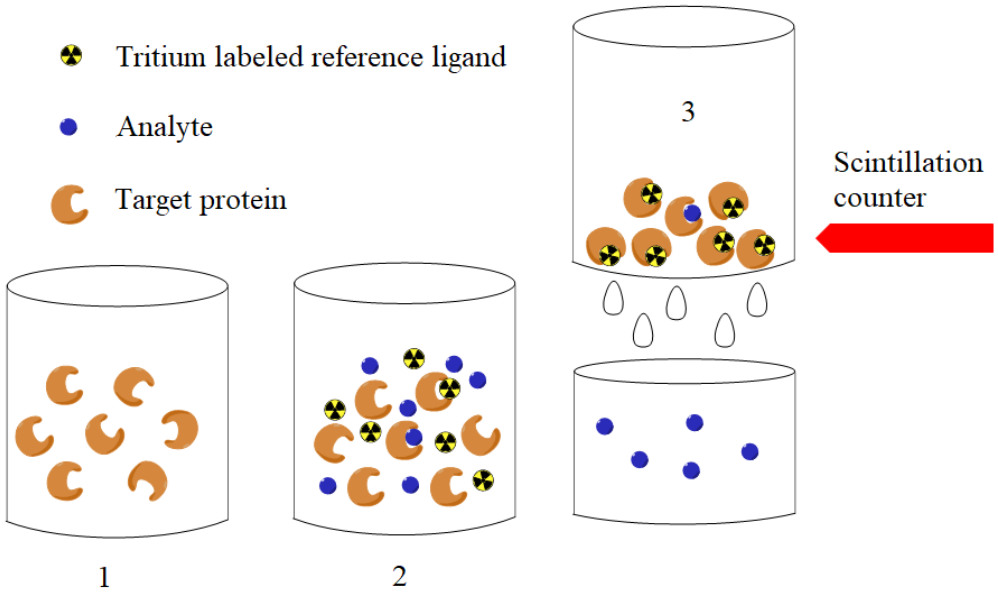

Figure 5. General principle of a competitive radioligand binding assay

Tritium labelled compounds also allow to monitor a compounds distribution and clearance from a body and single organs, which are additional features and probably the main objectives of ADME studies. One example is quantitative whole body audioradiography (QWBA) that visualizes the accumulation behavior of a tritiated drug candidate in the body of small animals. This allows to calculate and to estimate the maximum dose of the radioactively

labelled drug candidate that can be applied to a human test candidate in ongoing clinical ADME studies.

1.3 Analysis of molecules labelled by hydrogen isotopes

This section is going to explain how to determine whether the structure of an organic molecule contains a certain isotope (^{2}H or ^{3}H). Further, the question is addressed how to figure out at which position of its structure the isotope is situated. The quantification of the isotope labelling, in other words, the determination of the isotopic enrichment, will be also addressed in relation with the presented analytical methods. The isotopic enrichment is the percentage of molecules present in a given mixture of isotopologues and isotopomers which incorporates the isotope of interest at a certain position of the chemical structure. As chemical differences between hydrogenated and deuterated or tritiated small molecules are usually not measurable under clinical conditions, a chromatographic separation and isolation of every isotopologue and isotopomer of the same molecule is not possible. For this reason, isotope chemistry requires analytical methods being able to unambiguously indicate the presence of an atom and to quantify its abundance with high accuracy.

1.3.1 Mass spectrometry

Mass spectrometric analysis is the most reliant method to confirm the presence of compounds in complex mixtures and to determine their isotopic composition as already mentioned at the beginning of section **I**.*1.1.2* with **figure 3**. The principle of mass spectrometry is to ionize the molecules in the probe and to bring their ions into the gas phase, either by electrospray ionization (ESI) or matrix assisted laser desorption ionization (MALDI). For the ESI process the analyte solution is conducted through a metallic capillary and at its tip, an electrical field is applied that leads to an ionization of the molecules, either to positively charged species by a cation uptake (H^{+}, Na^{+} etc.) or to negatively charged species by proton releases. The ions migrate then to the counter electrode at the opposite of the capillary outlet. In MALDI, the analyte is embedded into an organic matrix together with inorganic salts. Molecules are excited and released for example by a nitrogen laser. Collisions in the gas phase lead to the formation of ions. Ions in the gas phase can be then accelerated by the application of an electrical field.[19] The ion separation and analysis by their mass to charge ratio (m/z) can

proceed on different ways. Quadrupole mass spectrometers conduct the ion beam through an oscillating voltage that is applied between four parallel metallic rods. Just ions with a defined m/z can pass the quadrupole at a given voltage. Thus, by tuning the quadrupole voltage, the whole m/z range of the analyte can be monitored. The time of flight (TOF) mass spectrometer gives the same initial energy to all ions by accelerating them over a short distance. Then, the time they need to cross a defined way is measured by a detector at the end. The higher the mass of the ion, the longer it needs to fly to the detector. Given that isotope incorporations always result in mass changes, mass spectrometry is used as the most current method in isotope chemistry because it is able to measure even the tiniest mass shifts. Consequently, isotopologue mixtures can be thoroughly analyzed, since isotopologues also manifest separation on MS spectra. On this path, the measurement of relative isotopic abundances (RIS) becomes possible, for example of naturally occurring isotopologues or after isotope labelling experiments. In a hydrogen isotope labelling experiment, the type and the quantity of hydrogen isotopes incorporated on the same molecule (+ ~1g/mol for the replacement of one hydrogen for one deuterium or + ~2g/mol for the replacement of one hydrogen for one tritium) can be determined by computer-assisted methods from the recorded MS-spectrum, given that the different intensities or integrals of the mass peaks reflect the ratio of isotopologues in a mixture. To this end, the isotopologue mass peaks are integrated before and after the deuterium incorporation and the contribution of the natural isotope abundance is subtracted from the integrals of the labelled molecule. An example is given in **figure 6** by ESI-MS. In order to determine the amount of D_1-isotopologue after the deuteration of a theoretical molecule (**figure 6b**, red spectrum), the integration value of the peak that appears in spectrum **a** at the same mass shift (161.2) needs to be subtracted from the integration value of the D_1-isotopologue in spectrum **b**. The same procedure is repeated for every isotopologue peak of the labelled material. The D_0 peak in spectrum **b** gives the amount of unlabelled starting material left after the deuteration experiment. The total isotope incorporation on the whole molecule is obtained by the sum of all deuterated isotopologue amounts relative to the amount of unlabelled starting material left.

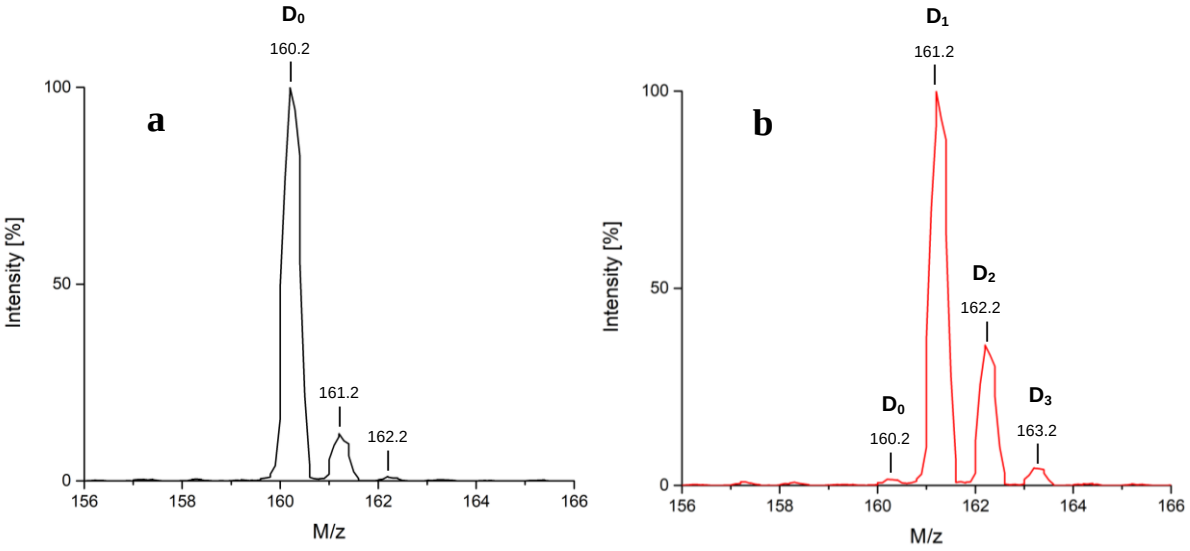

Figure 6. (**a**) Natural isotope pattern of a starting material (**b**) ESI-mass spectrum of the same molecule after deuterium incorporation

High-resolution mass spectrometry even allows differentiating other types of stable isotopes (^{2}H, ^{13}C, ^{15}N, ^{18}O). If a molecule contains different types of stable isotopes, higher mass isotopologues can be split into several interfering mass peaks. The slight shifts between different isotopes can be interpreted by the different gaps in mass, e.g. between protium and deuterium (M(^{2}H) - M(^{1}H) = 1.0063g/mol) and ^{12}C and ^{13}C (M(^{13}C) - M(^{12}C) = 1.0031g/mol). Thus, the peak of an isotopologue possessing just one deuterium would be shifted by 0.0032g/mol compared to the peak of an isotopologue possessing just one ^{13}C. These isotopic distances are related to the different sums of protons and neutrons in chemical elements. The high-resolution potential of this technique resolves interferences between mass peaks, it indicates whether a mass shift results from the one or the other isotope and permits computer-assisted quantifications, which is also relevant for environmental geochemistry, earth- and planetary sciences.[20]

1.3.2 NMR spectroscopy

NMR spectroscopy provides information about the nuclei present in an organic molecule, their ratios in the molecular framework and their electronic situations. An NMR spectrometer consists of a magnet that can generate a strong and homogeneous magnetic field and a source of electromagnetic radiation from the radiofrequency range. When an analyte is placed into the magnetic field, atomic nuclei with a nuclear spin $I = \frac{1}{2}$, as hydrogen for example, form two different energetic levels $m_I = +\frac{1}{2}$ and $-\frac{1}{2}$ with the transition $\Delta E = \gamma\hbar B_0$ between both (γ is

the gyromagnetic ratio, $\hbar = \frac{h}{2\pi}$ with h as the Planck constant, B_0 is the strength of the magnetic field, **figure 7**). At this stage, the nuclei are able to absorb electromagnetic radiation to undergo excitation from one level to the other if the condition $h\nu_L = \gamma\hbar B_0$ is fulfilled. The frequency ν_L that is needed to excite the nucleus is called Larmor-frequency.[21]

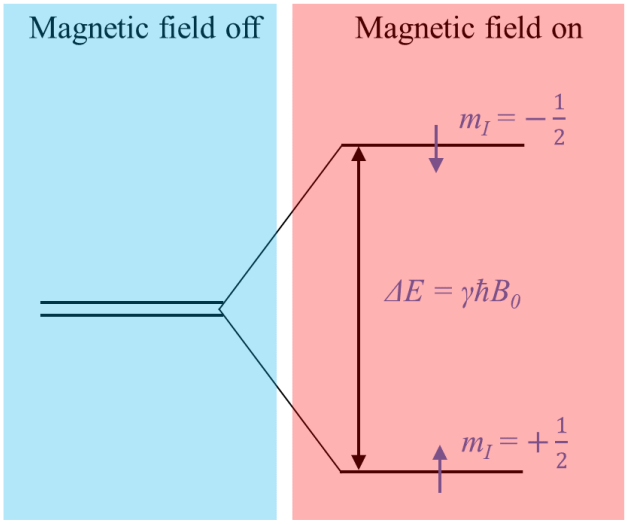

Figure 7. Split of the energetic levels of a nucleus with the spin $I = \frac{1}{2}$ in a magnetic field

Further, the applied magnetic field interacts with the electrons of every atom and induces an additional little magnetic field that contributes to the local magnetic field at the nucleus. As a result, the local magnetic field at the nucleus of every atom is never equal to the applied magnetic field. Thus, if B_0 is replaced for B_{local}, the condition for resonance turns into $h\nu_L = \gamma\hbar B_{local}$ and the Larmor-frequency depends now on the strength of the local magnetic field which is different for every nucleus of the molecule, regulated by the electronic situation. For this reason, same atoms that are situated at different positions of a molecule usually have different Larmor-frequencies. When a measured resonance is converted to the NMR spectrum by a "Fourier transformation", the chemical shift of every nucleus can be then related to its electronic situation. The less a nucleus is shielded by its electrons, the more downfield the NMR signal appears in the spectrum. However, exact attribution of NMR signals to corresponding nuclei usually succeeds through coupling effects. Coupling, the spreading of signals into multiplets, occurs because magnetic moments of neighboring nuclei interact. The formula to calculate the multiplicity is $2nI+1$, where I is the spin and n the number of equivalent nuclei the considered nucleus is coupling with. ^{1}H-NMR spectroscopy is used in hydrogen isotope labelling in order to reveal the exact positions of the incorporated isotope in

the structure of a molecule, as demonstrated on 1-phenyl-1*H*-1,2,4-triazole in **figure 8**. By comparing the spectra of the non-labelled protio-analogue (**figure 8**, top) with the deuterium labelled molecule (**figure 8**, bottom), we will see that integration values diminish for the signals where hydrogen is exchanged for deuterium (**figure 8** bottom, positions **1**, **2** and **3**), because deuterium does not resonate at the frequency of ^{1}H-NMR. Precise isotopic enrichment values of a certain position can be then derived from the integration values (**figure 8**, square brackets). Certain positions can be also assigned by considering the change in multiplicity when hydrogen is exchanged for deuterium on neighboring positions. Since the two **3**-positions are deuterated to 80%, the multiplicity of the **4**-positions changes from a doublet of a doublet (dd) to a doublet (d) as it can be seen in **figure 8** when both ^{1}H-NMR spectra are compared against each other.

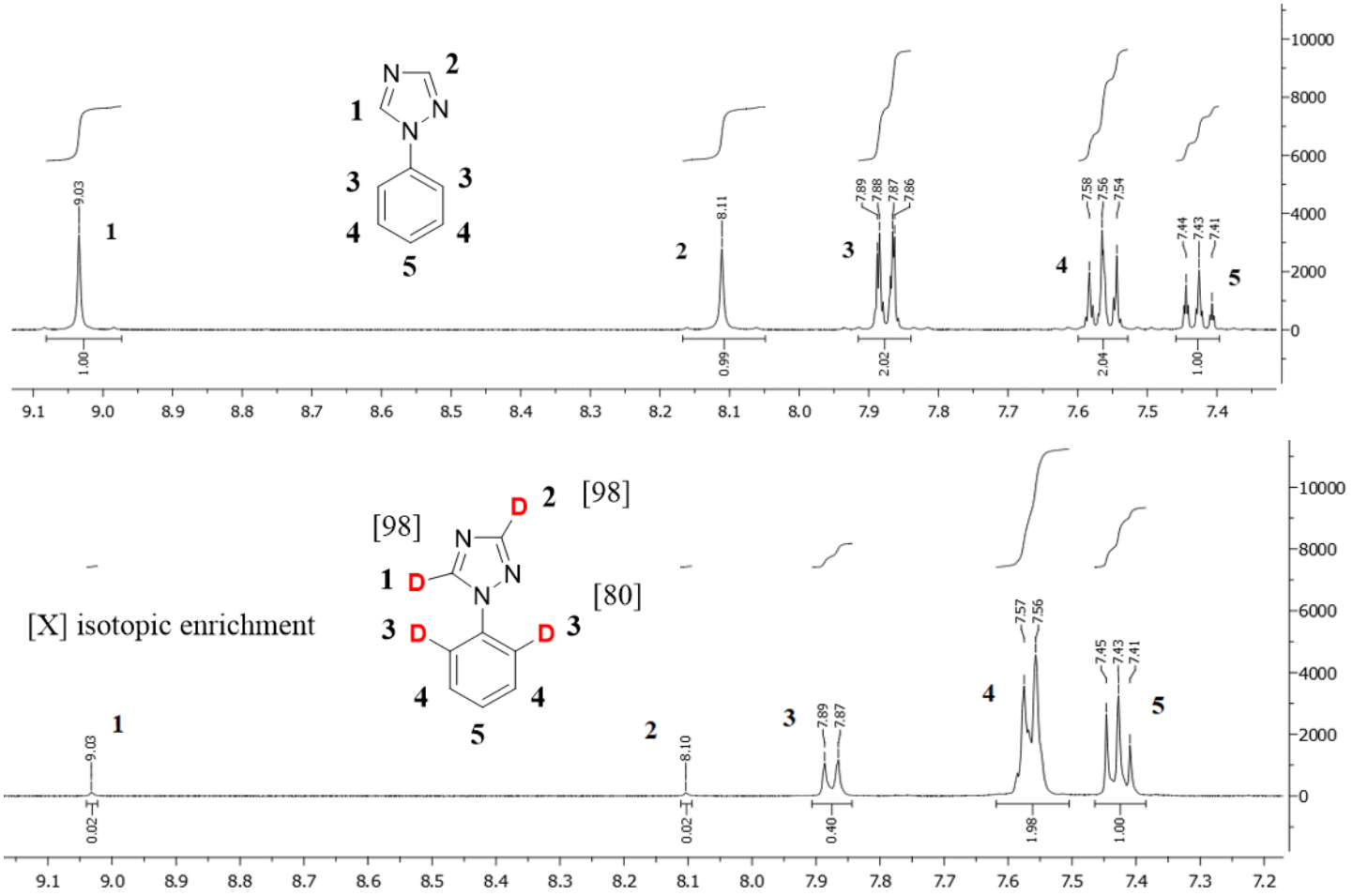

Figure 8. ^{1}H-NMR spectra of 1-phenyl-1*H*-1,2,4-triazole (top) and deuterated 1-phenyl-1*H*-1,2,4-triazole (bottom) with signal assignment, chemical shifts are given in ppm

Proton decoupled ^{13}C-NMR (^{13}C{^{1}H}-NMR) also helps to confirm the deuteration of a position because the multiplicity of a carbon signal where deuteration takes place changes

from a singlet into a triplet, due to the spin of deuterium (I_D = 1). ^{2}H- and ^{3}H-NMR analysis stay the most indispensable tools to thoroughly determine the positions of hydrogen isotopes in a molecule. However, the deuteron has a 6.15 times lower gyromagnetic ratio than the proton which diminishes the resolution in ^{2}H-NMR. For this reason, it is rather common to use high-field NMR instruments and ^{2}H selective cryogenic probes to obtain qualitative ^{2}H-NMR spectra. Additionally, several other technical advances turned ^{2}H-NMR into a very sensitive analytical method that is even able to detect the natural abundance of deuterium. The high sensitivity makes it a very convenient method for hydrogen isotope labelling experiments because every deuterated position in an organic molecule can be thoroughly determined. Further, ^{2}H-NMR is an excellent purity control as it shows the presence of small amounts of deuterated side-products which is not an easy task for other methods.[22] The triton is related to as the most sensitive nucleus for NMR-analysis due to its high gyromagnetic ratio. Additionally, the extremely low natural abundance of tritium leads to an efficient suppression of background signals which facilitates the analysis of ^{3}H-NMR spectra.[23] In order to diminish the fine structure of ^{2}H- and ^{3}H-NMR spectra, it is important to decouple the protons of the molecule from the ^{2}H- and ^{3}H-nuclei and to generate proton-decoupled deuterium- (^{2}H-{^{1}H}) NMR or proton-decoupled tritium (^{3}H-{^{1}H}) NMR spectra. In the following a comparative overview of the properties of the hydrogen isotope nuclei is illustrated (**table 1**).

	^{1}H	**^{2}H**	**^{3}H**
Usual notation	H	D	T
Radioactivity	No	No	Yes (β^--emitter)
Half-life **(Days)**	NA	NA	4540
Natural abundance **(%)**	99.985	0.015	10^{-18}
Spin quantum number **(no unit)**	1/2	1	1/2
Gyromagnetic ratio γ **(MHz.T^{-1})**	42.576	6.536	45.403
Quadrupolar moment **(10^{-24} cm^2)**	0	+2.87 10^{-3}	0
Larmor frequency at 14.09 T **(MHz)**	600.00	92.10	639.98

Relative sensibility[(a)] **(no unit)**	1.00	$9.65\ 10^{-3}$	1.21
Absolute sensibility[(b)] **(no unit)**	1.00	$1.45\ 10^{-6}$	-
Typical Chemical shift range **(ppm)**	0 to 20	0 to 20	0 to 20
Typical T_1 range **(s)**	0.1 to 20	0.1 to 10	0.1 to 10
Typical T_2 range **(s)**	0.1 to 20	0.1 to 10	0.1 to 10
Typical $J_{(H,X)}$ scalar coupling range **(Hz)**	0 to 20	0 to 3 [(c)]	0 to 22 [(d)]
NOE effect by ^1H decoupling	Yes	Negligible	Yes

(a) Value at constant magnetic field or equal number of nuclei
(b) Product of the relative sensitivity and natural abundance
(c) $J_{(D,H)} = J_{(H,H)} \times (\gamma_D / \gamma_H)$
(d) $J_{(T,H)} = J_{(H,H)} \times (\gamma_T / \gamma_H)$

Table 1. Comparison of the hydrogen, deuterium and tritium nucleus[23]

Moreover, due to the radioactive decay of tritium, molecules which contain tritium atoms in their structure are analyzed by scintillation counting. The measured parameter gives the specific activity [Ci/mg] or the molar activity [Ci/mmol] that indicates the amount of tritium atoms present in the structure of a purified molecule.

2. *N*-Based heterocycles: promising bioactive targets for the introduction of deuterium and tritium

The following chapter demonstrates a manifold of important targets for the incorporation of hydrogen isotopes. As we will see, aromatic heterocycles containing nitrogen atoms in their structures (*N*-heterocycles) appear to be highly relevant compounds or structural patterns in many fields of our life as pharma- and food industry. Heterocyclic scaffolds are involved as building blocks in the majority of commercial drugs, with nitrogen containing heterocycles being the most popular among them.[24] 59% of FDA approved drugs contain at least one nitrogen-based heterocycle.[25] For every compound of biological or technological relevance, it is favorable to have available methods that allow labelling by deuterium and tritium. For this

purpose, the most relevant *N*-heterocyclic scaffolds for this work will be classified and the nomenclature of their rings will be explained. Further, light will be shed on their chemical properties and on the advantages or drawbacks to incorporate hydrogen isotopes on certain *N*-heterocyclic sites. Finally, this chapter will analyze in more detail the presence of *N*-heterocyclic scaffolds in Active Pharmaceutical Ingredients (APIs) and the motivation of drug discovery and development to introduce *N*-heterocyclic cores into these agents.

2.1 Nomenclature and numbering of heterocyclic rings

The most relevant scaffolds for the follow-up of this work are introduced in this section. The focus lies on nitrogen-containing five-membered aromatic heterocycles and on structural analogues thereof with attached benzene rings, which are going to be called "benzo-derivatives". Benzimidazole, for example, is a benzo-derivative of imidazole and indole a benzo-derivative of pyrrole (**figure 9**). The numbering starts at the heteroatom that has the highest atomic number in the periodic table, e.g. in oxazole at the oxygen. In imidazole, the N–H has a higher priority than the nitrogen atom without hydrogen. An exception is carbazole which is not considered to be a classical *N*-heterocycle and numbering is started at the attached benzene ring next to the N–H moiety. The numbering continues towards the next heteroatom that is localized closest to the first one. For this reason, the C_2-atom lies between the oxygen and the nitrogen atom in oxazoles and benzoxazoles. Angular atoms are usually referred to with the number of the precedent position and an "a" or "b" is added (**figure 9**). Just angular carbon atoms of nucleobases get own numbers, but this is due to historical reasons.[26]

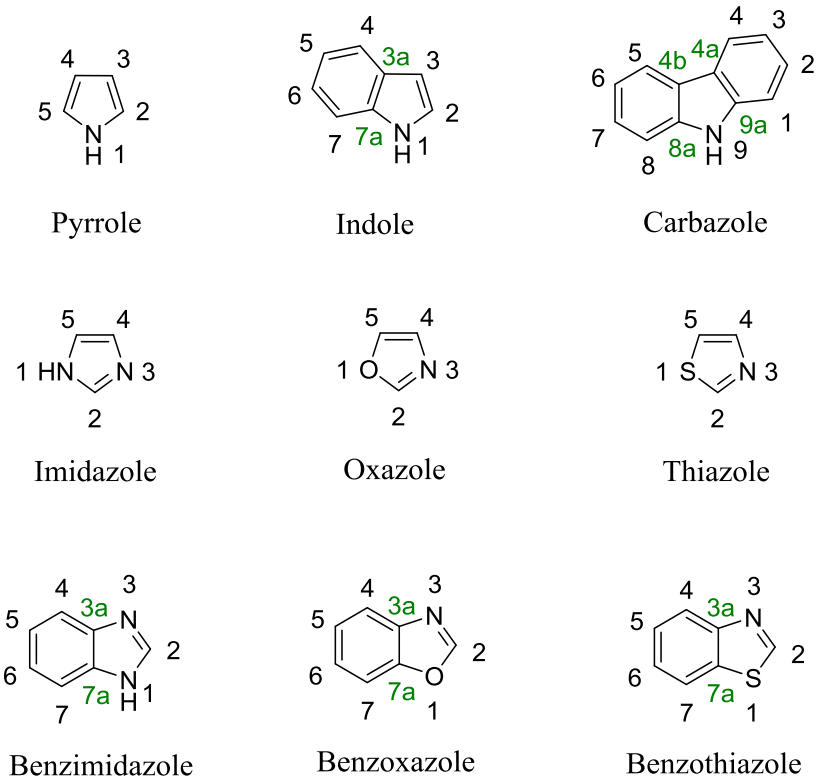

Figure 9. Nitrogen containing heterocyclic scaffolds (*N*-heterocycles) and the numbering of their positions

Sometimes the labels “α”, “β” or “γ” are used to indicate a position on a heterocycle relative to a heteroatom. In this context, “α”, “β” or “γ” would refer to the distance of the considered position from the heteroatom. If we follow this system, the C_2 atom of benzimidazole is the neighboring atom of the two nitrogens, thus, it would be the α position. The C_4 and C_7 atoms would be the β positions relative to the two nitrogen atoms. Positions situated on the third carbon with respect to a heteroatom are referred to as γ positions. The *ortho* positions of the phenyl ring on 2-phenyl-benzimidazole, for example, are γ positions (**figure 10**).

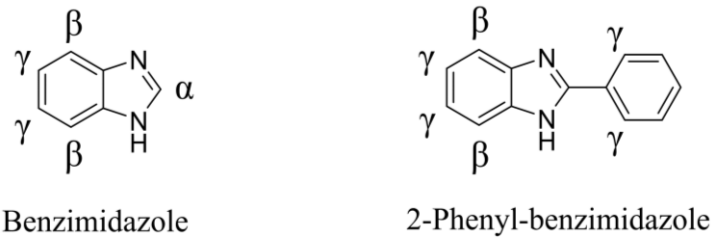

Figure 10. α-, β- and γ positions on benzimidazole and 2-phenyl-benzimidazole as example

Triazoles are named by the arrangement of their nitrogen atoms in the 5-membered heterocycle. This can be a 1,2,3- or a 1,2,4-constellation. In addition, the nomenclature has to

contain the position of the nitrogen atom that carries the proton because tautomerization takes place on both isomers (1,2,3- and 1,2,4-triazole) that leads to tautomers which are chemically different (**figure 11**).[27]

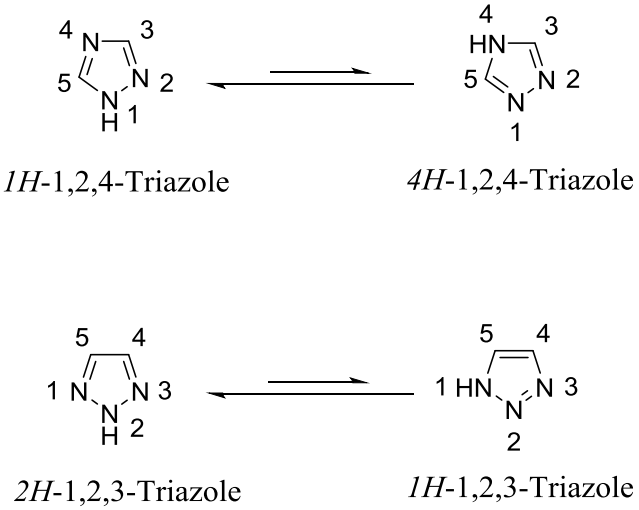

Figure 11. Tautomerism of 1,2,3- and 1,2,4-triazole

Analogous to triazoles, the hydrogen of the N-H moiety in imidazole is also exchangeable and migrates in solution by tautomerism from one to the other nitrogen atom. However, this proton migration yields two equivalent tautomers, thus, the protons on the C_4 and C_5 positions of imidazole also become chemically equivalent and give one signal in ^{1}H-NMR. The same goes for benzimidazole (one signal for C_4–H and C_7–H, another signal for C_5–H and C_6–H).

2.2 Basicity/acidity of N-Heterocycles

Every position in a *N*-heterocycle's structure displays a certain acidity, say, a tendency to be deprotonated or to exchange the proton in the presence of a proton acceptor. Acidity depends on several factors, but if we first just have a look at unsubstituted or simply substituted *N*-heterocycles, it is mostly the electronic situation of the considered position that defines the pK_a. Generally speaking, sites next to a heteroatom or between two heteroatoms, i.e. in the α position of heteroatoms, display the highest acidity from every other position in the ring, reasoned in the higher electronegativity and electron-withdrawing effect of the heteroatoms (**figure 12**).[28]

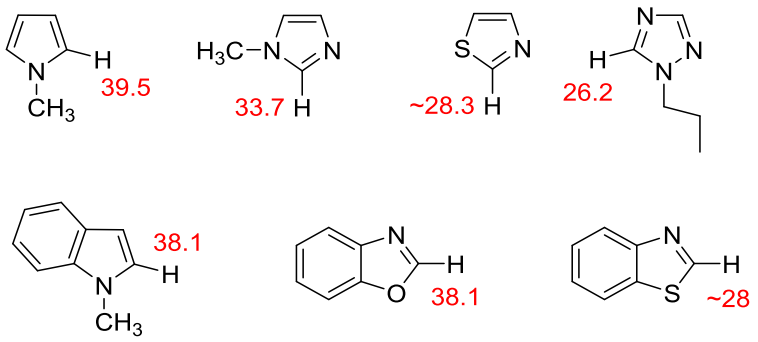

Figure 12. pK_a values of some acidic *N*-heterocyclic protons measured in THF

For the upcoming work, the provided pK_a values by Fraser *et al.* in **figure 12** are just benchmarks because they do not take into account further substituent effects on the conjugated aromatic rings. Consequently, they do not replace test experiments at higher temperatures by adding deuterated solvents (D_2O, CD_3OD), bases, acids etc. to estimate the acidic or basic character of a given *N*-heterocyclic derivative. The isotopic enrichment within such a test experiment, will indicate the positions on the *N*-heterocycle where also back-exchange can be theoretically expected in the presence of proton acceptors, even after successful introduction of the isotope label, e.g. by one of the methods that are going to be shown in the next chapter (**I**.*3*). Consequently, targeting *N*-containing heterocyclic moieties for the chemical incorporation of hydrogen isotopes bears the risk to lose a label that has been introduced over cost and time demanding chemical transformations. In the case of a tritium back-exchange, the impediment would be even twofold. On the one hand, undoubtedly, the loss of the tritium label from the labelled candidate is everything else than encouraging, and on the other hand, the formation of a potentially volatile and radioactive solvent represents an additional safety issue. Apart from that, it can be in so far reasonable to label *N*-heterocycles by hydrogen isotopes as we consider that the majority of *N*-heterocyclic sites exhibits practically no acidity, many of them are even known to be relatively stable towards metabolism. Last but not least, it is mainly due to the vast presence and application of *N*-heterocycles in pharmaceutical-, agrochemical- and material sciences that methodological research for the incorporation of hydrogen isotopes is needed for this group of compounds.

2.3 Implementation as therapeutics, in agricultural chemistry & material sciences

Among all other fields of application, *N*-heterocyclic scaffolds are mostly represented in bioactive molecules. The latter comprise natural products like nucleobases, amino acids,

hormones, cofactors, poisons etc. but also synthetic substances like drugs and agrochemicals. Since the structures of numerous natural bioactive molecules are built up of *N*-heterocycles, drug discovery often aims at mimicking a natural structure by preserving the same heterocyclic core and endowing it with a different substitution pattern to achieve or to enhance the desired effects. A medicinal chemist could call such a bioactive natural product the "lead structure". The term "lead structure" refers to a molecule that has attracted interest because of its promising effects and that serves as template in the ongoing drug development and optimization process. Popular examples for this strategy of drug design are nucleoside analogues, mostly used as anti-tumor agents (cytostatics).[29] An example, for copying the imidazole scaffold of a natural neurotransmitter into a drug´s structure that is supposed to have a higher affinity to the same receptor, is demonstrated in **figure 13**. The design of the drug cimetidine, an antagonist of the H_2 receptor, was based on the structure of the natural ligand histamine.[30]

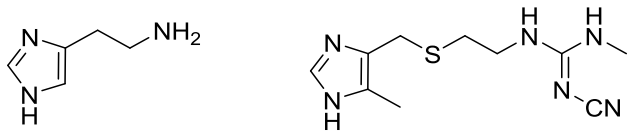

Histamine Cimetidine

Figure 13. Structures of histamine, the natural ligand of the $H_{1\text{-}4}$ receptors (left), and the H_2 antagonist cimetidine (right)

Another common strategy in drug discovery and development is the substitution of functionalities in a lead structure by heterocycles to form bioisosters, also called biomimetics, which is probably the broadest application of the shown *N*-heterocyclic scaffolds in section **I**.*2.2* for drug development, because some of them such as triazoles are mostly absent in natural molecules. The objective of using a bioisoster is to achieve either a stronger interaction between the drug and the desired target in the body or more convenient pharmacological drug properties.5 In most cases the introduction of an aromatic *N*-heterocyclic scaffold in the structure of a drug development candidate is considered to establish hydrogen bonds, more efficient metal ion complexation or π-interactions in the binding pocket of an enzyme. This can be achieved by presenting conformationally restricted proton donors or -acceptors, aromatics for π-interactions or chelating groups for metal complexation. Indeed, each of these properties is accommodated by one or several *N*-heterocyclic scaffolds. **Figure 14** shows an example for the replacement of a *cis*-olefin by an

oxazole during a development process of inhibitors of ADP- and collagen induced blood platelet aggregation.5 Indeed, it was crucial for the drug´s efficiency to introduce a central oxazole. This modification furnished BMY-45778, the compound in middle with a much lower EC_{50} value, compared to the olefin on the left (**figure 14**). EC_{50} is a pharmacological parameter that indicates a ligand concentration at which 50% of the expected effect is observed. Based on several data, the oxazole unit of BMY-45778 in the red box is most probably involved in a decisive hydrogen bonding with the PGI_2 receptor. Further, this hypothesis is reinforced by the EC_{50} of the isomeric compound on the right (**figure 14**). The drug candidate loses its efficiency almost completely as soon as the nitrogen atom of the central oxazole, being the stronger hydrogen bond acceptor inside the 5-membered heterocycle, is exposed to the opposite side (see the trend of EC_{50} values, **figure 14**).

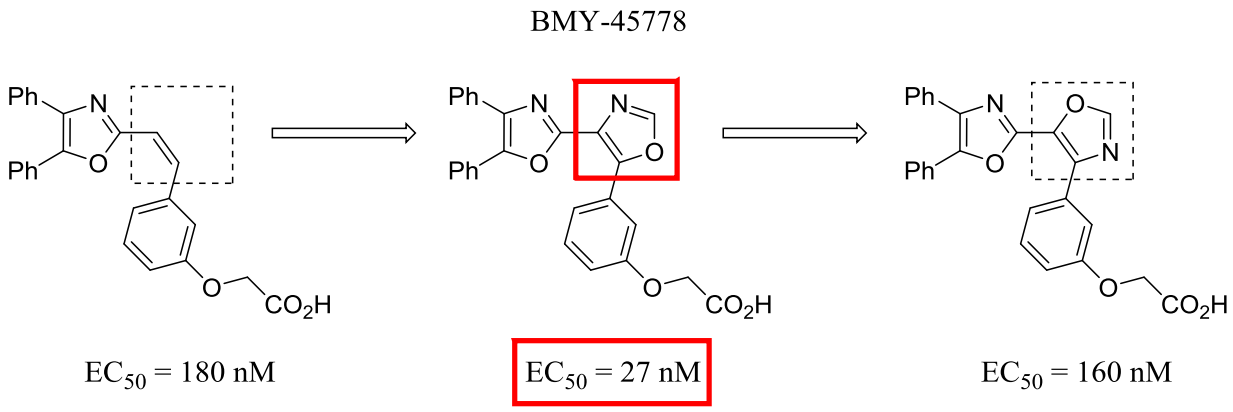

Figure 14. EC_{50} dependence on the C – C double bond - oxazole substitution on PGI_2 receptor ligands.

In the following, the interest in *N*-heterocycles, which are relevant for this work, is going to be explained and exemplified by illustrating popular bioactive compounds that accommodate the respective *N*-heterocyclic unit in their structure. As already alluded with **figure 14**, the oxazole unit is utilized as a versatile hydrogen bond acceptor in drug development, because it has two different heteroatoms for doing so. Further, the C_2-H position of oxazole is able to establish weak interactions by acting as H-bond donor.5 Since many oxazole-based drugs are well-established on the market,[31] oxazole is considered to be a perspective scaffold for the discovery of new drugs. The work with oxazoles is an emerging field given the wide range of newly synthesized aryl derivatives which manifested promising potency as anti-tuberculosis and patented anti-cancer agents.[32] Consequently, an upcoming request for the synthesis of isotopically labelled analogues for ADME studies can be expected.[33] Moreover, the oxazole

core is accommodated in the structures of natural alkaloids, e.g. pimprinine, pimprinoles A-C and many others[34]. Pimprinine in particular has gained attention with regard to its important anticonvulsant[35] and antiviral activity (left, **figure 15**).[36]

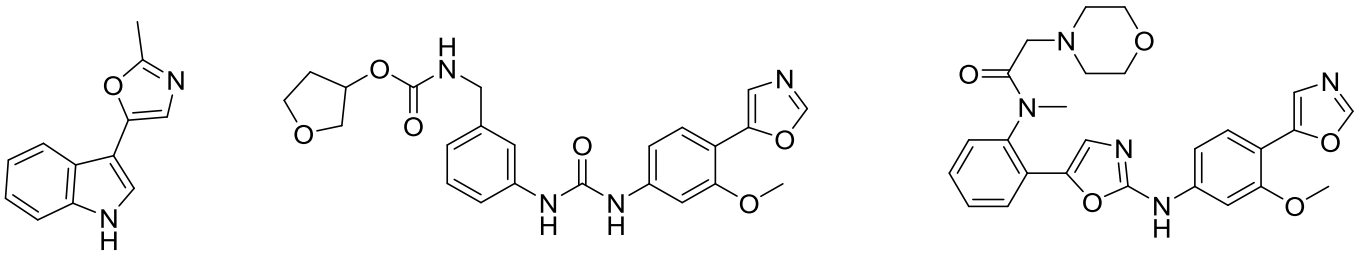

Pimprinine Merimepodib BMS-337197

Figure 15. Examples of an oxazole-based natural product (left) a commercial drug (middle) and a patented drug development candidate (right).

The Imidazole scaffold can play the role of a hydrogen bond donor and a hydrogen bond acceptor at the same time within drug design. Apart from cimetidine in **figure 13**, imidazole is a widespread nucleus in the structures of many other commercial drugs as it can be seen in **figure 16**, e.g. in drugs for the treatment of osteoporosis (zoledronic acid)[37], spinocerebellar degeneration (taltirelin);[38] but also in sedative-analgesic agents (midazolam, dexmedetomidine)[39] and antifungal drugs (bifonazole).[40] A few molecules of the latter do not even display complex functionalization, like bifonazole or the α_2 agonist dexmedetomidine (**figure 16**).

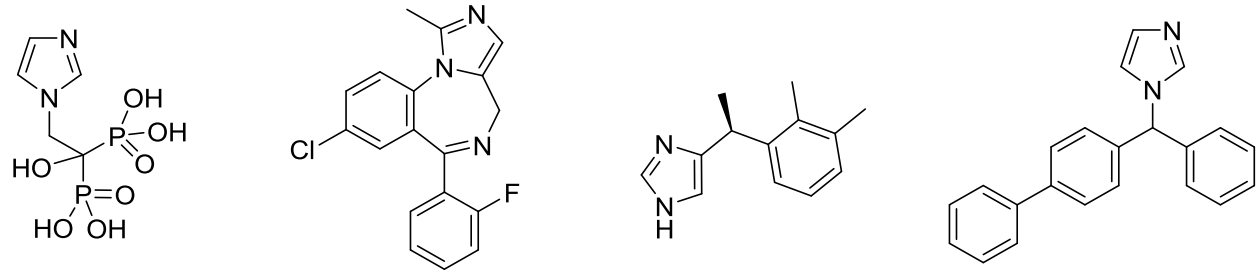

Zoledronic acid Midazolam Dexmedetomidine Bifonazole

Figure 16. Marketed imidazole-based bioactive molecules

1,2,4-triazoles are also prominent structural motives in many fields of life as medicine and agrochemistry. Some reviews present a synopsis of their recurrence in several antifungal drugs, fungicides, pesticides and sedative agents.[41] Additionally, the 1,2,4-triazole group can be also found in anti-tumor-[42] and anti-migraine agents (**figure 17**).[43] Due to the frequent occurrence of the 1,2,4-triazole scaffold in all those types of molecules, there is an obvious

and high interest in the preparation of hydrogen isotope labelled analogues of 1,2,4-triazole containing bioactive molecules.

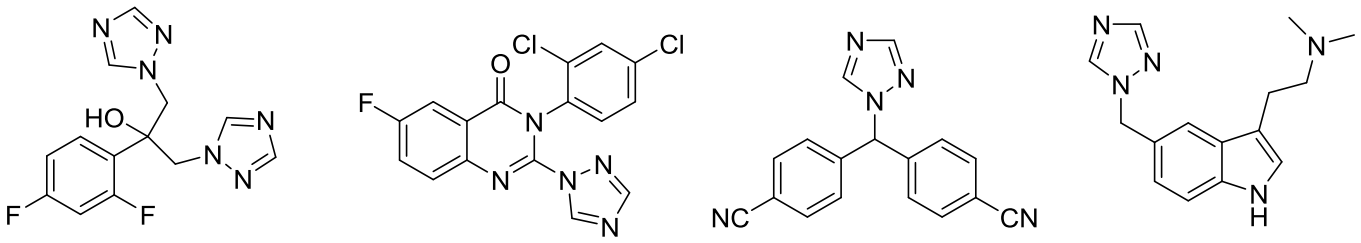

Fluconazole Fluquinconazole Letrozole Rizatriptan

Figure 17. *1H*-1,2,4-triazole-based antifungal drug (first from left), -fungicide (second from left), -anti-tumor- (third compound) and anti-migraine agent (fourth compound)

The popularity of *N*-heterocyclic benzoderivatives especially refers to their implementation as bioisosteres in drug design, reasoned in their low basicity and capability to form hydrogen bonds at the same time. This is manifested in the high ranking of benzimidazole derivatives in the top 25 of the most frequent nitrogen heterocyclic drugs approved by the FDA. The benzimidazole motif contributes to the affinity of drugs to their target by acting as a bioisostere for phenols, catechols, amidines and guanidines.5 Benzoxazoles can serve as conformationally restricted biomimetics for *N*-aryl amides. The H_1-antihistamine astemizole is representative for benzimidazole-based drugs (**figure 18**). Although it was withdrawn from the market in 1997,[44] astemizole and tritium labelled astemizole stayed important benchmark compounds for ADME studies, as shown in chapter **I**.*1.2*. Two benzoxazole-based drug examples are tafamidis, used for the treatment of transthyretin amyloidosis, and benoxaprofen, an anti-inflammatory drug which was also withdrawn from the market due to its hepatotoxicity (**figure 18**). Deuterated benoxaprofen in particular could be even applied by a pharmaceutical company as an internal standard for metabolism studies in man.[45]

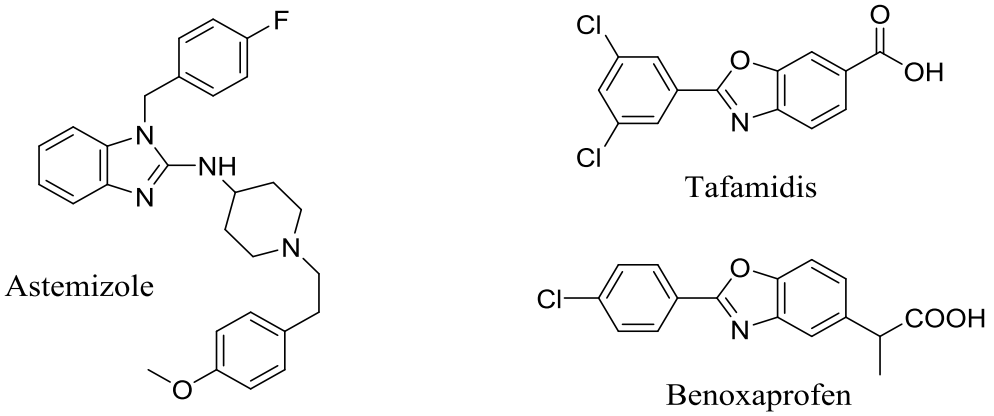

Figure 18. Molecular structures of astemizole, tafamidis and benoxaprofen

The placement of a sulfur atom inside a heterocycle, like in the case of benzothiazole, thiazole and thiophene, gives one additional opportunity for inducing conformational constraints in the design of drug structures. Electron-rich atoms such as carbonyl oxygen- or heterocyclic nitrogen atoms are able to interact with heterocyclic sulfur atoms through $n_0 \rightarrow \sigma^*$ donations. The underlying explanation for this attraction between two heteroatoms is the electronic situation of sulfur atoms which are embedded in aromatic systems. Given that sulfur and carbon have the same electronegativity, heterocyclic sulfur atoms receive a partial positive charge due to the -M effect of neighboring sp^2 carbon atoms (**figure 19**, bottom). This effect paves the way to control the three-dimensional conformation of a drug e.g. by biasing coplanar conformation of two aromatic heterocyclic moieties. This principle was demonstrated within the optimization of p38α MAP kinase inhibitors (**figure 19**). X-ray cocrystal analysis of both isomers shown in **figure 19** with the enzyme confirmed the sulfur-nitrogen interaction and the coplanarity of the thiazole- and diazine groups. In this context, the isomer on the left revealed to be the more efficient ligand because its conformation was more adapted to the enzymatic binding pocket, which is manifested in the lower IC_{50} value (compare IC_{50} values in **figure 19**). IC_{50} is the half maximum inhibitory concentration that defines the concentration of ligand needed to inhibit 50% of the targets present in a system.

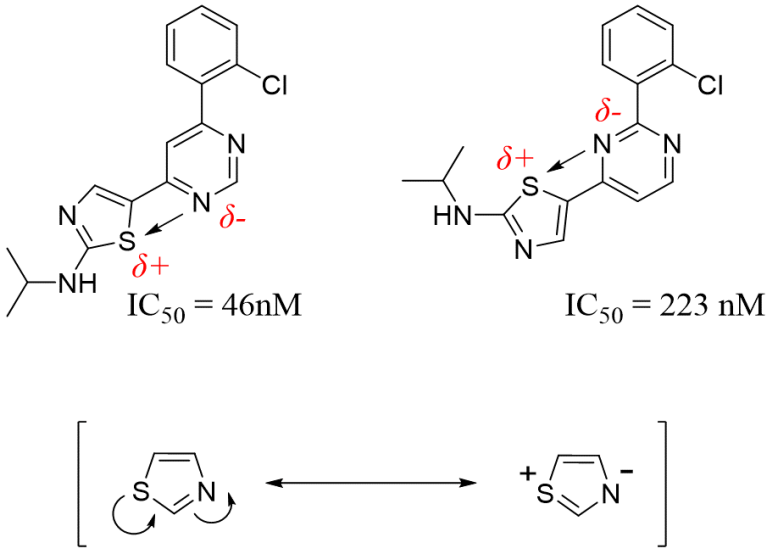

Figure 19. The effect of thiazole on the conformation of drugs.

The carbazole scaffold is encountered in many natural products owning interesting pharmaceutical properties. One example that attracted the attention of many researchers was staurosporine (**figure 20**, left).[46] From a therapeutic point of view, the carbazole-containing drug carvedilol is used as a nonselective beta and alpha-1 blocker for treating congestive heart failure, left ventricular dysfunction and high blood pressure (**figure 20**, middle). Carprofen is an anti-inflammatory drug for animals (**figure 20**, right). Carbazoles are also frequently used in material science as fluorescent molecules, where deuterium incorporation may be interesting in order to enhance their fluorescence properties.[47]

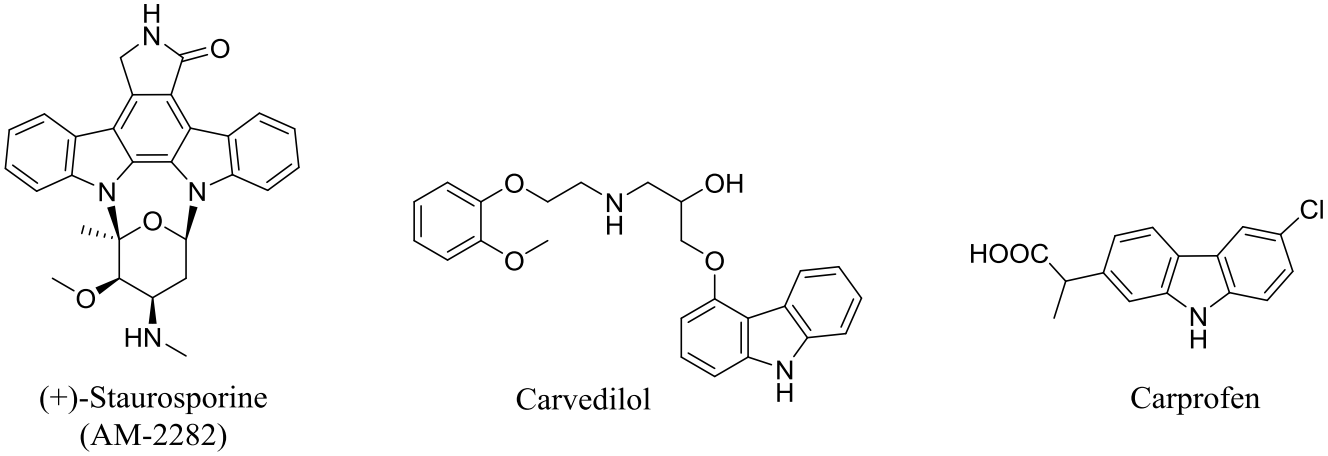

Figure 20. Carbazole-based natural product (left) and two commercial carbazole drugs (middle and right)

Deuterated analogues of carbazole based drugs like deuterated carvedilol are recurrent in literature because they are required for a manifold of different studies connected to the metabolism of this kind of compounds.[48]

3. Existing methods for the incorporation of hydrogen isotopes into organic substrates

The precedent chapters of this work have shown that the incorporation of hydrogen isotopes into organic molecules is of multifaceted interest. Further, it was demonstrated that *N*-heterocycles are relevant and perspective targets to be labelled by deuterium and tritium. The upcoming chapter is going to show and discuss methods for the preparation of molecules whose hydrogen atoms are replaced by hydrogen isotopes. A synopsis of general methods for the introduction of hydrogen isotopes through chemical transformations will be given. However, a particular focus will lie on methods adapted for the deuterium and tritium labelling of *N*-heterocycles. In this context, it will be also outlined that existing methods for the hydrogen isotope labelling of *N*-heterocycles shown in chapter **I**.*2* are scarce and suboptimal in certain aspects.

3.1 The synthetic approach

Synthetic approaches refer to methods that need more than one reaction step to generate the deutero- or tritio-analogue of the molecule of interest. Owing to the availability of modern catalytic exchange methods, nowadays (see chapter **I**.*3*.*2*), synthetic approaches are rather considered to be conventional approaches. Acid-base reactions are the most logical way to exchange hydrogen for deuterium on many heterocycles, based on the pK_a values of *N*-heterocycles provided in chapter **I**.*2*.*2*. However, an efficient deprotonation of the C_2–H position of oxazoles for example, can be just achieved by strong bases like organolithium reagents[49] or sodium methoxide (NaOMe).[50] The deuteration then occurs through quenching with deuteroxide (D_2O) or D_4-acetic acid for the deprotonation with organolithium reagents (equation (1), **figure 21**) or in an equilibrium with deutero-methanol (MeOD) as solvent in the case of NaOMe (equation (2), **figure 21**).

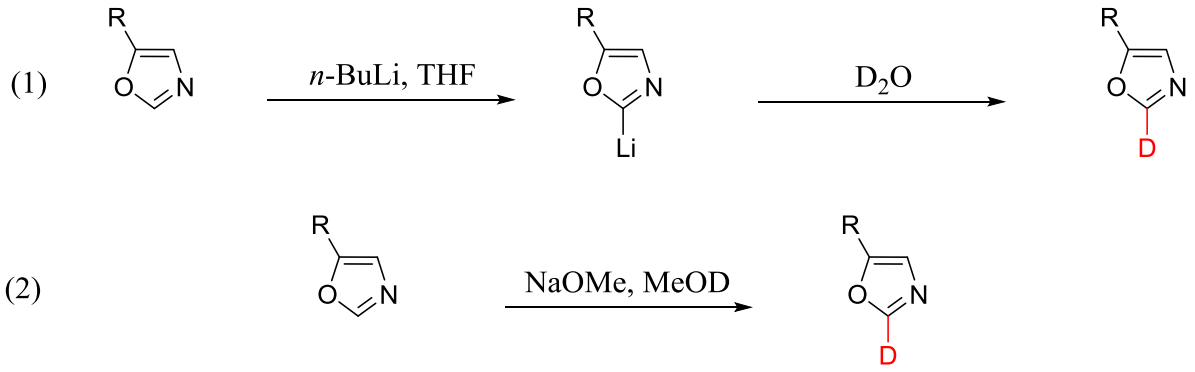

Figure 21. Deuteration of oxazole derivatives through acid-base reactions with deuterated solvents

As discussed in chapter **I**.*2.2*, the risk of labelling such positions is to lose the hydrogen isotope gradually through back-exchange in the presence of moisture and other protic solvents. Another strategy would be to label a certain position through an acid-base reaction in the course of a multi-step synthesis and to stabilize it by removing the acidic character of the position carrying the isotope label in further reaction steps. An example is illustrated in **figure 22** that shows the multi-step syntheses of deuterated fluconazole. Deuterium is incorporated in step (2) through an enol-carbonyl equilibrium. In step (3), the carbonyl is transformed into an epoxide by a Corey-Chaykovsky reaction and stable deuterium labelled fluconazole is obtained after one more nucleophilic substitution in step (4) (**figure 22**).[51]

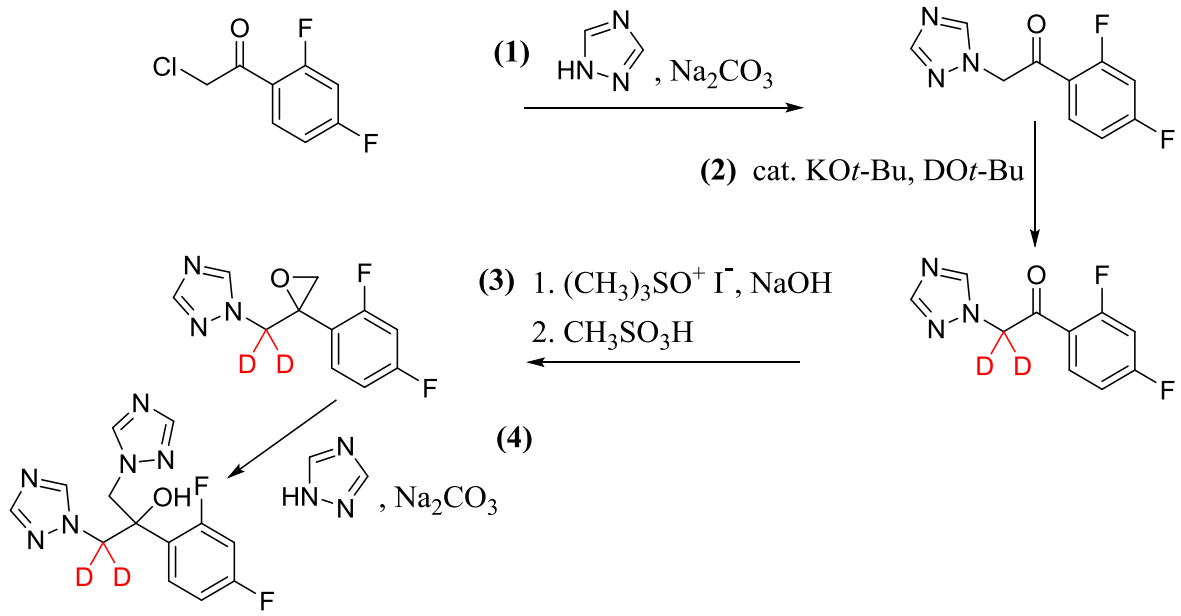

Figure 22. Synthesis of deuterated fluconazole

In general, up to now, in order to obtain many hydrogen isotope labelled drugs, a synthesis from labelled precursors is required. For the generation of a drug compound, being endowed with a tritium label, other strategies than the one from **figure 22** are required that circumvent the use or the formation of tritiated water, any other tritiated volatile species and tritiated acids. In order to synthesize tritium labelled carvedilol and astemizole, halogenation-dehalogenation methods were developed in the past.[52] For the synthesis of the two tritium labelled enantiomers of carvedilol, the carbazole moiety was halogenated with bromine (Br_2) in the first step. Subsequently, the two tritium labelled carvedilol enantiomers were delivered after hydrogenolysis of the tribromo-carvedilol with tritium gas and palladium on carbon as catalyst to give a molar activity of 35.2 Ci/mmol for the R-enantiomer and 61.0 Ci/mmol for the S-enantiomer (**figure 23**).

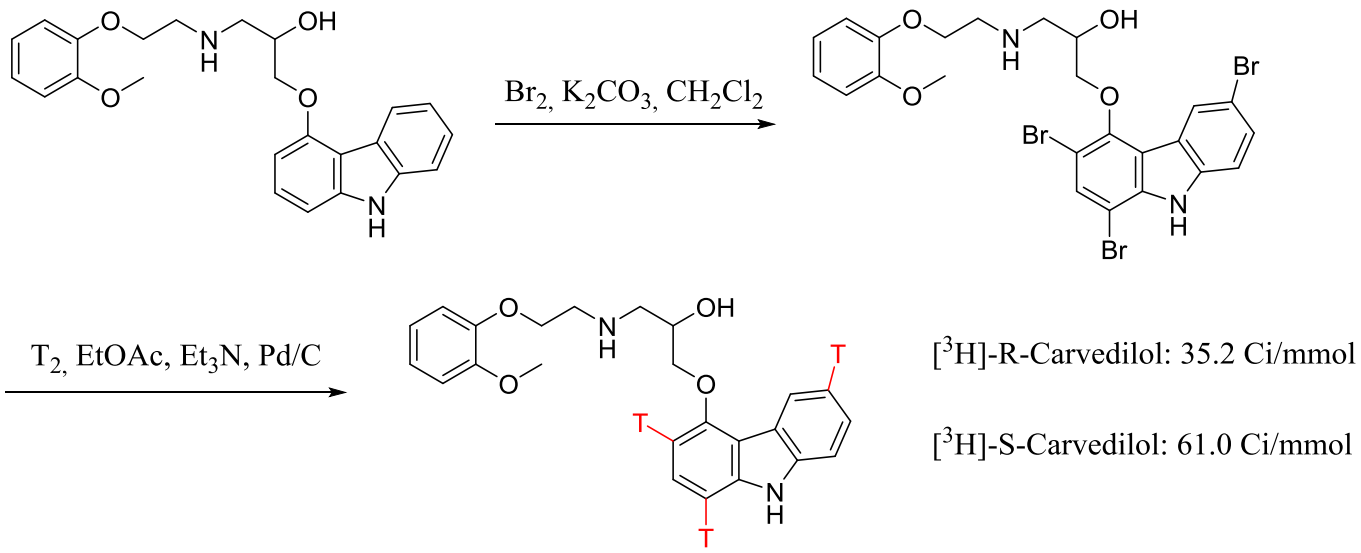

Figure 23. Synthesis of tritium labelled carvedilol through bromination and hydrogenolysis with tritium gas

Very often synthetic approaches employ harsh reaction conditions by using reactive reagents which might be not compatible with other functionalities in the molecule's structure. Nevertheless, the biggest drawback of the approaches mentioned above is the fact, that they all require an appropriate precursor molecule, i.e. a small building block being already labelled, a halogenated derivative or a derivative that contains double or triple bonds. Consequently, additional synthetic steps for obtaining the precursor itself and to build up a complex molecule can become time consuming, extremely challenging and deleterious for the overall yield. Additionally, high amounts of radioactive waste are produced if a tritium label

is introduced in an early step during synthesis. Owing to the given enormous efforts made in the past, a burning request for methods that circumvent these conventional multi-step syntheses can be anticipated.

3.2 Late-stage modifications

A stronger demand for isotopically labelled compounds clearly came up with the technological advances made in mass spectrometry which gave new opportunities to analyze complex mixtures. During the last three decades, this demand has prompted an intensive development of more rapid methods that yield SILS and radioligands. Chemical research started to seek methods that deliver deuterium or tritium labelled compounds in one operationally simple step, comparable to an acid-base reaction where exchangeable protons are subjected to an equilibrium with a source of deuterons, as it could be done on a position of the fluconazole precursor that undergoes a ketone-enole tautomerization (**I**.*3.1*, **figure 22**). These methods are also known under the name "late-stage modifications" because they use the molecule of interest as a substrate to introduce an isotope label in it, at the end of every other synthetical step. A simple form of such a hydrogen isotope exchange (HIE) and a tentative for doing so are illustrated in **figure 24**. A few little pyridine derivatives could be deuterated efficiently on several positions in deuterium oxide without additional acids or bases in a closed vessel (**figure 24**, top).[53] However, the required temperatures for the activations of these C-H bonds and the subsequent hydrogen/deuterium (H/D) exchange are remarkably high. At the bottom of **figure 24**, it is demonstrated that the necessity of high temperatures is a clear disadvantage for late-stage modifications. During an attempt to deuterate dextromethorphan with pyridiniumdeuterochloride, demethylation of the drug substrate occurred and deuterated dextrorphan was obtained in 95% yield.[54]

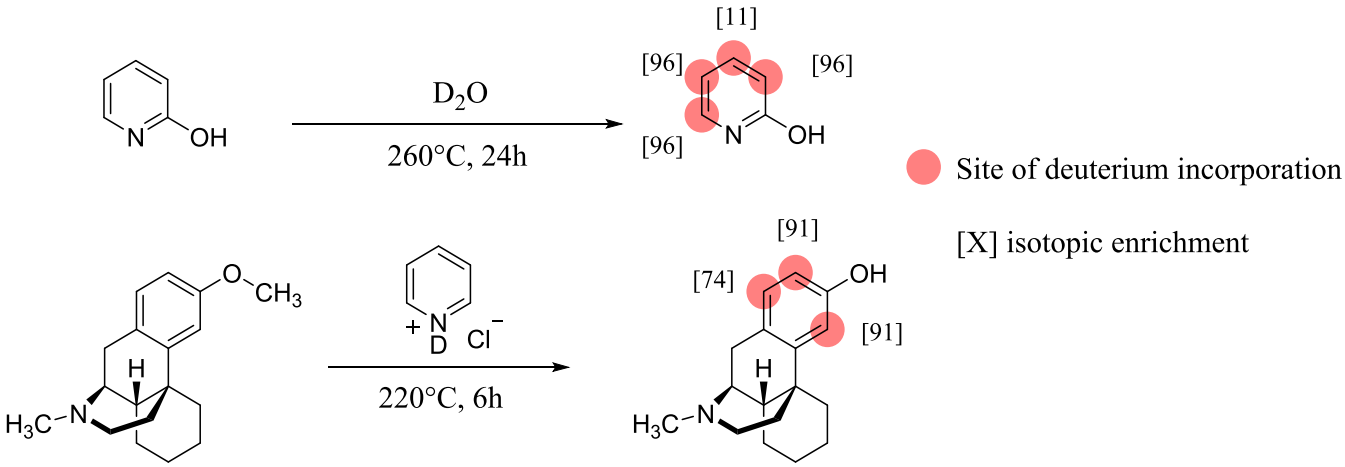

Figure 24. HIE on a pyridine derivative in D_2O (top) and a HIE attempt on dextromethorphan

As we could see, harsh reaction conditions can lead to the formation of undesired side products or to the complete loss of a valuable substrate e.g. due to demethylations, decarboxylations, eliminations, hydrolysis etc. Consequently, methods that require harsh reaction condition are not favorable or even applicable for HIE on complex molecules like drugs. Moreover, a significant drawback is the poor selectivity of deuterium incorporation in both cases (**figure 24**). Selective isotope incorporations are sometimes necessary which is going to be detailed later on.

3.2.1. Heterogeneous transition metal catalyzed HIE

Several reviews give excellent summaries on existing HIE methods, especially on reactions catalyzed by commercially available supported heterogenous transition metal catalysts (Pd/C, Pt/C, PtO_2, Raney nickel etc.), which were originally used for hydrogenations of unsaturated moieties and hydrogenolyses of halogens and protecting groups.9,[55] The reviewed HIE reactions, that also work with these catalysts, include hydrothermal -, microwave assisted reactions, pre-activations of the catalyst and so on. Many aromatics like carbazole could be deuterated at all positions of the aromatic rings under hydrothermal conditions in D_2O with PtO_2 as catalyst (**figure 25**, top).[56] Nonetheless, the emphasis in this chapter will lie on more selective HIE methods that work under mild reaction conditions, since they are more preferred for the late-stage labelling of complex and biologically relevant molecules. Correspondingly, the prerequisite of mild reaction conditions also justifies the use of transition metal catalysis. The first aim in using a transition metal catalyst is to establish a

mechanistic pathway that overcomes a relatively high activation barrier more easily. In this way, C–H bonds can be activated for HIE where activation and exchange does not occur with metal-free methods under mild reaction conditions. Indeed, drastic differences in terms of selectivity emerge during palladium catalyzed HIE that is performed under different temperatures (**figure 25**, bottom). 5-Phenylvaleric acid was deuterated with Pd/C in D_2O under a H_2 atmosphere at 160°C on every site of the molecule. The same HIE reaction at ambient temperature selectively deuterated the benzylic position of the molecule. Given that the substrate can be potentially degraded under high temperatures as shown for dextromethorphan in **figure 24**, this result demonstrated that the possibility to lower the temperature for HIE is a benefit of transition metal catalysis. Despite the lower deuterium incorporation in total, a selectively labelled deutero-analogue could be obtained from the deuteration at room temperature, containing an amount of deuterium which might be still sufficient for certain applications.

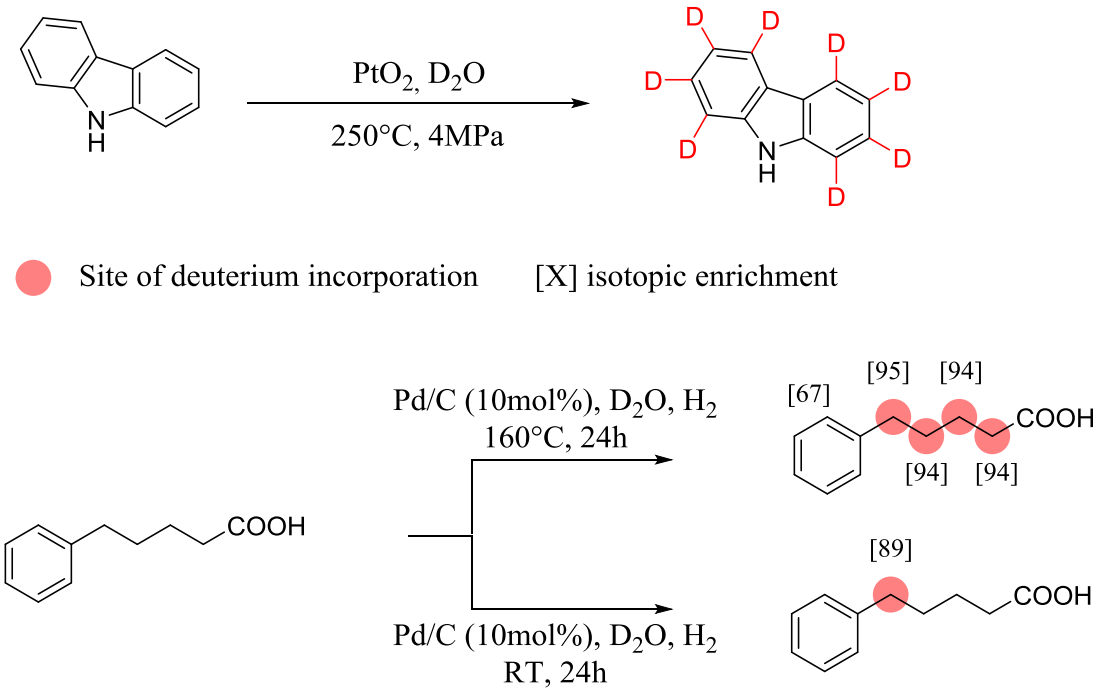

Figure 25. Deuteration of carbazole under hydrothermal conditions (top), and deuteration of 5-phenylvaleric acid at different temperatures (bottom)

As already alluded in the discussion after **figure 24**, regioselectivity in HIE can be a real benefit because it has positive impacts on the application of a deuteroanalogue as internal MS-standard. Selective H/D exchange methods are often preferred because they result in narrow distribution patterns of isotopologues in mass spectra (**figure 26c**), in contrast to unselective methods that tend to give isotope clusters (**figure 26b**). The broader the isotope

cluster, the higher the probability of an overlap with background ions and impurities or with the non-labelled analyte, which complicates quantitative analysis.

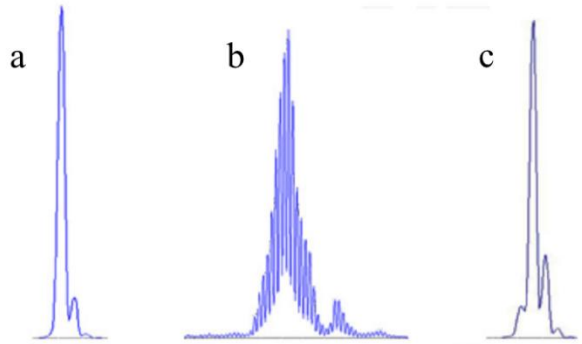

Figure 26. (a) Unlabelled starting material (b) Broad isotope cluster after unselective HIE method (c) Narrow MS pattern of labelled internal standard generated by selective HIE method (exemplary MS patterns extracted from reference 9; no precise molar masses attributed)

Other heterogeneous HIE catalysts consist of the earth-abundant metal nickel, such as "nickel Kieselguhr" or "Raney nickel". Correspondingly, the advantage of nickel over noble metals is the lower price. However, the results obtained from HIE reactions carried out with Raney nickel were dependent on the pre-activation procedure of the catalyst which is achieved by washing and sonication. Different sonication times of the catalyst, for example, were reported to give different isotopic enrichments on the substrate.[57] On top of that, most of the known nickel catalyzed HIE reactions were just carried out in D_2O which would render tritiations under the same conditions difficult. Further, the substrates were labelled with low selectivity.[58] Consequently, these methods are of low relevance for this work. Nevertheless, a much longer time ago, in 1971, probably the first selective HIE method was reported that exchanged selectively two deuterium atoms on pyridine at 42°C under a D_2 atmosphere catalyzed by a metallic nickel film on a glass surface.[59] Compared to previously discussed methods (**figure 24**), the major advantage of this elder procedure was its efficiency in the absence of deuteroxide. This suggests that it could have been theoretically also applied to tritiation reactions without employing or generating tritiated water (HTO, T_2O). Elemental metals from the platinum group of the periodic table (Ru, Rh, Pd, Os, Ir, Pt) are known to catalyze hydrogen isotope scrambling between hydrogen/deuterium/tritium gas and water.[60] For this reason, most of laboratories try to avoid using protic solvents for tritiations. Over the course of time, further selective HIE methods were developed by Alexakis *et al.*[61] These methods worked on a broader selection of *N*-containing heterocycles in tetrahydrofuran (THF)

without D_2O using commercial heterogeneous catalysts (Ru black, Rh black & Rh on alumina) and D_2 gas as isotopic source. *N*-heterocyclic model compounds like pyridine-, quinoline derivatives and isoquinoline were efficiently deuterated at α positions relative to nitrogen atoms of the heterocyclic systems. It has to be noted that the deuterium gas atmosphere was replaced twice during the course of each reaction. The authors mentioned that the tritiation of 4,4'-bipyridyl was also possible by employing deuterium tritide gas (DT) as isotopic source yielding the tritiated compound with a low specific activity.

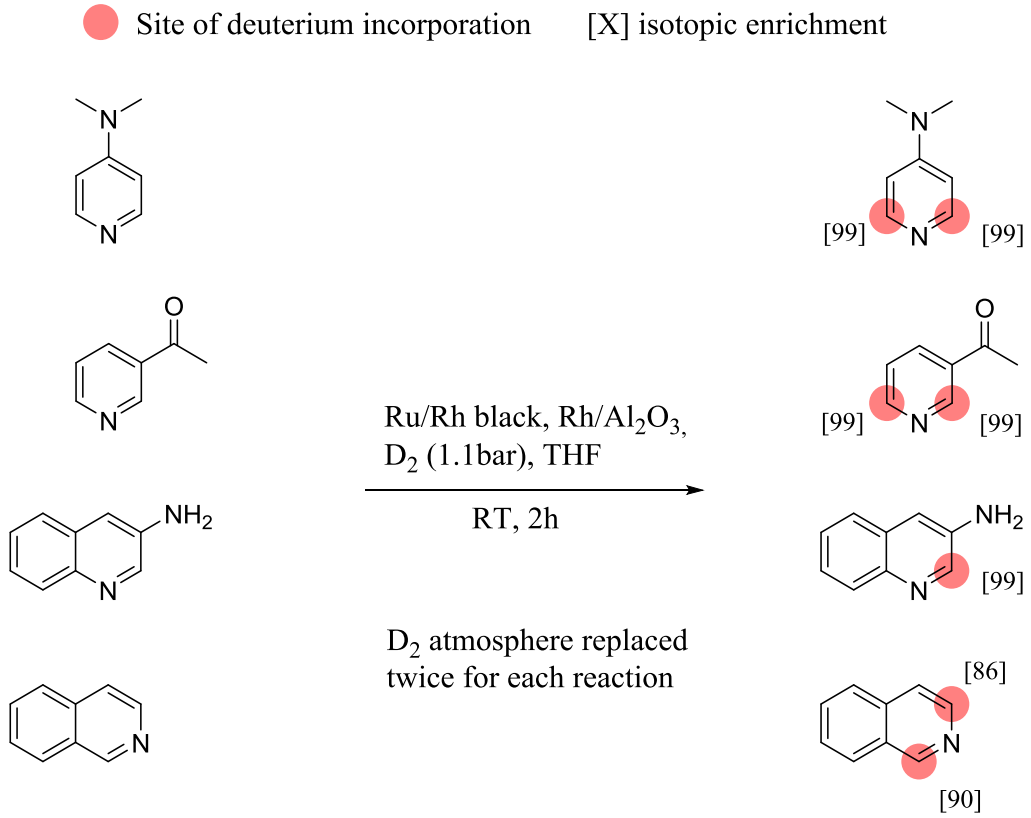

Figure 27. Selective HIE on *N*-heterocycles with heterogeneous catalysts and D_2 gas as isotopic source

In most cases, drug development processes are confronted with the task to obtain tritio-analogues of higher structural complexities than in **figure 27**. Inconveniences occurring at this stage are reasoned in the lack of labelling methods that efficiently tritiate a drug candidate of a given molecular structure in an organic aprotic solvent like THF with T_2 gas as isotopic source. Research on this field is insofar relevant as we consider that several aforementioned methods employed D_2O as isotopic source, as for example hydrothermal methods but also the labelling through supported nickel catalysts. Thus, their application to tritium labelling is not feasible by most of laboratories. T_2 gas as isotopic source is largely preferred over T_2O

reasoned in the 1000-fold higher radioactivity per volume unit of the latter. Further, there are modern absorption and storage techniques that render T_2 gas the easiest raw material to handle for tritium labelling. Typically, reactions involving gaseous tritium are conducted using subatmospheric pressure of T_2 in order to minimize the risk of leakage and radioactive releases. The difficulty to find such a method for the tritium labelling of drugs is due to the fact that the incorporation of tritium proceeds less efficiently, due to the kinetic hydrogen isotope effect. In some cases, the translation from deuteration to tritiation reactions can be even very poor. To a certain extent, this explains the rarity of reported successful tritium labelling under mild reaction conditions by heterogeneous transition metal catalysts and hydrogen isotope exchange. After all, a few concrete applications are known, where heterogeneous transition metal catalysts permitted to perform satisfying tritium labelling. Since the advent of the ruthenium and rhodium catalyzed HIE method by Alexakis *et al.* (**figure 27**), Rh black and T_2 gas gained certain popularity for the tritium labelling of *N*-heterocycles. For example, this catalytic system was used by Walji and coworkers in order to obtain tritiated *N*-heterocyclic PET tracers for further protein binding assays.[62] Analogous to the work of Alexakis *et al.*, selective tritium labelling took place on the *N*-heterocyclic cores in α positions relative to the nitrogen atoms (**figure 28**, top). In the same manner, Hesk and coworkers also succeeded to tritiate the drug candidate "SCH D" (**figure 28**, bottom).[63]

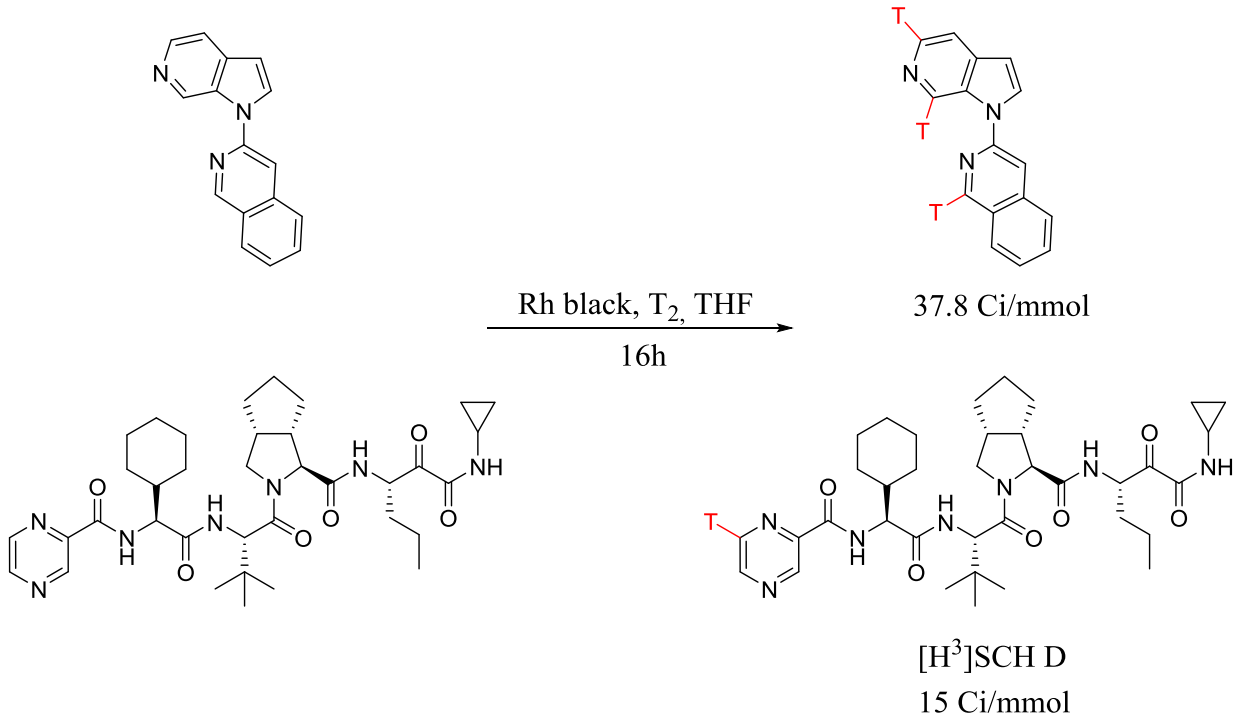

Figure 28. Tritiations of *N*-heterocycles by Rh black and T_2 gas in THF

It has to be noted that two equivalents of catalyst were needed for the tritiation of the complex SCH D, which represents a very high catalytic charge (**figure 28**). We have to bear in mind that high catalytic charges favor the degradation of the substrate. Further, the authors pointed out that significant amounts of T_2 gas got lost through absorption, when high catalytic charges were used. Last but not least, the major problems of commercial heterogeneous catalysts are batch to batch differences that usually lead to unreproducible results. They emerge because catalytic activity depends on particle size, dispersion, degree of purity and surface functionalization or poisoning. Commonly, these parameters are not precisely determined for marketed supported and unsupported heterogeneous transition metal catalysts.

3.2.2. Homogeneous transition metal catalyzed HIE

Two main conclusions from the precedent chapters have to be noted at this stage because they are the most relevant for the upcoming work. Firstly, many preclinical and clinical studies of the drug development process can be potentially mastered by means of deuterium labelled drugs and metabolites which supports the great usefulness of deuterium. Secondly, tritiated drugs are still indispensable since they are preferred for ADME studies, but complications to prepare them from tritium gas stay a significant obstacle for drug development. However, within the following HIE methods that employ homogeneous metal complexes as catalysts, considerably more examples of successful tritiations of complex molecules are known. Several organosoluble transition metal complexes have garnered considerable interest as HIE catalysts because they overcome many problems related to previously described heterogeneous methods. Metalorganic compounds are synthesized and purified after well-established protocols, characterized by NMR, stored and marketed as crystalline substances. As a consequence, batch to batch differences are not that enormous as for heterogeneous catalysts. Further, in many reported cases the metal center coordinates and activates hydrogen, deuterium and tritium gas at relatively low partial pressures. In contrast, from literature no cases are known where HIE succeeded by heterogeneous catalysts under comparable deuterium or tritium gas pressures. For these reasons, homogenous metal catalyses are very often the labelling methods of choice for tritiation reactions. Richard Heys discovered in 1992 that an iridium (I) complex catalyzes the exchange of hydrogen for deuterium in the presence of deuterium gas on *N*-heterocyclic compounds and compounds with carbonyl substituents.[64] Nowadays, there are several commercially available mononuclear homogeneous Ir(I)

complexes with Crabtree's and Kerr's catalyst as two examples. In the further course of time, it was found that Crabtree's catalyst was applicable to the *ortho* deuteration of acetanilides[65] and Kerr's catalyst was an efficient catalyst for the *ortho* deuteration of adjacent phenyl substituents of *N*-heterocycles.[66] The deuteration with Kerr's catalyst revealed impressive isotopic enrichments on a big variety of *N*-heterocyclic compounds, e.g. on oxazoles, imidazoles, thiazoles and benzoderivatives thereof (**figure 29**). Some drug-like examples of higher structural complexity could be also deuterated in dichloromethane (DCM) and THF (**figure 29**, bottom).

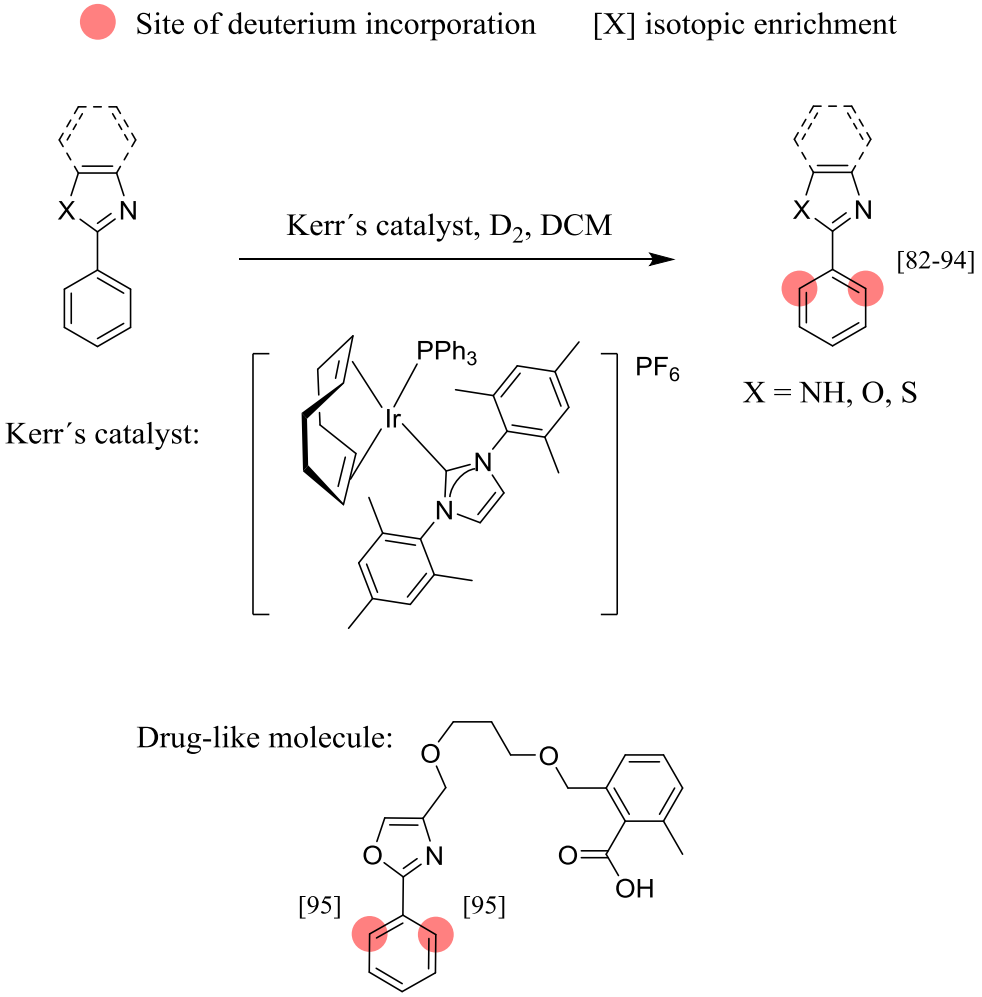

Figure 29. *Ortho* deuterations of phenyl rings on different *N*-heterocycles by Kerr´s catalyst

However, *N*-heterocycles which are not endowed with an aryl group in an adequate position, as benzimidazole, could not be labelled at all by this method because the regioselectivity is restricted to certain γ-positions relative to a coordinating atom. This γ-selectivity of Ir(I) catalysts can be interpreted by looking at the reaction mechanism and the formed key intermediates. The reaction mechanism for the HIE by Ir(I) catalysts was already proposed in

previous works.[67] In order to draw the HIE mechanism for *N*-heterocycles, a *N*-heterocyclic unit was assumed as the directing group. A corresponding pathway is illustrated in **figure 30** with the substrate 2-phenylimidazole as an example. First of all, the cyclooctadiene (COD) ligand is hydrogenated under the D_2 atmosphere under the formation of d_4-cyclooctane. Then, the catalyst activates a D_2 molecule and receives two deuteride ligands which confers the oxidation state +III to the iridium center. Additionally, the substrate is coordinated through a nitrogen atom and a C–H bond in *ortho* of the phenyl group through a side-on coordination. These processes lead to the formation of the octahedral complex **A** (**figure 30**).

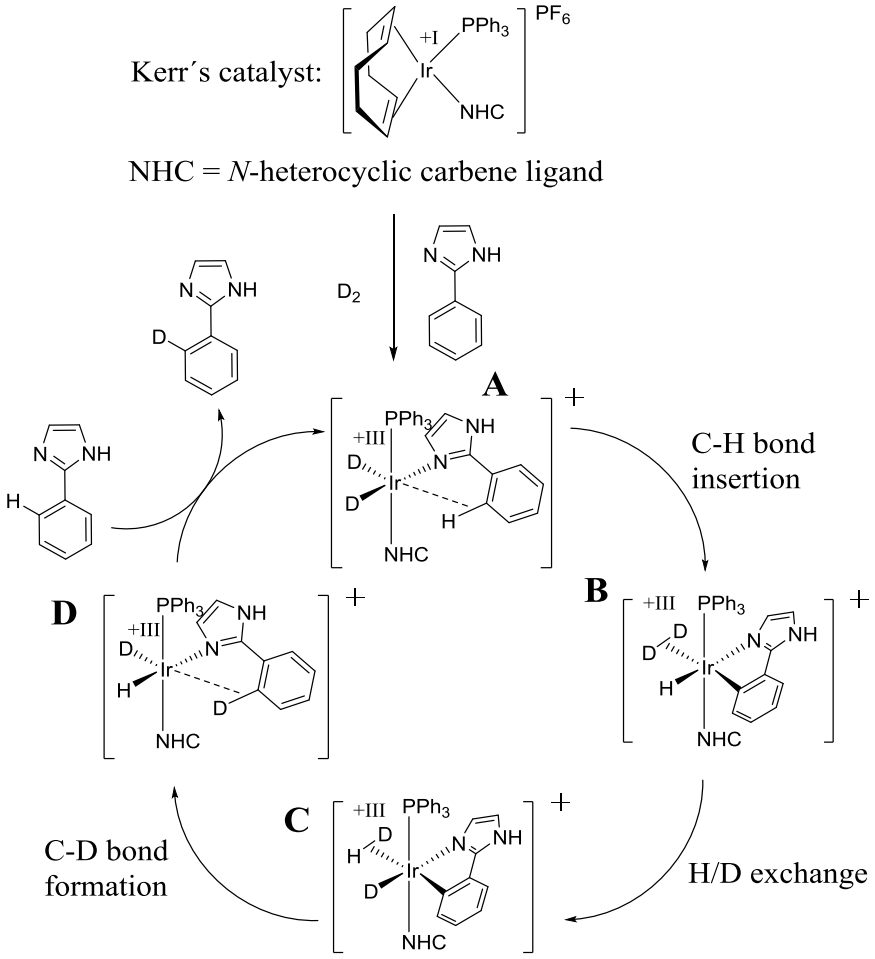

Figure 30. Reaction mechanism for the Ir(I)-catalyzed HIE stemming from reference 67, that was adapted to an exemplary HIE reaction on 2-phenylimidazole

Two covalently bound hydride or deuteride ligands can be eliminated at any time to obtain a side-on coordinated D_2, HD or H_2 molecule. Therefore, an equilibrium is established between deuterium or hydrogen gas and hydride or deuteride ligands on the catalyst. This also allows the C–H activation to occur through the insertion of the Ir-center into the C–H bond. On this

path, a covalent bond is formed between the *ortho* position of the phenyl ring and the metal resulting in a 5-membered metallacycle key intermediate (complex **B**, **figure 30**). As already alluded, the hydride ligand that is coordinated in *cis* relative to the phenyl ligand can be exchanged for a deuteride ligand through the equilibrium with the gas phase (complex **C**, **figure 30**). Subsequently, the *N*-heterocyclic substrate and the deuteride ligand are eliminated to give a C-D bond in *ortho* of the phenyl group (complex **D**, **figure 30**). Thus, the deuterated *N*-heterocyclic substrate can dissociate which permits the catalytic cycle to start again by coordinating another substrate molecule (complex **D** to **A**, **figure 30**). As we could see, the regioselectivity of Ir(I) is a product of the directing effect of the imidazole scaffold and the 5-membered metallacycle key intermediate formed after C–H activation. This can be also considered as a drawback of the method because it is a structural limitation. Since HIE merely takes place at *ortho* positions of phenyl groups adjacent to a *N*-heterocycle at a certain position, many *N*-heterocyclic molecules cannot be labelled at all, as it was the case for unsubstituted benzimidazole in the described work in **figure 29**. Further, owing to the production of SILS for metabolism studies, drug molecules would undergo insufficient deuterium incorporation in most cases, because two deuteriums per molecule might be not enough. Nevertheless, Ir(I) complexes stay indispensable HIE catalysts in terms of many tritiations. In a recent work, it was shown on the drug suvorexant that HIE with Crabtree´s catalyst leads to efficient and selective tritiation in *ortho* of the phenyl substituent, directed through the 1,2,3-triazole unit (**figure 31**, top). In the same work, Chirik and coworkers presented a mononuclear Fe(0) complex as a new homogeneous HIE catalyst (**figure 31**, bottom left).[68] Interestingly, in contrast to Ir(I), tritiations catalyzed by the Fe(0) catalyst always proceeded on the less sterically encumbered positions of complex molecules. If we have a look at the tritium incorporation selectivity on the two other examples cinacalcet and MK-7246, one can assume that the C-H activation via the Iron catalyst takes place in a non-directed way, although the mechanistic pathway was not proposed, yet (**figure 31**, bottom right).

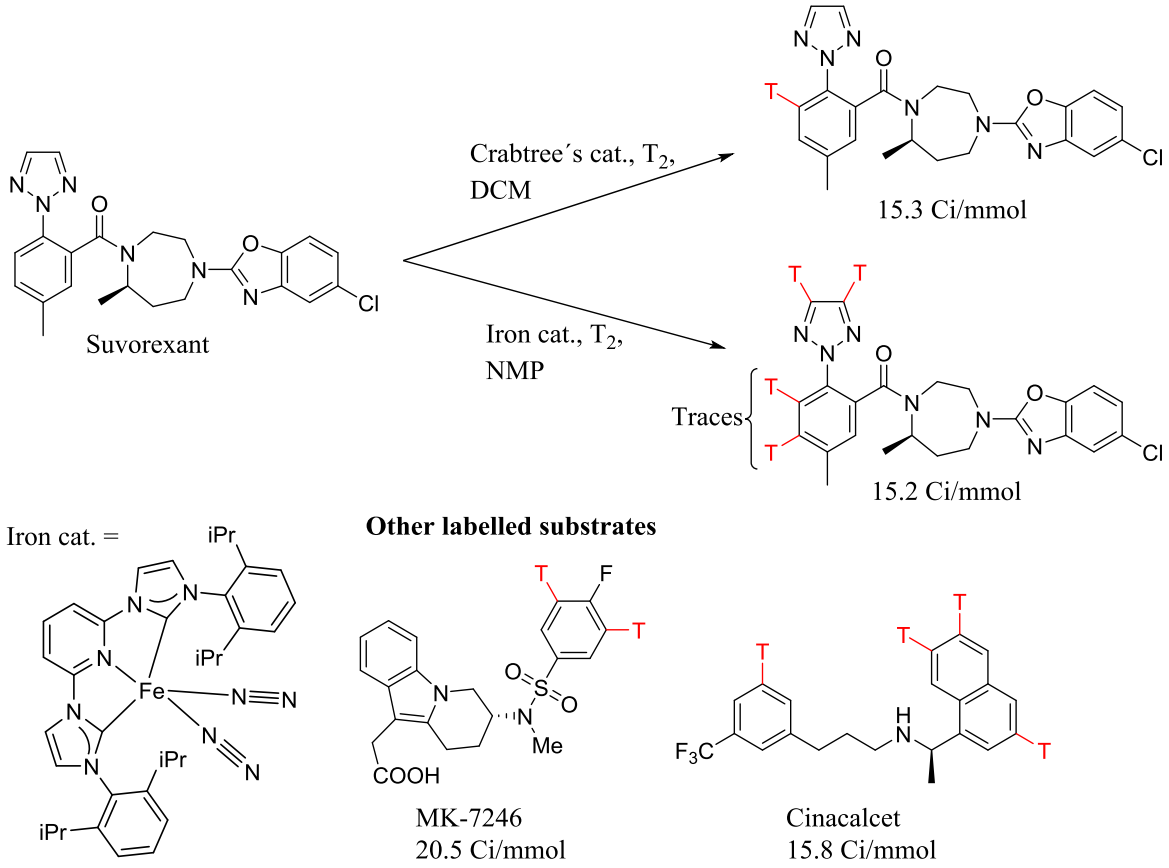

Figure 31. Tritiations of drugs catalyzed by a homogeneous Fe(0) catalyst

The possibility to use an earth-abundant metal like iron for efficient catalytic transformations is a clear plus of this work. The high air sensitivity of the iron catalyst and the need to synthesize it by using sodium amalgam Na(Hg) as reducing agent are still significant inconveniences of the method.[69] Soon after, Chirik and coworkers discovered a dinuclear nickel hydride complex to be another active homogeneous earth abundant metal catalyst for tritiations of APIs (**figure 32**).[70] The advantage of the Ni catalyst over the Fe(0) complex is the easier preparation that just includes the mixing of an air stable nickel precursor complex with the diimine ligand ^{iPr}DI = [2,6-^{i}Pr$_2$–C$_6$H$_3$N═C(CH$_3$)]$_2$ and HSi(OEt)$_3$ in THF. Tritiations of drug compounds took place at low pressures of tritium gas (0.15bar) and predominantly in α positions of nitrogen atoms on *N*-heterocyclic motifs, comparable to Ru/C and Rh black as in chapter **I**.*3.2.1* (**figure 27**), or on adjacent phenyl groups, in γ positions relative to nitrogen atoms, comparable to Ir(I) catalysts. Owing to the HIE selectivities observed, the authors assumed the C–H activations to be directed in this case. All in all, pyridine- and diazine containing radiolabelled drugs manifested satisfying molar activities. Unfortunately, a rather low molar activity was obtained for the purine-based drug famciclovir.

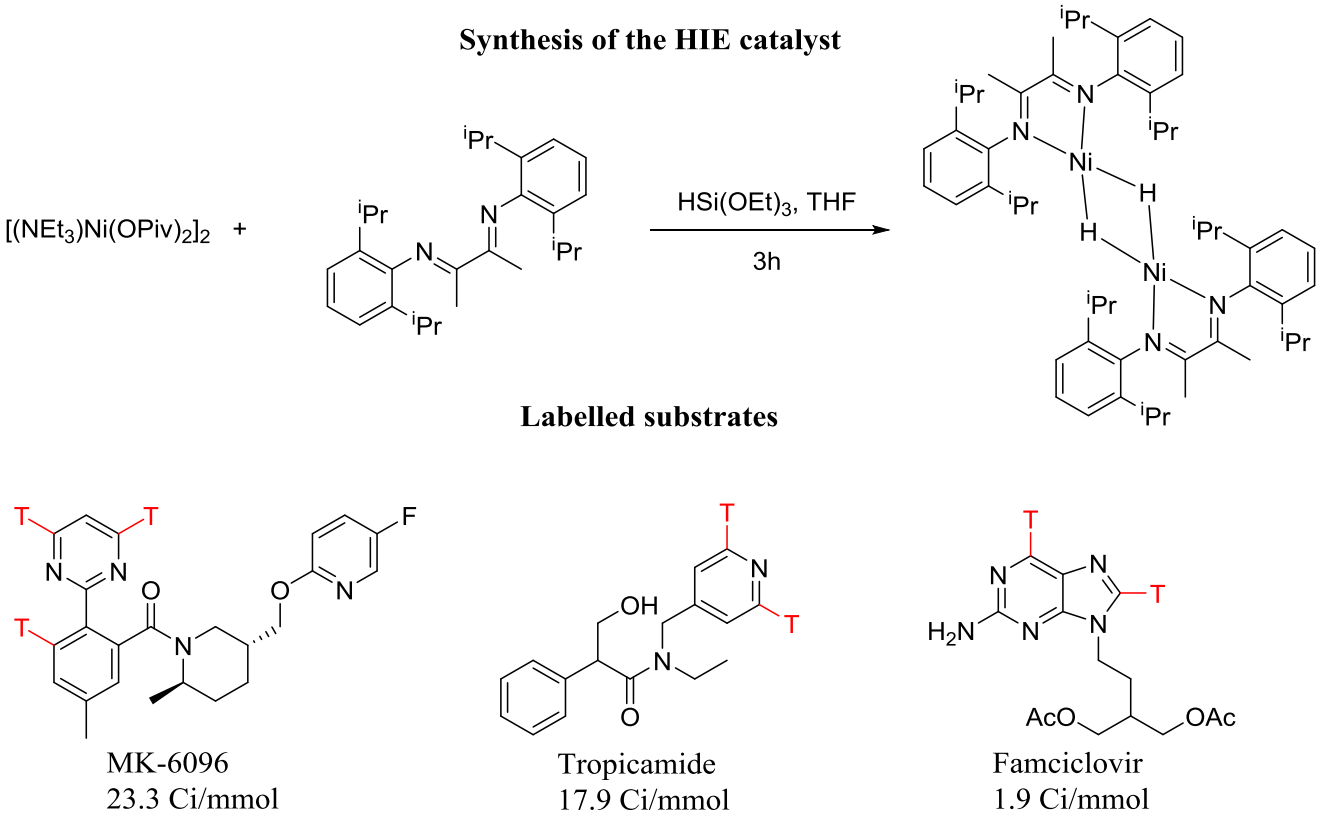

Figure 32. Tritiations of APIs catalyzed by a nickel complex

In an ongoing work, the same working group developed another more sterically encumbered Ni(I)-complex that was found to be even more active as HIE catalyst under the same pressure of T_2 gas as in **figure 32**. In this case, the tritiation of MK-6096 yielded a molar activity of 99.2Ci/mmol. The new Ni(I)-catalyst promoted also the deuteration of other *N*-heterocycles like oxazole and thiazole (**figure 33**)[71].

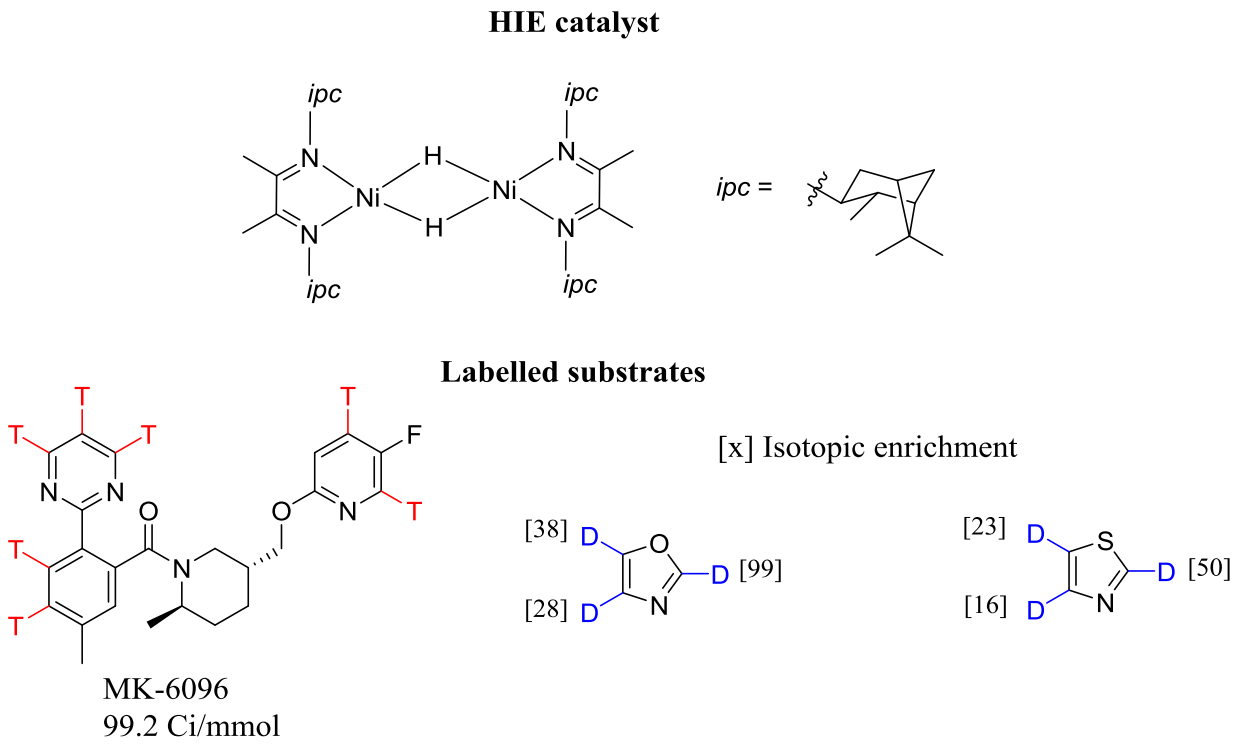

Figure 33. Dinuclear Ni(I)-complex with bulky substituents as HIE catalyst for the efficient tritiation of pharmaceuticals and the deuteration of oxazole and thiazole

To sum up, in the recent past, several homogeneous metal complexes were described as innovative and efficient HIE catalysts. Up to date, HIE through homogeneous catalysis is even the most efficient and rapid way to obtain tritiated drugs. However, a crucial point that was neglected in the course of the discussion is a potential formation of stable complexes between the transition metal and substrate molecules endowed with strongly coordinating functionalities. Thus, there is a permanent risk of metal contamination that can require additional purification steps of the isotopically labelled molecules which has to be taken into account within biological applications.

3.2.3 Metal nanoparticles-based methods for HIE

The last section of this chapter will introduce another type of HIE catalyst, that has the highest relevance for us, because this work is dedicated to the development of these methods. Undoubtedly, the latest discovery in the field of HIE catalysis are metal nanoparticles. In the context of this work, the emphasis will lie on nanosized spherical particles which consist of a catalytically active metal with the oxidation state zero. They are not deposited on a support

like carbon, graphene monolayers, $CaCO_3$ etc. as it was the case for heterogeneous catalysts in chapter **I**.*3.2.1*. In the ideal case, these nanoparticles are well-dispersed in a solvent because they are able to form stable solutions without getting into contact with each other. In other words, they could be also referred to as metal colloids. The word "colloid" describes a tiny solid object in the nanometer range that tumbles in a liquid without precipitating. Due to the little size and the low mass of the solid object, the Brownian motion of the solvent molecules prevents it from sinking to the ground. Metal nanoparticle solutions in particular are also stabilized by other effects. The precise methods for synthesis and stabilization will be detailed in the next chapter. In 2009, a HIE method was developed for the deuteration of *N*-heterocyclic substrates in D_20 using palladium nanoparticles embedded in a matrix of polyvinylpyrrolidone, as catalyst.[72] Polyvinylpyrrolidone (PVP) is a water-soluble polymer that has a stabilizing effect and prevents the metallic nanoparticles from aggregation. Pieters and coworkers demonstrated then that ruthenium nanoparticles, stabilized in a matrix of the same polymer, are performant catalysts for the deuteration of aliphatic amines, pyridine- and indole derivatives in THF under mild reaction conditions and D_2 gas as isotopic source (**figure 34**).[73] Polyvinylpyrrolidone stabilized ruthenium nanoparticles (RuNp@PVP) as catalyst promoted the exchange of hydrogen for deuterium at α- and β positions relative to nitrogen atoms, as in the previous work of Alexakis *et al.*[61] described in **I**.*3.2.1*.

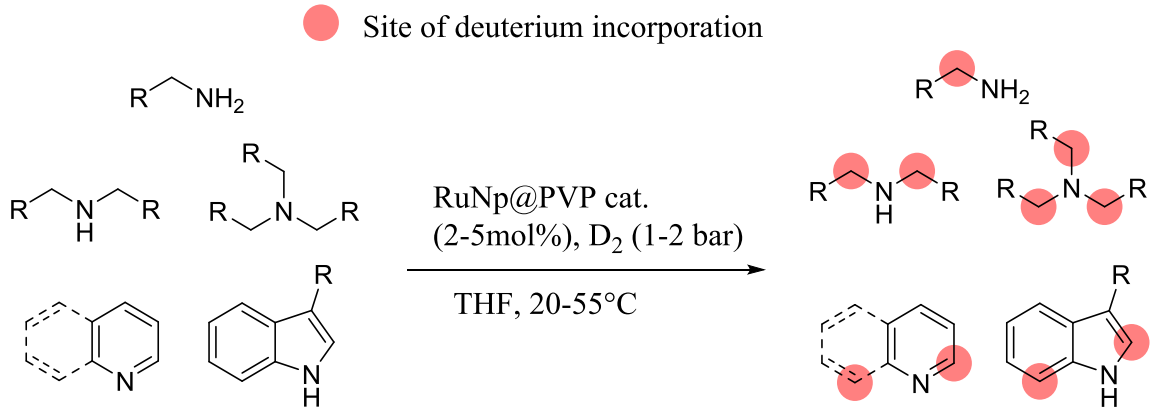

Figure 34. HIE on amines, pyridine, quinoline and indole catalyzed by RuNp@PVP under D_2 gas in THF

Nevertheless, in the work presented in **figure 34**, the RuNp@PVP catalyzed HIE was still limited to a small range of *N*-heterocyclic substrates being soluble in THF as the only organic solvent. Tritiations catalyzed by ruthenium nanoparticles appeared in a separate work with the focus on nucleobase derivatives. In this context, ruthenium nanoparticles stabilized by *N*-heterocyclic carbene ligands (Ru-*ICy* Np) were employed as catalyst to conduct tritiations of

didanosine and idelalisib, two drugs that contain nucleobases in their molecular structures (**figure 35**).[74]

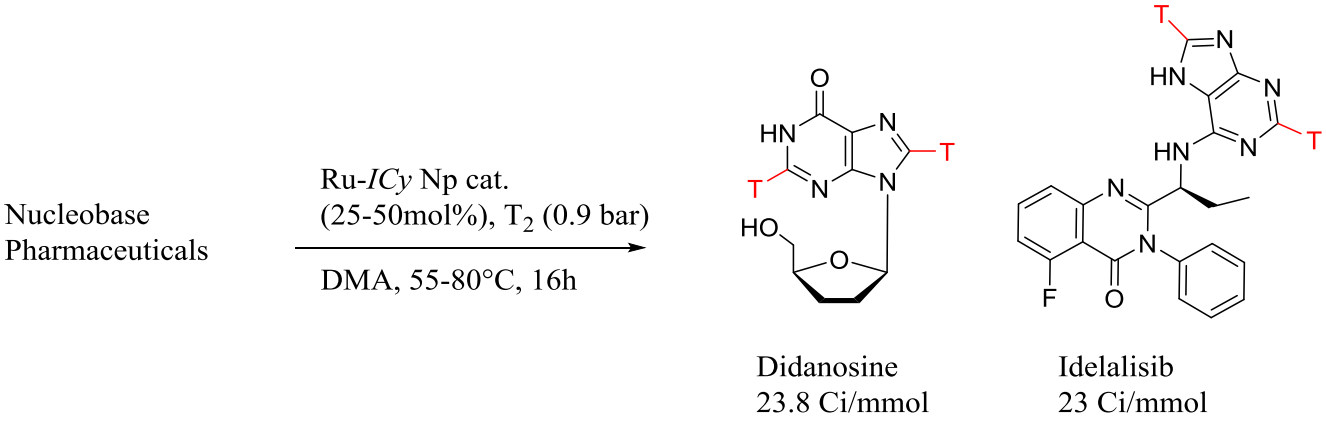

Figure 35. Tritiation of didanosine and idelalisib under T_2 catalyzed by Ru-*ICy* Np

In summary, encouraging results were obtained for ruthenium nanoparticles catalyzed HIE. In contrast to heterogeneous catalysts like rhodium black, ruthenium nanoparticles rendered tritiations of *N*-heterocyclic scaffolds possible at lower catalytic charges. On the one hand, the higher efficiency of metal nanoparticles in comparison to commercial heterogeneous catalysts can be reasoned in their nanometric size which confers a higher active surface for catalysis. On the other hand, like already mentioned in the context of homogeneous transition metal catalysts, also the synthesis of metal nanoparticles proceeds under controlled conditions and their storage and handling under glove box conditions. As a consequence, their surface should be covered by far less impurities. However, the substrate scope in terms of *N*-heterocycles stays restricted, if we consider the diversity of presented heterocyclic scaffolds in chapter **I**.*2*. Further, the removal of Ru-*ICy* Np from the reaction mixture is still difficult because this type of nanocatalyst is soluble in every common organic solvent, thus, it cannot be removed by simple precipitation and filtration and requires a preparative separation through high-pressure liquid chromatography (HPLC).

4. Metal nanoparticles

This chapter is exclusively dedicated to existing syntheses of catalytically active metal nanoparticles being soluble in common organic solvents. Recent highlights in metal nanoparticle synthesis will be presented and concomitant interest for our work will be outlined. In particular, metal nanoparticles will be shown that gave a hint for the development

of new metal nanoparticles applicable to HIE within this work. The course will proceed to fundamental investigations of these modern and rather unknown catalysts.

4.1 Synthesis, stabilization and analysis

Metal nanoparticles (MNp) are very little frameworks built up from metal atoms. Their synthesis is usually realized from a dissolved compound that contains the corresponding metal. To this end, a stimulus is given to the metal atoms to undergo assembly to a cluster of metal atoms being connected through metallic bonds, which represents a metal nanoparticle. Possible stimuli can be the reduction of a metal ion or the removal of ligands that form a complex with the metal atom. This is achieved, e.g. through thermal decomposition of organometallic precursors, as it was shown for the production of bimetallic iron/platinum nanoparticles from iron carbonyl $Fe(CO)_5$ and platinum acetylacetonate $Pt(acac)_2$.[75] Much milder methods to synthesize metal nanoparticles were discovered by Chaudret and coworkers. In this context, ways and means were developed to synthesize ruthenium nanoparticles (RuNp) through reductive decomposition of the organometallic precursor Ru(COD)(COT), with H_2 gas. However, without any other additive the formed RuNps can be just stabilized by the organic solvent. Thus, the colloid solution is not stable over a long time, and nanoparticles agglomerate with each other and tend to form a ruthenium sponge.[76] A big advantage of the produced nanoparticles by Chaudret *et al.* was still the absence of other reagents like surfactants which were added in conventional Np syntheses to form micelles as nanoreactors. However, every additional component can lead to impurities and poisoning of the Nps surface or even to the formation of an oxide shell around the Np being deleterious for the catalytic activity. Perfectly soluble MNp in common organic solvents could be achieved through the stabilization by polymers. For this purpose, the reductive decomposition of the organometallic precursor is carried out in THF in the presence of a cellulose derivative[77] or PVP[78] in order to synthesize RuNp@PVP that was discussed in section **I**.*3*.*2*.*3*. Full solubility is of high importance for an application of the MNp within catalysis because this property leads to a big active metallic surface and delivers all the available catalytic sites on the Np surface. The mobility of hydride and deuteride ligands at the surface of RuNp and their dynamic equilibrium with hydrogen and deuterium gas in the gas phase was proven by NMR experiments. Undoubtedly, this is the most crucial quality of a catalyst for an application in HIE.[79] An excellent overview of a big repertory of different stabilizing small-molecule ligands for ruthenium nanoparticles is provided in a review by Chaudret *et al.*[80] The most

important thing to be pointed out is that the stabilization through ligands like amines and thiols does not lead to RuNp which are stable in solution over a long time. Due to the low affinity and dynamic exchange behavior of these ligands at the metal surface, nanoparticles rather have the tendency to form aggregates and superstructures.[78] Surface ligands that provided stable and well-dispersed ruthenium nanoparticles in solution, additionally with excellent catalytic properties, are *N*-heterocyclic carbenes (NHCs). In general, carbenes have a high affinity for transition metals. In any case, they are assumed not to show strong exchange at the metallic surface because they do not easily dissociate from the metal they are coordinated to. The synthesis of NHC stabilized RuNp was demonstrated by Lara and coworkers.[81] The characterization of metal nanoparticles can be achieved by several analytical methods usually employed in chemistry and material science. Transmission electron microscopy (TEM) is used to determine the shape, size, size distribution and dispersion-or aggregation state of the Np. The size distribution points out in how far the synthesized badge of nanoparticles is monodisperse. Wide-angle X-ray scattering (WAXS) is used to determine the composition and the crystalline structure of the nanocatalyst. Further, the surface of nanoparticles can be characterized through the quantification of surface hydrides through titration with 2-norbornene. Another important surface study is the absorption of ^{13}C-labelled carbon monoxide (^{13}CO) on the MNp. Subsequent analysis by Fourier-transform infrared (FTIR) and magic-angle-spinning (MAS) NMR spectroscopy yields the strength of absorption and the coordination modes of the CO molecules (side-on or end-on). In this manner, information is obtained about the nature of potentially active sites for catalysis.[82]

4.2 DFT calculations on metal nanoparticles

Density functional theory (DFT) employs computational methods that approach the orbitals of atoms and molecules as mathematical functions. In this fashion, DFT calculations are able to provide numerical and empirical information about reactivity and reaction pathways. If a theoretical nanoparticle model is established, chemical processes taking place on the surface of metal nanoparticles can be also studied by DFT calculations. This is best realized by considering a cluster of metal atoms which are connected through metallic bonds and display hydride or deuteride ligands bound to the surface metal atoms. It was found in a previous study that the HIE reaction in the α position of the nitrogen atom of 1-methyl-*iso*-butylamine on a RuNp surface follows a Langmuir-Hinshelwood mechanism, that refers to the reaction

between two components which are both absorbed at the surface. In this case, this would be the coordinating amine and a surface deuteride. In contrast, a mechanism where one component is absorbed on the catalyst and reacts with a compound from the gas phase is called an Eley–Rideal mechanism. The most relevant finding of this study was that the HIE reaction passes through a four-membered dimetallacycle key intermediate which is formed after the C–H activation step and explains the selective deuteration on α positions of nitrogen-containing compounds (**figure 36**).[83]

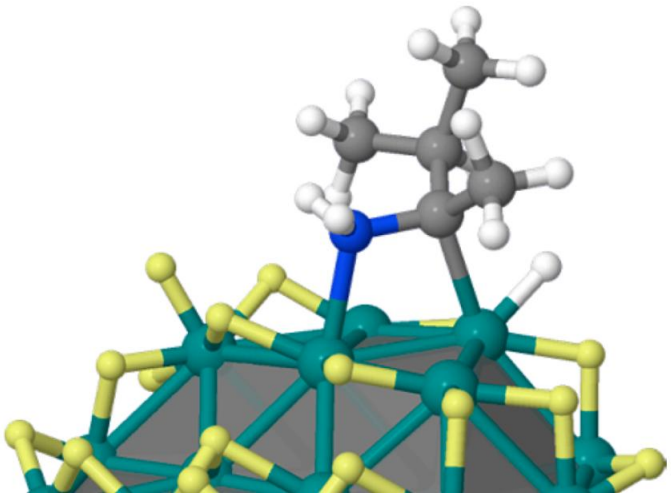

Figure 36. Modeled image of the 4-membered dimetallacyclic key intermediate that is formed after C–H activation on a secondary amine at the surface of a deuterated RuNp (figure extracted from reference 84).

II. Development of new metal nanoparticles-based HIE methods

Metal nanoparticle catalyzed HIE was outlined to be a promising method to label certain nitrogen containing compounds in the vicinity of their nitrogen atoms. However, none of the known metal nanoparticles was extensively used for the labelling of biologically interesting molecules by hydrogen isotopes. Various *N*-heterocyclic scaffolds were presented to be attractive and biologically relevant targets for HIE. Existing methods are just able to introduce hydrogen isotopes into oxazoles and imidazoles under structural limitations. For a mild and selective HIE on 1,2,4-triazoles and carbazoles, it still doesn´t exist any method. Owing to all these reasons, we believed that metal nanoparticle catalyzed HIE is worth to be further developed on *N*-heterocyclic substrates which were listed in chapter **I**.*2*. Therefore, the practical section of this work is segmented into two principle parts. The first part is the

synthesis of metal nanoparticles consisting of ruthenium that were already described and new metal nanoparticles that consist of nickel. In the second part, the objective is it to find and to develop new, efficient and generally applicable metal nanoparticle catalyzed deuteration and tritiation methods for a broad scope of *N*-heterocyclic substrates (**Figure 37**). In this context, DFT-based investigations will help us to understand the processes taking place in HIE at the surface of a nanocatalyst.

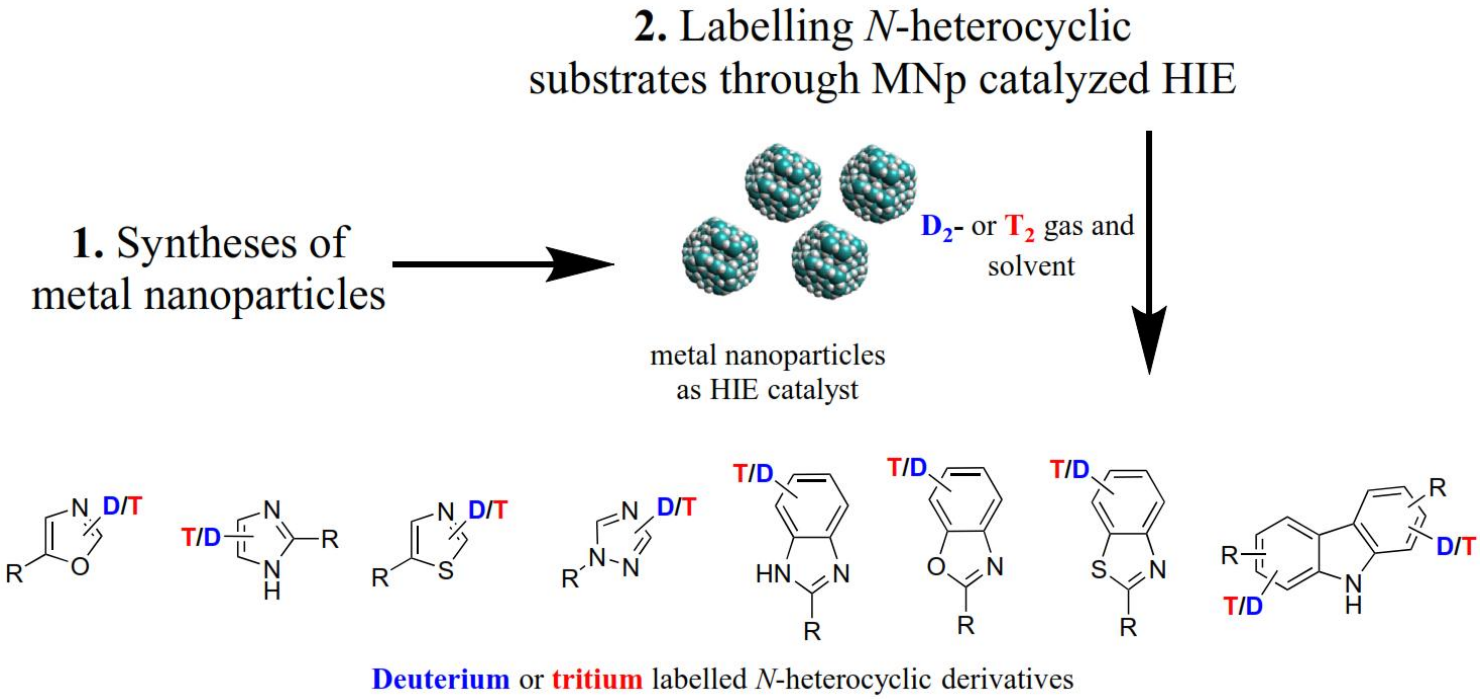

Figure 37. General scheme illustrating of the objectives of the upcoming work

1. Syntheses of metal nanoparticles

This chapter will present and explain the syntheses of metal nanoparticles which was performed within this work. In order to carry out comparative studies on the hydrogen isotope labelling of *N*-heterocycles afterwards, we synthesized four different types of metal nanoparticles. The metal ruthenium continues to be of high interest also for this work. On this account, RuNp@PVP and ruthenium nanoparticles stabilized by a NHC ligand (Ru-*ICy* Np) were synthesized. Then, the nanoparticle syntheses proceeded to NHC stabilized nickel nanoparticles (Ni-*ICy* Np and Ni-*IMes* Np).

1.1 Synthesis of RuNp@PVP

First, RuNp@PVP was prepared because this ruthenium-based nanocatalyst yielded already good results on the area of HIE. To this end, the crystalline organometallic compound Ru(COD)(COT) and the polymer PVP are dissolved in THF. Afterwards, Ru(COD)(COT) is reduced under a low pressure of H_2 gas (3bar) and vigorous stirring, according to the procedure of Chaudret *et al.* as already alluded in the theoretical part **I**.*4.1*.[78] The reductive decomposition of the organometallic precursor with H_2 gas proceeds at room temperature. The two ligands of the Ru(0) complex, 1,5-cyclooctadiene (COD) and the 1,3,5-cyclooctatriene (COT), undergo ruthenium catalyzed hydrogenation to give cyclooctane that dissociates from the complex and goes into solution. The Ru(0) atoms then form metallic bonds to each other and get stabilized as ruthenium nanoparticles. In this case, the metal nanoparticles are supposed to be accommodated in nanoreactors formed by PVP which prevents them from aggregating. The synthesis of RuNp@PVP with the corresponding conditions is depicted in **figure 38**.

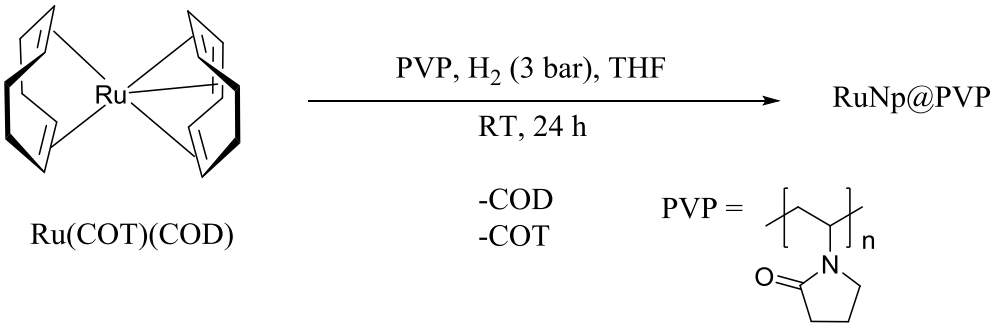

Figure 38. Synthesis of ruthenium nanoparticles in a PVP matrix

Given that the synthesis of RuNp@PVP proceeded after a well-established protocol, recording a TEM image of the product was the only analytical method to confirm the presence of well-dispersed and nano-sized metallic particles. Although the resolution was poor due to the high percentage of PVP, separated black spots on the image could be attributed to dispersed ruthenium nanoparticles with a size of around 1.1nm (**figure 39**). The ruthenium content of RuNp@PVP prepared after this procedure was found to be around 7.6%. WAXS analysis supported a hexagonal close-packed (hcp) structure of the ruthenium nanoparticles.

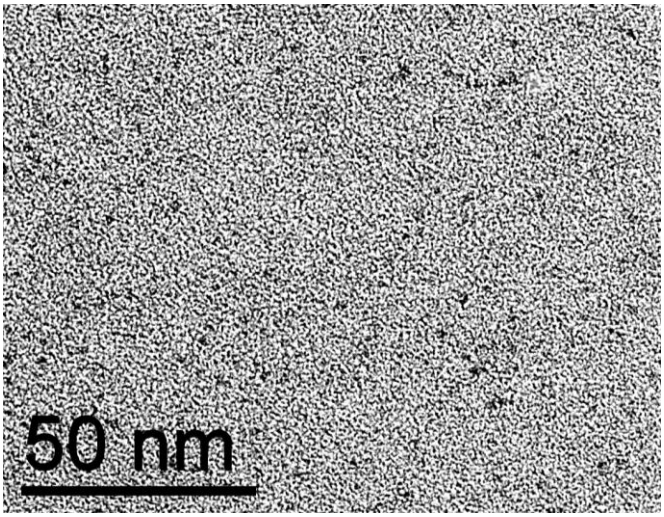

Figure 39. TEM image of RuNp@PVP

1.2 Synthesis of Ru-*ICy* Np

For the synthesis of NHC-stabilized RuNps, the reduction of Ru(COD)(COT) requires to be performed in the presence of the carbene ligand as it was previously reported.[81] For this purpose, 0.25 stoichiometric equivalents of the carbene ligand 1,3-dicyclohexylimidazol-2-ylidene (*ICy*) were prepared separately by deprotonating the imidazolium salt 1,3-dicyclohexylimidazolium chloride with potassium *tert*-butanolate (**figure 40**).

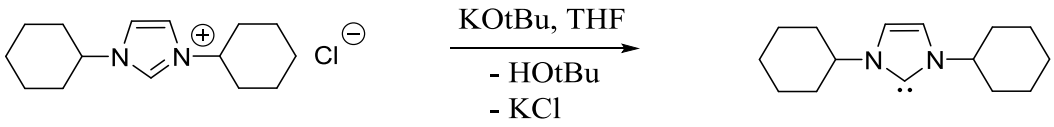

Figure 40. Preparation of a *N*-heterocyclic carbene ligand through the deprotonation of an imidazolium salt.

Subsequently the carbene solution was added to one equivalent the organometallic precursor solution and the reduction with H_2 gas was started. Within a short time, the reaction mixture turned into a deep black homogeneous solution, evidencing the formation of soluble ruthenium colloids (**figure 41**).

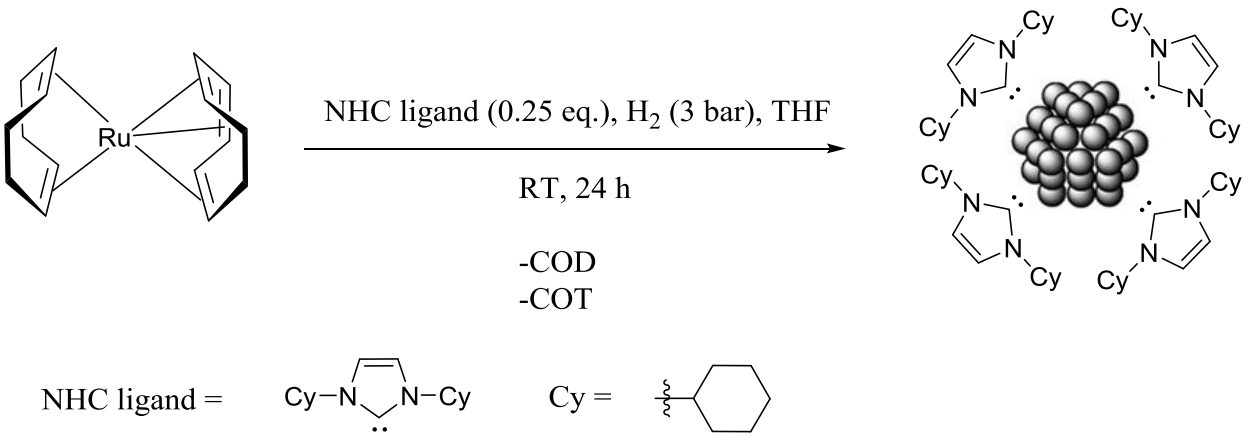

Figure 41. Synthesis of RuNp stabilized by *N*-heterocyclic carbenes

The successful formation of RuNp was confirmed also in this case over TEM. The distribution of the particle size was plotted in a histogram. The nanoparticles manifested a mean size of 1.2nm with a distribution of around ±0.5nm (**figure 42**).

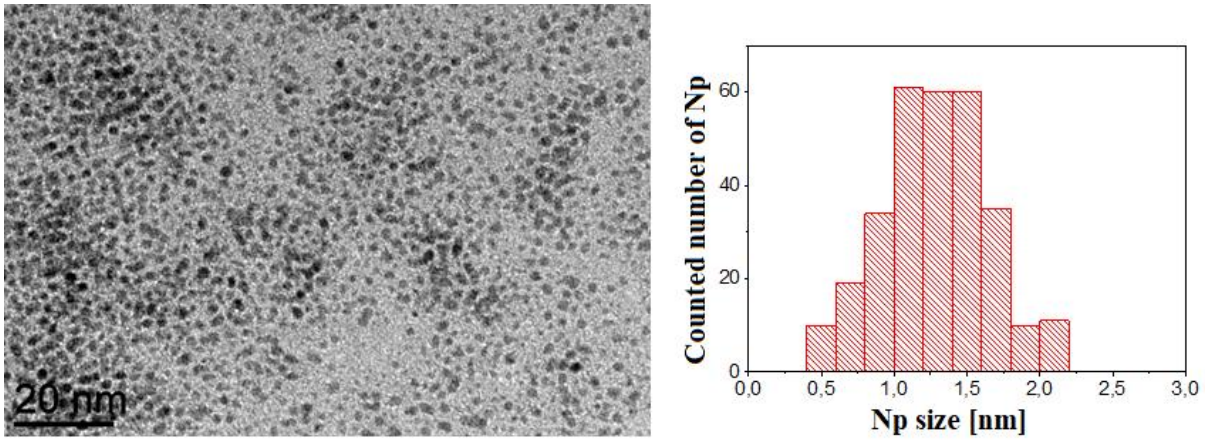

Figure 42. TEM image of Ru-*ICy* Np (left) and histogram showing the nanoparticle size distribution (right)

Nanoparticles were also analyzed by thermal gravimetric analysis (TGA) to determine the content of ruthenium relative to organic matter. Heating of the synthesized nanoparticles to around 600°C lead to a mass decrease of 29%. Consequently, synthesized Ru-*ICy* Np are supposed to contain 71wt% of ruthenium (see experimental section for TGA data).

1.3 Synthesis of Ni-*ICy* Np

The synthesis of nickel nanoparticles (NiNp) was of high interest, because a principle aim of this work was also the study of the reactivity of a different metal than ruthenium. Nickel is a non-noble, earth-abundant and much cheaper metal than noble metals as ruthenium. Being non-noble, well-dispersed Ni(0) manifests high oxygen sensitivity which is a drawback towards the work with ruthenium because it makes thorough operation of Ni(0) catalyzed reactions under inert conditions mandatory. Metallic Ni(0) films are already known to be active HIE catalysts under D_2 gas as mentioned earlier in chapter **I.***3.2.1*.[59] Nonetheless, with the synthesis of well-defined nickel nanoparticles we intended to generate a more active and efficient HIE catalyst, that operates under mild reaction conditions using D_2 or T_2 gas as isotopic sources. For this purpose, nickel nanoparticles were synthesized, stabilized by 0.25 stoichiometric equivalents of the NHC-ligand *ICy* that was prepared as stated in **figure 40**. A suitable nickel-based organometallic precursor proved to be bis(1,5-cyclooctadiene) nickel ($Ni(COD)_2$). However, the reduction of $Ni(COD)_2$ with H_2 gas demanded a higher temperature than in the case of Ru(COD)(COT). The formation of nickel nanoparticles (Ni-*ICy* Np) could be observed at 70°C (**figure 43**).

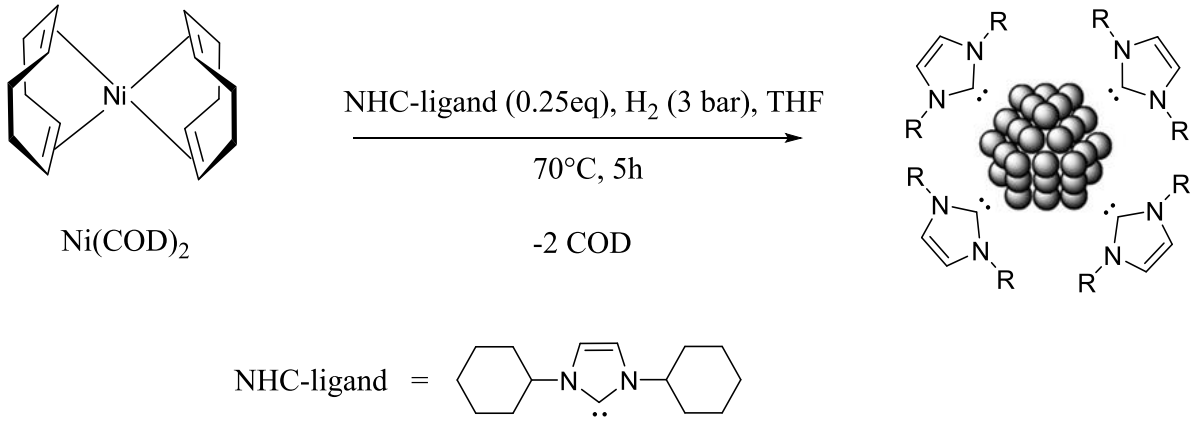

Figure 43. Synthesis of NiNp stabilized by *N*-heterocyclic carbenes (Ni-*ICy* Np)

The nanoparticle solution was again concentrated and washed by precipitation in *n*-pentane in order to remove non-volatile impurities. The analysis of the nanocatalyst by TEM supported the formation of NiNp displaying a bigger diameter then the aforementioned RuNp. The size of Ni-*ICy* Np was around 2nm with a size-dispersion of ±1nm (**figure 44**).

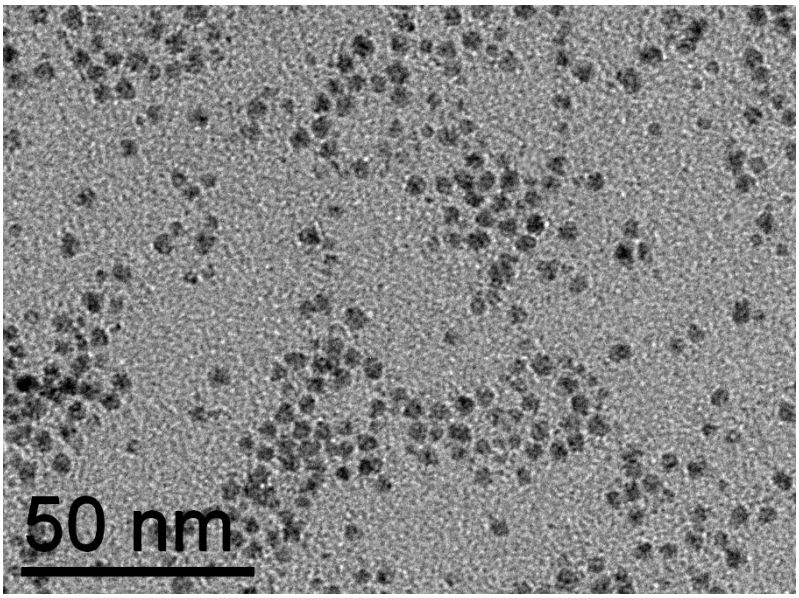

Figure 44. TEM image of NiNp stabilized by 0.25 stoichiometric equivalents of *ICy*

The metal content in NiNp was determined by inductively coupled plasma-mass spectrometry (ICP-MS) in all cases, because TGA proved to be not as suitable as ICP-MS for nickel-based probes. In this context, the mass of the synthesized nanocatalyst was found to be composed to 69wt% of nickel. The crystal structure analysis of Ni-*ICy* Np by wide-angle X-ray scattering (WAXS) evidenced a face-centered-cubic (*fcc*) unit-cell for the nickel metal (see experimental part for complete analytical data).

1.4 Synthesis of Ni-*IMes* Np

With regard to NiNp, it was also necessary to test the influence of a different NHC ligand on the reactivity within HIE reactions in the ongoing work. 1,3-Dimesitylimidazol-2-ylidene (*IMes*) was a very convenient NHC-ligand to work with, because it was commercially available as free carbene and ready to use for MNp syntheses. In this section, two batches of NiNp were synthesized which were stabilized by different amounts of *IMes*, in order to figure out a possible steric or electronic impact of the NHC-ligand attached to the catalyst surface. Ni-*IMes* Np were synthesized under the same conditions as Ni-*ICy* Np in **figure 43**. One batch was stabilized by 0.25 equivalents of NHC-ligand and the other one by 0.5 equivalents (**figure 45**). The obtained nanoparticle solutions were again precipitated twice in *n*-pentane and dried under vacuum prior to storage in the glove box.

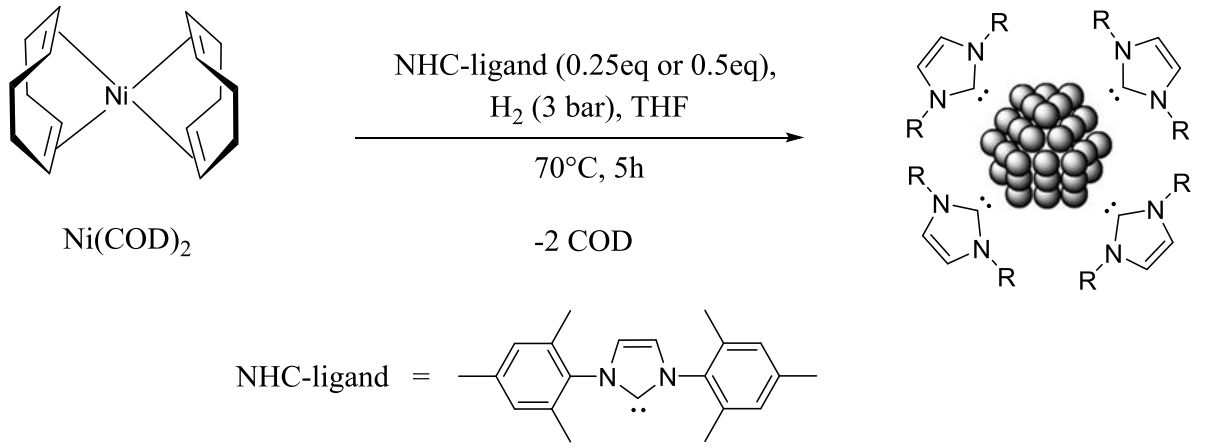

Figure 45. Synthesis of NiNp stabilized by *N*-heterocyclic carbenes (Ni-*IMes* Np)

TEM images pointed out that the syntheses furnished well-dispersed NiNp with a mean size of 1.8±0.6nm in the case of 0.25 equivalents NHC ligand (**figure 46**, left) and smaller NiNp with 0.5 equivalents NHC-ligand (**figure 46**, right). The precise determination of the nanoparticle size was difficult for the latter, due to the poor resolution of the TEM image.

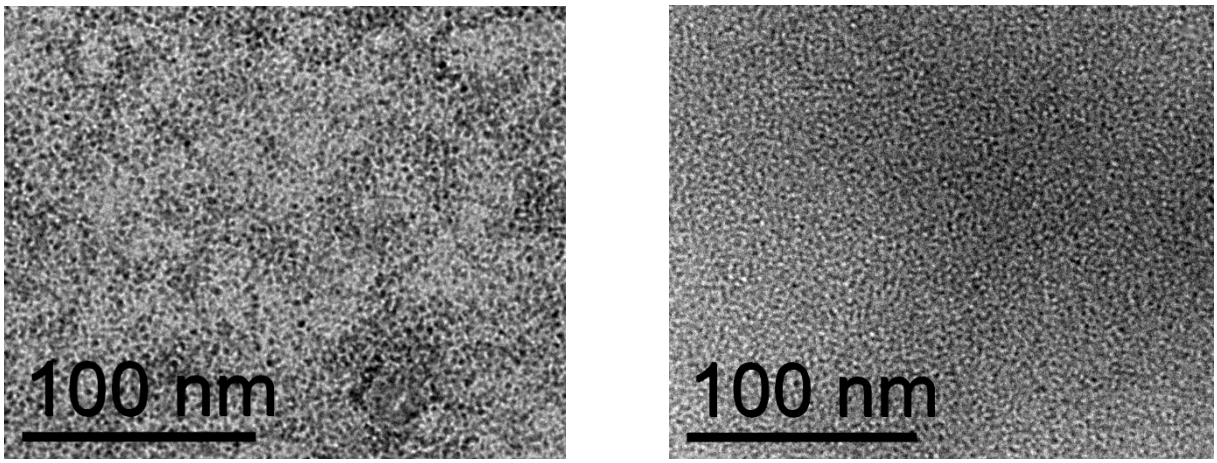

Figure 46. TEM images of Ni-*IMes* Np stabilized by 0.25eq. (left) and 0.5eq. of NHC-ligand (right)

WAXS analysis witnessed *fcc*-Ni(0) also in the case of Ni-*IMes* Np. The determination of the metal content in the two batches through ICP-MS delivered 36wt% (0.25eq of *IMes*) and 29wt% nickel (0.5eq of *IMes*).

2. HIE on *N*-Heterocycles catalyzed by metallic nanoparticles

2.1 HIE catalyzed by ruthenium nanoparticles

In this chapter, ruthenium nanoparticles are going to be explored for their potential to incorporate hydrogen isotopes into several types of *N*-heterocycles. In recent articles, we demonstrated that the use of RuNp allows the deuteration of nitrogen-containing compounds in bioactive molecules, including the indole and pyridine moiety as *N*-heterocyclic substrates, and by using D_2 as isotopic source. Thereafter, we envisioned that the nanocatalysts synthesized in **II**.*1*.*1* and **II**.*1*.*2* might be used for an efficient and selective deuteration of a larger variety of nitrogen containing heterocycles. Based on this theory, we anticipated that this would also provide a new method for the late-stage tritiation of many pharmaceuticals under mild reaction conditions.

2.1.1 Initial considerations

The first aim was to determine experimentally in how far compounds, which are of interest for us, can be deuterated by D_2O as solvent or co-solvent without any metal catalyst under a moderate temperature of 80°C. Thermal exchange experiments in the protic (co-)solvent D_2O on some selected model compound examples, carrying additional acidic or basic moieties themselves, lead to a low percentage of exchanged hydrogen at C_2 of the oxazole ring of an oxazole derivative (**figure 47**, top). The exchange in the presence of D_2O replaced hydrogen at C_2 of imidazolyl-acetic acid to 74% for deuterium (**figure 47**, center) and almost quantitatively at C_5 of the 1,2,4-triazolic moiety (**figure 47**, bottom).

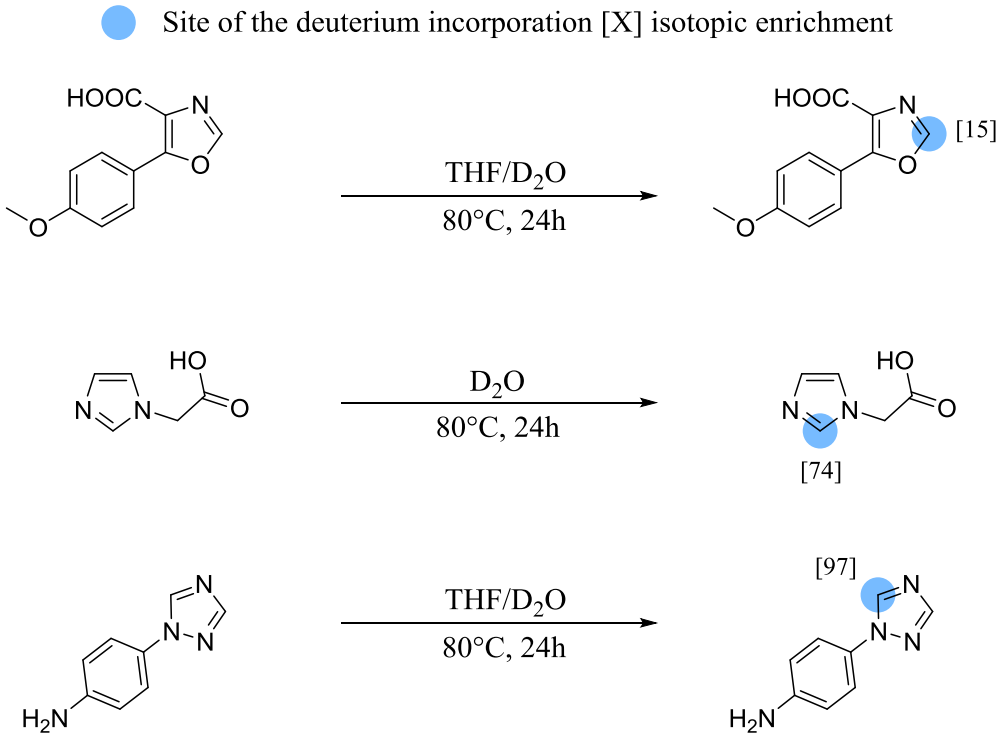

Figure 47. Deuteration on acidic sites of *N*-heterocyclic derivatives in D_2O.

Consequently, the C_2 position of the depicted oxazole derivative is still worth to be targeted by transition metal catalyzed HIE because it is shown to be deuterated not efficiently under relatively mild conditions through D_2O alone. On top of that, it is worth to develop a suitable and efficient HIE method for heterocyclic cores because there are several other sites like the C_4 and C_5 position on imidazoles and the C_3 position of 1,2,4-triazoles which are not deuterated at all by protic deuterated solvents. A back-exchange to the protio form should also not occur since these positions do not display low pK_a values (**I**.*2.2*, **figure 12**). At any rate, a novel method is needed for the tritium labelling of such compounds. Despite the satisfying H/D exchange at one position of 1,2,4-triazole, a corresponding tritium labelling by T_2O is of very low interest. Hence, a method being able to activate T_2 gas to use it as isotopic source is strongly necessitated if tritium labelling is intended on these types of substrates. Further, it was necessary to test the reactivity of various *N*-heterocyclic substrates within other transition metal catalyzed methods in order to draw a comparison between HIE methods that already exist and metal nanoparticle catalysis that is going to be investigated. This will allow us to list advantages and drawbacks based on experimental results. As already mentioned previously in **I**.*3.2.2*, an option to conduct regioselective HIE by using D_2 or T_2 as isotopic source on *N*-heterocyclic derivatives is homogenous Ir(I) catalysis. 2,5-diphenyloxazole revealed to be an attractive substrate to initiate our studies. In another context, it appeared as a biologically

relevant reference compound for affinity assays, since it showed efficient antimycobacterial activity.[85] Crabtree´s catalyst [(COD)Ir(py)PCy_3]PF_6 (COD = 1,5-cyclooctadiene; py = pyridine; Cy = cyclohexyl), was found to give a complete exchange at the *ortho* positions of one phenyl ring of 2,5-diphenyloxazole (**figure 48**, top). The HIE selectivity on this substrate is in line with the result obtained with another Ir(I) catalyst[86] confirming the reproducibility of our applied reaction conditions. Positions located in α and β relative to the nitrogen, however, did not change in terms of isotopic ratio at all, which was also confirmed for 2-methyl-benzoxazole (**figure 48**, center). Moreover, to the best of our knowledge, no Ir(I)-complex is known that addresses HIE on substrates containing 1,2,4-triazole scaffolds. In our case, the attempt to deuterate a hydroxylic triazole derivative via the same Crabtree catalyzed exchange protocol resulted in the full conversion to an undesired side-product (**figure 48,** bottom). This observation brought about the conclusion that a different catalytic method is required being also compatible with triazolic compounds.

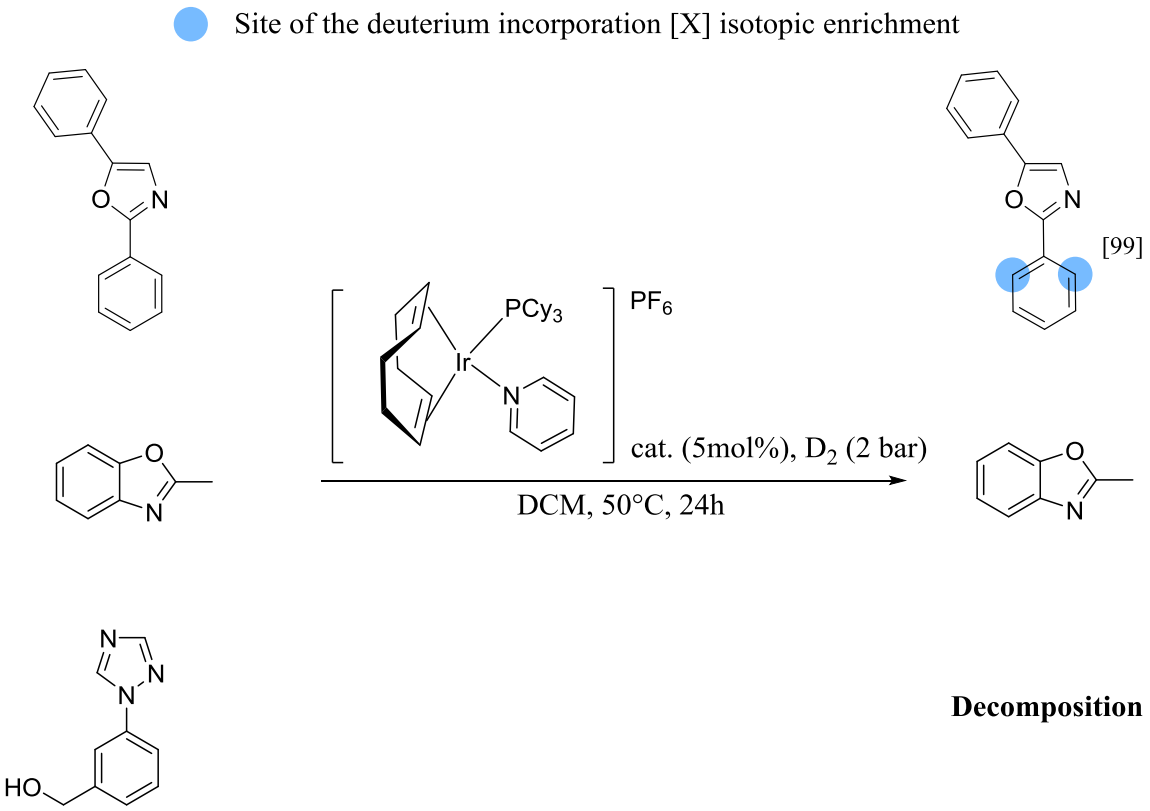

Figure 48. Reactivity tests on different *N*-heterocyclic derivatives with Crabtree catalyst and D_2 gas in DCM.

2.1.2 Deuterations of oxazoles

In the next step, we intended to figure out the most convenient ruthenium catalyst and reaction conditions for our HIE reactions on oxazoles. On this account, we submitted the oxazole-based compound 2,5-diphenyloxazole to deuteration experiments with three different catalysts under the same reaction conditions (2bar of D_2 gas, 5mol% Ru in each case, 2mL of solvent, 50°C, 24h): commercially available ruthenium on charcoal (Ru/C), RuNp@PVP and Ru-*ICy* Np. We must bear in mind that transition metal catalysts as Ru(0) originally found application for the reduction of various functionalities through hydrogenation with H_2. Thus, when combining an unsaturated organic substrate with a metallic ruthenium catalyst and a hydride donor as H_2 gas or one of its isotope analogues (D_2, T_2), several other undesired reactions might take place apart from HIE through C–H activation. Not surprisingly, hydrogenation of the phenyl rings of 2,5-diphenyloxazole took place in parallel to the HIE reaction, leading to complex mixtures of several isomers and their isotopomers after every described test reaction (the experiment was also run with H_2 instead of D_2 gas in order to simplify the analysis. In this manner, every side-product could be precisely characterized by ^{1}H-NMR and ESI-MS, **figure 49**).

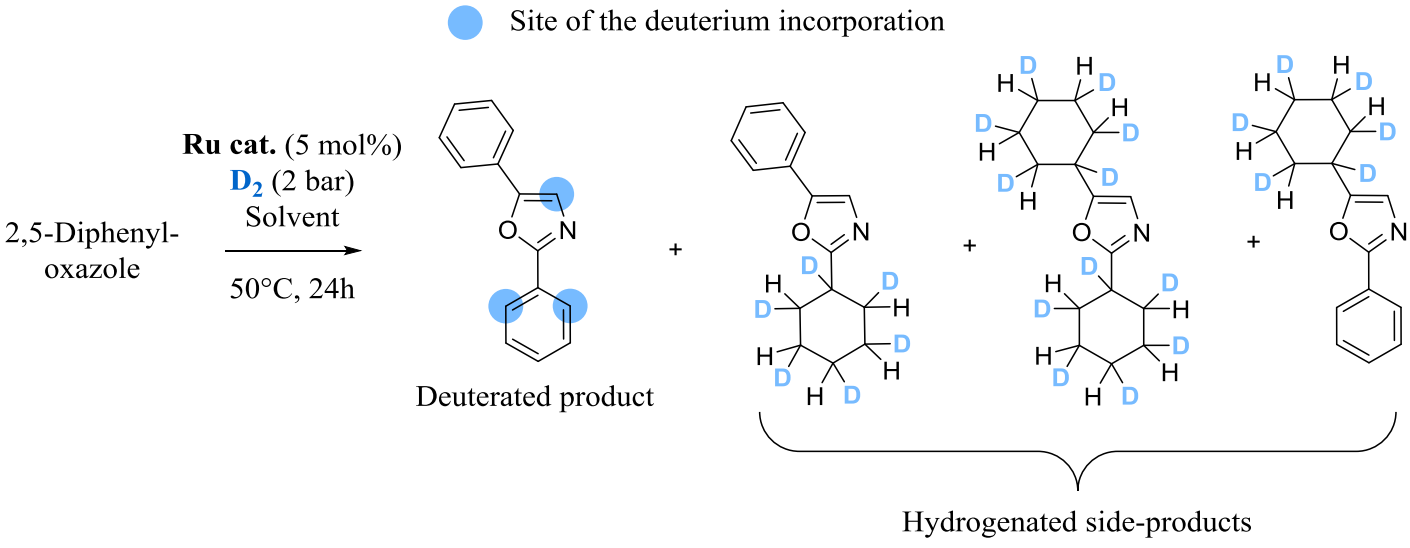

Figure 49. HIE on 2,5-diphenyloxazole by Ru catalysts and its reduction to undesired side-products.

^{1}H-NMR analysis of the crude products was used to quantify the formation of the major side-product in every experiment in order to select the best reaction conditions (**figure 50**). In each case, the integration was calibrated towards the signal in the middle that could be attributed to

the *ortho* hydrogens of the phenyl ring on position 5 of 2,5-diphenyloxazole where deuteration did not take place. The signal on the left was attributed to the *ortho* positions of the phenyl ring on position 2 where HIE took place. The signal on the right arises from two hydrogens of the major side-product that overlaps with the hydrogen on the C_4 position of the oxazole. However, this did not perturbate the analysis because the differences between the amounts of formed side-product within the three experiments were still significant. When the HIE was run with commercial Ru/C in THF, the isotopic enrichment was very high, evidenced by the little integration value of the signal on the left (**figure 50a**). However, the side-product was formed in a significantly higher amount than the labelled product (compare integration value in the middle and on the right, **figure 50a**). This finding witnessed a low chemospecificity of the charcoal supported heterogeneous ruthenium catalyst. The deuteration of the substrate with Ru-*ICy* Np still yielded an amount of side-product that was equal to the deuterated substrate (**figure 50b**). When 2,5-diphenyloxazole was deuterated with RuNp@PVP in THF, reduction of the substrate was also concomitant but to a much lower degree (**figure 50c**). Within this approach, the isotopic enrichment in *ortho* slightly dropped (compare 0.07 on the left integral in **a** and **b** with 0.28 in **c**, **figure 50**). The solvent was changed from THF to DMA and the HIE with RuNp@PVP was repeated (**figure 50d**). In this manner, the deuteration in *ortho* could be boosted compared to **c**, corresponding to 93% of isotopic enrichment at the *ortho* positions as it can be seen in the spectrum **d**. Astonishingly, the amount of generated side-product in **d** was just half the amount observed for the reaction catalyzed by Ru/C in **a** and also lower than in **b** with Ru-*ICy* Np. Owing to the higher chemospecificity and the satisfying efficiency achieved with RuNp@PVP, this catalyst was determined to be the most suitable for our ongoing plans. Further, we found that HIE reactions can be also carried out in the solvent DMA which offers the possibility to dissolve a broader variety of substrates.

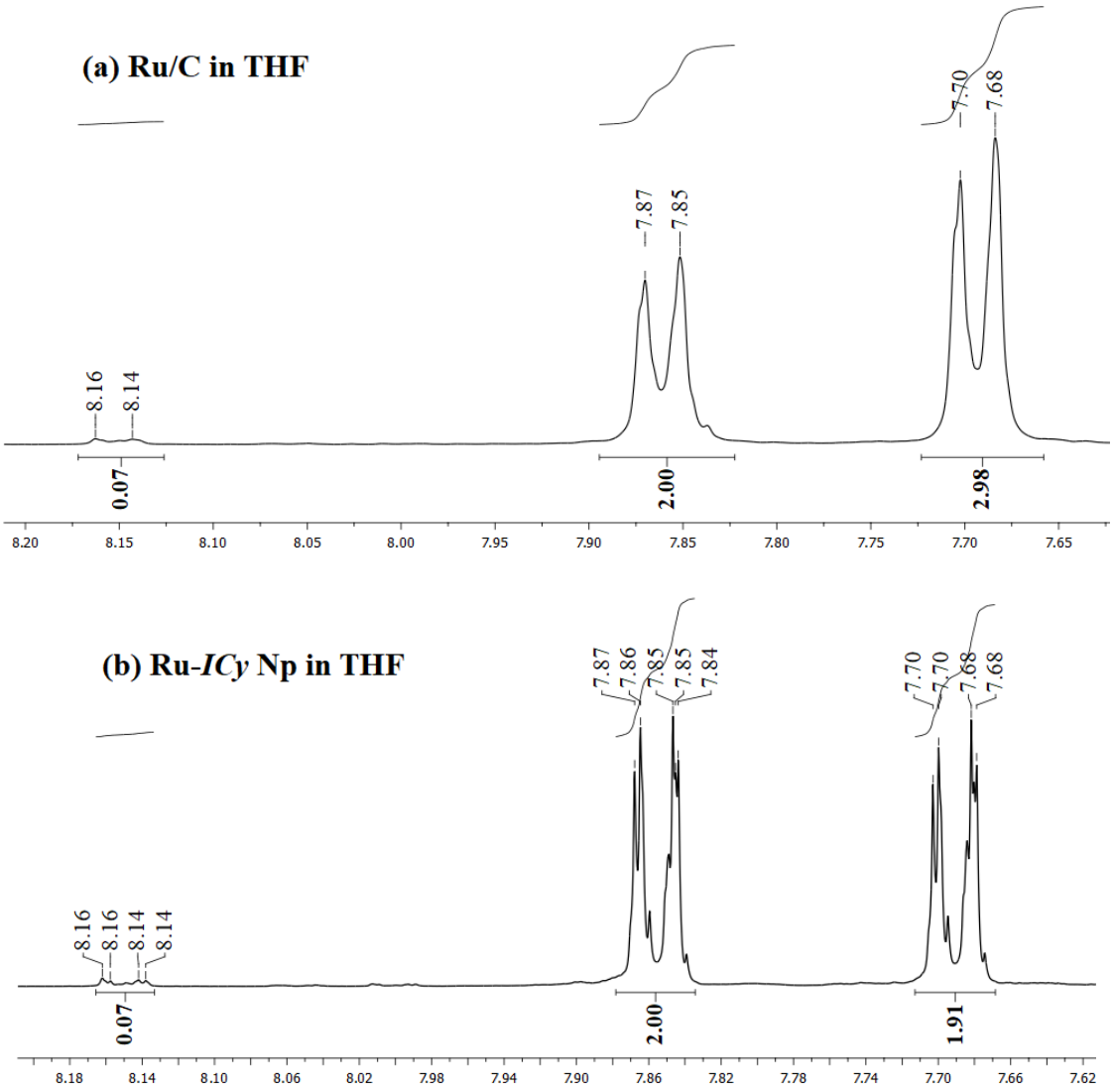

Figure 50. (a)-(d) ^{1}H-NMR spectra of the crude mixtures after HIE on 2,5-diphenyloxazole with different Ru catalysts **(e)** spectrum after HPLC-purification (chemical shifts in ppm)

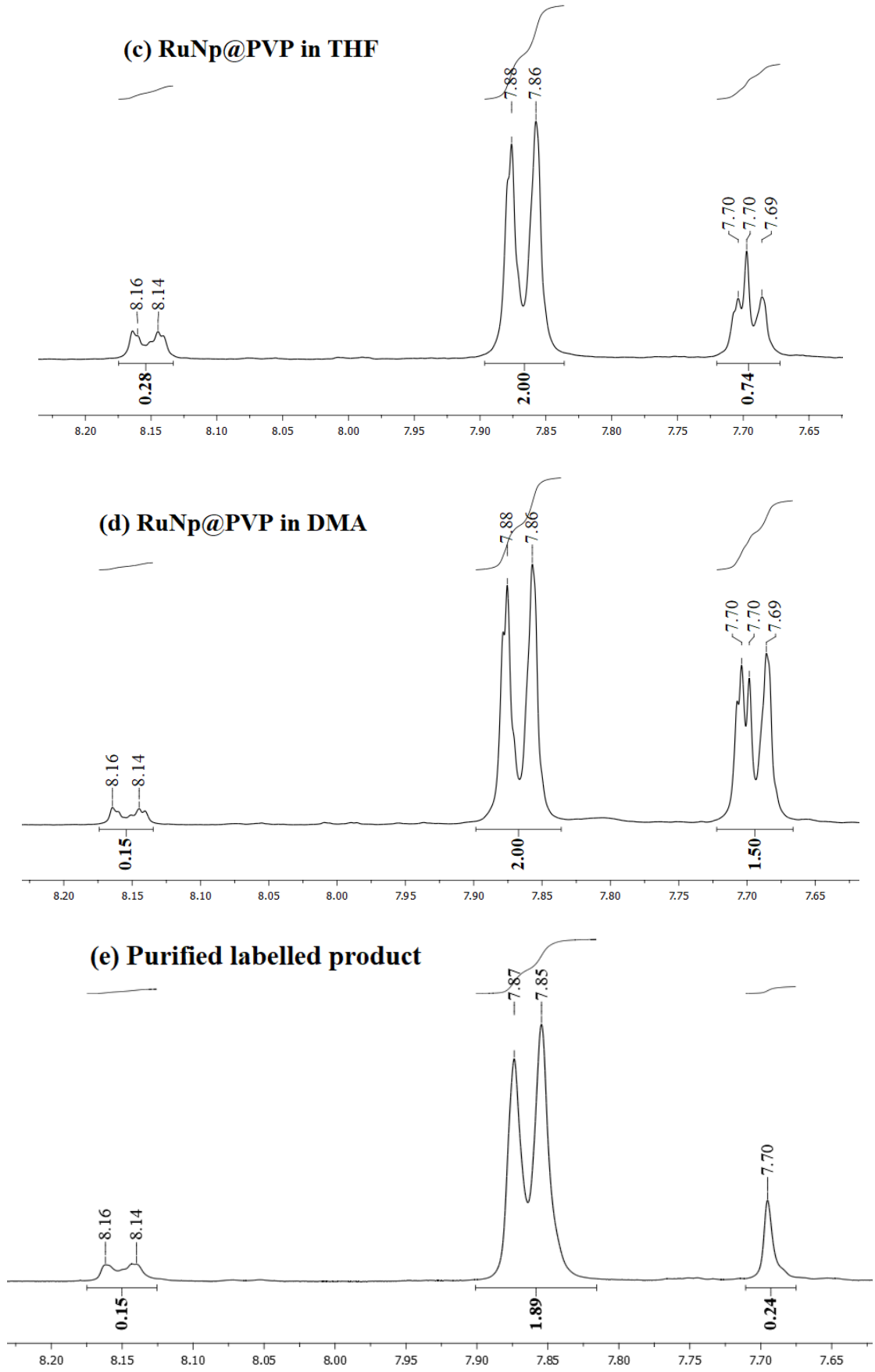

Figure 50. (a)-(d) ^{1}H-NMR spectra of the crude mixtures after HIE on 2,5-diphenyloxazole with different Ru catalysts **(e)** spectrum after HPLC-purification (chemical shifts in ppm)

After HPLC of the crude reaction mixture from **figure 50d**, spectrum **e** was obtained where the labelled C_4 position of the oxazole arises at 7.70 ppm. Deuterated 2,5-diphenyloxazole **1** was afforded in an isolated yield of 25% with a total uptake of 2.4 deuterium atoms incorporated at the oxazole core and in the *ortho* positions of the phenyl group attached to the C_2 position, i.e. in α- and in γ-positions to the nitrogen atom (**figure 51**). The utility of the RuNp@PVP-based approach to label oxazoles by hydrogen isotopes could be confirmed by furnishing other successfully deuterated model compounds **2** – **4**, whose hydrogen isotope labelling cannot be achieved via Ir(I)-catalysis (**figure 51**). Deuteration reactions were also conducted in tetrahydrofurane (THF) or dimethylacetamide (DMA) as solvents and with RuNp@PVP as catalyst (5mol% of ruthenium nanoparticles) at 50°C under D_2 atmosphere (2bar). It is noteworthy that isotopic enrichments on oxazoles with strongly polar functionalities as **3** and **4** were higher in the solvent dimethylacetamide (DMA) than in THF. It is likely that DMA represents a better coordination competitor for polar moieties like $–NH_2$ and –COOH on the surface of the catalyst, due to the presence of a nitrogen atom in its molecular structure that coordinates stronger to the ruthenium surface than the oxygen atom of THF. This solvent property probably favored the dissociation of the amino group of **3** and the carboxyl group of **4** from the catalyst surface and established a more favorable coordination/decoordination equilibrium to increase the turnover number (TON) for the C–H activation on the oxazole ring. Moreover, regio- and chemoselective labelling at C_2 of compound **4** was realized without forming the decarboxylated side product. Interestingly, Compounds **2** and **3** displayed high deuterium uptakes at the C_2- and just moderate uptakes at the C_4 positions of the oxazole ring (both α-positions relative to the same coordinating nitrogen atom, **figure 51**).

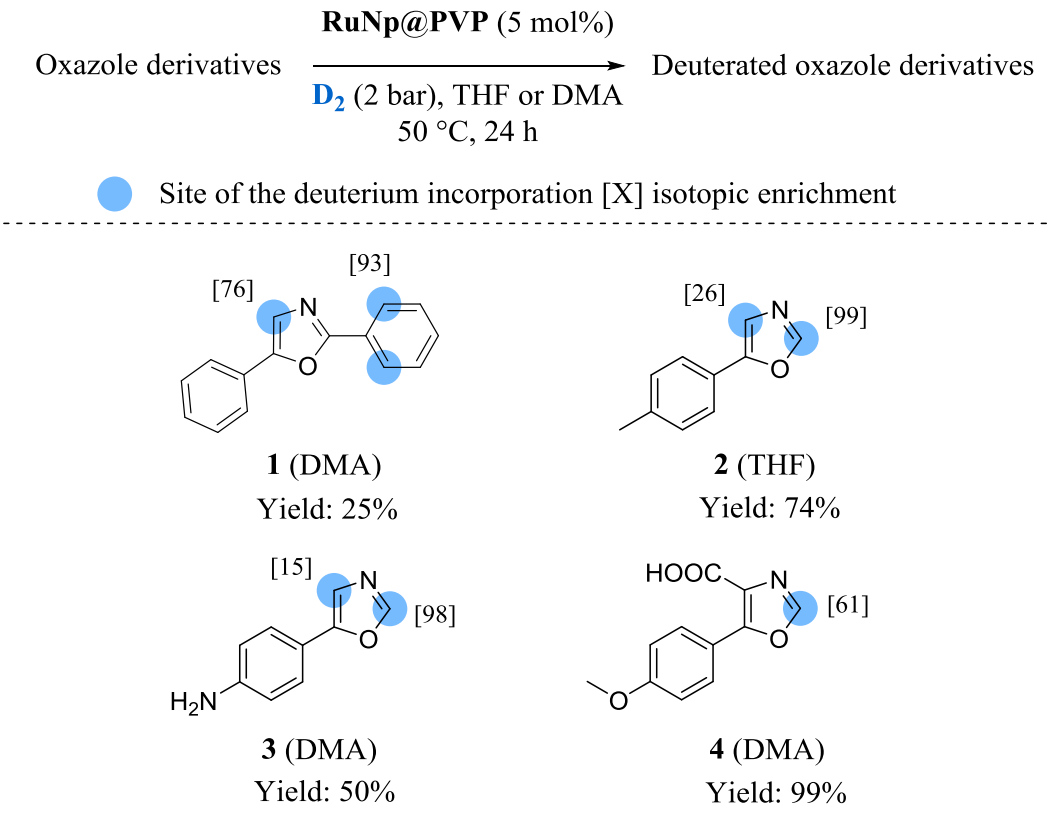

Figure 51. Examples of deuterated oxazole derivatives

From a fundamental point of view, we were further interested in exploring the considerable difference in isotopic enrichment between the C_2- and the C_4 position on compound **3** as an example. In order to study the reaction pathway leading to the C(sp^2)-H activation at the α positions of the nitrogen atom on oxazoles, theoretical calculations at the DFT-PBE level of theory were conducted by Romuald Poteau and coworkers. Every other DFT-based calculation in the following sections was also carried out in the working group of Romuald Poteau. For this purpose, a 0.5 nm ruthenium cluster with 1.4 H atoms *per* Ru surface atom ($Ru_{13}H_{17}$) was used as a model for a ruthenium nanoparticle.[83, 87] As we can see in **figure 52**, the coordination of **3** to the RuNP model through the lone pair of the nitrogen atom is an exothermic process ($\mathbf{3}^{N*}$: *ca.* -19 kcal.mol^{-1}). From this intermediate a stabilizing agostic interaction can be established between the C_2-H ($\mathbf{3}^{N*,C2H*}$, green pathway) or C_4-H ($\mathbf{3}^{N*,C4H*}$, blue pathway) groups and one of the first-neighbored ruthenium atoms to the one that interacts with the nitrogen atom. The formation of this three-center two electron bond between a C-H bonding orbital and an empty metal orbital is evidenced by the slight carbon pyramidalization (accompanied by the lifting of the hydrogen atom out of the plane of the oxazole ring). From both 4-membered dimetallacycle intermediates $\mathbf{3}^{N*,C4H*}$ and $\mathbf{3}^{N*,C2H*}$, the C−H bond activation is a kinetically accessible process with an activation barrier of 6.0

kcal/mol on C_4 position ($\mathbf{3}^{N^*,C4H‡^*}$) and of 4.2 kcal/mol on C_2 position ($\mathbf{3}^{N^*,C2H‡^*}$). However, from a thermodynamic point of view, the C - H bond breaking is an almost athermic process at C_2 position ($\mathbf{3}^{N^*,C2^*}$**:**+1 kcal/mol with respect to $\mathbf{3}^{N^*,C2H^*}$) whereas it is clearly endothermic at the C_4 position ($\mathbf{3}^{N^*,C4^*}$**:**+4.3 kcal/mol w.r.t. $\mathbf{3}^{N^*,C4H^*}$). However, the formation of the 4-membered dimetallacyle is just one key parameter in both pathways. Owing to the small barrier heights, a second crucial key parameter is the competition between the (C-H)* → (C)*(H)* reaction (*i.e.* $\mathbf{3}^{N^*,CXH^*}$ → ($\mathbf{3}^{N^*,CX^*}$)(H*)) and the (C)*(H)* → (C-H)* back reaction. The lower deuterium incorporation at the C_4 position ([15]) *vs* at the C_2 position ([98]), experimentally observed for compound **3,** can therefore be explained by the small barrier (only 1.7 kcal/mol) for the back reaction (from $\mathbf{3}^{N^*,C4^*}$ to $\mathbf{3}^{N^*,C4H^*}$), thereby reducing the efficiency of the overall process. A similar explanation can probably be invoked for compound **2**, where the isotopic labelling at the C_2 position ([99]) was also found to be higher than the one encountered at the C_4 position ([26]).

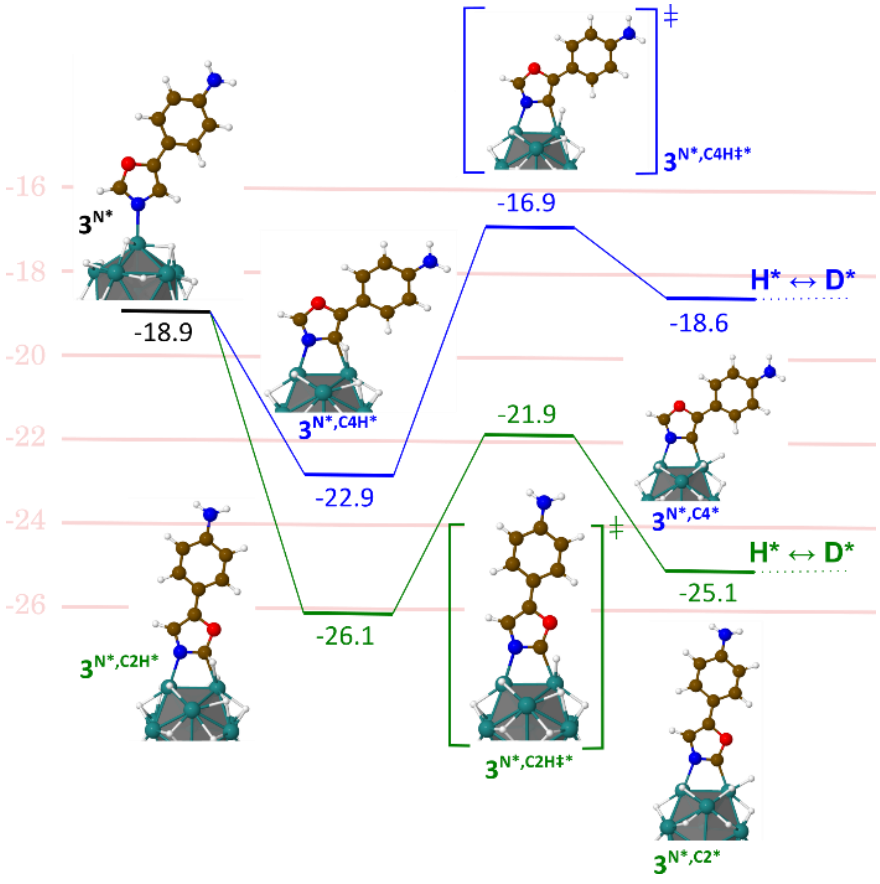

Figure 52. Energy diagram for the Langmuir–Hinshelwood-type H/D exchange on the C_2 (green pathway) and C_4 (blue pathway) position of the oxazole ring of compound 3; energies are given in kcal.mol^{-1}

The exchange of hydrogen for deuterium was found to take place at α-, β- and γ-positions relative to the nitrogen atom of the oxazole scaffold within RuNp@PVP catalyzed deuterations. This property of Ru nanoparticles permitted to provide several examples of deuterated oxazole derivatives that cannot be labelled by other HIE methods as homogeneous Ir(I) catalysis at all. Further, the HIE catalyst RuNp@PVP proved to be compatible with very polar and protic functionalities, in contrast to the Fe(0) catalyst of Chirik *et al.* where the carboxyl group of a drug had to be deprotonated prior to hydrogen isotope exchange.[68] DFT-based mechanistic studies deciphered a four-membered dimetallacyclic adduct as the key intermediate for the labelling of α positions relative to nitrogen atoms on aromatic rings. Additionally, when monitoring the energetic profiles of the C–H activations on C_2 and C_4 of an oxazole compound, the preference of RuNp for the C_2- over the C_4 position could be interpreted. Nonetheless, the reduction of sensitive substrates still persisted which prompted the conclusion that employing a different metal as HIE catalyst like the nickel nanoparticles from **II**.*1.3* - **II**.*1.4* could probably circumvent this problematic side-reaction.

2.1.3 Deuterations of imidazoles

Owing to the ubiquity of the imidazole scaffold in biologically relevant molecules as demonstrated in chapter **I**.*2.3*, we subjected various imidazole derivatives to the RuNp@PVP-based HIE approach (**figure 53**). 2-Phenylimidazole **5** showed high deuterium incorporation on the phenyl, in *ortho* to the imidazole nucleus. Moreover, deuteration occurred at the *α*-positions relative to the nitrogen atoms of the imidazole itself, which are not labelled by Kerr´s catalyst.[66] Thus, in contrast to this homogeneous Ir(I) catalyst, the Ru nanocatalyst permitted the isotopic labelling of two additional positions which can be significant for the successful synthesis of SILSs (**figure 53**).

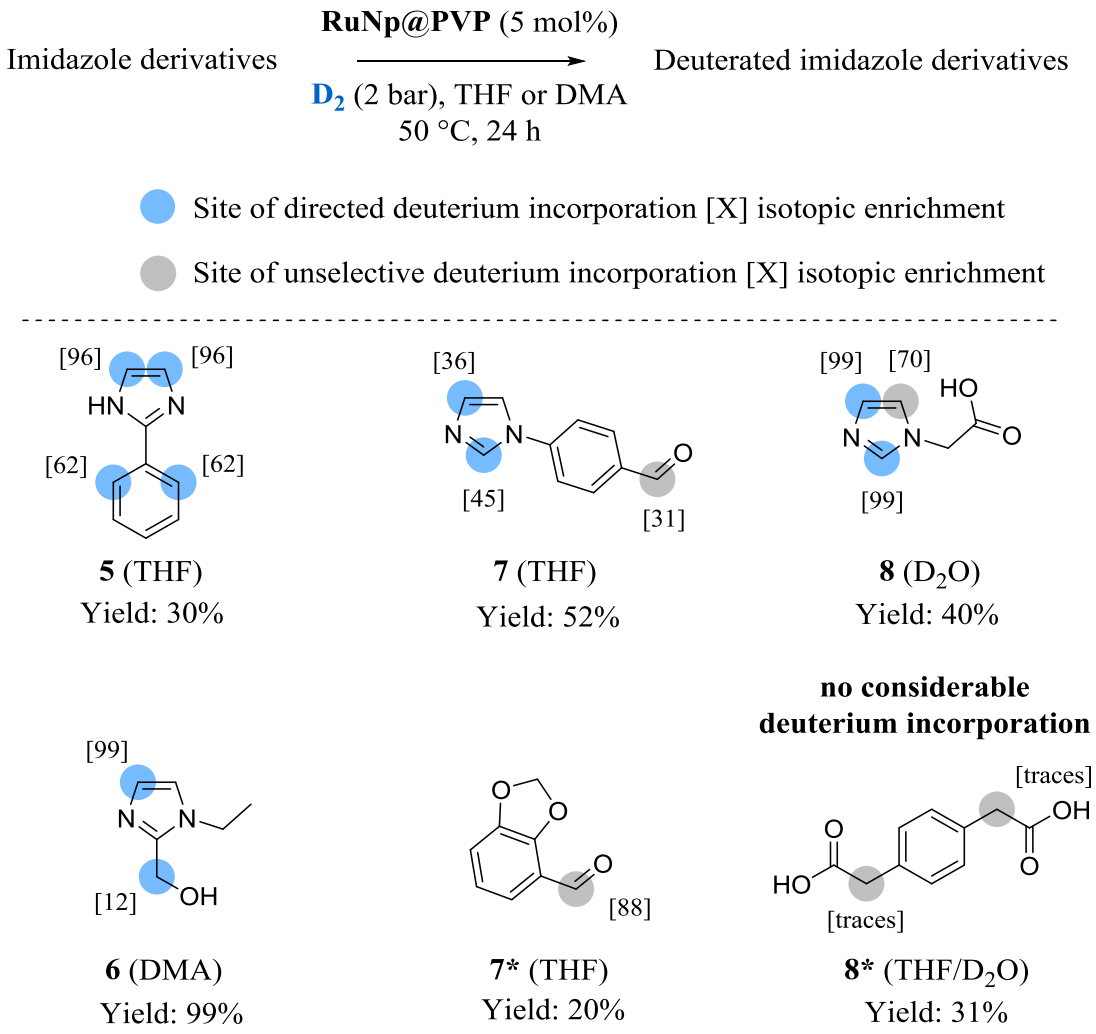

Figure 53. Examples of deuterated imidazole derivatives and diverse test compounds

The deuterium incorporation on both sites of **5** was considered from a theoretical point of view, especially in order to identify the key intermediate leading to the labelling at the *γ*-positions of the coordinating nitrogen, i.e. **γ1** and **γ2** in **figure 54**. Two competitive pathways were investigated (**γ1** in red and **γ2** in blue, **figure 54**). In any case, compound **5** is initially adsorbed at the Ru nanoparticle surface through the lone pair of the N_3 nitrogen atom to give $\mathbf{5}^{\mathbf{N*}}$. Then, the C–H bond in *ortho* of the phenyl ring also coordinates to the ruthenium catalyst by the formation of a stabilizing agostic interaction. It is noteworthy that two different adsorptions of the substrate can occur, either on one ruthenium atom ($\mathbf{5}^{\mathbf{N*,\gamma 1H*}}$) or on two neighboring ruthenium atoms ($\mathbf{5}^{\mathbf{N*,\gamma 2H*}}$). They lead respectively to a five-membered metallacyle (a key intermediate analogue to the one proposed in homogeneous catalysis) or a six-membered dimetallacycle adduct.

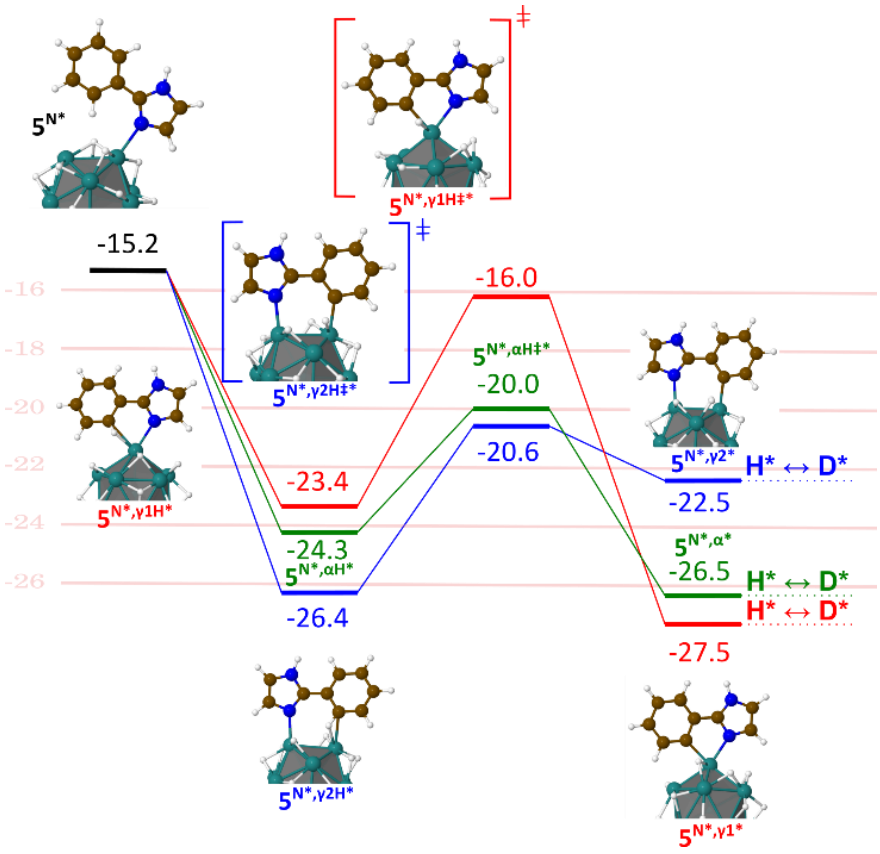

Figure 54. Energy diagram for the Langmuir–Hinshelwood-type H/D exchange on **5** in the *ortho*-position of the phenyl (blue and red pathways) and at α-positions relative to the imidazole nitrogen atoms (green pathway; for the sake of clarity the geometries are not given, see also SI); energies are given in kcal.mol^{-1}.

The pathway that involves a six-membered dimetallacycle is both endothermic and kinetically accessible (blue pathway, **figure 54**). This mechanism cannot be excluded for the deuterium incorporation but it is probably inefficient due to the small barrier (1.9 kcal/mol) and the exothermicity (*ca.* -4 kcal/mol) of the (C)*(H) * ↔ (C-H)* back reaction (*i.e.* $\mathbf{5}^{\mathbf{N*,\gamma 2*}}\leftrightarrow\mathbf{5}^{\mathbf{N*,\gamma 2H*}}$). The C-H activation involving a five-membered metallacyle (red pathway, **figure 54**) is also kinetically accessible, with an activation barrier of 7.4 kcal/mol, but thermodynamically more favorable (-4.1 kcal/mol) on the contrary to the **γ2** case. The C-H activation equilibrium is now in favor of (C)*(H)* ($\mathbf{5}^{\mathbf{N*,\gamma 1*}}$). Thus, the deuterium incorporation at the γ-position of the nitrogen is most probably due to a process that goes through a five-membered metallacyle intermediate such as in homogeneous catalysis. The very efficient HIE in *α* to the nitrogen atoms ([96]) corresponds to a thermodynamically favorable mechanism (-2.1 kcal/mol w.r.t. (C-H)*, green pathway in **figure 54**) involving a 4-membered dimetallacycle as key intermediate and a low activation barrier for the C-H bond breaking step (4.3 kcal/mol). Thus, the competition between the (C)*(H)* ↔ (C-H)* back reaction (*i.e.*

($\mathbf{5}^{\mathbf{N*,\alpha*}}$)(H*) ↔ $\mathbf{5}^{\mathbf{N*,\alpha H*}}$) and the (C)*(D*)* ↔ (C-D)* (*i.e.* ($\mathbf{5}^{\mathbf{N*,\alpha*}}$)(D*) ↔ $\mathbf{5}^{\mathbf{N*,\alpha D*}}$) isotopic exchange is in favor of the latter. An explanation of the difference between the 62% and 96% conversion yields is somewhat beyond the chemical accuracy of DFT, even though, interestingly, the barrier that leads to the (C^{ortho}-D)* turns out to be higher than its (C^{α}-D)* counterpart in agreement with the observed lower experimental isotopic enrichment at this position. Compound **6** in **figure 53** was deuterated at the α-position of the N_3 nitrogen atom with 99% of isotopic enrichment accompanied by a slight deuterium incorporation on the hydroxymethyl group, which is a *β* position of the coordinating nitrogen atom. At this point, the observation was made, that *β* positions on sp^3 carbons can be also targeted for HIE by ruthenium nanoparticles, although the obtained isotopic enrichment for this position was quite moderate. An attempt to explain the incorporation of 0.24D at the hydroxymethyl group is illustrated in **figure 55**. The coordination of the nitrogen and the oxygen atom to the surface of the catalyst at the same time provides a large gain in energy because a chelate is formed. This constraint immobilizes the substrate in a certain conformation where the hydrogen atoms of the methylene group are directed opposite to the surface of the RuNp, making a C-H activation through the RuNp impossible on this position (**figure 55**, structure on the left). In order to allow a rotation of the hydroxylic side-chain for a C-H activation to occur, the hydroxyl group is supposed to dissociate from the surface (**figure 55**, structure on the right), which must be energetically less favored than the chelate conformation on the left. This seemed to be the most plausible rationalization of the lowered deuterium incorporation at the C(sp^3) center.

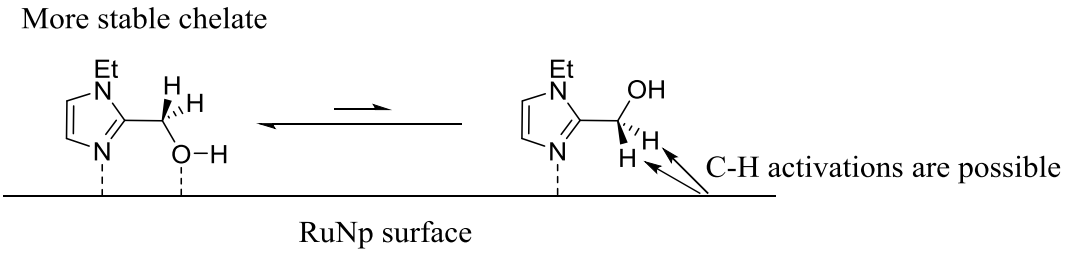

Figure 55. Proposed chelate-based explanation for the low isotopic enrichment on the hydroxymethyl group of **6**

Against our expectations, besides the imidazole labelling of **7**, an exchange of the formyl proton for deuterium was concomitant. In order to confirm the ability of RuNp to procure HIE on aldehyde groups in general, the model compound **7*** was subjected to deuteration that was functionalized with an aldehyde moiety but did not contain any nitrogen atom in its structure.

Indeed, hydrogen was selectively exchanged for deuterium on **7*** yielding an isotopic enrichment of 88% on the aldehyde moiety. However, this HIE reaction took place in parallel with the reduction of the aldehyde to an alcohol that was formed in a ratio of 2:1, relative to the deuterium labelled aldehyde **7***. These findings were also made by Kerr *et al.* for Ir(I) complexes.[88] Apparently, the surface of Ru nanoparticles shows a similar behavior towards aromatic aldehydes as Crabtree's catalyst, where the transition metal performs a C-H activation over oxidative addition of the –CHO group and regenerates the deuterated aldehyde. Further, it is noteworthy, that compounds **6** and **7** were both selectively deuterated on the imidazole cycle in *α*-positions to the unsubstituted nitrogen atoms with the C_5-positions remaining almost unchanged in both cases. The C_5-positions of **6** and **7** merely manifested some traces of deuterium incorporation which could be perceived by ^{2}H-NMR; but they were too little to be precisely quantified. In all cases, the C-H activation was mostly directed by the unsubstituted nitrogen atom N_3 inside the imidazole core, whereas aromatic tertiary nitrogen (N_1 in **6** & **7**) can be assumed not to be a directing atom. A loss of this selectivity rule was clearly encountered for **8**. The deuteration of **8** took place in D_2O, because of its poor solubility in organic solvents. Besides the expected and efficient labelling of C_2 and C_4, the non-exchangeable C_5 position of **8** was also deuterated to 70%, which gave rise to three different aromatic signals in the ^{2}H-NMR spectrum (see experimental part). First, the deuterium incorporation at C_5 was related to a directing group effect arising from the carboxylic side chain that coordinated to the catalyst and directed the C–H activation to the C_5 position. To test this hypothesis, an acetic acid derivative needed to be subjected to RuNp@PVP catalyzed deuteration being endowed with an aromatic ring and no other functionality that could coordinate to the catalyst. Although these criteria are fulfilled by *p*-phenylenediacetic acid **8***, this compound did not show any deuterium incorporation at aromatic positions with RuNp@PVP (**figure 53**). Consequently, the theory, that the acetic acid side-chain could direct the C–H activation in **8**, was withdrawn. In view of this result, the unexpected exchange at C_5 of **8** was rather related to its tendency to undergo C–H activation through a non-directed agnostic interaction with the catalyst. In the next sections, such positions will be also identified on other *N*-heterocyclic compounds. To sum up, several imidazole derivatives were deuterated successfully by RuNp@PVP in α, β and γ positions relative to coordinating nitrogen atoms and even aromatic aldehydes were revealed to be suitable substrates for the deuteration by RuNp. The method proved again to incorporate more deuterium atoms per molecule than previously reported methods like Ir(I) catalysis and to be more tolerant for substrate functionalization. For the first time, the discrimination through a

DFT-based study was successful between a five-membered metallacycle and a six-membered dimetallacycle adduct which is formed on the surface of the metal nanoparticle after the C–H activation for the HIE in γ. The comparison of the energetic profiles led to the conclusion that the HIE in γ passes through a five-membered metallacycle key-intermediate.

2.1.4 Deuterations of *N*-heterocyclic benzoderivatives

In the next step, several N-heterocyclic benzoderivatives were subjected to ruthenium nanoparticles catalyzed HIE. Given the results of Atzrodt *et al.*, benzimidazole **9** did not show any reactivity with Kerr's catalyst in terms of deuteration.[66] However, RuNp@PVP permitted to deuterate this substrate on C_2, in α to the N_1 and N_3 nitrogen. C_4 and C_7, the two β positions of the nitrogen atoms on **9**, manifested also very efficient deuterium uptake (**figure 56**). The deuteration of sp^2 carbons in β to nitrogen atoms was already observed on indoles, in one of our previous works with Ru nanoparticles.[73] Herewith it could be also confirmed on another class of *N*-heterocycles. Analogously, deuteration succeeded on 2-phenyl-benzimidazole **10** on the β positions. Further the *ortho* positions of the adjacent phenyl moiety were also addressed for HIE, since they are located in γ to the same coordinating nitrogen atoms. Prompted by the result on compound **6** in the previous section (**figure 53**), where deuterium incorporation succeeded on a sp^3 carbon in β to a coordinating nitrogen atom, we employed other model compounds having a substituent on similar positions of the N-heterocyclic scaffold. Unfortunately, compound **11** showed just traces of deuterium incorporation on its hydroxymethyl group, as in the case of **6**. For a better understanding of this result, 2-Me-benzoxazole **12** was tried, as it does not carry a hydroxy group which could prevent the C-H activation on the sp^3 carbon through the coordination of the oxygen atom to the catalyst surface. Indeed, the methyl of **12**, which is a sp^3-hybridized β position of the benzoxazole nitrogen, displayed an isotopic enrichment of 38% corresponding to a considerably higher amount of deuterium than it was found for the sp^3-positions in **6** and **11**. Nonetheless, the β positions on the *N*-heterocyclic cores of **11** and **12** were deuterated very efficiently and quite selectively. Unselective deuterations in **11** and **12** were encountered and also confirmed by ^{2}H-NMR on one more position of the *N*-heterocyclic scaffold, respectively (grey dots, **figure 56**). These are two more examples where the deuterium uptake could be rather related to non-directed agostic interactions and subsequent C–H activation on the ruthenium catalyst.

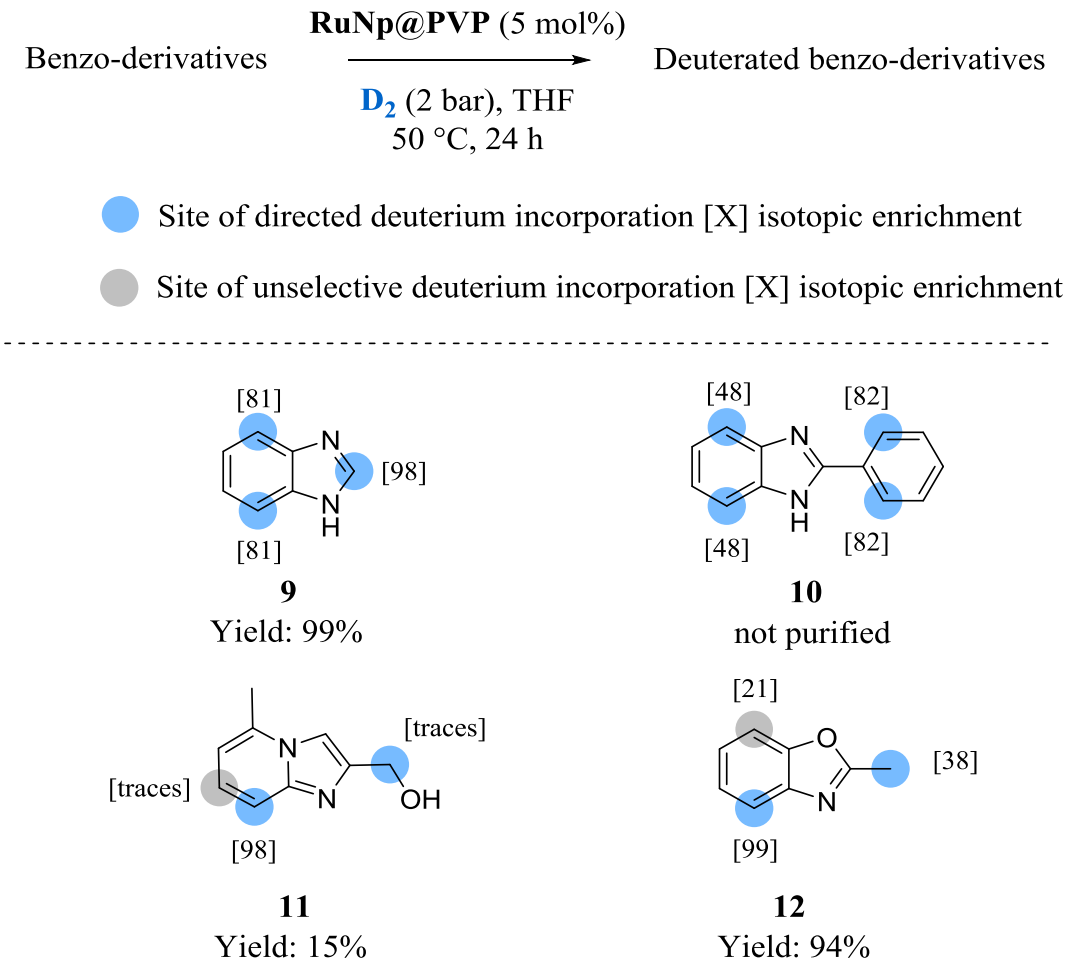

Figure 56. Examples of deuterated *N*-heterocyclic benzoderivatives

Having elicited the possibility to label β positions on sp^2 and on sp^3 carbons relative to a coordinating nitrogen atom with RuNp@PVP and D_2 gas, the objective was set to incorporate high deuterium amounts on 2-methyl-benzimidazole **13** and to show that this method is also suitable for the generation of stable isotopically labelled internal standards (**figure 57**). A first deuteration run on 2-methyl-benzimidazole in THF gave almost complete deuteration of the β positions and an exchange of hydrogen for deuterium at the methyl group to 57% (**figure 57**, molecule **13I**). The incomplete deuteration of the methyl suggested that there must be still a possibility to boost the overall isotopic enrichment on this molecule. Thus, the isolated product was resubmitted to a second deuteration run with new catalyst under the same reaction conditions. In this manner, the deuteration of the methyl could be raised to 80%, which gave a total deuterium incorporation of 4.3 deuteriums in ESI-MS (4.4 deuteriums determined by ^{1}H-NMR) (**figure 57**, molecule **13II**).

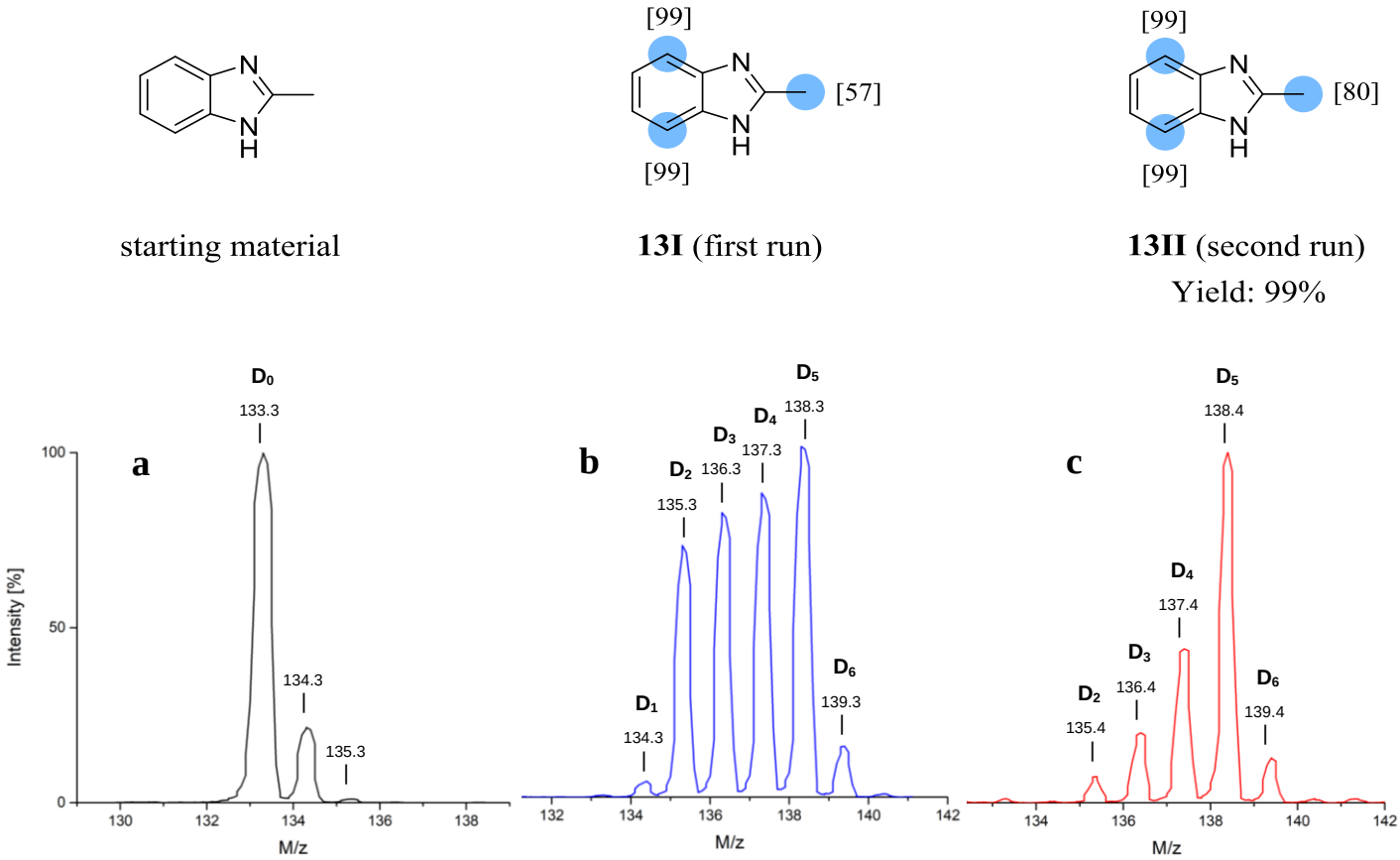

Figure 57. Isotopic enrichment on 2-methyl-benzimidazole after two runs of deuteration (top) and corresponding ESI-mass spectra (bottom)

Additionally, the deuteration progress was followed by ESI-MS after every deuteration run in order to monitor the disappearance and formation of every isotopologue. When unlabelled 2-methylbenzimidazole with the natural isotope pattern **a** was submitted to a first deuteration run, the broad isotope pattern **b** was obtained, being composed of 4 peaks of similar intensities that can be assigned to the isotopologues $\mathbf{D_2}$-$\mathbf{D_5}$. It is noteworthy, that the $\mathbf{D_0}$-peak wasn´t visible any more after this deuteration run (**figure 57**, compare black and blue spectrum). A second run, under the same reaction conditions with new catalyst, tightened the distribution pattern by decreasing the amounts of lower deuterated isotopologues ($\mathbf{D_2}$-$\mathbf{D_4}$) to form a major amount of the $\mathbf{D_5}$-isotopologue being the representative peak (**figure 57**, compare blue and red spectrum). The amount of $\mathbf{D_0}$ material after the second run was at <0.1%. The percentage of the unselectively generated isotopologue $\mathbf{D_6}$ was determined to be 1,8%. Consequently, it could be supported by mass spectrometry that RuNp@PVP catalyzed HIE clearly has a regioselective character because a narrow mass distribution was obtained instead of a broad isotope cluster. Last but not least, the total incorporation of 4.3 deuterium atoms (ESI-MS) also renders this method attractive for the synthesis of SILS for metabolism

studies (see also chapter **I**.*3.2.1*).9 A DFT-based investigation, was conducted for compound **9** in order to identify the key intermediate involved in the labelling at the β- (**figure 58**, blue pathway) and α- (green pathway) positions of the nitrogens. Again, the reaction starts with a favorable σ-donation of the N_3 nitrogen lone pair ($\mathbf{9}^{N*}$) and a further stabilization of the adduct as a result of a C^{α}-H ($\mathbf{9}^{N*,\alpha H*}$) or C^{β}-H ($\mathbf{9}^{N*,\beta H*}$) agostic interaction. The C^{β}-H HIE reaction involves a 5-membered dimetallacycle and is favored by an exothermic (C-H)* ↔ (C)*(H)* reaction ($\mathbf{9}^{N*,\beta*}$ is more stable than $\mathbf{9}^{N*}$ by -4.8 kcal/mol) leading to the H/D exchange (*vide supra* the discussion for compound **3**, **II**.*2.1.2*) and a relatively low C-H activation barrier ($\mathbf{9}^{N*,\beta H‡*}$: 5.6 kcal/mol). As shown in **figure 58**, the C^{α}-H HIE reaction is characterized by a profile (in green), very similar to the profiles calculated for the two other H/D exchanges in α, described above for oxazole and imidazole substructures (**II**.*2.1.2* & **II**.*2.1.3*).

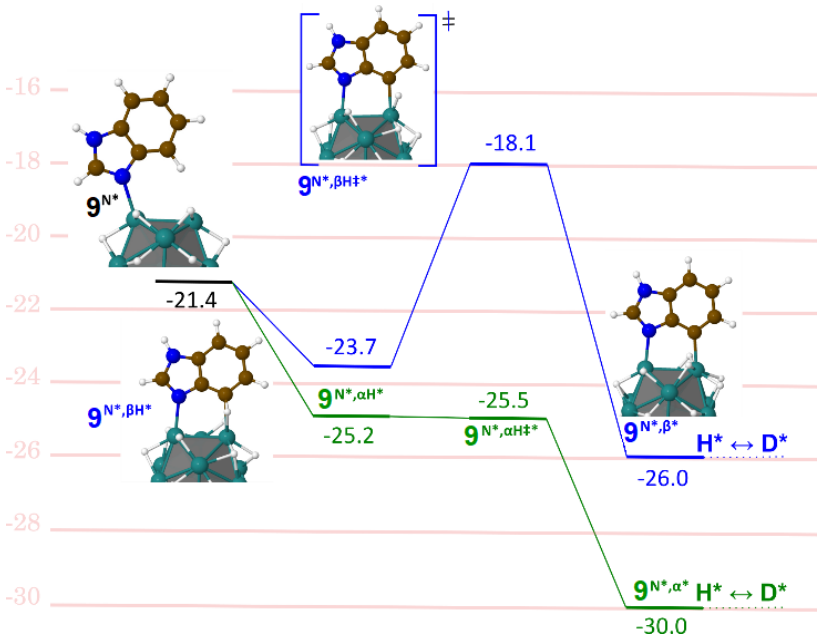

Figure 58. Energy diagram for the Langmuir–Hinshelwood-type H/D exchange on **9** in α (green pathway; for the sake of clarity the geometries are not given, see also SI) and β (blue pathway) positions of the nitrogen atoms; energies are given in $kcal.mol^{-1}$

The postulated α and β processes excelled in three key factors which characterize an efficient HIE at C(sp^2) centers, *i.e.* the formation of metallacycle intermediates, a low-barrier and an exothermic C-H activation process. It is noteworthy that the most efficient labelling process (98%) goes through an almost barrierless (C)*(H)* pathway whereas the (C-D)* bonding also requires to overcome the lowest barrier (4.5 kcal/mol vs. 7.9 kcal/mol). In summary, RuNp@PVP allowed to deuterate α, β and γ positions relative to coordinating nitrogen atoms

on C(sp^2) and on C(sp^3) of *N*-heterocyclic benzoderivatives which could not be labelled by other HIE methods before. It was shown that the incorporation of deuterium could be almost completed on the targeted positions by conducting the HIE reaction twice on 2-methyl-benzimidazole. DFT calculations paved the way to the discovery of a new key intermediate in catalysis. In this context, it was found that a five-membered dimetallacycle adduct is formed after the C–H activation in β of a coordinating nitrogen atom.

2.1.5 Deuterations of 1,2,4-triazoles

To the present day, it still did not exist a suitable method for the late-stage isotope labelling of the 1,2,4-triazole scaffold despite its high frequency in the structures of bioactive agents and therapeutics. Gratifyingly, the same HIE conditions used for oxazoles, imidazoles and their benzoderivatives, resulted in very positive results on various 1,2,4-triazolic derivatives. Since both triazolic protons are situated in *α*-positions relative to coordinating nitrogen atoms, they were exchanged very efficiently for deuterium atoms in all cases (compounds **14-19**, **figure 59**). Similar to previous findings, it appeared very likely, that the underlying C–H activations for the labelling at the α positions of the triazolic scaffold pass through four-membered dimetallacyclic key intermediates. In contrast to the targeted C_2–H and C_4–H of oxazoles, the C_3–H and C_5–H of the 1,2,4-triazole unit display almost the same reactivities in most cases, which was reflected in identical isotopic enrichments on C_3 and C_5 of compounds **14-19** (**figure 59**). Moreover, exchange of hydrogen for deuterium appeared in *ortho* positions of adjacent phenyl rings, since they are situated in γ to the triazolic N_2 atom for examples **14-18**, however not for example **19**. An explanation of the result on **19** is given below. Logically, C–H activations in *ortho* of adjacent phenyl substituents in compounds **14-18** must also proceed through five-membered metallacyclic key intermediates as in the case of 2-phenylimidazole (**figure 54**). If a comparison is made between compounds **14** and **15**, we notice that a methoxy group in the *para* position did not have any impact on the isotopic enrichment in the *ortho* positions. When comparing **14** with **16** and **17**, it turns out that the presence of protic and strongly polar moieties, like the hydroxyl group in **16** and the amino group in **17**, lowers the isotopic enrichment values in *ortho* positions of the phenyl units. In addition, the hydroxymethyl side chain in the *meta* position of **16** shields one *ortho* site more than the other. Thus, diminished isotopic enrichments can emerge from competitive and steric substituent effects. This hypothesis could be confirmed by subjecting compound **18** to the

same HIE conditions. The acetylation of the -NH_2 group in **17** furnished the acetyl amide **18**. The HIE on **18** with RuNp@PVP resulted again in a higher deuterium uptake in the *ortho* positions. The most reasonable interpretation of this result is that the extension of the amino group by an electron withdrawing acetyl has a deleterious impact on the coordination ability, depriving the aniline nitrogen of its ability to compete with the triazole unit for the catalyst surface.

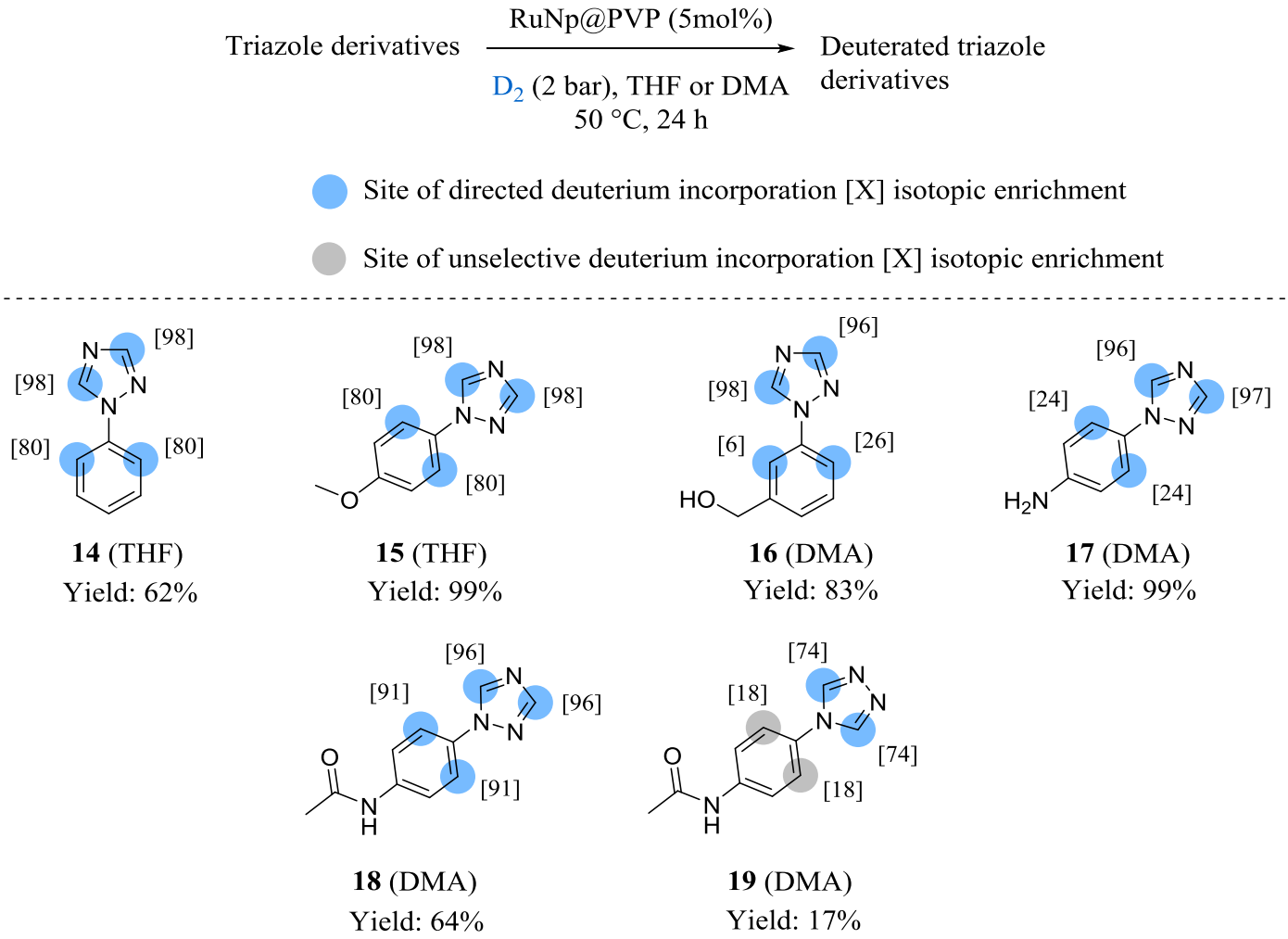

Figure 59. Examples of deuterated 1,2,4-triazole derivatives

Just when derivative **19** was considered, where the 1*H*-1,2,4-triazole in **18** is replaced for a 4*H*-1,2,4-triazole unit, the acidity of the triazole protons increased remarkably. As a consequence, a certain amount of incorporated deuterium got lost through back-exchange after the HIE during the recrystallisation of **19** from methanol and ethylacetate, giving a slight decrease in isotopic enrichment (74%). Deuterations were also observed in *ortho* positions of phenyl groups, i.e. in γ-sites of coordinating nitrogen atoms. These enrichments were considered to be non-directed, since those protons cannot be reached for C–H through the

coordination of N_1 and N_2 to the ruthenium surface. Hence, the interpretation of the non-directed HIE on these both *ortho* positions could reside in their ability to directly coordinate to the catalyst through an agostic interaction (see also chapter **II**.*2.1.6*, **figure 64**, for a more detailed explanation). To sum up, the first method with a high functional group compatibility was found to perform efficient HIE on 1,2,4-triazole-based molecules. In every considered case, intensive exchange was observed at both α positions of the 1,2,4-triazole unit, highlighting its role as a reliable handle for the incorporation of two deuterium atoms at a minimum which could be supported by successful labelling of model compounds **14-19**. Except acetyl derivative **19**, deuterium atoms were never observed to exchange backwards at other model compounds in methanol after being stored at room temperature, since the values for total isotope incorporation generated by ESI-MS were mostly in line with those from ^{1}H-NMR. Based on the DFT-results in the precedent chapters, the labelling in α on the triazole scaffold was attributed to a reaction mechanism that passes through a four-membered dimetallacyclic key intermediated and the labelling in γ on adjacent phenyl rings to a reaction mechanism that goes through a five-membered metallacyclic key intermediate.

2.1.6 Deuterations of carbazoles

Up to date, only few HIE methods were reported for the deuteration of carbazoles. All of them are accompanied by harsh reaction conditions and unselective isotope incorporation (chapter **I**.*3.2.1*, **figure 25**).[56] The catalysis by RuNps in this work allowed more selective deuterium labelling in the solvents THF and ethylacetate. For compounds **20** to **23**, high isotopic enrichments (72% – 89%) occurred at the *β*-positions relative to the nitrogen using smooth reaction conditions (**figure 60**). However, the deuterium incorporation selectivity on carbazoles stayed moderate, if we consider that other positions of the *N*-heterocycles manifested unselective incorporations up to 13% (grey dots on compound **20**, **figure 60**). As already noticed on other *N*-heterocycles (e.g. compounds **8**, **11**, **12**, **19**) the positions C_2, C_3, C_6 and C_7 of the carbazole scaffold are also prone to undergo C-H activations which cannot be directed by a σ-coordination of the nitrogen atom. This hypothesis is reinforced by the fact that using *N*-methylcarbazole **24** as a substrate led exclusively to weak deuterium incorporations in positions C_2, C_3, C_6 and C_7 but not in β to the nitrogen atom (**figure 60**). Another major problem was the reduction of compounds **20**-**24** which required a purification

through chromatography or recrystallization in every case, furnishing a decreased yield of deuterated products (**figure 60**).

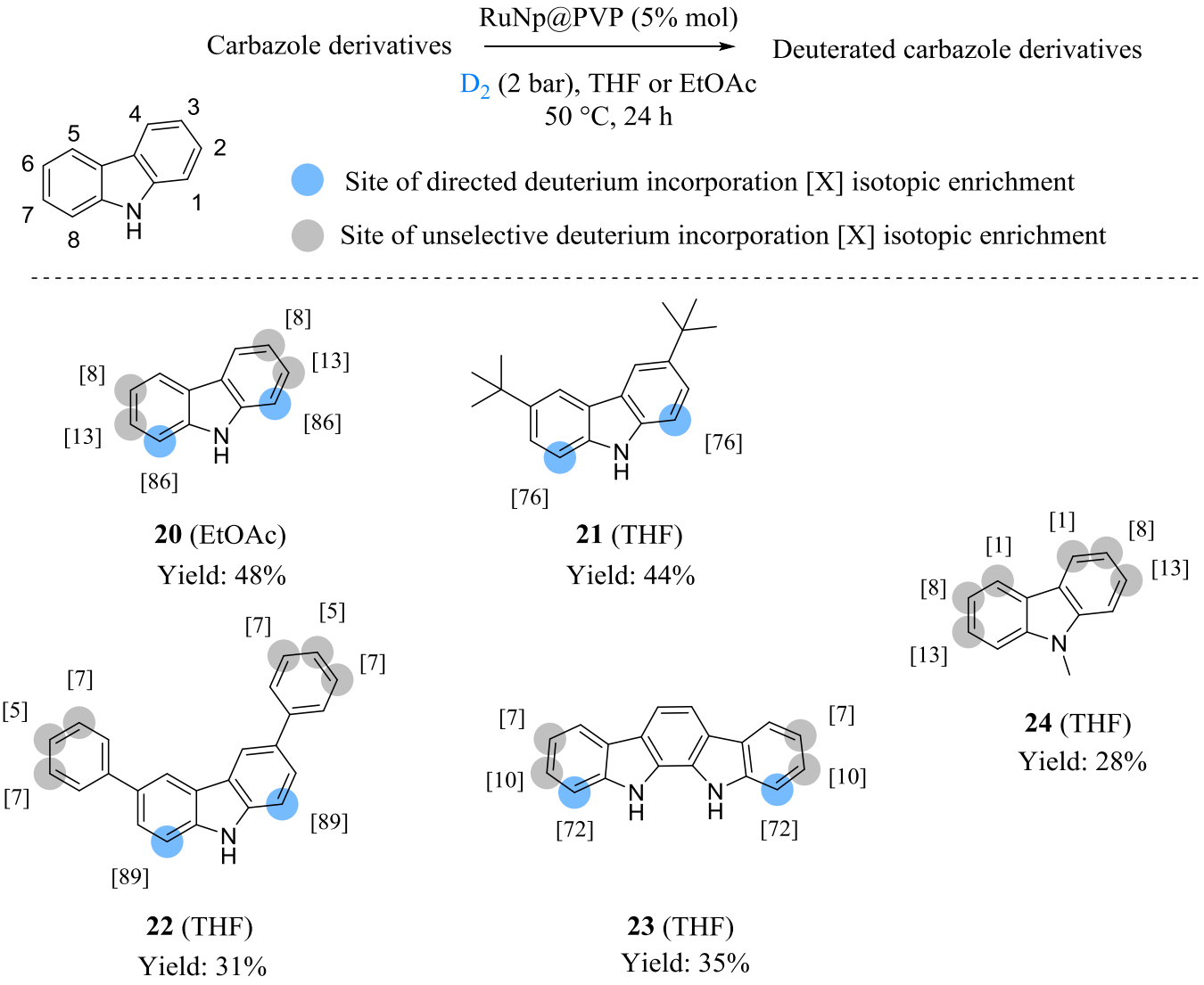

Figure 60. Examples of carbazole derivatives deuterated under neutral conditions.

To shed some light on this topic from a theoretical point of view, a DFT-based investigation was performed using carbazole as model compound. Three coordination modes have been considered, either by the nitrogen atom (**20**^{NH*}, blue pathway, **figure 61**), by the carbon in position 1 (**20**$^{\beta H*}$, red level, **figure 61**), and the simultaneous coordination of N and C_1-H (**20**$^{NH*,\beta H*}$, black pathways, **figure 61**). **20** revealed to be weakly coordinated to the surface, by -5 to 9 kcal/mol, if we compare it to *ca.* -25 kcal/mol in the previous cases. This is consistent with a π coordination instead of a σ coordination. Apparently, the latter is less favored because it would break the conjugation of the carbazole scaffold. Since the **20**$^{\beta H*}$ adsorption mode is the less favored one, a subsequent C_1-H activation has not been explored.

The **20**^{NH*} coordination leads to a direct N-H activation with a rather low 13.3 kcal/mol barrier height and a **20**^{N*} product more stable by 7.9 kcal/mol than the adsorbed carbazole. Thus, after H/D exchanges at the surface, a (N–D)* carbazole (or **20**^{ND*}) could be obtained by overcoming a 21.2 kcal/mol kinetic barrier. Although significantly higher than in the previous cases, it can be probably overcome in mild conditions. Two other pathways were considered from the **20**$^{NH*,\beta H*}$ dimetallacycle: the N-H activation (**20**$^{N*,\beta H*}$, dashed black line) followed by the C_1-H activation (**20**$^{N*,\beta*}$) and the C_1-H activation (**20**$^{NH*,\beta*}$, plain black line) followed by the N-H activation (**20**$^{N*,\beta*}$). These both exothermic reactions involve moderate barrier heights and the C-H activation seems easier through these two pathways. In summary, the optimal reaction consists in the coordination of a 5-membered dimetallacycle that partially breaks the conjugation and that preludes a possible HIE both on N and on C_1 through two pathways that require to overcome a 17.8 kcal/mol apparent barrier in order to go to **20**$^{ND*,\beta D*}$.

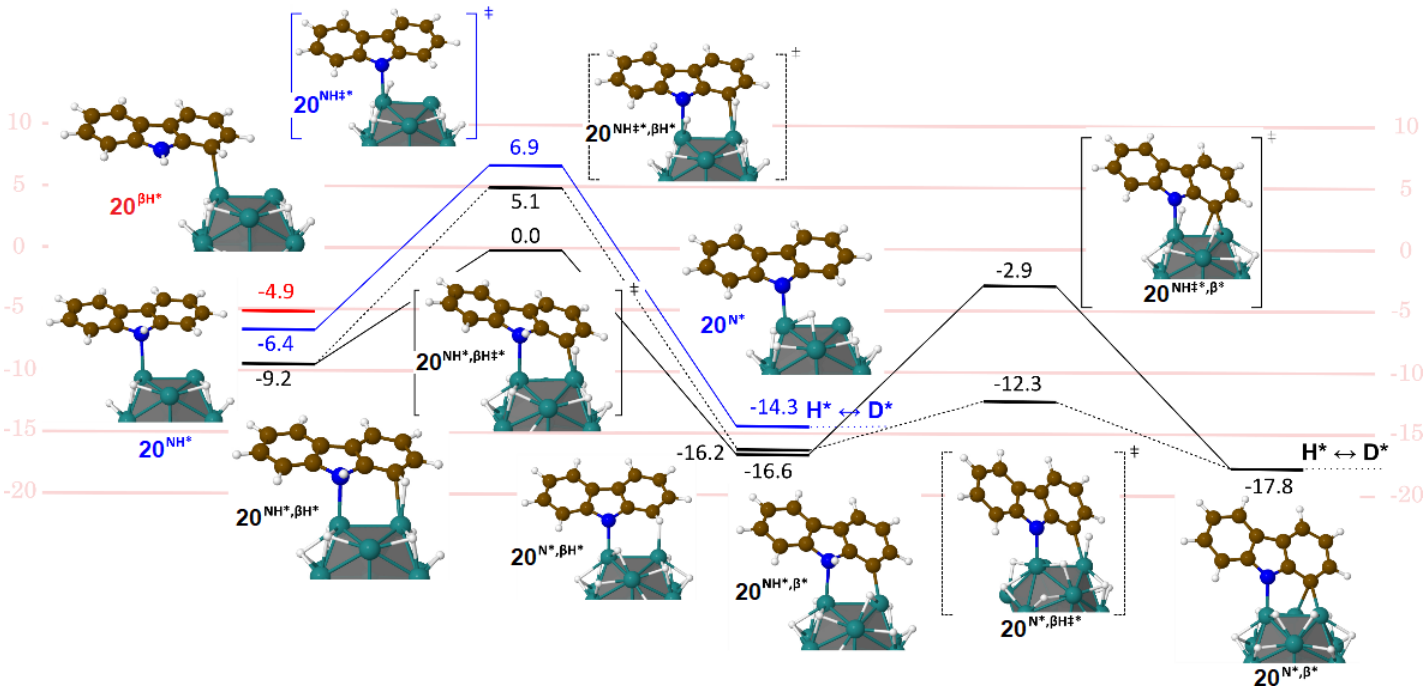

Figure 61. Energy diagram for the first steps of the Langmuir–Hinshelwood-type H/D exchange on **20**: on N and then in β (dashed black pathway); in β and then on N (black pathway); directly on N (blue pathway). The π adsorption energy in β is also given in red. Energies are given in kcal.mol^{-1}.

Surprisingly, the use of one equivalent of the base Cs_2CO_3 clearly enhanced the efficacy, regio-and chemoselectivity of the deuterium incorporation. The HIE on carbazoles in the presence of Cs_2CO_3 was insofar much more chemoselective as undesired reduced side

products were not formed anymore and the deuterated products could be obtained in nearly quantitative yields without further purification (**figure 62**).

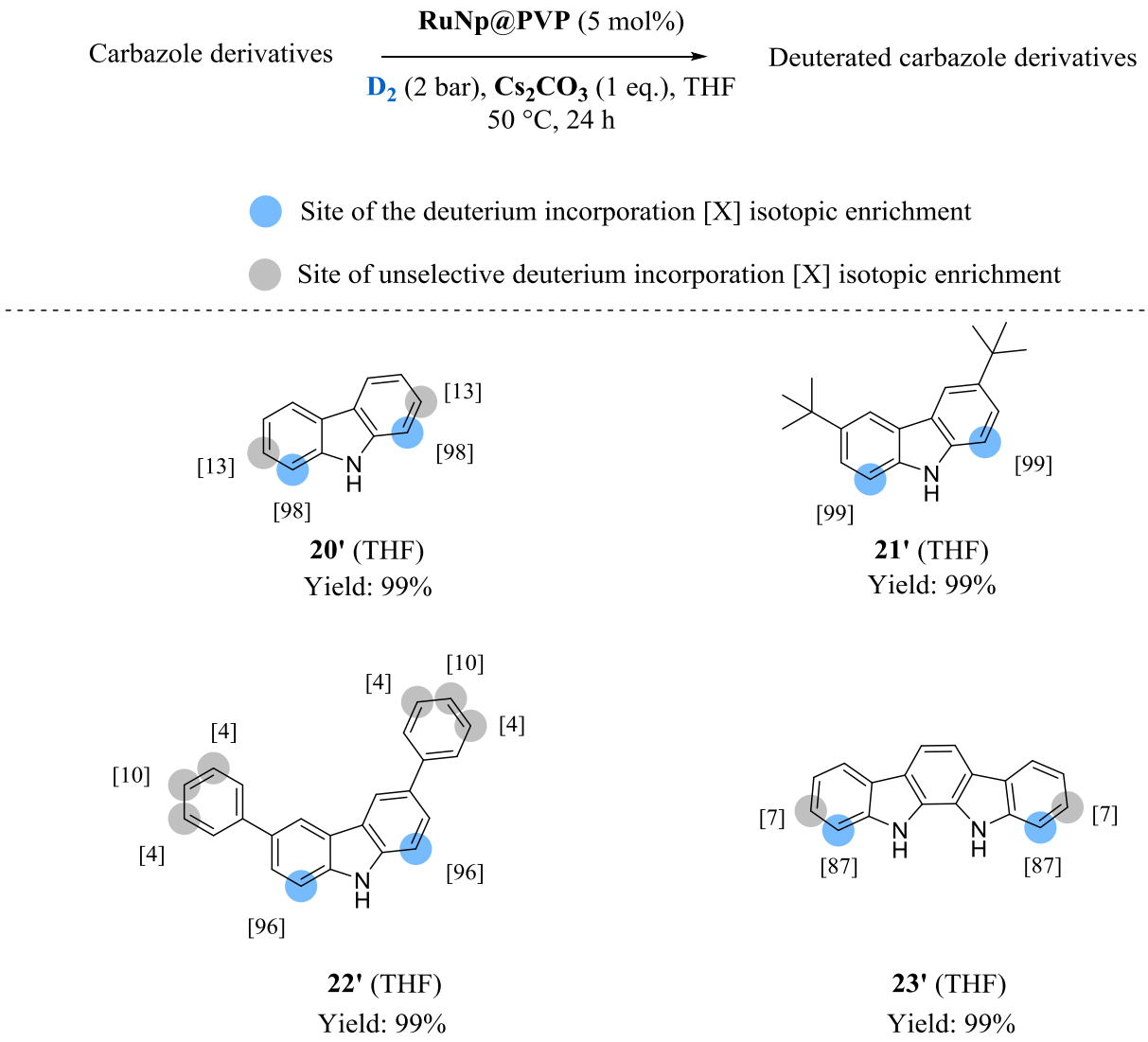

Figure 62. Examples of deuterated carbazoles under basic conditions

Further, the labelling proceeded in a slightly more regioselective manner because traces of deuterium incorporations nearly disappeared in positions 3 and 6 of carbazole **20'** and in positions 3 and 8 of compound **23'** (**figure 62**). The increase in regio- and chemoselectivity might be explained by a base assisted N-H activation leading to the formation of a N-Ru bond which would inhibit non-directed agostic interactions of positions C_2, C_3, C_6 and C_7 of the carbazole scaffold and π-interactions of the aromatic rings with the surface of the catalyst. We also anticipated that the base could facilitate the C-H activation process itself which would explain the more efficient deuterium incorporation and the higher isotopic enrichments in the β positions. In any case, this represented the first method allowing an efficient and quite

selective deuterium incorporation on carbazole substructures using an HIE approach, to the best of our knowledge. Prompted by the obtained results we were eager to study the role of cesium carbonate on these activation processes. The exploration of these pathways in the presence of a base is not an easy task for transition-state search algorithms. It is however possible to give some energetic and structural clues regarding the role of Cs_2CO_3 on the C–H and N–H activation on compound **20'**. As shown in **figure 63(a)**, Cs_2CO_3 can favorably interact with both the surface and the nanoparticle bound intermediate **20'$^{NH*,\ \beta H*}$**. Interestingly, this **Cs_2CO_3 / 20'$^{NH*,\ \beta H*}$** complex is more stable by *ca*. 20 kcal/mol than two separate species on the surface. However, this is an energy minimum, i.e. geometry optimizations do not involve a barrierless H transfer from C_1 or N toward the base.

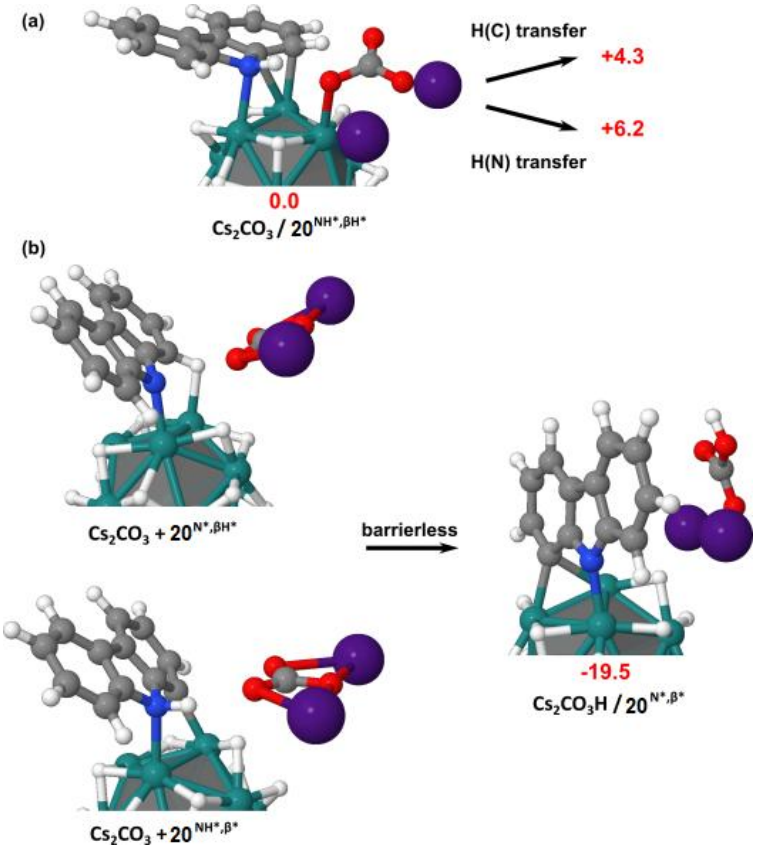

Figure 63. Ability of Cs_2CO_3 to coordinate to the catalyst surface and to adapt the role of a proton acceptor in the N–H and C–H activation step.

Given that the species resulting from this transfer are thermodynamically less stable by ~4 kcal.mol^{-1} and ~6 kcal.mol^{-1}, such pathways would not facilitate the deuterium incorporation. However, we should also consider the possible role of the base after a first C-H or N-H activation by the metal surface of the RuNp. As shown in **figure 63(b)**, a Cs_2CO_3 in the vicinity of the **20'$^{NH*,\ \beta*}$** or **20'$^{N*,\ \beta H*}$** intermediates spontaneously – and hence efficiently –

abstracts the hydrogen of the N-H and C_1-H bonds. The reactions are exothermic by ~19.5 kcal.mol^{-1} and do not display any energetic barrier. These proton abstractions give rise to the formation of the adduct **20'$^{N*, \beta*}$** where the carbazole is bound perpendicularly to the surface of the nanoparticle (**figure 63(b)**) Given the C and N coordination on the surface, the H/D exchange can then occur from the resulting **20'$^{N*, \beta*}$** compound. All in all, the easier and faster formation of σ-coordinations to the catalyst surface in the presence of a base, could explain the higher efficiency, chemo- and regioselectivity of the deuterium incorporation on the substrates **20'-23'**. First of all, the higher efficiency i.e. the almost complete deuterium incorporations at β positions of carbazoles can be referred to the easier transfer of protons during the activation of N-H and C-H bonds which is barrierless with Cs_2CO_3. Undoubtedly, the most striking effect of adding Cs_2CO_3 on the HIE was the absence of reduced side-products. It is very likely that π-coordinations of aromatic C–C double bonds are indispensable to let the reduction of aromatic rings occur as a side-reaction. However, in the presence of Cs_2CO_3 the N–H and C–H activated adduct **20'$^{N*, \beta*}$** from **figure 63(b)** is favored because its formation proceeds in a barrierless fashion. Since the aromatic substrate has adapted a perpendicular position relative to the catalyst surface in this case, π-interactions disappear and the formation of reduced side-products is circumvented, explaining the increase in chemoselectivity. Apparently, Cs_2CO_3 also slightly influenced the regioselectivity i.e. the unselective deuterations of other positions than C_1 and C_8, but this effect was not enormous. As already mentioned above, the deuteration at positions 3 and 6 of carbazole, for example, decreased from 8% to 0% (compare compounds **20** and **20'** in **figure 60** and **figure 62**). A possible mechanism is illustrated in **figure 64** to shed some light on these unselective deuterations which are not driven by the coordination of a nitrogen atom to the catalyst. Although energetically less favored, but still possible, it is likely that C–H bonds on other aromatic carbons than C_1 or C_8, interact with the catalyst through agostic interactions (**figure 64**, step **A**). An absorption mode without the participation of the nitrogen atom was already invoked with the red level **20$^{\beta H*}$** in **figure 61**. The coordination of such a position is followed by the insertion of a surface ruthenium atom into the C–H bond. This generates the C–H activated organometallic species i.e. a carbazole that is covalently bound through the C_3 or C_6 position to the metal surface (**figure 64**, step **B**). Since the surface hydrides and deuterides are mobile at the catalyst surface, the hydride gets exchanged for a deuteride in the vicinity of the carbazole (**C**). The subsequent reductive elimination with a surface deuteride leads to the final hydrogen-deuterium exchange on position 3 of carbazole (**figure 64**, step **D**). In any case, **figure 64** could serve as a general explanation for non-directed ruthenium catalyzed HIE for

every other *N*-heterocycle in the precedent chapters (compounds with grey dots, **8**, **11**, **12**, **19**, **20**, **22**, **23** and **24**). For a deeper understanding of this type of deuteration and the underlying mechanism, further experiments under different reaction conditions are required.

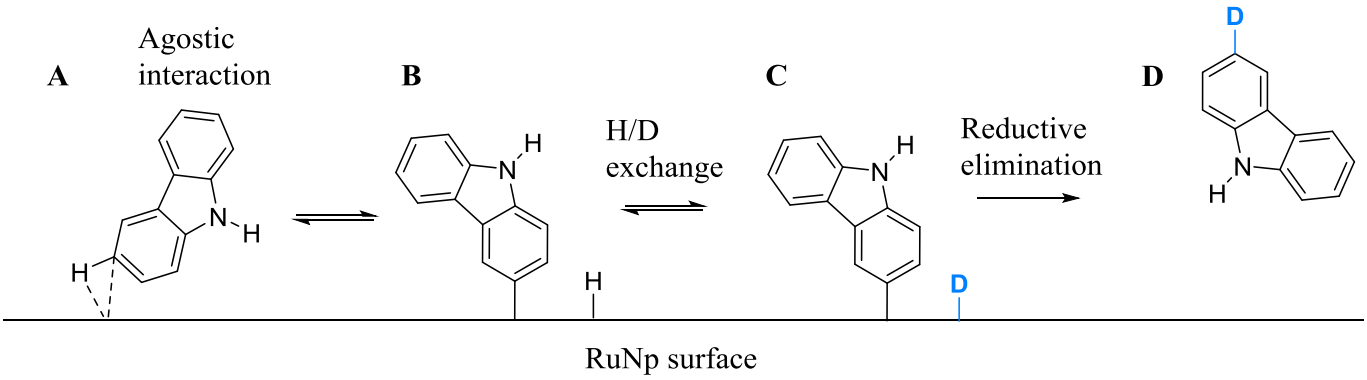

Figure 64. Proposed Ru-catalyzed mechanism for non-directed labelling; exemplified on carbazole

2.1.7 Deuterations of N-heterocyclic bioactive molecules

Deuteration experiments on *N*-heterocycles of medical relevance and higher molecular complexity should provide a more profound evaluation of the potential usefulness of Ru nanoparticle catalyzed hydrogen isotope labelling. Besides suvorexant **31**, biologically active substances were chosen whose deuterium or tritium labelling wasn't carried out within a late-stage modification approach, to the present day. For the antifungal drug fluconazole and the H_1 antagonist astemizole just conventional synthetical approaches from labelled precursors are known to generate the final drug compounds being endowed with a deuterium or tritium label as discussed in chapter **I**.*3.1*.[52] Deutero- or tritioanalogues of the natural product pimprinine, the agrochemical fluquinconazole and the TLR7 agonist Imiquimod should exist because two of these examples are marketed drugs but HIE methods for their synthesis did not appear in literature. This might be reasoned in a lack of HIE methods with an appropriate functional group tolerance for the labelling of highly sensitive and badly soluble substrates like these. The deuteration of pimprinine catalyzed by RuNp appeared at the indole with a moderate isotopic enrichment, at C_4 of the oxazole ring and the methyl with isotopic enrichments of 89% and 63%. The HIE yields a total uptake of 3.5 deuteriums (compound **25I**, **figure 65a**).

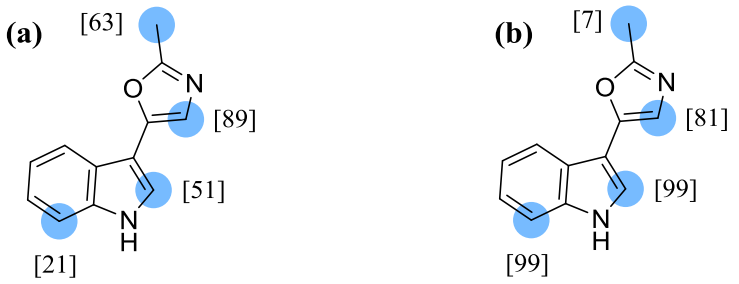

25I (MeOD)
Yield: 20%

25II (MeOD, Cs_2CO_3)
Yield: 15%

Figure 65. Deuteration of pimprinine by RuNp@PVP with different selectivities

A different selectivity was achieved under the same reaction conditions by adding one equivalent of Cs_2CO_3. By adding Cs_2CO_3, the labelling efficiency on the indole could be boosted to 99% in α and β to the N-H group, analogous to the findings made with carbazoles **20'** – **23'** (**figure 62**). As a result, the HIE efficiency on the methyl group was lower and the isotopic enrichment diminished from 63% to 7%. With this HIE protocol, a total amount of 3.1 deuteriums could be still incorporated. Repeatedly, the addition of Cs_2CO_3 brought about the advantage that reduced side-products were not formed in contrast to the previous protocol without base (compound **25II**, **figure 65b**). Attempts to interpret the change in selectivity on pimprinine without and with Cs_2CO_3 are given in **figure 66**. First of all, in order to be reduced to side-products, the substrate needs to undergo π-interactions with the catalyst. This is best achieved when the molecule is not covalently bound to the nanoparticle; thus it can get flat on the surface. As discussed on carbazoles, this situation is given under neutral conditions (**figure 66(a)**, top). Moreover, under neutral conditions the indole N–H moiety and the oxazole nitrogen atom compete for coordination sites on the RuNp. In the context of imidazole- and benzimidazole scaffolds, DFT calculation revealed that the nitrogen on position 3 has a higher affinity to the catalyst than the (benz)imidazole N–H group (**II**.*2.1.3* & **II**.*2.1.4*). Consequently, the oxazole nitrogen is assumed to be the better coordination competitor in this case which is also justified by the much higher deuterium incorporation on the oxazole- than on indole group under neutral conditions (**figure 66(a)**, bottom). Whereas, an explanation for the almost complete deuteration of the α- and β position on the indole moiety in the presence of Cs_2CO_3 was seen in the formation of a covalent Ru–N bond between the indole and the RuNp (**figure 66(b)**), which is generated through a base-assisted N–H activation as for carbazole in **figure 63**. Being covalently bound to the surface, this intermediate was supposed to be sufficiently stable to bring about the efficient deuteration

of the indole group in **25II** (**figure 66**, **(b)**). Interestingly, the isotopic enrichment was not affected at the α position of the oxazole group (**figure 65**, compare **(a)** and **(b)**), which proved that the oxazole nitrogen is still a good coordination competitor. These results rather indicated that Cs_2CO_3 has the ability to assist in C–H activations on every sp^2-hybridized carbon atom but not on sp^3-carbons which explains the decreased isotopic enrichment at the methyl group in **25II**.

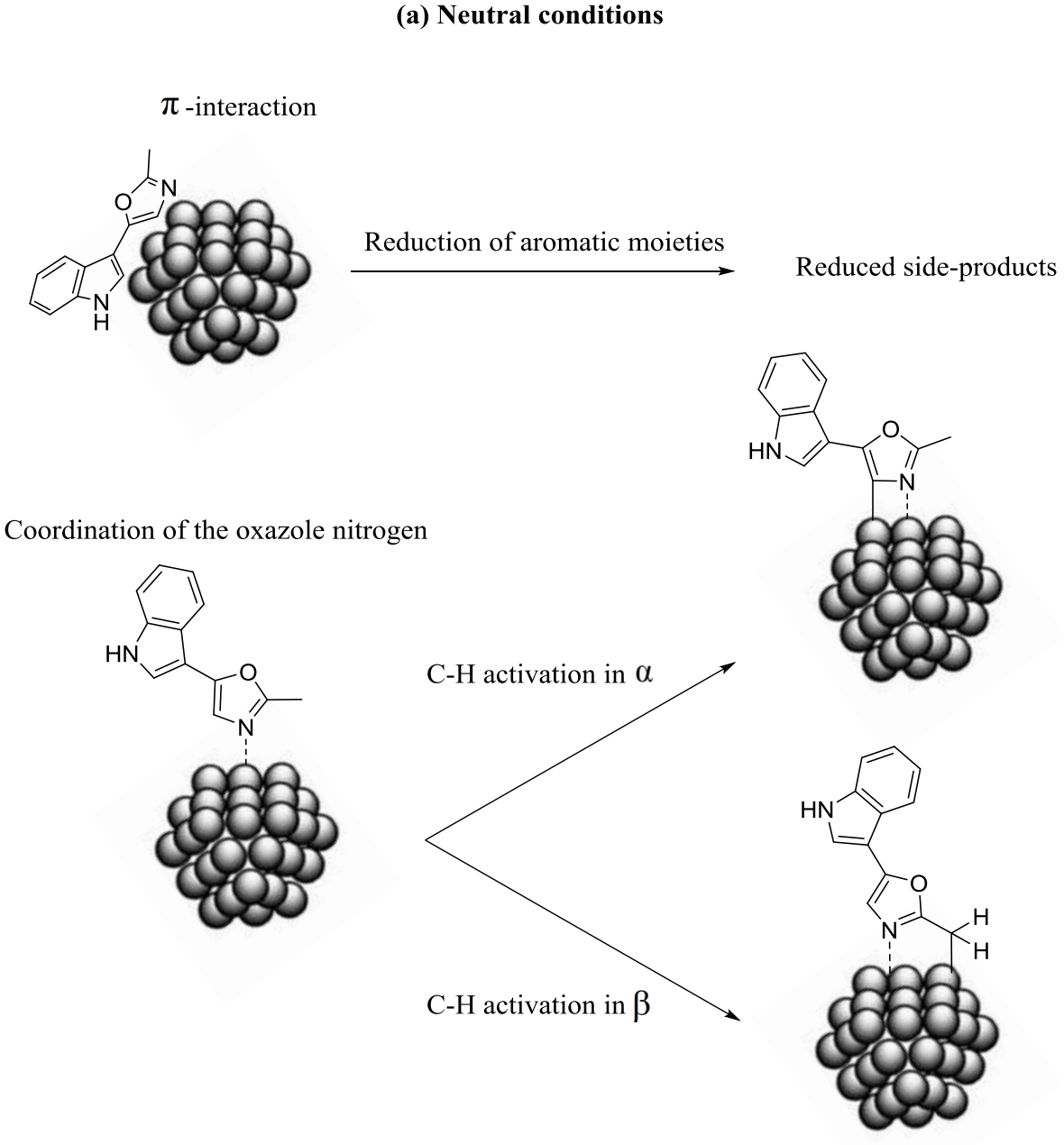

Figure 66. Propositions of favored key-intermediates for the RuNp@PVP catalyzed deuteration of pimprinine **(a)** without and **(b)** with Cs_2CO_3

(b) Basic conditions (1eq. of Cs_2CO_3)

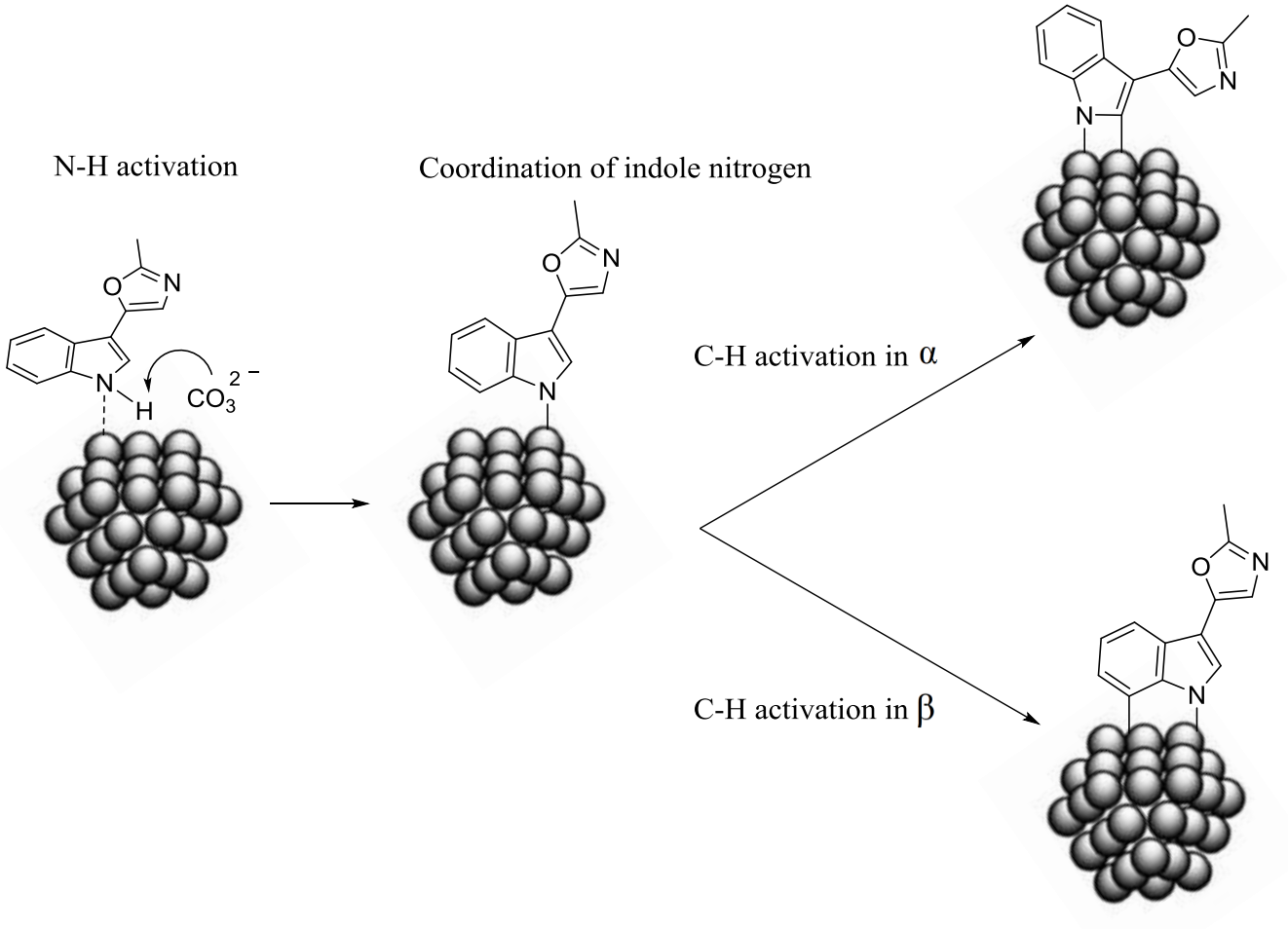

Figure 66. Propositions of favored key-intermediates for the RuNp@PVP catalyzed deuteration of pimprinine **(a)** without and **(b)** with Cs_2CO_3

When handling this oxazolic natural product, we confirmed that it is prone to turn rapidly into degradation products at 40°C and in the presence of oxygen and light.[89] For this reason, it is indispensable having the possibility to perform isotopic labelling under mild reaction conditions, as we have shown herein. Finally, the possibility to switch the deuterium incorporation selectivity renders this HIE method interesting for the preparation of stable isotopically labelled internal standards for metabolic studies. Carvedilol is a drug example that contains a carbazole scaffold in its molecular structure (**figure 67**). Using carvedilol as substrate led to the deuteration on both α positions of the secondary amine nitrogen with an isotopic enrichment of 90% respectively (**figure 67**, **26I**, signals at 3.10 ppm and 2.99 ppm in ^{2}H-NMR). In contrast, the targeted carbazole moiety merely showed low deuterium uptakes (14% and 17%) on the β positions relative to the carbazolic N–H group (**figure 67**, signals at

7.45 ppm and 7.09 ppm in ^{2}H-NMR). This difference in isotopic enrichment on two different coordinating units inside the same molecule clearly reflected a competition for the catalyst surface between both. Apparently, the alkylamine showed much higher deuteration because its nucleophilic nitrogen has the ability to undergo a strong σ-coordination to the catalyst surface, whereas the carbazole scaffold is just able to interact through a weak π-coordination with the ruthenium catalyst. Thus, the deuterated drug **26I** was representative for the obtained results from the DFT-studies for the HIE on carbazoles in chapter **II**.*2.1.6* which told us that the level of isotopic enrichment goes hand in hand with the tendency of the directing nitrogen atom to coordinate to the Ru catalyst surface.

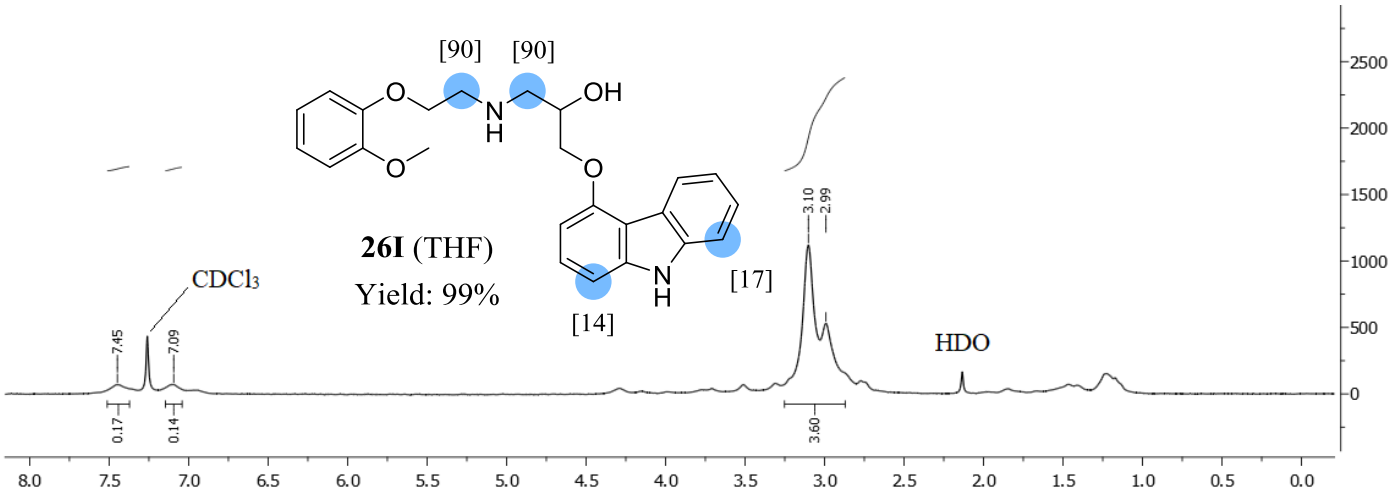

Figure 67. Labelled positions in the molecular structure of carvedilol **25I** and ^{2}H-NMR spectrum; chemical shifts are given in ppm

However, if we imagine a clinical trial situation within a drug development process which absolutely requires a deutero- or tritio-analogue of a drug candidate that carries the hydrogen isotope label exclusively on its carbazole moiety (e.g. for the investigation of the precise metabolism sites of the molecule and the place of metabolism in the body), a different strategy would be needed for achieving such a HIE on a molecule as carvedilol. Logically, if we don´t want the amine to be labelled, we have to completely withdraw its affinity to the catalyst; and if the carbazole moiety is supposed to be enriched by deuterium or tritium as efficiently as possible, its affinity to the catalyst needs to be increased. In any case, we already figured out how to boost the isotopic enrichment on the carbazole moiety in chapter **II**.*2.1.6*. Indeed, by simply protecting the aliphatic amine with a *Boc*-group and adding one equivalent of Cs_2CO_3, we were able to exclusively label the carbazole moiety with RuNp@PVP and to obtain *N-Boc*-protected carvedilol with high isotopic enrichments on both β positions on the carbazole unit (99%) (**figure 68**, **26II**, signals at 7.45 ppm and 7.10 ppm in ^{2}H-NMR). The

additional signals in the aromatic region at 7.29 and 6.87 ppm arouse from unselective labelling of positions 2, 3 and 5 of the carbazole unit. Gratifyingly, deuterium incorporation wasn´t detected at all in the proximity of the protected amine nitrogen. The possibility to modify the regioselectivity of the isotope incorporation on a complex structure by using simple protecting group strategies, highlights once more the versatility of our RuNps catalyzed HIE reactions for the synthesis of labelled compounds used in metabolic studies.

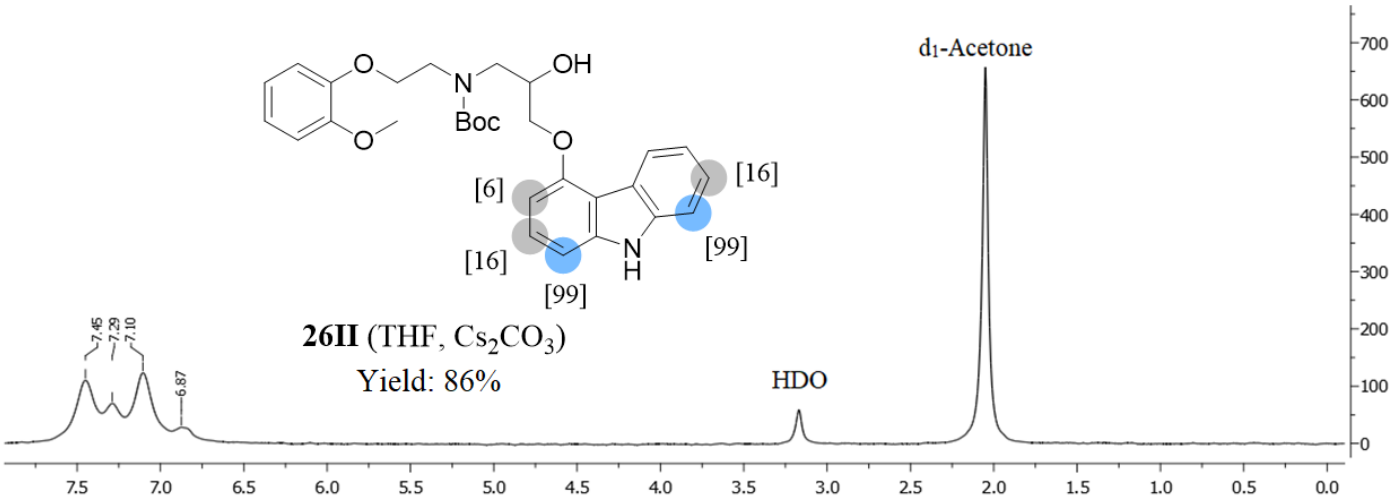

Figure 68. Labelled positions in the molecular structure of *N-Boc*-protected carvedilol **25II** and ^{2}H-NMR spectrum; chemical shifts are given in ppm

In the next step, the deprotection of deuterated *N-boc*-protected carvedilol **26II** was carried out in order to obtain carvedilol that displays deuteration exclusively at the carbazole moiety. Removal of the *boc*-group succeeded with 25 equivalents of trifluoroacetic acid in DCM (**figure 69**, top). Unfortunately, the deuterium labelling on deprotected carvedilol **26III** proved to be stable just at position 7 and 8 of the carbazole group (**figure 69**, bottom). The big signal at 7.10ppm in **figure 68** corresponds to the deuterated position 1 of the carbazole scaffold. Taken into account that chemical shifts of the carbazole group in **26II** and **26III** do not significantly differ, the signal at 7.10ppm of **26II** disappeared after removal of the *boc*-group, which could be related to a back-exchange of deuterium for hydrogen at positions 1 and 2 of the carbazole nucleus under acidic conditions (compare aromatic regions of ^{2}H-NMR spectra in **figure 68** and **figure 69**). The third signal at 6.87 ppm in the ^{2}H-NMR spectrum in **figure 69** corresponds to traces of deuterium on aromatic positions of the methoxyphenyl group.

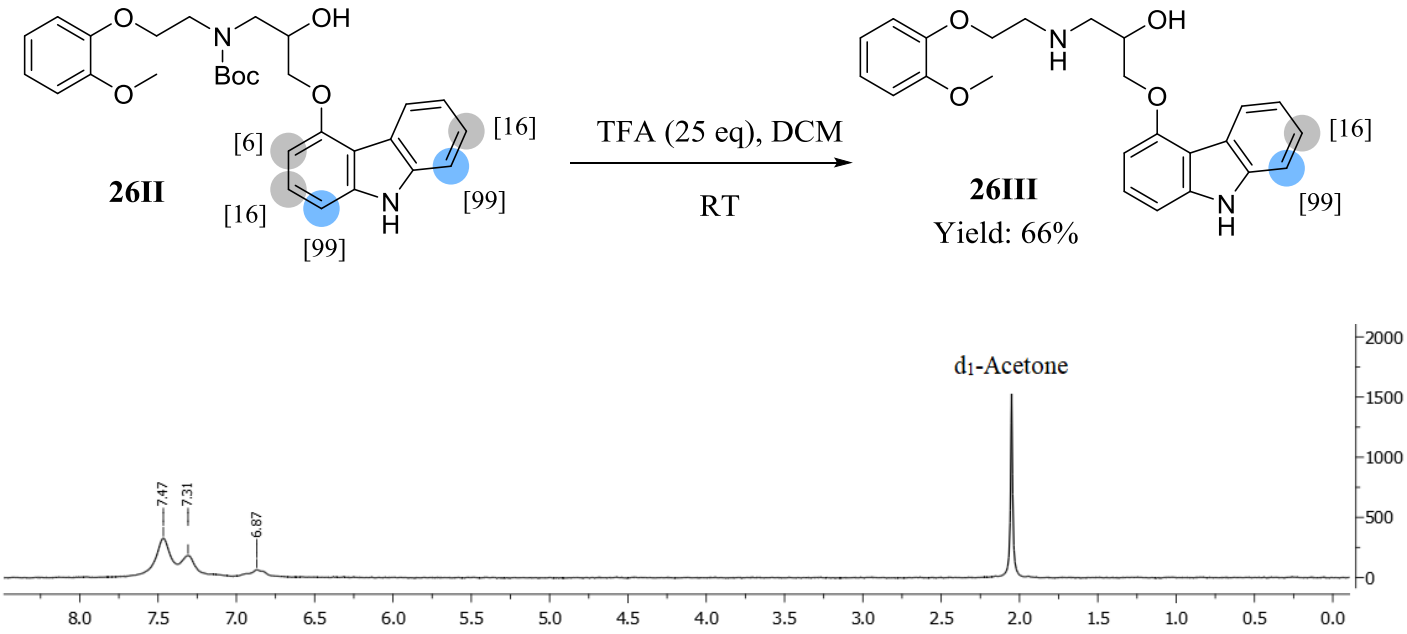

Figure 69. Deprotection of deuterated *N*-boc-carvedilol **26II** to deuterated carvedilol **26III** (top) ^{2}H-NMR spectrum of deuterium labelled carvedilol **26III** (bottom); chemical shifts are given in ppm

Moreover, many other *N*-heterocyclic drugs and agrochemicals could be successfully deuterated under neural conditions by RuNp@PVP. The benzimidazole containing drug astemizole has been a commercial drug in the treatment of allergies (**figure 70**).[90] Deuteration within our method occurred at the benzimidazole scaffold in β to the unsubstituted nitrogen with an isotopic enrichment of 87%. Furthermore, the ^{2}H-NMR spectrum also supported slight H/D exchange on one α-methylene of the tertiary amine (22%). Seemingly, the two protons of this α-methylene are diastereotopic protons which gives rise to a different chemical shift and to the appearance of two signals in ^{2}H-NMR at 2.64ppm and 2.47ppm when the methylene group is deuterated (**figure 70**). The deuteration of other positions on the side-chain could be excluded because ESI-MS analysis of the labelled product did not show any isotopologues with more than three deuteriums.

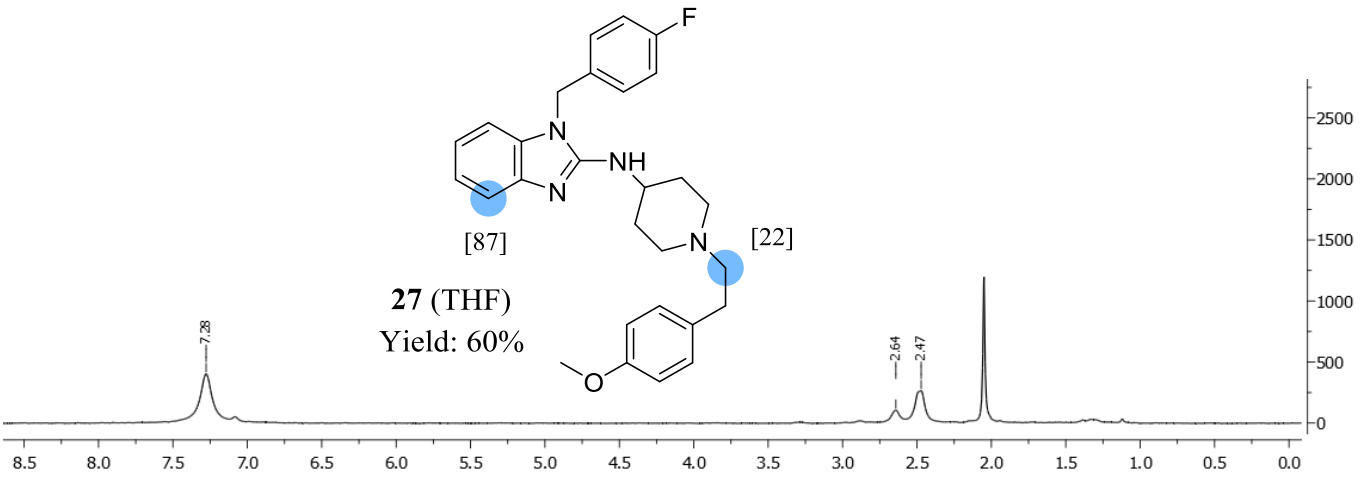

Figure 70. Labelled positions in the molecular structure of astemizole **26** and ^{2}H-NMR spectrum; chemical shifts are given in ppm

The deuteration selectivity at the aliphatic side-chain can be related to the chair conformation of the piperidinyl moiety which necessitates its two big substituents to be equatorial. As a consequence, certain hydrogens of the 6-membered aminocycle, especially those which are situated on α-positions relative to the nitrogen atoms, cannot be exposed to the metal surface. Most probably this conformational constraint prevents a C–H activation at those positions (**figure 71**).

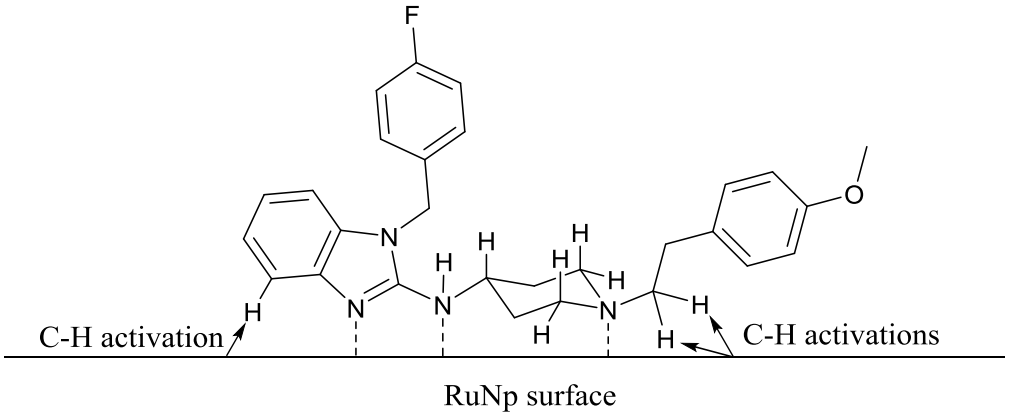

Figure 71. Structural conformation of astemizole, dictating the deuteration selectivity

Imiquimod exerts convincing efficacy against malignant melanoma, with a mode of action on different pathways (**figure 72**).[91] It displays very poor solubility in common organic solvents like THF or ethylacetate and needed to be dissolved in DMA for a satisfying deuteration. High deuterium incorporation could be encountered at two positions of the *N*-heterocyclic system, in α and β to the heteroatoms, leading to isotopic enrichments of 86% on the α- and to 89% on the β position. The low solubility also complicated NMR-analysis by broadening the signals and decreasing the resolution.

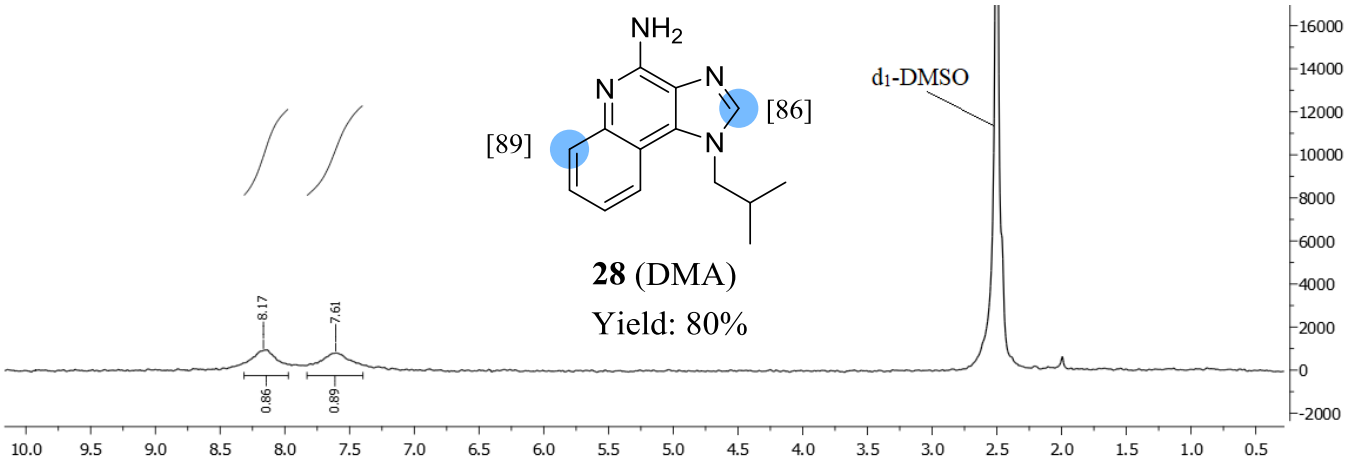

Figure 72. Labelled positions in the molecular structure of imiquimod **28** and ^{2}H-NMR spectrum; chemical shifts are given in ppm

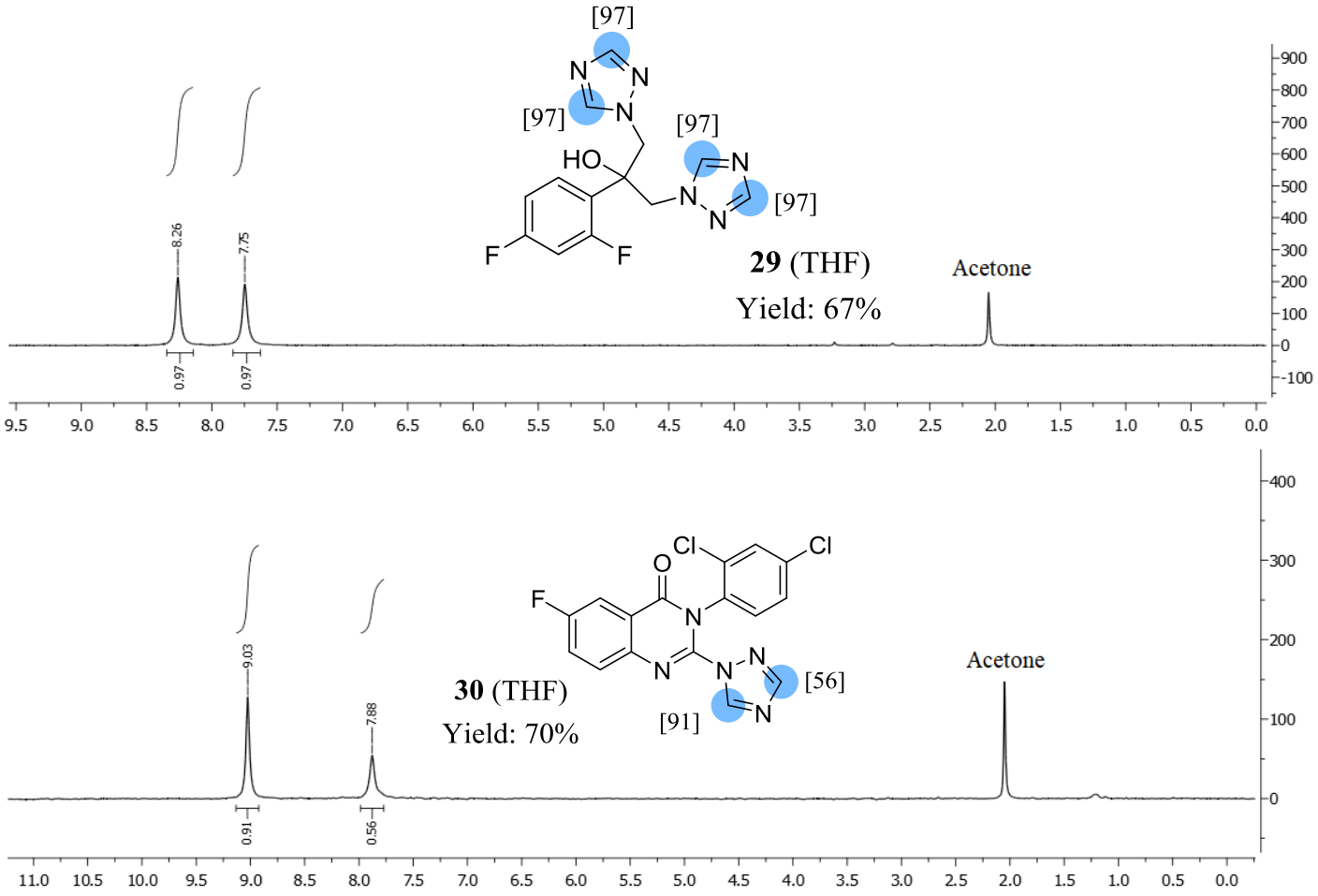

Figure 73. Labelled positions in the molecular structure of fluconazole **29** (top) and fluquinconazole **30** (bottom) with ^{2}H-NMR spectra; chemical shifts are given in ppm

The HIE on the antifungal drug fluconazole and the agricultural fungicide fluquinconazole was representative for the high functional group tolerance of the Ru nanoparticle catalyzed method (**figure 73**). Respectively, triazolic protons were exchanged efficiently for deuterium

and the deutero-analogues of both 1,2,4-triazole containing bioactive compounds could be obtained through simple filtrations (**figure 73**, compounds **29** and **30**). The ^{2}H-NMR spectra were then recorded without further purifications after the deuteration reactions (**figure 73**). This rapid deuterium labelling is insofar beneficiary as we consider that stable isotopically labelled internal standards of fluconazole were originally synthesized from deuterated precursors over four steps (**I**.*3.1*).[51] The 1,2,3-triazole drug suvorexant is administered for insomnia treatment and is already known to be labelled by hydrogen isotopes within other methods (**figure 74**). Significant exchange occurs either on the 1,2,3-triazole with a homogeneous Fe(0) catalyst (leading to the incorporation of 0.6D) or in *ortho* of the adjacent phenyl with Crabtree´s catalyst (theoretically limited to the incorporation of 1D).[68] In this work, the use of RuNp@PVP as catalyst allowed for deuterium labelling of both, the 1,2,3-triazole group (1.6D) and the adjacent phenyl ring (0.3D) which gave a considerably higher deuterium incorporation as a whole, than the ones obtained using the previously described HIE procedures. The successful deuteration of these positions was approved by ^{2}H-NMR. The signal at 7.86ppm corresponds to triazolic deuterons and the smaller signal at 7.31ppm to the *ortho* position. The latter manifests broadening because suvorexant usually shows different rotamers in NMR-spectra. Contrary to the findings made with model compound **12**, the benzoxazole moiety of suvorexant stayed unlabelled, which was related to the steric hindrance arising from the chlorine substituent that prevented a coordination of the benzoxazole nitrogen to the ruthenium nanoparticle. All in all, these results manifested an excellent and general compatibility of triazolic units with RuNp@PVP, completely circumventing side-reactions like reductions of unsaturated groups and hydrogenolyses e.g. of halogen substituents.

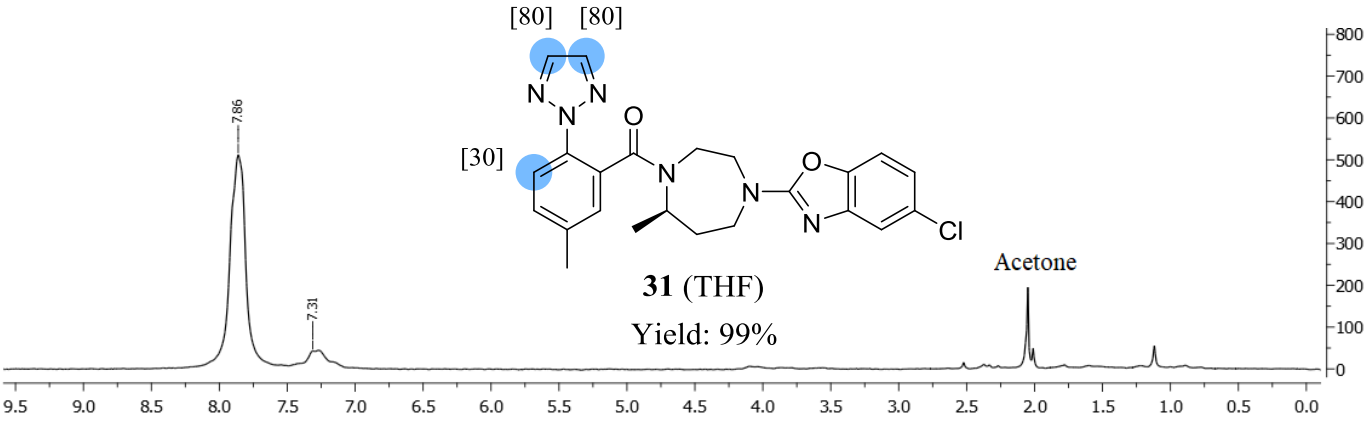

Figure 74. Labelled positions in the molecular structure of suvorexant **31** with ^{2}H-NMR spectra; chemical shifts are given in ppm

2.1.8 Tritiations of *N*-heterocyclic Drugs

Owing to the mentioned limitations in tritium labelling of drugs previously discussed in chapter **I**.*3.2.1*, the possibility to introduce a tritium label into complex *N*-heterocyclic pharmaceuticals through our RuNp@PVP-based method would be a real benefit. For this reason, in the first step, we tried to optimize the deuteration conditions for the three selected drug examples *N*-Boc-protected carvedilol, astemizole and fluconazole in order to apply them to the tritiations of these drugs with T_2- instead of D_2 gas. The objective was to develop tritiation protocols that can generate radioactive analogues of these three drug examples with RuNp@PVP as catalyst under tritium gas pressures inferior to 1.0 bar in THF. *N*-Boc-protected carvedilol was deuterated in the precedent chapter with 10 mol% RuNp@PVP under a D_2 gas pressure of 2 bar in THF with 99% isotopic enrichment on both β positions. For the optimization of the reaction conditions under lower gas pressures, the catalytic loading was raised to 20 mol%. In this manner, the deuteration still proceeded with high isotopic enrichments (80%) at 936 mbar, which already represented an appropriate gas pressure for a potential tritiation reaction (**table 2**, entry 1).

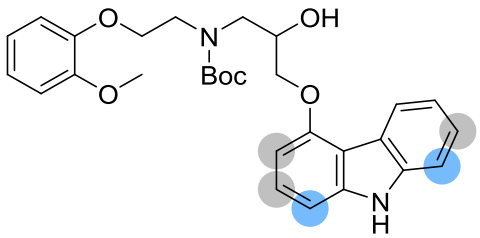

Entry	Applied pressure of D_2 gas (RT)	Isotopic enrichment at β positions (^{1}H-NMR)	Deuterium uptake in total (ESI-MS)
1	936 mbar	80%	1.8D
2	795 mbar	53%	1.2D
3	578 mbar	59%	1.4D
4	549 mbar	60%	1.3D

Table 2. Deuterium uptakes on *N*-Boc-carvedilol under different D_2 gas pressures (isotopic enrichment values were equivalent on both β positions), experiments were carried out in 2.5mL Fisher-Porter tubes using the reaction conditions: 20mol% RuNp@PVP, 10µmol substrate, 1 eq. Cs_2CO_3, 0.3mL THF, 50°C, 24h

When the pressure of deuterium gas was decreased to lower values, the deuterium uptakes settled at 50-60% on both β positions of the carbazole scaffold (**table 2**, entry 2-4). The deuterium uptakes were also followed by ESI-MS and listed in the last column of **table 2**. These values refer to the sum of all deuterium atoms that were incorporated on every labelled position of the molecule (blue and grey dots). As it was shown in **table 2**, more than one deuterium atom could be incorporated into *N*-Boc-protected carvedilol under D_2 pressures which were slightly above 500 mbar. The objective was also to incorporate approximatively one tritium atom into the molecule within a tritiation reaction with T_2- instead of D_2 gas. For this reason, the tritiation of *N*-Boc-protected carvedilol was conducted under a T_2 pressure from the same range (519 mbar) in a Fisher-Porter tube of 2.5 mL with a gas volume of 5.0 mL in the presence of one equivalent Cs_2CO_3, taking into account a KIE that usually leads to a lower tritium incorporation. The total activity of T_2 used was 6.6 Ci. Unfortunately, the tritium uptake in **26*** merely corresponded to 0.3T i.e. an isotopic enrichment of 13% per β position. Thus, the achieved molar activity (9 Ci/mmol) of the tritiated drug was still within an acceptable range but much lower than expected. With regard to the deuteration of *N*-Boc-protected carvedilol under the same conditions, where still more than one deuterium could be incorporated on the carbazole, the impact of the kinetic isotope effect was assumed to be tremendous for the tritiation described herein. In order to find an explanation for this large drop of the isotopic enrichment on *N*-Boc-protected carvedilol within the tritiation reaction and if we want to figure out in how far the kinetic isotope effect plays a role in this case, further experiments need to be conducted. Nevertheless, a purification of the tritiated product through HPLC was not necessary at all since side-products resulting from reduction or radiolysis were not formed. Further, ^{3}H-NMR evidenced a fully selective labelling at the β positions of the carbazole nucleus (two singulets) which could be considered as a clear asset (**figure 75**).

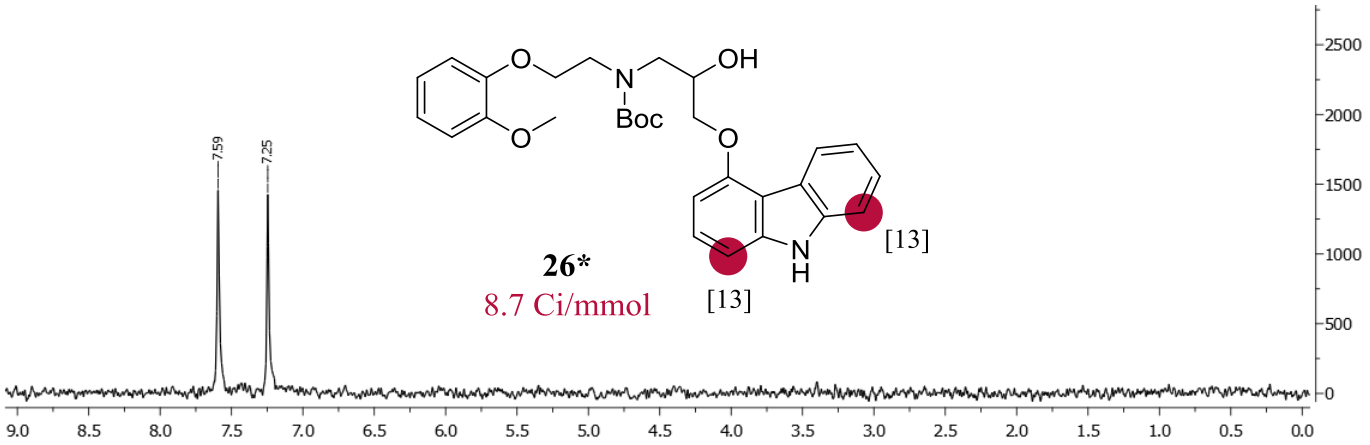

Figure 75. Tritiated *N*-Boc-carvedilol and the corresponding ^{3}H-NMR spectrum

In order to exclude leakage and other preparative errors, the tritiation of *N*-Boc-carvedilol was repeated with a higher pressure and bigger volume of T_2 gas of 882 mbar in a Fisher-Porter tube of 5.0 mL (gas volume of 7.3 mL) which was equal to 16.9 Ci of T_2 gas inside the reaction vessel. Under these conditions, the tritium uptake on the molecule even dropped to a molar activity of 4.4 Ci/mmol, according to 7% of isotopic enrichment per β position on the carbazole scaffold. This result reconfirmed within a tritiation that HIE catalyzed by RuNp@PVP under gas pressures below 1.0 bar depends less on the gas pressure than on other factors. Despite of all, further experiments are required for a full comprehension of the low isotopic enrichment in these tritiations.

When the deuteration conditions were optimized for astemizole, the deuterium uptake was monitored by the isotopic enrichment at the β position of the benzimidazole scaffold through ^{1}H-NMR and verified by ESI-MS (**table 3**). The optimization of the reaction conditions was started at 948 mbar of D_2 and with 46 mol% of catalytic loading in THF. Under these conditions, the deuterium incorporation of 0.5D was too low, if we consider that at least one deuterium was needed (**table 3**, entry 1). The deuteration was repeated under the same conditions in DMA. Although the pressure at room temperature with the less volatile solvent DMA (**table 3**, entry 2) was 110 mbar lower than in entry 1, both initial pressures at -196 °C were the same. Owing to the deuterium uptake, the change from THF to DMA did not give any difference. Thus, the deuteration was repeated in THF with a higher catalytic loading (92 mol% RuNp@PVP). Gratifyingly, the deuterium uptake could be more than doubled in this manner (**table 3**, entry 3). A second experiment under the same conditions ensured the reproducibility of the result (**table 3**, entry 4).

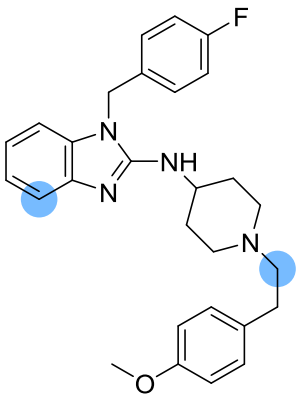

Entry	Applied pressure of D_2 gas (RT)	Isotopic enrichment at the β position of the benzimidazole group (^{1}H-NMR)	Deuterium uptake in total (ESI-MS)
1	948 mbar *a*	31%	0.5D
2	838 mbar *b*	29%	
3	991 mbar *c*	50%	1.2D
4	980 mbar *c*	54%	1.2D

Table 3. Deuterium uptakes on astemizole under different D_2 gas pressures (isotopic enrichment values of the β position on benzimidazole were chosen as a reference point), experiments were carried out in 2.5mL Fisher-Porter tubes using the reaction conditions: (**a)** 46mol% RuNp@PVP, 11µmol substrate, 0.5mL THF, 50°C, 24h, **(b)** 46mol% RuNp@PVP, 11µmol substrate, 0.5mL DMA, 50°C, 24h, **(c)** 92mol% RuNp@PVP, 11µmol substrate, 0.4mL THF, 50°C, 24h

Since the deuteration of astemizole with 92 mol% RuNp@PVP and a D_2 pressure that was slightly below 1 bar incorporated more than one deuterium atom, the same conditions were chosen for a corresponding tritium labelling. The tritiation of astemizole was conducted with a total activity of 12.4 Ci, being equal to a tritium gas pressure of 970 mbar with a gas volume of 5 mL. To our delight, the obtained molar activity of **27*** (24 Ci/mmol) clearly outperformed the prerequisites for ADME studies, which usually range form 10-20 Ci/mmol (**figure 76**). In this case, the isotopic enrichment values did not significantly differ between deuteration and tritiation reaction under the same conditions, evidencing the absence of a KIE for the tritiation of astemizole.

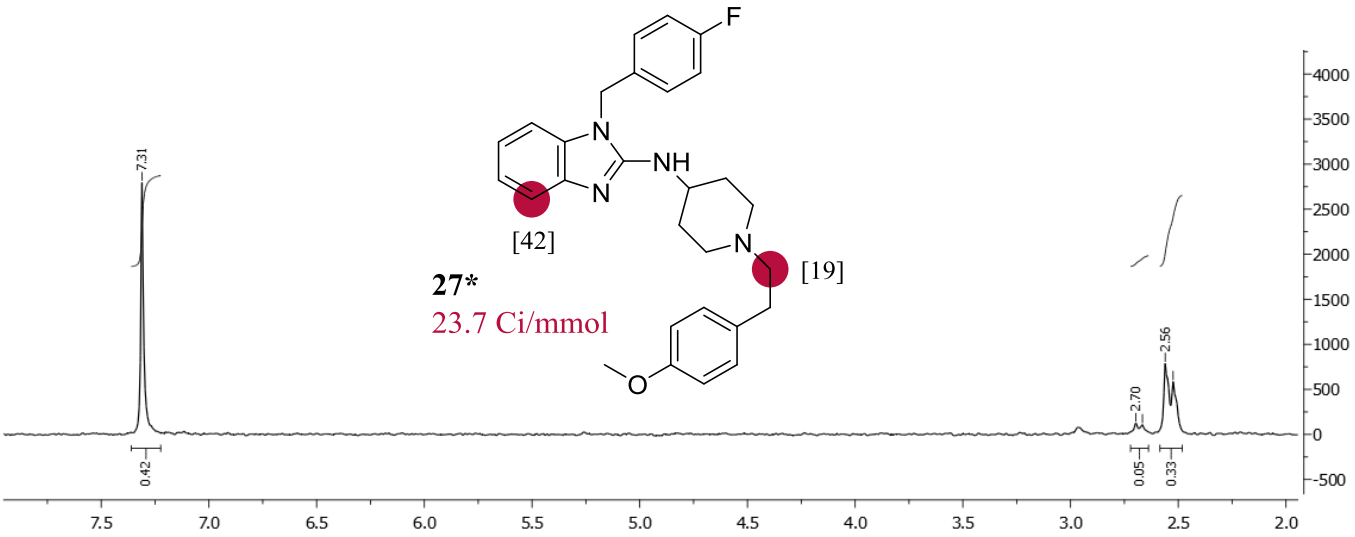

Figure 76. Tritiated astemizole and the corresponding ^{3}H-NMR spectrum

When the deuteration conditions were optimized for fluconazole, the deuterium uptake was followed by the isotopic enrichment through ^{1}H-NMR at the α positions of the 1,2,4-triazole scaffolds and verified once by ESI-MS (**table 4**). The first try at 625mbar and 30°C delivered 50% of isotopic enrichment on each labelled position (**table 4**, entry 1). Increasing the temperature to 50°C did not give any change in isotopic enrichment (**table 4**, entry 2). When gradually increasing the D_2 gas pressure from 600-900mbar we encountered that 10mol% or 13mol% of catalyst nearly operated with the same efficiency at 30°C and 50°C (**table 4**, entries 1-4). Just a higher catalyst loading of 30mol% raised the isotopic enrichment to 91% per α position (**table 4**, entry 5).

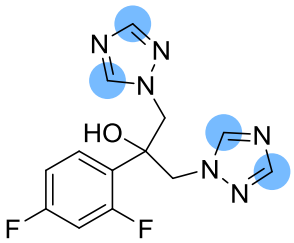

Entry	Applied pressure of D_2 gas (RT)	Isotopic enrichment at α positions (^{1}H-NMR)	Deuterium uptake in total (ESI-MS)
1	625 mbar ***a***	50%	
2	636 mbar ***b***	51%	
3	840 mbar ***b***	56%	
4	~900 mbar ***c***	50%	1.7D
5	~900 mbar ***d***	91%	

Table 4. Deuterium uptakes on fluconazole under different D_2 gas pressures (isotopic enrichment values were mostly equivalent for every α position), experiments were carried out in 2.5mL Fisher-Porter tubes using the reaction conditions: (**a)** 10mol% RuNp@PVP, 50µmol substrate, 1mL THF, 30°C, 24h, **(b)** 10mol% RuNp@PVP, 50µmol substrate, 1mL THF, 50°C, 24h, **(c)** 13mol% RuNp@PVP, 17µmol substrate, 0.5mL THF, 50°C, 24h, **(d)** 30mol% RuNp@PVP, 17µmol substrate, 0.5mL THF, 50°C, 24h

Given that the reaction condition from entry 4 in **table 4** already incorporated a sufficient amount of 1.7D into fluconazole, this was the reaction condition of choice for the tritiation reaction. However, the reaction temperature was set to 30°C because it was found not to have any impact on the deuterium uptake in this case. The tritium labelling of fluconazole was performed under 869mbar of T_2 gas (gas volume of 5mL) which corresponds to a total activity of 11.1Ci. This procedure yielded tritium labelled fluconazole with a molar activity of 24.7 Ci/mmol (**figure 77**). If we have a look at the isotopic enrichment, a KIE is perceivable but it did not appear in a drastic fashion, if we compare 1.7D to 0.8T and take also in account that the tritiation reaction was conducted under a lower temperature of 30°C instead of 50°C. All in all, the result was satisfying because the obtained molar activity was again in full compliance with the requirements for ADME studies.

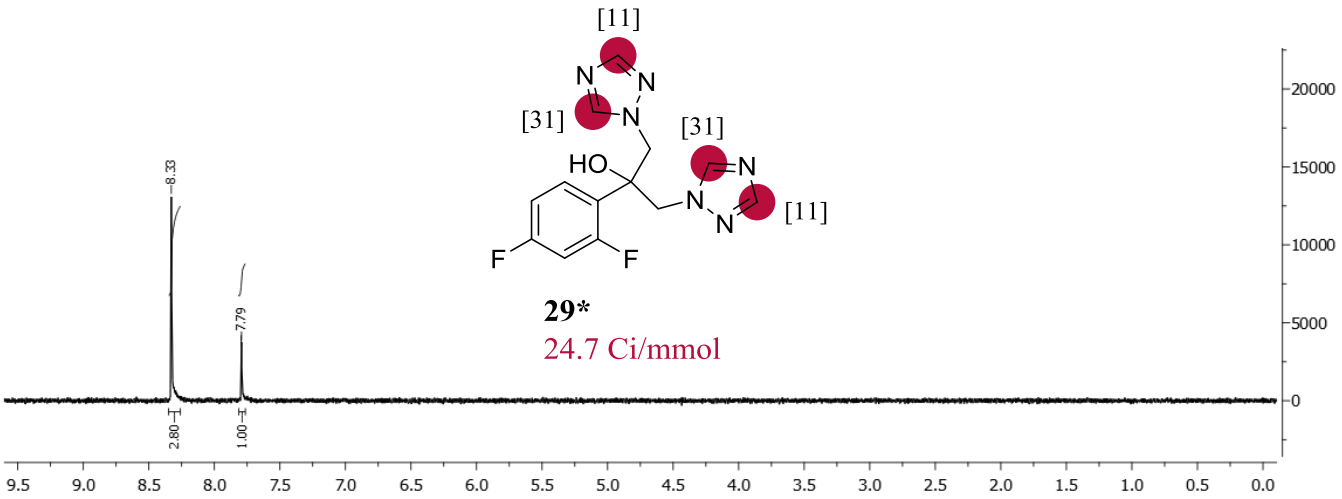

Figure 77. Tritiated fluconazole and the corresponding ^{3}H-NMR spectrum

To sum up, a moderate KIE emerged between the deuteration and tritiation reaction of fluconazole **29***. Comparing the deuteration and tritiation reaction of astemizole **27***, rather no KIE could be encountered. Changing the isotopic source from D_2 to T_2 did not significantly diminish the tritium uptakes on the two drugs owing to the satisfying molar activities of around 24 Ci/mmol for both tritium labelled drug analogues **27*** and **29***. However, the tritium uptake of *N*-Boc-carvedilol manifested a much stronger KIE due to the large drop in isotopic enrichment compared to the deuteration under the same conditions. Probably, the strongly divergent result on *N*-Boc-carvedilol can be related to a different type of KIE that arose from the base Cs_2CO_3 that showed a specific reactivity with T_2 gas on the RuNp surface. In order to figure out in how far Cs_2CO_3 is involved in the drop of isotopic enrichment in this tritiation reaction, we could imagine to conduct the tritiation of a different substrate, which showed higher tritium uptakes with RuNp@PVP (e.g. astemizole), in the presence of Cs_2CO_3 as a test experiment. Interestingly, in none of the three cases, the amount of incorporated deuterium or tritium strongly depended on the gas pressure. It was rather the increase in catalytic loadings that gave rise to higher deuteration at gas pressures inferior to 1.0bar as demonstrated for astemizole and fluconazole. The tritium uptake in *N*-Boc-carvedilol did not depend at all on the applied total activity or pressure of tritium gas. However, for the illumination of this topic, further studies on the KIE between hydrogen, deuterium and tritium are required. In any case, the low dependence of isotopic enrichment on the applied D_2- or T_2 gas pressure could be an evidence that the catalyst loses the capacity to activate deuterium or tritium gas under gas pressures below 1.0bar once the *N*-heterocyclic substrate gets absorbed on the surface. There are still several crucial assets of our method to be outlined in terms of tritium incorporation in complex pharmaceuticals. Compared to every existing heterogeneous transition metal catalyzed HIE method, it could be demonstrated that

the catalyst RuNp@PVP was applicable to the broadest variety of *N*-heterocyclic drugs to efficiently prepare tritiated analogues thereof. This is further evidenced by the fact that, to the present day, the simplest way to label the *N*-heterocyclic substructures of astemizole and carvedilol by tritium was the transformation of halogenated precursors with Pd/C and T_2, a procedure that consisted of several other reaction steps (**I**.*3.1*).[52] Furthermore, it is noteworthy that in every case (**26***, **27***, **29***) tritium labelling took place on positions which are not major metabolism sites.[92] Undoubtedly, these achievements confirmed the potential of our method to accelerate drug discovery and development processes.

2.1.9 Limitations of RuNp@PVP as HIE catalyst

Despite the great success delivered with RuNp@PVP in HIE on *N*-heterocyclic scaffolds, certain drawbacks and restrictions were figured out on different levels of application. As already noticed at the beginning of section **II**.*2.1.2*, 2,5-diphenyloxazole and several other compounds from chapters **II**.*2.1.2* – **II**.*2.1.7* were reduced to undesired side-products. Further, it is also possible that hydrogenolysis of halogenated- and benzylic moieties occurred. The degree of these side-reactions with RuNp@PVP was still acceptable but a purification would be required at any rate since isotopically labelled internal standards are supposed to have a high degree of purity, prior to a potential application e.g. in biological assays. Another problem is that the hydrogenation of phenyl- to cyclohexyl groups very often gives side-products which do not significantly differ in polarity compared to the main-product. Thus, in some cases a HPLC purification was required to remove undesired components properly from the crude reaction mixture. Beyond the presented classes of *N*-heterocycles whose hydrogen isotope labelling was very satisfying and efficient (**II**.*2.1.2* – **II**.*2.1.8*), there is another interesting *N*-heterocyclic scaffold that didn´t show any exchange of hydrogen for deuterium through our ruthenium nanoparticle-based method. Unfortunately, the substrates thiazole and benzothiazole did not show any reactivity in the presence of RuNp@PVP and D_2 gas, neither hydrogen isotope exchange nor decomposition (**figure 78**). The failure of our catalyst to label thiazole and benzothiazole scaffolds by hydrogen isotopes could be very likely attributed to the presence of sulfur atoms in their molecular structures. Such organic molecules are known to undergo very strong coordination to transition metals through their sulfur atom. Thus, complete covering of a transition metal catalyst surface results in poisoning, i.e. deactivation of the catalyst. On the one hand, sulfur poisoning can have a steric impact by preventing other

(benzo-)thiazole molecules from coordinating with their nitrogen atom to the Ru nanoparticle for further C-H activation. On the other hand, when heterogeneous transition metal catalysts are poisoned by sulfur, their electronical properties are modified so far that they lose their ability to absorb and activate H_2 gas.[93]

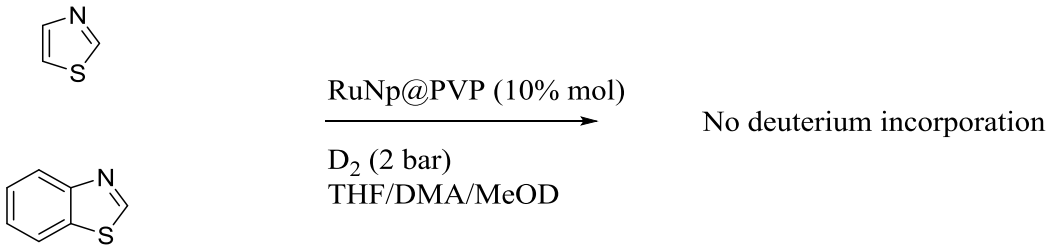

Figure 78. Thiazole and benzothiazole did not show any reactivity with RuNp@PVP

The precedent chapters of this work showed a large range of *N*-heterocyclic derivatives endowed with a certain variety of functional groups which did not significantly perturbate our HIE method and satisfying isotopic enrichments could be still achieved. In other words, those functionalities were compatible with our ruthenium nanoparticles catalyzed HIE approach, which finally allowed the successful hydrogen isotope labelling of many drugs (methoxy-, amino-, carboxyl-, chlorine substituents etc., **II**.*2.1.2* – **II**.*2.1.7*). Non the less, the functionalization in drugs' molecular structures might be even more complex. Thus, there are many other interesting drugs on the market built up from *N*-heterocyclic units which offer several sites for a potential selective hydrogen isotope incorporation through Ru nanoparticles (benzimidazole in albendazole and omeprazole, 1,2,4-triazole in letrozole, imidazole in metronidazole, benzoxazole in tafamidis, carbazole in carprofen, **figure 79**) Non the less, none of these drugs displayed satisfying exchange of hydrogen for deuterium under a D_2 atmosphere and in the presence of RuNp@PVP. The strongly divergent behavior of those specific cases in **figure 79** from previously labelled drugs in **II**.*2.1.2* – **II**.*2.1.8* could be reasoned in their substitution patterns. Sulfur containing functions like the thioether in albendazole and the sulfoxide in omeprazole most probably had a poisoning effect on the catalyst again and prevented heterocyclic units from interacting with the catalyst. The nitrile functionalities of letrozole are probably also strongly ligating and have a higher affinity to the ruthenium surface than nitrogen atoms in whose vicinity H/D exchange is expected to take place. Apparently, the other drugs metronidazole, tafamidis and carprofen (second line, **figure 79**) do not display any problematic functionality in their molecular structures, since the carboxyl groups in compounds **4** and **8** (**II**.*2.1.2* & **II**.*2.1.3*) did not inhibit the deuterium

uptakes. Chlorine substituents were also tolerated in fluquinconazole and suvorexant and did not undergo hydrogenolysis (**30** and **31**, **II**.*2.1.7*). Nevertheless, as it could be already encountered on deuterium labelled suvorexant **31**, HIE did not take place on the benzoxazolyl group carrying a chlorine substituent. Analogously, not just the type of substitution but also the substitution pattern seemingly modifies the electronic properties of the *N*-heterocyclic cores in metronidazole, tafamidis and carprofen to such an extent, that coordination through the nitrogen atom and C–H activations were not possible any more. Finally, dependent on the stability of certain functionalities, side reactions as hydrogenolysis of C–Cl or C–S bonds may also occur. Hydrogenolysis can be a minor side-reaction which is not detectable by current analytical methods (^{1}H-, ^{13}C-NMR, ESI-MS), since those methods are merely able to analyze the filtered solution and dissolved species. However, cleaved species could be potentially bound irreversibly to the catalyst surface, without any opportunity for elimination. This can be considered as another poisoning effect on the catalyst.

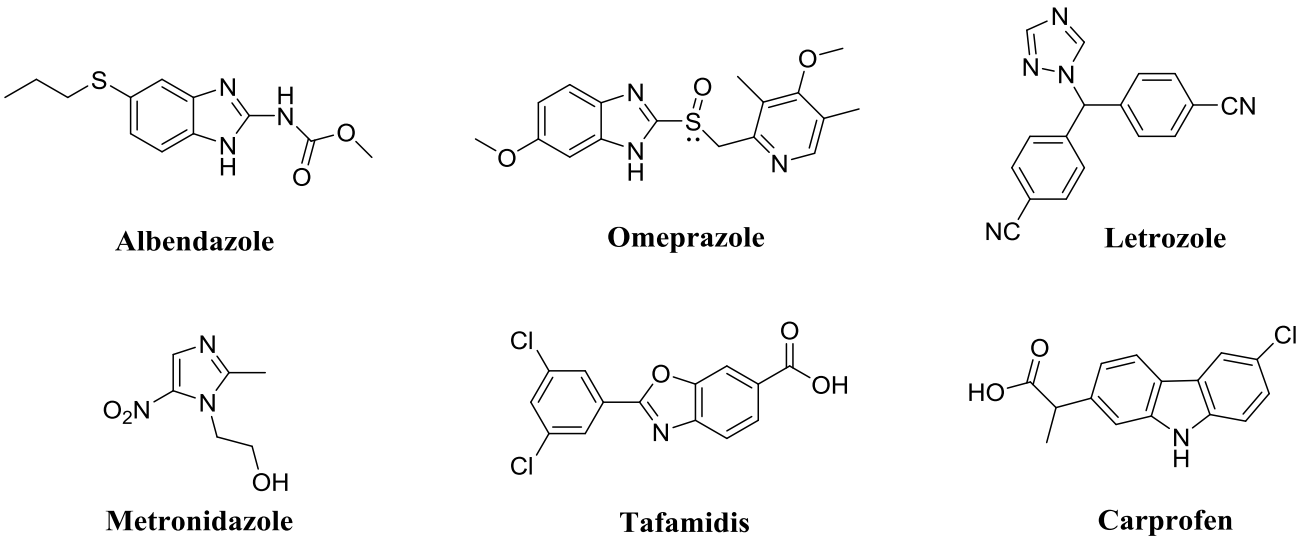

Figure 79. Heterocyclic drugs which cannot be labelled by RuNp@PVP

2.2 HIE catalyzed by nickel nanoparticles

The next aim in this thesis was it to test different metallic nanoparticles for HIE on *N*-heterocyclic substrates and to make out their utilities, respectively. The catalytic behavior of ruthenium nanoparticles for HIE was already well-explored in this work and other aforementioned publications and the limitations of this method were also discussed. One major disadvantage was the reduction of some substrates lowering the yield of deuterated product. Thereafter, a way was presented to inhibit undesired reductions of unsaturated moieties during the deuterium labelling of carbazoles in chapter **II.***2.1.6.* The addition of an inorganic base favored the formation of σ-bonds between carbazole derivatives and the catalyst surface by facilitating the proton abstraction from the N-H and C-H bonds. However, there are many other listed examples that do not have a N-H moiety in their molecular structures, being sensitive to reduction anyhow, like 2,5-diphenyloxazole. This model substrate underwent strong reduction with different ruthenium catalysts. The isotopic enrichments on deutero analogue **1** with RuNp@PVP were not very high, as well (**II**.*2.1.2*). Moreover, ruthenium nanoparticles revealed to be very sensitive towards poisoning through compounds displaying sulfur atoms in their molecular structures. These limitations gave the impetus to try nanoparticles that preferably consisted of a different metal as catalyst for HIE on some selected *N*-heterocyclic examples. For this reason, NHC-stabilized nickel nanoparticles, which were synthesized in **II**.*1.3* and **II**.*1.4*, are going to be tested for HIE in this chapter. The investigation started again with 2,5-diphenyloxazole. Deuterations of the substrate were conducted with 9mol% of every synthesized batch of NiNp under a D_2 atmosphere of 2bar in THF at 50°C with a reaction time of 24 hours, respectively. The catalyst Ni-*ICy* Np (0.25eq NHC) deuterated efficiently the α position of the substrate but it gave just an isotopic enrichment of 43% on both γ positions (**table 5**, entry 1). The deuteration of 2,5-diphenyloxazole with NiNp being stabilized by 0.25 equivalents *IMes*-ligand (Ni-*IMes* Np) led to an almost full deuteration in α and in γ to the nitrogen atom of the oxazole scaffold (**table 5**, entry 2). The third attempt with Ni-*IMes* Np being stabilized by 0.5 equivalents *IMes*-ligand lead to a slightly lower deuterium incorporation in α than in the precedent case (**table 5**, entry 3). It is noteworthy, that the regioselectivity was the same as observed for RuNp@PVP with every batch of NiNp. However, in contrast to ruthenium catalysts, reduced side-products were not formed at all with NiNp and deuterated 2,5-diphenyloxazole could be obtained in 99% yield without any further purification.

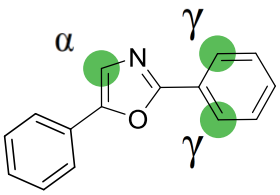

Site of deuterium incorporation catalyzed by NiNp

Entry	Catalyst (equivalents of NHC-ligand)	Isotopic enrichment in α (^{1}H-NMR)	Isotopic enrichment in γ (^{1}H-NMR)
1	Ni-*ICy* Np (0.25eq NHC)	97%	43%
2	Ni-*IMes* Np (0.25eq NHC)	98%	99%
3	Ni-*IMes* Np (0.5eq NHC)	93%	99%

Table 5. Deuteration of 2,5-diphenyloxazole with different NiNp using the reaction conditions: 9mol% Ni, 200µmol substrate, D_2 (2bar), 2mL THF, 50°C, 24h

Due to the highest isotopic enrichment values obtained with Ni-*IMes* Np (0.25eq NHC), this catalyst was also used for the next experiments. In order to ensure the reproducibility of the results with the new nickel nanoparticles, the HIE on 2,5-diphenyloxazole was repeated after having stored the NiNp for six months in the glove box. Unfortunately, we had to encounter an activity loss of the catalyst of 39% for the α position and 56% for the γ positions (**figure 80**). Apparently, metallic Ni(0), being the active species in this HIE process, was gradually oxidized during the storage period, even if just traces of oxygen were present.

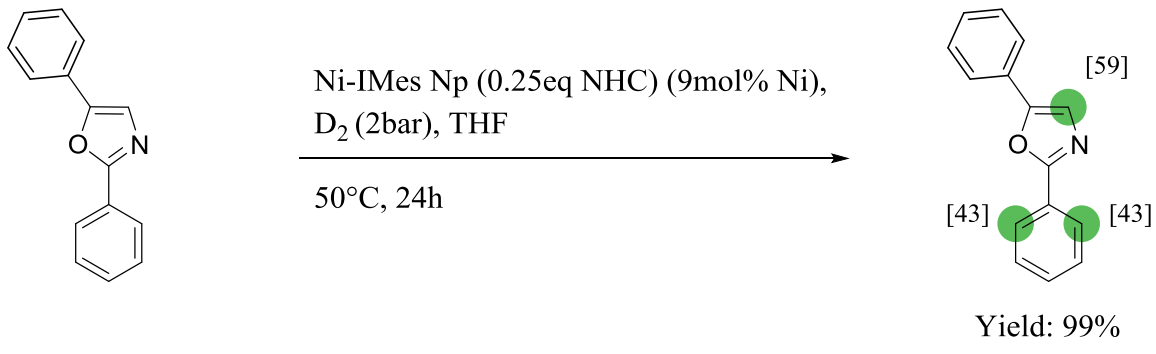

Yield: 99%

Site of deuterium incorporation [X] isotopic enrichment

Figure 80. Decreased isotopic enrichment on 2,5-diphenyloxazole after having stored the catalyst Ni-*IMes* Np (0.25eq NHC) for six months

Regarding the high sensitivity of the nickel nanocatalyst towards storage in the solid state, a smaller amount of Ni-*IMes* Np was prepared according to the procedure from section **II**.*1.4* and used directly after synthesis as catalyst stem solution for the next deuteration reactions. Since most of deuterations of *N*-heterocyclic derivatives worked in THF, there was no need to remove the solvent under reduced pressure or vacuum. Astonishingly, the deuteration of 2,5-diphenyloxazole with the freshly prepared Ni-*IMes* Np stem solution gave the same result as in the beginning with freshly prepared Ni-*IMes* Np (0.25eq NHC) which were washed by precipitation in *n*-pentane and dried prior to use (see **II**.*1.4* for catalyst synthesis and **table 5**, entry 2 and compound **32** in **figure 81** for deuteration results). Prompted by this positive result, other *N*-heterocyclic derivatives were subjected to deuteration with the freshly prepared solution of Ni-*IMes* Np (0.25eq NHC) under a D_2 atmosphere. 2-Phenylimidazole was deuterated very efficiently in *ortho* on the phenyl group. The positions in α to the nitrogen atoms on the imidazole scaffold showed moderate deuterium incorporation (**33**, **figure 81**). 1-Phenyl-1,2,4-triazole manifested different isotopic enrichment levels on the C_3 and C_5 position on the triazole scaffold (**34**, **figure 81**). The C_5 position revealed to be the more reactive one for nickel nanoparticle catalyzed HIE. Interestingly, deuterium uptakes in *ortho* of the adjacent phenyl ring did not appear. Gratifyingly, none of the considered cases (**32-34**, **figure 81**) underwent reduction through hydrogenation within the NiNp-based HIE method.

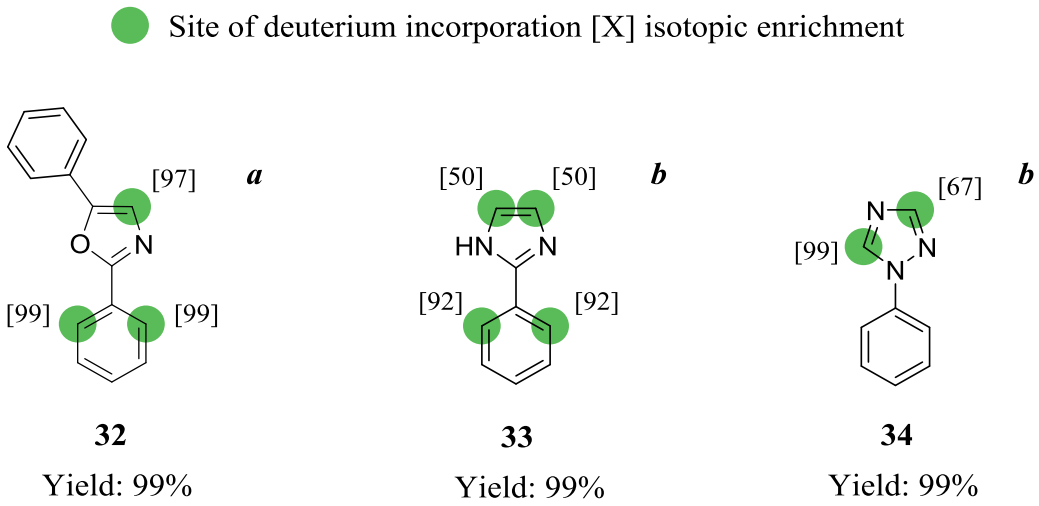

Figure 81. *N*-heterocyclic substrates deuterated with a freshly prepared stem solution of Ni-*IMes* Np (0.25eq NHC) using the reaction conditions: (**a**) 10mol% Ni, 100µmol substrate, D_2 (2bar), 2mL THF, 50°C, 24h (**b**) 5mol% Ni, 200µmol substrate, D_2 (2bar), 2mL THF, 50°C, 24h

In the past, Raney-Ni was reported to be a current catalyst for the reduction of benzene to cyclohexane[94] but apparently the reaction conditions described herein are too mild for a Ni(0)-catalyzed hydrogenation of aromatic moieties. Consequently, the higher chemospecificity in HIE delivered with nickel nanoparticles in this work is not just beneficial for the yield of deuterated products, but it might be also the reason for the higher isotopic enrichments on many positions of the shown *N*-heterocyclic model substrates compared to RuNp@PVP. By changing the metal from ruthenium to nickel, probably not just the reduction of phenyl rings but also reductions and hydrogenolyses of *N*-heterocyclic cores were inhibited, which resulted in a lower formation of protic side-products like amines for example. In this manner, the nanoparticle surface got less poisoned as it has been supposed for ruthenium (**II**.*2.1.9*) and higher TONs could be achieved with nickel, leading to higher isotopic enrichments on the marked positions of **32** (**figure 81**). In addition, the regioselectivity on every subjected *N*-heterocyclic substrate revealed to be the same as in the case of ruthenium, except on compound **34**. This is likely due to the fact that the nickel nanocatalyst operates after the same reaction mechanisms in terms of HIE reactions with D_2 gas as isotopic source as described for ruthenium nanoparticles in chapters **II**.*2.1.2* - **II**.*2.1.6*. For the triazolic deutero analogue **34,** the mechanism that leads to the C-H activation in γ to nitrogen is seemingly unfavorable with the nickel catalyst or it cannot compete with the much higher affinity of the triazole moiety to the nickel catalyst surface. Further, Ni-*ICy* Np allowed to deuterate benzothiazole for the first time. Benzothiazole displayed a deuterium uptake of 85% on the C_2 position with 19mol% of NiNp (**35**, **figure 82**), indicating that the substrate did not irreversibly coordinate to the catalyst surface and a TON could be achieved superior to 1. This result stands in stark contrast to the limitations observed for RuNp@PVP (**II**.*2.1.9*). Consequently, nickel nanoparticles can be assumed to be less sensitive towards sulfur poisoning.

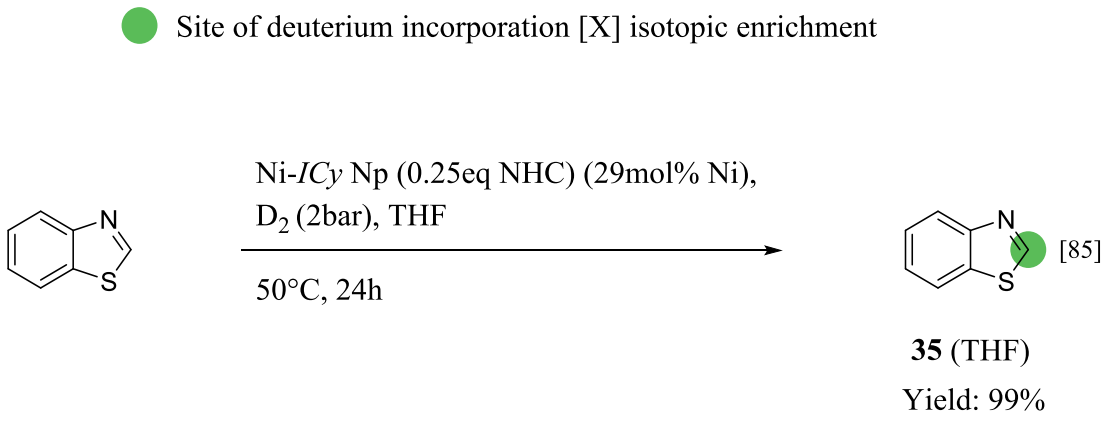

Figure 82. Deuteration of benzothiazole by Ni-*IMes* Np on the C_2 position

During the attempt to deuterate benzimidazole with Ni-*IMes* Np, the nanocatalyst aggregated a few minutes after getting into contact with benzimidazole dissolved in THF. The metallic nanoparticles also gradually lost their black color and turned white. After stirring for 24 hours, no transformation of the organic substrate was observed by ^{1}H-NMR, neither deuteration, nor degradation (**figure 83**). This observation pointed towards an insufficient stability of nickel nanoparticles with this kind of substrates. Since nickel is a less noble metal than ruthenium for example, it undergoes redox reactions more easily. The degradation of the metallic catalyst in this case might be due to its oxidation through an acidic moiety. The N-H moiety of benzimidazole could be acidic enough to react with well-dispersed metallic nickel to give a nickel salt and H_2 gas.

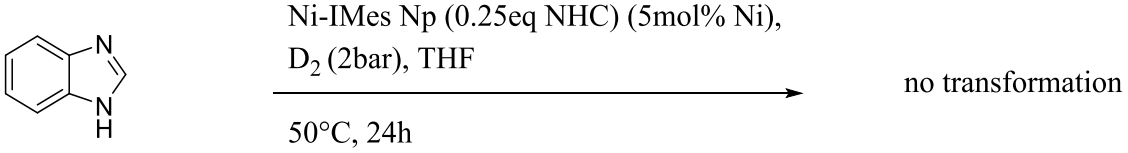

Figure 83. Ni-*IMes* Np proved to be unstable when getting into contact with benzimidazole

Nickel nanoparticles stabilized by *N*-heterocyclic carbenes proved to be efficient, regio- and chemoselective catalysts for the deuteration of some *N*-heterocyclic substrates. In terms of efficiency and regioselectivity, results could be achieved which were very similar to the deuteration of these substrates by ruthenium nanoparticles embedded in a PVP matrix. This similarity points towards the fact that C-H activations must pass through the same reaction mechanisms with metallic Ni catalysts as discussed in the context of DFT-calculations on ruthenium nanoparticles (**II**.*2.1.2* - **II**.*2.1.6*). However, a huge difference to Ru catalyzed HIE from previous sections was the much higher chemoselectivity of the Ni catalysts because reduced side-products were completely absent in this case. In order to study the fundamental background of nickel catalyzed hydrogenations and to explain why reductions did not happen under a D_2 atmosphere with these nickel nanocatalysts, the performance of other investigations and experiments would be needed. The second difference compared to RuNp@PVP was the deuteration of benzothiazole that succeeded with Ni-*IMes* Np. Apparently, NiNp were not poisoned by the sulfur atom of benzothiazole, witnessed by the deuteration of the C_2 position. Nevertheless, β positions relative to the nitrogen or the sulfur atom were not activated, as it was observed for HIE catalyzed by RuNp on *N*-heterocyclic benzoderivatives (**II**.*2.1.4*). A third difference relative to RuNp@PVP could be figured out within NiNp catalyzed HIE. The NHC-stabilized NiNp revealed to be unstable when getting

into contact with benzimidazole, which can be probably related to the acidity of the N–H bond.

Summary and perspectives

This work triggered several meaningful achievements in isotope chemistry and organic chemistry. The results were accompanied and elucidated by DFT-calculations to a large extend which revealed new fundamental aspects in transition metal catalysis. First of all, means and ways were demonstrated how to generate numerous biologically relevant stable deuterium and tritium labelled *N*-heterocyclic compounds over ruthenium nanoparticle catalyzed C-H activations using D_2 and T_2 gas as the only isotopic sources. This HIE method furnished a broad repertory of drug-like model compounds and structurally complex commercial drugs, one agrochemical and one natural product from the oxazole, imidazole, triazole and carbazole families which are highly deuterated at the expected sites, employing RuNp@PVP as a catalyst. The exchange of hydrogen for deuterium was found to take place on sp^2- and sp^3-carbon atoms at α-, β- and γ-positions relative to a nitrogen atom. This property of Ru nanoparticles permitted to provide plenty examples of deuterium labelled *N*-heterocyclic compounds that cannot be labelled by other HIE methods as homogeneous Ir(I) catalysis at all. The nitrogen associated selectivity of RuNp for α- β- and γ-positions allowed to incorporate up to 5 deuterium atoms per molecule, representing up to date the only mild HIE method that is suitable for a rapid SILS synthesis of many bioactive *N*-heterocyclic substrates. However, a clear drawback of RuNp@PVP-catalyzed HIE was the concomitant reduction of many substrates to undesired side-products, which required HPLC purification of the labelled products. The capacity of RuNp to operate on α-, β- and γ-positions relative to a nitrogen atom was studied by DFT-based calculations. In the light of the above, it was found that nitrogen atoms inside the aromatic heterocycles show coordination to the RuNp surface. Nitrogen atoms at position 3 of imidazoles and benzimidazoles coordinate stronger to the ruthenium catalyst than the N–H group at position 1. This coordination directs the subsequent C–H activations. C–H activations at α-positions relative to the coordinating nitrogen atom result in a four-membered dimetallacycle key intermediate. C–H activations on β-positions succeed under the formation of a five-membered dimetallacycle key intermediate and C–H activations on γ-positions give a five-membered metallacycle key intermediate which is formed between the substrate and the ruthenium nanoparticle. This gain in mechanistic

knowledge will certainly help to derive and understand many other reaction pathways in nano- and heterogeneous catalysis. Moreover, the regioselectivity of HIE on *N*-heterocyclic scaffolds could be controlled by changing the coordination affinity of certain structural moieties. Thus, the isotopic enrichment could be almost completed at α- and β positions of carbazole- and indole moieties in presence of the base Cs_2CO_3. On this path, the reduction of aromatic groups as a side-reaction was also completely inhibited. DFT again provided important hints for the clarification of these results by pointing out the important role of the carbonate ion as a proton acceptor on the nanoparticle surface during the N–H and C–H activation steps. In this context, the additive Cs_2CO_3 allowed both activation steps to occur without the need to overcome an energetic barrier. Owing to the drug carvedilol, the affinity of a secondary amine could be withdrawn by protecting it with a Boc-group and the regioselectivity of the HIE was completely shifted to the carbazole moiety by adding one equivalent of Cs_2CO_3. This strategy paved the way to deuterium labelled carvedilol with the deuterium label exclusively on the carbazole moiety. With the aim to enhance the hydrogen isotope labelling of other molecules, especially of those which could not be labelled within this work (**II**.*2.1.9*), similar additive strategies could be also applied to the protection or masking of other functionalities in the near future, that interfere in MNp catalyzed HIE because they strongly bind to the catalyst. Furthermore, RuNp@PVP catalyzed HIE permitted to perform tritiations of astemizole, fluconazole and *N*-Boc protected carvedilol which were achieved in one rapid and practically simple step for the first time, to the best of our knowledge.

Tritiation reactions were conducted under tritium gas pressures below one bar and the tritium labelled drugs displayed satisfying molar activities. Undoubtedly, these features fulfill the requirements of most laboratories for tritiation protocols. The encouraging results achieved with RuNp@PVP as HIE catalyst prompted the conclusion, that the established deuteration and tritiation protocols from this work will garner a lot of attention from the academic and industrial sphere. Owing to the presented large substrate scope, these methods can be certainly transferred to the synthesis of SILSs and radioligands of many other *N*-heterocyclic molecules that circulate in drug development and life-science. In order to explore other metallic nanoparticles as HIE catalysts, new NHC-stabilized nickel nanoparticles were synthesized. These NiNp also revealed to be efficient HIE catalysts for the deuteration of *N*-heterocyclic model compounds displaying the same regioselectivity as RuNp in most cases. The most remarkable property of the Ni-based catalysts was the high chemoselectivity of the deuterations. In contrast to RuNp, the nickel nanocatalysts did not reduce the aromatic groups

of any tested substrate. This was a huge asset compared to every other Ru-based catalyst. Another unusual finding was the deuteration of benzothiazole, a sulfur-containing substrate that did not show any reactivity with RuNp. For this reason, other molecules with sulfur atoms in their molecular structures need to be subjected to NiNp catalyzed HIE soon. Nevertheless, there was also evidence that the substrate scope of NiNp catalyzed HIE can be more limited than the substrate scope of RuNp, which was reflected in the decomposition of the nickel catalyst with benzimidazole as substrate. This result was refered to a side-reaction where Ni(0) was oxidized by the protic N–H group of the substrate. On this account, it will be indispensable to figure out the compatibility of NiNp with other protic or acidic compounds and functionalities in future experiments. Undoubtedly, the results obtained for nickel catalyzed HIE in this work offered a fundament which will render nickel nanoparticles an important and perspective subject for future studies in hydrogen isotope labelling.

Experimental part

Reagents and instrumentation. Metal nanoparticle syntheses and catalyses were carried out in Fischer-Porter glassware under argon. Metal nanoparticles were stored in a glove box under an argon atmosphere (O_2 < 0.1 ppm). Organometallic precursors, ligands and substrates were purchased from commercial suppliers (Aldrich, Acros Organics, Alfa Aesar, Maybridge, abcr, Ark Pharm Inc., Cayman Chemical) and used without further purification. THF was dried over sodium and benzophenone and distilled before use. DMA was stored in a Schlenck tube over molecular sieves (4Å, previously activated by microwave treatment). CD_3OD was used without further purification. ^{1}H NMR (400 MHz), ^{13}C NMR (100 MHz) & ^{3}H NMR (427 MHz) spectra were recorded on a (400 MHz) Bruker Avance spectrometer. Proton-decoupled deuterium (^{2}H-{^{1}H}) 1D NMR (92 MHz) spectra were recorded on a 14.1 T (600 MHz) Bruker Avance II NMR spectrometer equipped with a 5-mm selective ^{2}H observe cryogenic probe. Proton signals were eliminated using the WALTZ-16 CPD sequence. Chemical shifts are reported in parts per million (ppm) downfield from residual solvent peaks and coupling constants are reported in Hertz (Hz). Splitting patterns are designated as singlets (s), doublets (d) or triplets (t). Splitting patterns that could not be interpreted or easily visualized are designated as multiplets (m). Electrospray (ESI) mass spectra were recorded using a Waters ZQ 2000 LCMS System. GC-MS analysis was carried out using a Waters GCT Premier TOF Mass spectrometer equipped with a DCI probe tip.

H/D exchange quantification. Deuterium incorporation was quantified by the decrease of ^{1}H-NMR integral intensities at the specified positions compared to the starting material. Integral intensities were calibrated against hydrogen signals that did not undergo H/D-exchange. Incorporations of deuterium and tritium could be further determined by ^{2}H- and ^{3}H-NMR. Mass spectrometry quantification was performed by subtraction of the mean molecular masses of the product and substrate isotopologue clusters in order to eliminate the contribution of the natural isotope abundance to the total mass.

General Procedure for H/D exchanges. A 100 mL Fischer–Porter bottle was equipped with a magnetic stir bar. The catalyst (RuNp@PVP or nickel nanoparticles) and Cs_2CO_3 were charged in a glove box into the Fischer–Porter bottle. The substrate was dissolved in the appropriate solvent; the solution was then degassed and added to the catalyst in the Fischer–Porter bottle under an argon atmosphere. Argon was removed under reduced pressure and the Fischer-Porter glassware was flushed with D_2 gas under stirring. The degassing-flushing cycle was repeated twice. The reaction mixture was then stirred at 50°C (sand bath) under D_2 (2 bar) for 24 hours. Amounts of substrates, catalyst, used solvents, work-up and purification procedures are individually indicated in all cases.

DFT calculations. The Ru_{13} model has previously been published and detailed elsewhere.[83] It has been successfully applied to rationalize the enantiospecific C-H activation using ruthenium nanocatalysts in terms of reaction pathways. It was shown that similar thermodynamic and activation energies are found on this model and on a larger hydrogenated 1nm Ru_{55} model. The surface of this Ru_{13} model is covered with 17 hydrides per surface ruthenium atom, *i.e*. 1.4 H/surface Ru atom, a usually measured coverage value on RuNPs.[95] DFT calculations were done with the Vienna ab initio simulation package, VASP.[96] spin polarized DFT; exchange-correlation potential approximated by the generalized gradient approach proposed by Perdew, Burke, and Ernzerhof (PBE);[97] projector augmented waves (PAW) full-potential reconstruction;[98] PAW data sets for Ru atoms treating the 4*p*, 4*d* and 5*s* states (14 valence electrons); kinetic energy cutoff: 500 eV; Γ-centered calculations;[99] Gaussian smearing of 0.02 eV width; geometry optimization threshold: residual forces on any direction less than 0.02 eV/Å; supercell size set to ensure a vacuum space of *ca*. 14 Å between periodic images of metal clusters, 30.5Å x 30.5Å x 31Å). Reaction barriers were estimated by the climbing image nudge elastic band (CINEB) method;[100] spring force between images: 5 eV; force tolerance of 0.02 eV/Å. The harmonic vibrational modes were systematically

calculated for in order to distinguish minima and saddle points by using the dynamical matrix code implemented in VASP as well as the VASPTST tools also developed by Henkelman's group.

Syntheses of metal nanoparticles

Synthesis of RuNp@PVP

A schlenk flask was charged with PVP (500mg). The PVP was dissolved in THF (15mL) under stirring at 50°C. Ru(COD)(COT) (79.0mg, 0.25mmol) was filled in a Fisher-Porter flask and dissolved in THF (15mL). The PVP solution was added to the Ru(COD)(COT) solution. Argon was removed under reduced pressure and the Fisher-Porter flask was charged with H_2 gas (3bar) under stirring. The reaction mixture was stirred overnight at ambient temperature. The solution was concentrated under vacuum to a volume of 3mL and *n*-pentane (30mL) was added under stirring. The mixture was stirred for 30min and then stored for 1h at room temperature without stirring to let deposit RuNp@PVP at the bottom. The supernatant was removed and the solid dried under vacuum overnight.

Yield: 400mg
The size and shape of the RuNp was confirmed by TEM.

Synthesis of ruthenium nanoparticles stabilized by 1,3-dicyclohexylimidazol-2-ylidene (Ru-ICy Np)

A schlenk flask was charged with 1,3-dicyclohexylimidazolium chloride (19.0mg, 0.08mmol, 0.25eq) and with potassium *tert*-butoxide (KO*t*Bu) (10.0mg, 0.09mmol, 0.28eq). THF (15mL) was added and the solution was stirred over night at room temperature to form the carbene ligand. Ru(COD)(COT) (100mg, 0.32mmol, 1eq) was filled in a Fisher Porter flask, dissolved in THF (15mL) and cooled down in a liquid nitrogen/acetone bath. The carbene ligand solution was filtered through a celite pad and added to the Ru(COD)(COT) solution. Argon was removed under reduced pressure and the Fisher Porter bottle was charged with H_2 gas (3bar). The reaction mixture was stirred over night at ambient temperature. The solution was

concentrated under vacuum to a volume of 3mL and *n*-pentane (30mL) was added under stirring. The mixture was stirred for 30min and then stored for 1h at room temperature without stirring to let deposit Ru-*ICy* Np at the bottom. The supernatant was removed and the solid dried under vacuum overnight.

Yield: 24mg

The size of the RuNp was measured by TEM. The determination of the mean size (1.2±0.5nm) was achieved by taking into account a population of at least 200 Np.

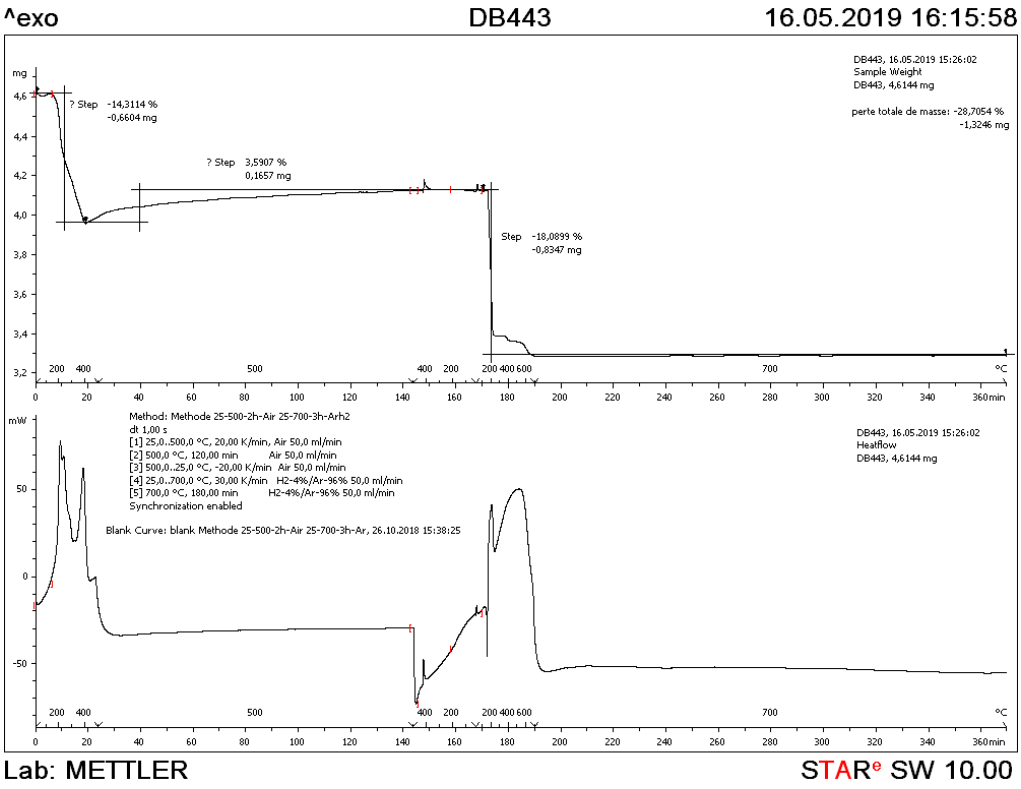

TGA of Ru-*ICy* Np

Synthesis of Nickel nanoparticles stabilized by 1,3-dicyclohexylimidazol-2-ylidene (Ni-ICy Np)

A schlenk flask was charged with 1,3-dicyclohexylimidazolium chloride (48.3mg, 0.18mmol, 0.25eq) and with KO*t*Bu (22.2mg, 0.20mmol, 0.28eq). THF (15mL) was added and the solution was stirred over night at room temperature to form the carbene ligand. $Ni(COD)_2$ (200mg, 0.73mmol, 1eq) was filled in a Fisher Porter flask, dissolved in THF (15mL) and cooled down in a liquid nitrogen/acetone bath. The carbene ligand solution was filtered

through a celite pad and added to the $Ni(COD)_2$ solution. Argon was removed under reduced pressure and the Fisher Porter bottle was charged with H_2 gas (3bar). The reaction mixture was stirred for 5h at 70°C. The solution was cooled down to room temperature, concentrated under vacuum to a volume of 1mL, *n*-pentane (30mL) was added and the mixture was stirred for 30min. The mixture was stored for 1h at room temperature without stirring to let deposit Ni-*ICy* Np at the bottom. The supernatant was removed and the solid dried under vacuum for 2h.

Yield: 29mg

The size of the NiNp was measured by TEM. The determination of the mean size (2±1nm) was achieved by taking into account a population of at least 200 Np.

Synthesis of Nickel nanoparticles stabilized by 1,3-Dimesitylimidazol-2-ylidene (Ni-IMes Np)

A schlenk flask was charged with 1,3-dimesitylimidazol-2-ylidene (*IMes*) (27.8mg, 90µmol, 0.25eq) or (55.6mg, 180µmol, 0.5eq). THF (10mL) was added and stirred until the solid completely dissolved. $Ni(COD)_2$ (100mg, 0.37mmol, 1eq) was filled in a Fisher Porter flask, dissolved in THF (15mL) and cooled down in a liquid nitrogen/acetone bath. The carbene ligand solution was added to the $Ni(COD)_2$ solution, argon was removed under reduced pressure and the Fisher Porter bottle was charged with H_2 gas (3bar). The reaction mixture was stirred for 5h at 70°C. The solution was cooled down to room temperature, concentrated under vacuum to a volume of 1mL, *n*-pentane (30mL) was added and the mixture was stirred for 30min. The mixture was stored for 1h at room temperature without stirring to let deposit Ni-*IMes* Np at the bottom. The supernatant was removed and the solid dried under vacuum for 2h.

Yield: 39mg, (0.25eq *IMes*)

The size of the NiNp (0.25eq *IMes*) was measured by TEM. The determination of the mean size (1.8±0.6nm) was achieved by taking into account a population of at least 200 Np.

Yield: 56mg, (0.5eq *IMes*)

Synthesis of pimprinine

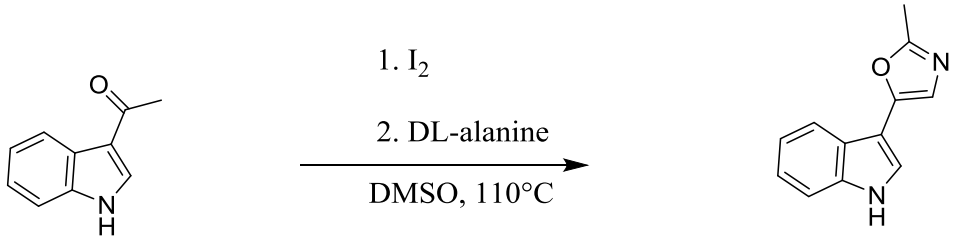

Chemical Formula: $C_{12}H_{10}N_2O$

Pimprinine was synthesized after a literature procedure.[34] 3-Acetylindole (1.6g, 10mmol) and I_2 (5.1g, 20mmol) were dissolved in DMSO (60mL) and stirred for 45min at 110°C. DL-alanine (1.8g, 20mmol) was added to the reaction mixture and the reaction was stirred for another 15min at 110°C. After cooling down to room temperature the reaction mixture was poured into a Na_2SO_3 solution (100mL, 10% in H_2O dist.). The aqueous phase was extracted three times with EtOAc (3 x 50mL). The combined organic phases were dried over $MgSO_4$ and the solvent was removed under vacuum. The crude product was purified over C18 functionalized SiO_2. Pimprinine was eluted with 1:1 MeOH : H_2O (0.1% TFA).

Yield: 160mg, 8%, light yellow solid

^{1}H NMR (400 MHz, Methanol-*d*$_4$): δ 7.80 – 7.75 (m, 1H), 7.59 (s, 1H), 7.46 – 7.40 (m, 1H), 7.23 – 7.12 (m, 3H), 2.51 (s, 3H).

^{13}C-{^{1}H}NMR (100 MHz, Methanol-*d*$_4$): δ 160.8, 150.1, 138.2, 125.3, 123.7, 123.4, 121.3, 120.4, 119.2, 112.8, 105.5, 13.5.

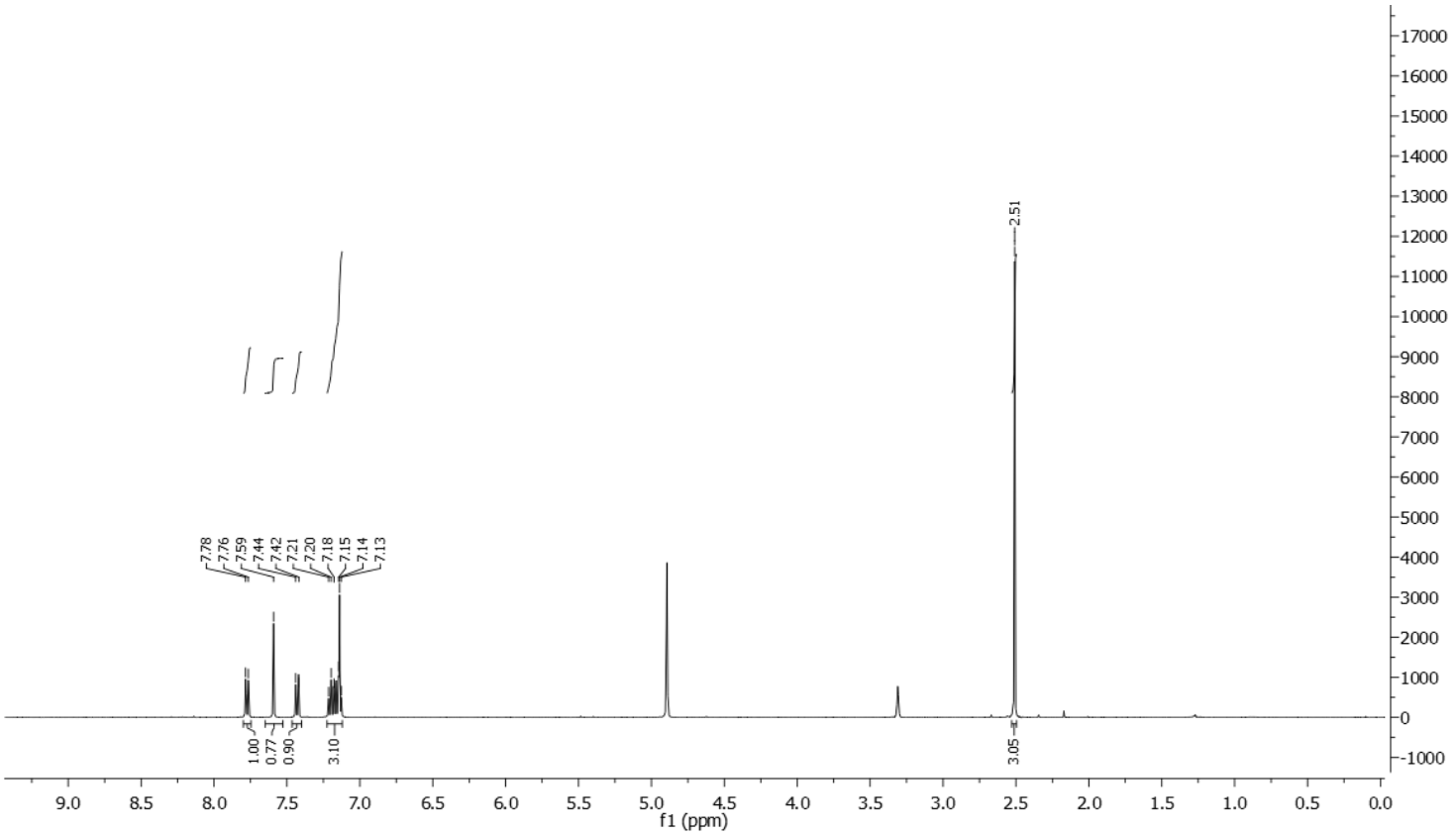

^{1}H-NMR spectrum of pimprinine

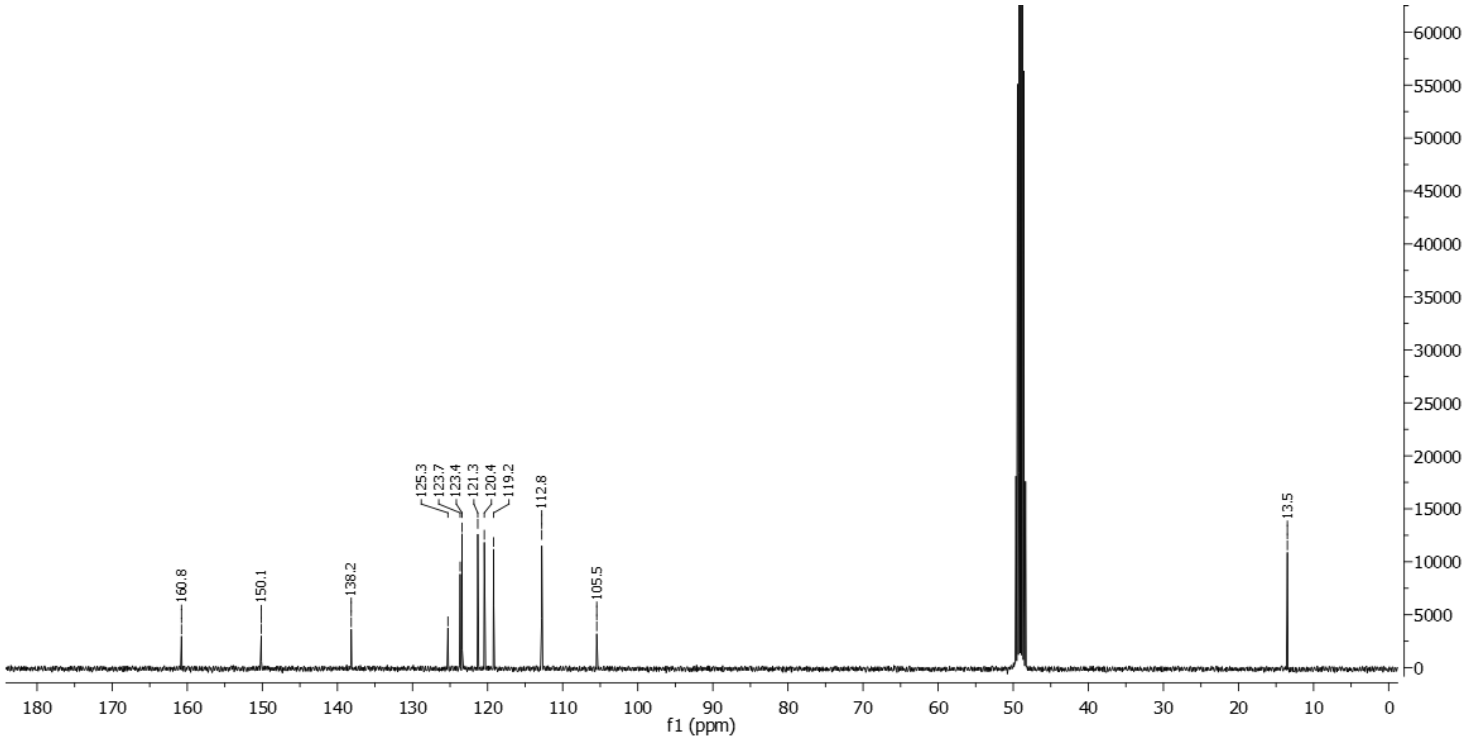

^{13}C-NMR spectrum of pimprinine

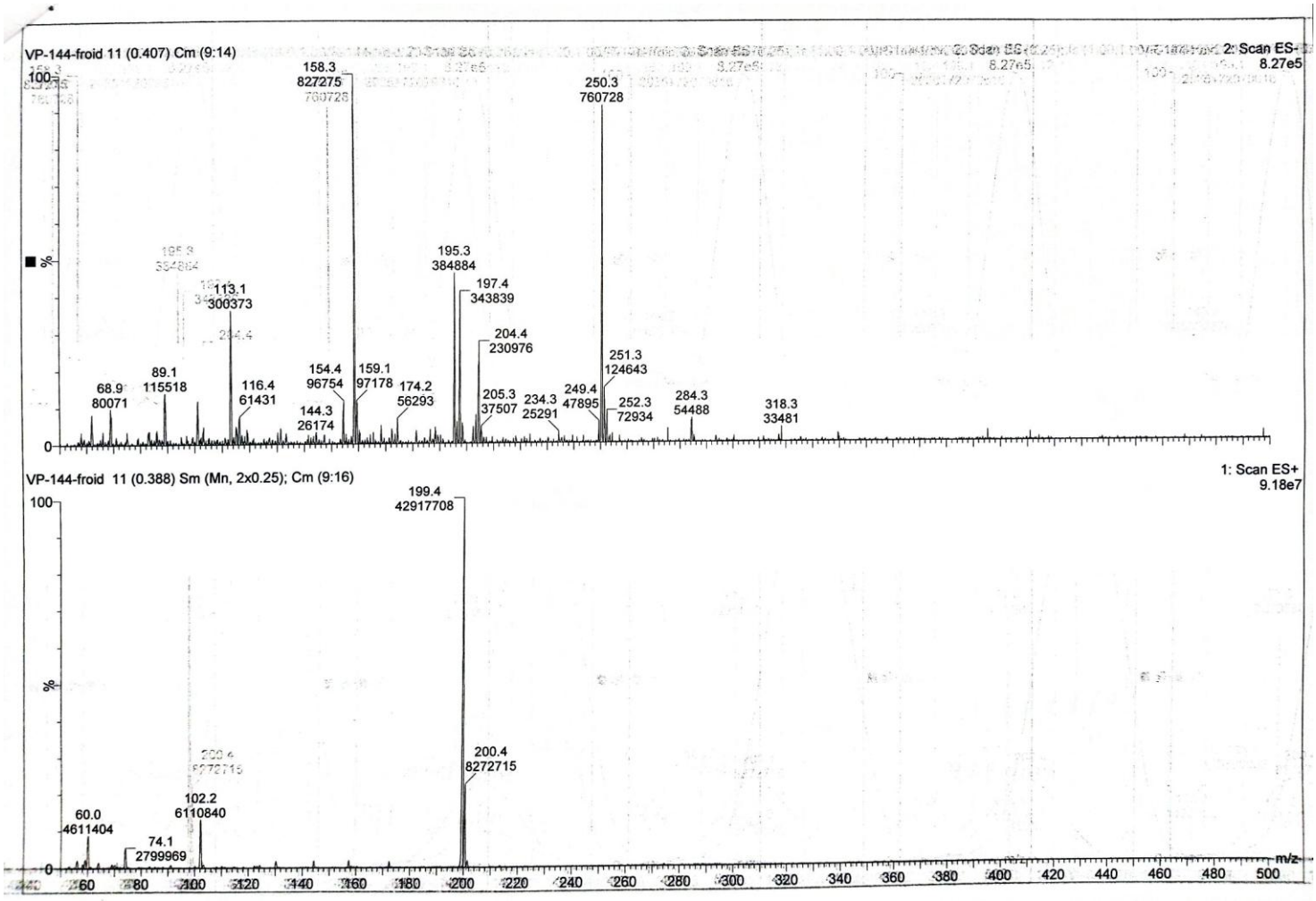

ESI spectrum of pimprinine

Synthesis of 4'-(1,2,4-Triazol-1-yl)acetanilide

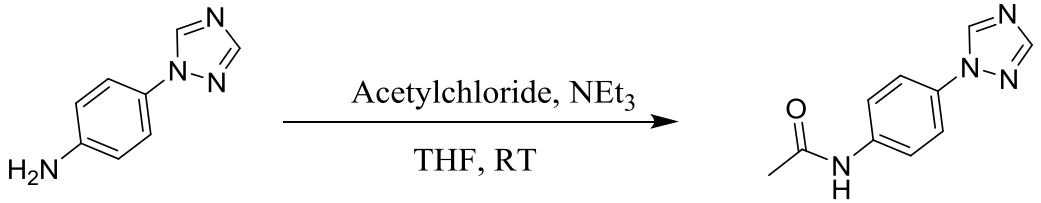

Chemical Formula: $C_{10}H_{10}N_4O$

4-(1*H*-1,2,4-Triazol-1-yl)aniline (150mg, 937µmol) was dissolved in THF (5mL) and NEt_3 (130µL, 937µmol) was added under stirring at RT. Acetylchloride (65µL, 937µmol) was added and the reaction mixture was stirred for 1h at room temperature. The reaction mixture was poured into H_2O dist. (100mL). The aqueous phase was extracted three times with DCM

(3 x 50mL). The solvent was removed under vacuum and the crude product was recrystallized from DCM/MeOH (3:1).

Yield: 65.0mg, 34%, white solid

^{1}H NMR (400 MHz, Methanol-*d*$_4$): δ 9.02 (s, 1H), 8.14 (s, 1H), 7.77 – 7.71 (m, 4H), 2.15 (s, 3H).

^{13}C-{^{1}H}NMR (100 MHz, Methanol-*d*$_4$): δ 171.8, 152.7, 142.8, 140.2, 134.0, 121.8, 121.6, 23.9.

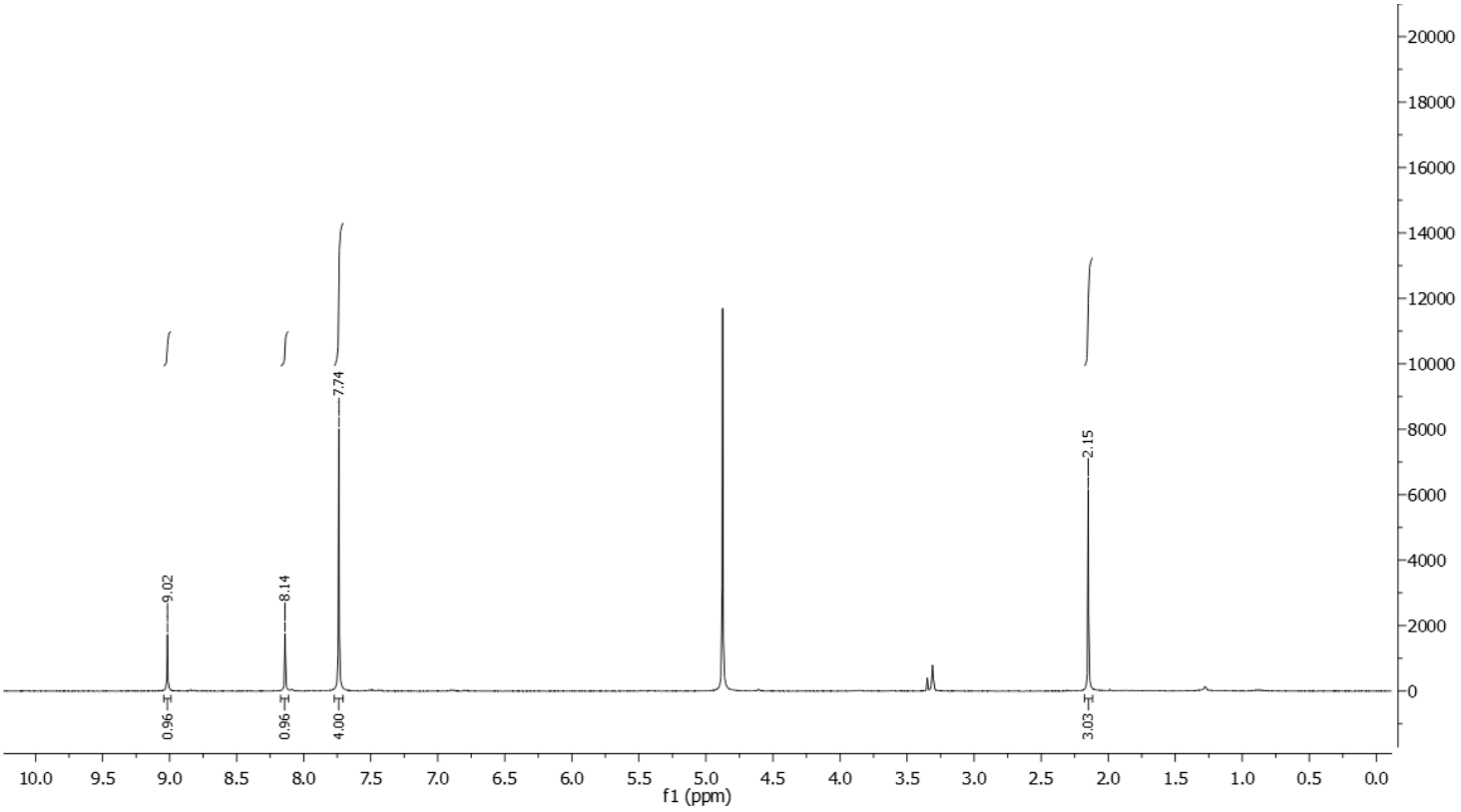

^{1}H-NMR spectrum of 4'-(1,2,4-Triazol-1-yl)acetanilide

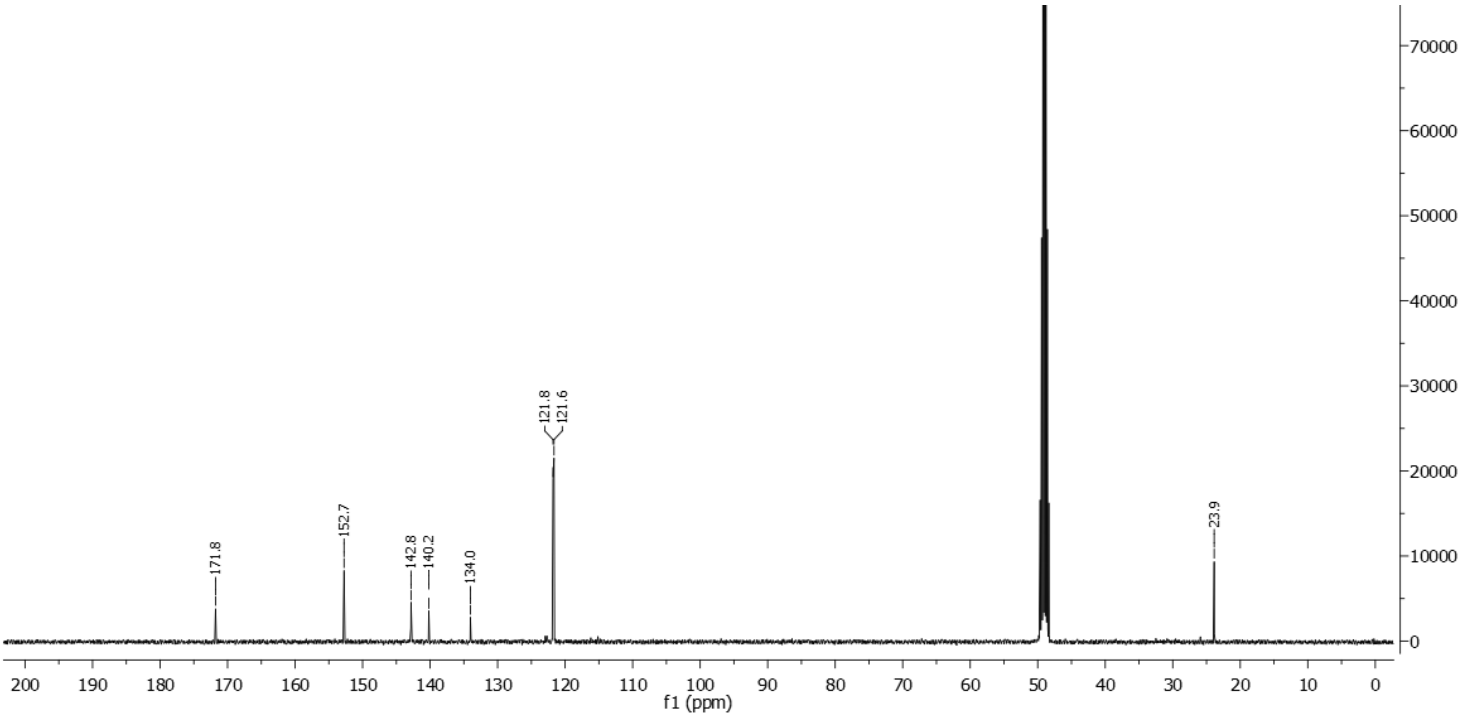

^{13}C-NMR spectrum of 4'-(1,2,4-Triazol-1-yl)acetanilide

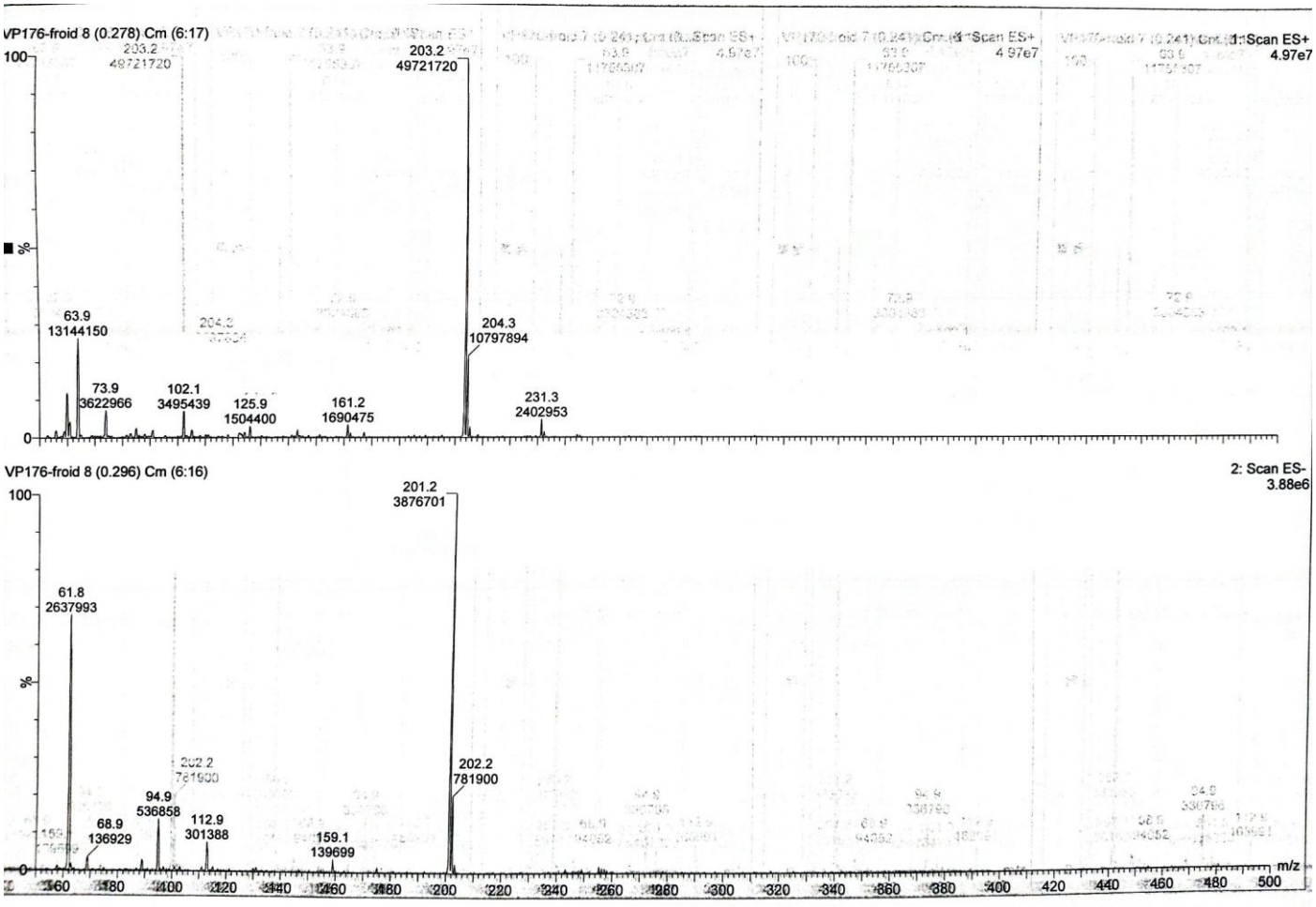

ESI-spectrum of 4'-(1,2,4-Triazol-1-yl)acetanilide

Synthesis of N-methylcarbazole

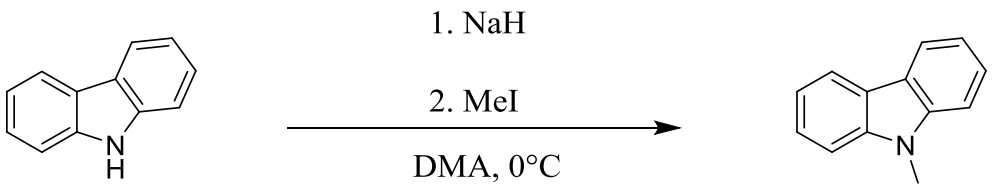

Chemical Formula: $C_{13}H_{11}N$

Carbazole (1.0g, 6mmol) was dissolved in DMA (2mL). A suspension of NaH (0.24g, 10mmol) in DMA (2mL) was added under stirring at 0°C. The mixture was stirred for 30min and methyliodide (0.37mL, 6mmol) was added and the reaction mixture was stirred for 1h at room temperature. The reaction mixture was poured into H_2O dist. (100mL). The aqueous phase was extracted three times with chloroform (3 x 20mL). The organic phase was dried over $MgSO_4$ and the solvent was removed under vacuum. The crude product was purified over SiO_2 where *N*-methylcarbazole was eluted with 20:1 cyclohexane : THF. The product was recrystallized from cyclohexane.

Yield: 590mg, 54%, white solid

^{1}H NMR (400 MHz, Acetone-d_6): δ 8.17 – 8.11 (m, 2H), 7.57 – 7.51 (m, 2H), 7.50 – 7.43 (m, 2H), 7.24 – 7.17 (m, 2H), 3.91 (s, 3H).

^{13}C-{^{1}H}NMR (100 MHz, $CDCl_3$): δ 141.1, 125.8, 122.9, 120.4, 118.9, 108.5, 29.2.

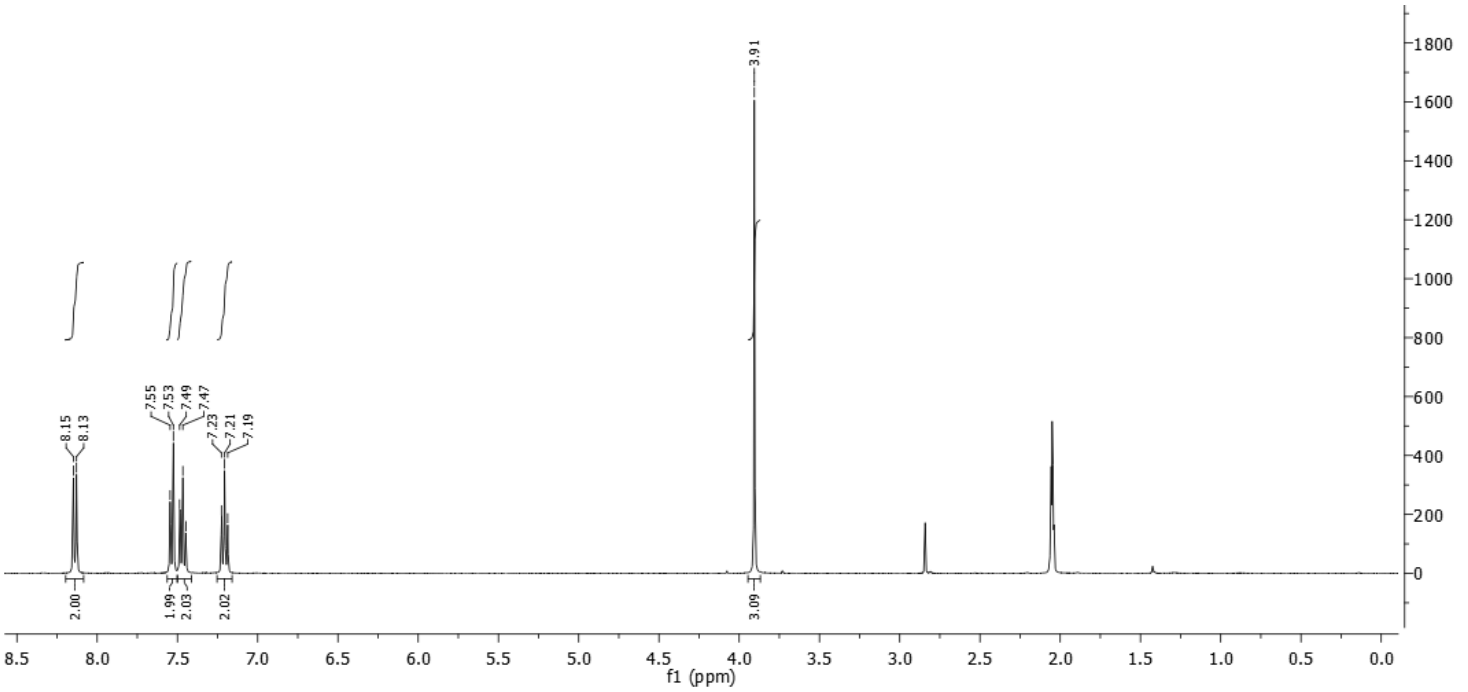

^{1}H-NMR spectrum of *N*-methylcarbazole

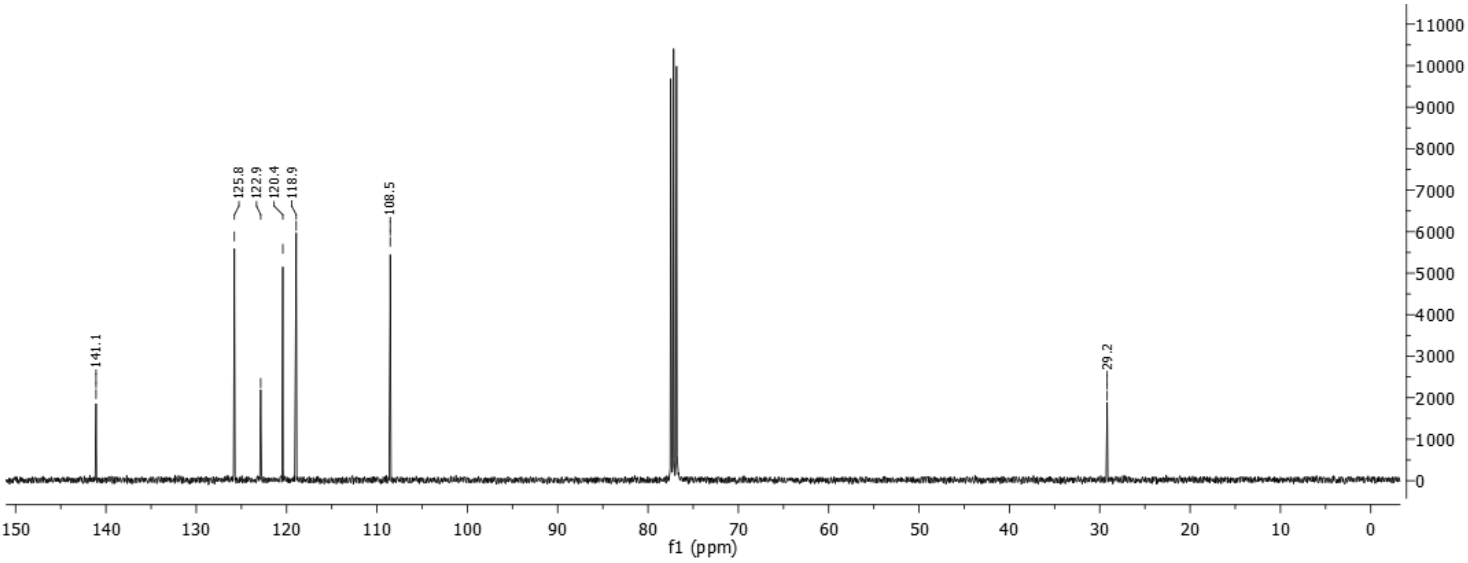

^{13}C-NMR spectrum of *N*-methylcarbazole

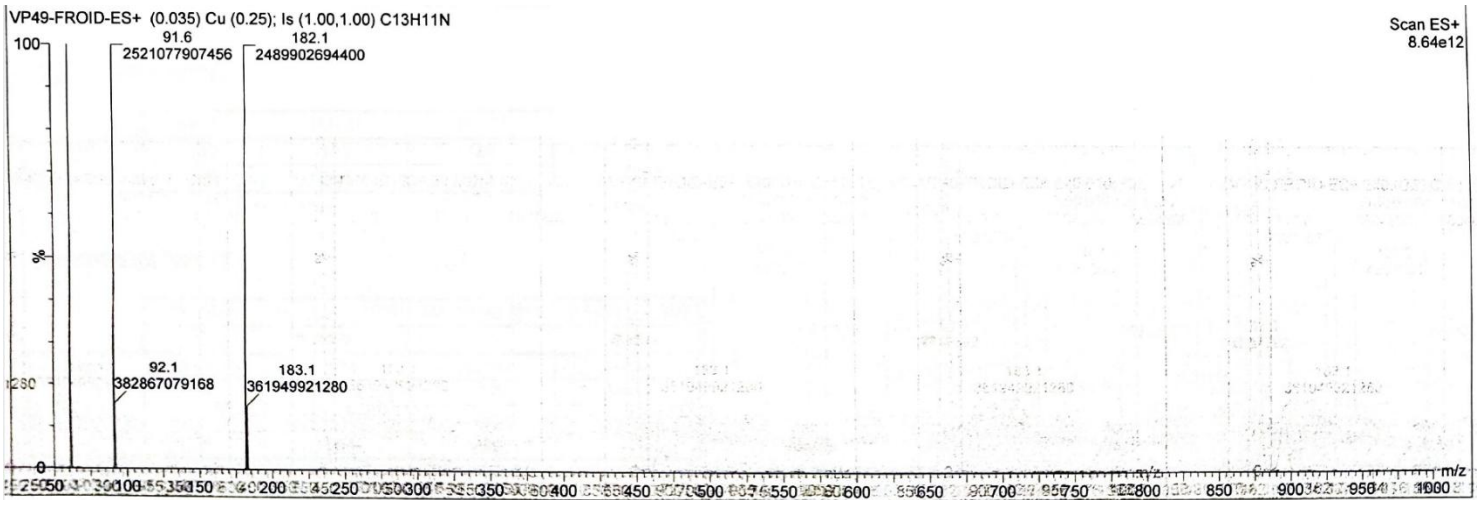

ESI-spectrum of *N*-methylcarbazole

Synthesis of N-Boc-carvedilol

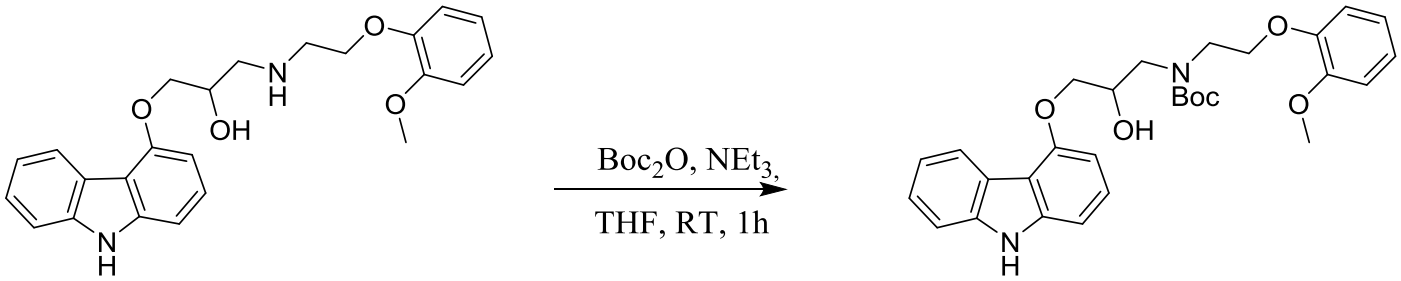

Chemical Formula: $C_{29}H_{34}N_2O_6$
Molecular Weight: 506,60

Carvedilol (1.0g, 2.5mmol) was dissolved in THF (20mL) and NEt_3 (377µL, 2.70mmol, 1.1eq) was added under stirring. A solution of di-*tert*-butyl dicarbonate (540mg, 2.50mmol, 1eq) in THF (15mL) was added slowly under stirring to the reaction mixture at room temperature. The reaction mixture was stirred 1h at room temperature and poured on a SiO_2 column. Elution was carried out with EtOAc/MeOH (50:3) and the solvent was removed under vacuum. The crude product was dissolved in THF (5mL) and precipitated in *n*-pentane (400mL).

Yield: 1.2g, 96%, white solid

^{1}H NMR (400 MHz, Acetone-d_6): δ 10.31 (bs, NH), 8.55 – 8.40 (m, 1H), 7.54 – 7.46 (m, 1H), 7.40 – 7.28 (m, 2H), 7.22 – 7.11 (m, 2H), 6.99 – 6.80 (m, 4H), 6.77 – 6.68 (m, 1H), 4.80 – 4.49 (m, 2H), 4.38 – 4.15 (m, 4H), 4.00 – 3.92 (m, 1H), 3.88 – 3.79 (m, 2H), 3.78 – 3.66 (m, 4H), 1.54 – 1.43 (m, 9H).

^{13}C-{^{1}H}NMR (100 MHz, Acetone-d_6): δ 157.1, 156.2, 150.7, 149.3, 142.4, 140.1, 127.3, 125.4, 124.1, 123.3, 122.2, 121.6, 119.7, 114.6, 113.3, 110.9, 104.7, 101.4, 80.3, 71.2, 70.4, 68.3, 56.0, 53.1, 49.2, 28.6.

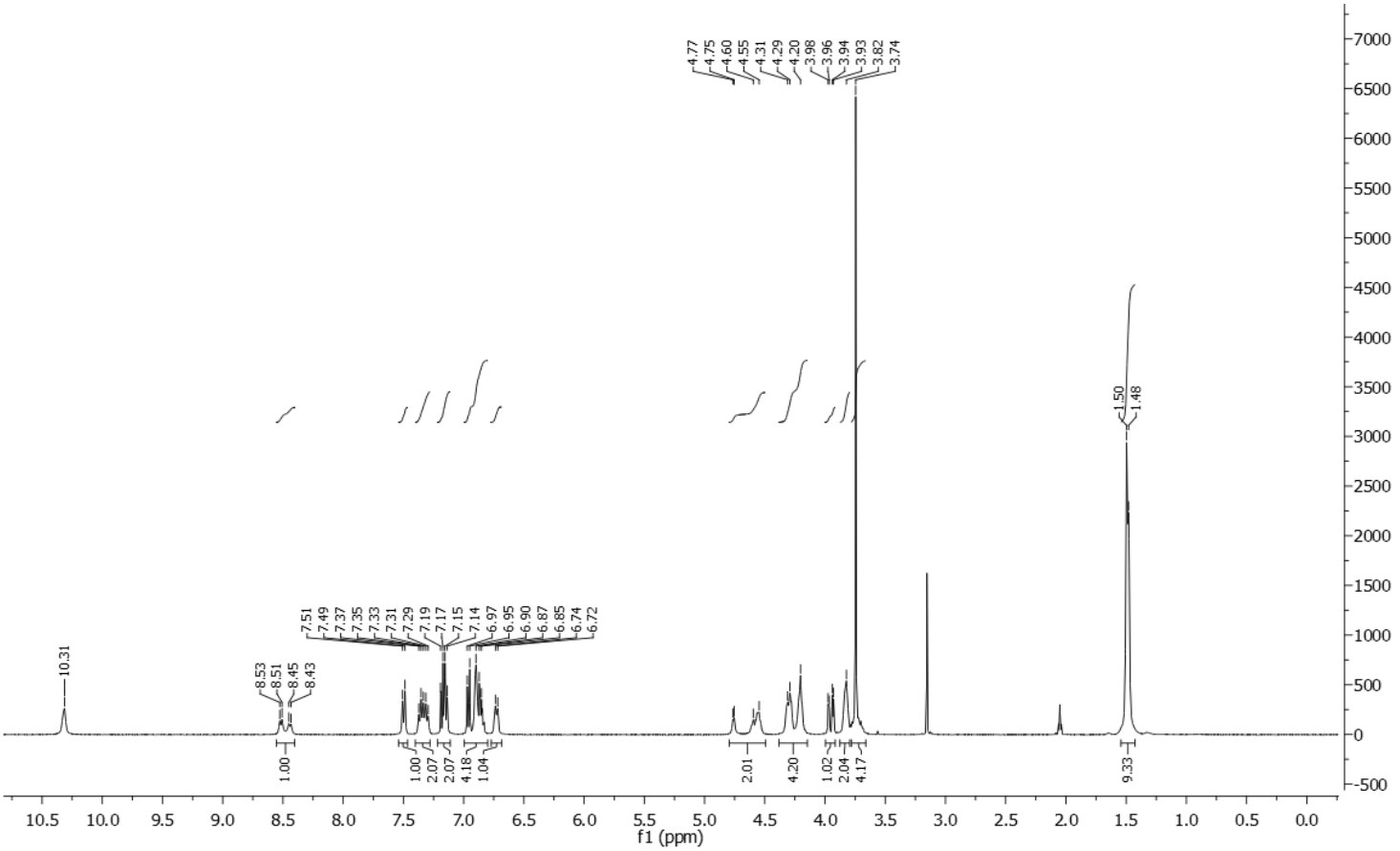

^{1}H-NMR spectrum of *N*-Boc-carvedilol

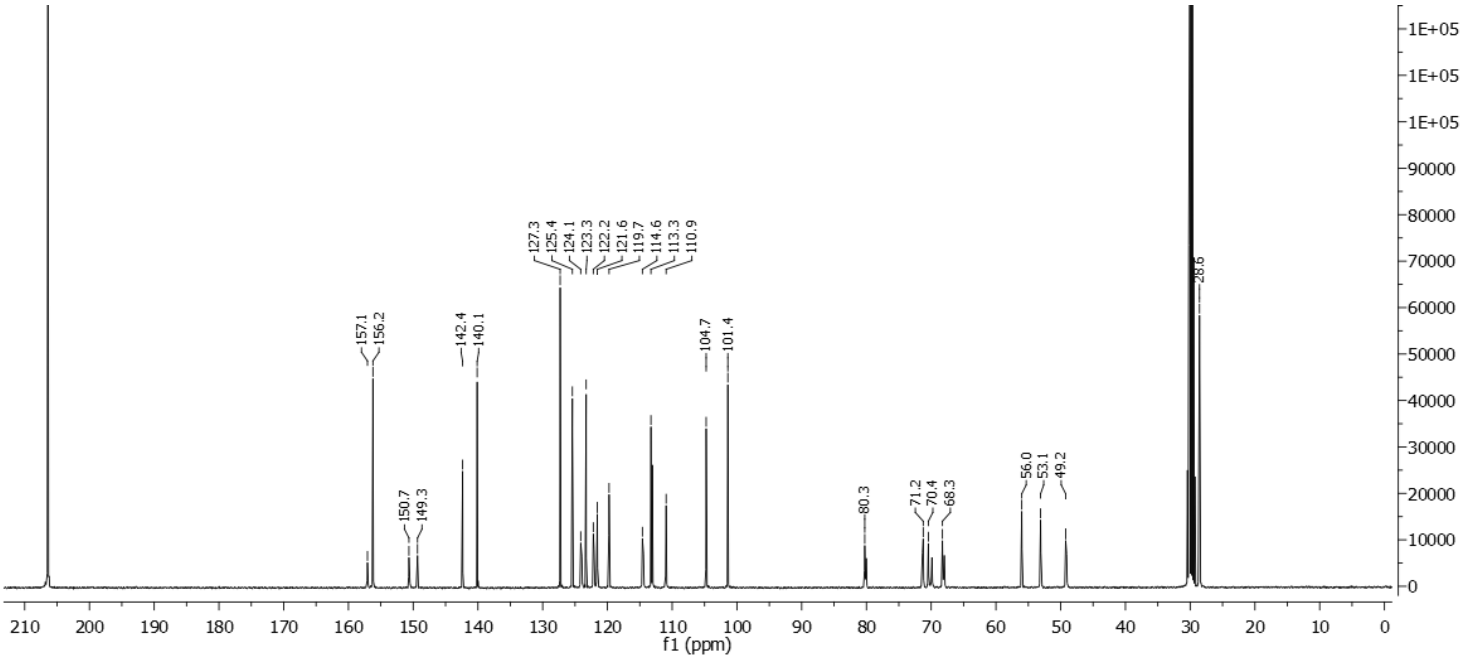

^{13}C-NMR spectrum of *N*-Boc-carvedilol

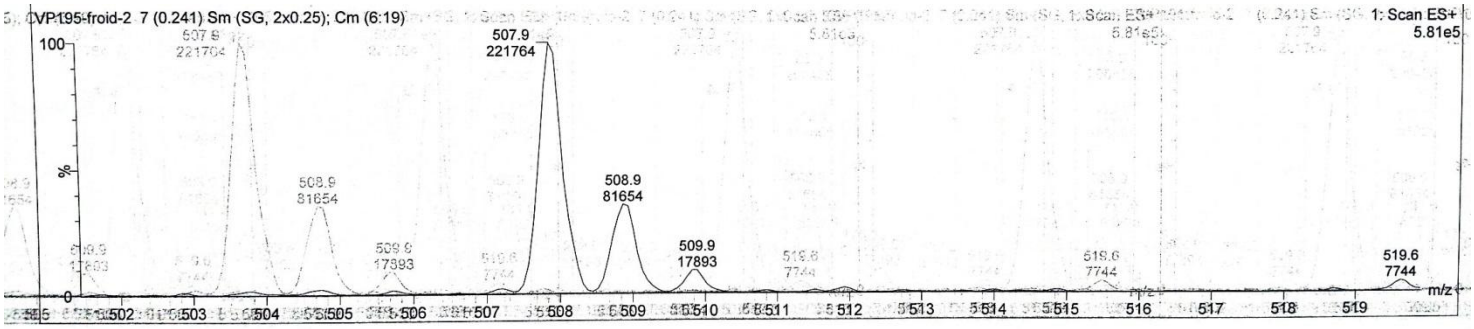

ESI-spectrum of *N*-Boc-carvedilol

Deuterations of oxazoles

2,5-Diphenyloxazole **1**

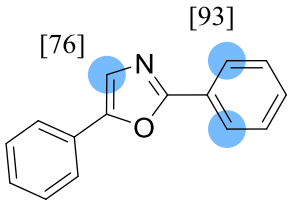

Chemical Formula: $C_{15}H_{11}NO$

Substrate	Solvent (Volume)	RuNp@PVP cat.
44.3mg, 0.2mmol	DMA (1mL)	14.4mg, 5mol%

Workup and purification:

After cooling down to room temperature ethylacetate : cyclohexane (1:1, 3mL) was added to the reaction mixture and stirred for 10min to let precipitate RuNp@PVP. The suspension was passed through a SiO_2 pad and the crude product was eluted with ethylacetate (5mL). The solvent was removed under vacuum and the crude product was purified by HPLC on an Interchim utisphere C18-HDO 5UM 150x21.2mm P REP-LC column. Condition: 1.7mL/min, UV & mass detection, 25°C, Solvents & gradients: Solvent A : H_2O + 0.1% HCOOH; Solvent B : ACN + 0.1% HCOOH

t (0)	95%A 5%B
t(24min)	50%A 50%B

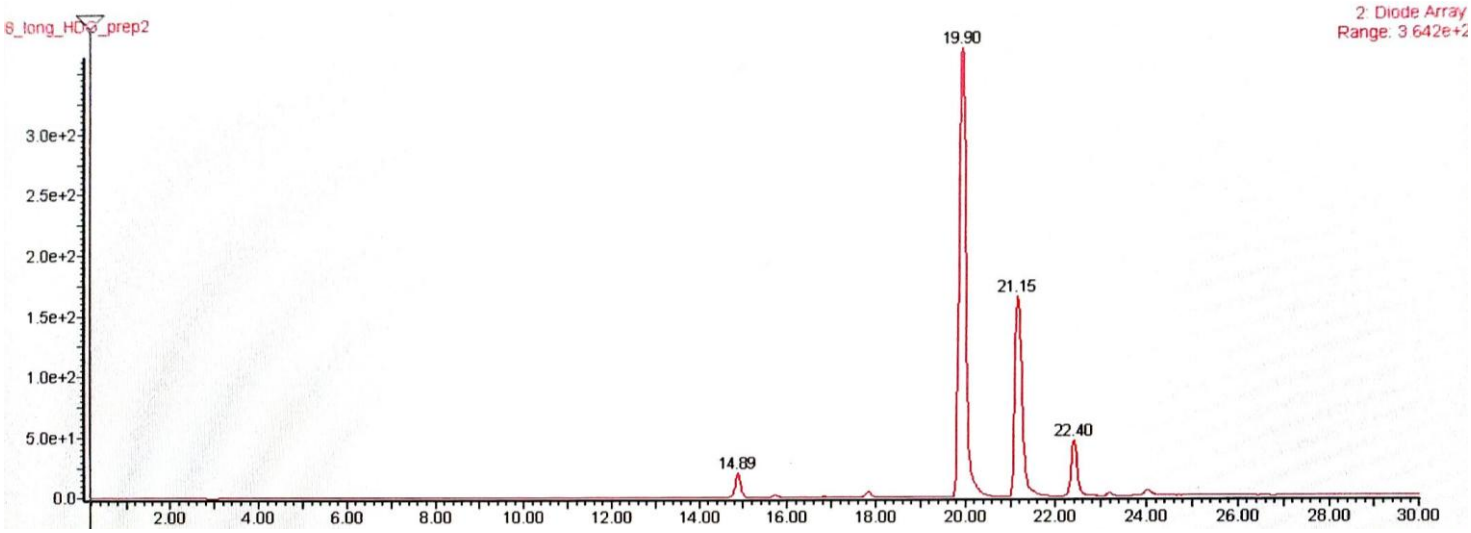

HPLC chromatogram

Yield: 11.0mg, 25%, white solid

^{1}H NMR (400 MHz, Acetone-d_6): δ 8.19 – 8.10 (m, 0.15H), 7.90 – 7.83 (m, 2H), 7.70 (s, 0.24H), 7.60 – 7.47 (m, 5H), 7.42 – 7.36 (m, 1H).

Deuterium incorporation was expected at δ 8.19 – 8.10 and at δ 7.70. Isotopic enrichment values were determined against the integral at δ 7.42 – 7.36.

^{2}H-{^{1}H}NMR (92 MHz, Acetone): δ 8.19 (s, 1.86D), 7.72 (s, 0.76D).

^{13}C-{^{1}H}NMR (100 MHz, Acetone-d_6): δ 161.6, 152.1 (m), 131.3, 129.9, 129.7, 129.3, 128.9, 128.3, 126.9 (m), 125.0, 124.7.

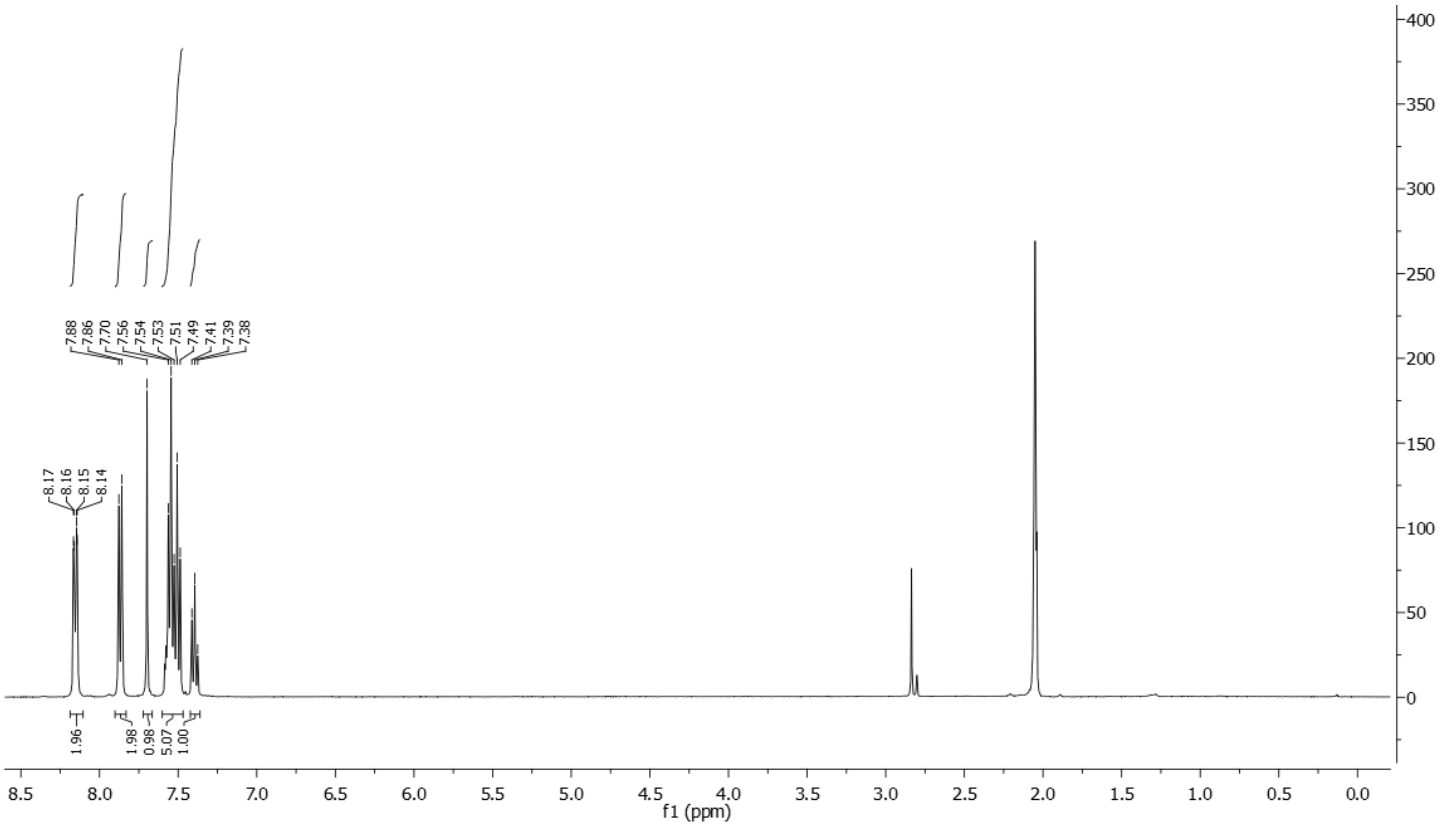

^{1}H-NMR spectrum of the non-deuterated starting material

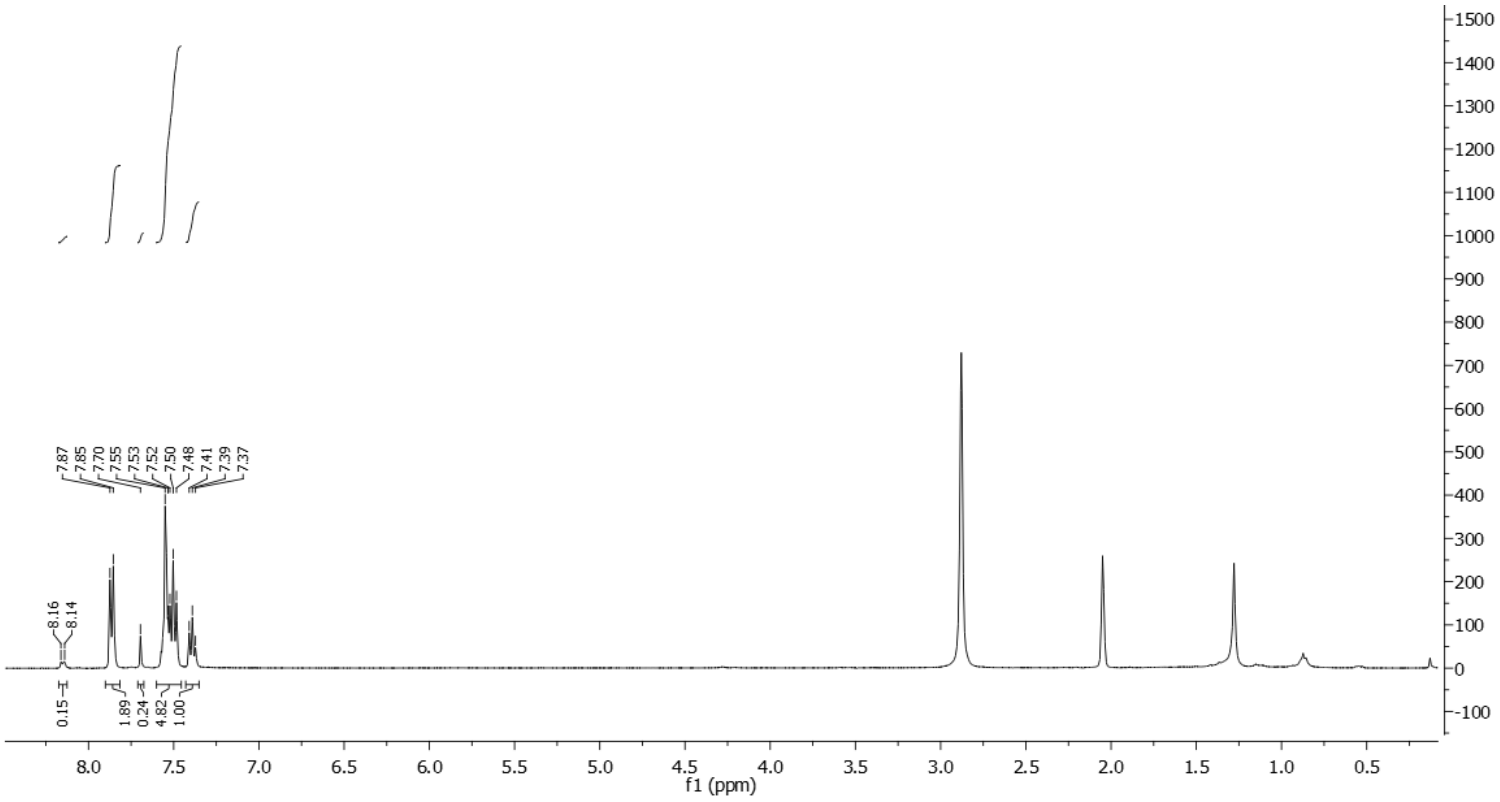

^{1}H-NMR spectrum of **1**

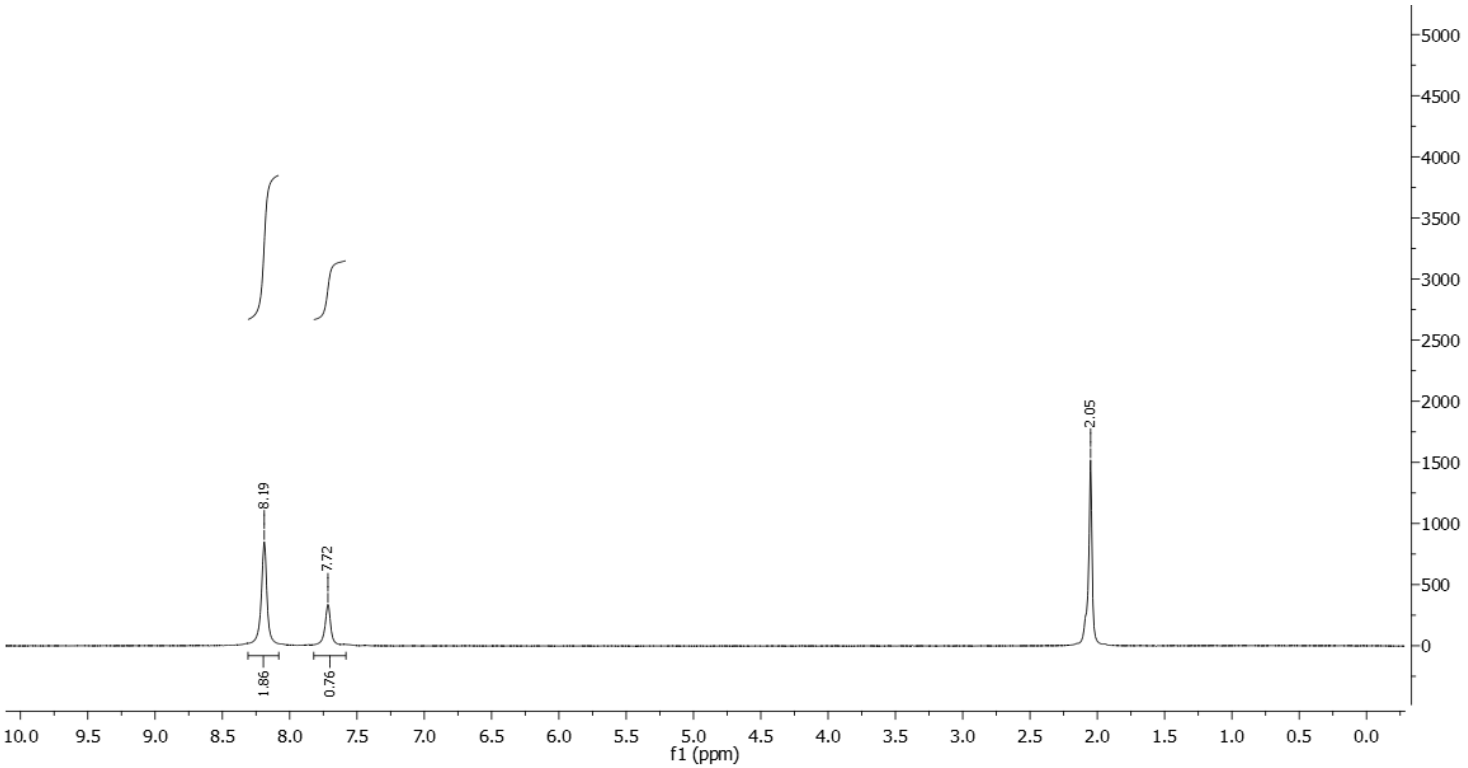

^{2}H-NMR spectrum of **1**

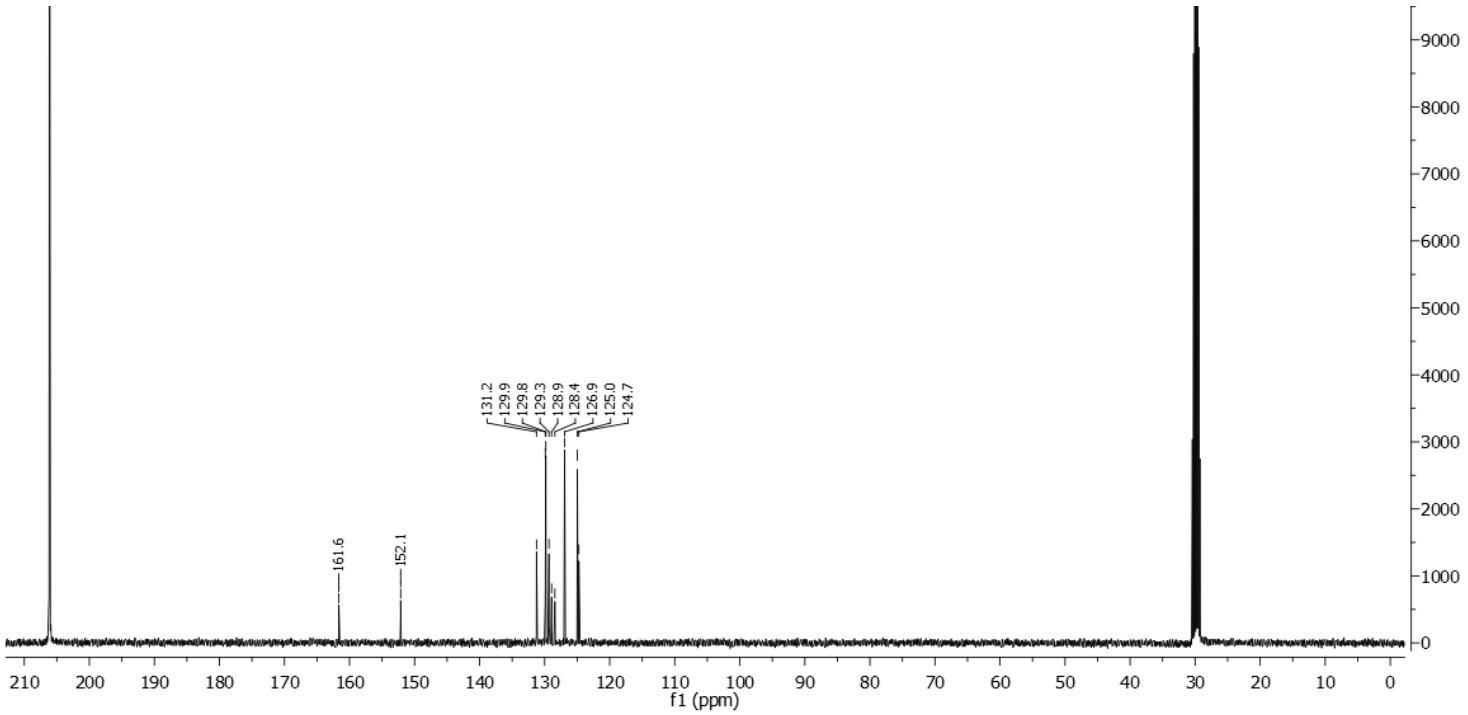

^{13}C-NMR spectrum of the non-deuterated starting material

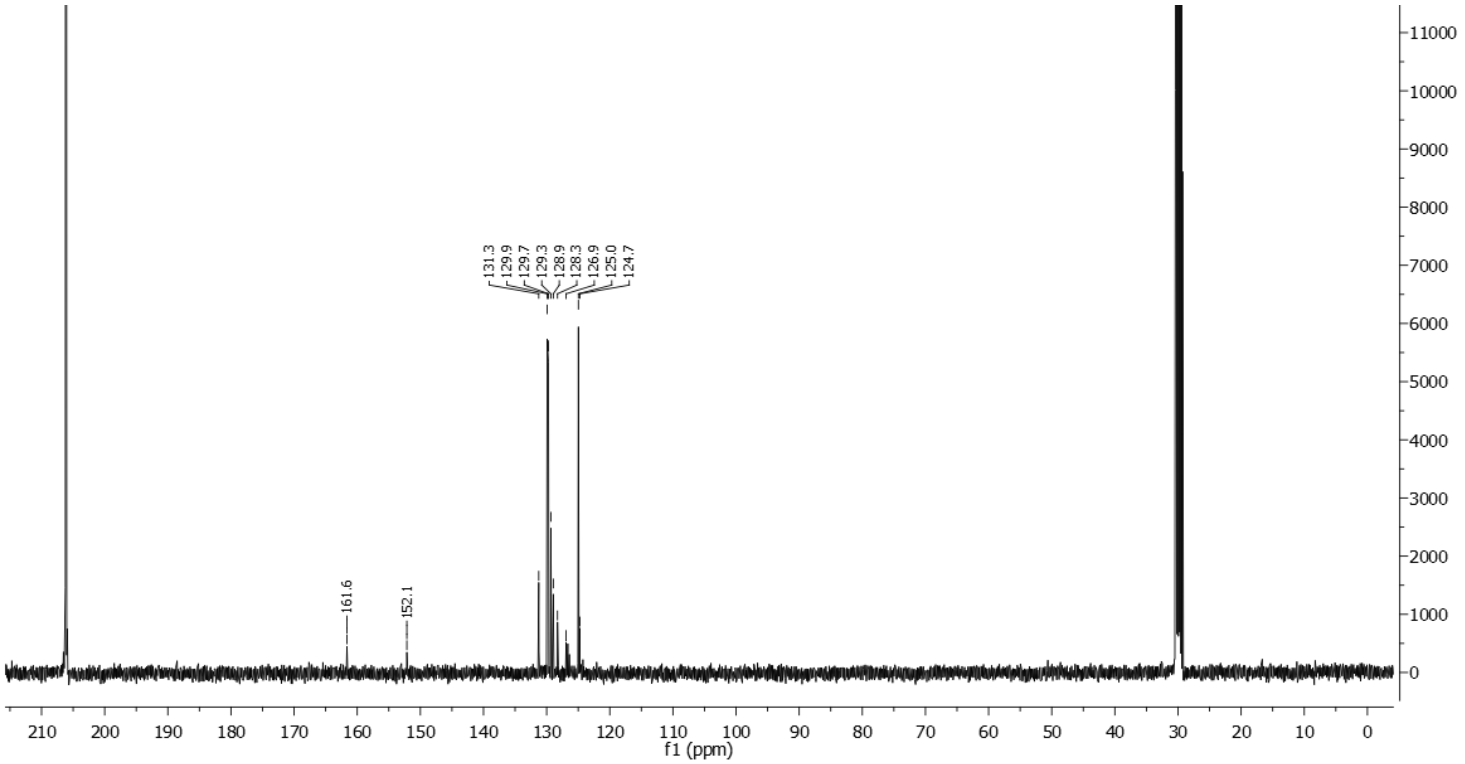

^{13}C-NMR spectrum of **1**

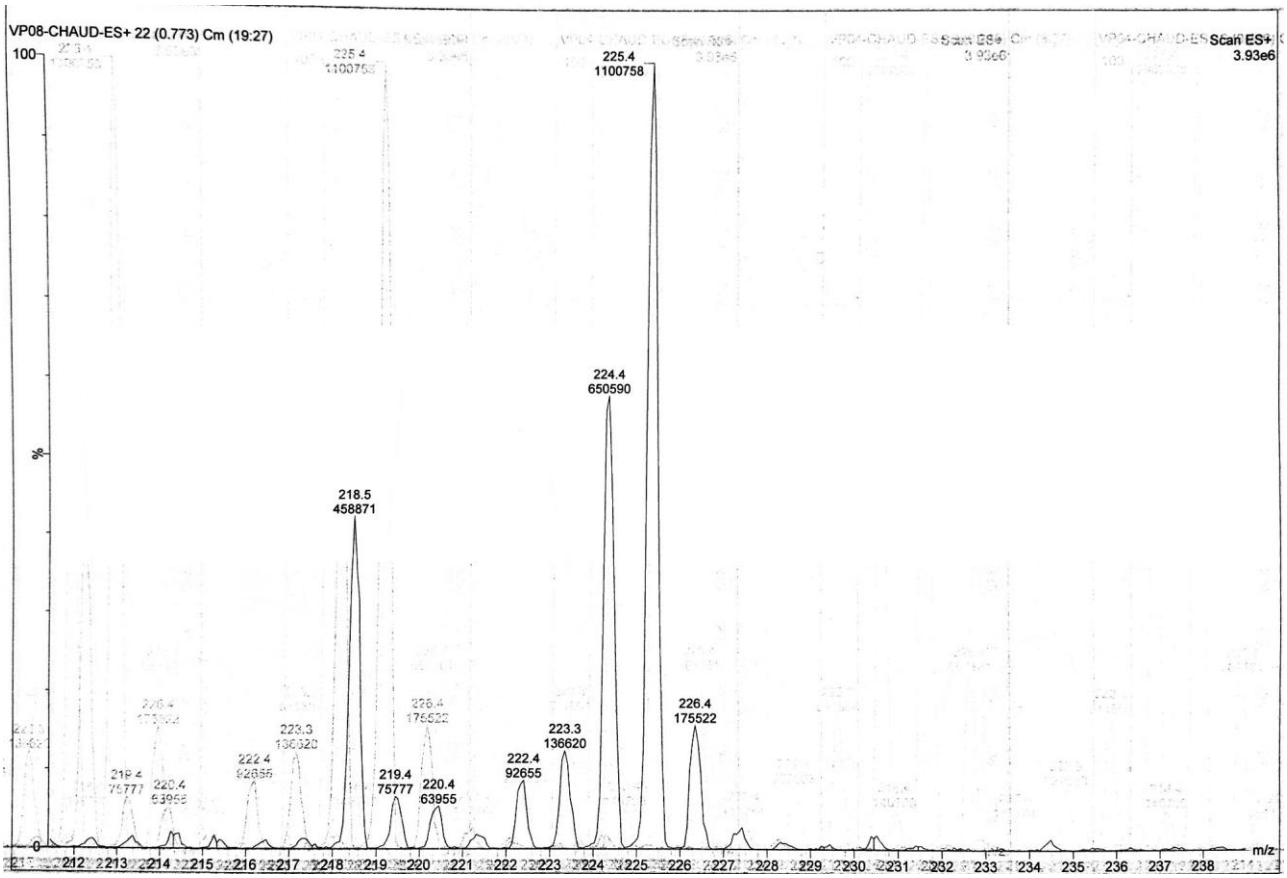

ESI spectrum of **1**

5-(4-Methylphenyl)-oxazole **2**

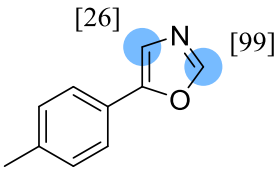

Chemical Formula: $C_{10}H_9NO$

Substrate	Solvent (Volume)	RuNp@PVP cat.
31.8mg, 0.2mmol	THF (2mL)	14.4mg, 5mol%

Workup and purification:

After cooling down to room temperature, cyclohexane (2mL) was added to the reaction mixture and stirred for 10min to let precipitate RuNp@PVP. The suspension was passed through a SiO_2 pad and the product was eluted with ethylacetate (5mL). The solvent was removed under vacuum.

Yield: 25.0mg, 79%, light yellow solid

^{1}H NMR (400 MHz, Acetone-d_6): δ 8.16 (s, 0.01H), 7.73 – 7.57 (m, 2H), 7.49 (s, 0.75H), 7.36 – 7.11 (m, 2H), 2.36 (s, 3H).

Deuterium incorporation was expected at δ 8.16 and at δ 7.49. Isotopic enrichment values were determined against the integral at δ 7.36 – 7.11.

^{2}H-{^{1}H}NMR (92 MHz, Acetone): δ 8.12 (s, 0.99D), 7.47 (s, 0.20D),

^{13}C-{^{1}H}NMR (100 MHz, Acetone-d_6): δ 152.2, 151.4 (m), 139.3, 130.4, 126.2, 125.0, 121.9, 21.2.

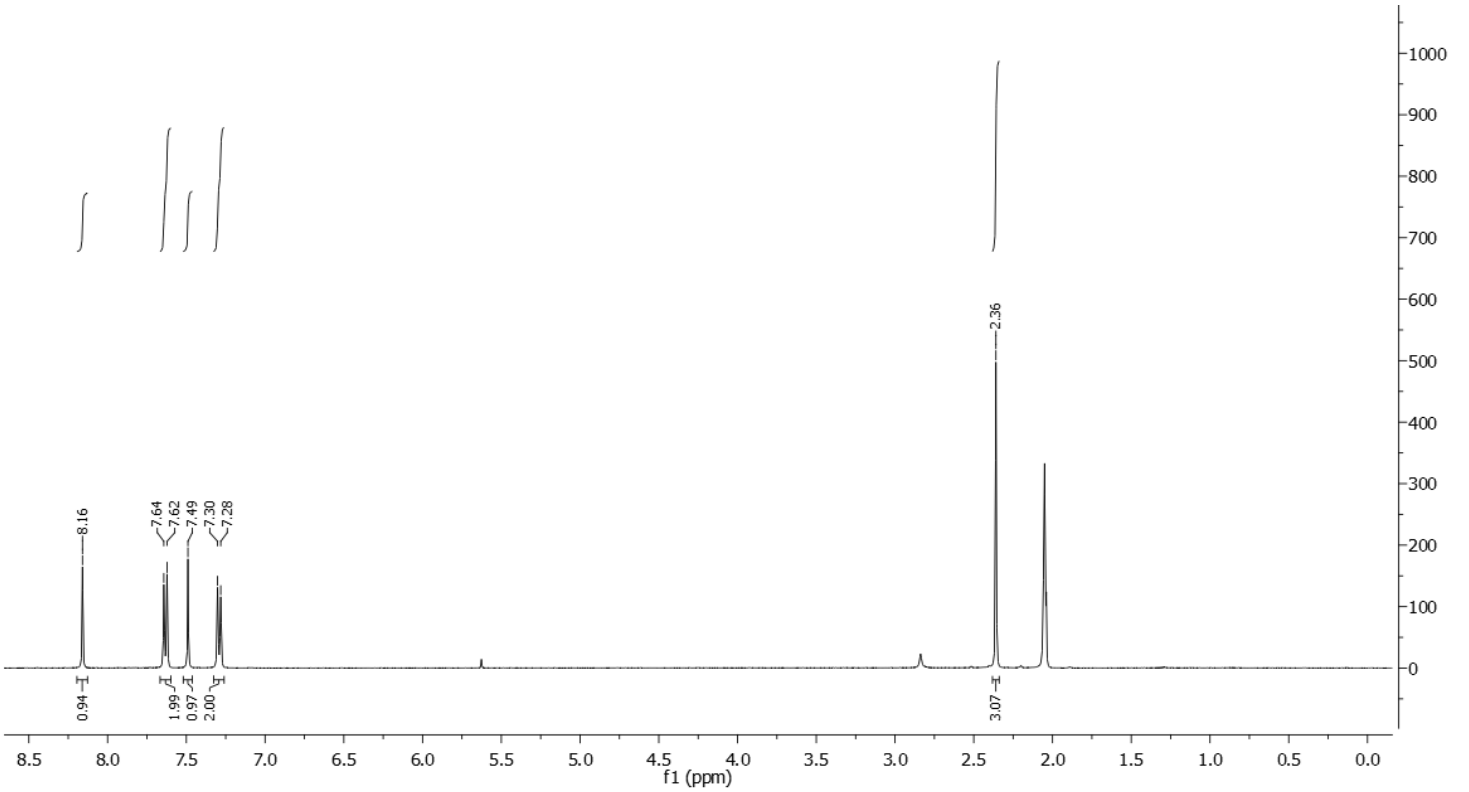

^{1}H-NMR spectrum of the non-deuterated starting material

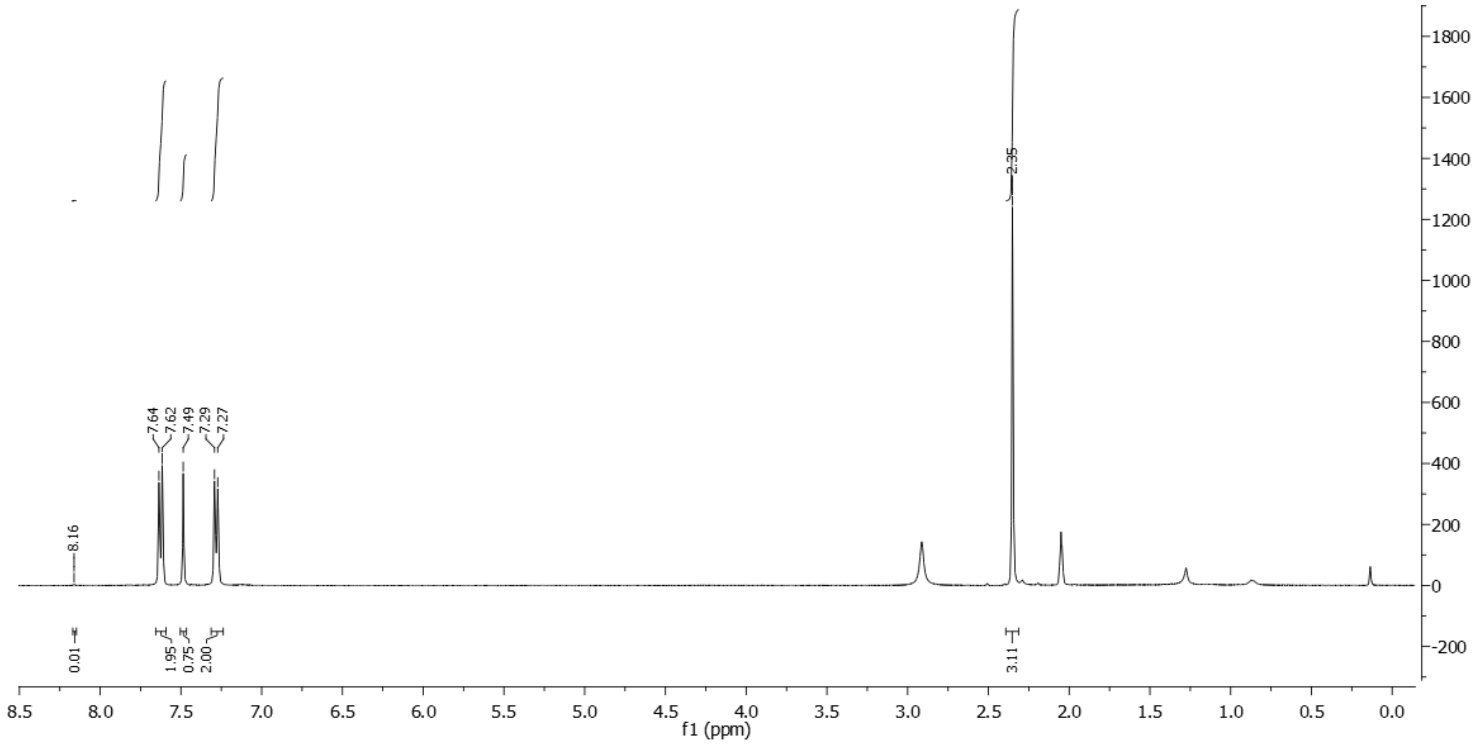

^{1}H-NMR spectrum of **2**

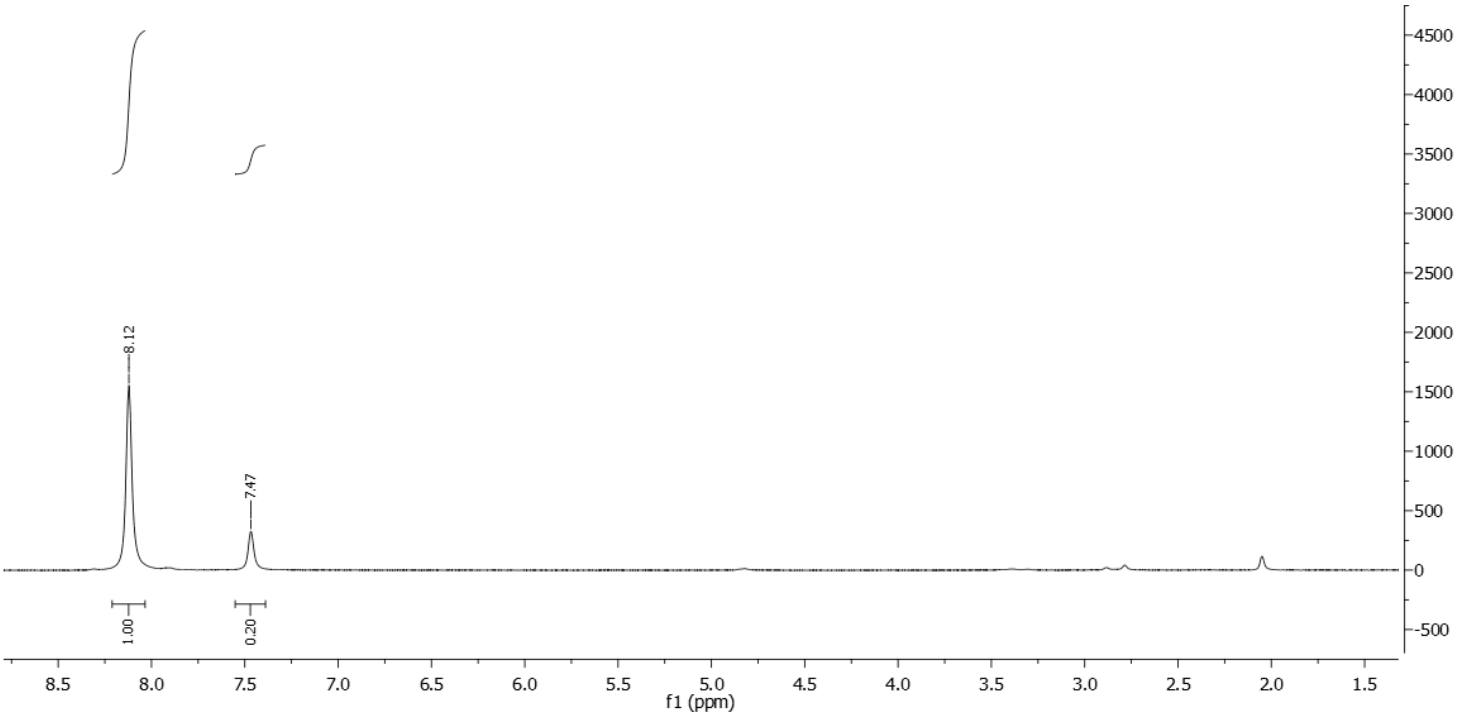

^{2}H-NMR spectrum of **2**

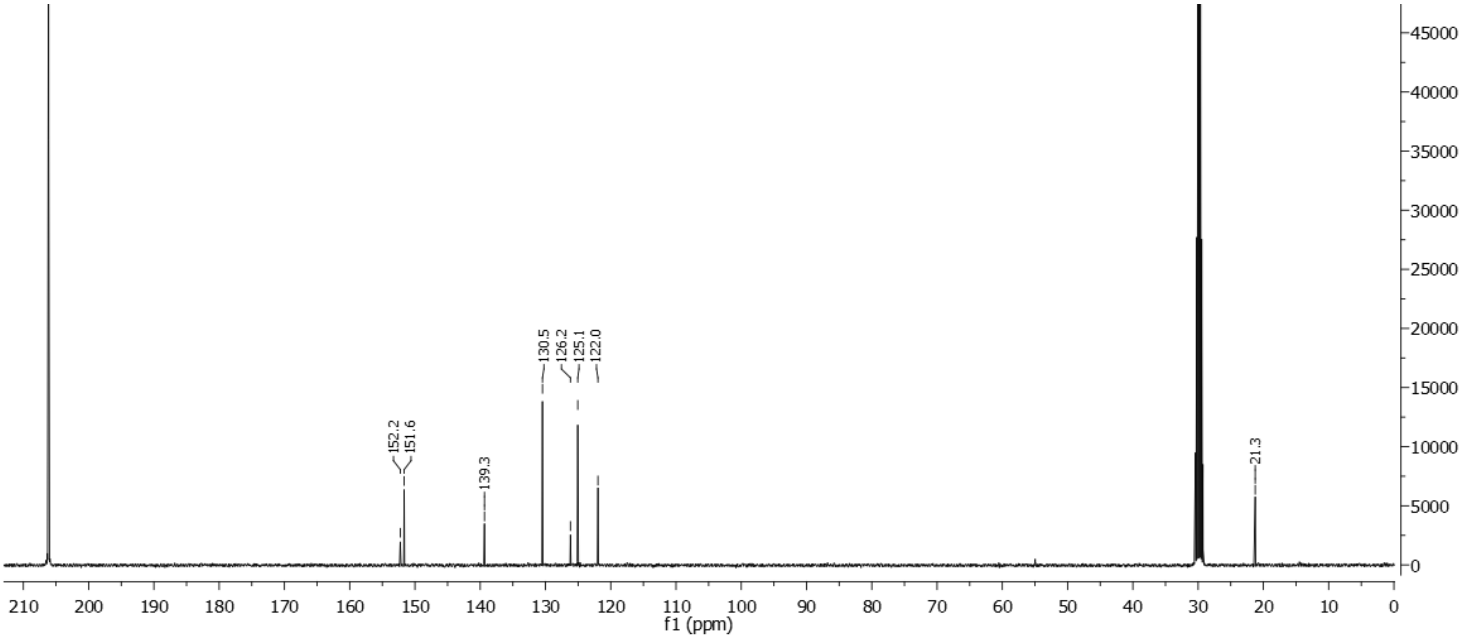

^{13}C-NMR spectrum of the non-deuterated starting material

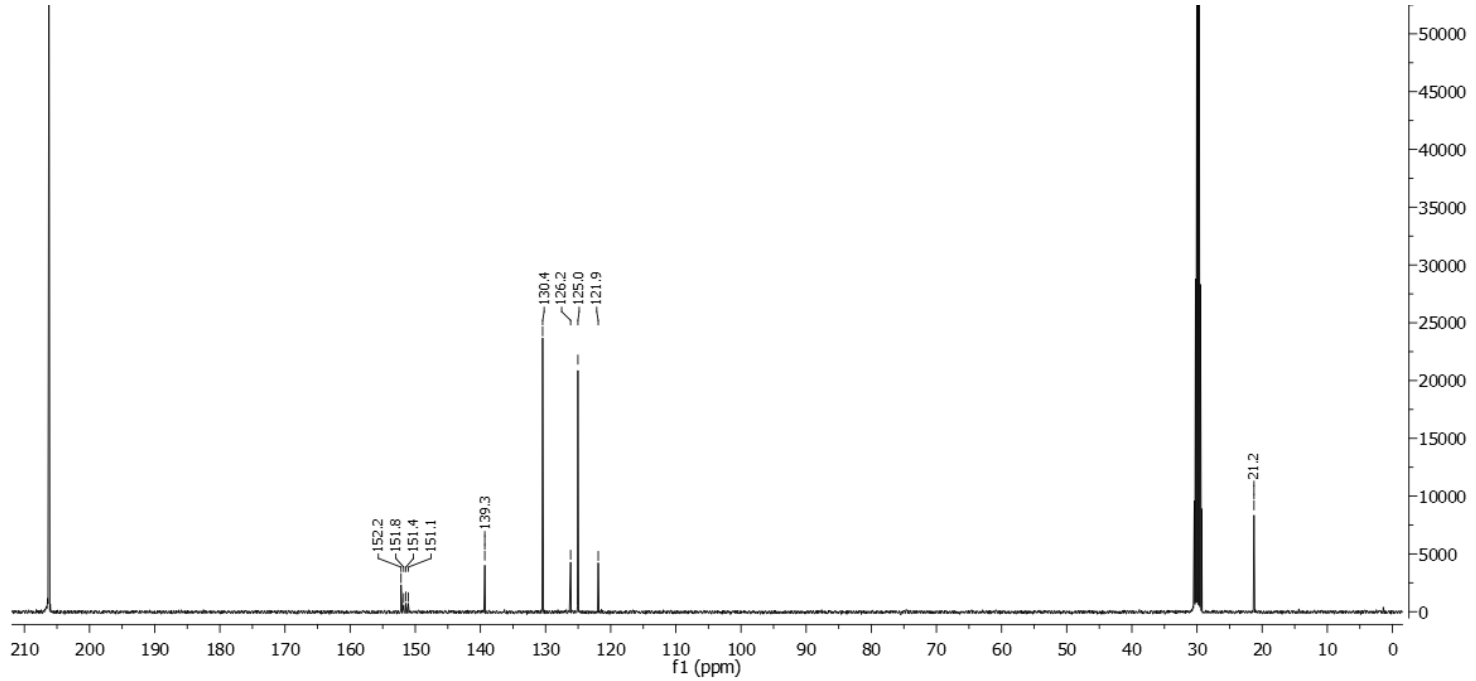

^{13}C-NMR spectrum of **2**

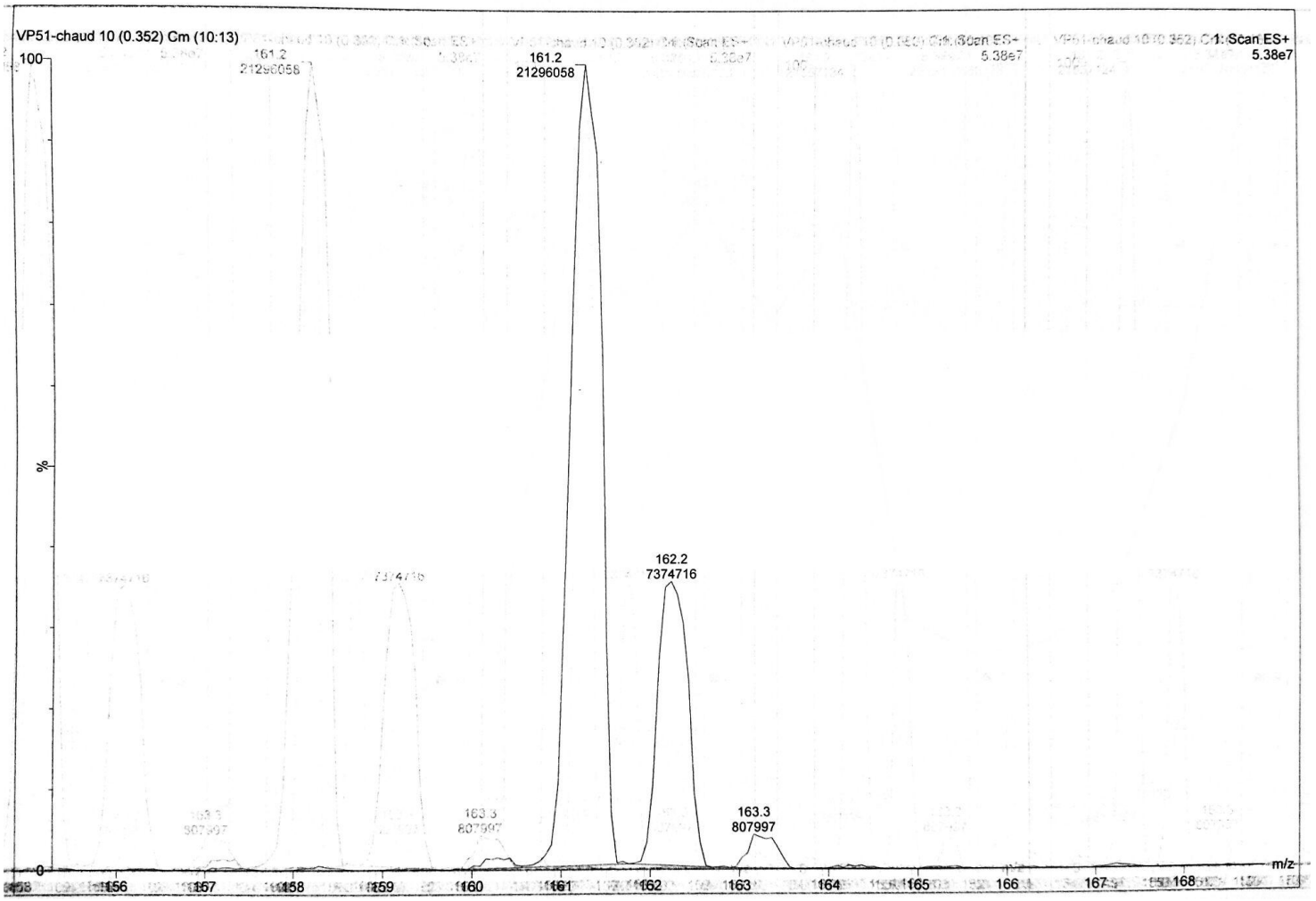

ESI spectrum of **2**

4-(Oxazol-5-yl)aniline **3**

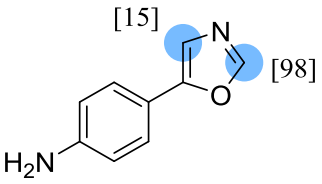

Chemical Formula: $C_9H_8N_2O$

Substrate	Solvent (Volume)	RuNp@PVP cat.
32.0mg, 0.2mmol	DMA (2mL)	14.4mg, 5mol%

Workup and purification:

After cooling down to room temperature, the reaction mixture was poured on a brine solution (50mL) in a separation funnel. The aqueous phase was extracted 3 times with a mixture of ethylacetate and cyclohexane (EtOAc : cyclohexane 3:1; 50mL). The organic phases were combined and dried over $MgSO_4$. The solvent was removed under vacuum.

Yield: 16.0mg, 50%, orange solid

^{1}H NMR (400 MHz, $CDCl_3$): δ 7.83 (s, 0.01H), 7.49 – 7.42 (m, 2H), 7.15 (s, 0.82H), 6.76 – 6.68 (m, 2H), 3.84 (bs, 1H).

Deuterium incorporation was expected at *δ* 7.83 and at *δ* 7.15. Isotopic enrichment values were determined against the integral at *δ* 7.49 – 7.42.

^{2}H-{^{1}H}NMR (92 MHz, $CHCl_3$): δ 7.86 (s, 0.99D), 7.19 (s, 0.18D).

^{13}C-{^{1}H}NMR (100 MHz, $CDCl_3$): δ 147.0, 126.0, 119.2, 118.5, 115.2.

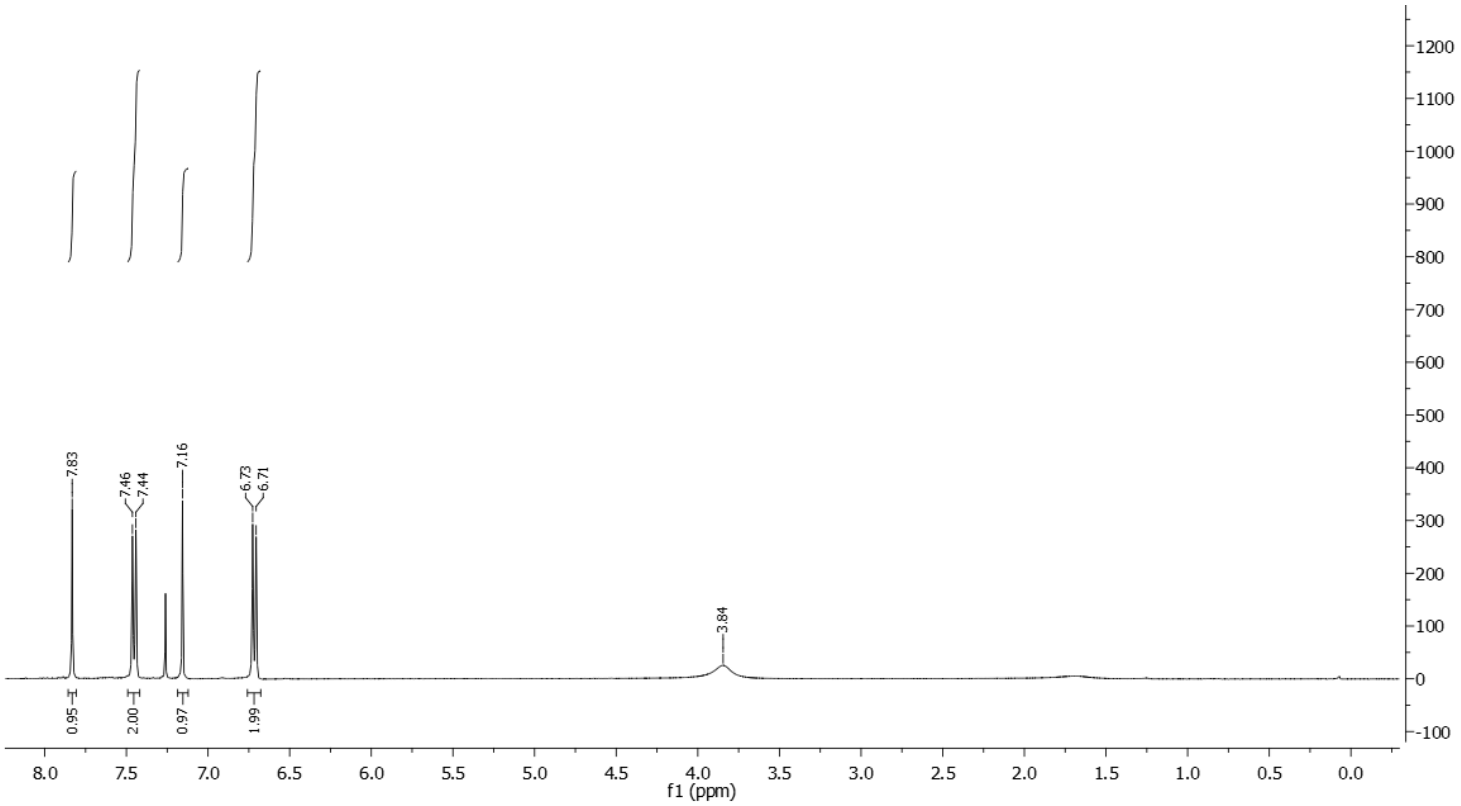

^{1}H-NMR spectrum of the non-deuterated starting material

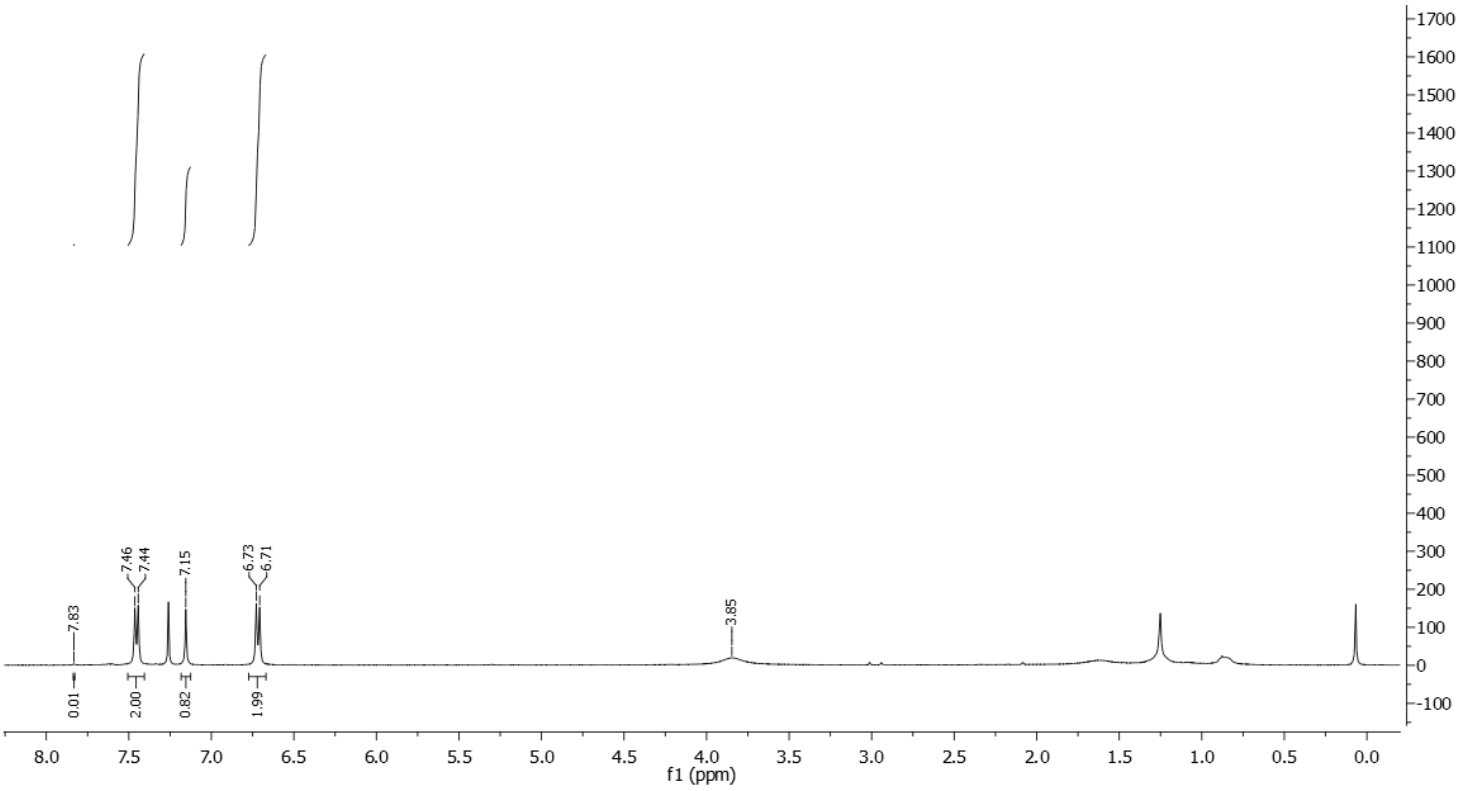

^{1}H-NMR spectrum of **3**

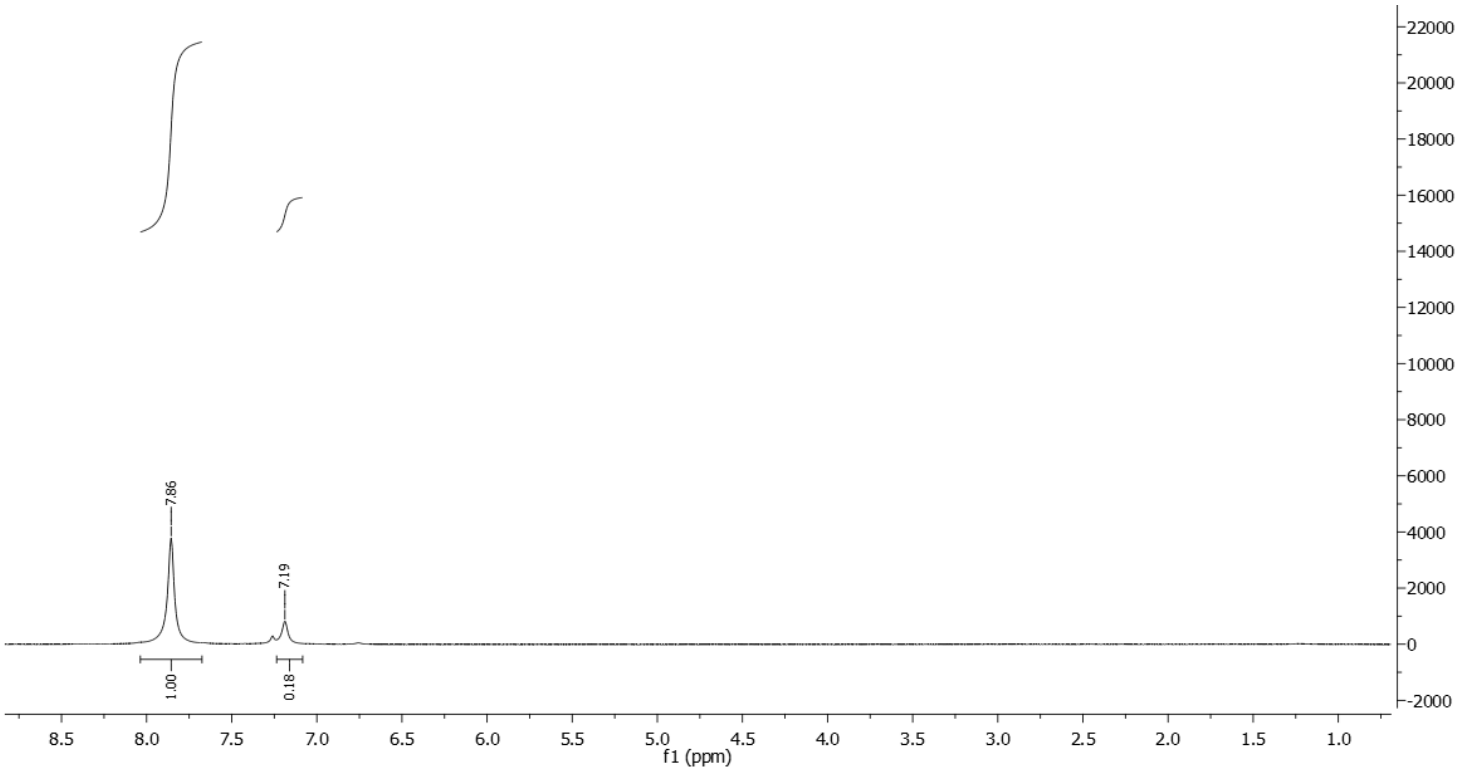

^{2}H-NMR spectrum of **3**

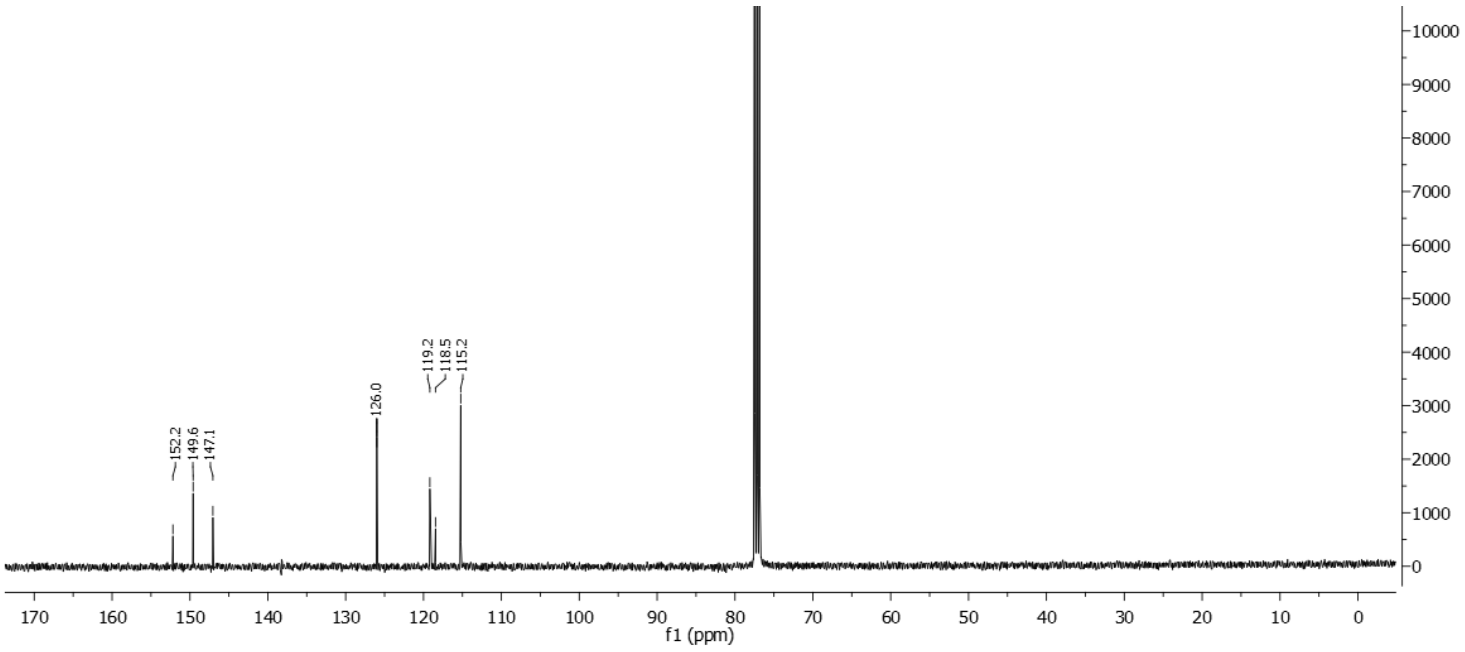

^{13}C-NMR spectrum of the non-deuterated starting material

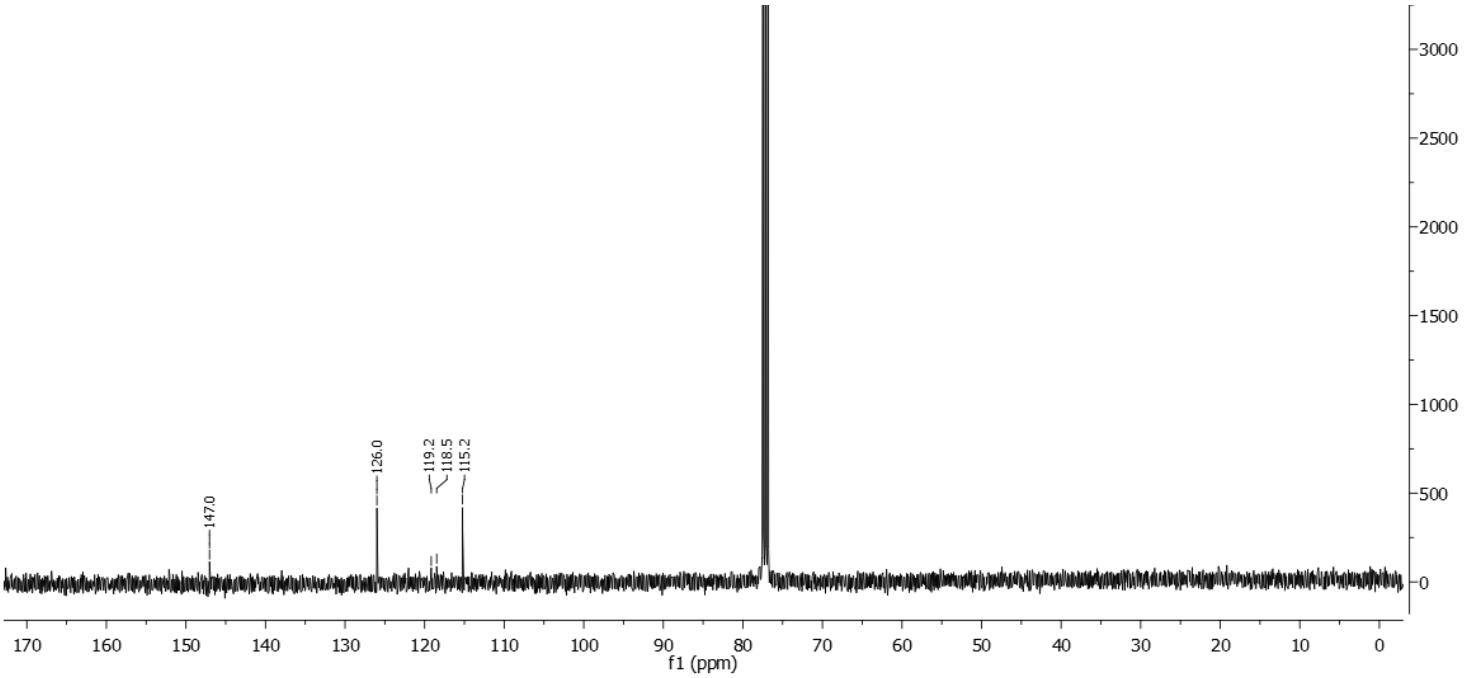

^{13}C-NMR spectrum of **3**

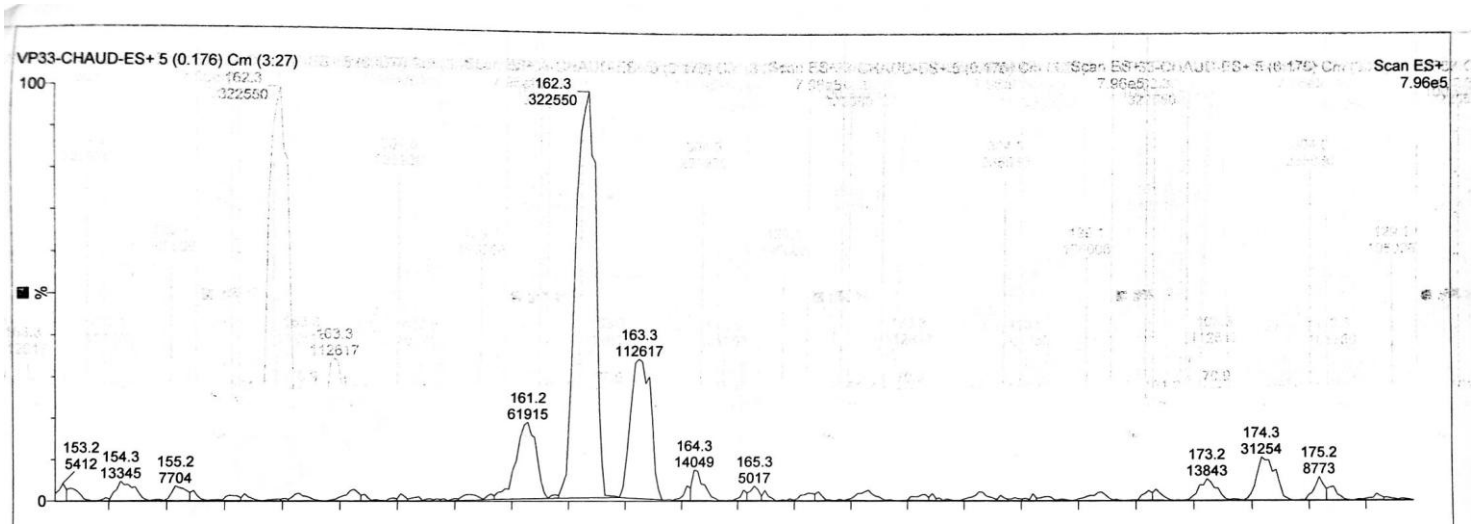

ESI spectrum of **3**

5-(4-Methoxyphenyl)-oxazole-4-carboxylic acid **4**

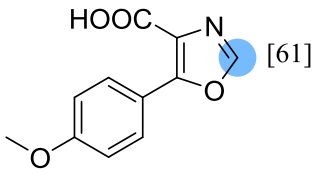

[61]

Chemical Formula: $C_{11}H_9NO_4$

Substrate	Solvent (Volume)	RuNp@PVP cat.
43.8mg, 0.2mmol	DMA (2mL)	14.4mg, 5mol%

Workup and purification:

After cooling down to room temperature, the reaction mixture was poured on a brine solution (50mL) in a separation funnel. The aqueous phase was extracted 3 times with a mixture of ethylacetate and cyclohexane (EtOAc : cyclohexane 3:1; 50mL). The organic phases were combined and dried over $MgSO_4$. The solvent was removed under vacuum.

Yield: 45.0mg, 99%, light yellow solid

^{1}H NMR (400 MHz, Acetone-d_6): δ 8.24 (s, 0.39H), 8.16 – 8.11 (m, 2H), 7.09 – 7.05 (m, 2H), 3.88 (s, 3H).

Deuterium incorporation was expected at δ 8.24. Isotopic enrichment values were determined against the integral at δ 7.09 – 7.05.

^{2}H-{^{1}H}NMR (92 MHz, Acetone): δ 8.19 (s)

^{13}C-{^{1}H}NMR (100 MHz, Acetone-d_6): δ 163.3, 162.2, 155.9, 150.0 (m), 130.9, 126.1, 120.3, 114.7, 55.8.

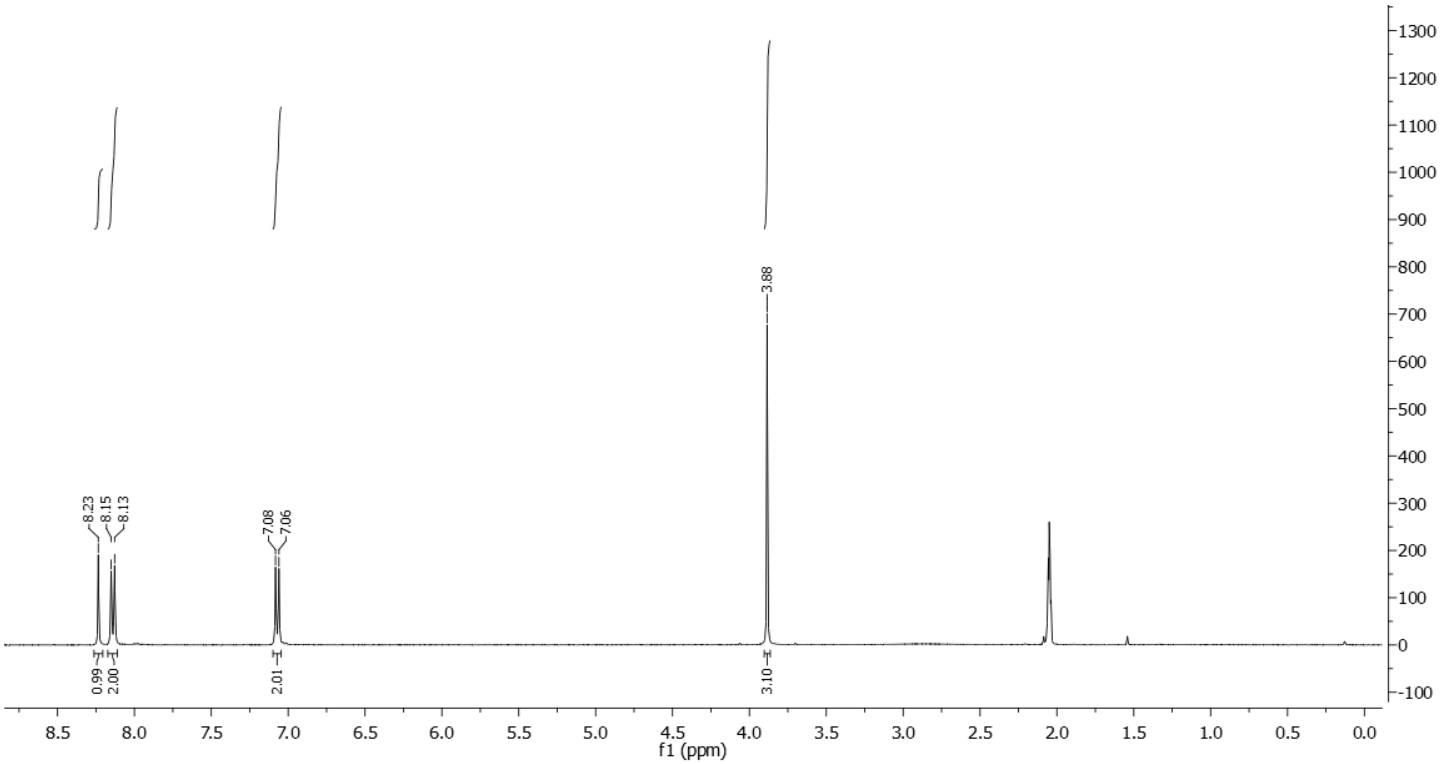

^{1}H-NMR spectrum of the non-deuterated starting material

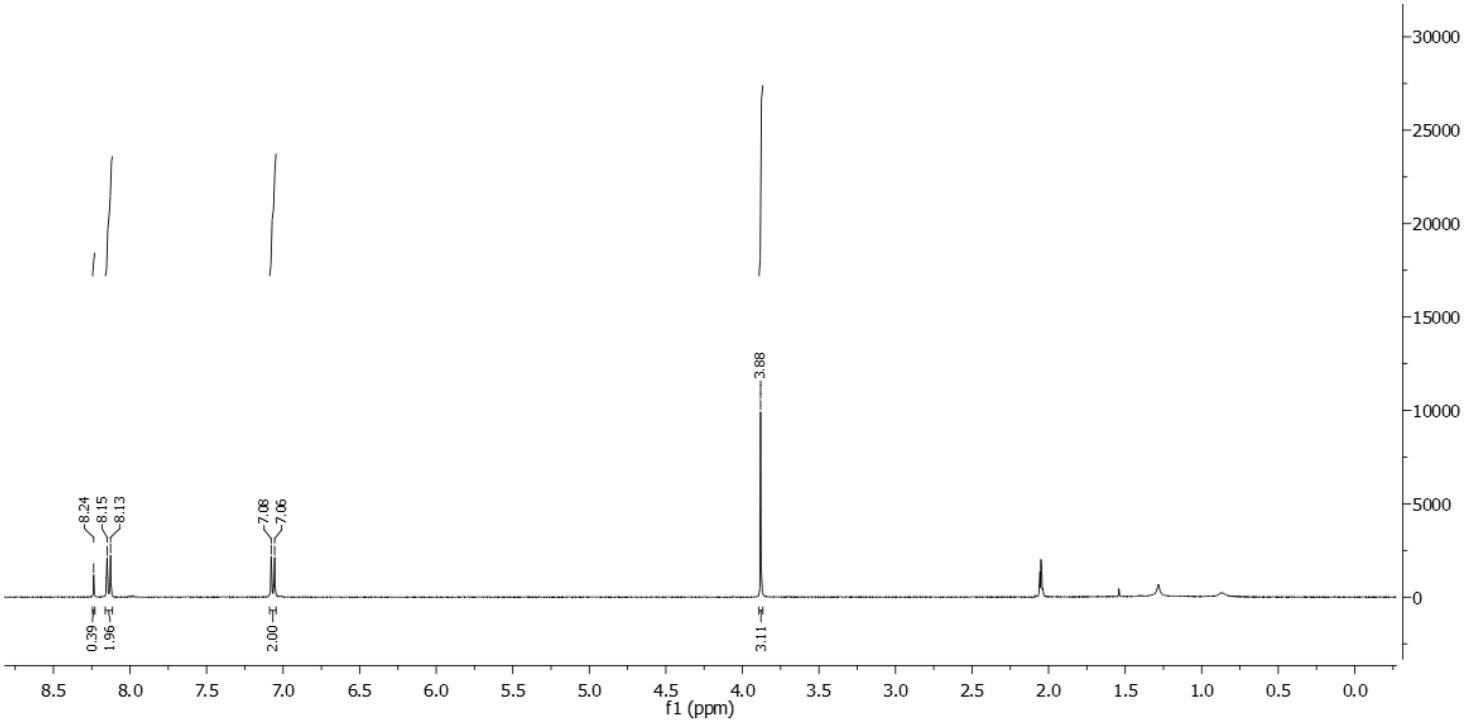

^{1}H-NMR spectrum of **4**

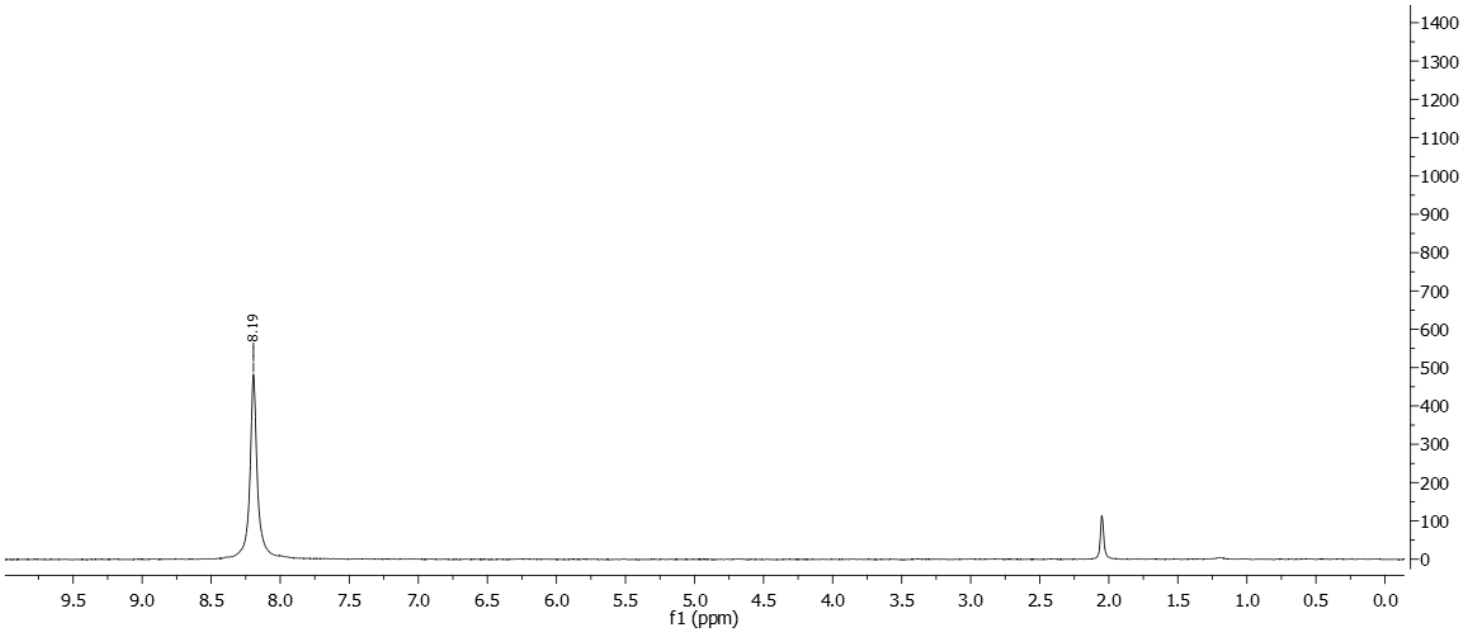

^{2}H-NMR spectrum of **4**

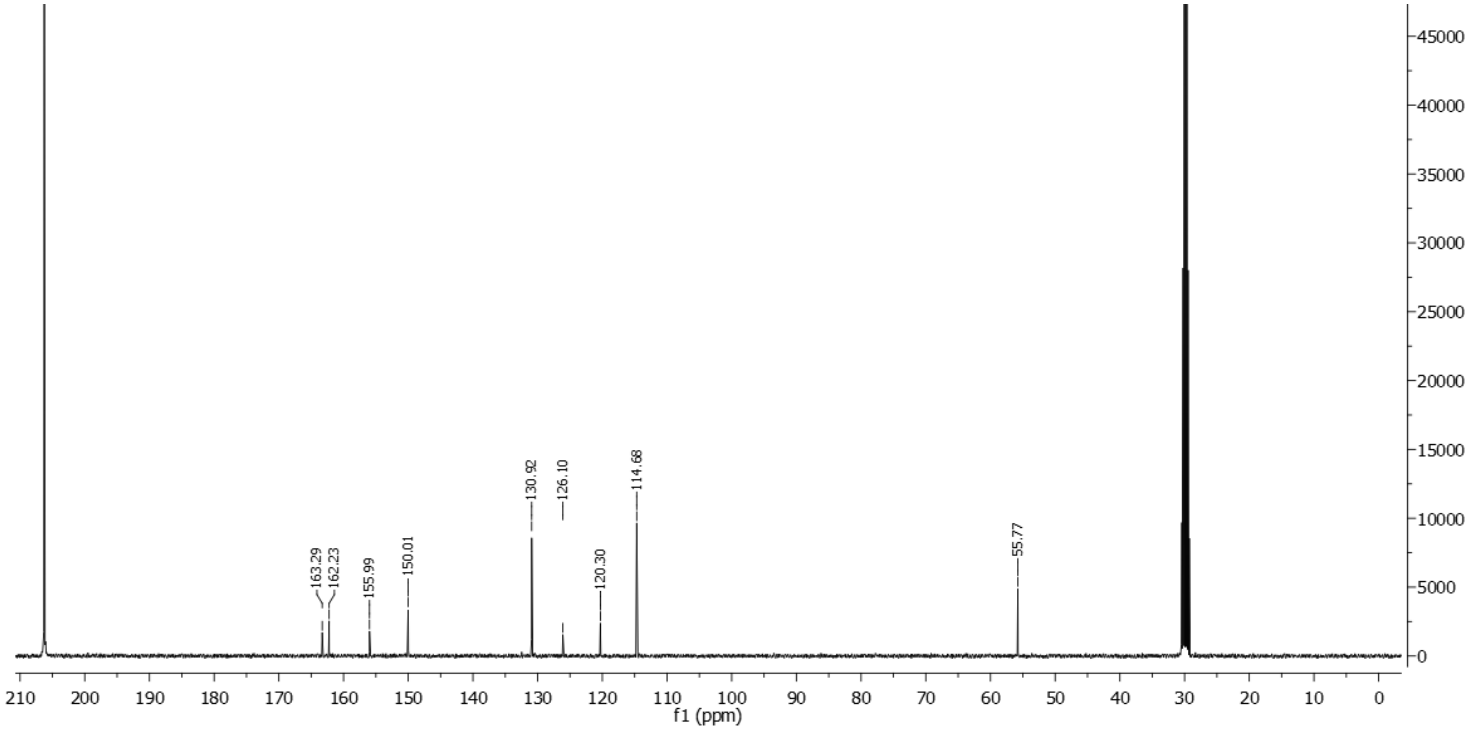

^{13}C-NMR spectrum of the non-deuterated starting material

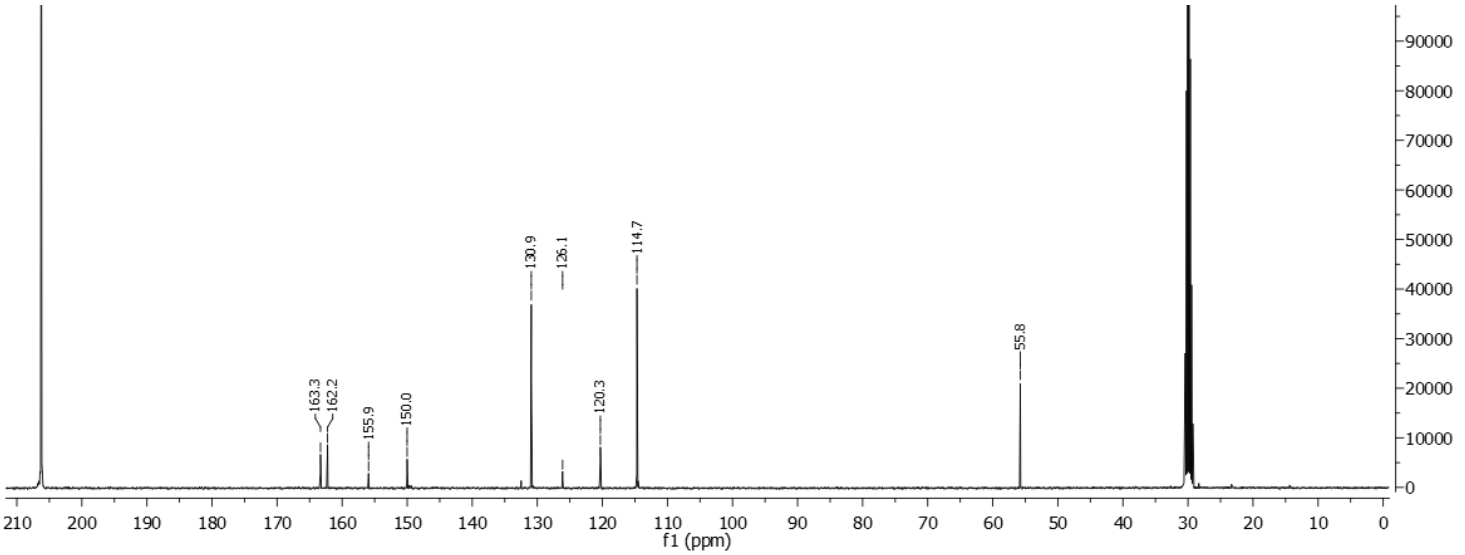

^{13}C-NMR spectrum of **4**

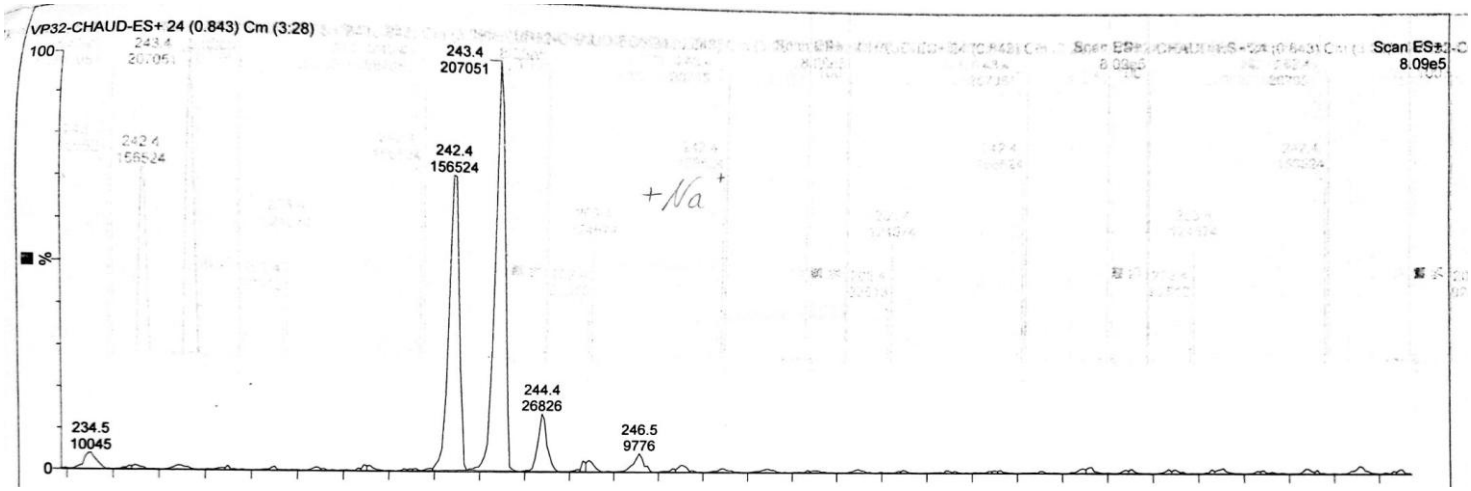

ESI spectrum of **4**

Deuterations of imidazoles

2-Phenylimidazole **5**

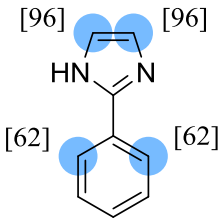

Chemical Formula: $C_9H_8N_2$

Substrate	Solvent (Volume)	RuNp@PVP cat.
28.8mg, 0.2mmol	THF (2mL)	14.4mg, 5mol%

Workup and purification:

After cooling down to room temperature, cyclohexane (2mL) was added to the reaction mixture and stirred for 10min to let precipitating RuNp@PVP. The suspension was passed through a pad of neutral Al_2O_3 and then eluted with ethylacetate (5mL). The solvent was removed under vacuum to obtain 31.0mg of crude product. The crude product (10mg) was purified by HPLC on an XBridge Prep Phenyl 5µm OBD 19x150mm column. Condition: 1mL/min, UV & mass detection, 25°C, Solvents & gradients: Solvent A : H_2O + 0.1% HCOOH; Solvent B : MeOH + 0.1% HCOOH

t (0)	95%A 5%B
t(24min)	50%A 50%B

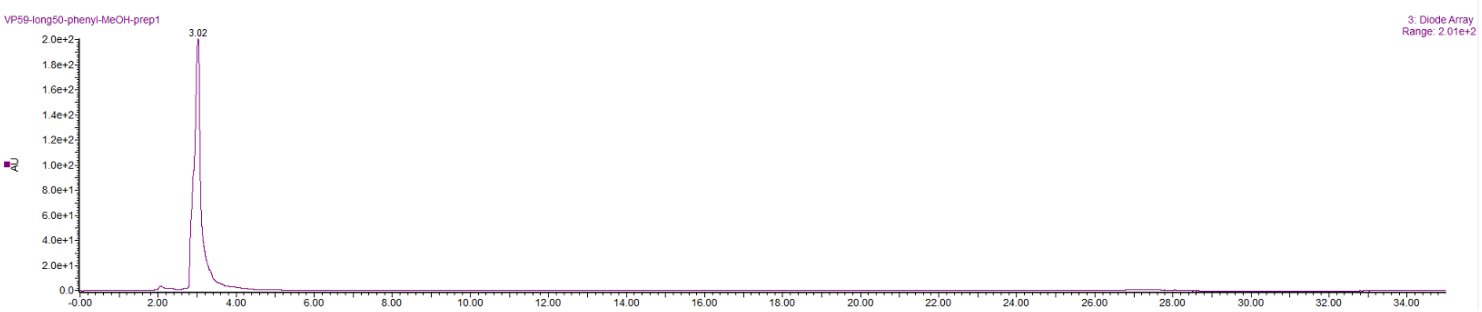

HPLC chromatogram

The obtained formiate salt was dissolved in methanol (1mL) and an aqueous K_2CO_3-solution (0.03M, 1mL) was added under stirring. The mixture was poured in H_20 dist. (50mL) in a separation funnel and extracted 3 times with ethylacetate (50mL). The organic phases were combined and the solvent was removed under vacuum. The neutralized product was purified on neutral Al_2O_3, where it could be eluted with EtOAc/cyclohexane (3:1).

Yield: 3.0mg, 30%, white solid

^{1}H NMR (400 MHz, Acetone-d_6): δ 11.64 (bs, NH), 8.01 – 7.96 (m, 0.79H), 7.46 – 7.40 (m, 2H), 7.36 – 7.30 (m, 1H), 7.20 (s, 0.04H), 7.06 (s, 0.04H).

Deuterium incorporation was expected at δ 8.01 – 7.96, δ 7.20 and δ 7.06. Isotopic enrichment values were determined against the integral at δ 7.36 – 7.30.

^{2}H-{^{1}H}NMR (92 MHz, Acetone): δ 7.98 (s, 1.24D), 7.14 (s, 1.92D)

^{13}C-{^{1}H}NMR (100 MHz, Acetone-d_6): δ 129.4 (m), 128.8, 125.8.

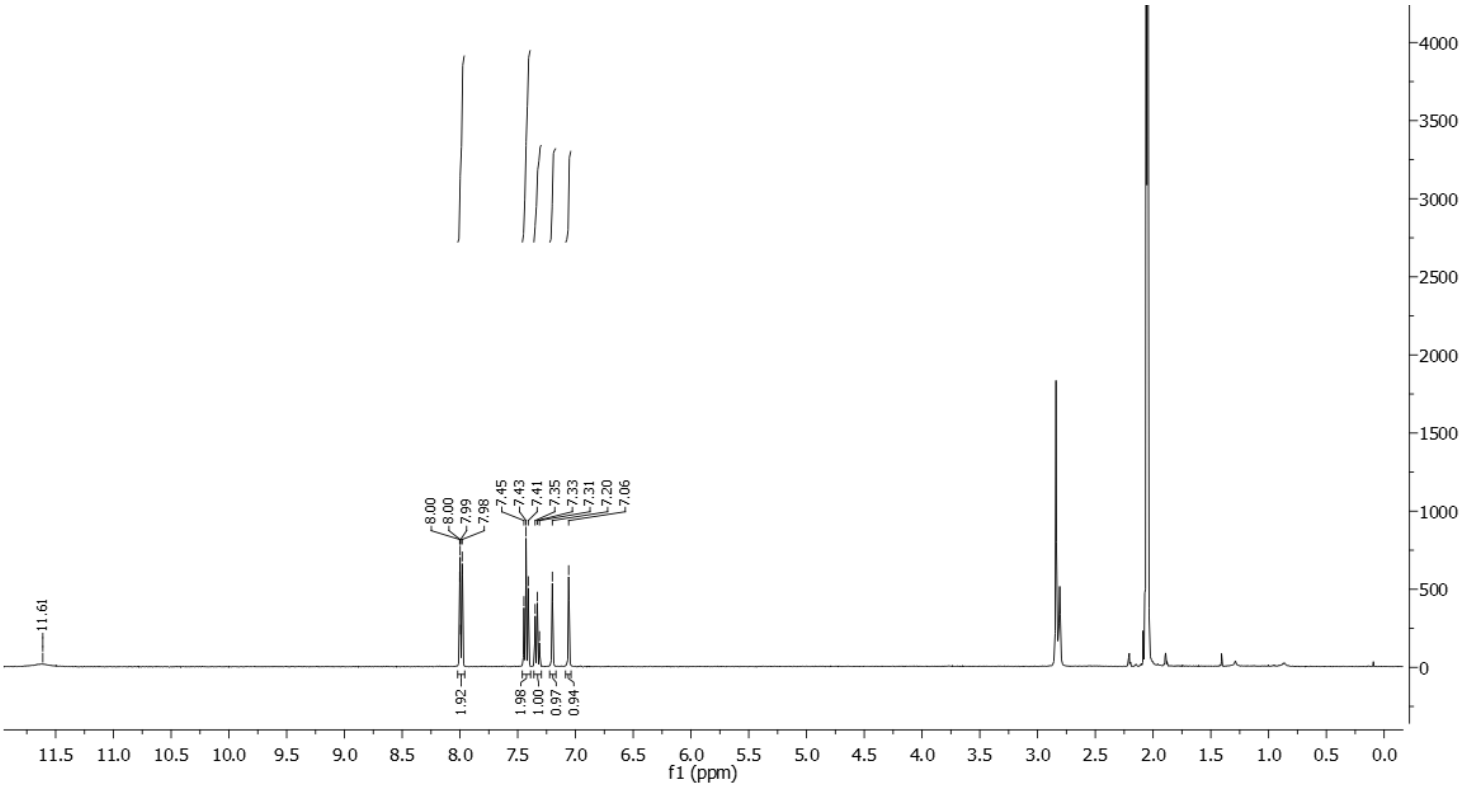

^{1}H-NMR spectrum of the non-deuterated starting material

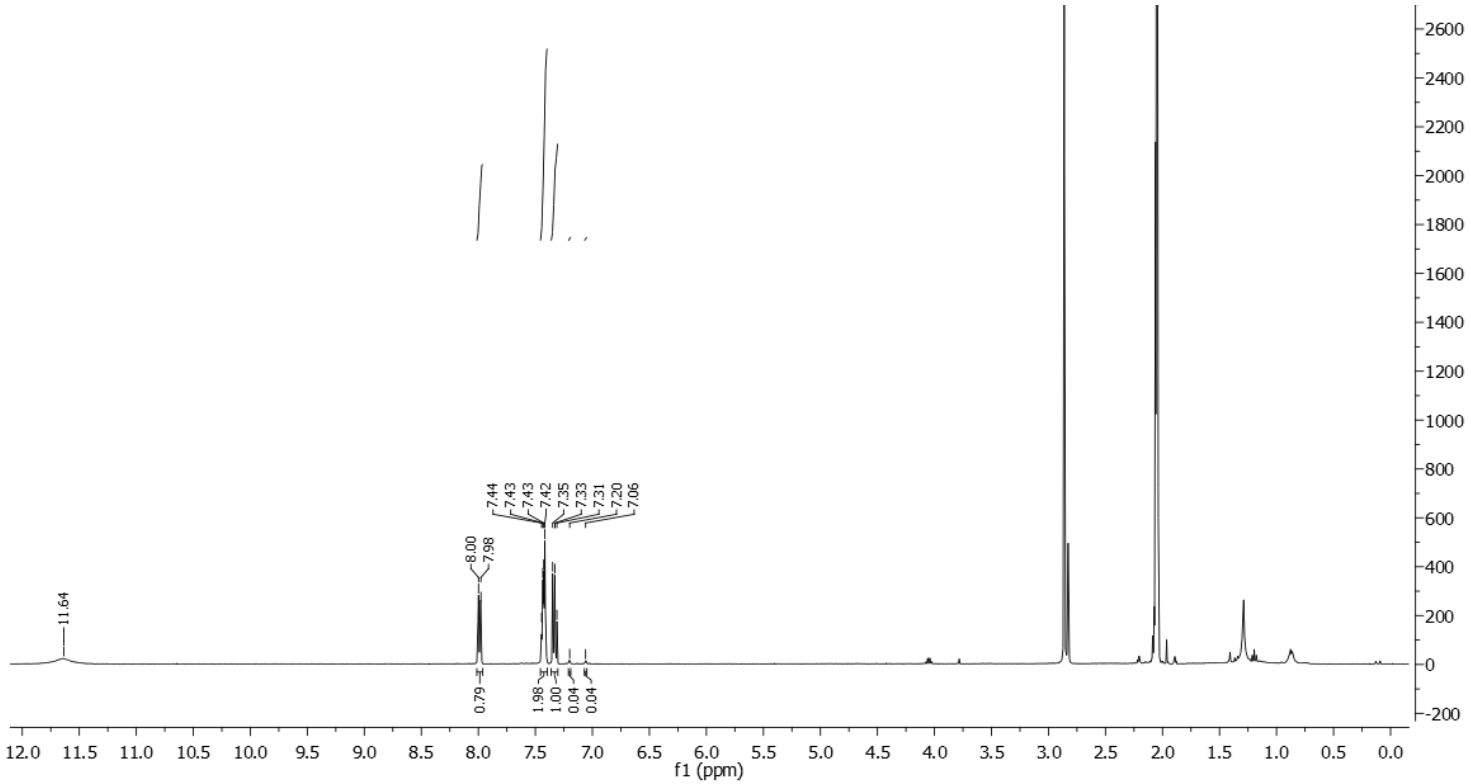

^{1}H-NMR spectrum of **5**

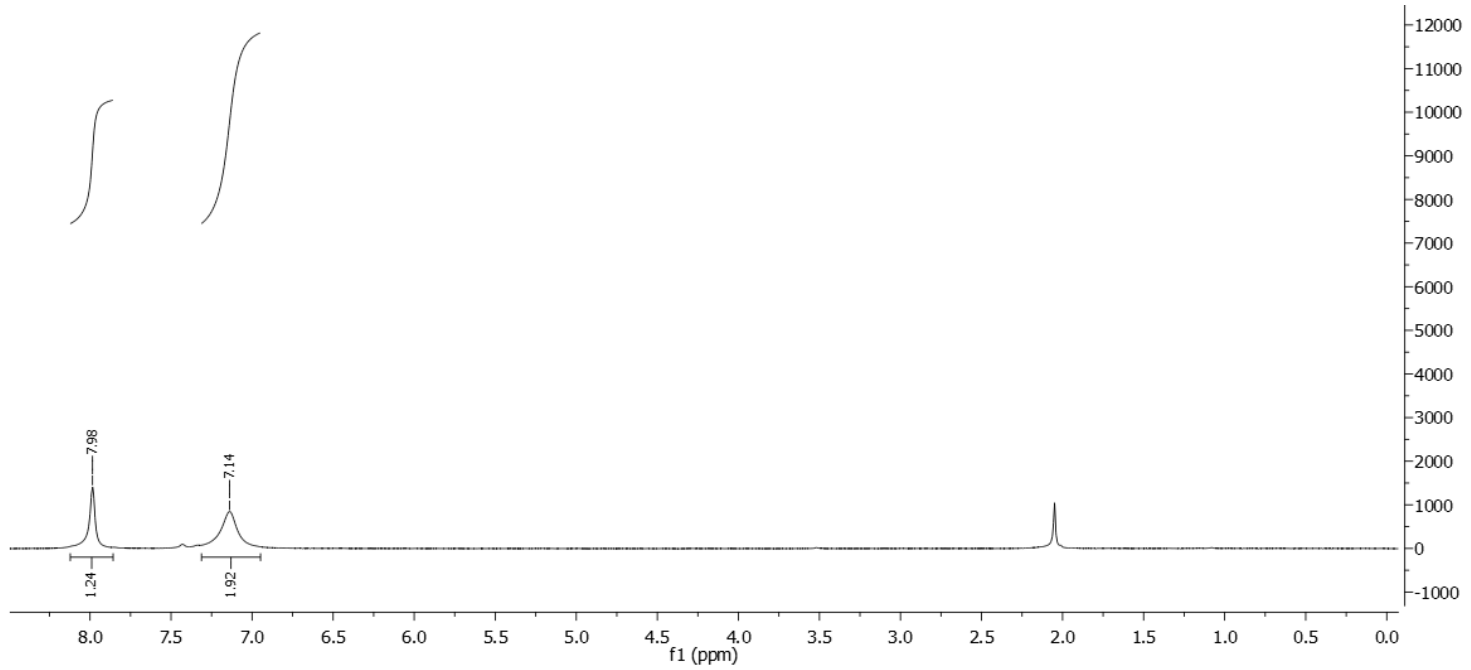

^{2}H-NMR spectrum of **5**

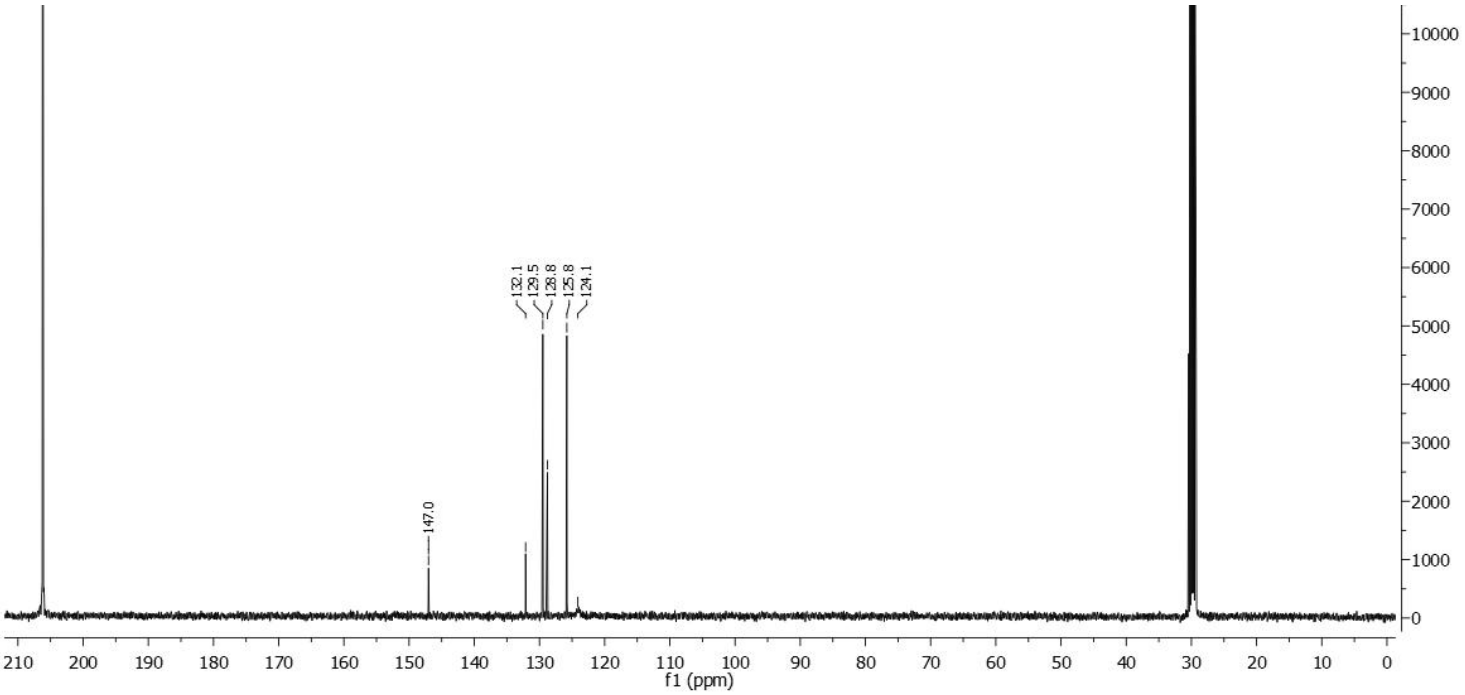

^{13}C-NMR spectrum of the non-deuterated starting material

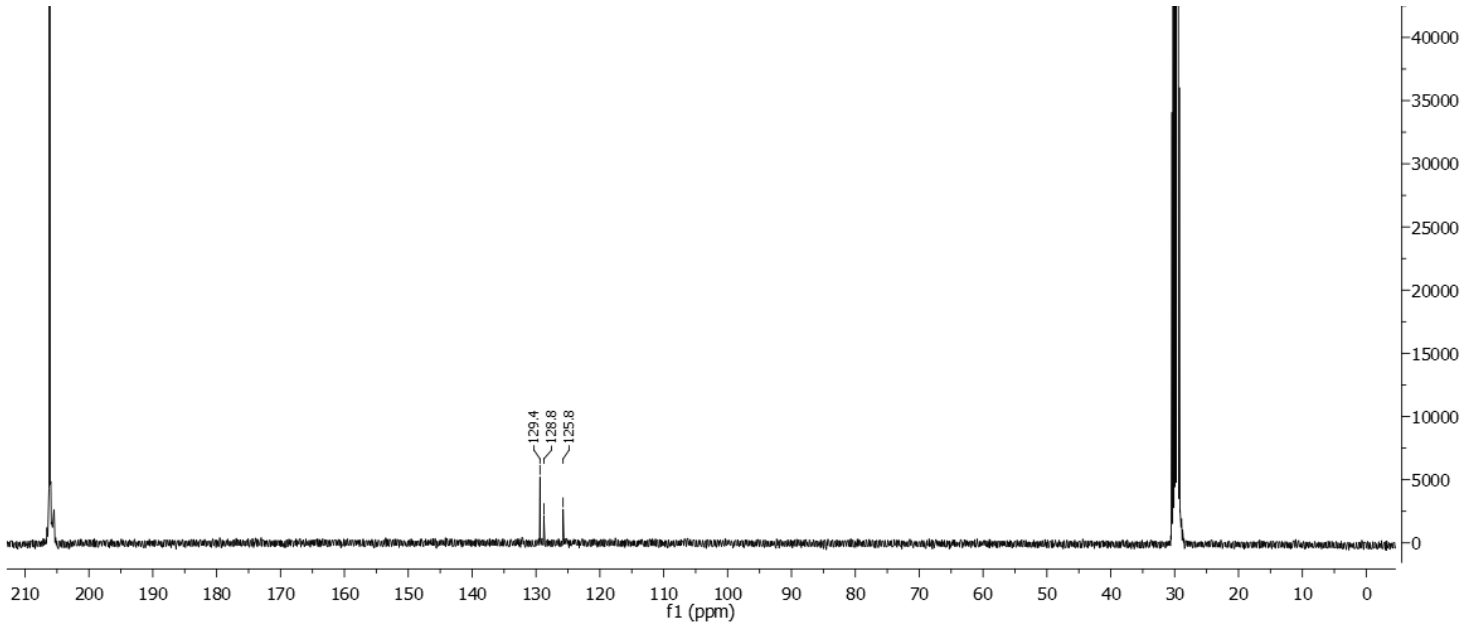

^{13}C-NMR spectrum of **5**

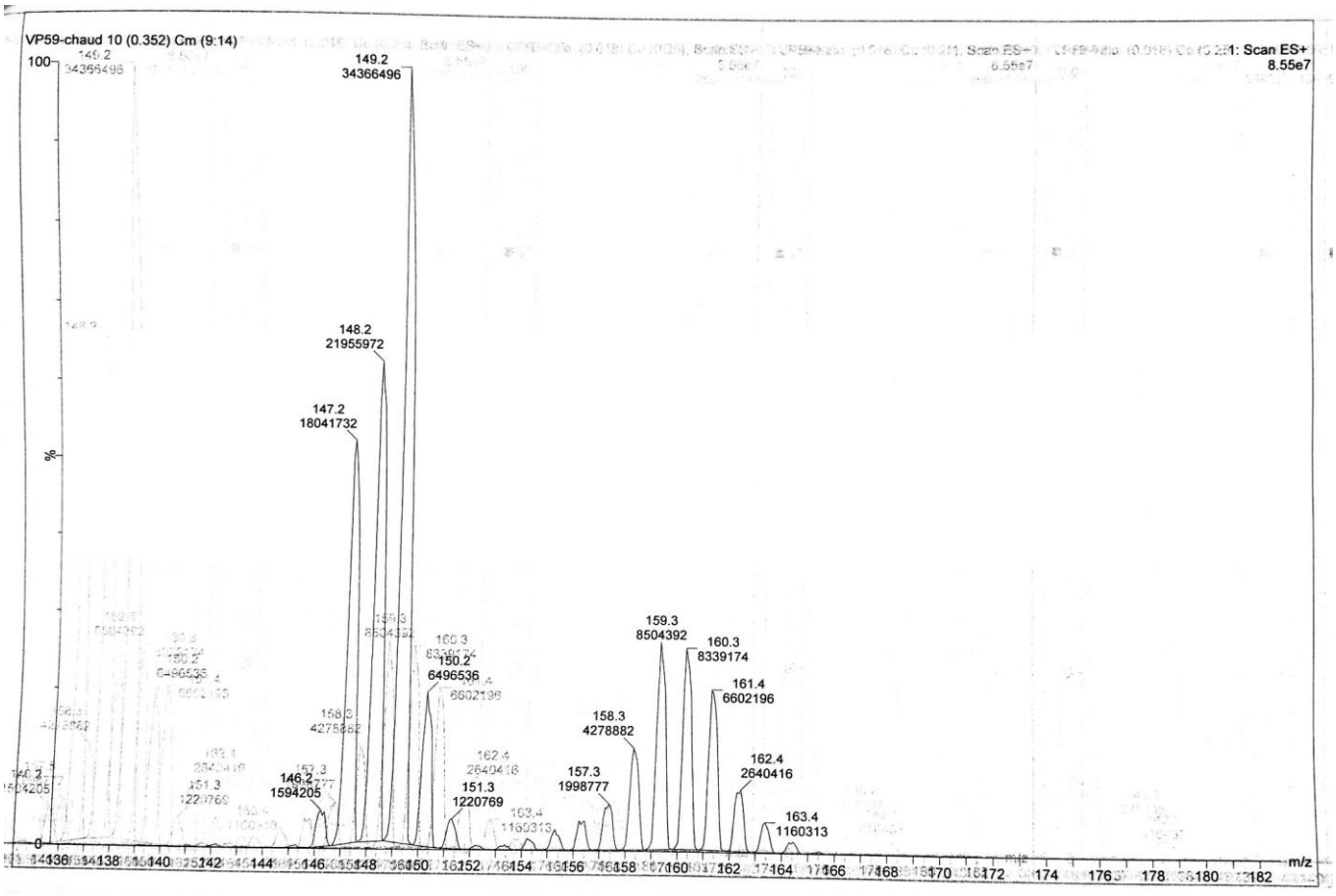

ESI spectrum of **5**

(1-Ethyl-imidazol-2-yl)methanol **6**

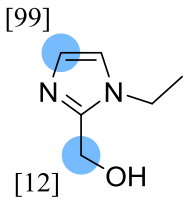

Chemical Formula: $C_6H_{10}N_2O$

Substrate	Solvent (Volume)	RuNp@PVP cat.
25.2mg, 0.2mmol	DMA (2mL)	14.4mg, 5mol%

Workup and purification:

After cooling down to room temperature, EtOAc/cyclohexane (1:1, 3mL) was added to the reaction mixture and stirred for 10min to let precipitating RuNp@PVP. The suspension was

passed through a Sep-Pak® C18 cartridge and then eluted with EtOAc/cyclohexane (1:1, 5mL). The solvent was removed under vacuum.

Yield: 25.0mg, 99%, colourless oil

^{1}H NMR (400 MHz, Acetone-d_6): δ 7.10 - 7.02 (m, 1H), 6.78 (s, 0.02H), 4.59 (s, 2H), 4.47 (bs, OH), 4.11 (q, J = 7.3 Hz, 2H), 1.39 (t, J = 7.3 Hz, 3H).

Deuterium incorporation was expected at δ 6.78 and at δ 4.59. Isotopic enrichment values were determined against the integral at δ 7.10 - 7.02.

^{2}H-{^{1}H}NMR (92 MHz, Acetone): δ 6.79 (s, 0.99D), 4.55 (s, 0.24D)

^{13}C-{^{1}H}NMR (100 MHz, Acetone-d_6): δ 148.1, 127.0 (m), 120.3, 56.5 (m), 41.4, 16.7.

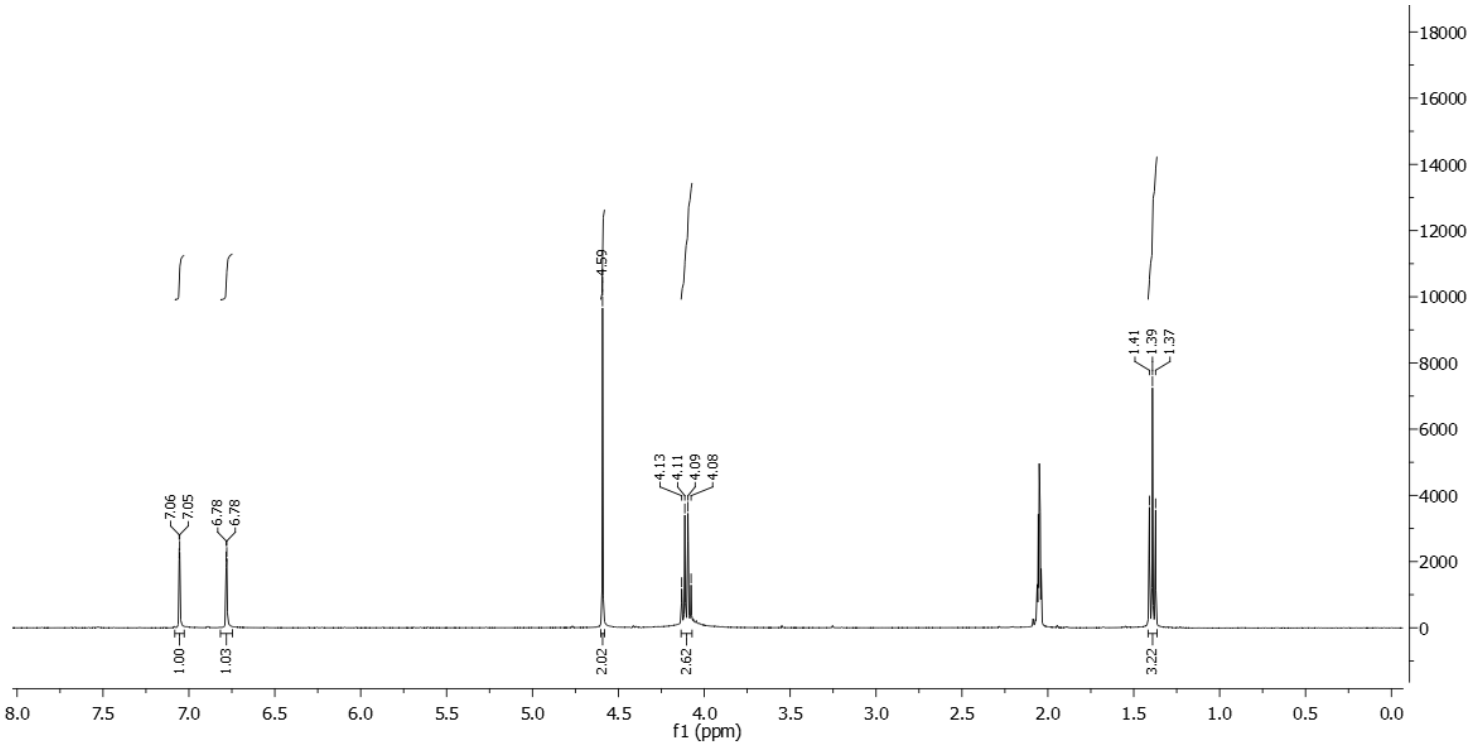

^{1}H-NMR spectrum of the non-deuterated starting material

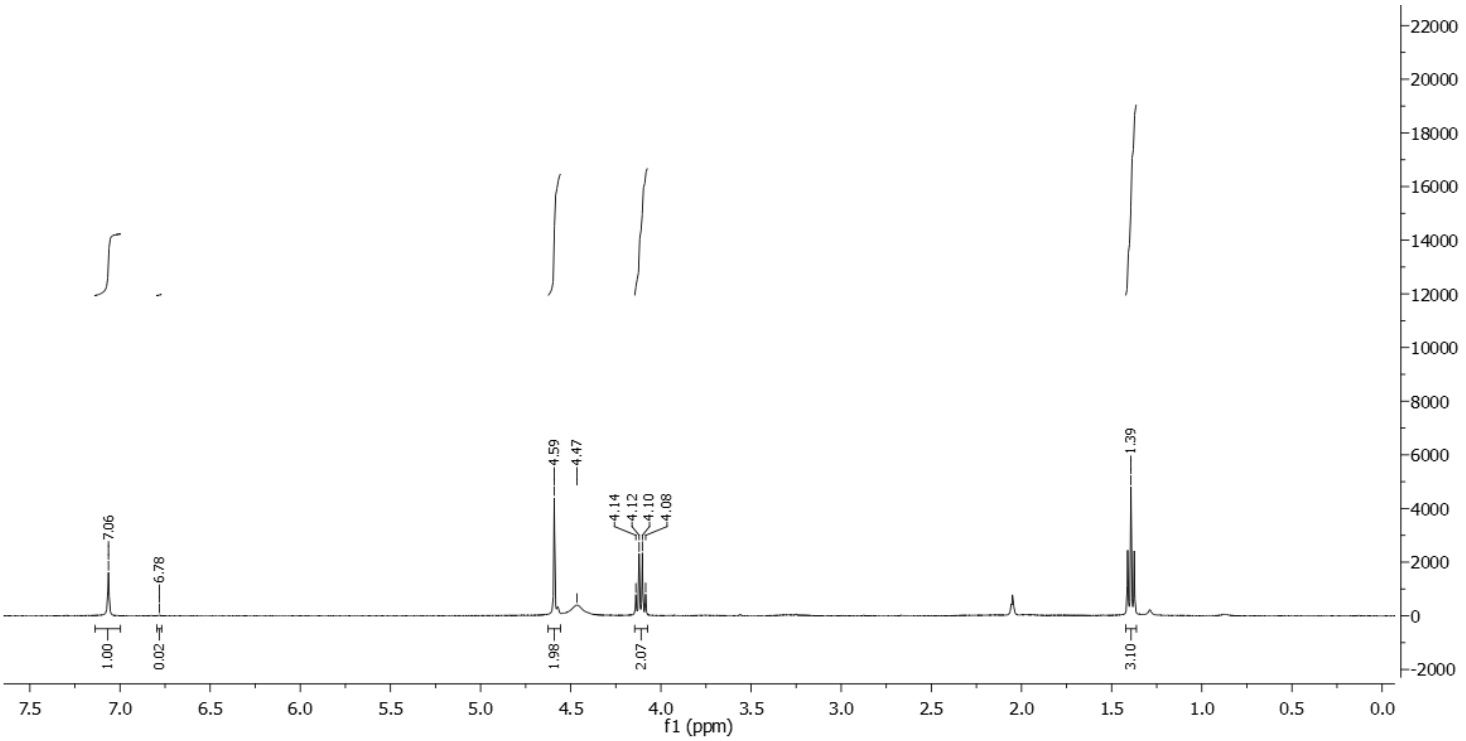

^{1}H-NMR spectrum of **6**

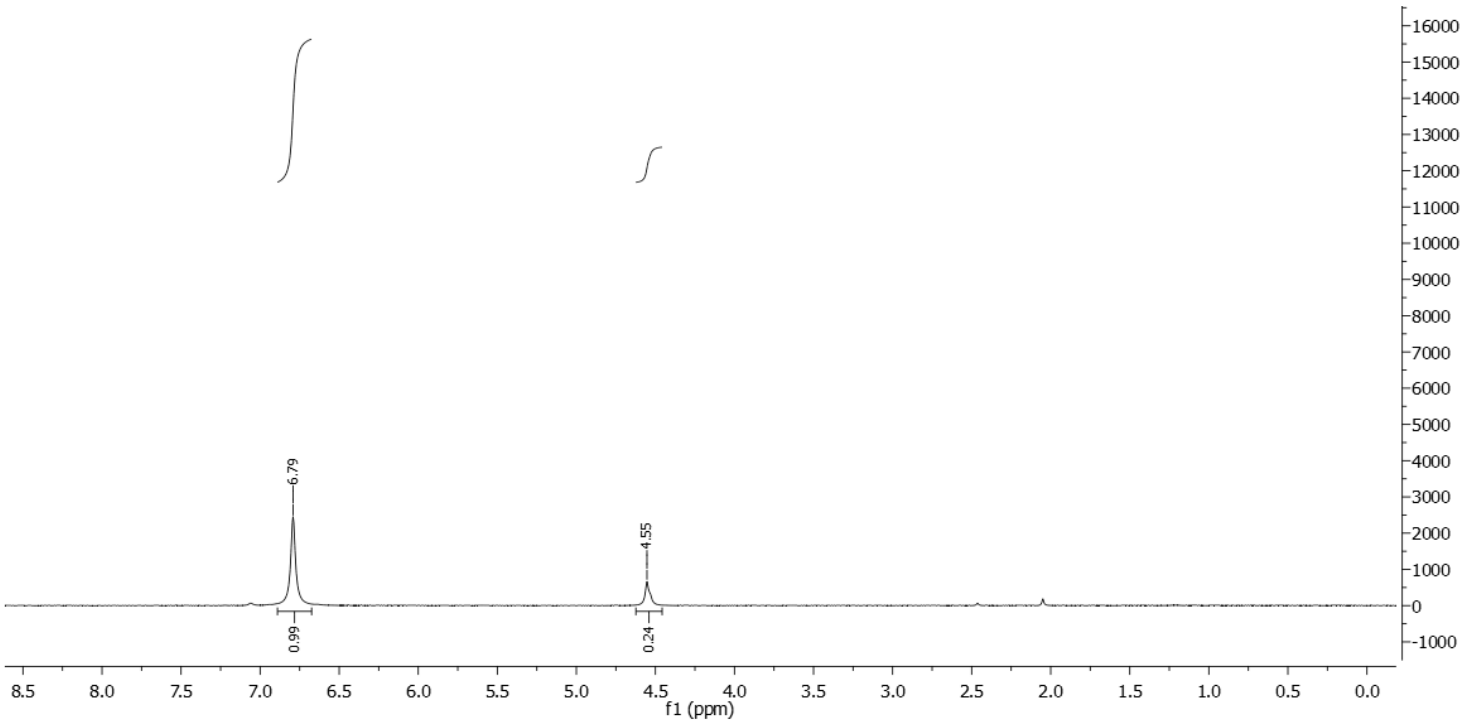

^{2}H-NMR spectrum of **6**

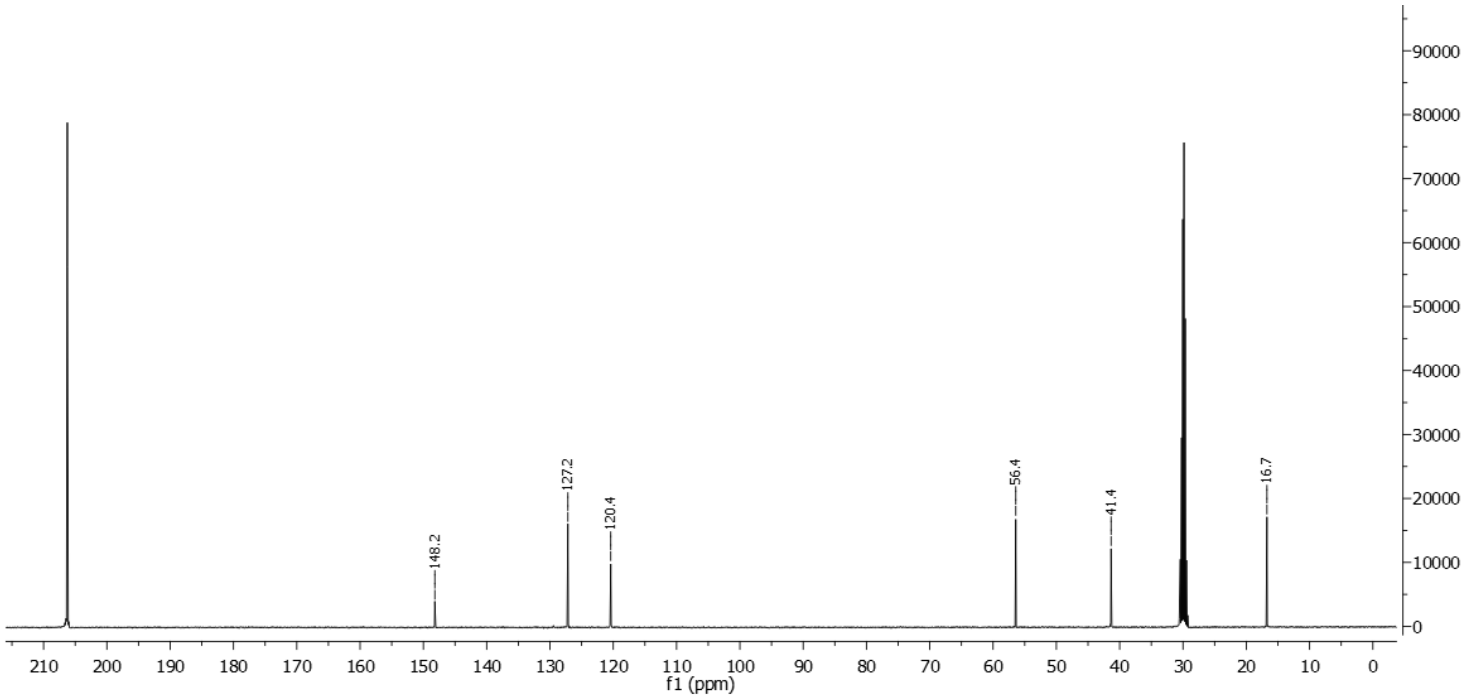

^{13}C-NMR spectrum of the non-deuterated starting material

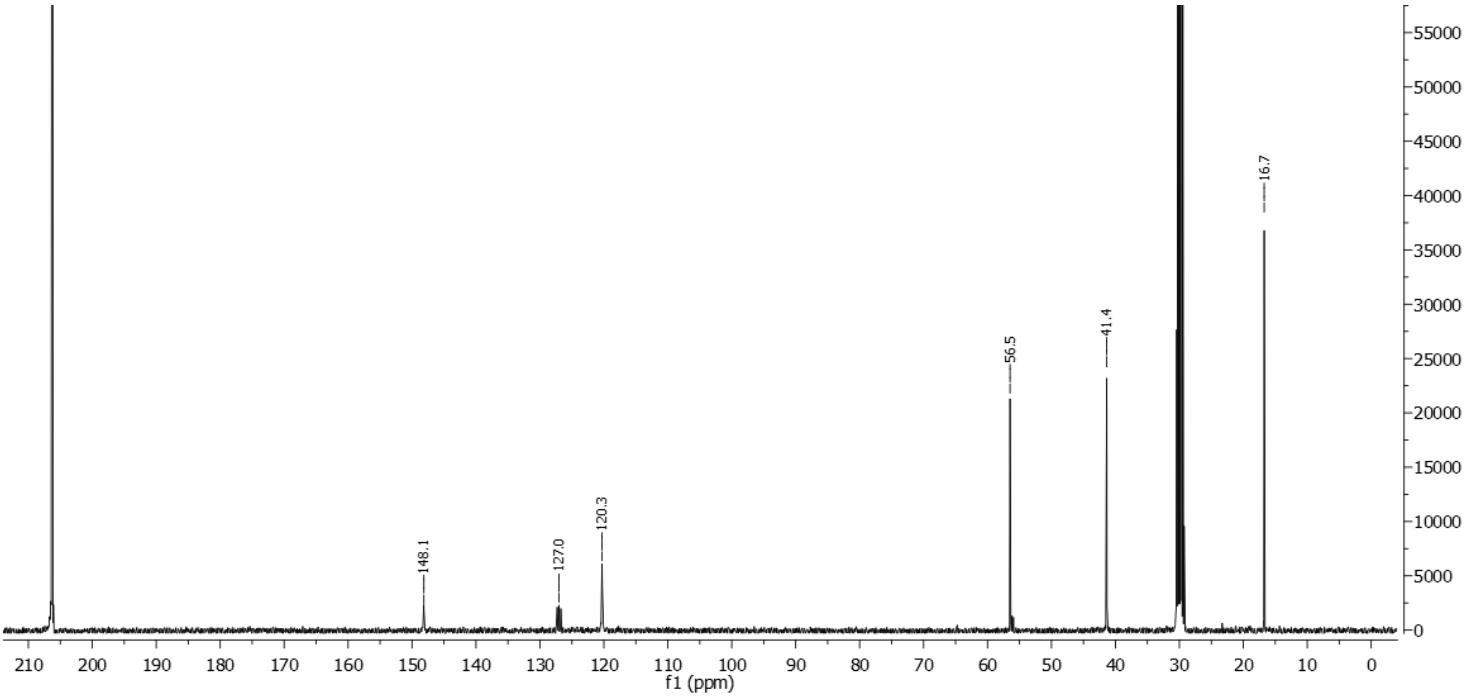

^{13}C-NMR spectrum of **6**

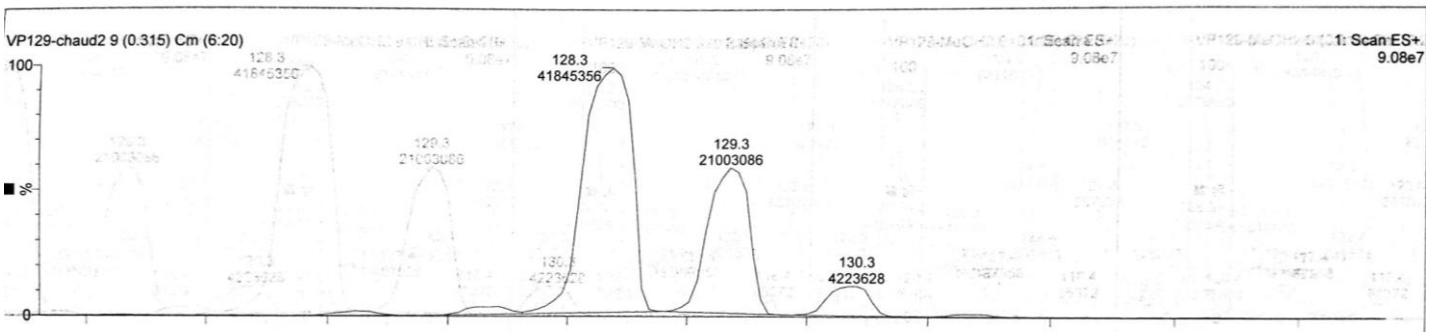

ESI spectrum of **6**

4-(Imidazol-1-yl)benzaldehyde **7**

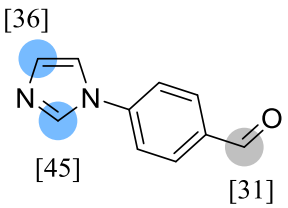

Chemical Formula: $C_{10}H_8N_2O$

Substrate	Solvent (Volume)	RuNp@PVP cat.
34.4mg, 0.2mmol	THF (2mL)	14.4mg, 5mol%

Workup and purification:

After cooling down to room temperature, EtOAc/cyclohexane (1:1, 3mL) was added to the reaction mixture and stirred for 10min to let precipitating RuNp@PVP. The suspension was passed through a Sep-Pak® C18 cartridge and then eluted with THF (3mL). The solvent was removed under vacuum. The product was recrystallized from THF/cyclohexane (1:1).

Yield: 18.0mg, 52%, yellow solid

^{1}H NMR (400 MHz, Acetone-d_6): δ 10.08 (s, 0.69H), 8.27 (s, 0.55H), 8.09 (d, J = 8.6 Hz, 2H), 7.89 (d, J = 8.6 Hz, 2H), 7.75 (s, 1H), 7.16 (s, 0.64H).

Deuterium incorporation was expected at δ 10.08, δ 8.27 and at δ 7.16. Isotopic enrichment values were determined against the integral at δ 7.89.

^{2}H-{^{1}H}NMR (92 MHz, Acetone): δ 10.11 (s, 0.29D), 8.28 (s, 0.45D), 7.20 (s, 0.36D)

^{13}C-{^{1}H}NMR (100 MHz, Acetone-d_6): δ 191.8, 142.7, 136.5, 135.9, 132.2, 131.7, 121.5, 118.4.

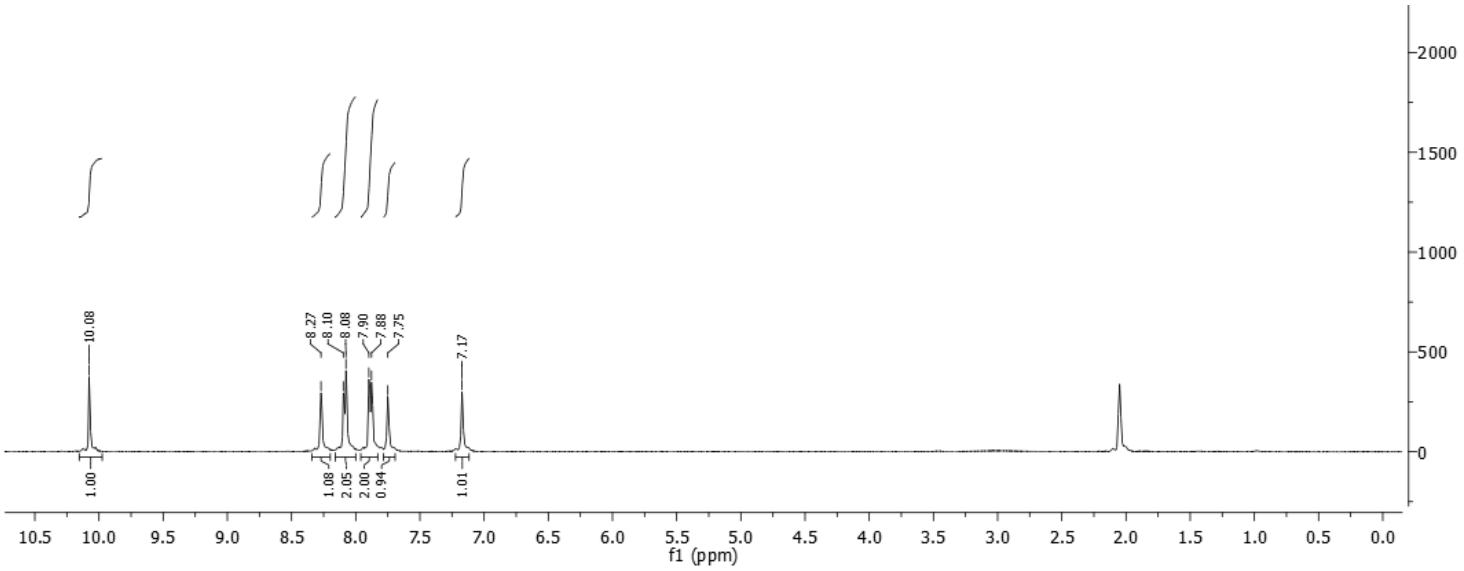

^{1}H-NMR spectrum of the non-deuterated starting material

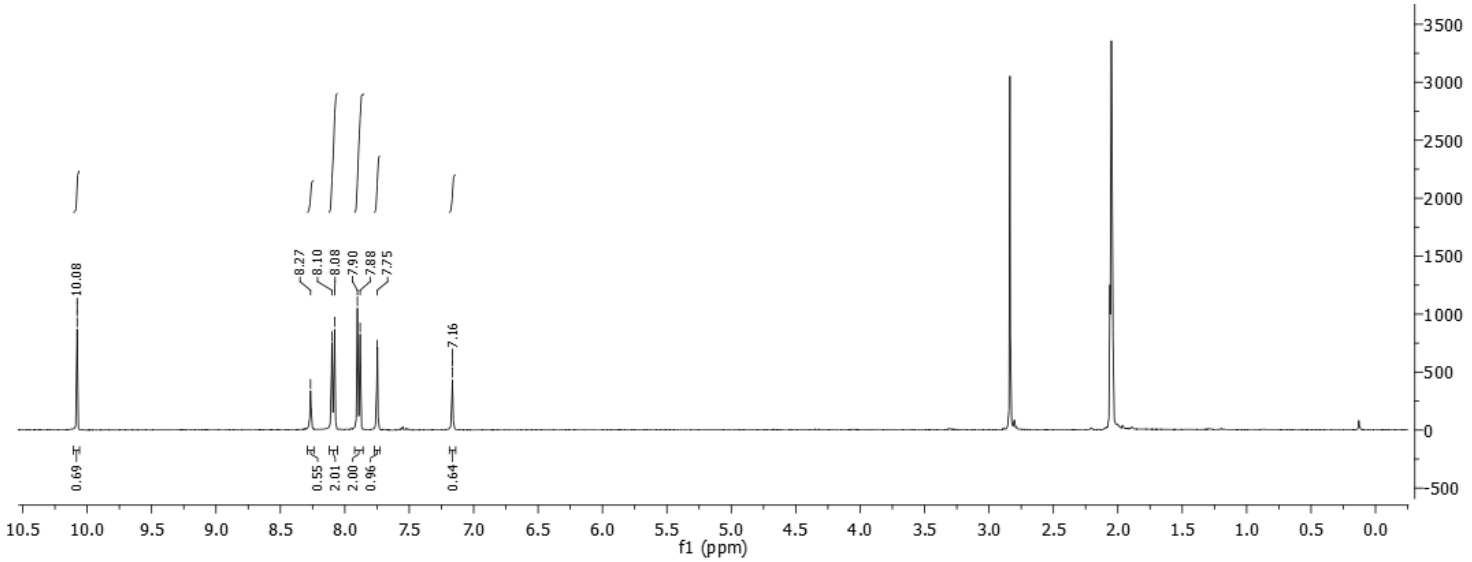

^{1}H-NMR spectrum of **7**

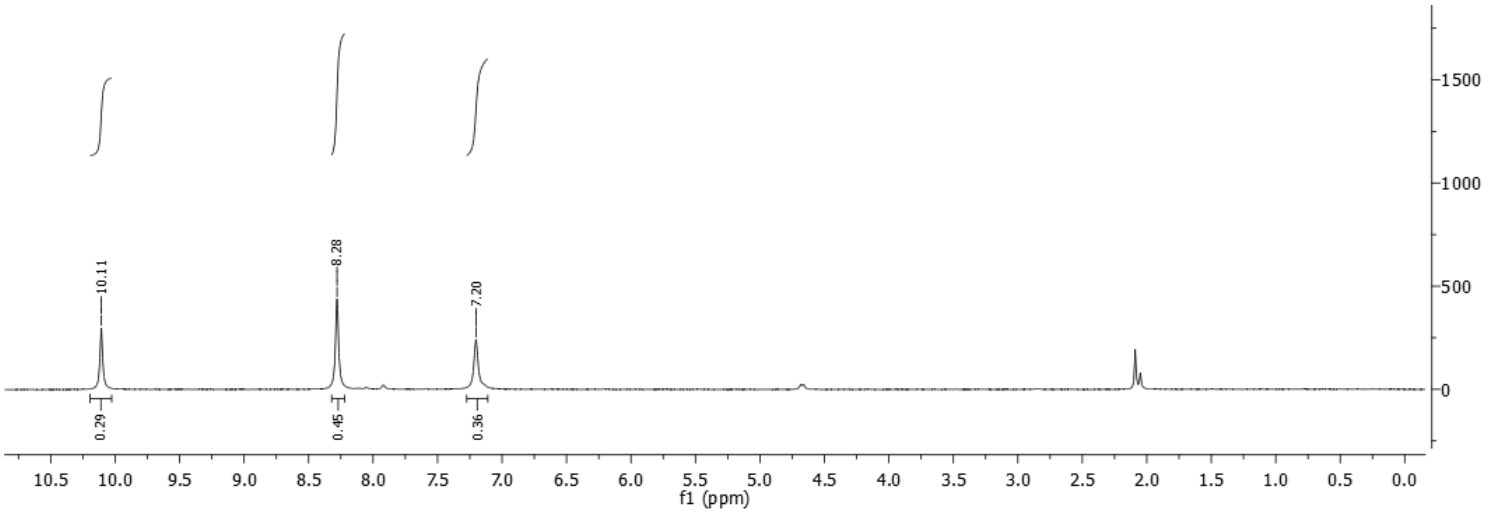

^{2}H-NMR spectrum of **7**

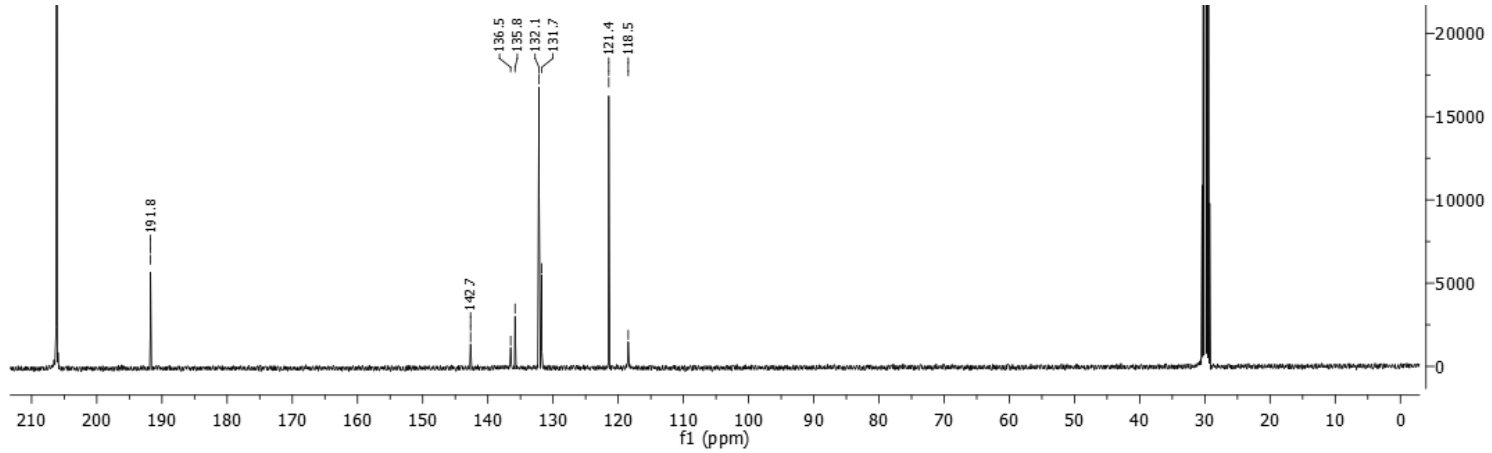

^{13}C-NMR spectrum of the non-deuterated starting material

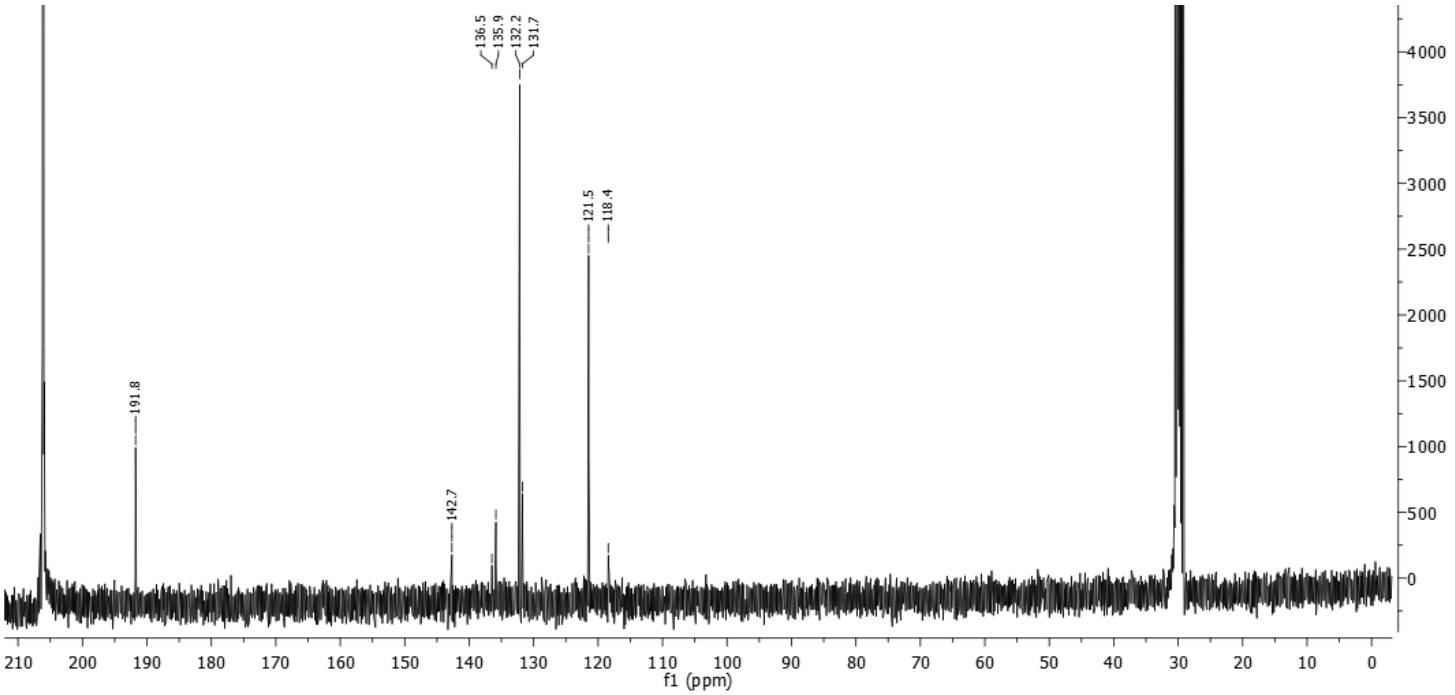

^{13}C-NMR spectrum of **7**

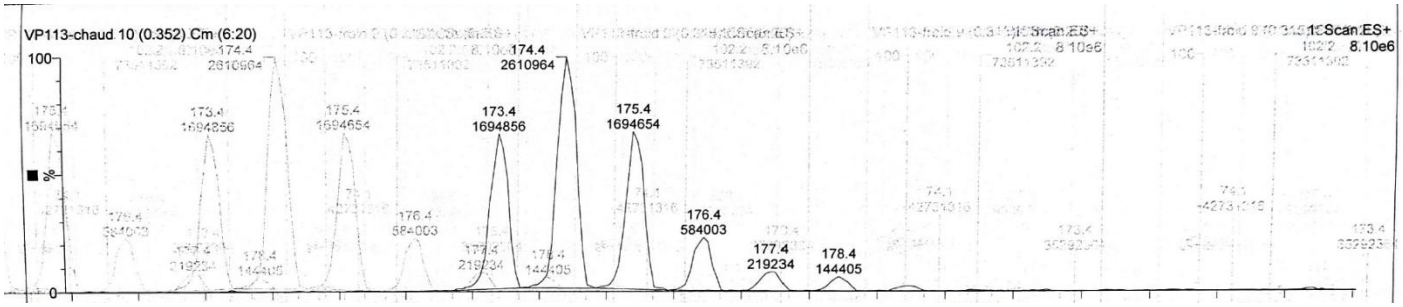

ESI spectrum of **7**

2,3-(Methylenedioxy)benzaldehyde **7***

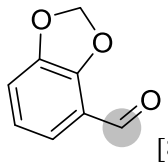

[88]

Chemical Formula: $C_8H_6O_3$

Substrate	Solvent (Volume)	RuNp@PVP cat.
30.0mg, 0.2mmol	THF (2mL)	14.4mg, 5mol%

Workup and purification:

After cooling down to room temperature, EtOAc/cyclohexane (1:1, 3mL) was added to the reaction mixture and stirred for 10min to let precipitating RuNp@PVP. The suspension was passed through SiO_2 pad and then eluted with EtOAc (5mL). The solvent was removed under vacuum and the crude product was purified over SiO_2. The labelled product was eluted with *n*-pentane/EtOAc (3:1).

Yield: 6.0mg, 20%, yellow solid

^{1}H NMR (400 MHz, Acetone-d_6): δ 10.14 (s, 0.11H), 7.36 – 7.20 (m, 1H), 7.18 – 7.07 (m, 1H), 7.04 – 6.91 (m, 1H), 6.20 (s, 2H).

Deuterium incorporation was expected at δ 10.14. Isotopic enrichment values were determined against the integral at δ 7.36 – 7.20.

^{2}H-{^{1}H}NMR (92 MHz, Acetone): δ 10.13 (s)

^{13}C-{^{1}H}NMR (100 MHz, Acetone-d_6): δ 187.7(m), 150.6, 150.0, 122.6, 120.7, 120.2, 114.0, 103.7.

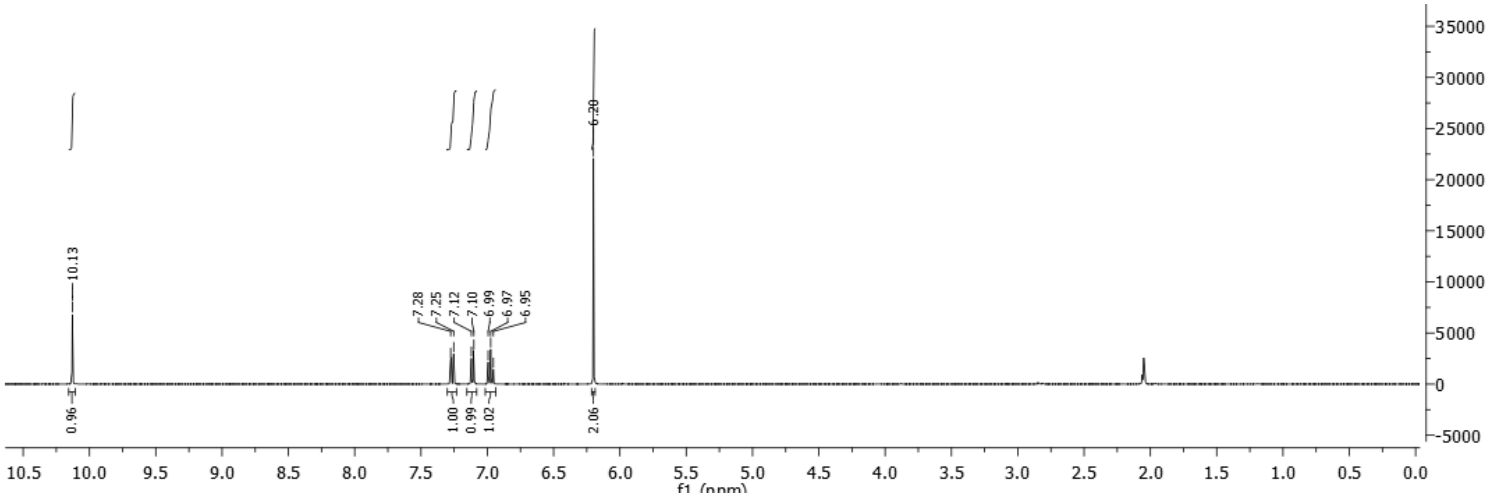

^{1}H-NMR spectrum of the non-deuterated starting material

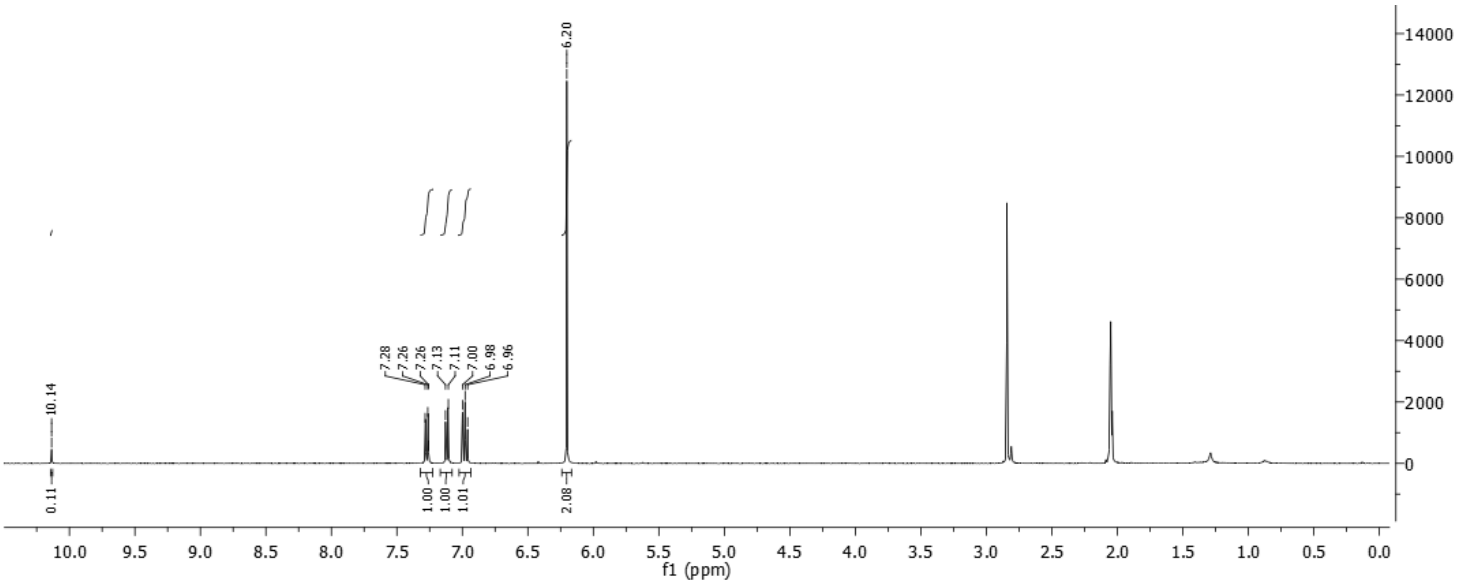

^{1}H-NMR spectrum of **7***

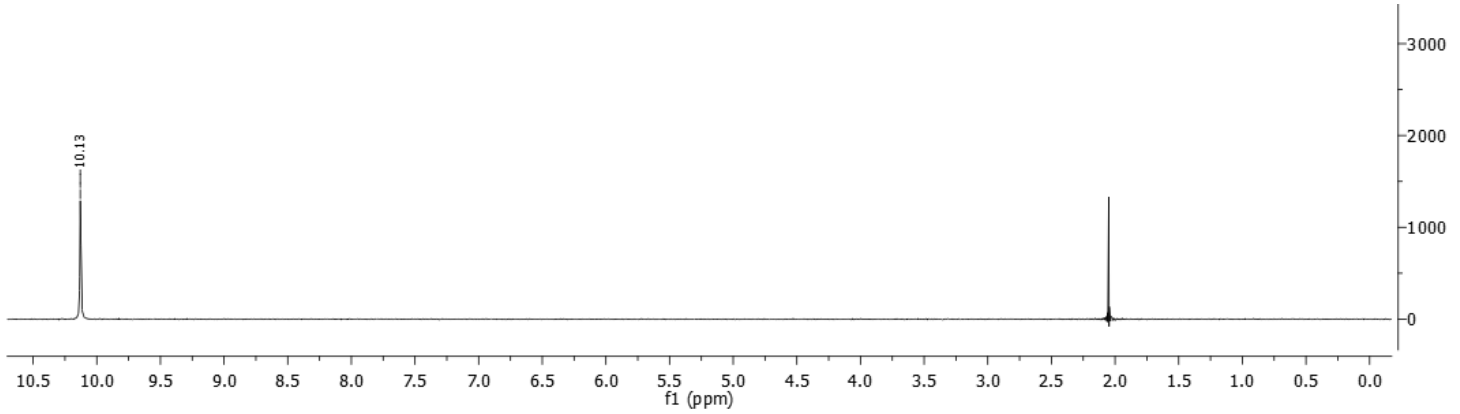

^{2}H-NMR spectrum of **7***

(Imidazol-1-yl)acetic acid ***8***

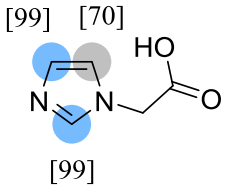

Chemical Formula: $C_5H_6N_2O_2$

Substrate	Solvent (Volume)	RuNp@PVP cat.
25.2mg, 0.2mmol	D_2O (2mL)	14.4mg, 5mol%

Workup and purification:

After cooling down to room temperature, the reaction mixture was incubated with "Amberlyst A21 free base" (5mL) for 1h. The liquid phase was removed and the resin was washed with MeOH (5mL). The labelled product was eluted with an aqueous HCl solution (1M, 10mL). The solvent was removed under vacuum.

Yield: 10.0mg, 40%, white solid

^{1}H NMR (400 MHz, DMSO-*d*$_6$): δ 4.86 (s, 2H)

Deuterium incorporation was expected at δ 7.62, δ 7.13 and at δ 6.88. Isotopic enrichment values were determined by ^{2}H-{^{1}H}NMR.

^{2}H-{^{1}H}NMR (92 MHz, DMSO): δ 7.95 (s, 1D), 7.36 (s, 0.66D), 7.14 (s, 1D)

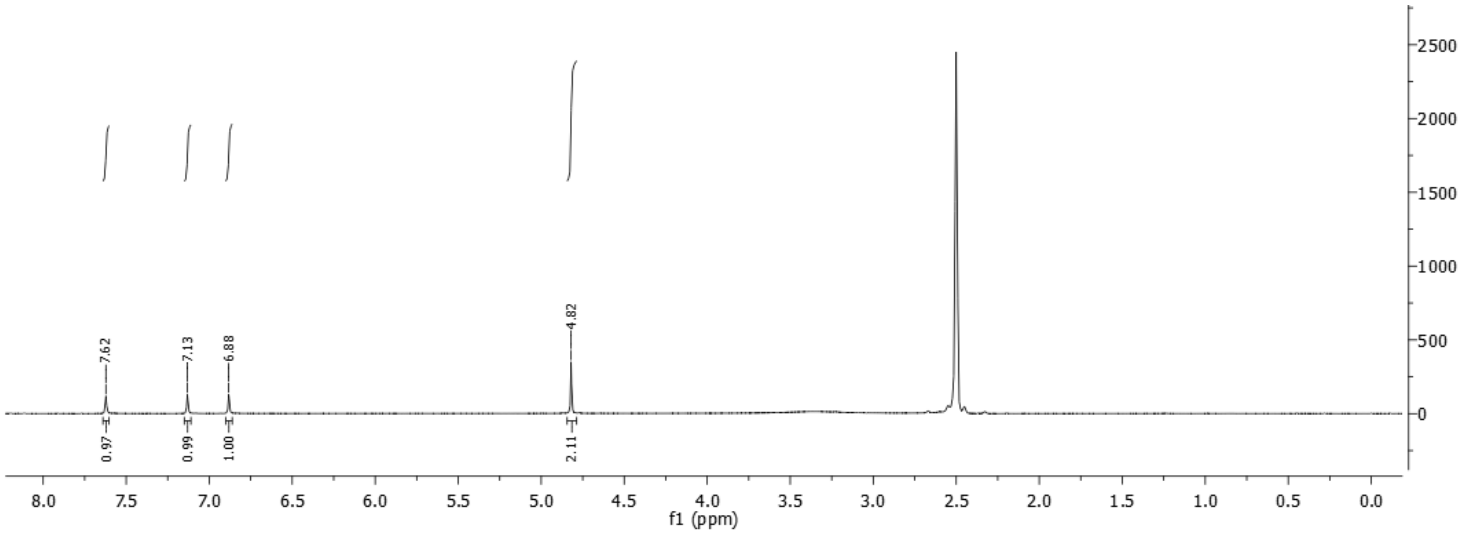

^{1}H-NMR spectrum of the non-deuterated starting material

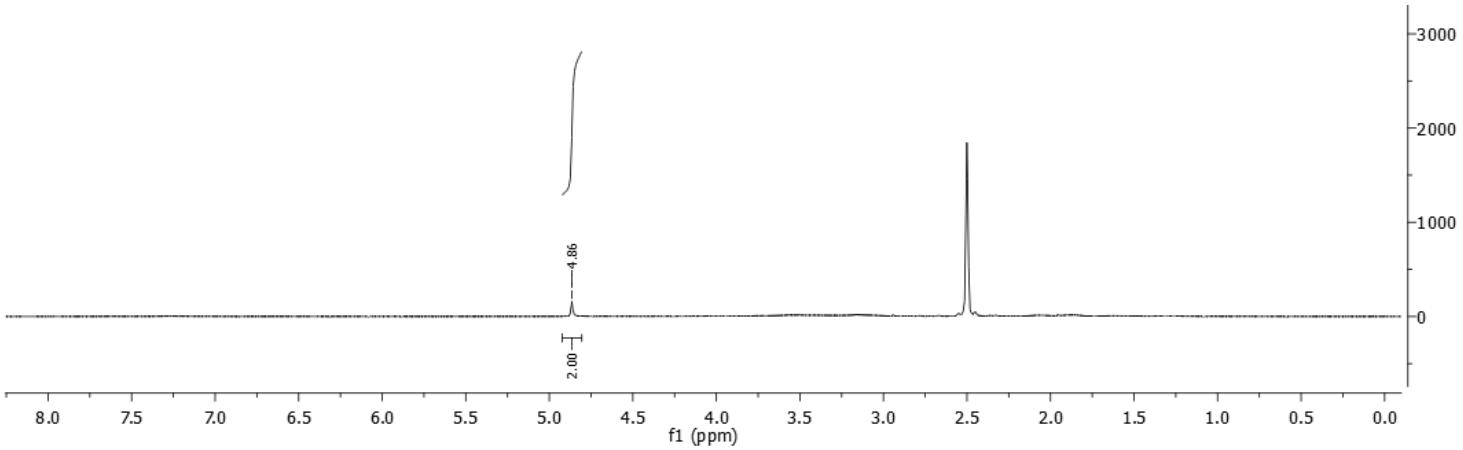

^{1}H-NMR spectrum of **8**

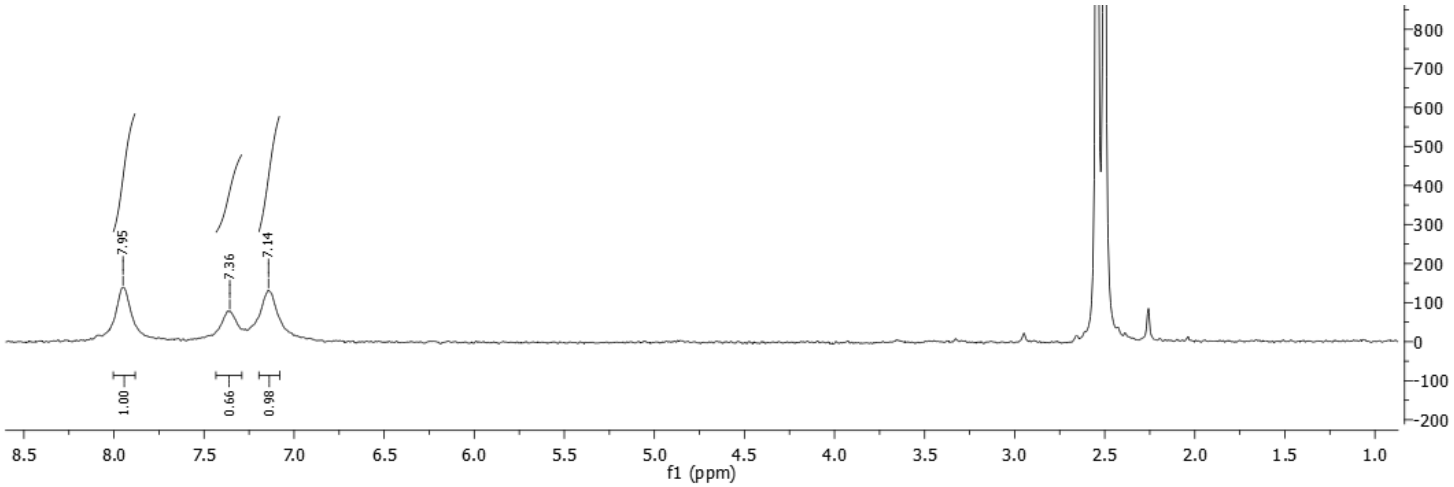

^{2}H-NMR spectrum of **8**

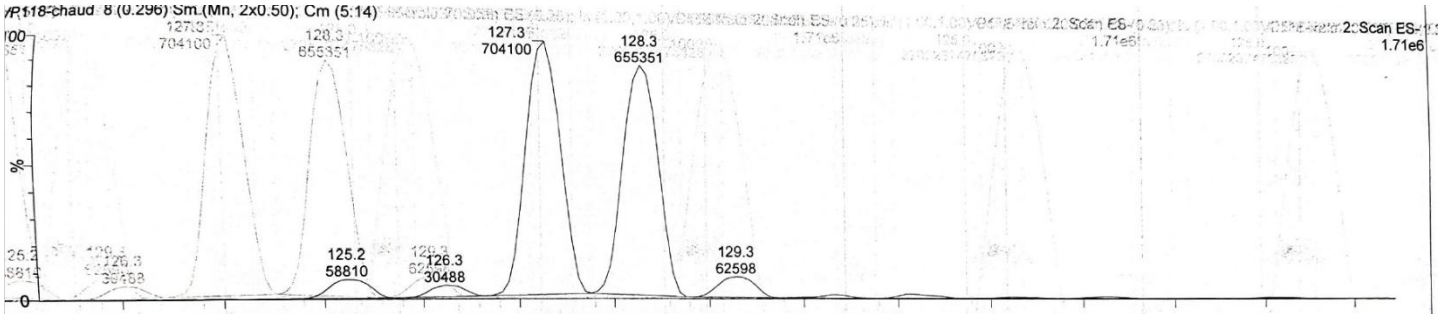

ESI spectrum of **8**

p-Phenylenediacetic acid ***8****

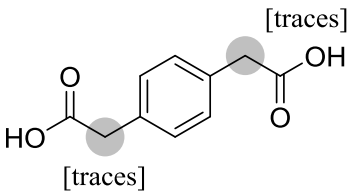

Chemical Formula: $C_{10}H_{10}O_4$

Substrate	Solvent (Volume)	RuNp@PVP cat.
38.8mg, 0.2mmol	D_2O/THF 1:1 (2mL)	14.4mg, 5mol%

Workup and purification:

After cooling down to room temperature, the reaction mixture was incubated with "Amberlyst A21 free base" (5mL) for 15 min. The liquid phase was removed and the resin was washed with MeOH (5mL). The compound was eluted with a 1:1 mixture of aqueous HCl solution (0.1M) and MeOH (10mL). The solvent was removed under vacuum.

Yield: 12.0mg, 31%, white solid

^{1}H NMR (400 MHz, methanol-*d*$_4$): δ 7.24 (s, 4H), 3.58 (s, 3.54H),

Deuterium incorporation was expected at *δ* 3.58 and confirmed by ^{2}H-{^{1}H}NMR.

^{2}H-{^{1}H}NMR (92 MHz, methanol): δ 3.59 (s)

The signal at δ 3.59 (s) ^{2}H-{^{1}H}NMR could be attributed to slight deuteration of the enolic positions. Signals emerging at lower chemical shifts could be related to reduced side-products.

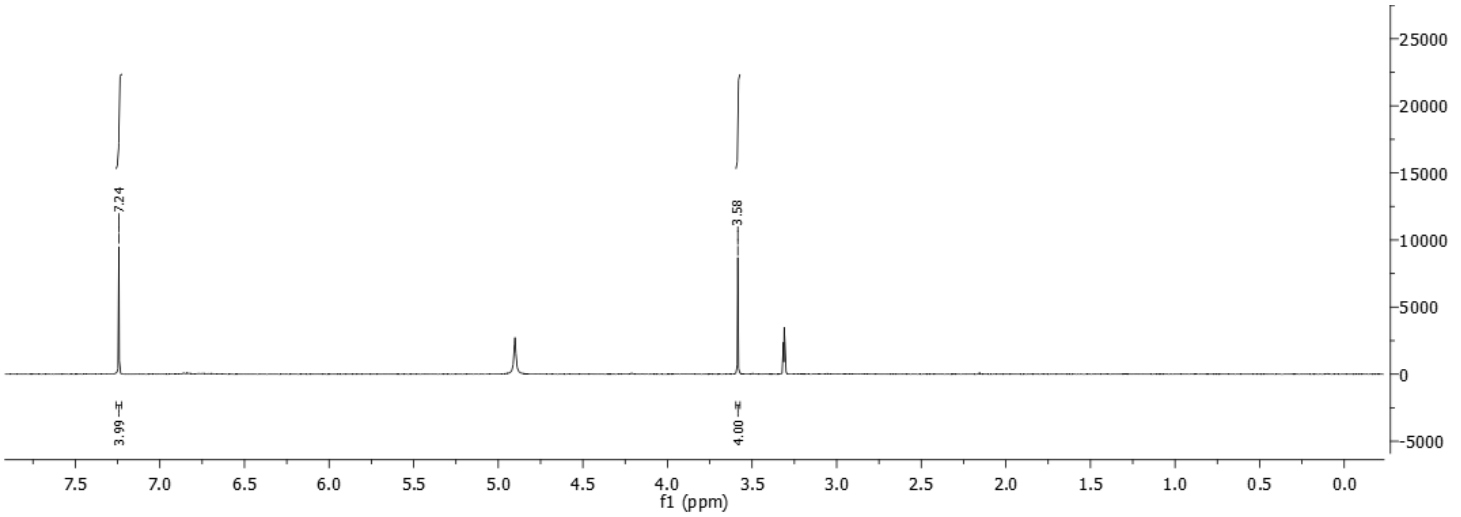

^{1}H-NMR spectrum of starting material

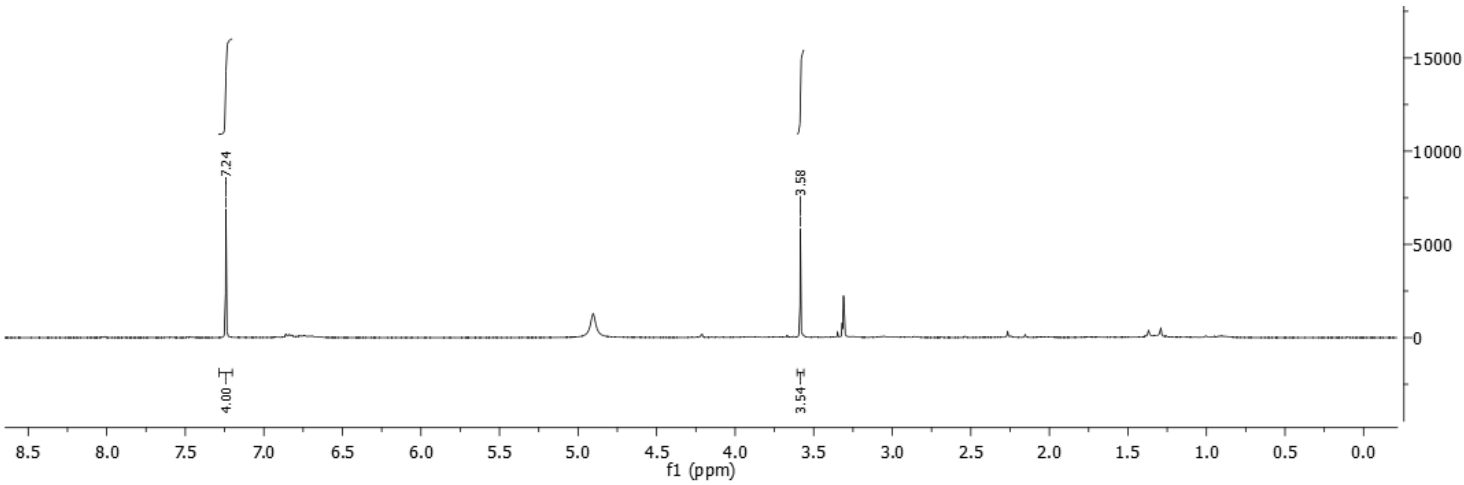

^{1}H-NMR spectrum of **8***

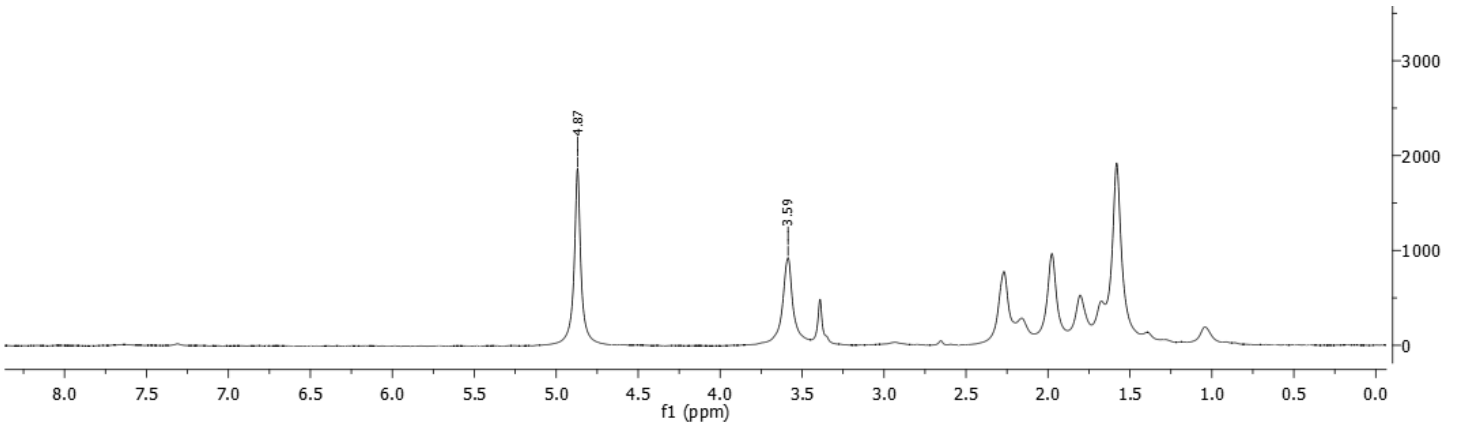

^{2}H-NMR spectrum of **8***

Deuterations of *N*-heterocyclic benzoderivatives

Benzimidazole ***9***

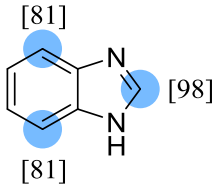

Chemical Formula: $C_7H_6N_2$

Substrate	Solvent (Volume)	RuNp@PVP cat.
23.6mg, 0.2mmol	THF (2mL)	14.4mg, 5mol%

Workup and purification:

After cooling down to room temperature, cyclohexane (2mL) was added to the reaction mixture and stirred for 10min to let precipitating RuNp@PVP. The suspension was passed through a Sep-Pak® C18 cartridge and then eluted with EtOAc/cyclohexane (1:1, 5mL). The solvent was removed under vacuum.

Yield: 25.0mg, 99%, white solid

^{1}H NMR (400 MHz, Acetone-*d*$_6$): δ 8.18 (s, 0.03H), 7.66 – 7.59 (m, 0.39H), 7.25 – 7.18 (m, 2H).

Deuterium incorporation was expected at *δ* 8.18 and at *δ* 7.66 – 7.59. Isotopic enrichment values were determined against the integral at *δ* 7.25 – 7.18.

^{2}H-{^{1}H}NMR (92 MHz, Acetone): δ 8.12 (s, 0.97D), 7.61 (s, 1.62D)

^{13}C-{^{1}H}NMR (100 MHz, Acetone-*d*$_6$): δ 142.0 (m), 122.8 (m).

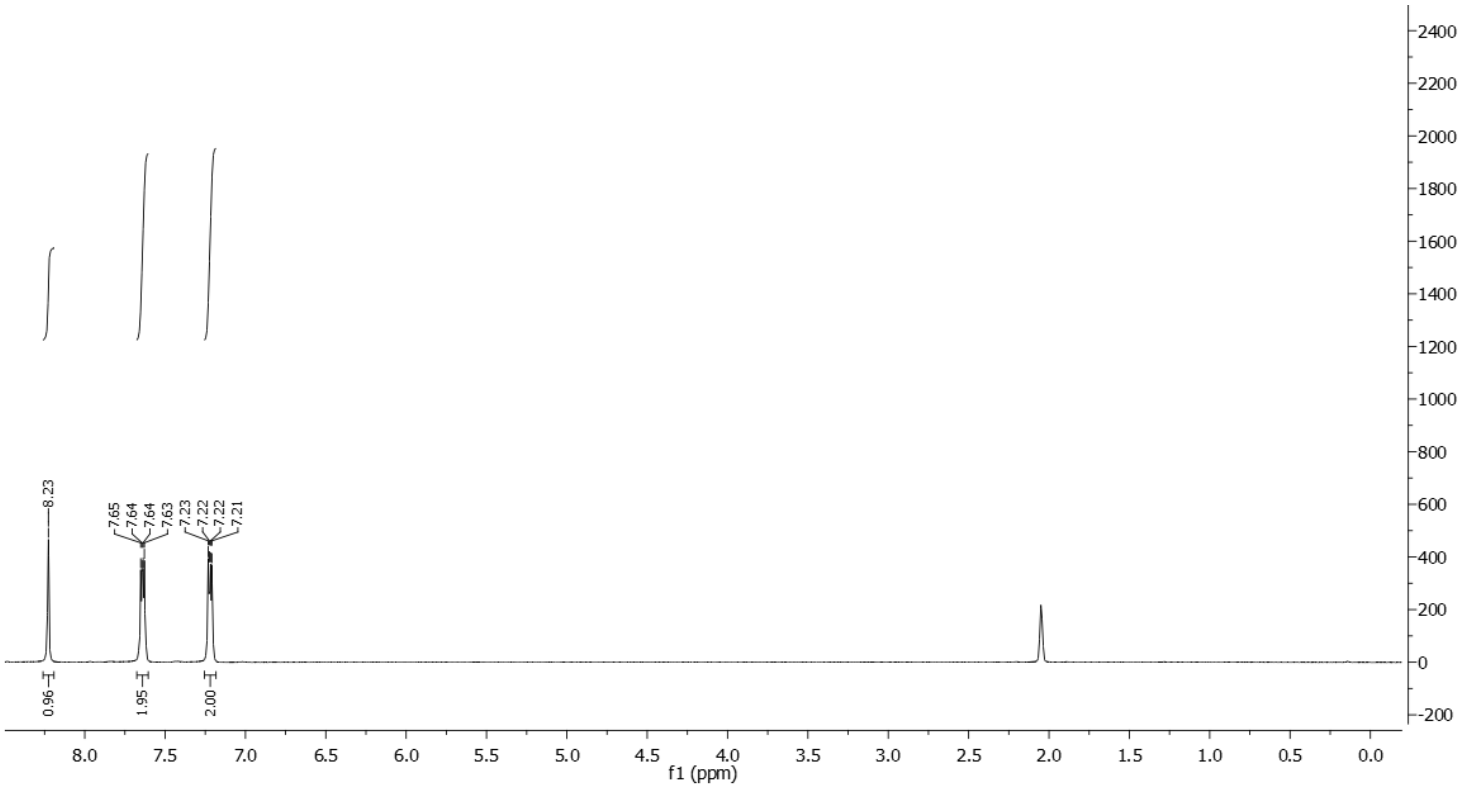

^{1}H-NMR spectrum of the non-deuterated starting material

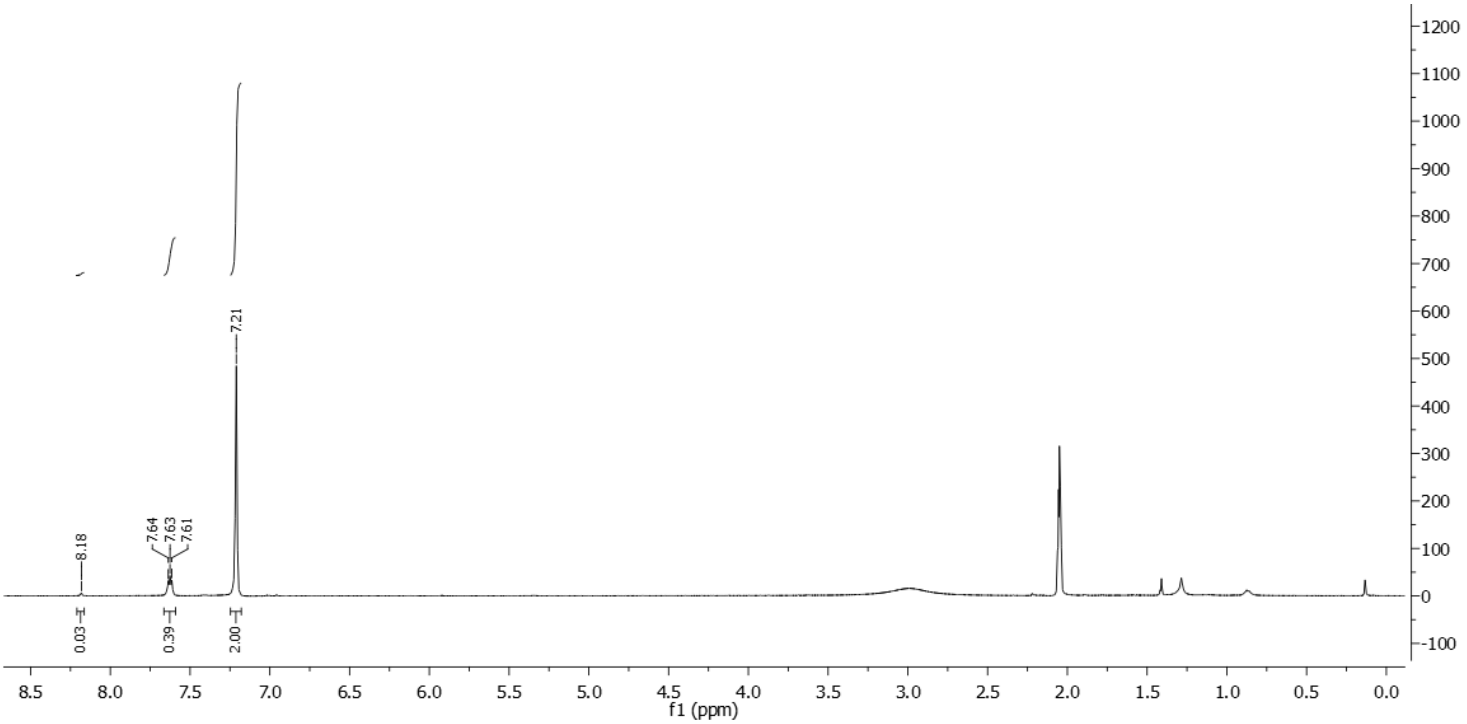

^{1}H-NMR spectrum of **9**

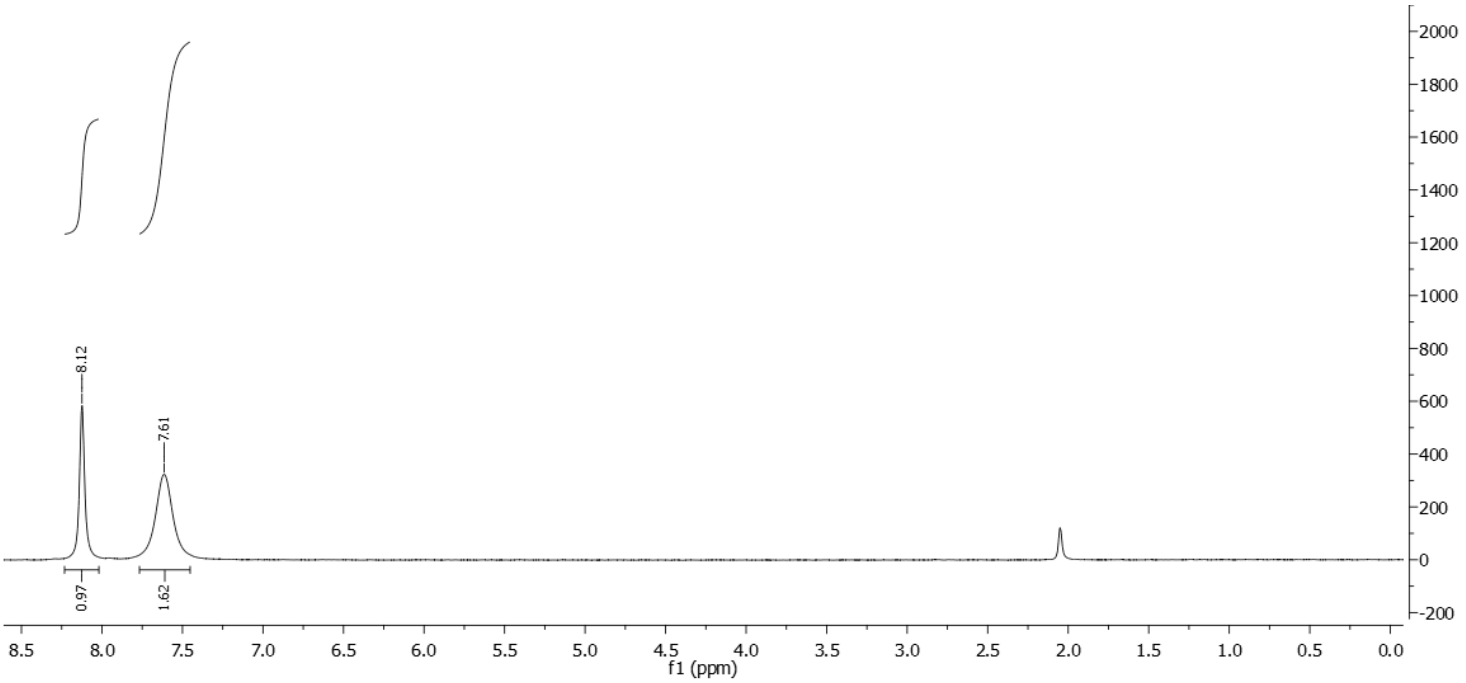

^{2}H-NMR spectrum of **9**

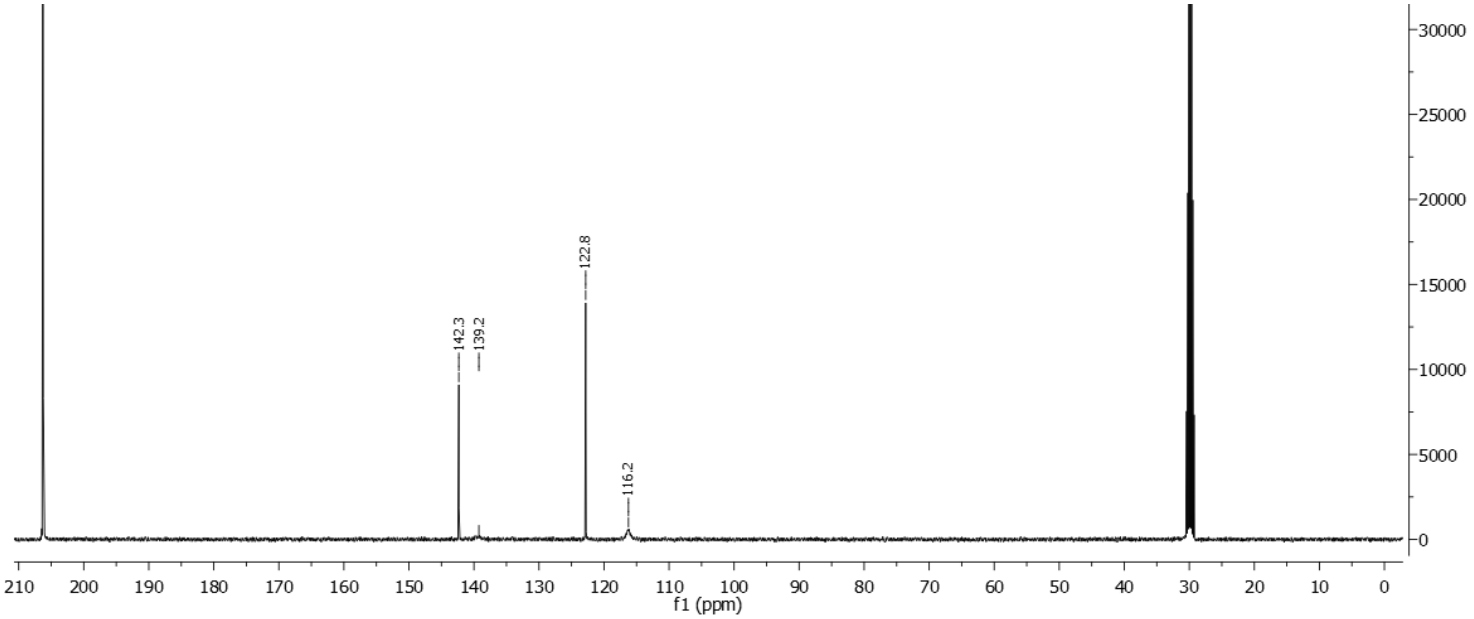

^{13}C-NMR spectrum of the non-deuterated starting material

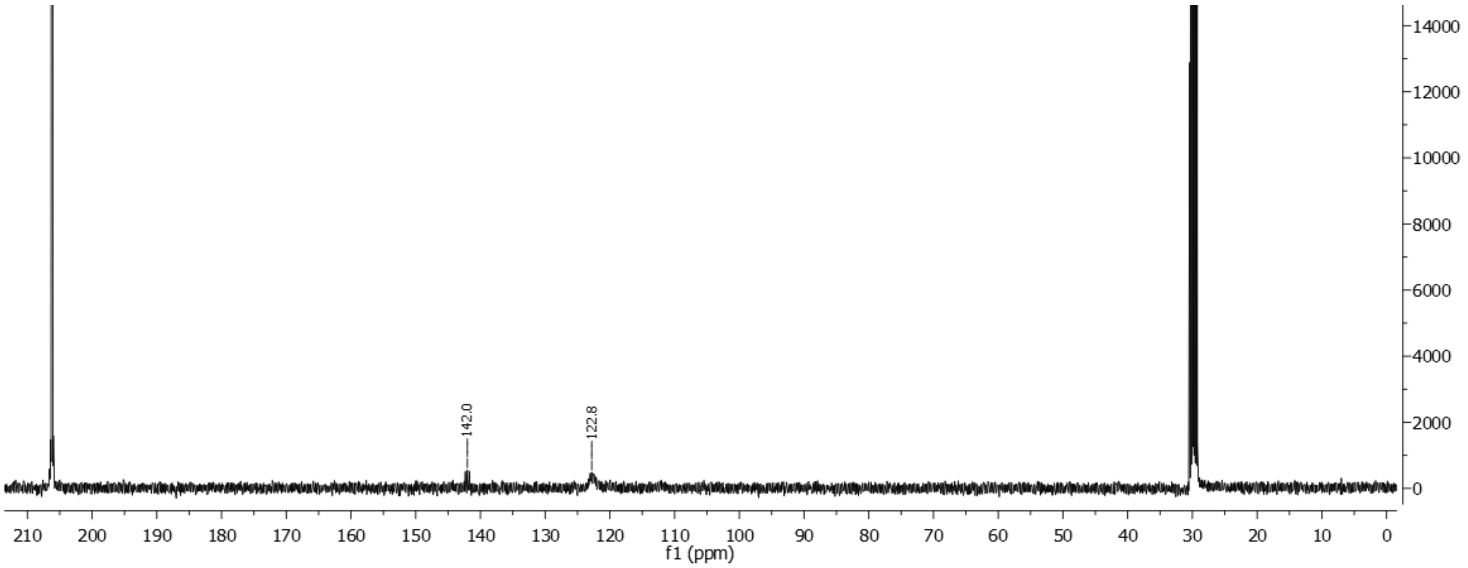

^{13}C-NMR spectrum of **9**

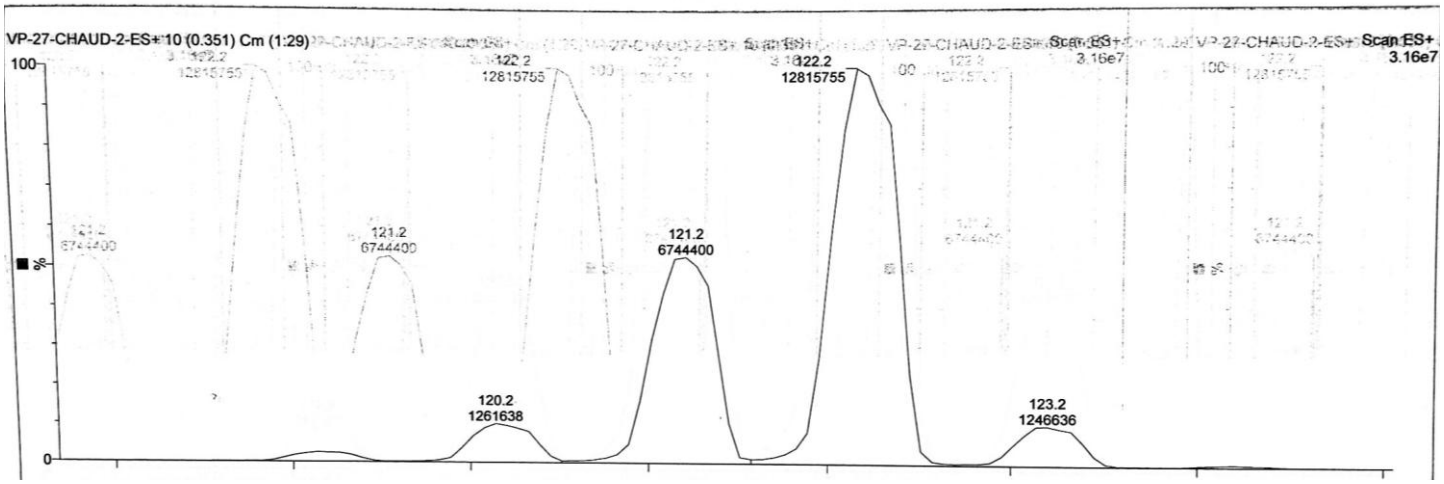

ESI spectrum of **9**

2-Phenylbenzimidazole **10**

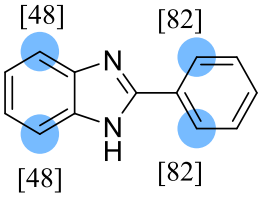

Chemical Formula: $C_{13}H_{10}N_2$

Substrate	Solvent (Volume)	RuNp@PVP cat.
38.8mg, 0.2mmol	DMA (2mL)	14.4mg, 5mol%

Workup and purification:

After cooling down to room temperature, cyclohexane (2mL) was added to the reaction mixture and stirred for 10min to let precipitating RuNp@PVP. The suspension was passed through a Sep-Pak® C18 cartridge and then eluted with EtOAc/cyclohexane (1:1, 5mL). The solvent was removed under vacuum. The crude was not further purified.

^{1}H NMR (400 MHz, Acetone-d_6): δ 8.28 – 8.21 (m, 0.37H), 7.65 – 7.45 (m, 4.05H), 7.24 – 7.17 (m, 2H).

Deuterium incorporation was expected at δ 8.28 – 8.21 and at δ 7.65 – 7.45. Isotopic enrichment values were determined against the integral at δ 7.24 – 7.17. The reduced side-product arises at δ 7.11.

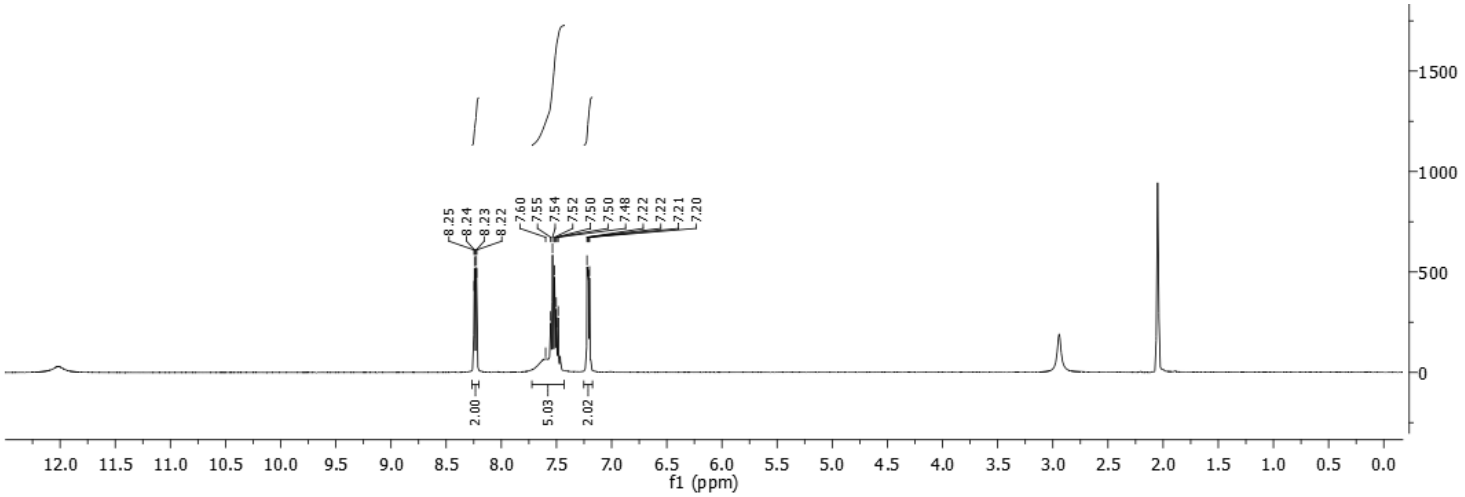

^{1}H-NMR spectrum of the non-deuterated starting material

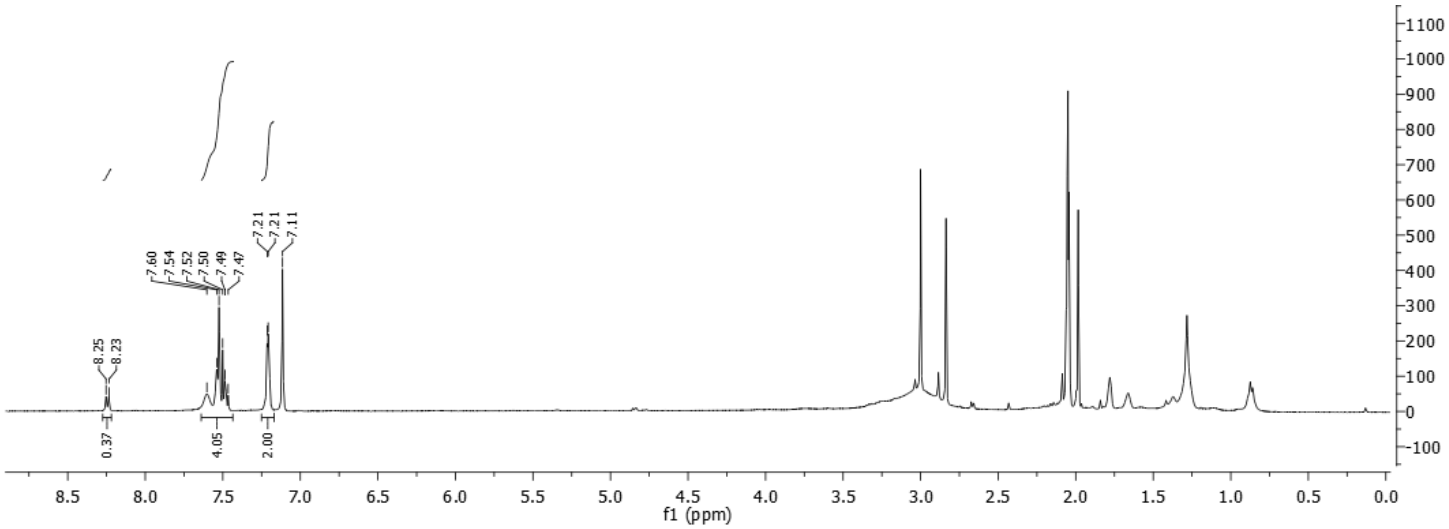

^{1}H-NMR spectrum of **10**

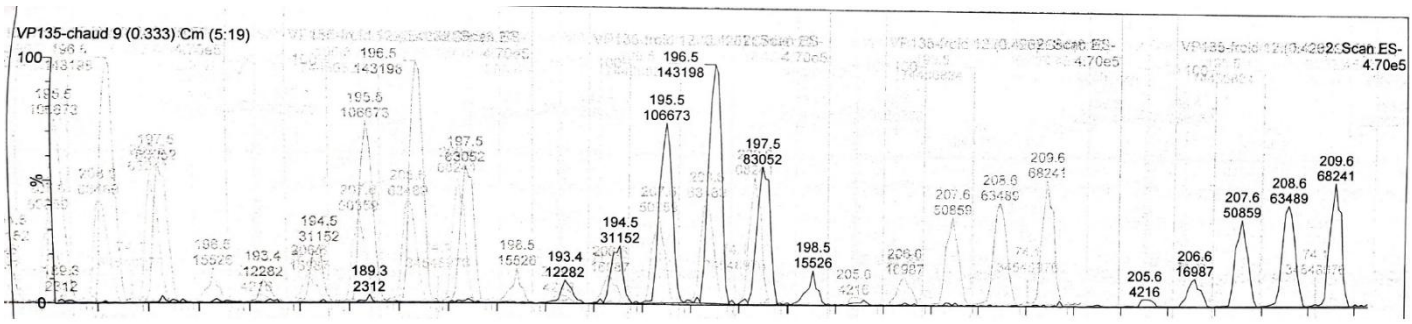

ESI spectrum of **10**

(5-Methylimidazo[1,2-a]pyridin-2-yl)methanol **11**

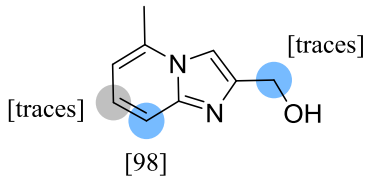

Chemical Formula: $C_9H_{10}N_2O$

Substrate	Solvent (Volume)	RuNp@PVP cat.
32.4mg, 0.2mmol	THF (2mL)	14.4mg, 5mol%

Workup and purification:

After cooling down to room temperature, cyclohexane (3mL) was added to the reaction mixture and stirred for 10min to let precipitating RuNp@PVP. The suspension was passed through a Sep-Pak® C18 cartridge and then eluted with THF (2mL). The solvent was removed under vacuum and the labelled product was recrystallized from acetone/MeOH (10:1).

Yield: 5.0mg, 15%, colourless crystals

^{1}H NMR (400 MHz, methanol-*d*$_4$): δ 7.68 (s, 1H), 7.44 – 7.37 (m, 0.02H), 7.30 – 7.21 (m, 1H), 6.80 – 6.72 (m, 1H), 4.78 (s, 2H), 2.63 (s, 3H).

Deuterium incorporation was expected at δ 7.44 – 7.37. Isotopic enrichment values were determined against the integral at *δ* 7.68.

^{2}H-{^{1}H}NMR (92 MHz, methanol): δ 7.43 (s), 4.77 (m)

^{13}C-{^{1}H}NMR (100 MHz, methanol-*d*$_4$): δ 147.7, 146.7, 136.9, 126.9, 114.0 (m), 112.8, 108.6, 59.6, 18.5.

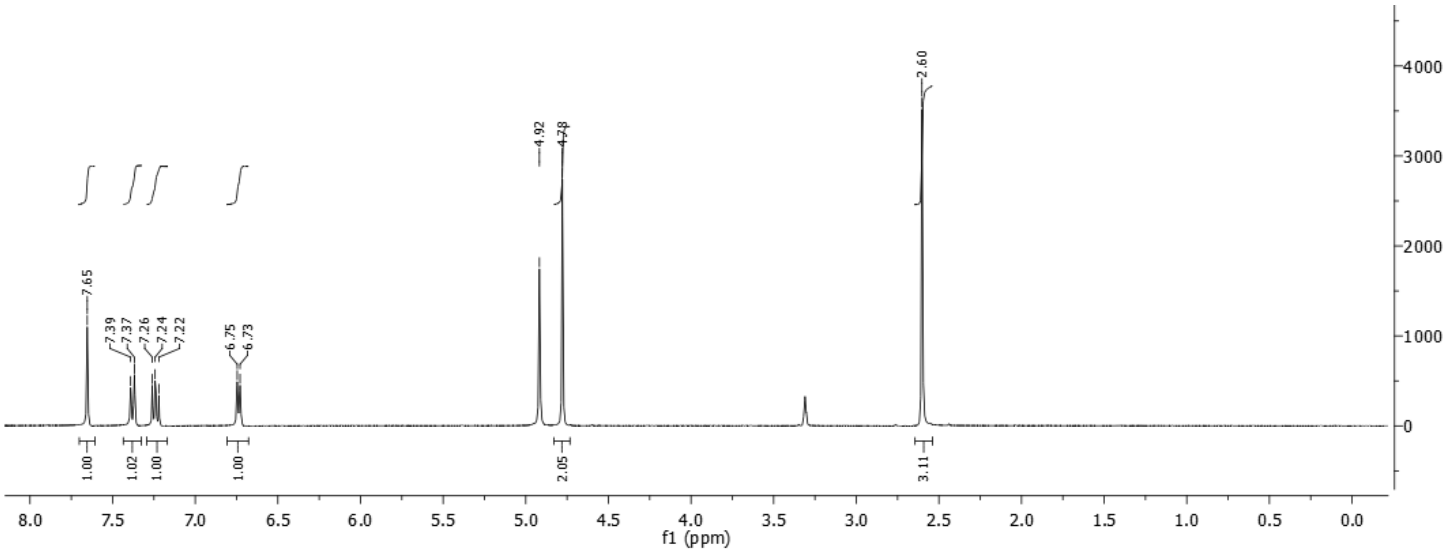

^{1}H-NMR spectrum of the non-deuterated starting material

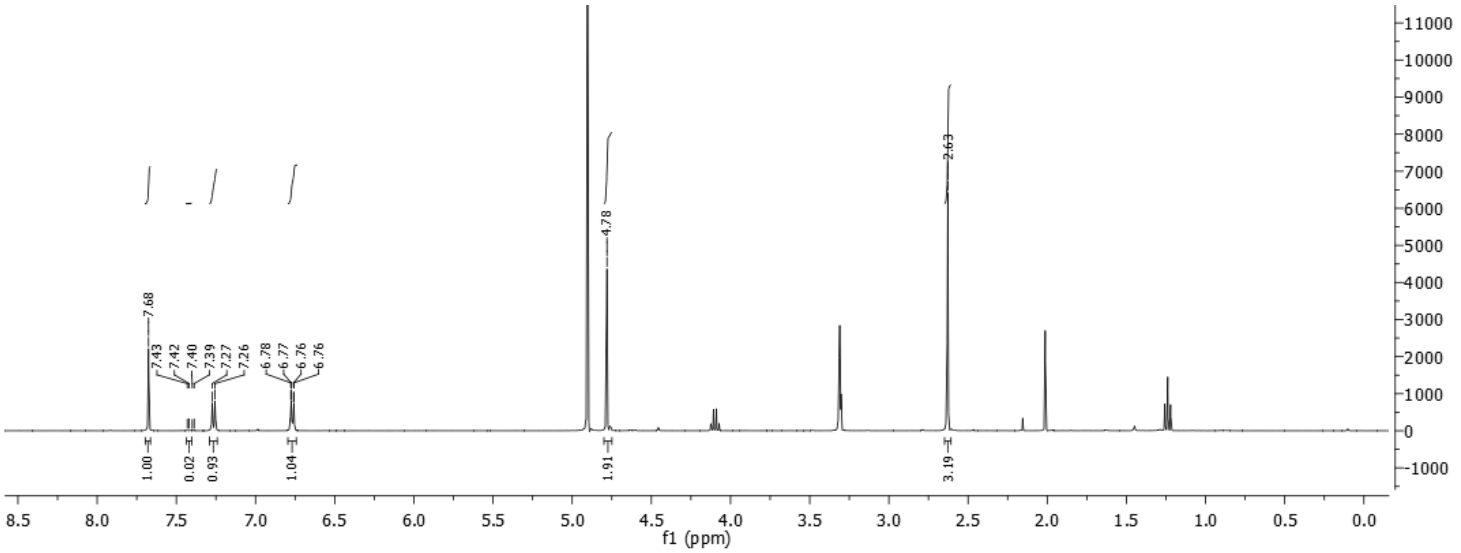

^{1}H-NMR spectrum of **11**

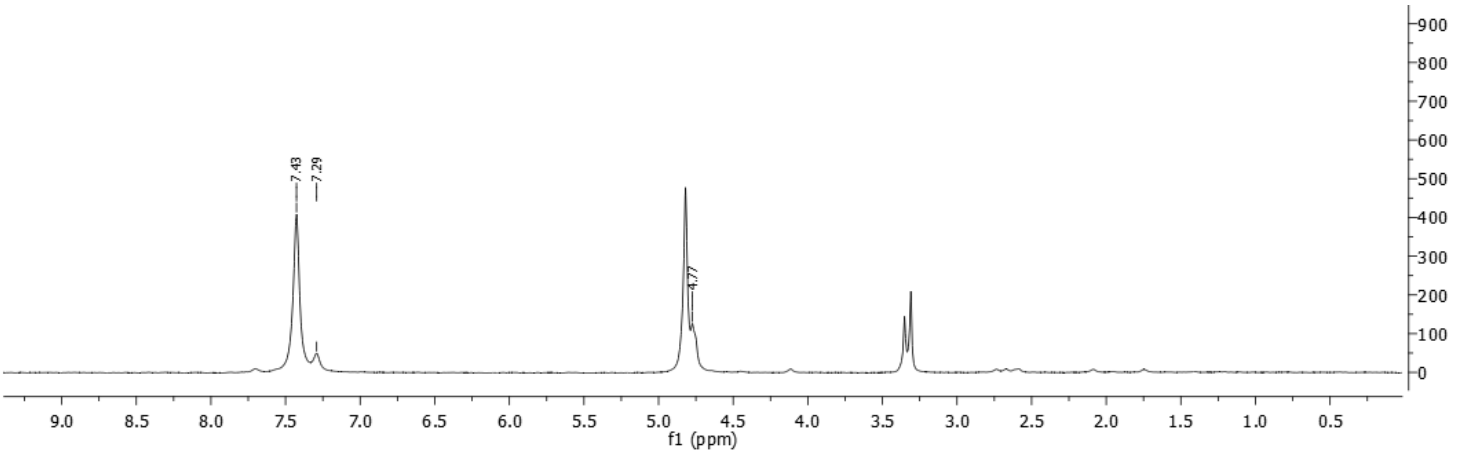

^{2}H-NMR spectrum of **11**

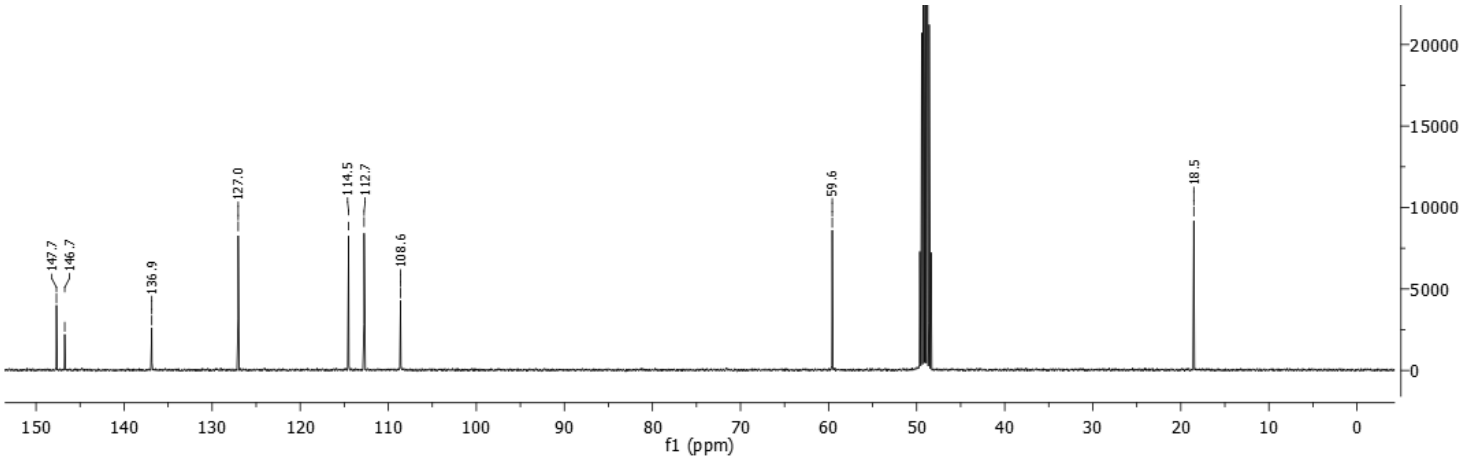

^{13}C-NMR spectrum of the non-deuterated starting material

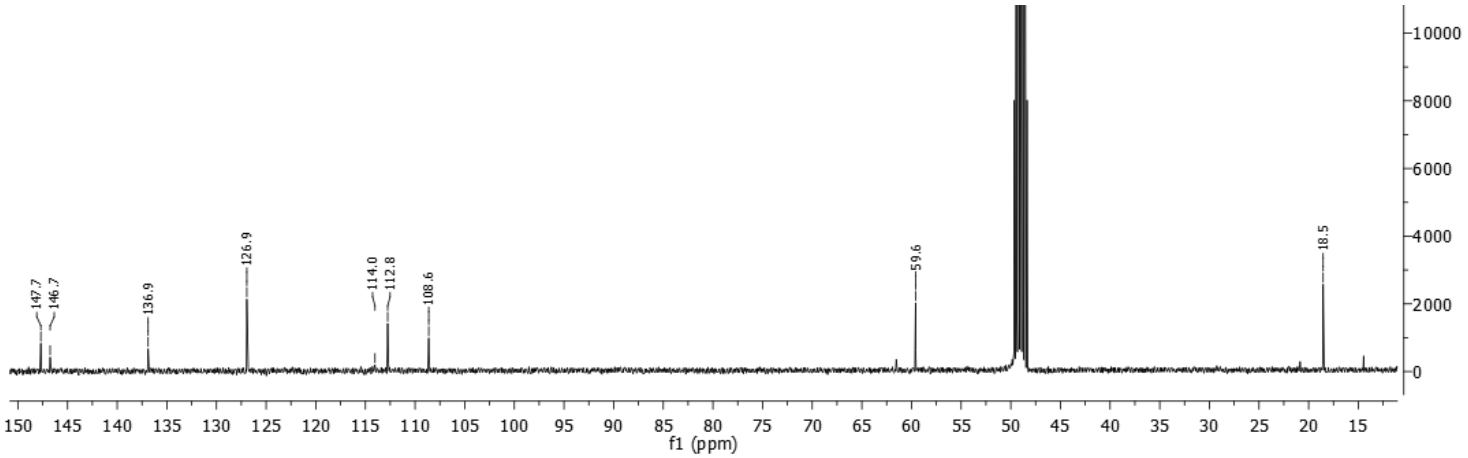

^{13}C-NMR spectrum of **11**

2-Methylbenzoxazole **12**

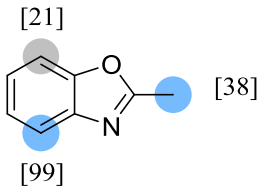

Chemical Formula: C_8H_7NO

Substrate	Solvent (Volume)	RuNp@PVP cat.
53.2mg, 0.4mmol	THF (2mL)	14.4mg, 2.5mol%

Workup and purification:

Once the reaction was set up and stirred for 24h under D_2 atmosphere (2bar), the gas phase was removed under reduced pressure and flushed again with D_2 gas to give a pressure of 2bar. The reaction mixture was stirred for another 24h. After cooling down to room temperature, the reaction mixture was absorbed on SiO_2. The product was eluted with *n*-pentane:THF (10:1, 50mL). The solvent was removed under vacuum.

Yield: 50.0mg, 94%, colourless liquid

^{1}H NMR (400 MHz, Acetone-*d*$_6$): δ 7.65 – 7.57 (m, 0.01H), 7.57 – 7.50 (m, 1H), 7.35 – 7.27 (m, 2H), 2.59 (s, 1.87H).

Deuterium incorporation was expected at δ 7.65 – 7.57 and at δ 2.59. Isotopic enrichment values were determined against the integral at δ 7.35 – 7.27.

^{2}H NMR (600 MHz, Acetone): δ 7.61 (s, 0.99D), 7.55 (s, 0.21D), 7.32 (s, 0.05D), 2.66 – 2.41 (m, 1.13D).

^{13}C-{^{1}H}NMR (100 MHz, Acetone-d_6): δ 164.7, 151.9, 142.7, 125.2, 124.8, 119.8 (m), 111.0, 14.2 (m).

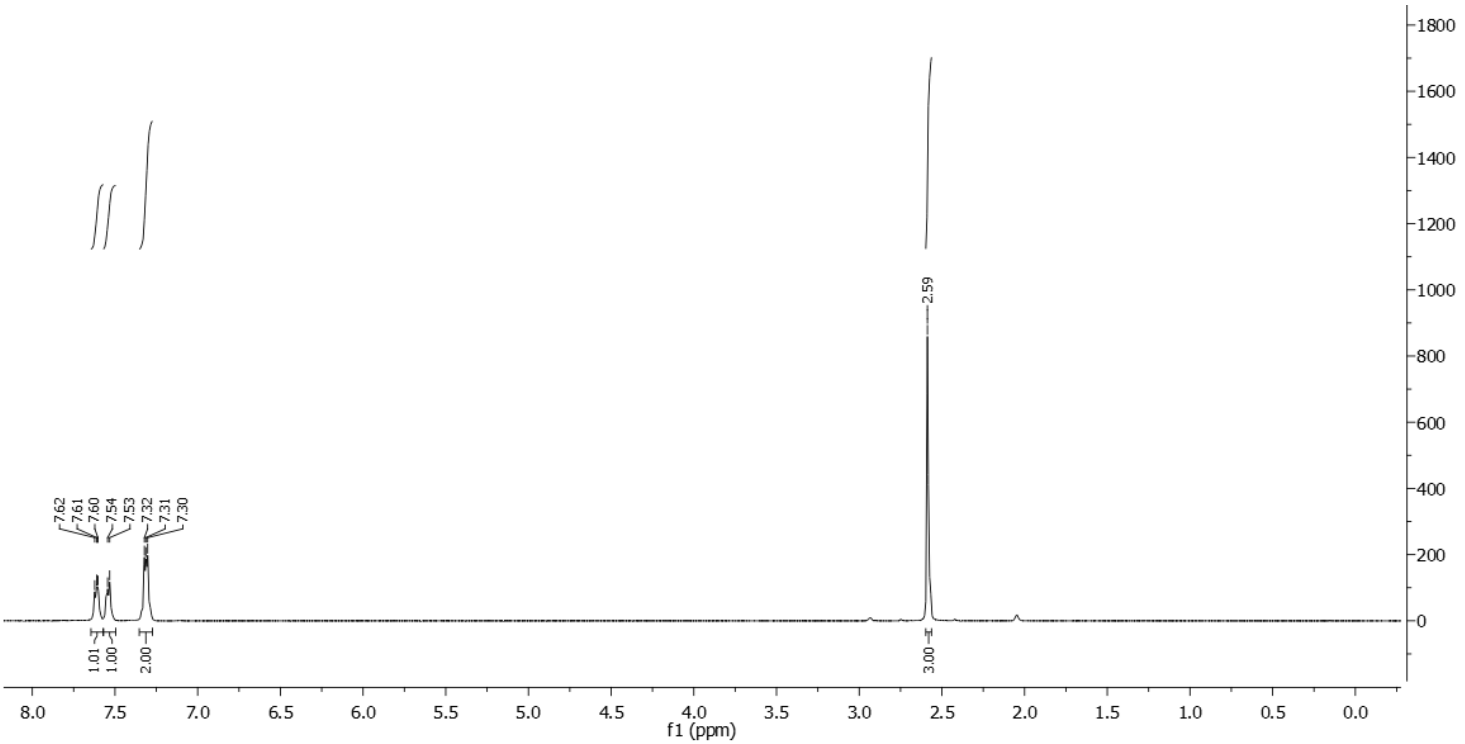

^{1}H-NMR spectrum of the non-deuterated starting material

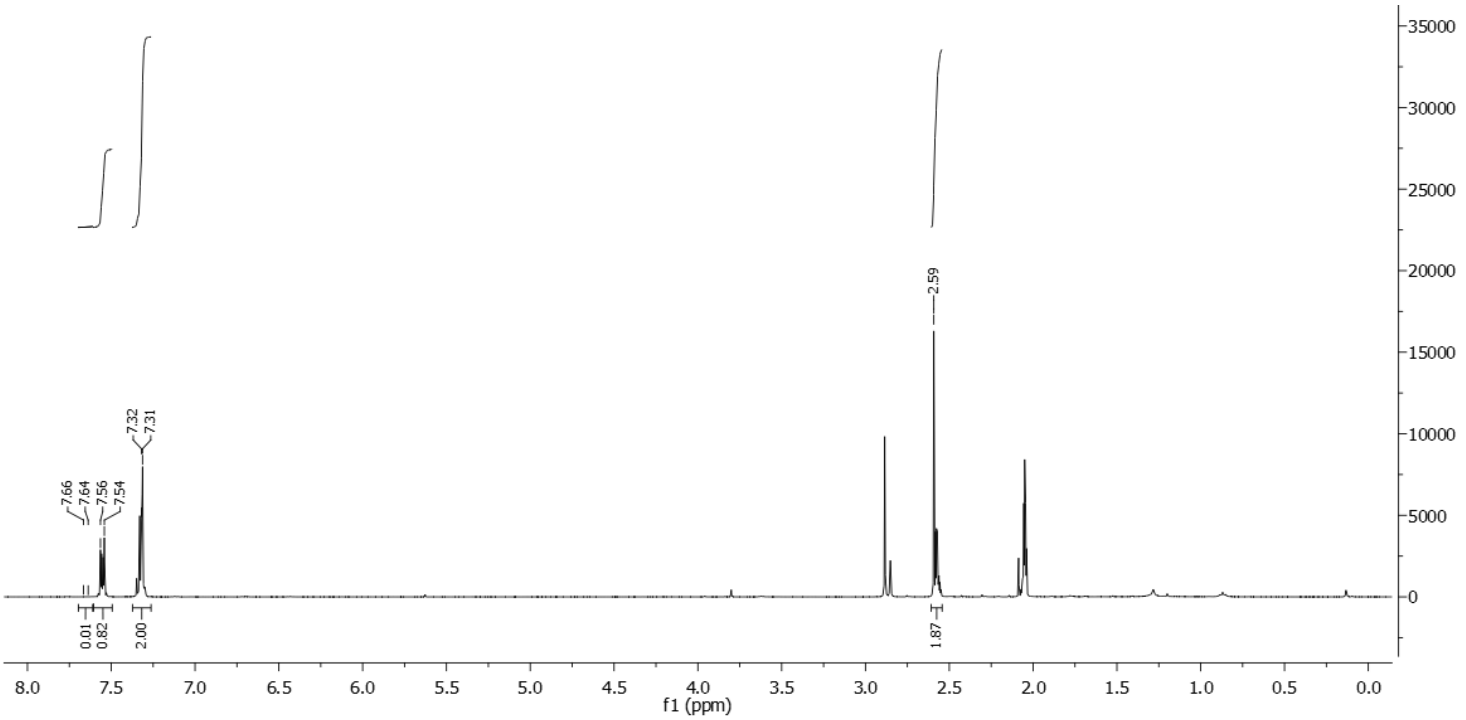

^{1}H-NMR spectrum of **12**

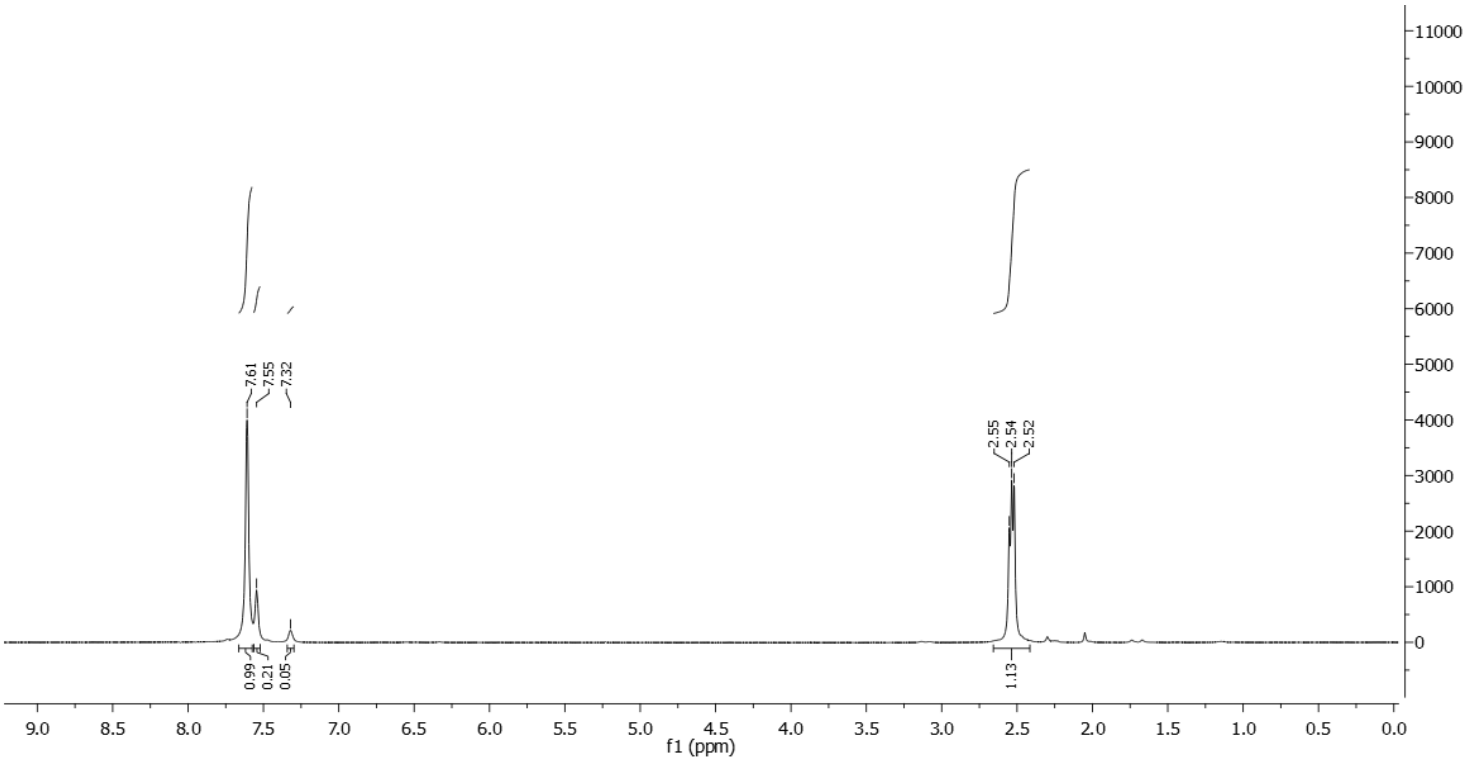

^{2}H-NMR spectrum of **12**

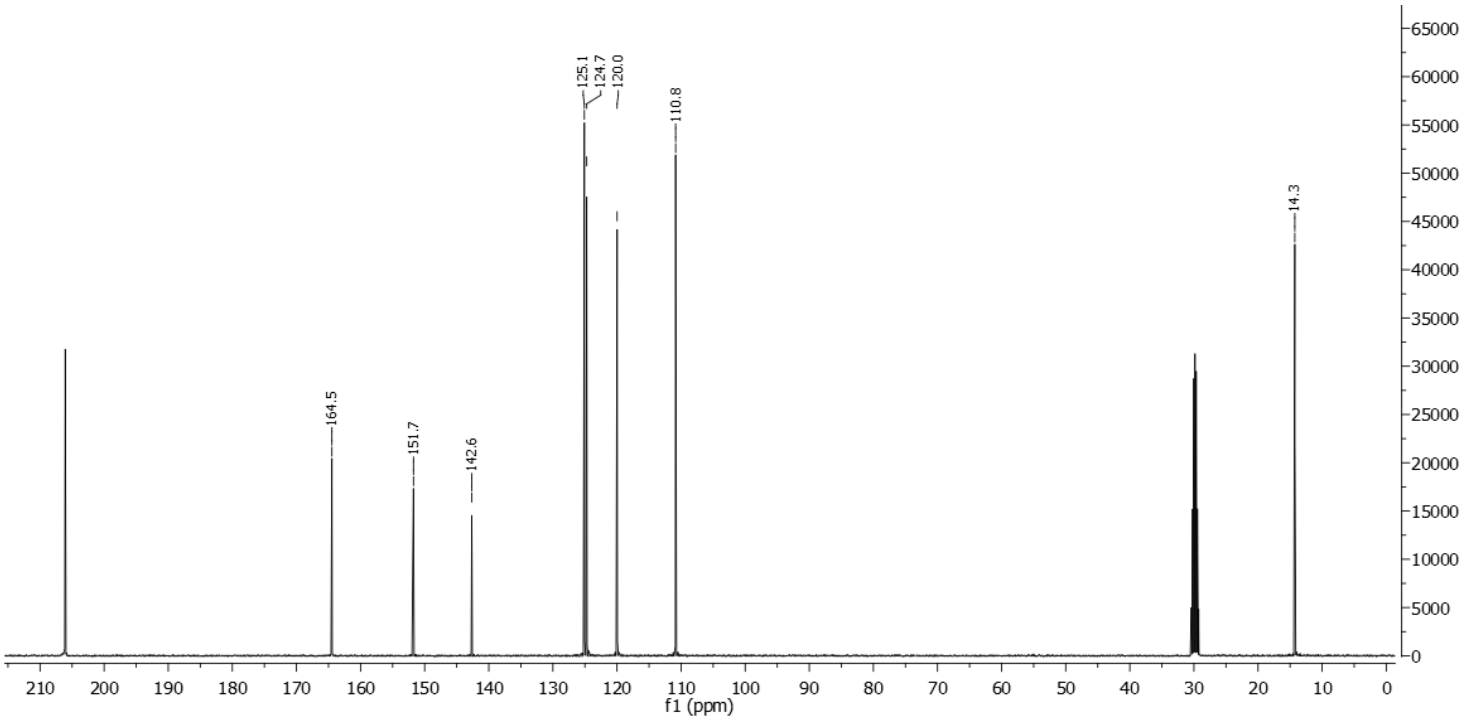

^{13}C-NMR spectrum of the non-deuterated starting material

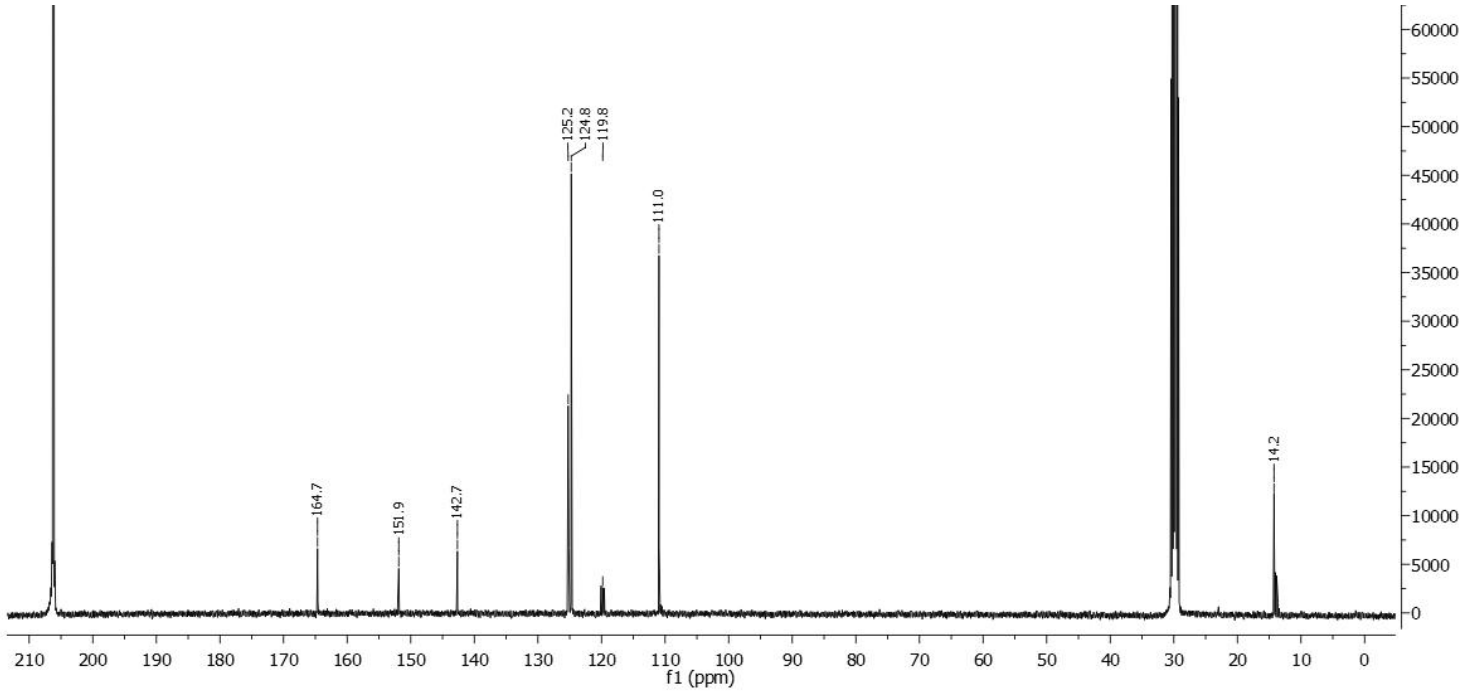

^{13}C-NMR spectrum of **12**

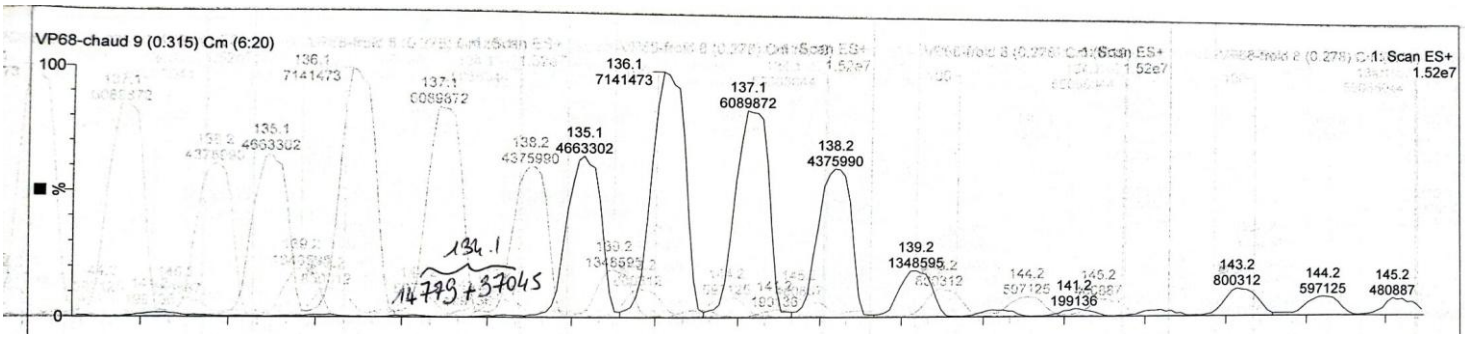

ESI spectrum of **12**

2-Methyl-benzimidazole **13I** *(first deuteration run)*

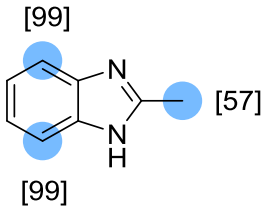

Chemical Formula: $C_8H_8N_2$

Substrate	Solvent (Volume)	RuNp@PVP cat.
26.4mg, 0.2mmol	THF (2mL)	14.4mg, 5mol%

Workup and purification:

After cooling down to room temperature, cyclohexane (2mL) was added to the reaction mixture and stirred for 10min to let precipitating RuNp@PVP. The suspension was passed through a Sep-Pak® C18 cartridge and then eluted with EtOAc/cyclohexane (1:1, 5mL). The solvent was removed under vacuum.

Yield: 26.0mg, 99%, white solid

^{1}H NMR (400 MHz, Acetone-d_6): δ 7.51 – 7.46 (m, 0.06H), 7.18 – 7.08 (m, 2H), 2.57 – 2.51 (m, 1.28H).

Deuterium incorporation was expected at δ 7.51 – 7.46 and at δ 2.57 – 2.51. Isotopic enrichment values were determined against the integral at δ 7.18 – 7.08.

^{13}C-{^{1}H}NMR (100 MHz, Acetone-d_6): δ 152.0, 122.0, 114.8 (m), 14.9 (m).

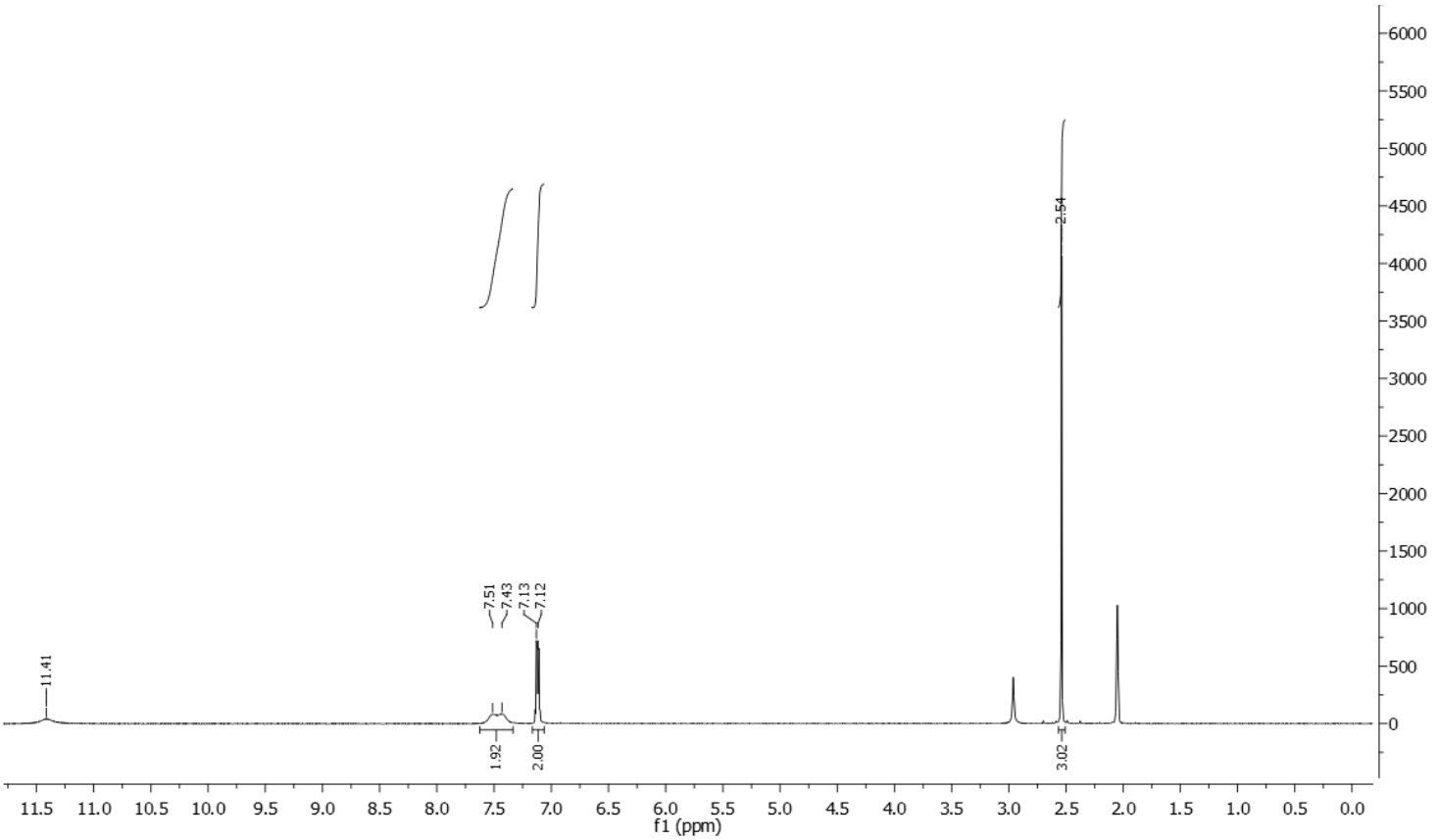

^{1}H-NMR spectrum of the non-deuterated starting material

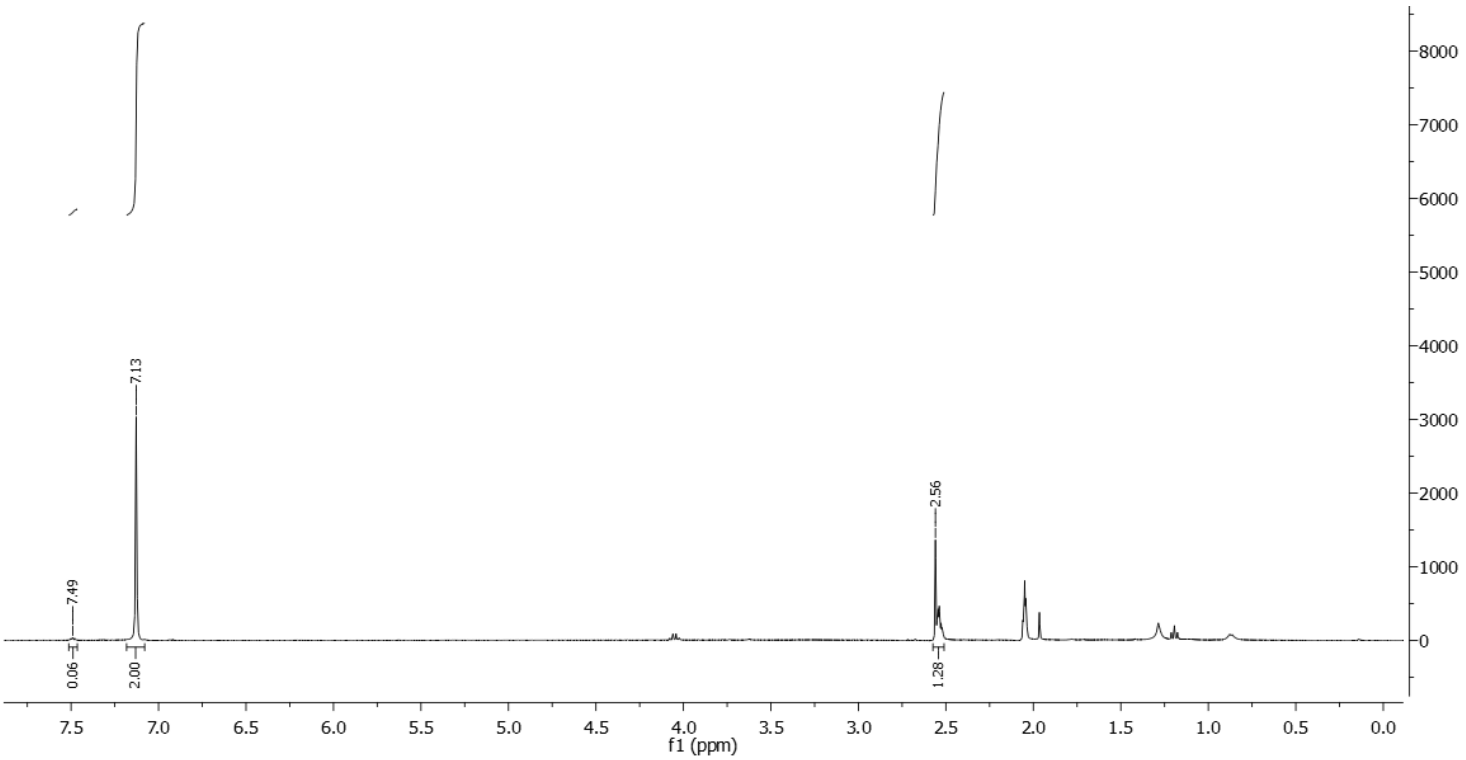

^{1}H-NMR spectrum of **13I**

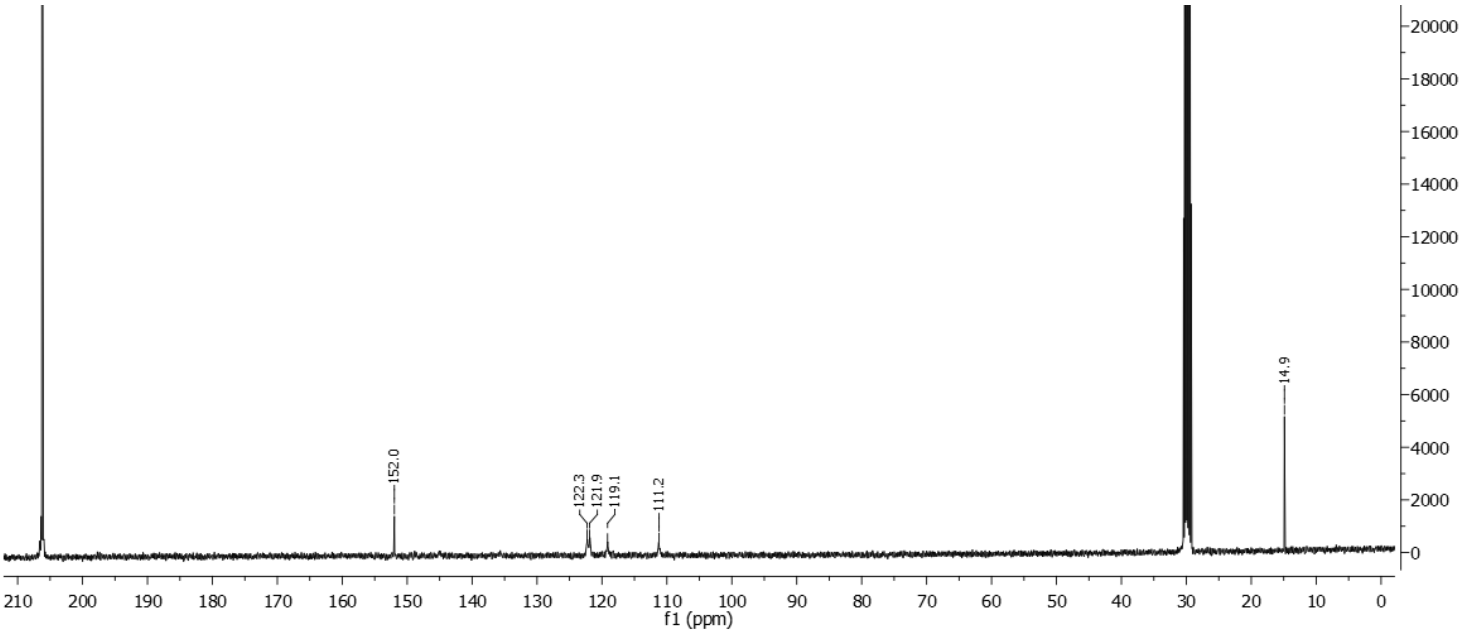

^{13}C-NMR spectrum of the non-deuterated starting material

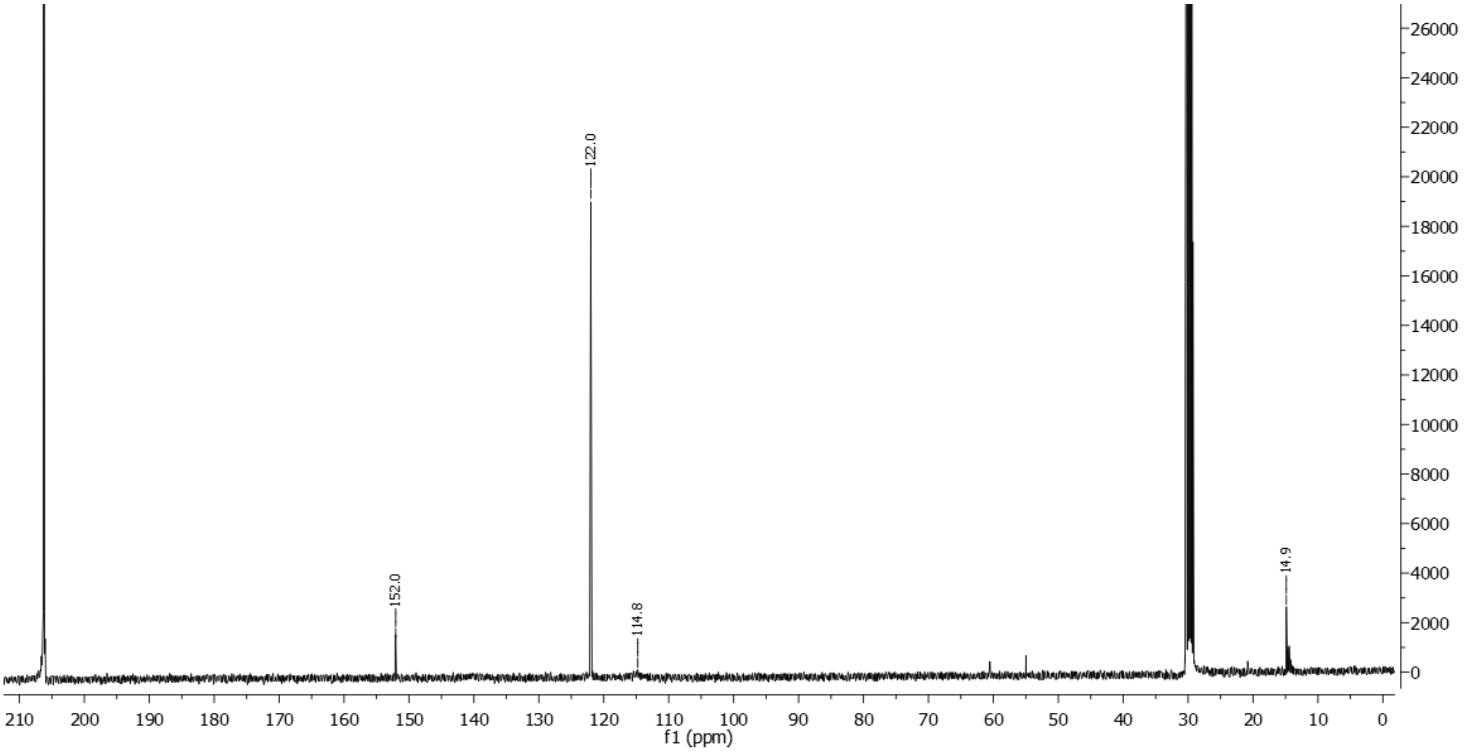

^{13}C-NMR spectrum of **13I**

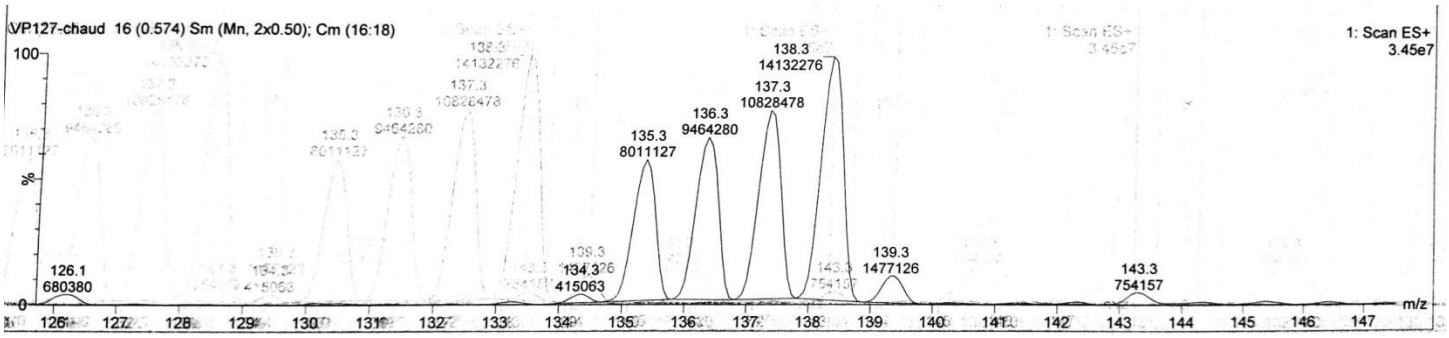

ESI spectrum of **13I**

2-Methyl-benzimidazole **13II** *(second deuteration run)*

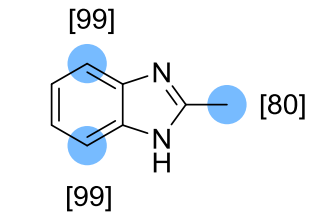

Chemical Formula: $C_8H_8N_2$

Substrate	Solvent (Volume)	RuNp@PVP cat.
26.0mg, 0.2mmol	THF (2mL)	14.4mg, 5mol%

Workup and purification:

After cooling down to room temperature, cyclohexane (2mL) was added to the reaction mixture and stirred for 10min to let precipitating RuNp@PVP. The suspension was passed through a Sep-Pak® C18 cartridge and then eluted with EtOAc/cyclohexane (1:1, 5mL). The solvent was removed under vacuum.

Yield: 26.0mg, 99%, white solid

^{1}H NMR (400 MHz, Acetone-d_6): δ 7.51 – 7.48 (m, 0.04H), 7.19 – 7.09 (m, 2H), 2.58 – 2.52 (m, 0.59H).

Deuterium incorporation was expected at δ 7.51 – 7.48 and at δ 2.58 – 2.52. Isotopic enrichment values were determined against the integral at δ 7.19 – 7.09.

^{2}H-{^{1}H}NMR (92 MHz, Acetone): δ 7.48 (s, 2D), 2.47 (s, 2.38D)

^{13}C-{^{1}H}NMR (100 MHz, Acetone-d_6): δ 152.0, 122.0, 114.9 (m), 14.4 (m).

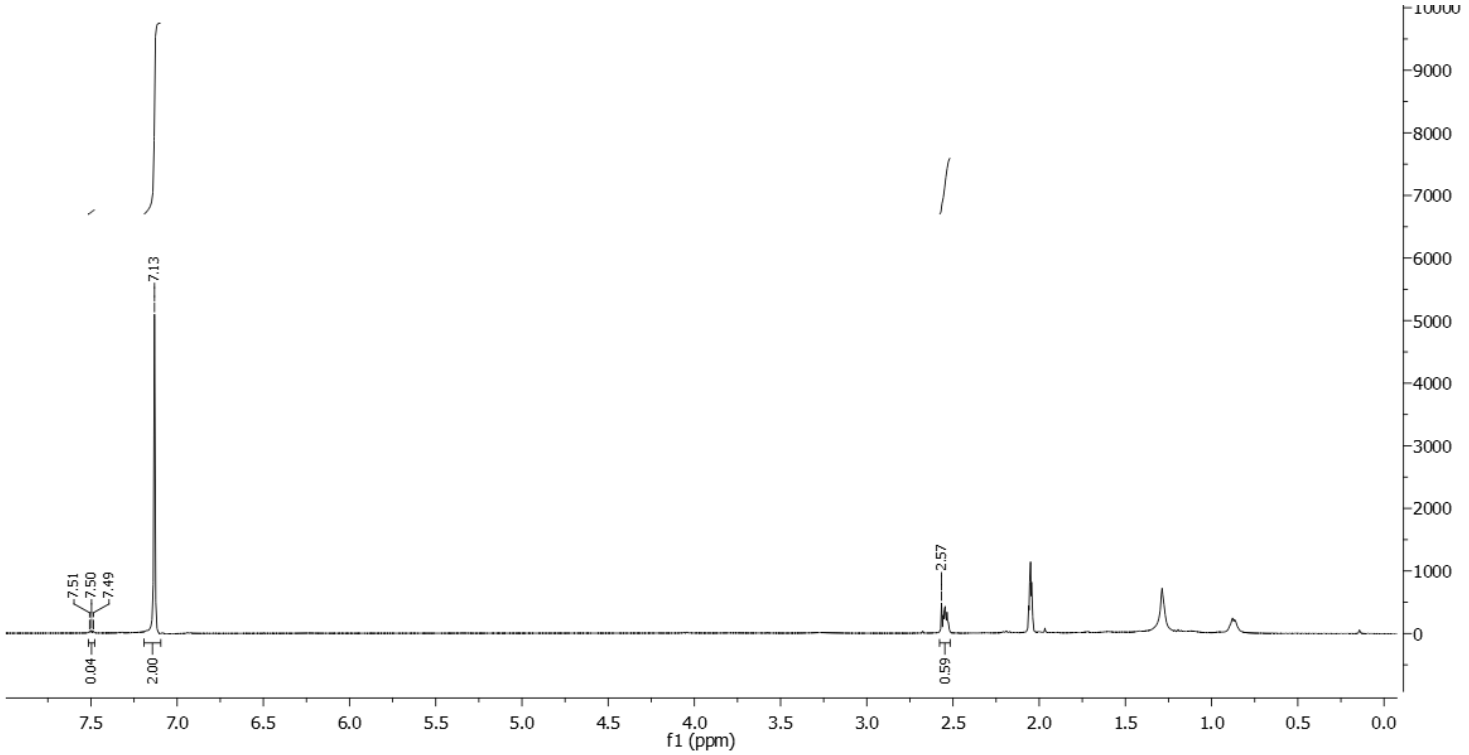

^{1}H-NMR spectrum of **13II** (2nd run)

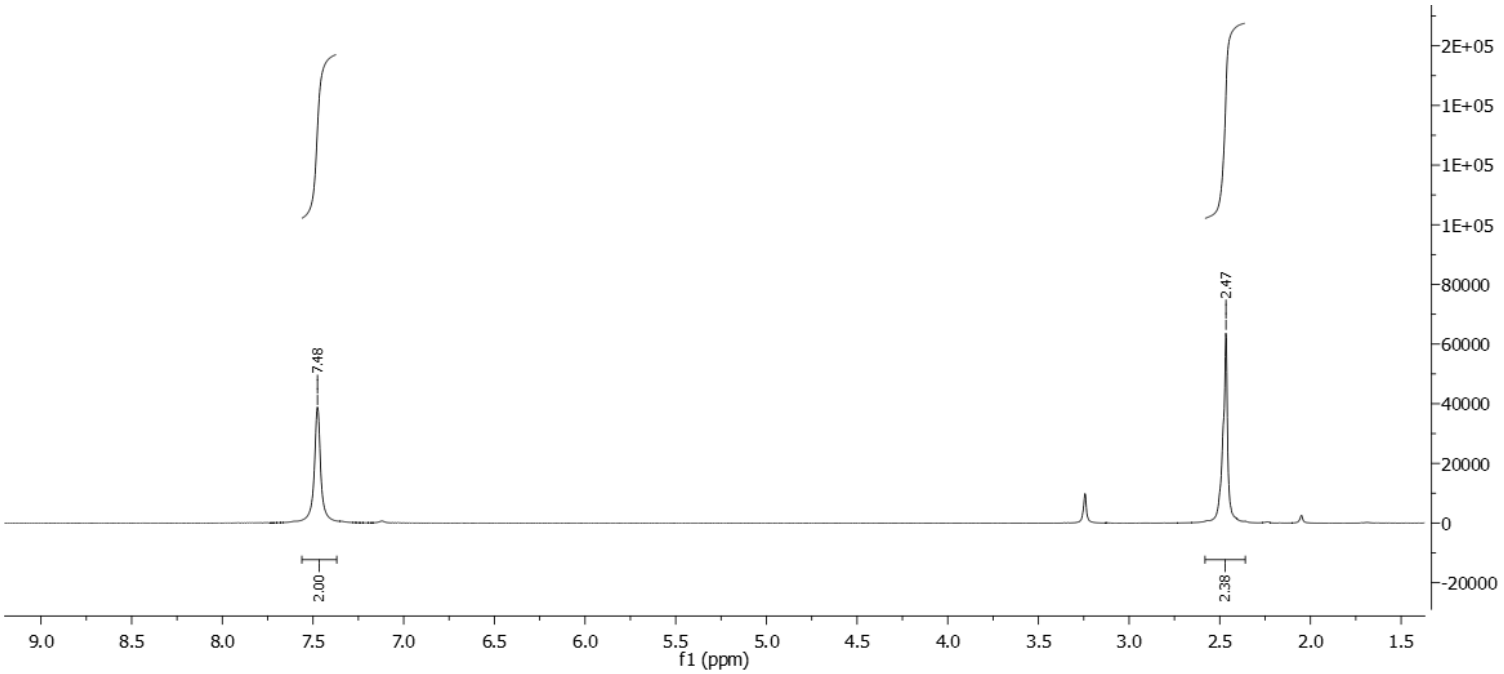

^{2}H-NMR spectrum of **13II** (2nd run)

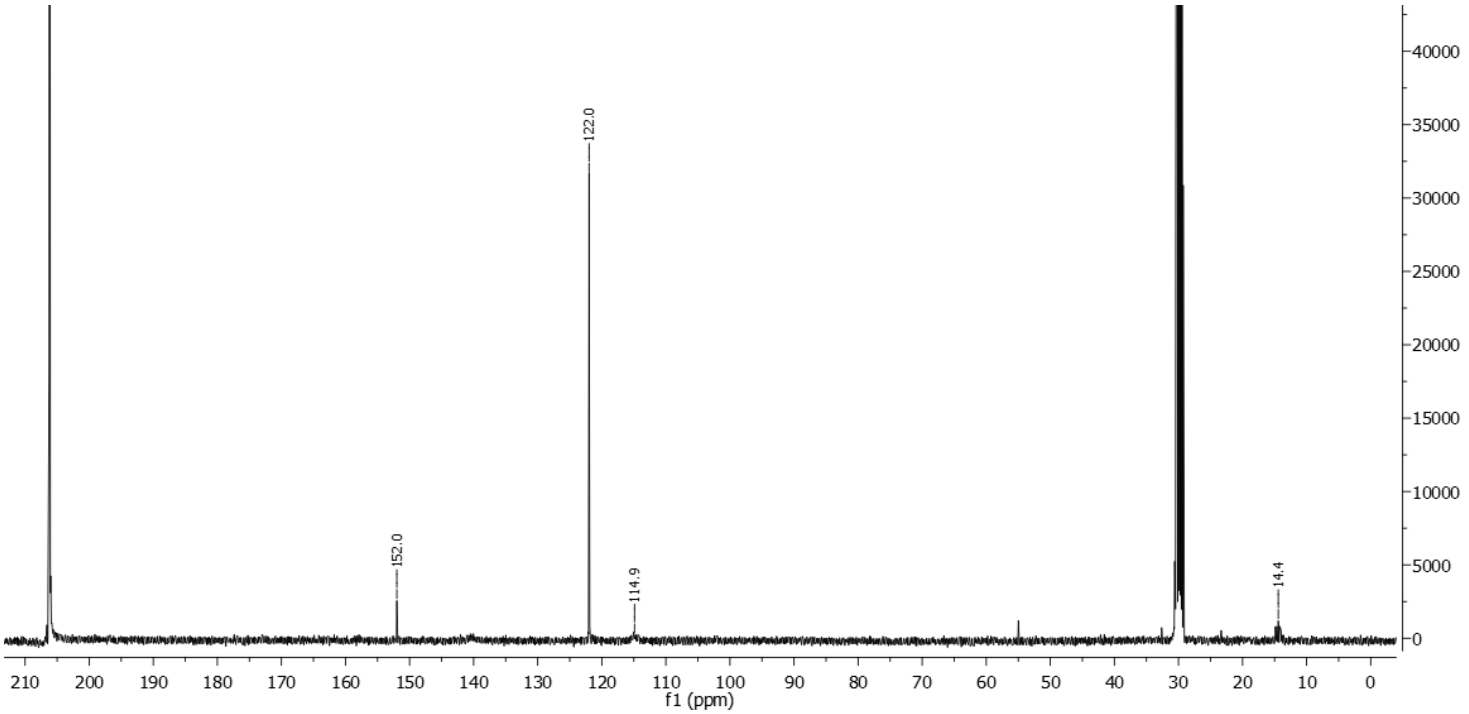

^{13}C-NMR spectrum of **13II** (2nd run)

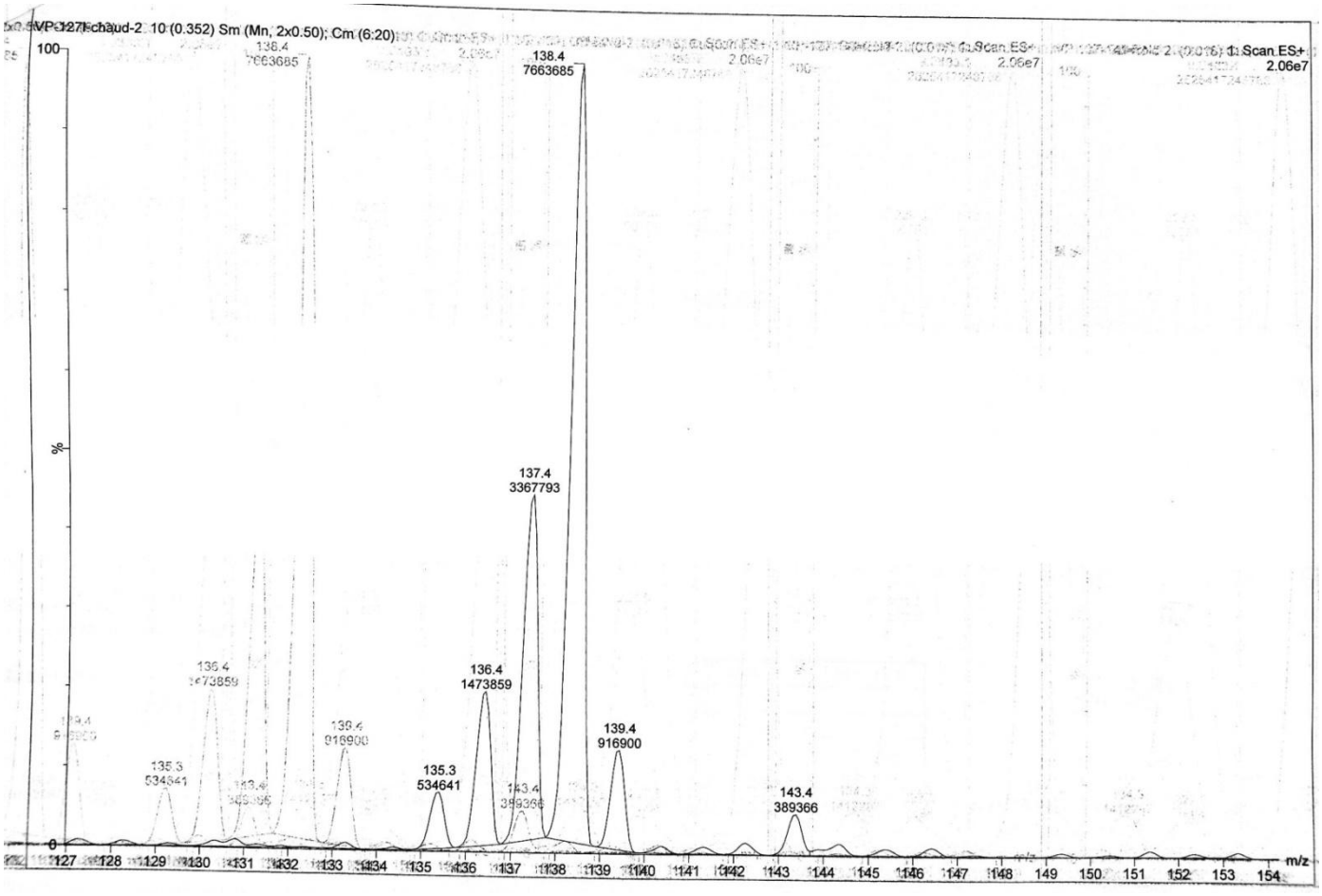

ESI spectrum of **13II** (2nd run)

Deuterations of 1,2,4-triazoles

1-Phenyl-1H-1,2,4-triazole **14**

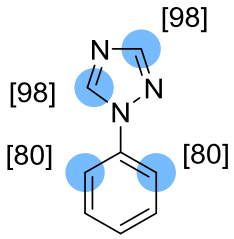

Chemical Formula: $C_8H_7N_3$

Substrate	Solvent (Volume)	RuNp@PVP cat.	Reaction time
29.0mg, 0.2mmol	THF (0.5mL)	14.4mg, 5mol%	48h

Workup and purification:

After cooling down to room temperature, EtOAc (3mL) was added to the reaction mixture and stirred for 10min to let precipitate RuNp@PVP. The suspension was passed through a basic Al_2O_3 pad and then eluted with EtOAc (3mL). The solvent was removed under vacuum. The crude product was recrystallized from acetone.

Yield: 18.0mg, 62%, white solid

^{1}H NMR (400 MHz, Acetone-d_6): δ 9.03 (s, 0.02H), 8.10 (s, 0.02H), 7.91 – 7.84 (m, 0.40H), 7.62 – 7.50 (m, 2H), 7.46 – 7.38 (m, 1H).

Deuterium incorporation was expected at δ 9.03, δ 8.10 and at δ 7.91 – 7.84. Isotopic enrichment values were determined against the integral at δ 7.46 – 7.38.

^{2}H-{^{1}H}NMR (92 MHz, Acetone): δ 9.01 (m, 0.98D), 8.09 (m, 0.96D), 7.88 (m, 1.60D)

^{13}C-{^{1}H}NMR (100 MHz, Acetone-d_6): δ 153.4 (m), 142.6 (m), 138.2, 130.5, 128.6, 120.4 (m).

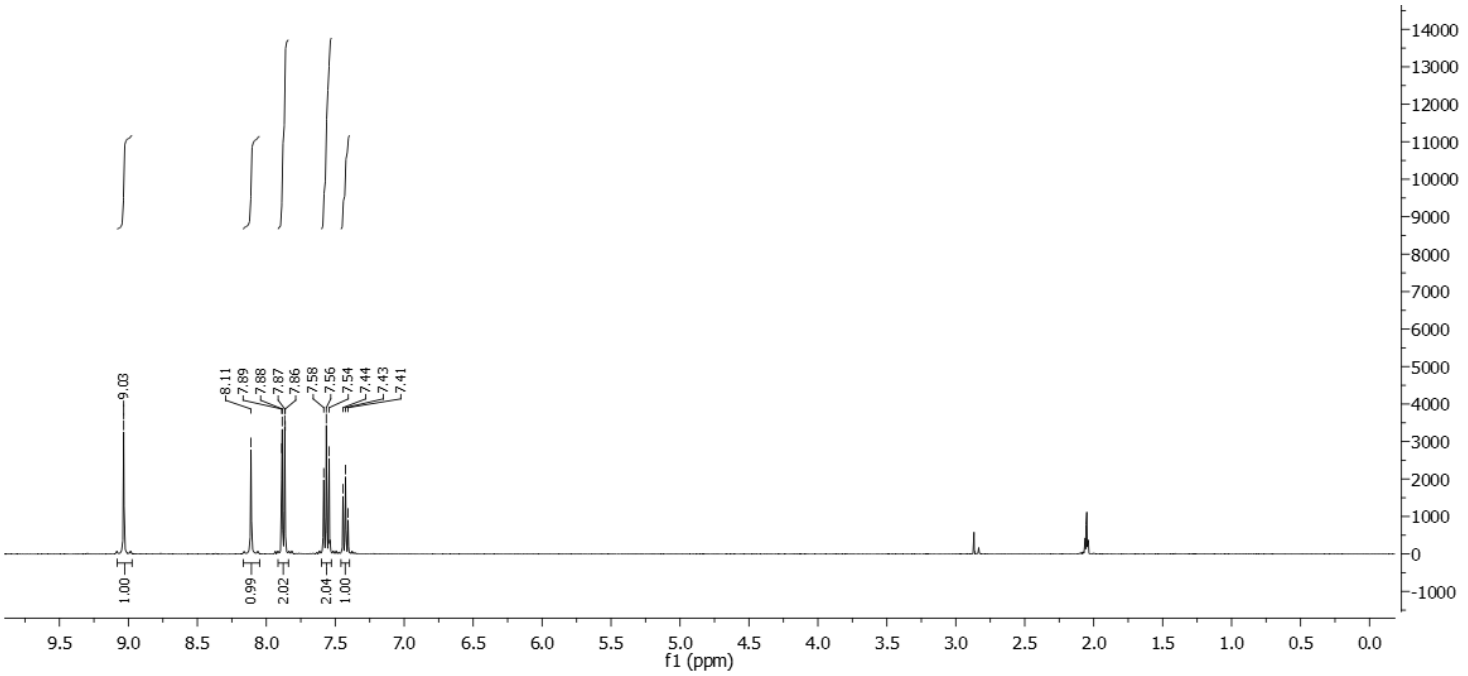

^{1}H-NMR spectrum of the non-deuterated starting material

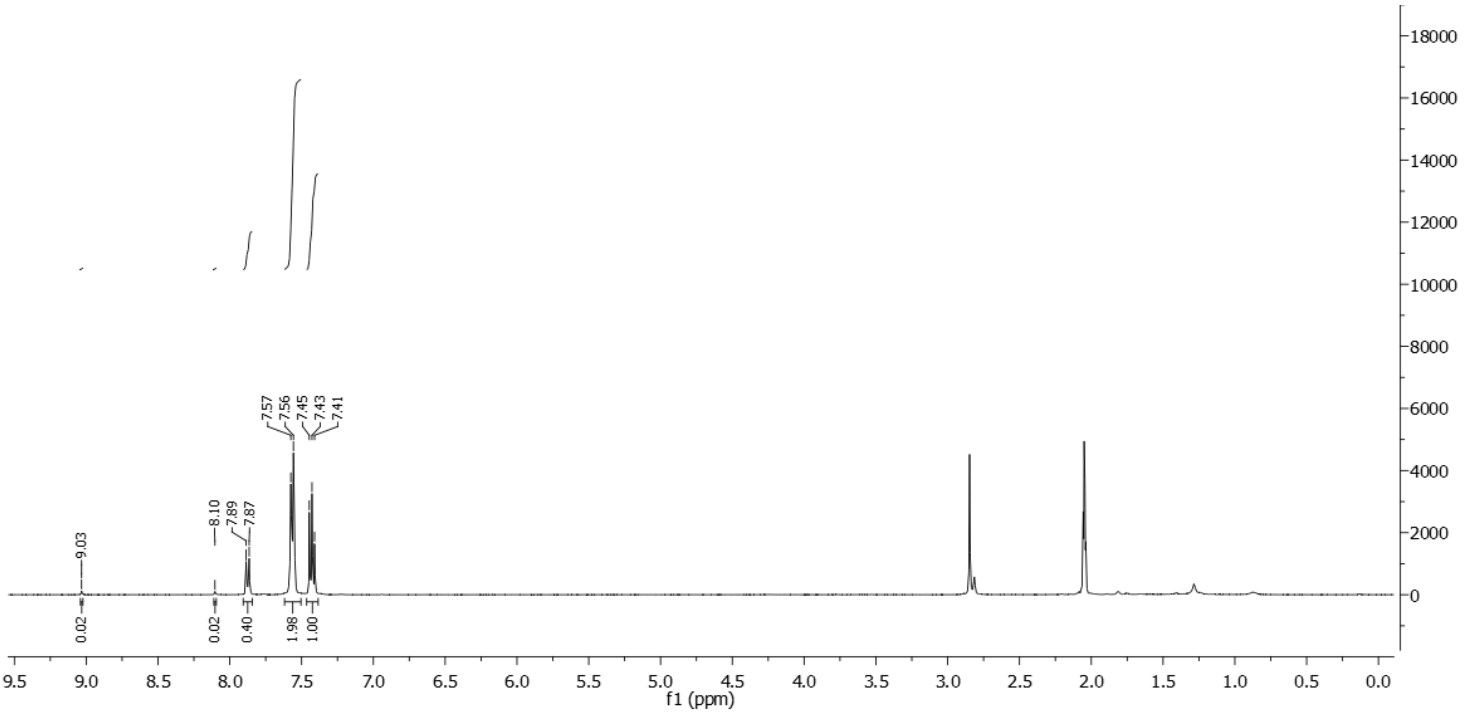

^{1}H-NMR spectrum of **14**

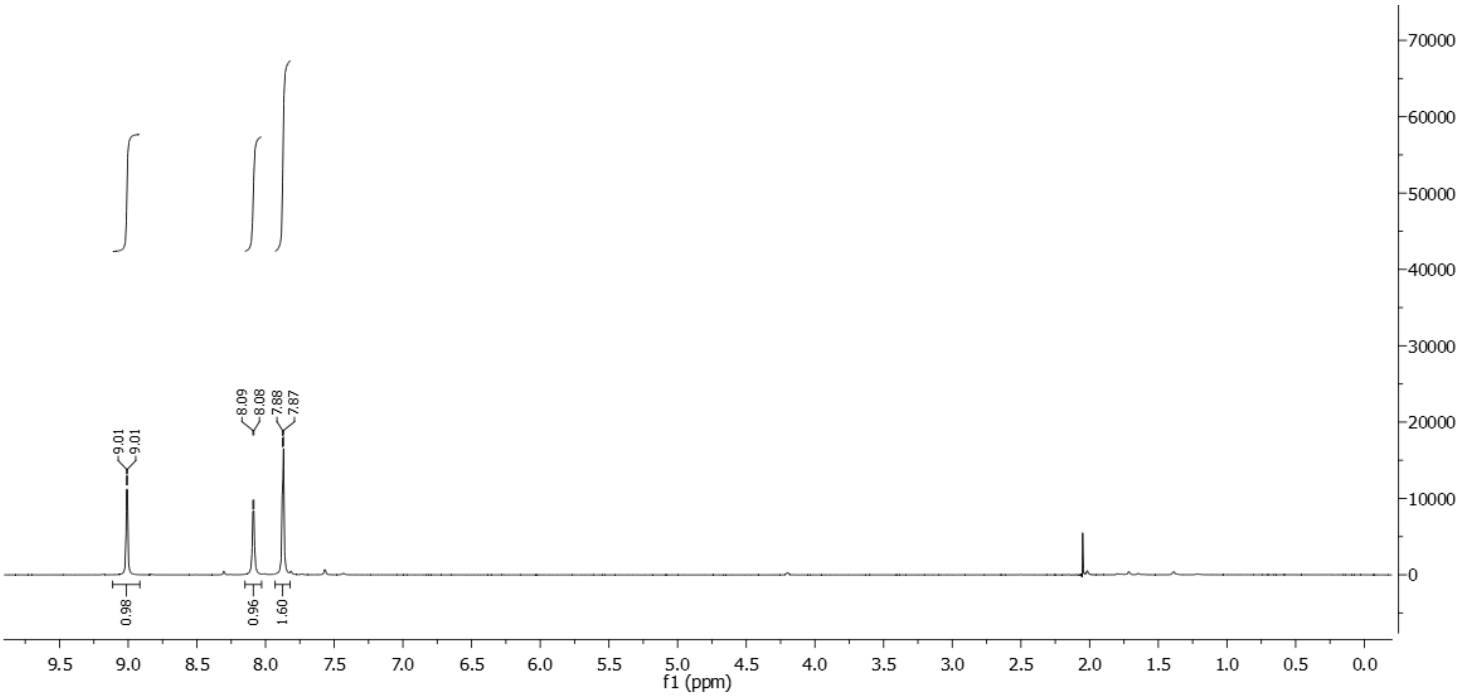

^{2}H-NMR spectrum of **14**

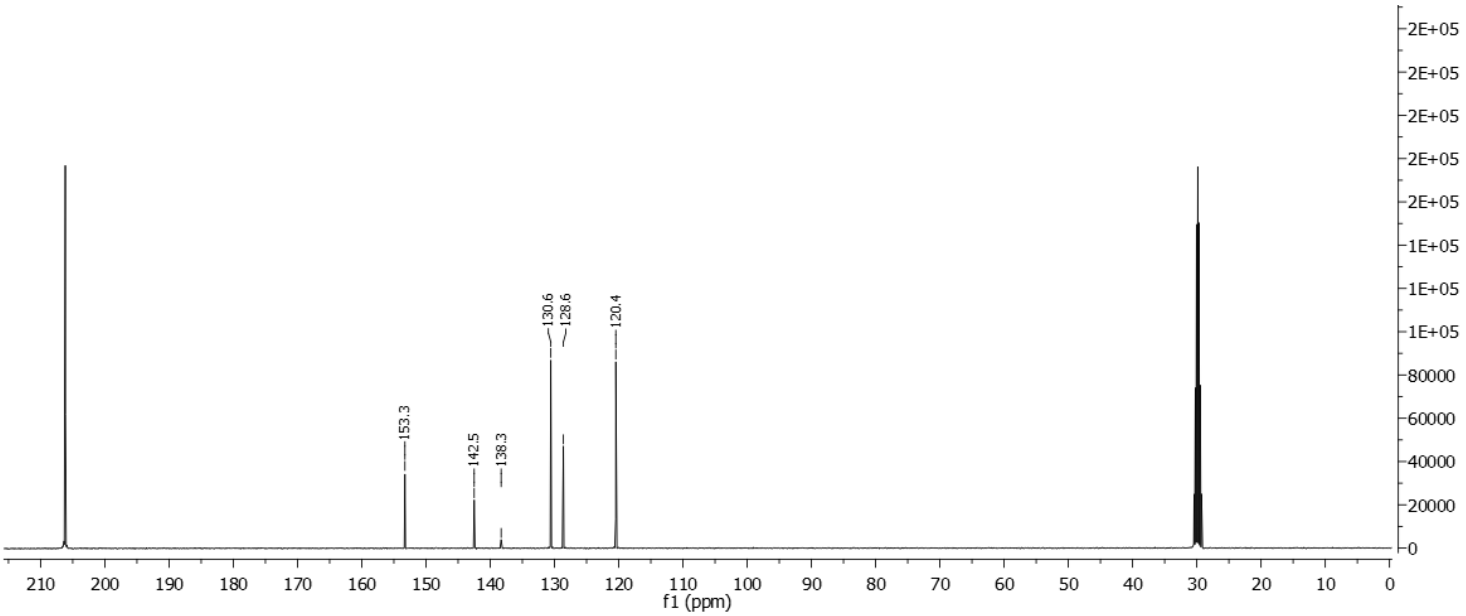

^{13}C-NMR spectrum of the non-deuterated starting material

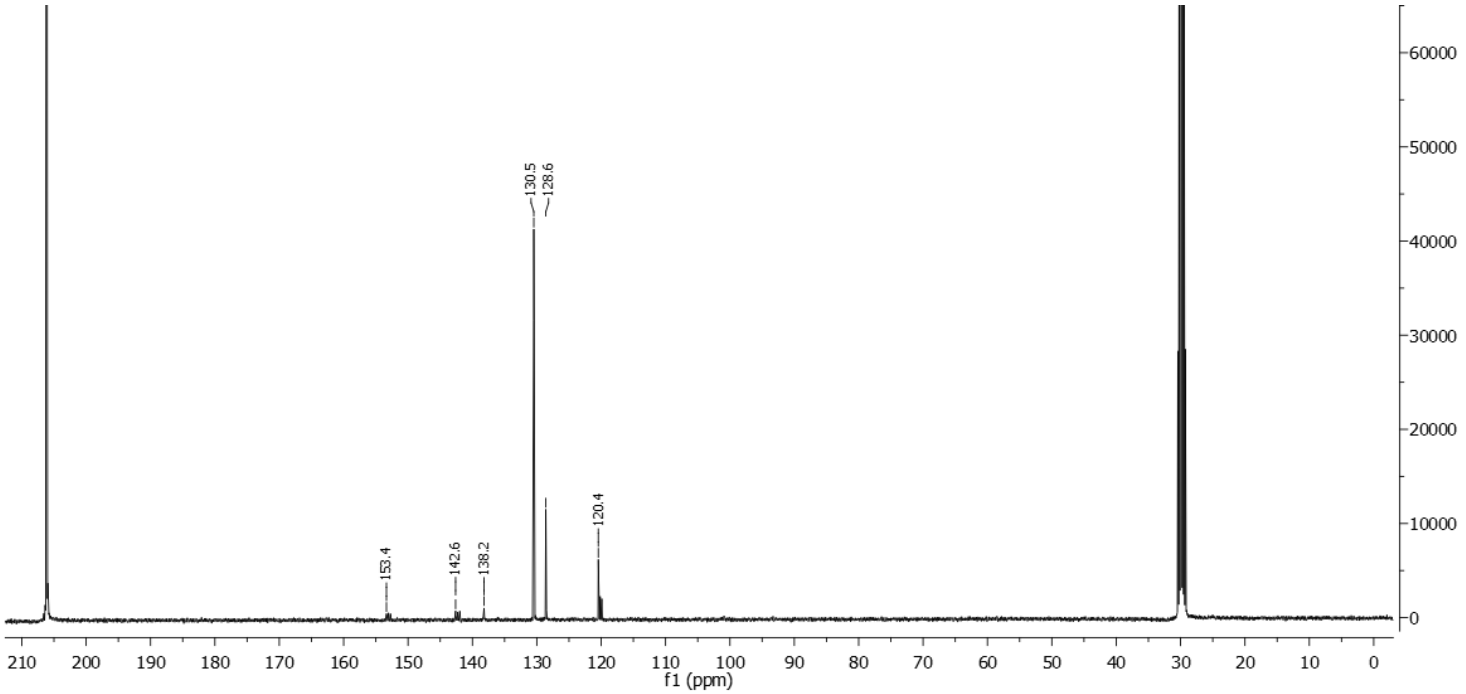

^{13}C-NMR spectrum of **14**

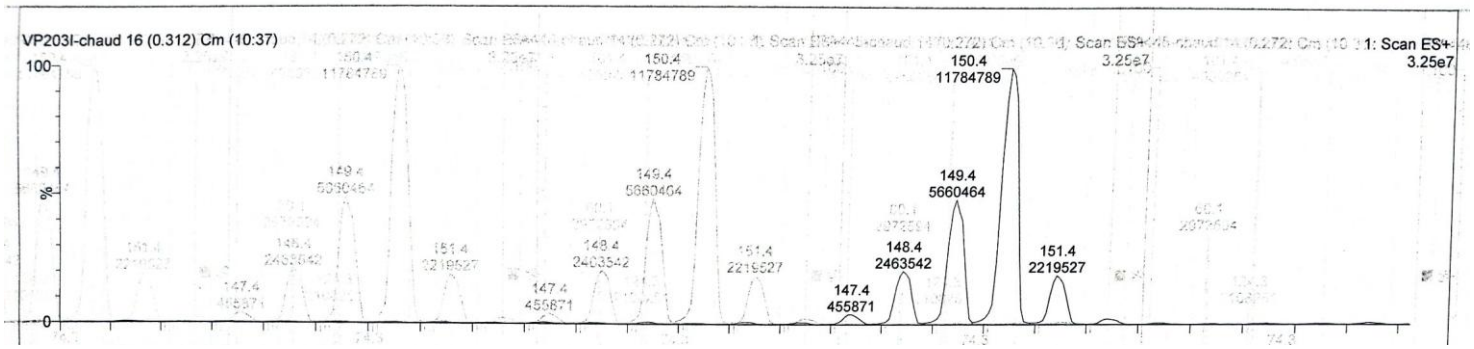

ESI spectrum of **14**

1-(4-Methoxyphenyl)-1H-1,2,4-triazole **15**

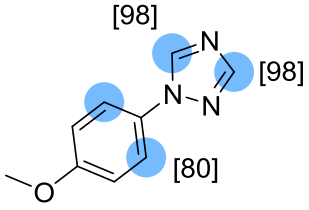

Chemical Formula: $C_9H_9N_3O$

Substrate	Solvent (Volume)	RuNp@PVP cat.
35.0mg, 0.2mmol	THF (2mL)	14.4mg, 5mol%

Workup and purification:

After cooling down to room temperature, EtOAc/cyclohexane (1:1, 3mL) was added to the reaction mixture and stirred for 10min to let precipitate RuNp@PVP. The suspension was passed through a Sep-Pak® C18 cartridge and then eluted with EtOAc/cyclohexane (1:1, 5mL). The solvent was removed under vacuum.

Yield: 37.0mg, 99%, white solid

^{1}H NMR (400 MHz, Acetone-d_6): δ 8.90 (s, 0.02H), 8.06 (s, 0.02H), 7.81 – 7.71 (m, 0.41H), 7.14 – 7.06 (m, 2H), 3.86 (s, 3H).

Deuterium incorporation was expected at δ 9.05, δ 8.90, δ 8.06 and at δ 7.81 – 7.71. Isotopic enrichment values were determined against the integral at δ 7.14 – 7.06.

^{2}H-{^{1}H}NMR (92 MHz, Acetone): δ 8.91 (s, 0.98D), 8.08 (s, 0.98D), 7.79 (s, 1.59D)

^{13}C-{^{1}H}NMR (100 MHz, Acetone-d_6): δ 160.1, 153.0 (m), 142.3 (m), 131.5, 122.1 (m), 115.4, 55.9.

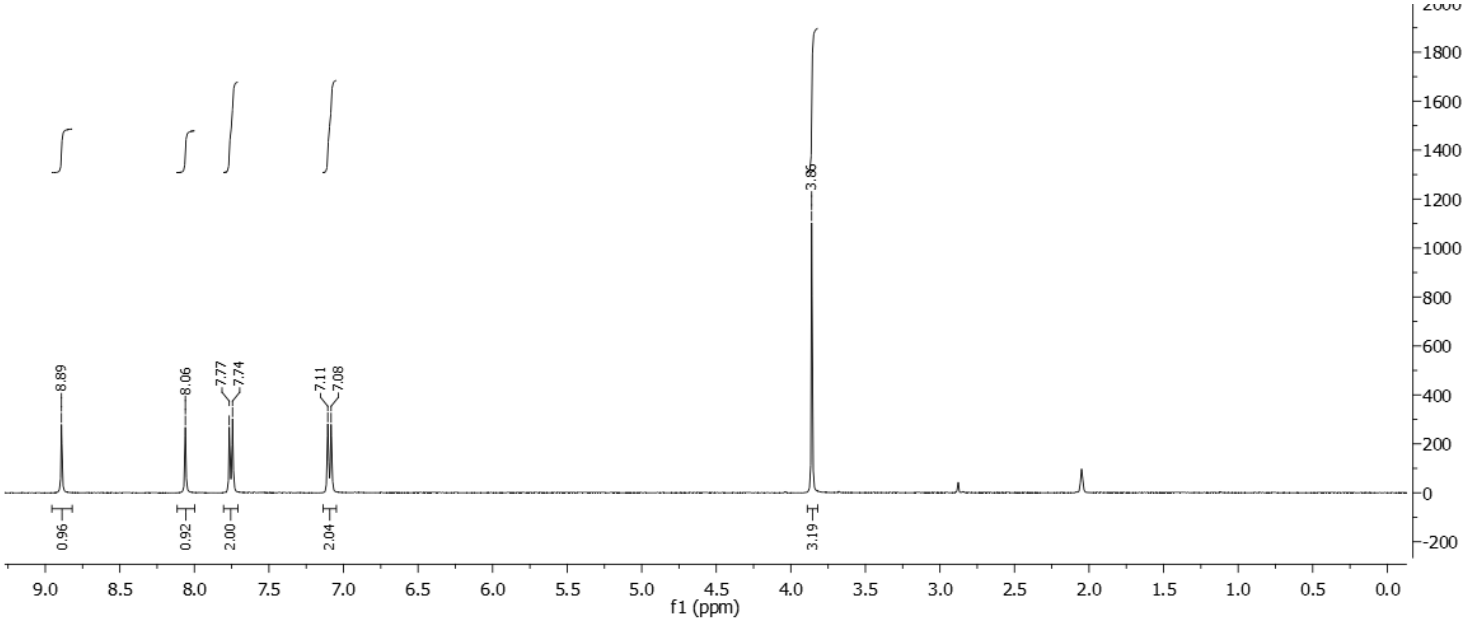

^{1}H-NMR spectrum of the non-deuterated starting material

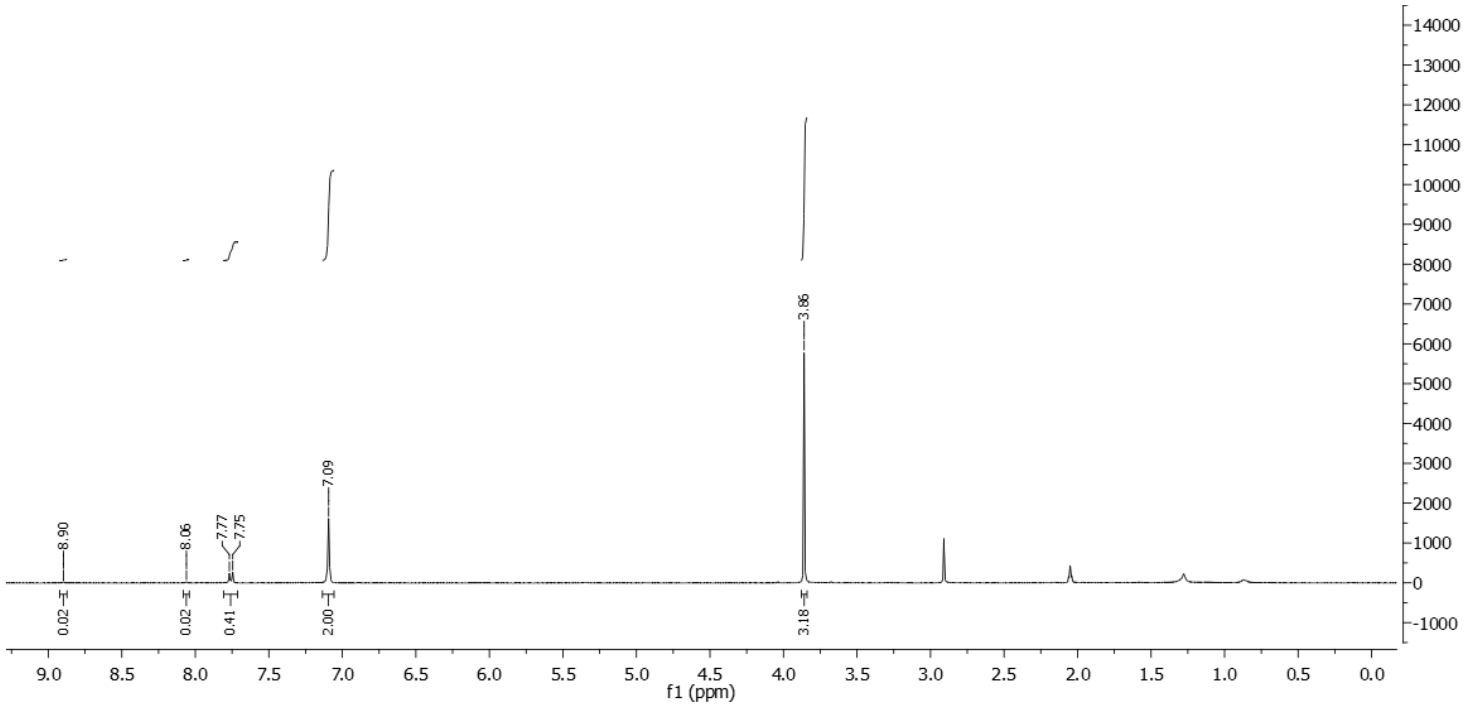

^{1}H-NMR spectrum of **15**

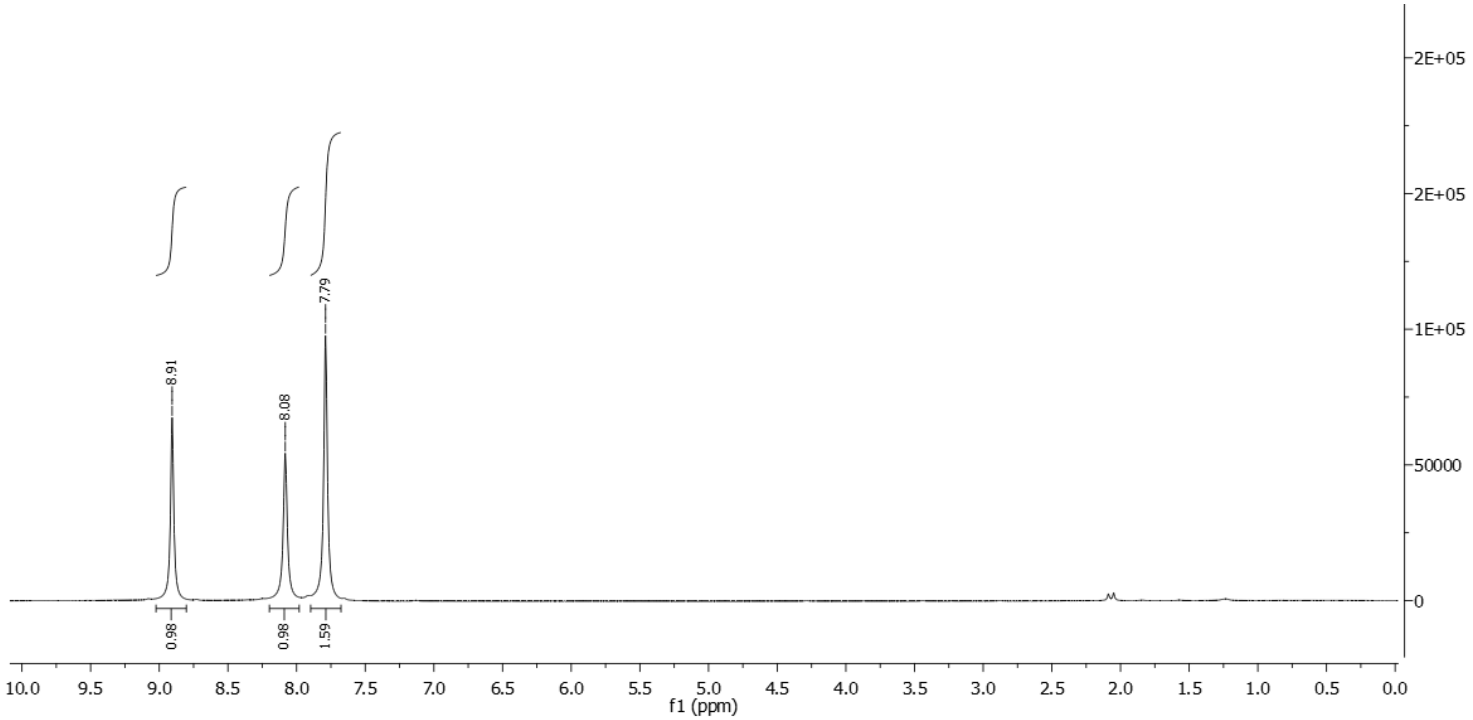

^{2}H-NMR spectrum of **15**

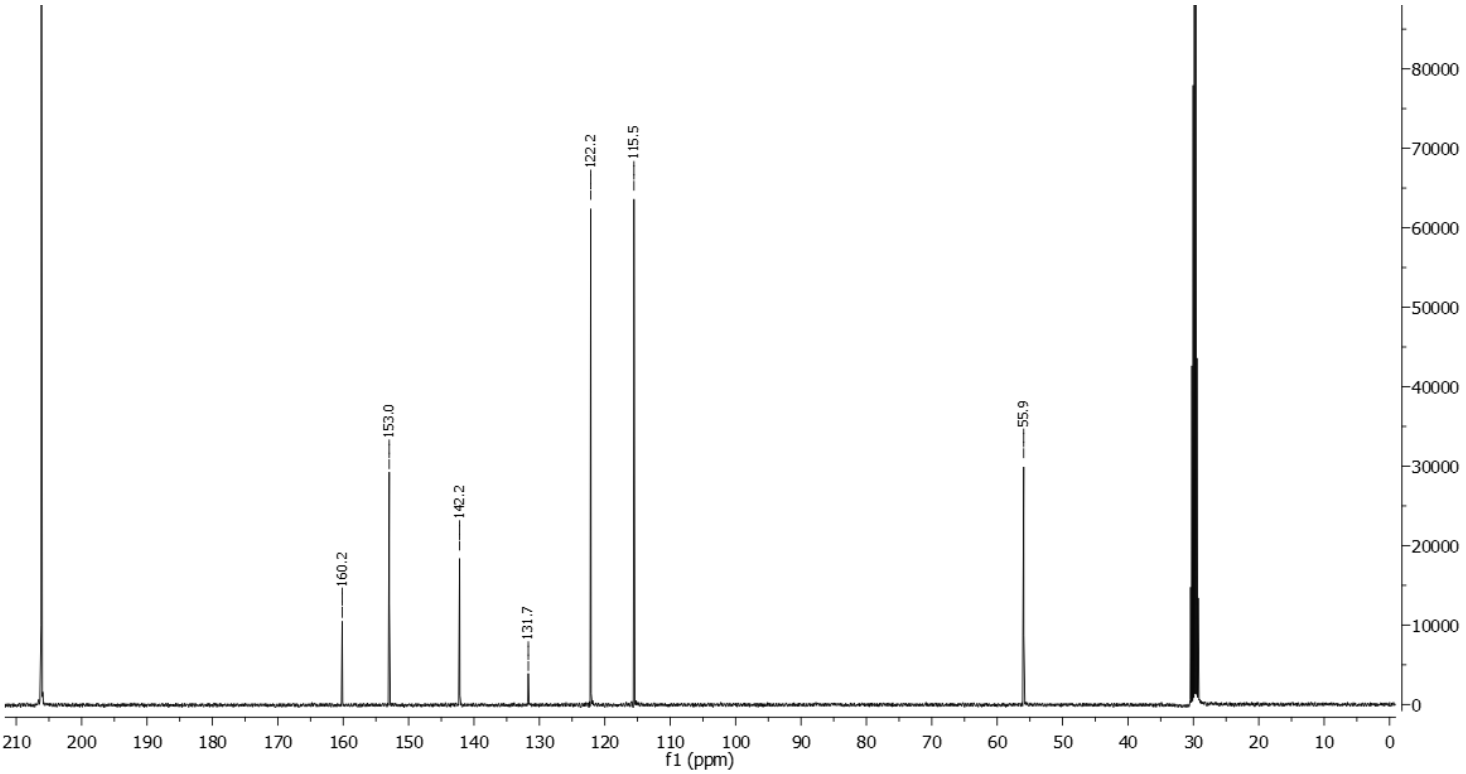

^{13}C-NMR spectrum of the non-deuterated starting material

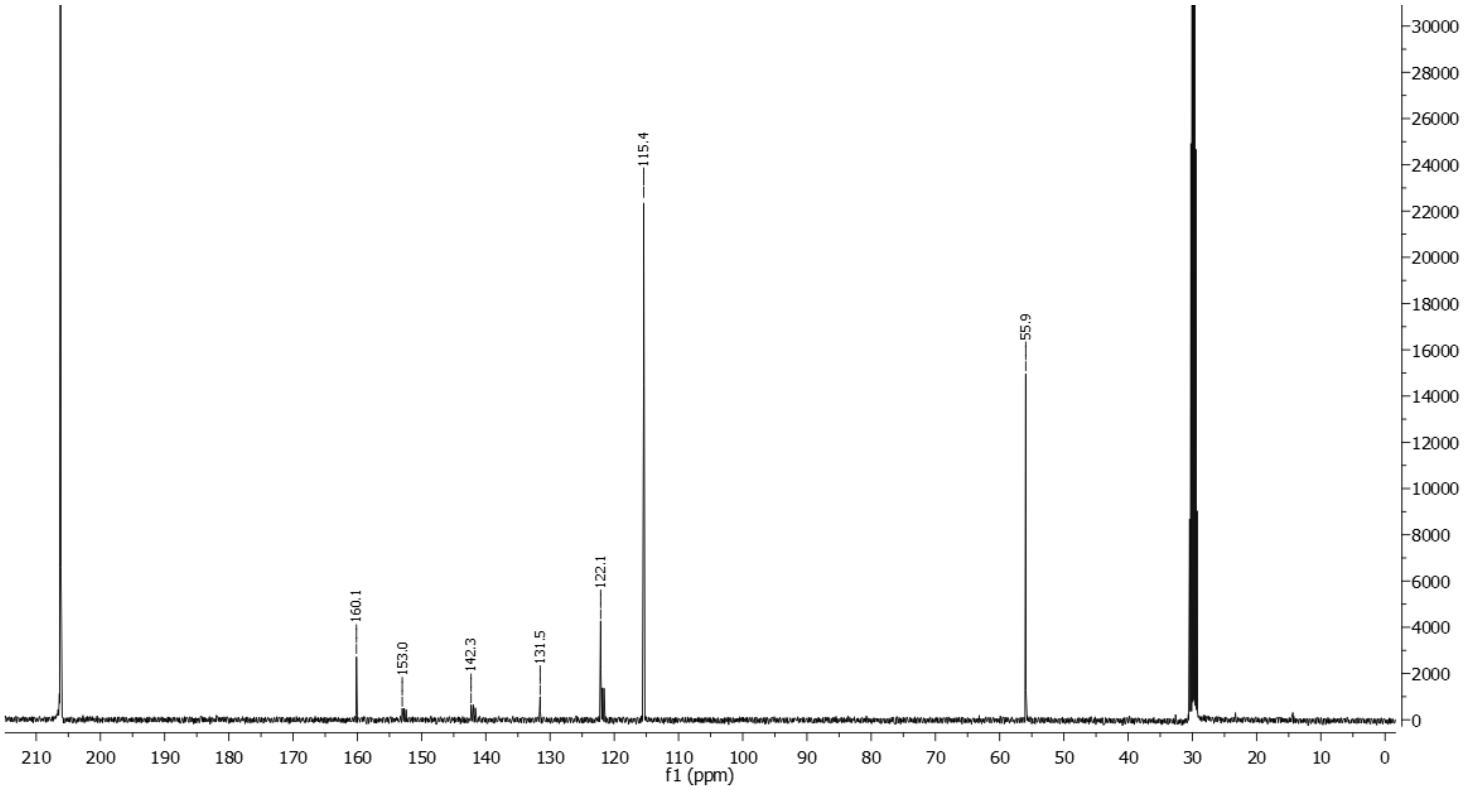

^{13}C-NMR spectrum of **15**

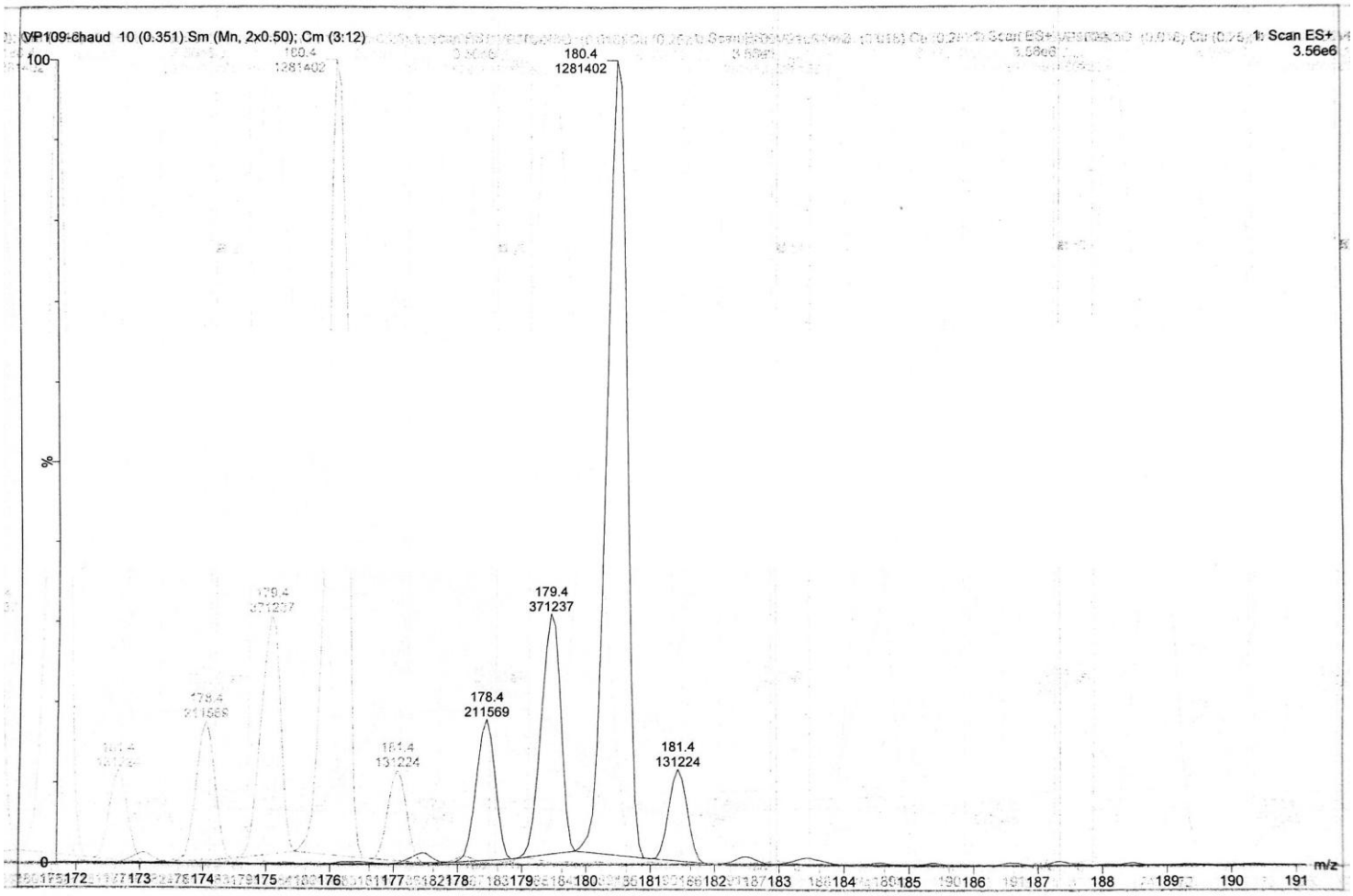

ESI spectrum of **15**

[3-(1H-1,2,4-Triazol-1-yl)phenyl]methanol **16**:

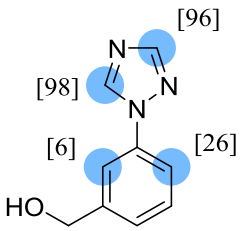

Chemical Formula:$C_9H_9N_3O$

Substrate	Solvent (Volume)	RuNp@PVP cat.
35.2mg, 0.2mmol	DMA (2mL)	14.4mg, 5mol%

Workup and purification:

After cooling down to room temperature, EtOAc/cyclohexane (1:1, 3mL) was added to the reaction mixture and stirred for 10mins to let precipitating RuNp@PVP. The suspension was passed through a Sep-Pak® C18 cartridge and then eluted with EtOAc/cyclohexane (1:1, 5mL). The solvent was removed under vacuum.

Yield: 29.0mg, 83%, grey solid

^{1}H NMR (400 MHz, Acetone-d_6): δ 9.05 (s, 0.02H), 8.11 (s, 0.04H), 7.88 (s, 0.94H), 7.76 – 7.70 (m, 0.74H), 7.55 – 7.47 (m, 1H), 7.44 – 7.38 (m, 1H), 4.74 (s, 2H), 4.59 (bs, OH).

Deuterium incorporation was expected at δ 9.05, δ 8.11, δ 7.88 and at δ 7.76 – 7.70. Isotopic enrichment values were determined against the integral at δ 7.44 – 7.38.

^{2}H NMR (600 MHz, Acetone): δ 9.00 (s, 0.98D), 8.07 (s, 0.96D), 7.86 (s, 0.07D) , 7.72 (s, 0.26D)

^{13}C-{^{1}H}NMR (100 MHz, Acetone-d_6): δ 152.0 (m), 144.7, 141.4 (m), 137.3, 129.5 (m), 125.6, 117.8, 117.5, 63.1.

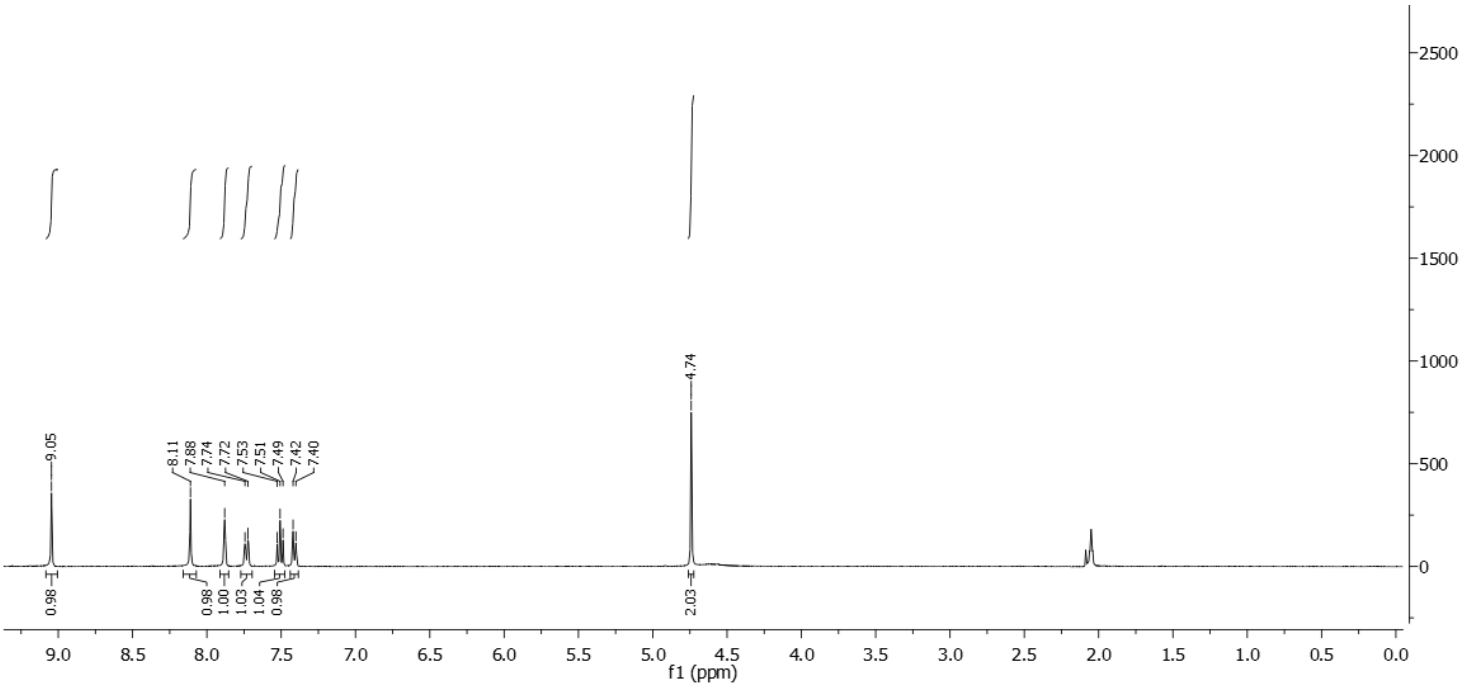

^{1}H-NMR spectrum of the non-deuterated starting material

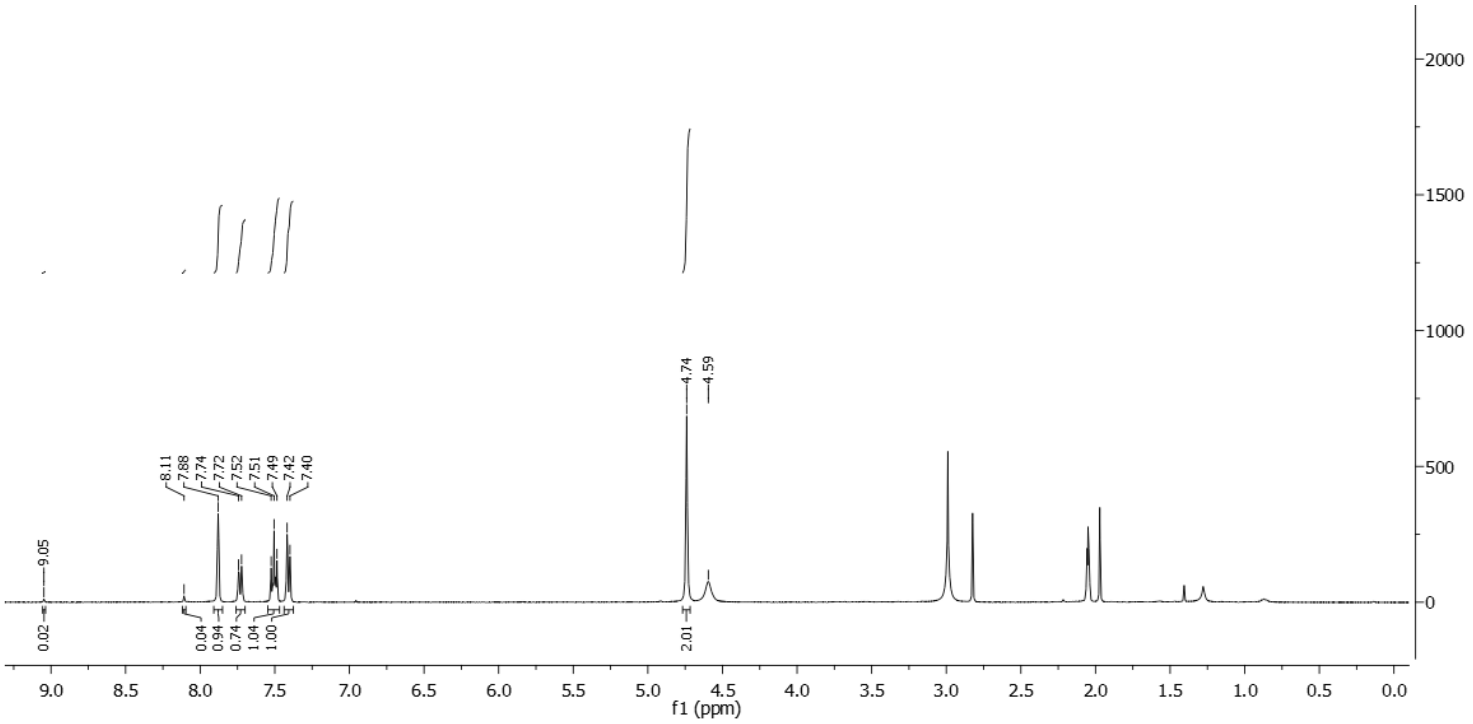

^{1}H-NMR spectrum of **16**

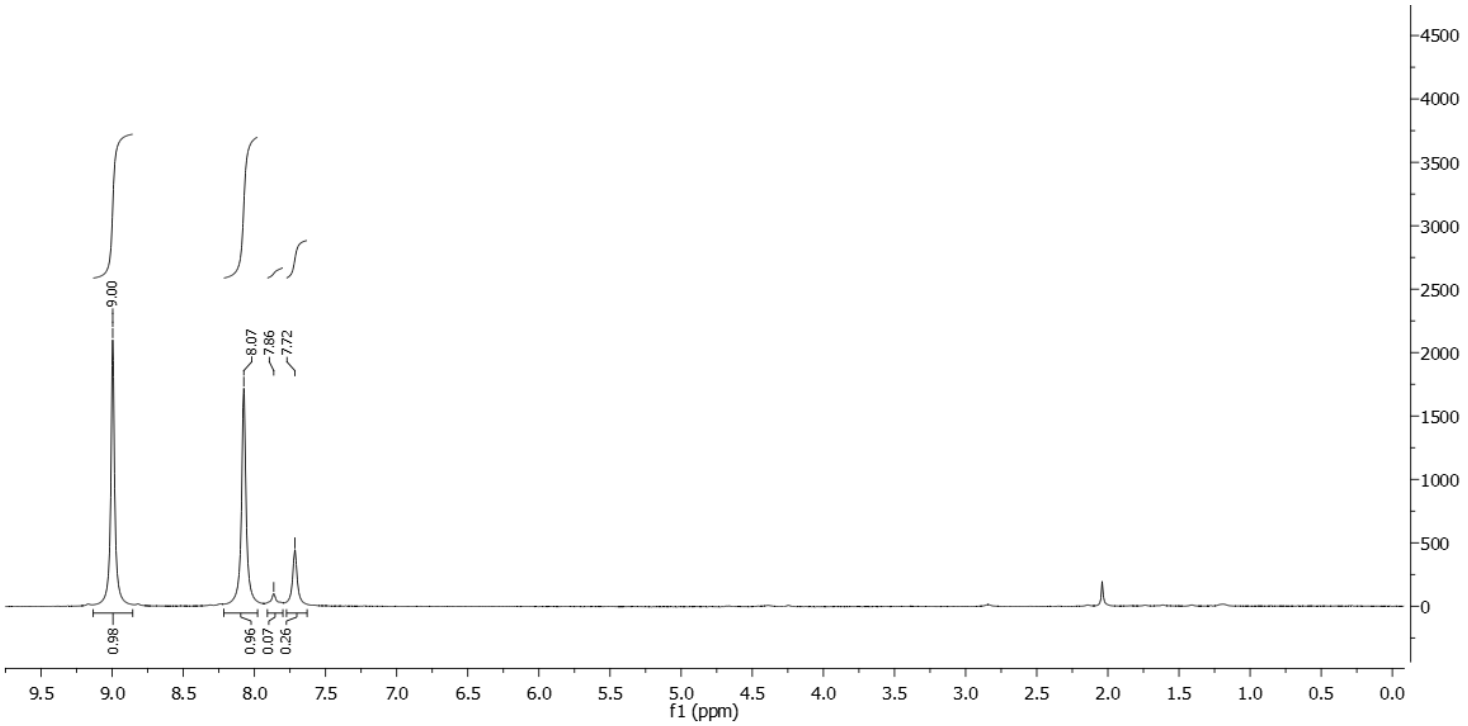

^{2}H-NMR spectrum of **16**

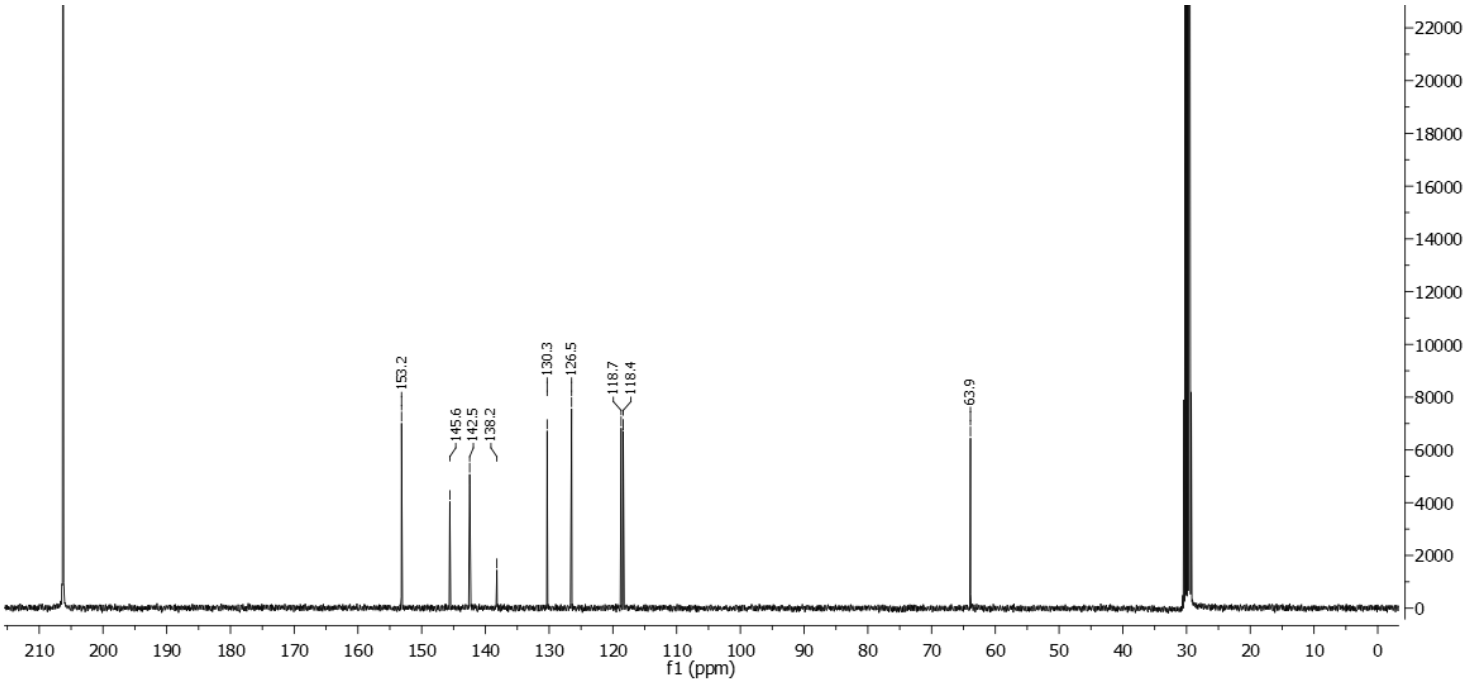

^{13}C-NMR spectrum of the non-deuterated starting material

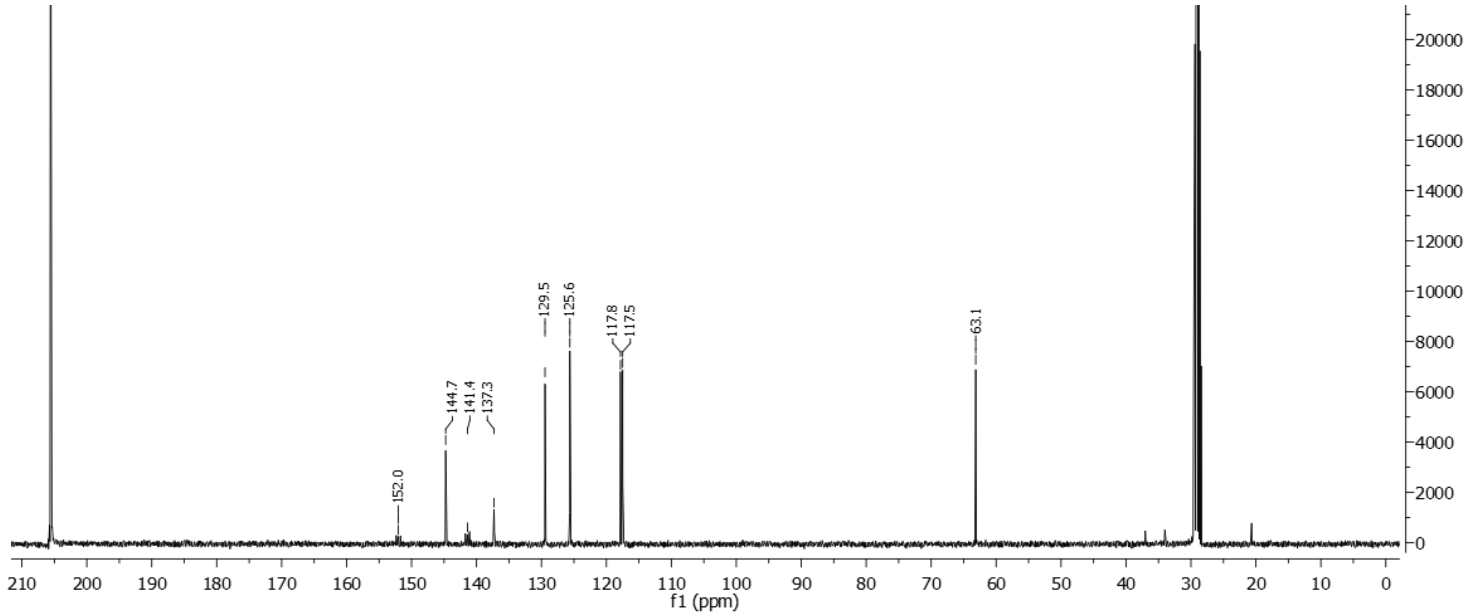

^{13}C-NMR spectrum of **16**

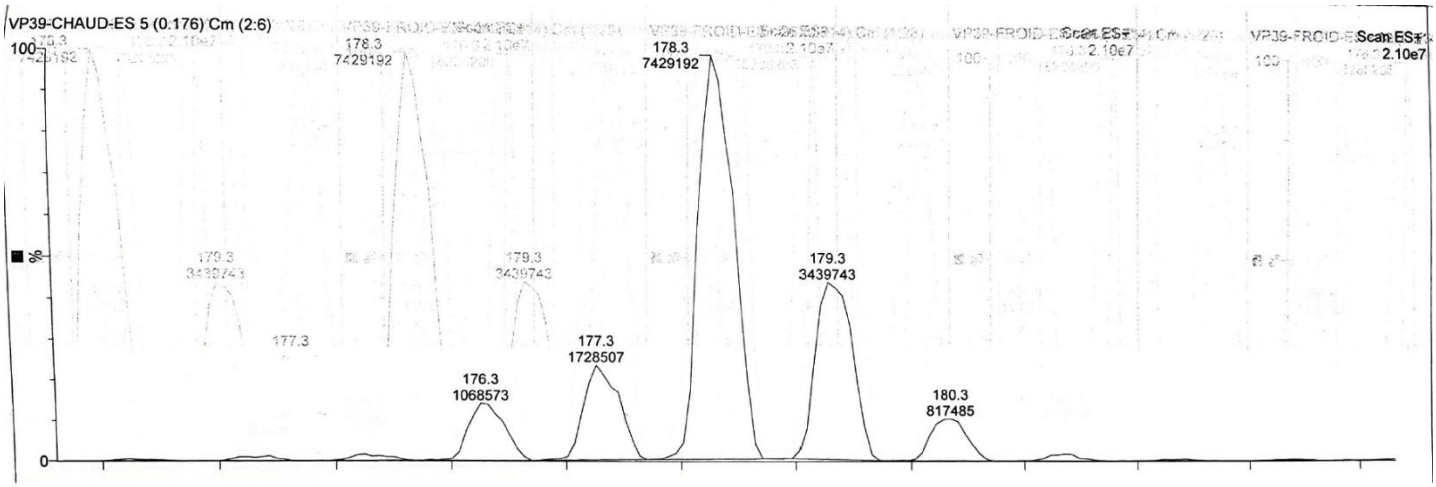

ESI-spectrum of **16**

4-(1H-1,2,4-Triazol-1-yl)aniline **17**

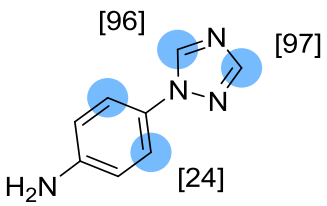

Chemical Formula: $C_8H_8N_4$

Substrate	Solvent (Volume)	RuNp@PVP cat.
32.0mg, 0.2mmol	DMA (2mL)	14.4mg, 5mol%

Workup and purification:

After cooling down to room temperature, EtOAc/cyclohexane (1:1, 3mL) was added to the reaction mixture and stirred for 10min to let precipitate RuNp@PVP. The suspension was passed through a Sep-Pak® C18 cartridge and then eluted with EtOAc/cyclohexane (1:1, 5mL). The solvent was removed under vacuum.

Yield: 33.0mg, 99%, grey solid

^{1}H NMR (400 MHz, $CDCl_3$): δ 8.38 (s, 0.03H), 8.04 (s, 0.04H), 7.45 – 7.34 (m, 1.53H), 6.80 – 6.69 (m, 2H), 3.87 (bs, NH_2).

Deuterium incorporation was expected at δ 8.38, δ 8.04 and at δ 7.45 – 7.34. Isotopic enrichment values were determined against the integral at δ 6.80 – 6.69.

^{2}H-{^{1}H}NMR (92 MHz, $CHCl_3$): δ 8.42 (s, 0.97D), 8.07 (s, 0.96D), 7.43 (s, 0.48D).

^{13}C-{^{1}H}NMR (100 MHz, $CDCl_3$): δ 152.2 (m), 146.8, 140.8 (m), 128.7, 122.1 (m), 115.5.

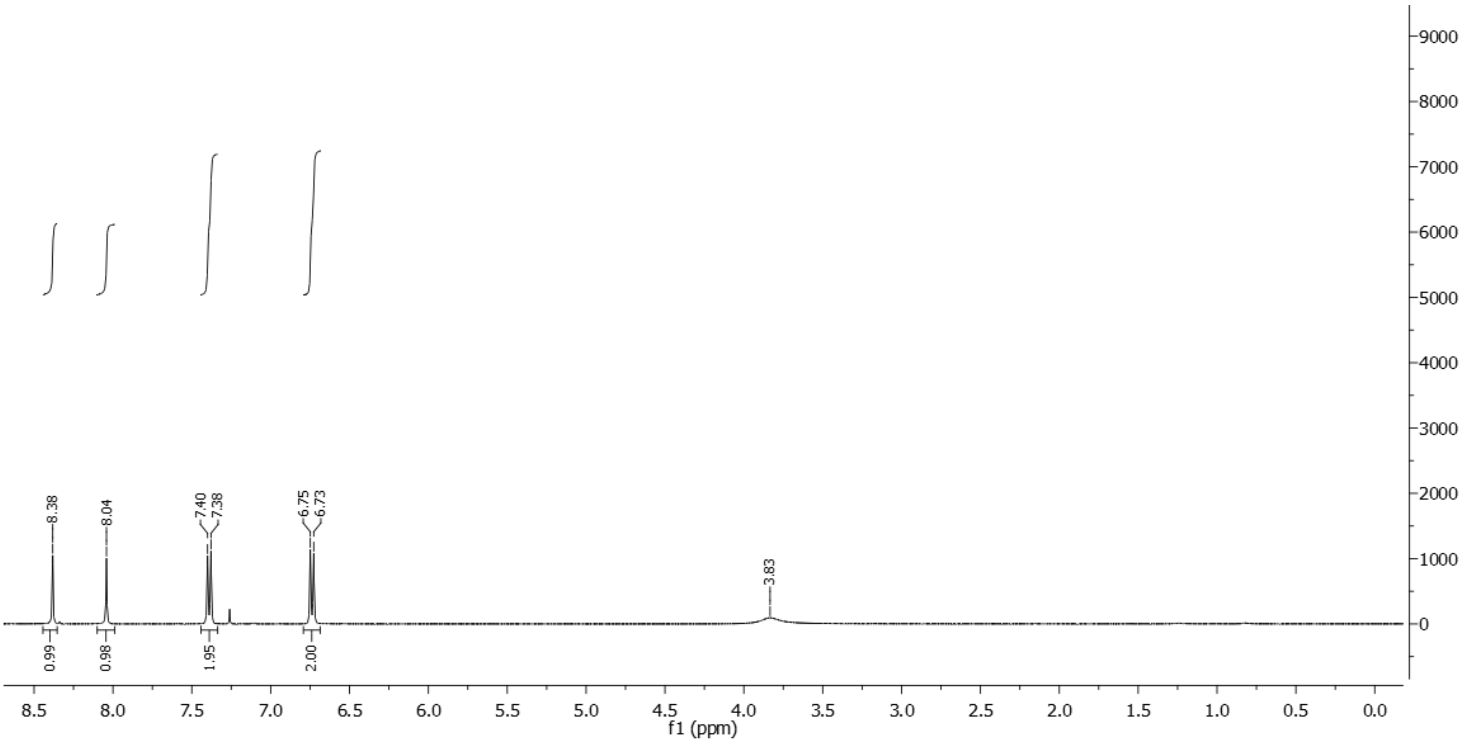

^{1}H-NMR spectrum of the non-deuterated starting material

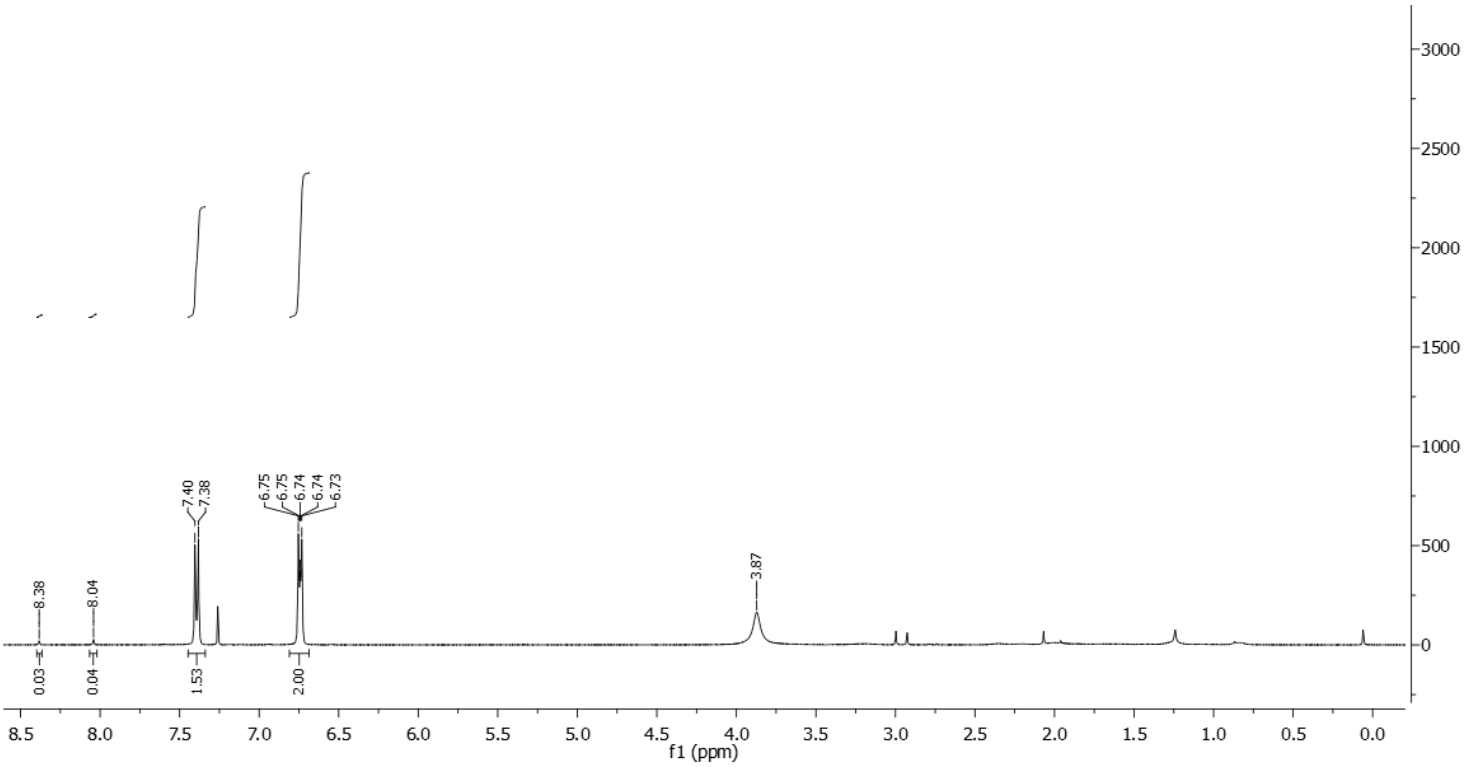

^{1}H-NMR spectrum of **17**

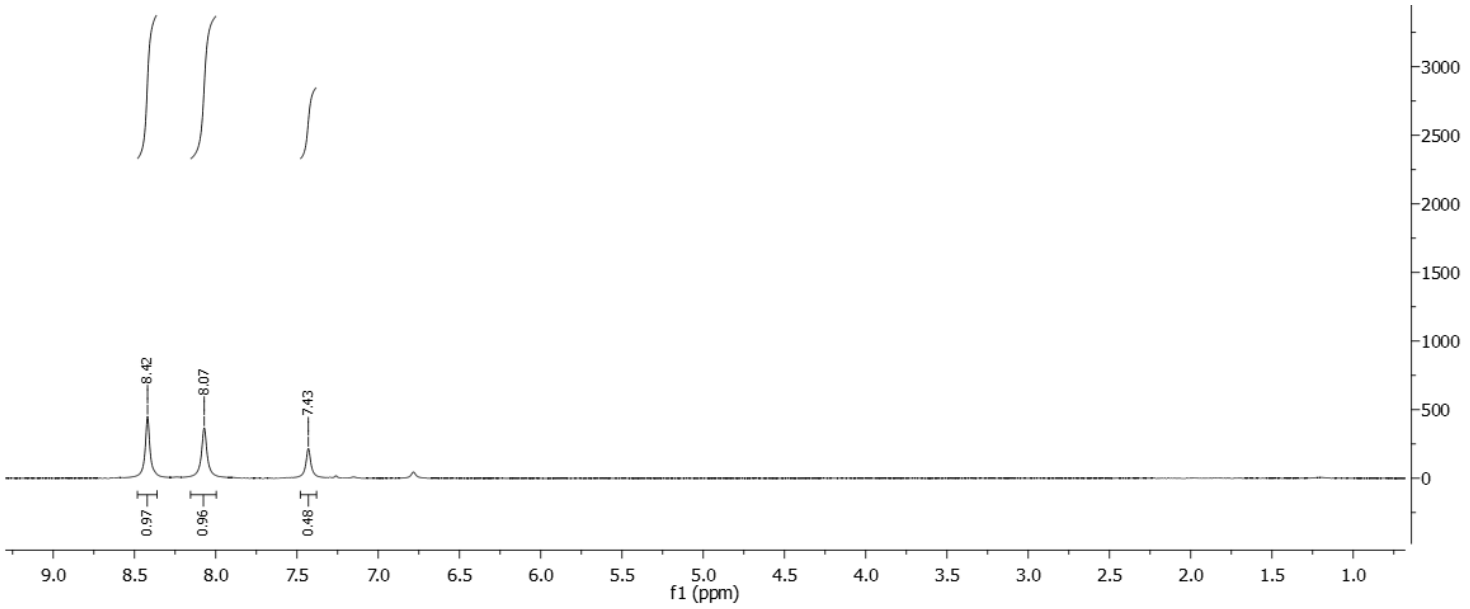

^{2}H-NMR spectrum of **17**

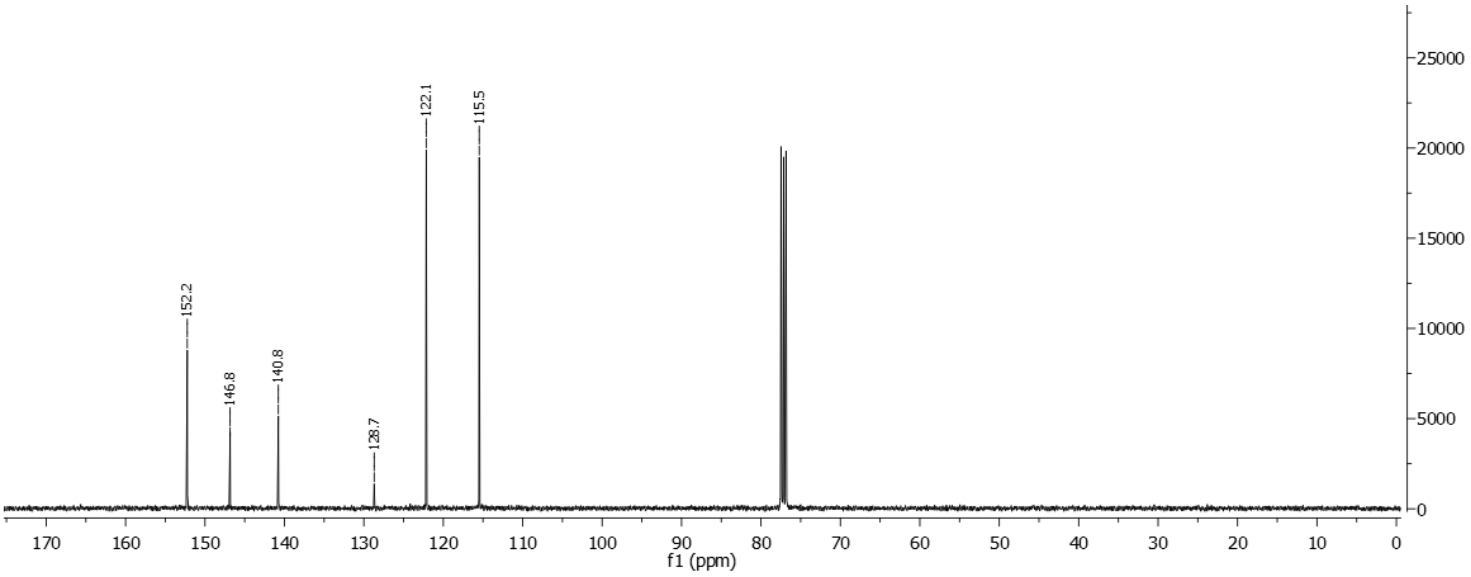

^{13}C-NMR spectrum of the non-deuterated starting material

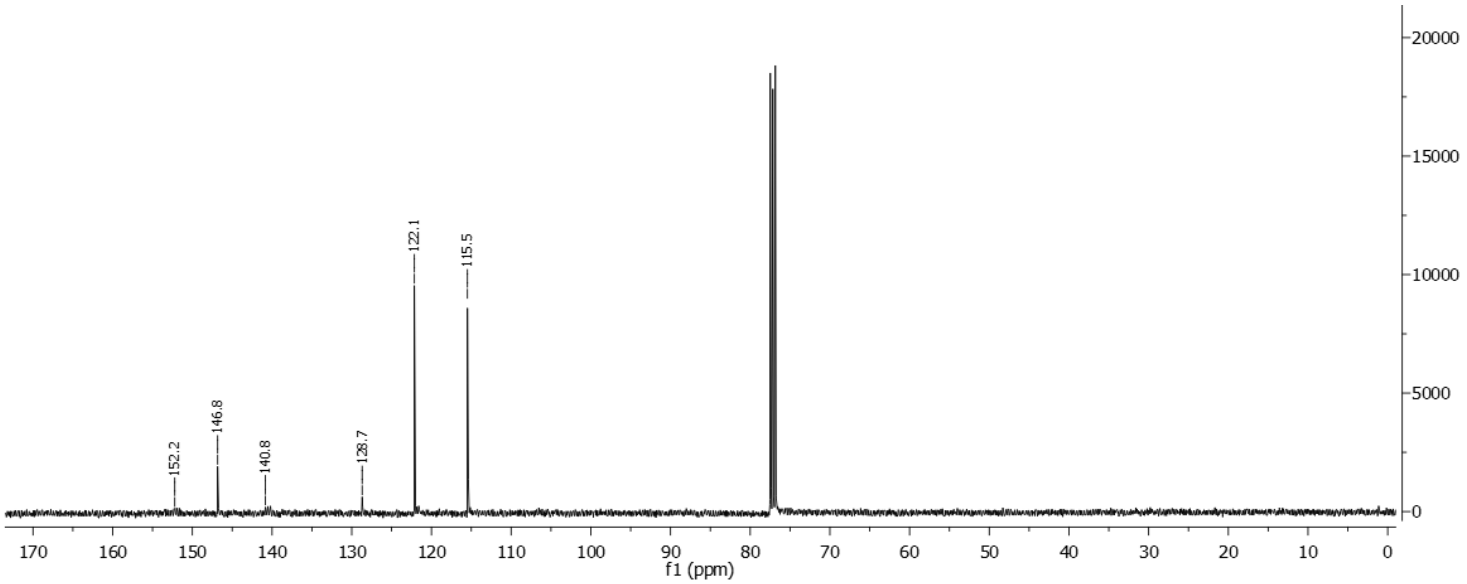

^{13}C-NMR spectrum of **17**

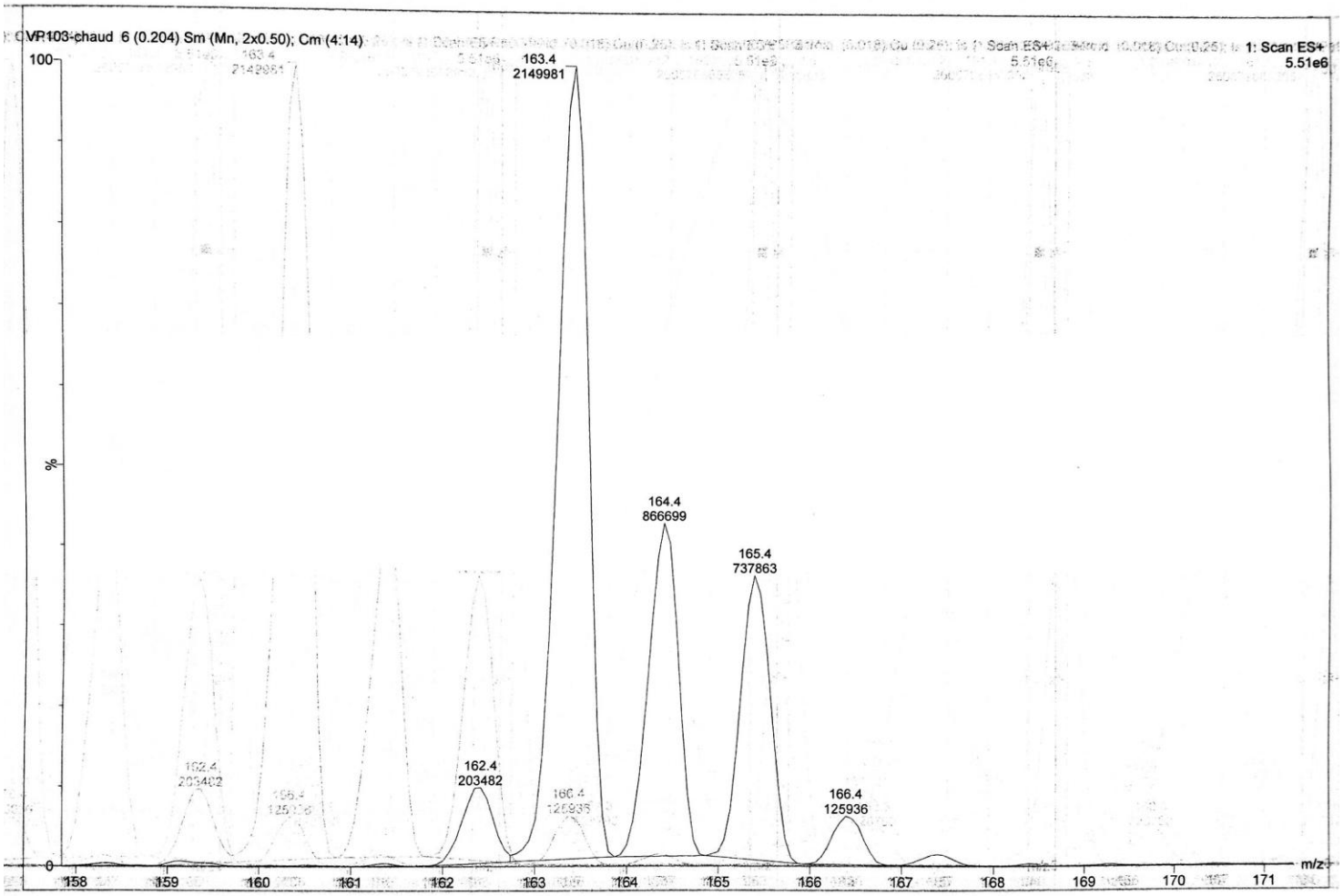

ESI-spectrum of **17**

4'-(1H-1,2,4-Triazol-1-yl)acetanilide **18**

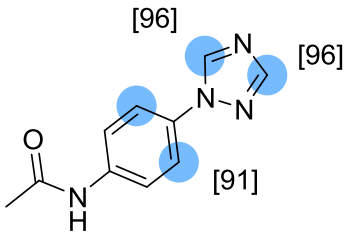

Chemical Formula: $C_{10}H_{10}N_4O$

Substrate	Solvent (Volume)	RuNp@PVP cat.
40.4mg, 0.2mmol	DMA (2mL)	14.4mg, 5mol%

Workup and purification:

After cooling down to room temperature, EtOAc/cyclohexane (1:1, 3mL) was added to the reaction mixture and stirred for 10min to let precipitate RuNp@PVP. The suspension was passed through a Sep-Pak® C18 cartridge and then eluted with ethylacetate (5mL). The solvent was removed under vacuum and the labelled product was recrystallized from DCM/MeOH (10:1).

Yield: 26.0mg, 64%, white solid

^{1}H NMR (400 MHz, methanol-*d*$_4$): δ 9.03 (s, 0.04H), 8.14 (s, 0.04H), 7.78 – 7.71 (m, 2.18H), 2.15 (s, 3H).

Deuterium incorporation was expected at *δ* 9.03, *δ* 8.14 and at *δ* 7.78 – 7.71. Isotopic enrichment values were determined against the integral at *δ* 2.15.

^{2}H-{^{1}H}NMR (92 MHz, methanol): δ 8.98 (s, 0.95D), 8.12 (s, 0.96D), 7.73 (s, 1.81D).

^{13}C-{^{1}H}NMR (100 MHz, methanol-*d*$_4$): δ 171.8, 152.8, 142.9 (m), 140.2 (m), 133.9, 121.8 (m), 121.7, 23.9.

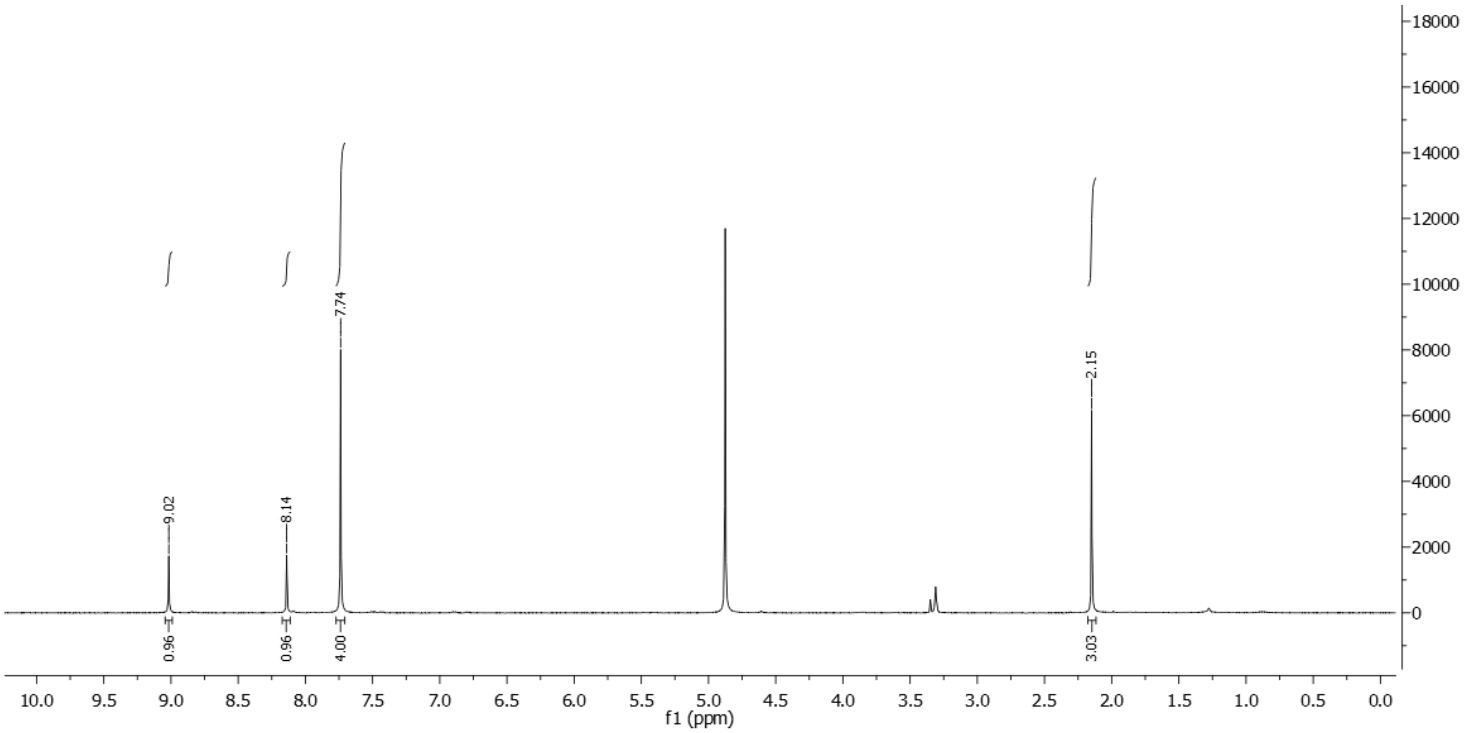

^{1}H-NMR spectrum of the non-deuterated starting material

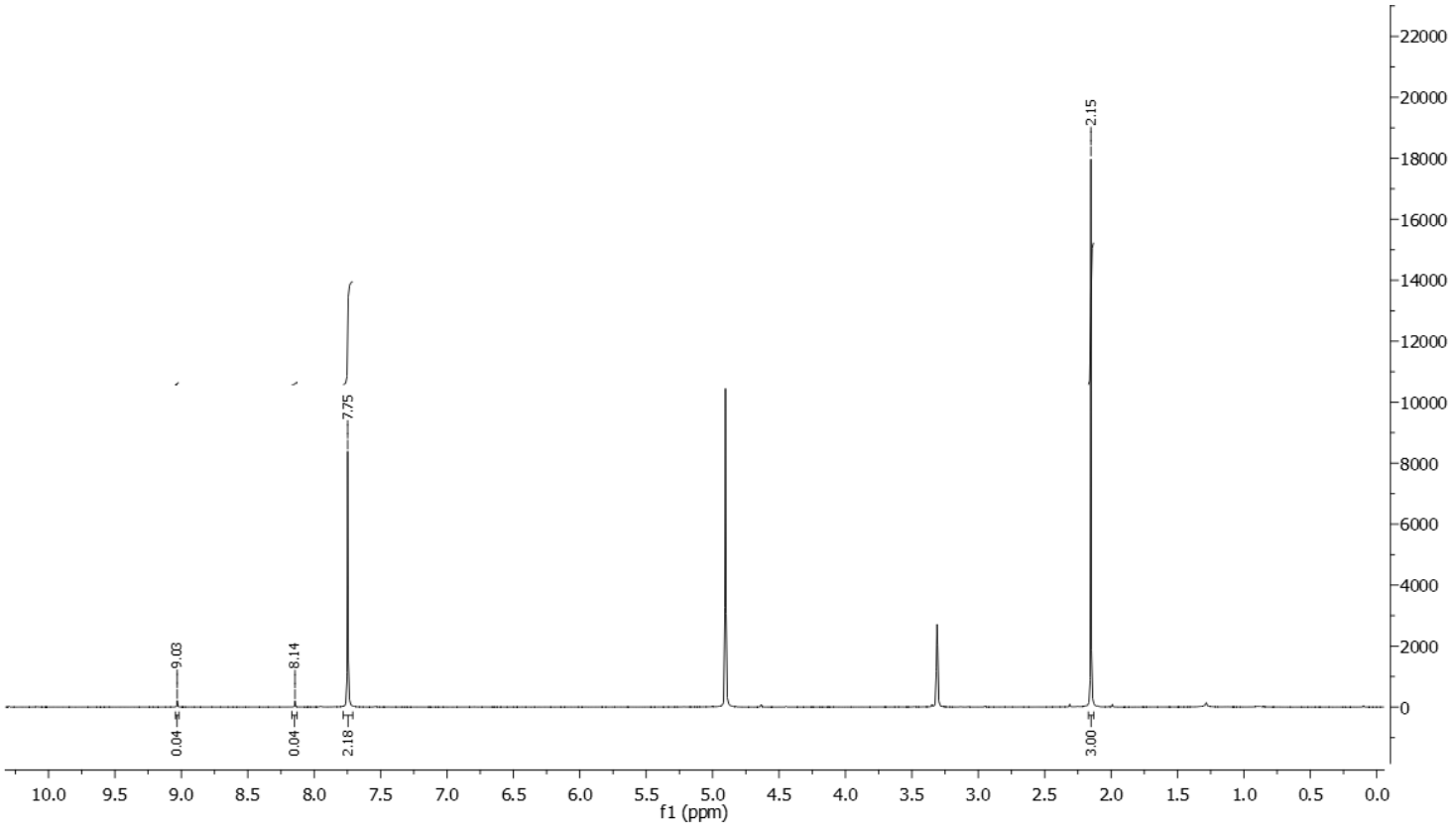

^{1}H-NMR spectrum of **18**

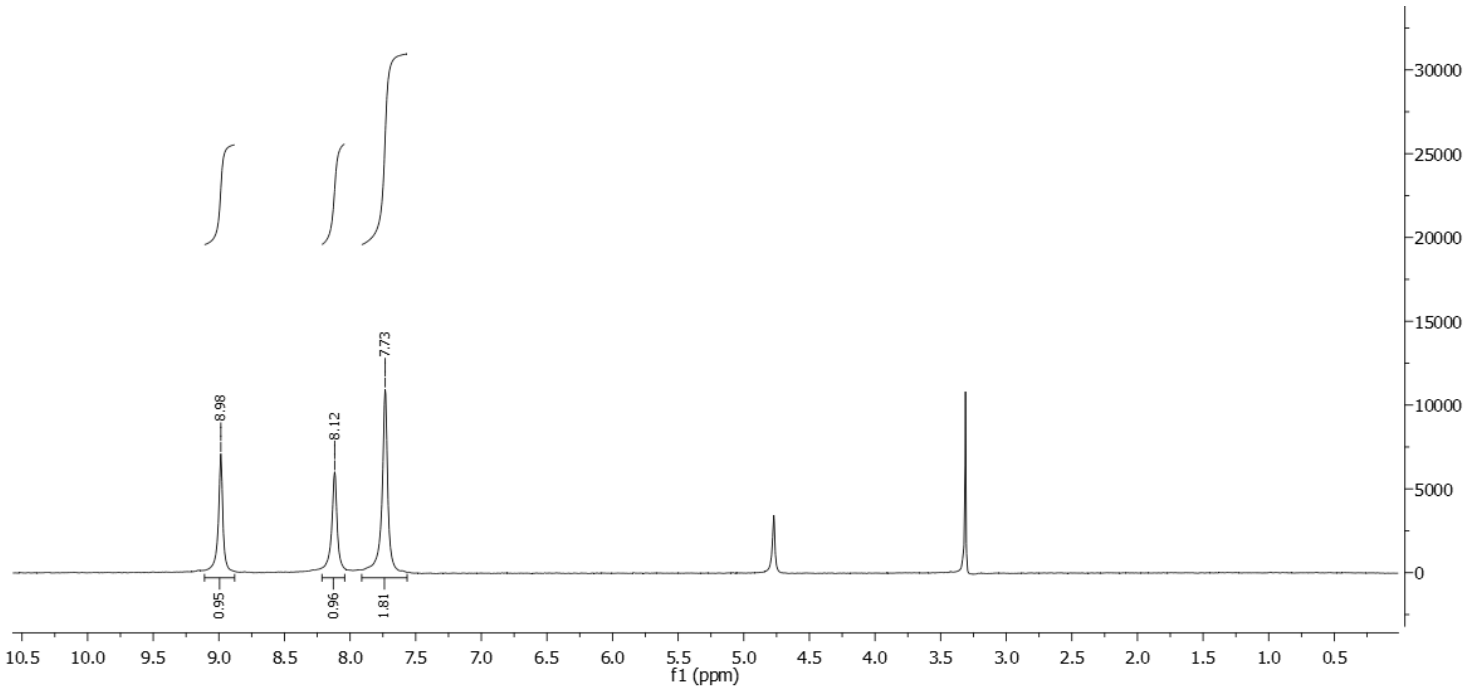

^{2}H-NMR spectrum of **18**

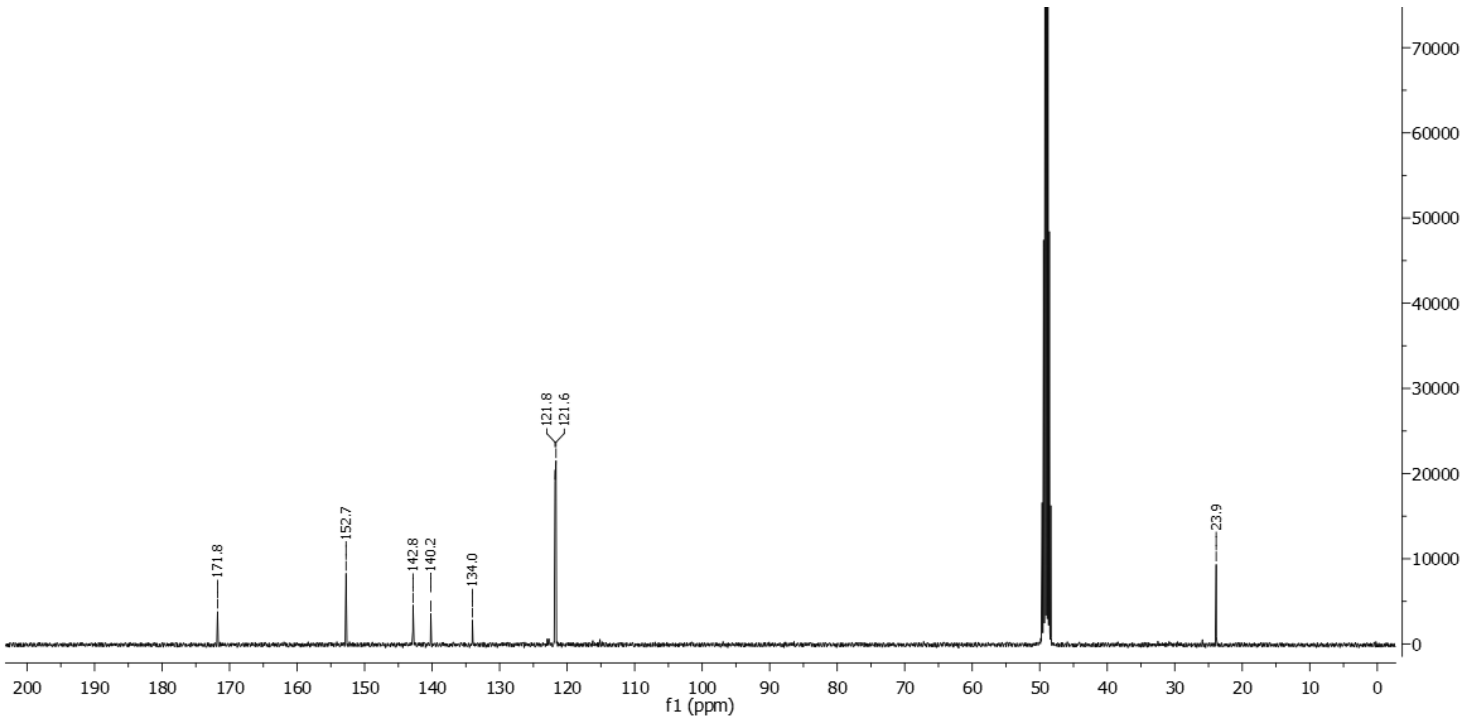

^{13}C-NMR spectrum of the non-deuterated starting material

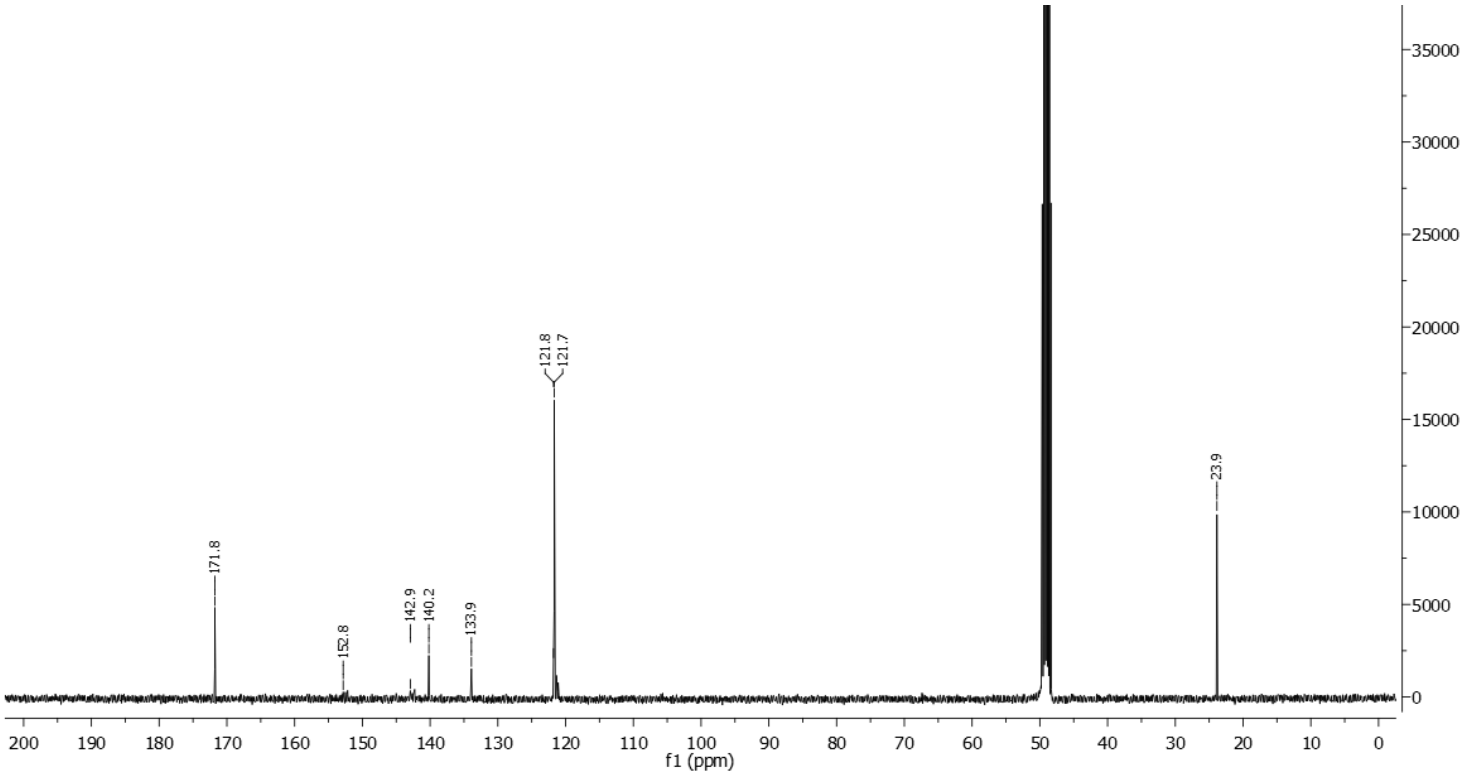

^{13}C-NMR spectrum of **18**

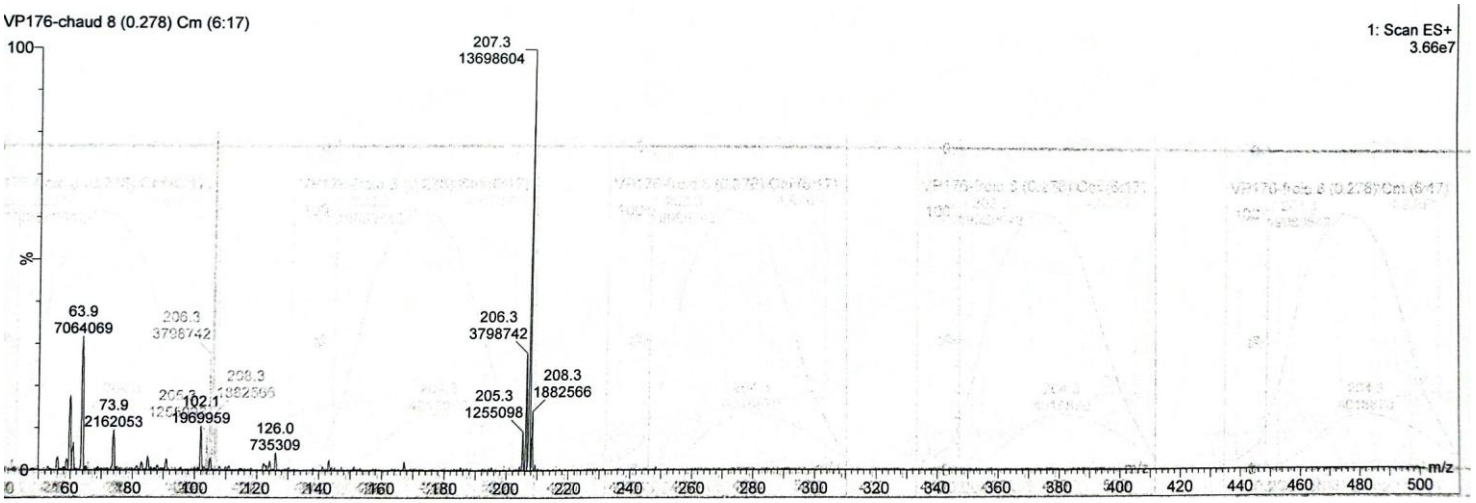

ESI-spectrum of **18**

4'-(4H-1,2,4-Triazol-4-yl)acetanilide **19**

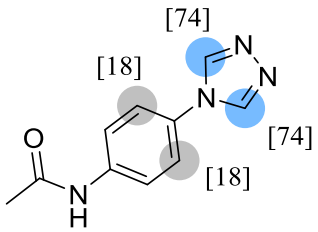

Chemical Formula: $C_{10}H_{10}N_4O$

Substrate	Solvent (Volume)	RuNp@PVP cat.
40.4mg, 0.2mmol	DMA (2mL)	14.4mg, 5mol%

Workup and purification:

After cooling down to room temperature, EtOAc/cyclohexane (1:1, 3mL) was added to the reaction mixture and stirred for 10min to let precipitate RuNp@PVP. The suspension was passed through a Sep-Pak® C18 cartridge and then eluted with DCM (2mL). The solvent was removed under vacuum and the labelled product was recrystallized from MeOH/EtOAc (10:1).

Yield: 7.0mg, 17%, white solid

^{1}H NMR (400 MHz, methanol-*d*$_4$): δ 8.95 (s, 0.53H), 7.85 – 7.72 (m, 2H), 7.64 – 7.48 (m, 1.64H), 2.16 (s, 3H).

Deuterium incorporation was expected at *δ* 8.95 and at δ 7.64 – 7.48. Isotopic enrichment values were determined against the integral at δ 7.85 – 7.72.

^{2}H-{^{1}H}NMR (92 MHz, methanol): δ 8.91 (s), 7.55 (s).

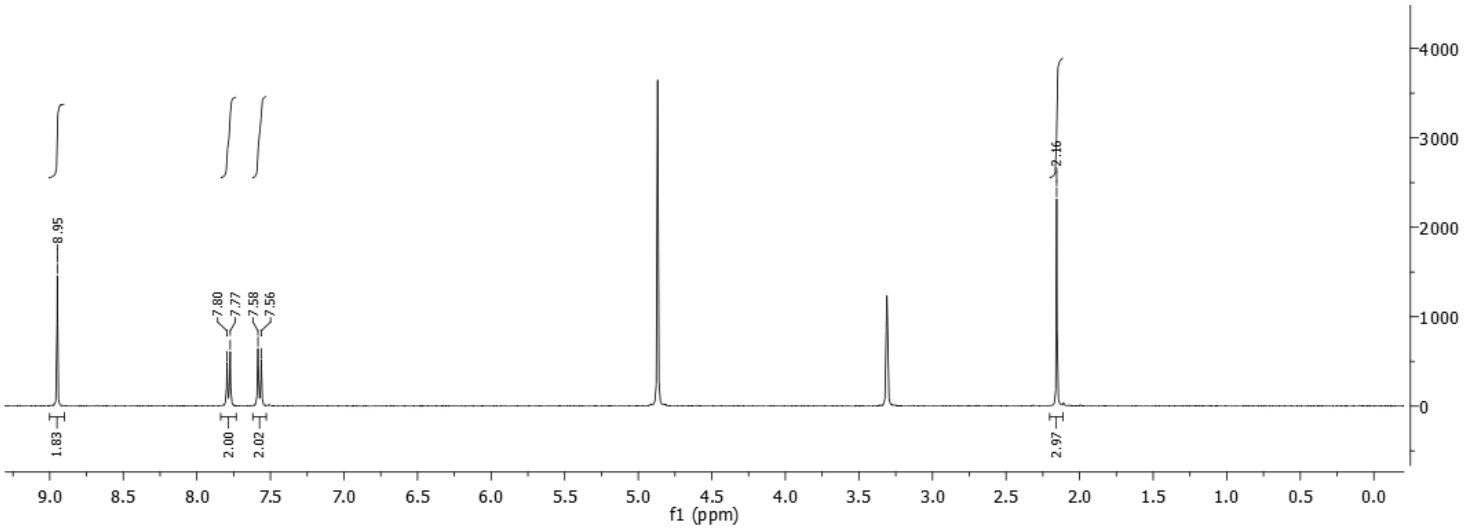

^{1}H-NMR spectrum of the non-deuterated starting material

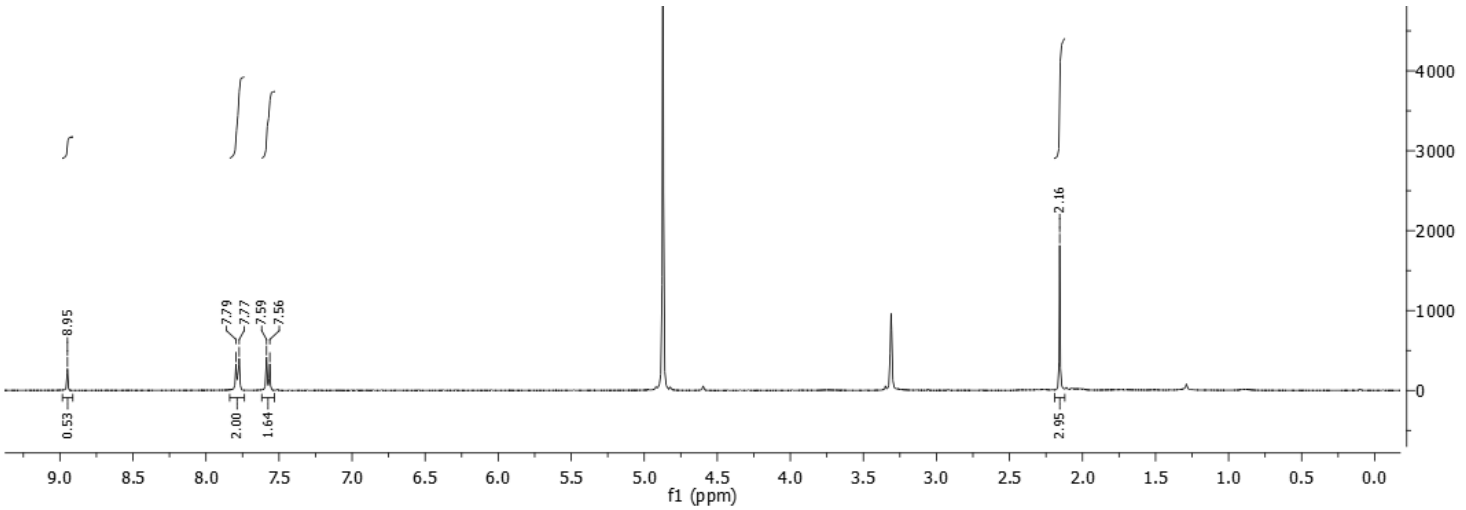

^{1}H-NMR spectrum of **19**

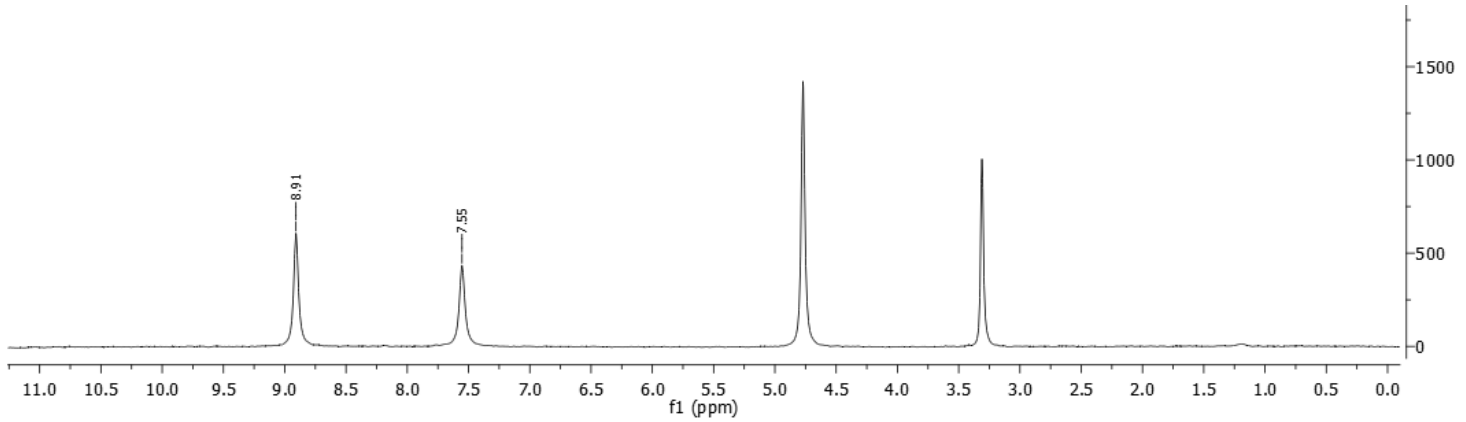

^{2}H-NMR spectrum of **19**

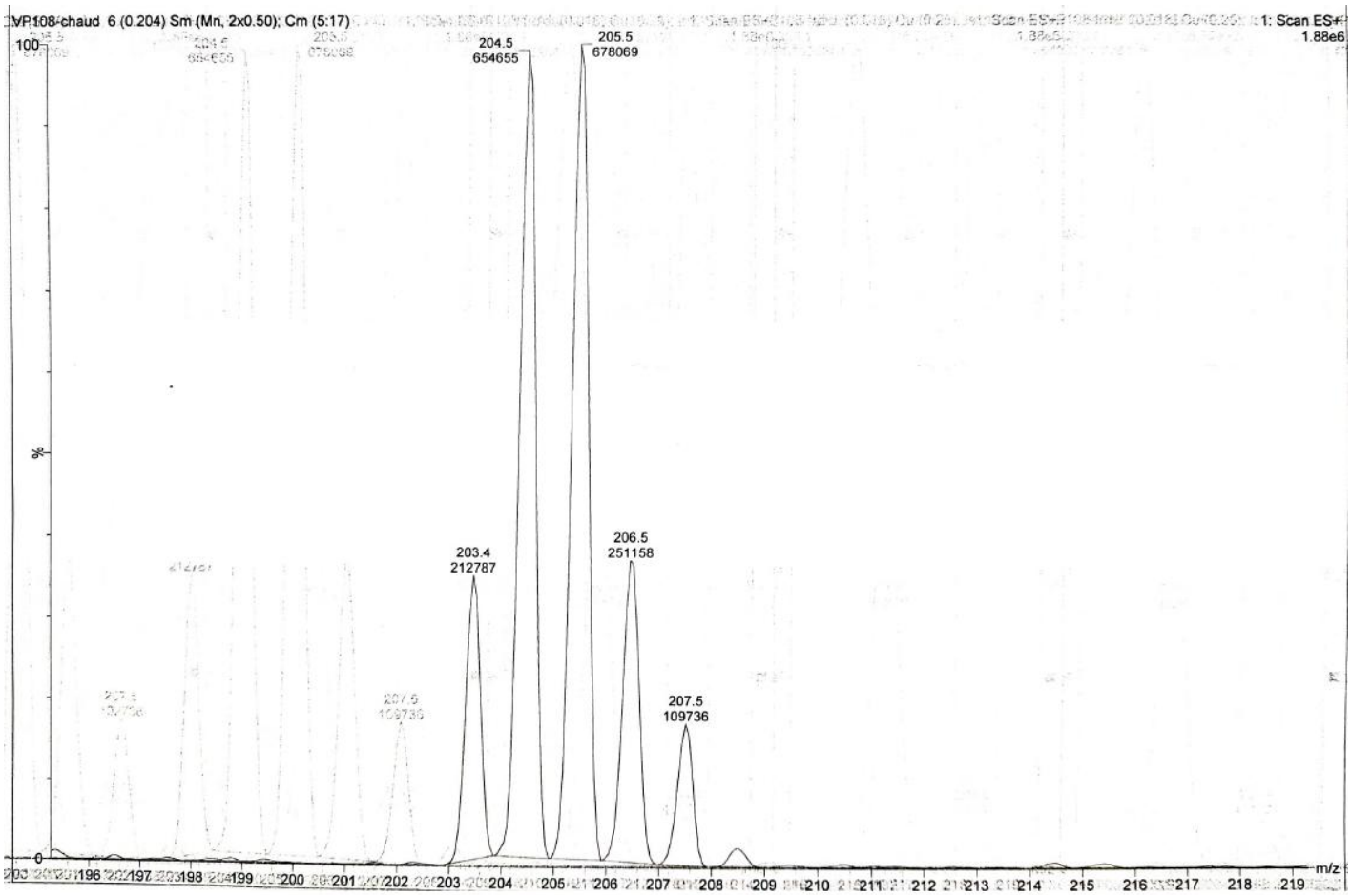

ESI-spectrum of **19**

Deuteration of carbazoles under neutral conditions

Carbazole **20**

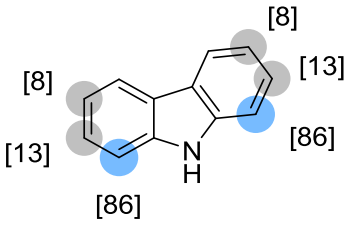

Chemical Formula: $C_{12}H_9N$

Substrate	Solvent (Volume)	RuNp@PVP cat.
33.4mg, 0.2mmol	EtOAc (2mL)	14.4mg, 5mol%

Workup and purification:

After cooling down to room temperature EtOAc/cyclohexane (1:1, 3mL) was added to the reaction mixture and stirred for 10mins to let precipitate RuNp@PVP. The suspension was passed through a SiO_2 pad and the crude product was eluted with THF (5mL). The solvent was removed under vacuum and the crude product was recrystallized from THF/MeOH (10:1).

Yield: 16.0mg, 48%, white solid

^{1}H NMR (400 MHz, Acetone-d_6): δ 10.35 (bs, NH), 8.14 – 8.09 (m, 2H), 7.53 – 7.49 (m, 0.28H), 7.41 – 7.35 (m, 1.74H), 7.21 – 7.15 (m, 1.87H).

Deuterium incorporation was expected at δ 7.53 – 7.49. Isotopic enrichment values were determined against the integral at δ 8.14 – 8.09.

^{2}H-{^{1}H}NMR (600 MHz, Acetone): δ 7.51 (s, 1.72D), 7.39 (s, 0.26D), 7.18 (s, 0.16D).

^{13}C-{^{1}H}NMR (100 MHz, Acetone-d_6): δ 140.8, 126.3, 123.9, 120.8, 119.6, 111.6 (m).

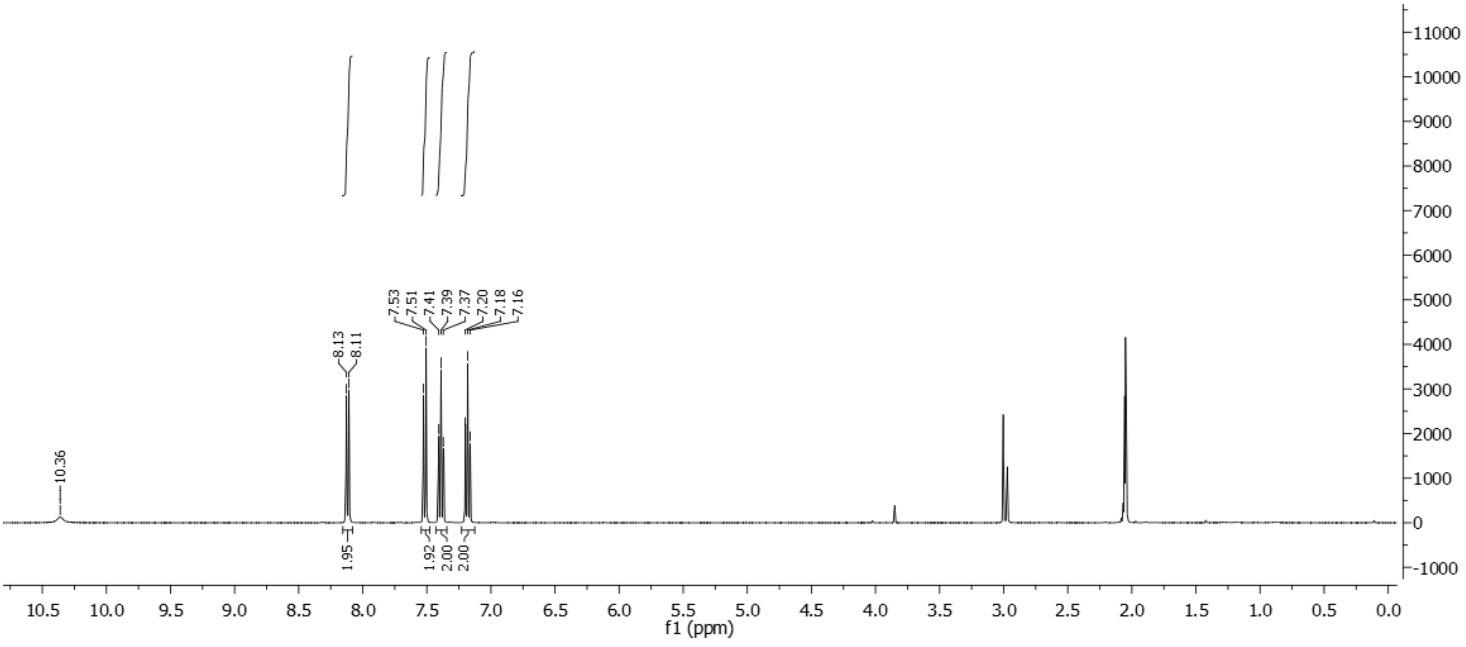

^{1}H-NMR spectrum of the non-deuterated starting material

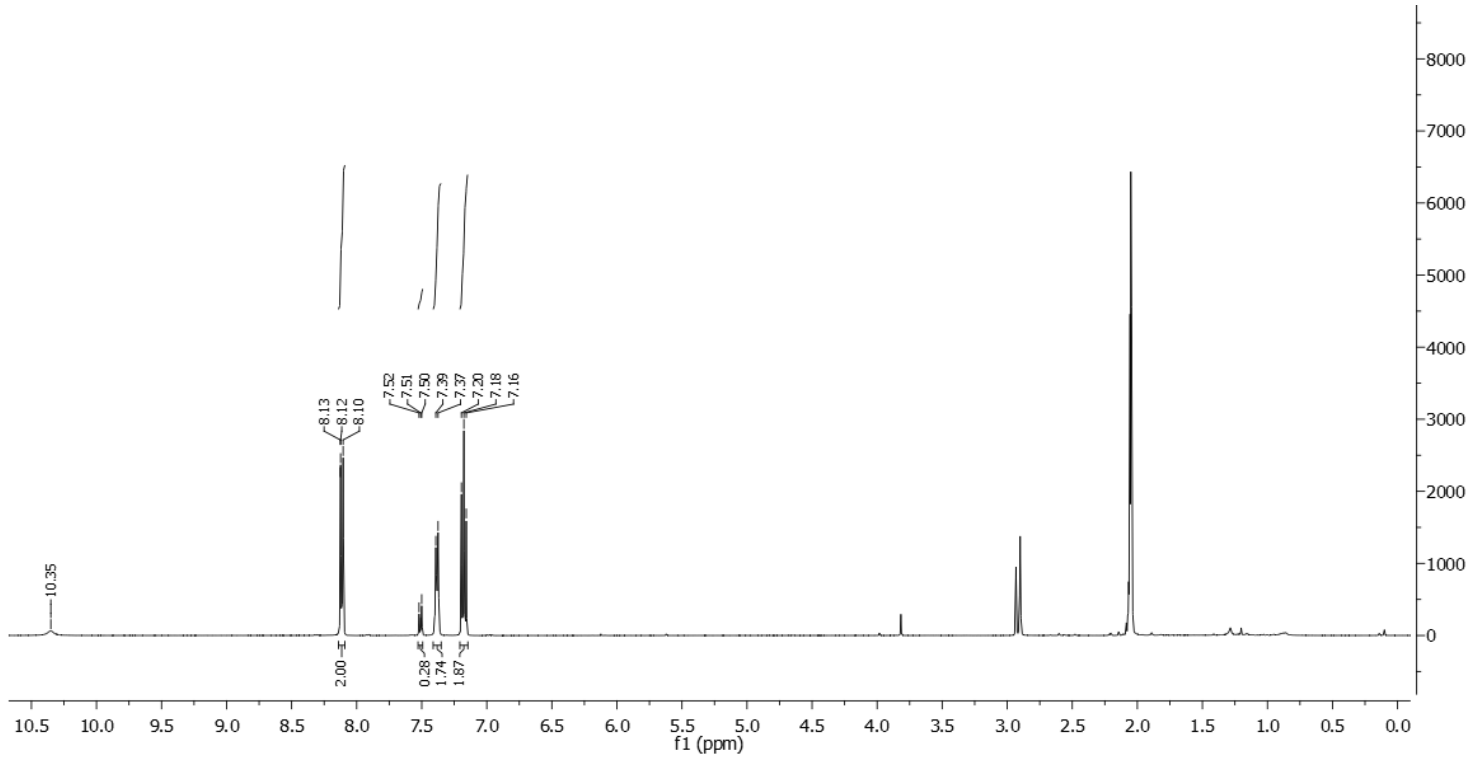

^{1}H-NMR spectrum of **20**

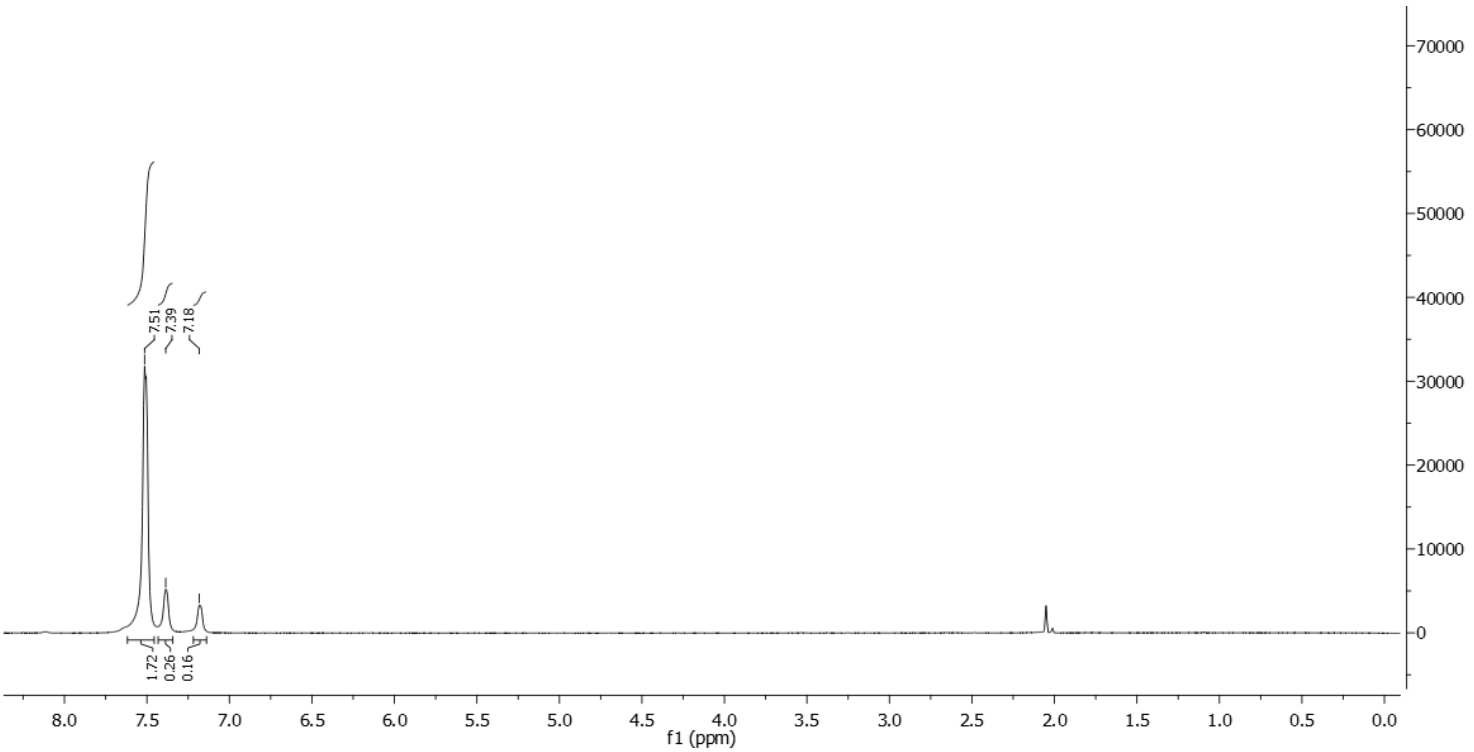

^{2}H-NMR spectrum of **20**

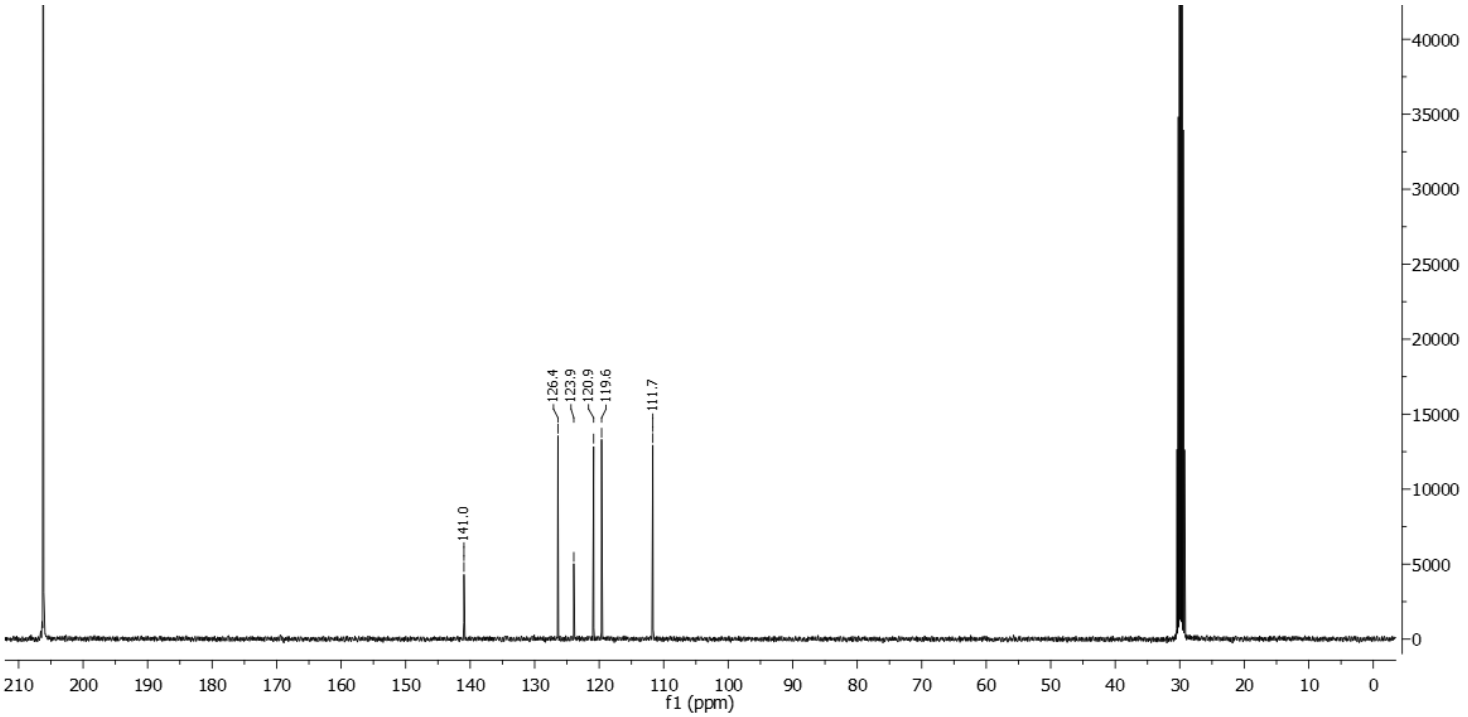

^{13}C-NMR spectrum of the non-deuterated starting material

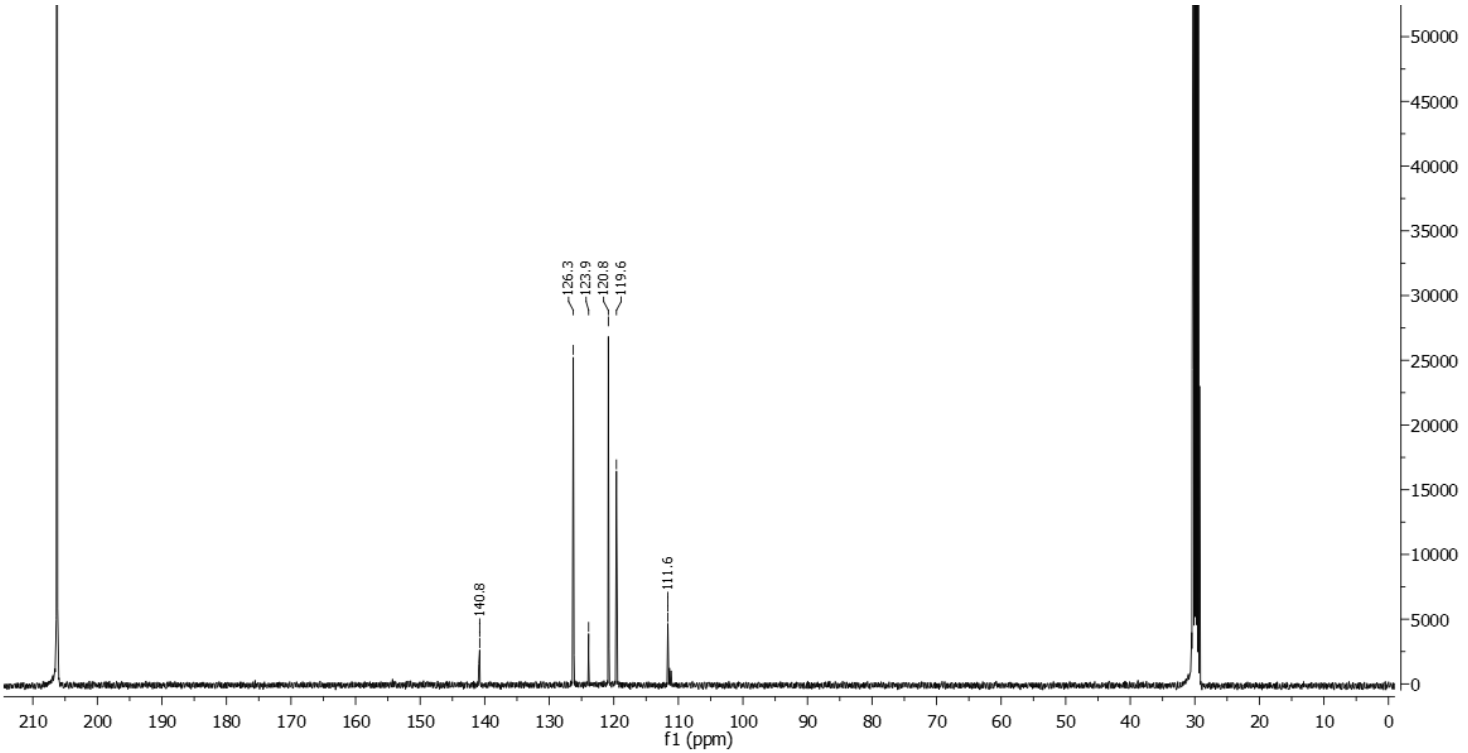

^{13}C-NMR spectrum of **20**

3,6-Di-tert-butylcarbazole **21**

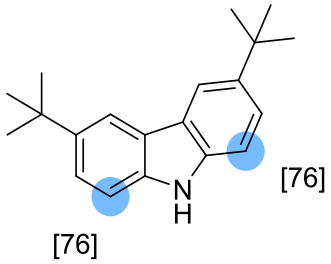

Chemical Formula: $C_{20}H_{25}N$

Substrate	Solvent (Volume)	RuNp@PVP cat.
22.9mg, 0.1mmol	THF (2mL)	14.4mg, 10mol%

Workup and purification:

After cooling down to room temperature EtOAc/cyclohexane (1:1, 3mL) was added to the reaction mixture and stirred for 10mins to let precipitate RuNp@PVP. The suspension was passed through a SiO_2 pad and the crude product was eluted with THF (5mL). The solvent was removed under vacuum and the crude product was recrystallized from THF/MeOH (10:1).

Yield: 10.0mg, 44%, white solid

^{1}H NMR (400 MHz, Acetone-d_6): δ 10.02 (bs, NH), 8.23 – 8.16 (m, 2H), 7.51 – 7.43 (m, 2H), 7.42 – 7.37 (m, 0.48H), 1.43 (s, 18H).

Deuterium incorporation was expected at δ 7.42 – 7.37. Isotopic enrichment values were determined against the integral at δ 8.23 – 8.16.

^{2}H-{^{1}H}NMR (600 MHz, Acetone): δ 7.39 (s).

^{13}C-{^{1}H}NMR (100 MHz, Acetone-d_6): δ 142.1, 139.5, 139.5, 123.9, 116.9, 111.1 (m), 35.2, 32.4.

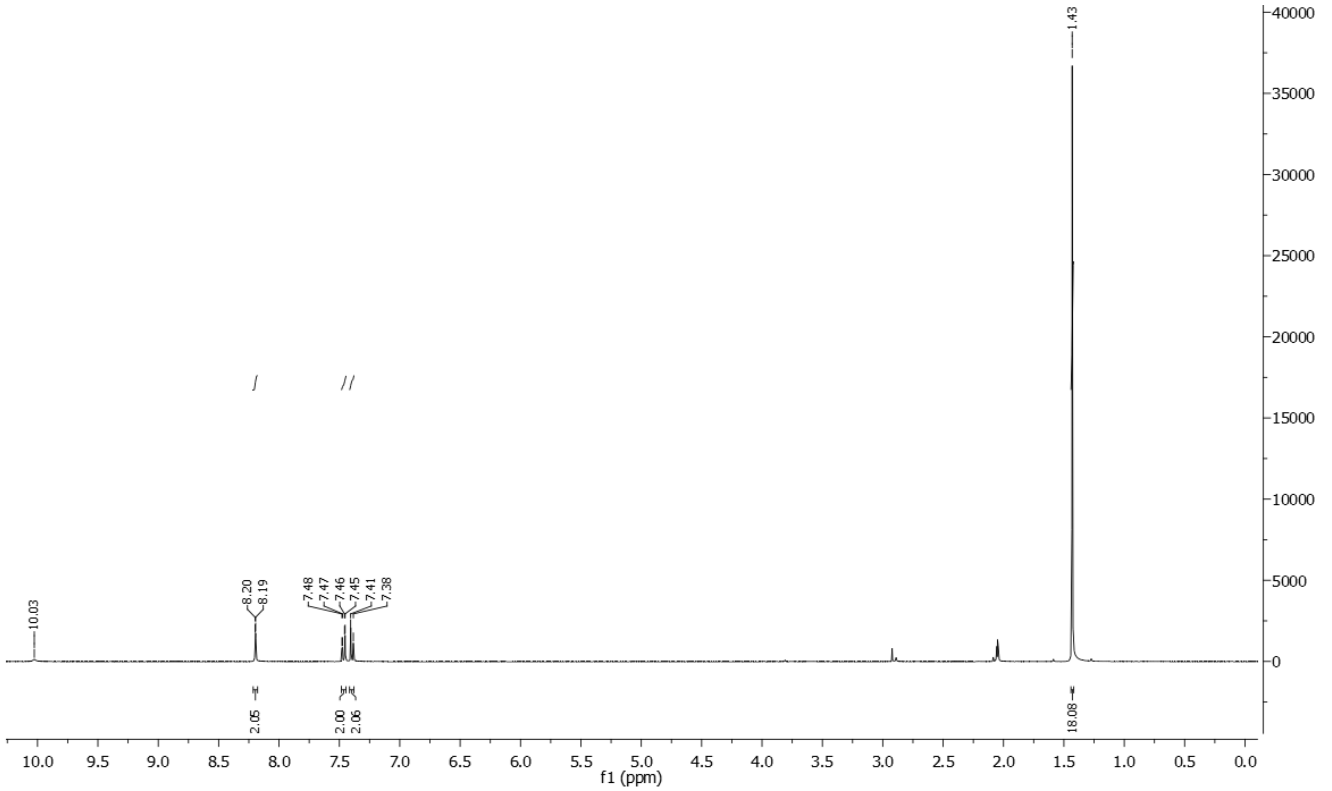

^{1}H-NMR spectrum of the non-deuterated starting material

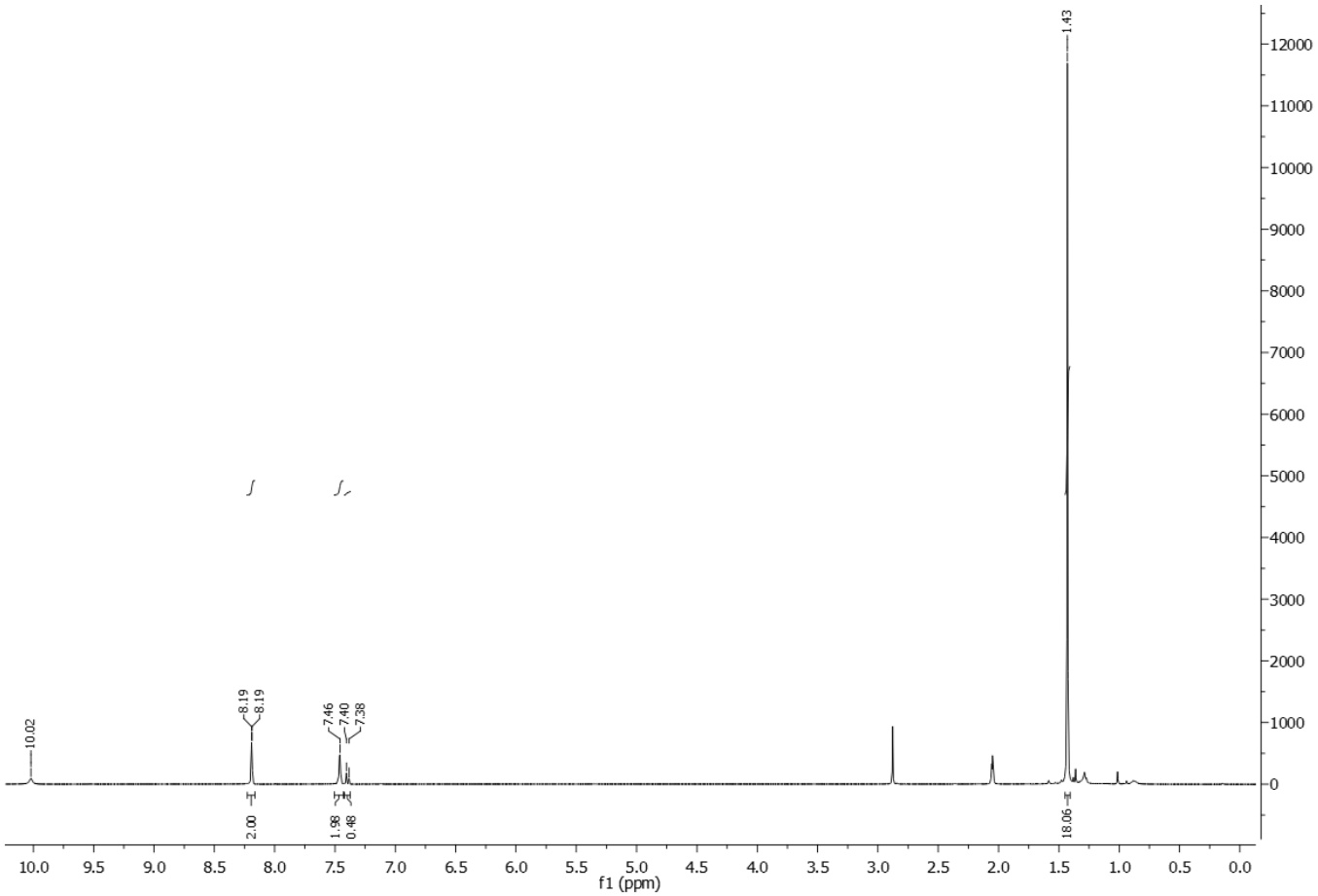

^{1}H-NMR spectrum of **21**

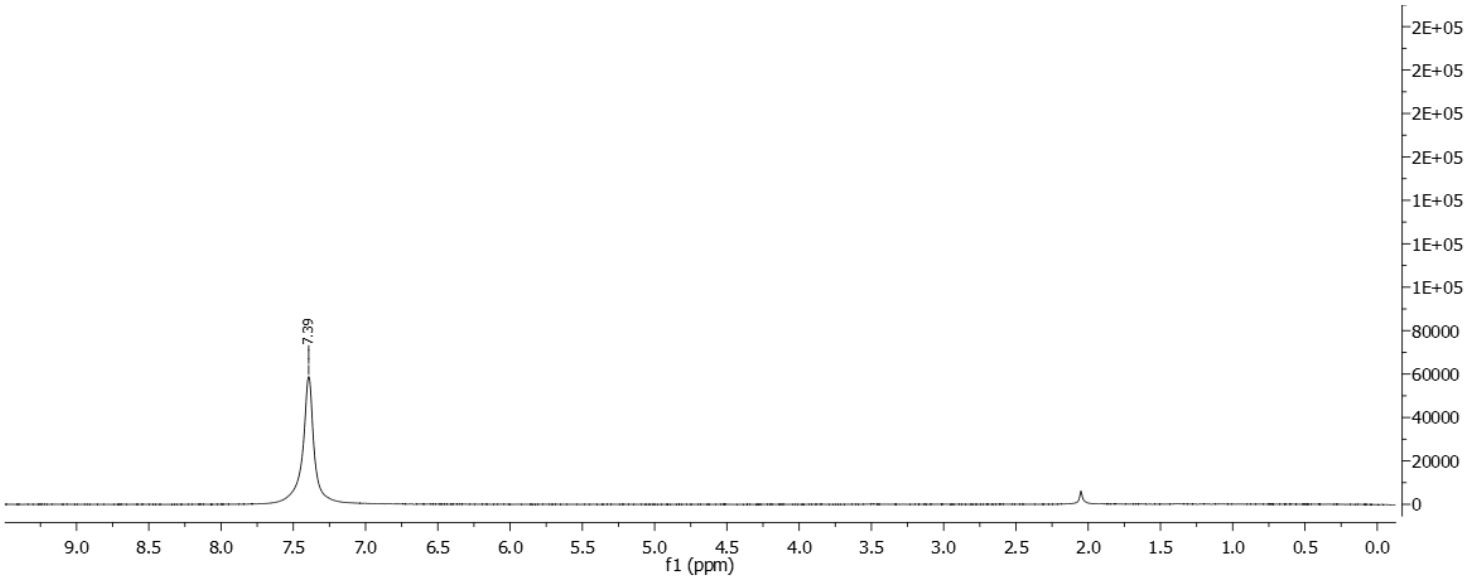

^{2}H-NMR spectrum of **21**

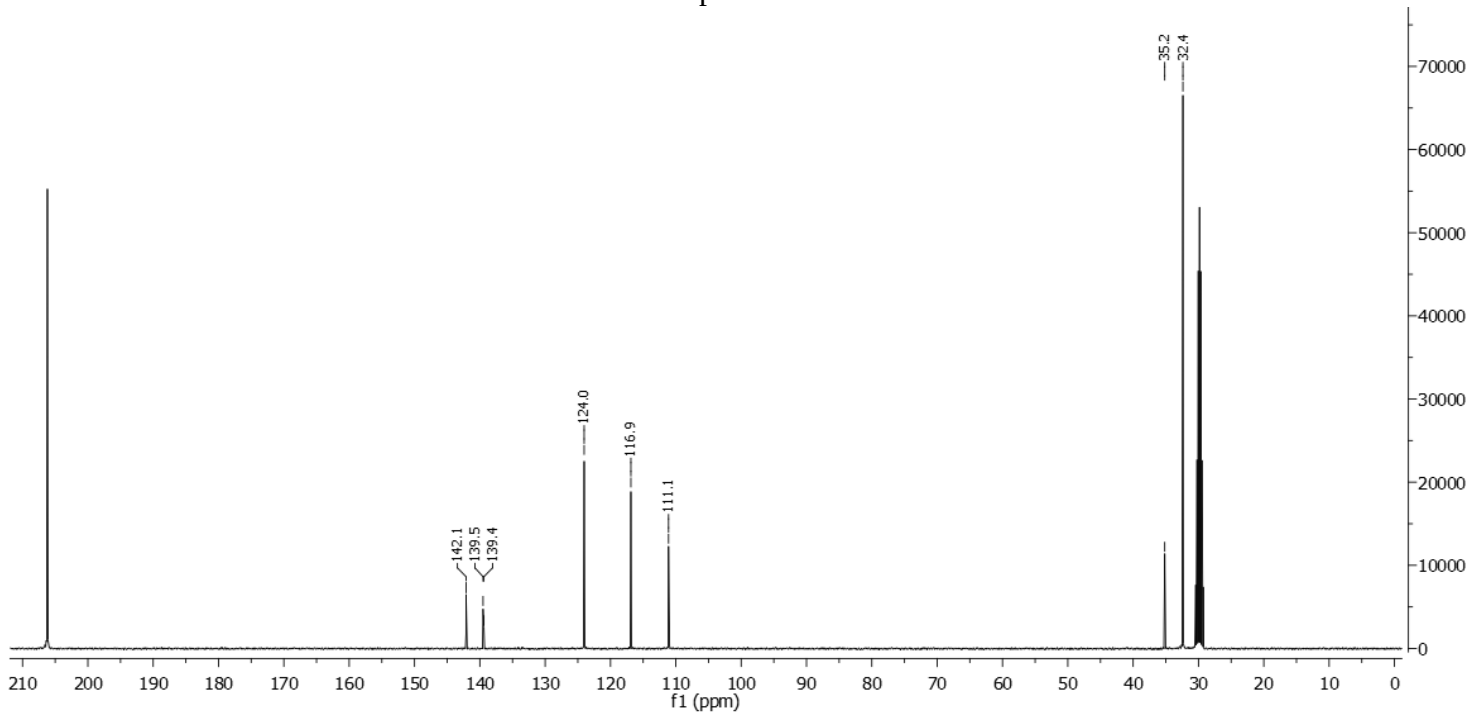

^{13}C-NMR spectrum of the non-deuterated starting material

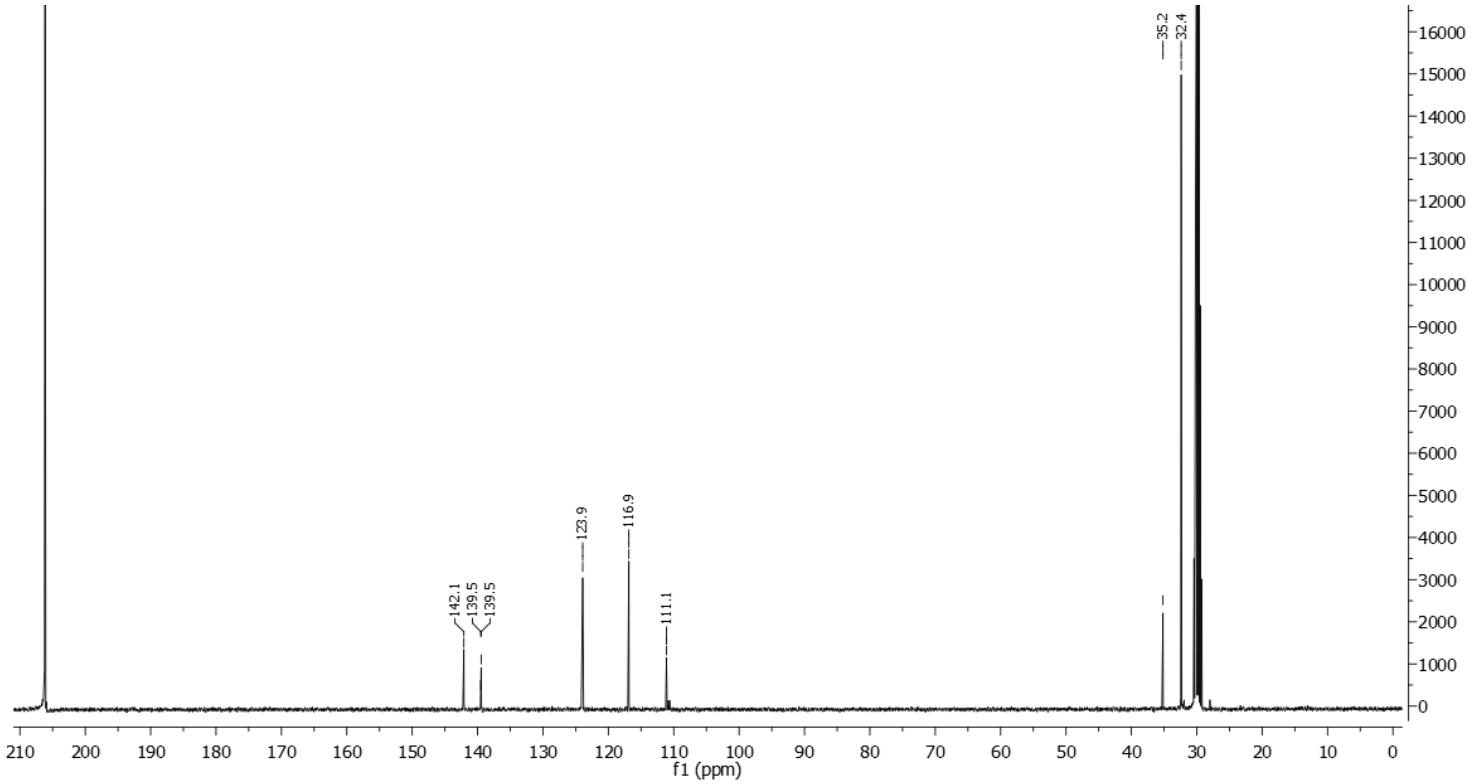

^{13}C-NMR spectrum of **21**

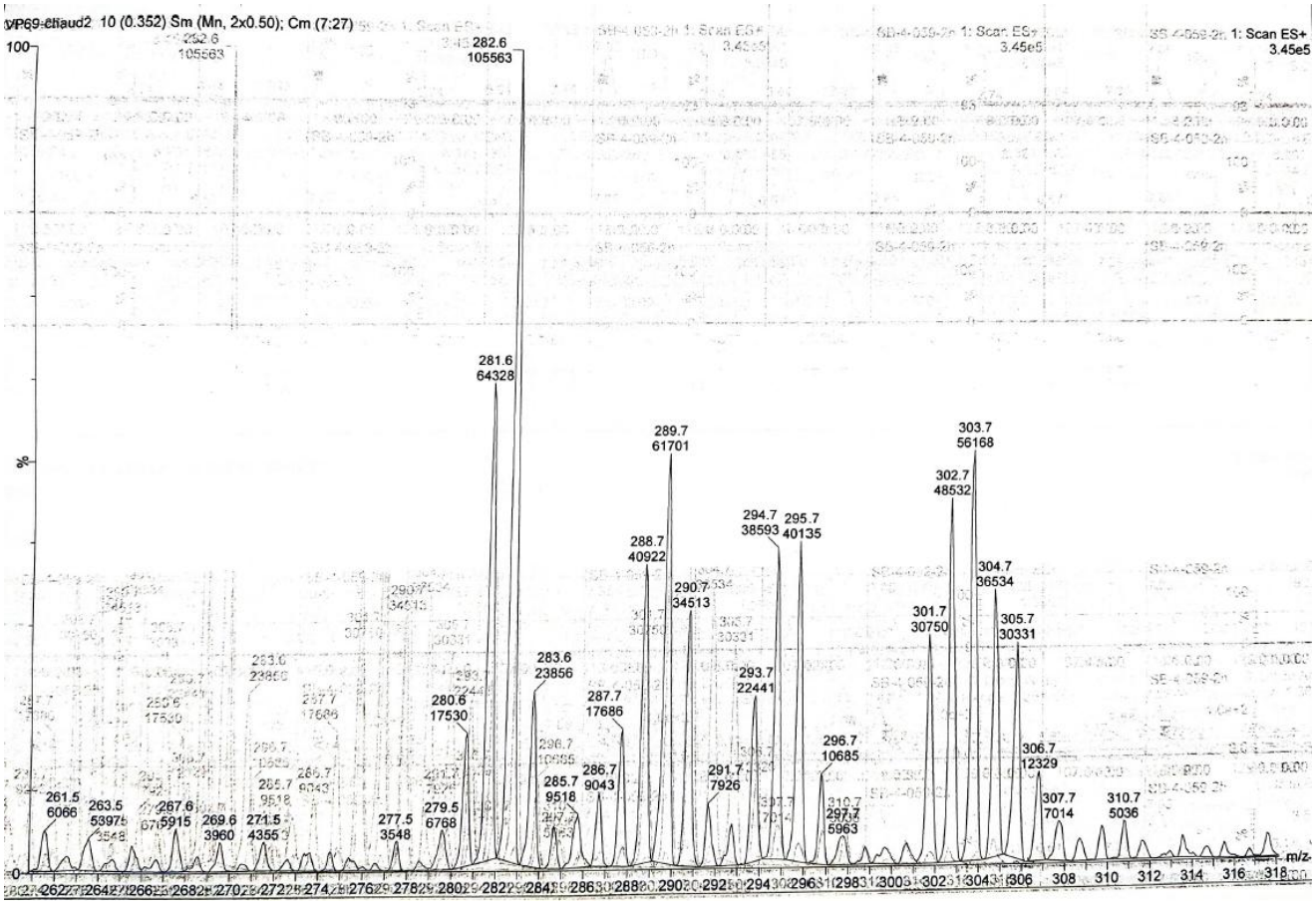

ESI-spectrum of **21**

3,6-Diphenylcarbazole **22**

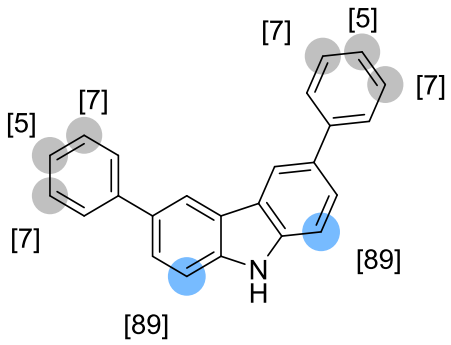

Chemical Formula: $C_{24}H_{17}N$

Substrate	Solvent (Volume)	RuNp@PVP cat.
31.9mg, 0.1mmol	THF (2mL)	14.4mg, 10mol%

Workup and purification:

After cooling down to room temperature EtOAc/cyclohexane (1:1, 3mL) was added to the reaction mixture and stirred for 10mins to let precipitate RuNp@PVP. The suspension was passed through a SiO_2 pad and the crude product was eluted with EtOAc (5mL). The solvent was removed under vacuum and the crude product was purified over SiO_2. The product was eluted with 10:1 cyclohexane/ethylacetate.

Yield: 10.0mg, 31%, white solid

^{1}H NMR (400 MHz, Acetone-*d*$_6$): δ 8.58 – 8.55 (m, 2H), 7.82 – 7.77 (m, 4H), 7.76 – 7.72 (m, 2H), 7.63 – 7.60 (m, 0.23H), 7.51 – 7.44 (m, 4H), 7.36 – 7.29 (m, 2H).

Deuterium incorporation was expected at *δ* 7.63 – 7.60. Isotopic enrichment values were determined against the integral at *δ* 8.58 – 8.55.

^{2}H-{^{1}H}NMR (600 MHz, Acetone): δ 7.62 (s).

^{13}C-{^{1}H}NMR (100 MHz, Acetone-*d*$_6$): δ 142.9, 140.9, 133.1, 129.6, 127.8, 127.2, 125.8, 124.8, 119.5, 112.2 (m).

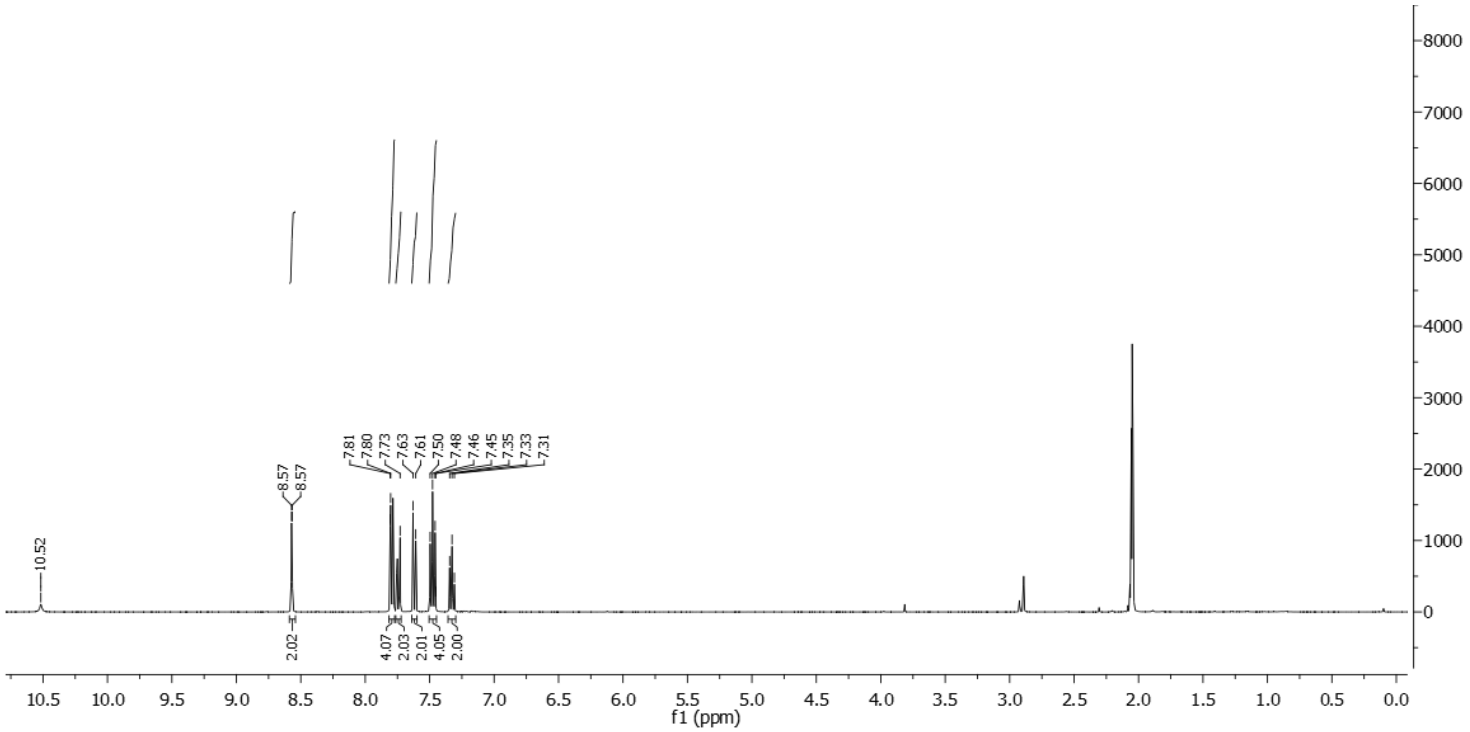

^{1}H-NMR spectrum of the non-deuterated starting material

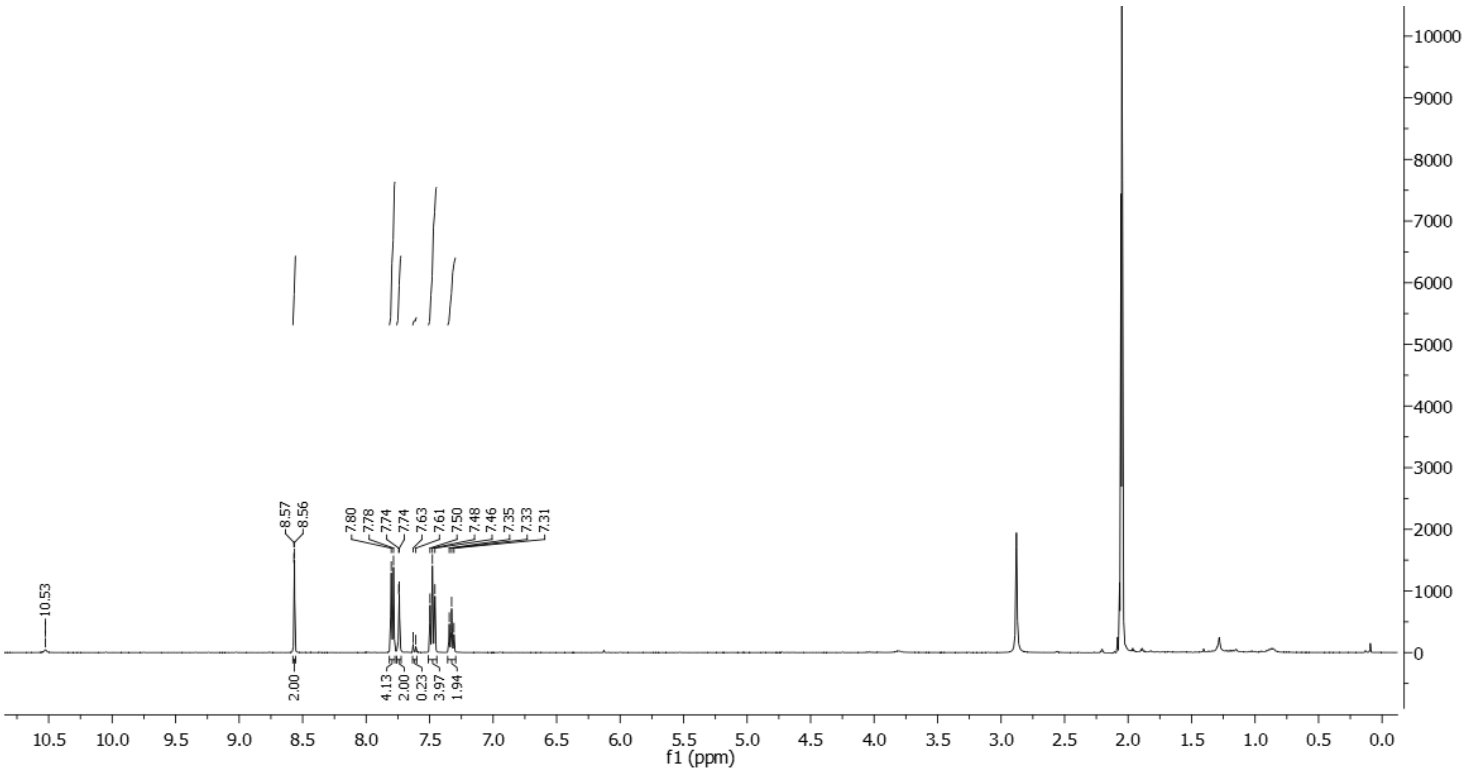

^{1}H-NMR spectrum of **22**

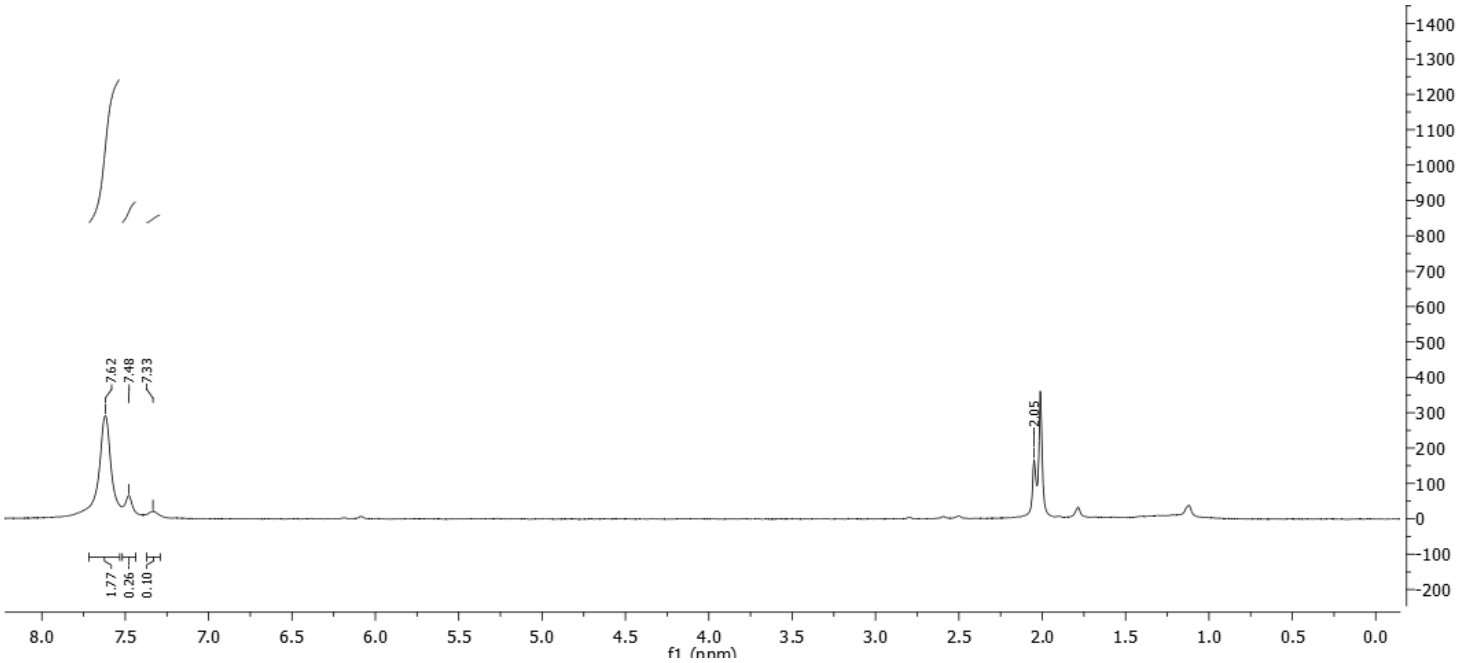

^{2}H-NMR spectrum of **22**

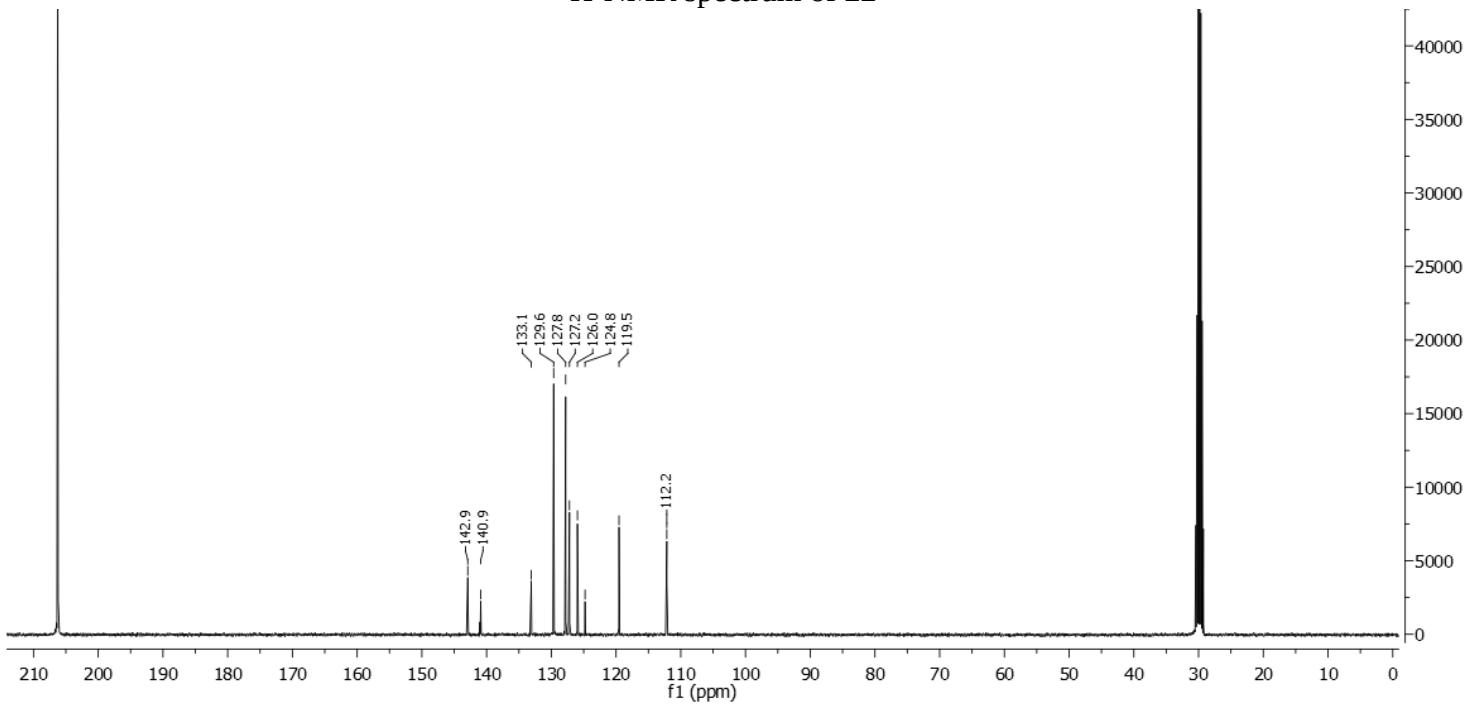

^{13}C-NMR spectrum of the non-deuterated starting material

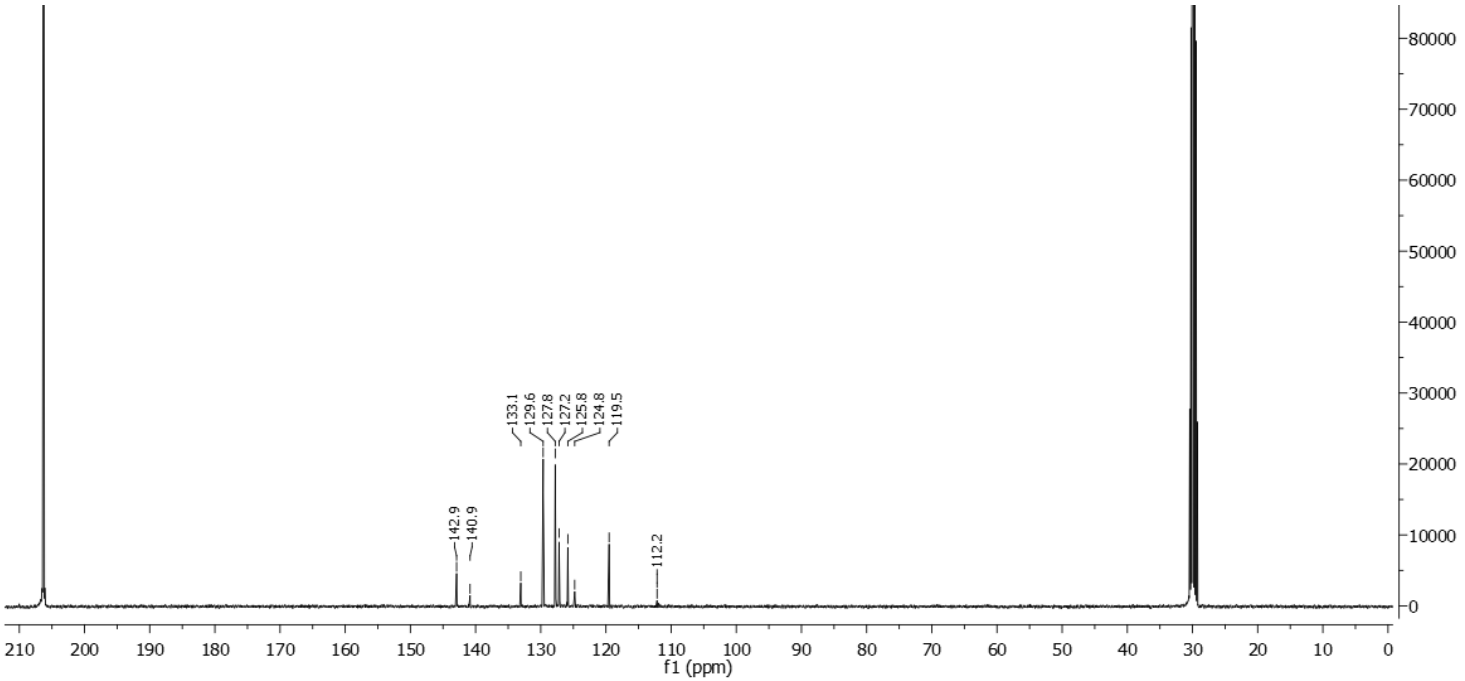

^{13}C-NMR spectrum of **22**

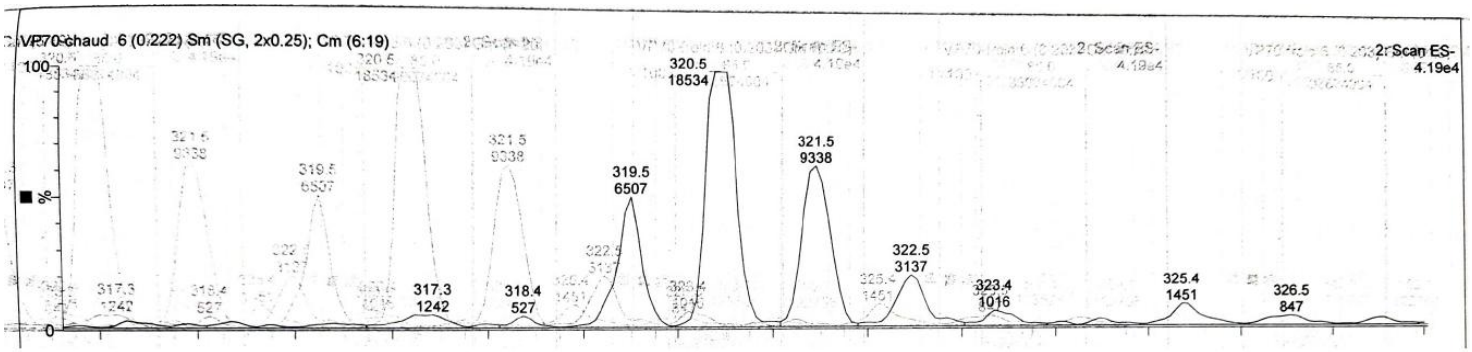

ESI-spectrum of **22**

11,12-Dihydroindolo[2,3-a]carbazole **23**

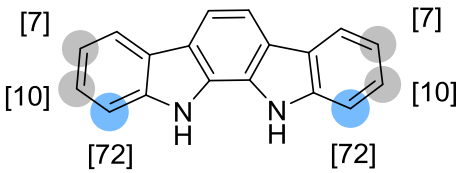

Chemical Formula: $C_{18}H_{12}N_2$

Substrate	Solvent (Volume)	RuNp@PVP cat.
51.2mg, 0.2mmol	THF (2mL)	28.9mg, 10mol%

Workup and purification:

After cooling down to room temperature EtOAc/cyclohexane (1:1, 3mL) was added to the reaction mixture and stirred for 10mins to let precipitate RuNp@PVP. The suspension was passed through a neutral Al_2O_3 pad and the crude product was eluted with THF (5mL). The solvent was removed under vacuum and the crude product was recrystallized from THF/MeOH (10:1).

Yield: 18.0mg, 35%, white solid

^{1}H NMR (400 MHz, Acetone-d_6): δ 10.41 (bs, NH), 8.19 – 8.14 (m, 2H), 7.98 – 7.94 (m, 2H), 7.63 – 7.59 (m, 0.56H), 7.40 – 7.35 (m, 2H), 7.25 – 7.19 (m, 2H).

Deuterium incorporation was expected at δ 7.63 – 7.59. Isotopic enrichment values were determined against the integral at δ 8.19 – 8.14.

^{2}H-{^{1}H}NMR (600 MHz, Acetone): δ 7.61 (s, 1.44D), 7.38 (s, 0.20D), 7.23 (s, 0.14D).

^{13}C-{^{1}H}NMR (100 MHz, Acetone-d_6): δ 140.3, 126.8, 125.5, 125.4, 121.9, 120.5, 120.0, 112.6, 112.1 (m).

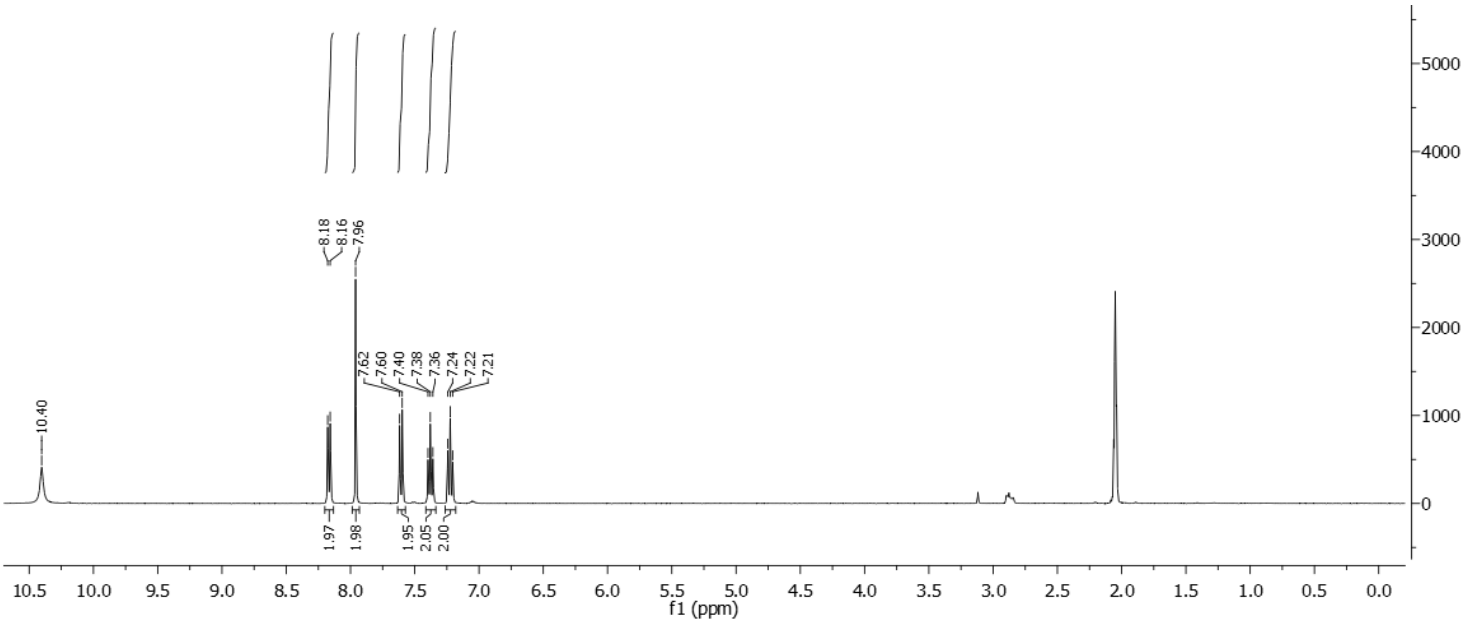

^{1}H-NMR spectrum of the non-deuterated starting material

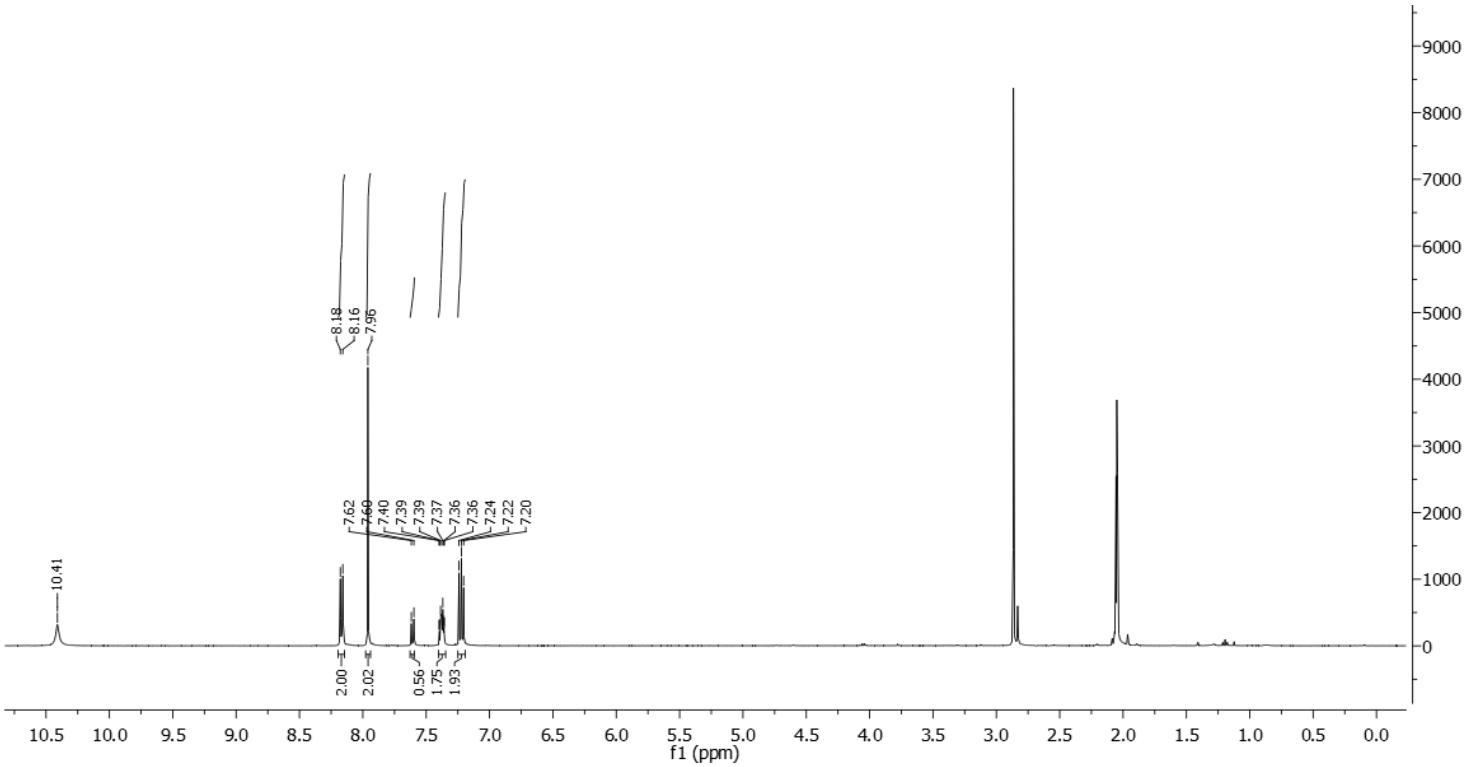

^{1}H-NMR spectrum of **23**

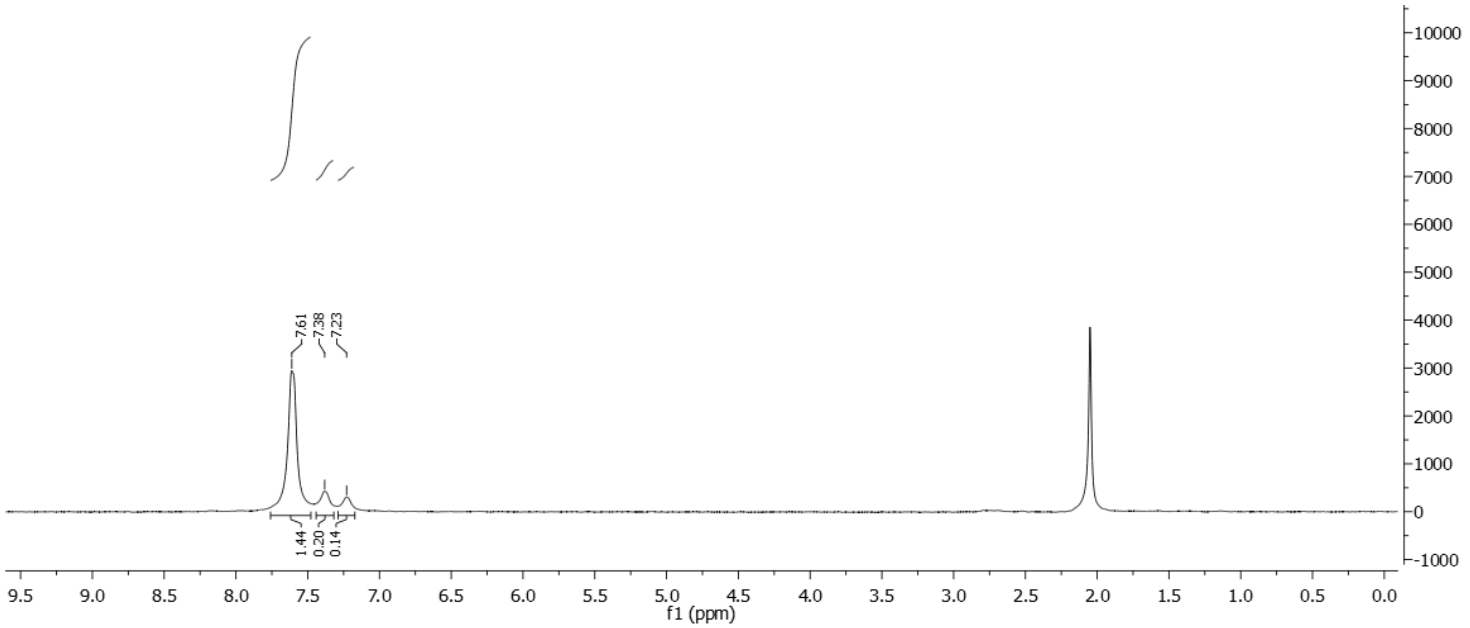

^{2}H-NMR spectrum of **23**

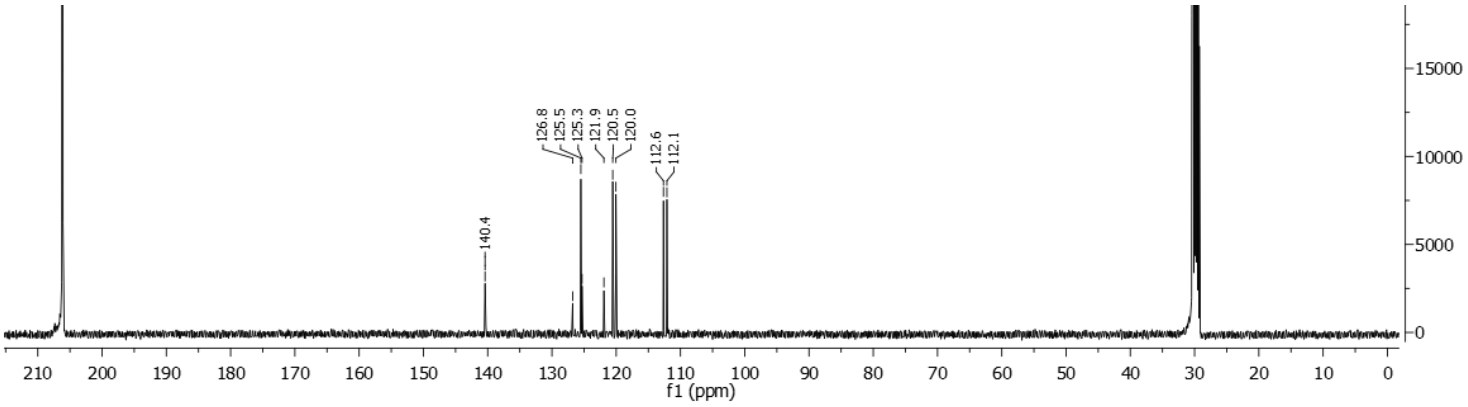

^{13}C-NMR spectrum of the non-deuterated starting material

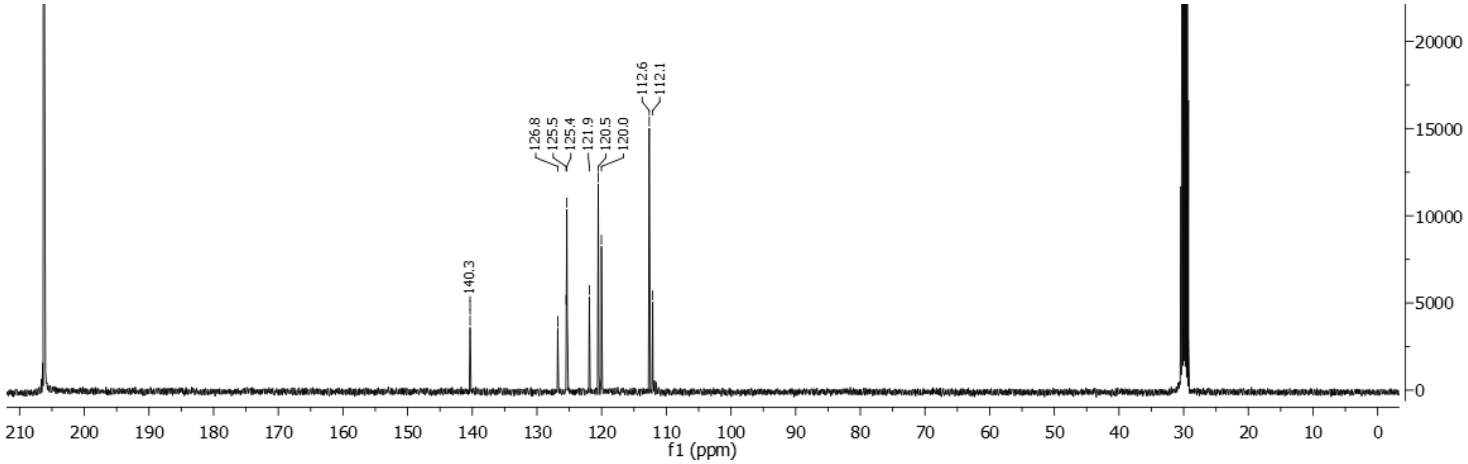

^{13}C-NMR spectrum of **23**

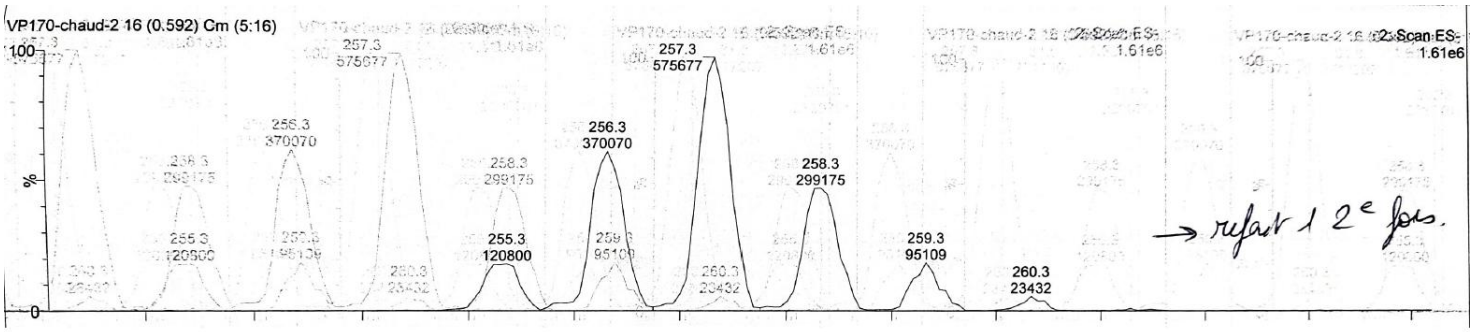

ESI-spectrum of **23**

N-Methylcarbazole **24**

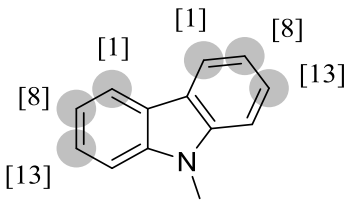

Chemical Formula: $C_{13}H_{11}N$

Substrate	Solvent (Volume)	RuNp@PVP cat.
36.2mg, 0.2mmol	THF (2mL)	14.4mg, 5mol%

Workup and purification:

After cooling down to room temperature cyclohexane (3mL) was added to the reaction mixture and stirred for 10mins to let precipitate RuNp@PVP. The suspension was passed through a SiO_2 pad and the crude product was eluted with EtOAc (5mL). The solvent was removed under vacuum and the crude product was recrystallized from THF/MeOH (10:1).

Yield: 10.0mg, 28%, white solid

^{1}H NMR (400 MHz, acetone-*d*$_6$): δ 8.17 – 8.11 (m, 2H), 7.57 – 7.51 (m, 2H), 7.50 – 7.43 (m, 1.73H), 7.23 – 7.18 (m, 1.83H), 3.90 (s, 3H).

Deuterium incorporation was expected at δ 7.50 – 7.43 and at δ 7.23 – 7.18. Isotopic enrichment values were determined against the integral at *δ* 7.57 – 7.51.

^{2}H-{^{1}H}NMR (600 MHz, acetone): δ 8.18 – 8.07 (m, 0.03D), 7.52 – 7.38 (m, 0.27D), 7.26 – 7.14 (m, 0.17D).

^{13}C-{^{1}H}NMR (100 MHz, acetone-*d*$_6$): δ 141.9, 126.5, 123.5, 120.9, 119.6, 109.6.

For ^{1}H- and ^{13}C-NMR spectrum of the non-deuterated starting material see “synthesis of compounds”

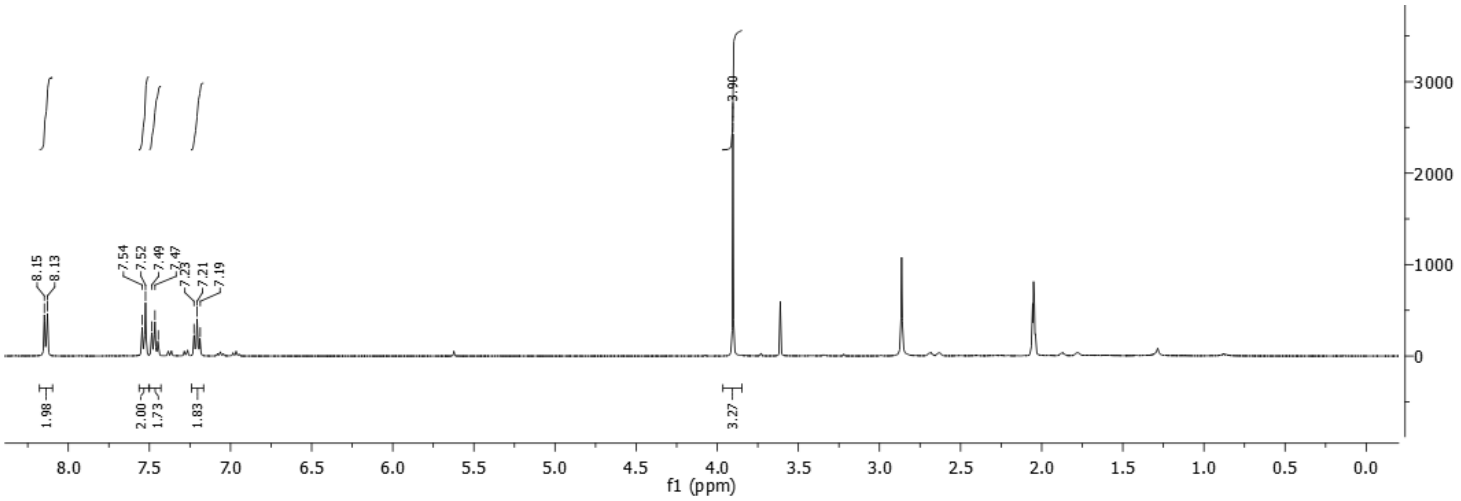

^{1}H-NMR spectrum of **24**

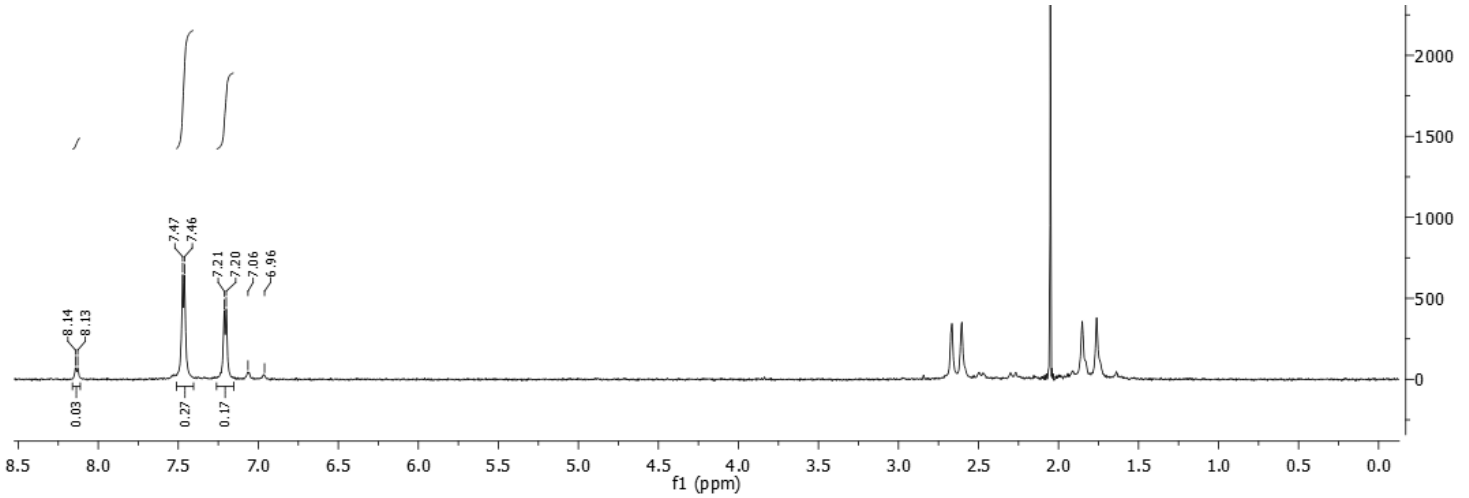

^{2}H-NMR spectrum of **24**

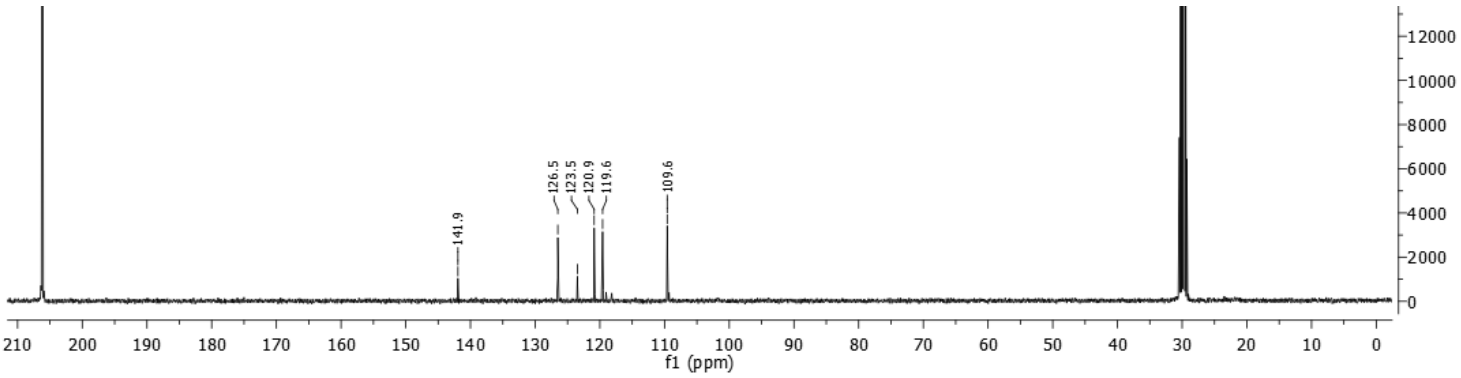

^{13}C-NMR spectrum of **24**

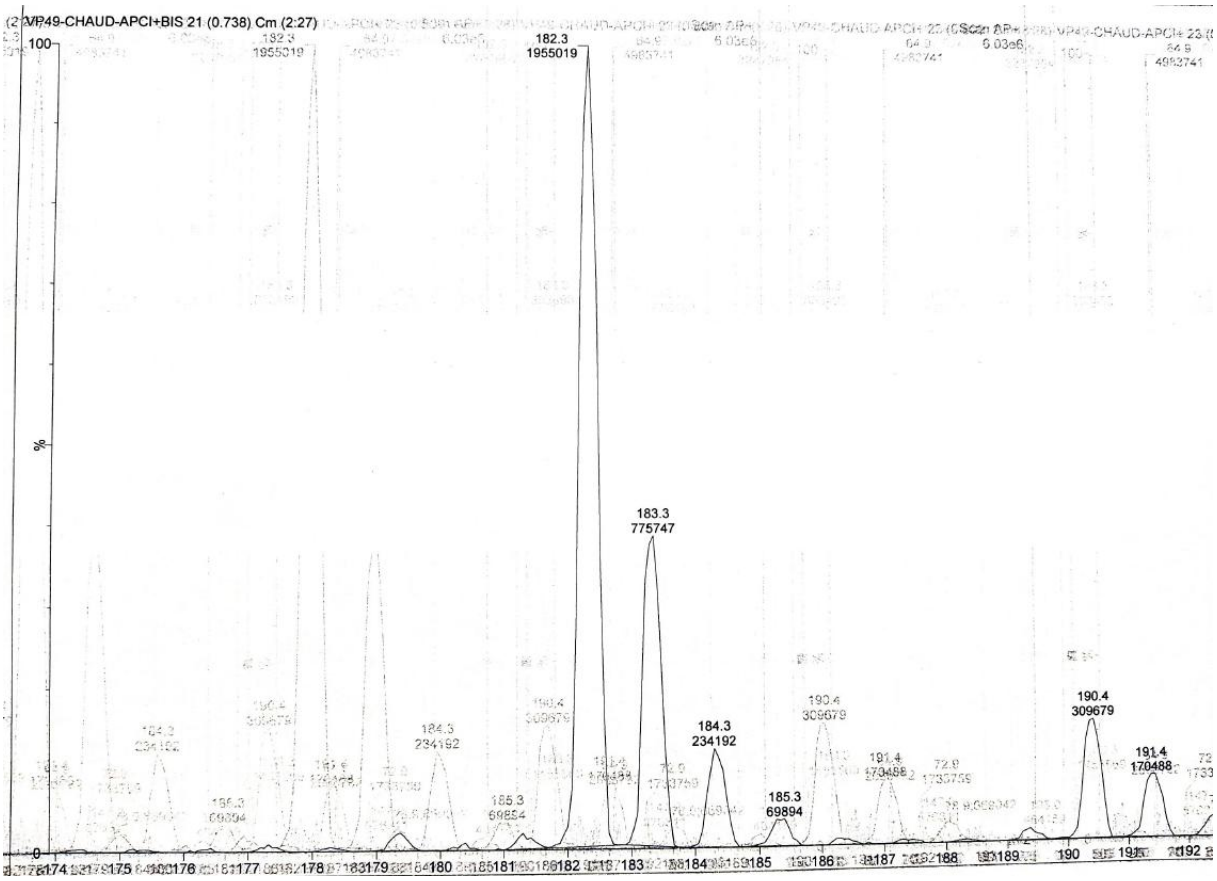

ESI-spectrum of **24**

Deuteration of carbazoles with RuNp@PVP and Cs_2CO_3

Carbazole **20'**

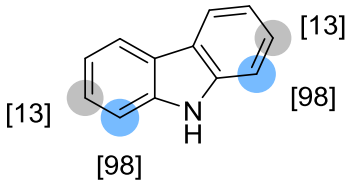

Chemical Formula: $C_{12}H_9N$

Substrate	Cs_2CO_3	Solvent (Volume)	RuNp@PVP cat.
33.4mg, 0.2mmol	65.2mg, 0.2mmol	THF (2mL)	14.4mg, 5mol%

Workup and purification:

After cooling down to room temperature the reaction mixture was poured on a 5mM solution of acetic acid in H_2O dist. (100mL). The aqueous phase was extracted three times with EtOAc (3 x 50mL) in a separation funnel. The solvent was removed under vacuum and the crude product was recrystallized from THF and MeOH (THF : MeOH, 10:1).

Yield: 34.0mg, 99%, white solid

^{1}H NMR (400 MHz, Acetone-d_6): δ 10.37 (bs, NH), 8.16 – 8.08 (m, 2H), 7.54 – 7.50 (m, 0.04H), 7.42 – 7.36 (m, 2H), 7.22 – 7.15 (m, 2H).

Deuterium incorporation was expected at δ 7.54 – 7.50. Isotopic enrichment values were determined against the integral at δ 8.16 – 8.08.

^{2}H-{^{1}H}NMR (92 MHz, Acetone): δ 7.52 (m, 1.96D), 7.39 (m, 0.27D).

^{13}C-{^{1}H}NMR (100 MHz, Acetone-d_6): δ 140.9, 126.3, 123.90, 120.8, 119.6, 111.7 (m).

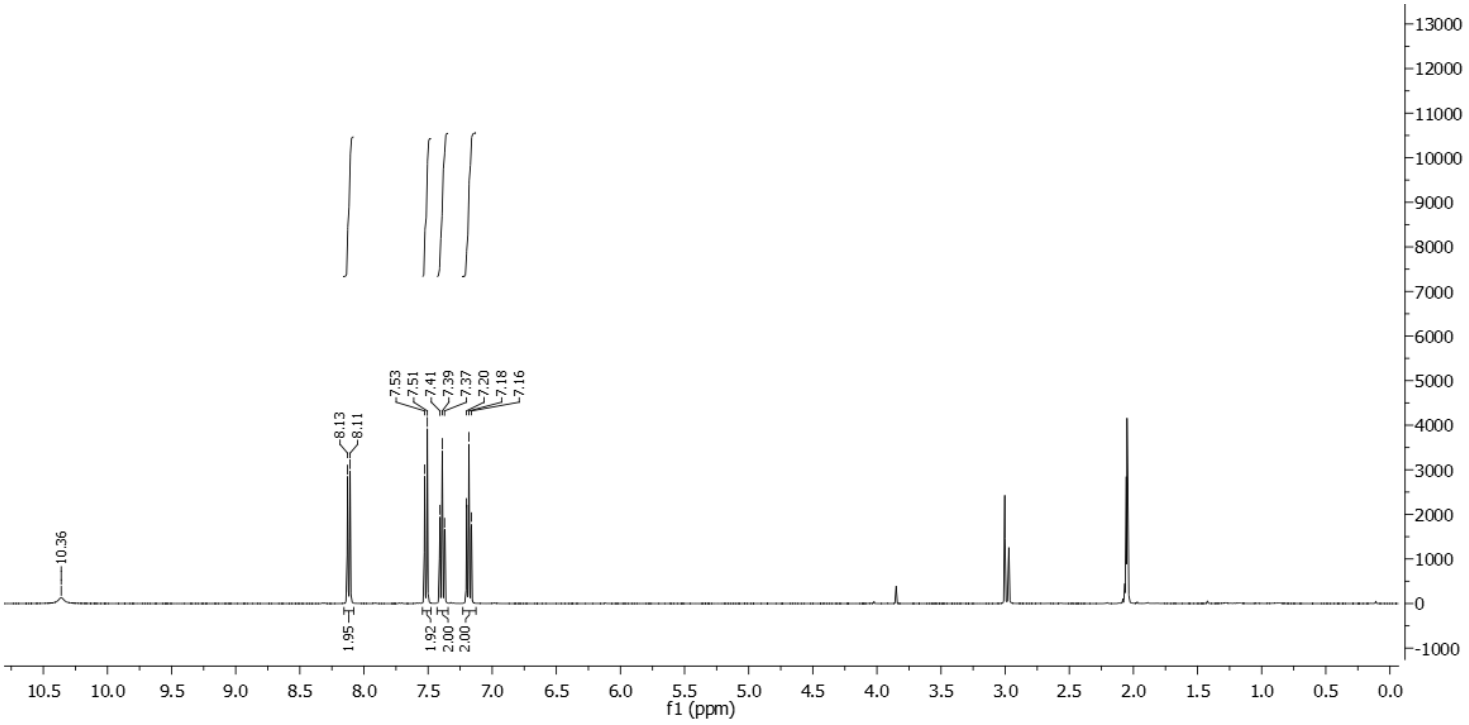

^{1}H-NMR spectrum of the non-deuterated starting material

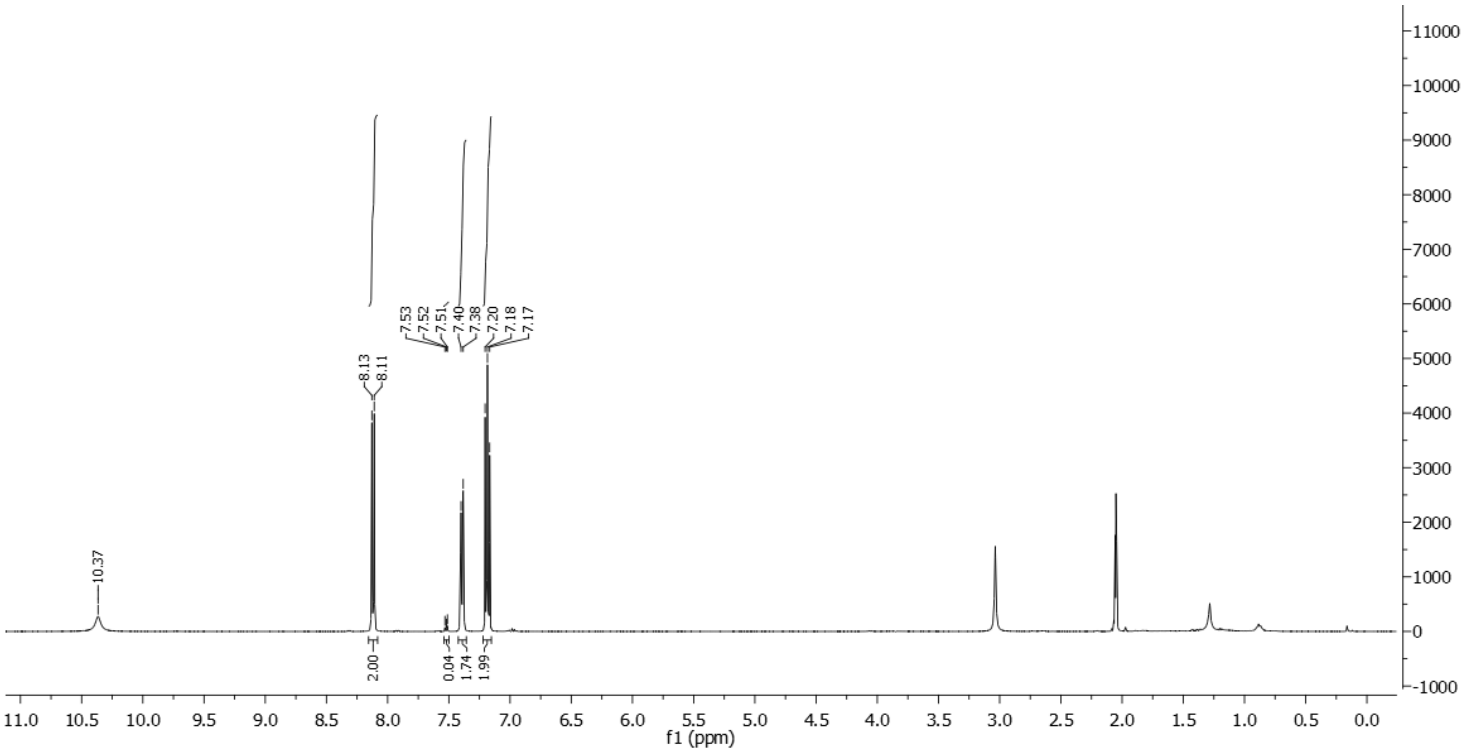

^{1}H-NMR spectrum of **20'**

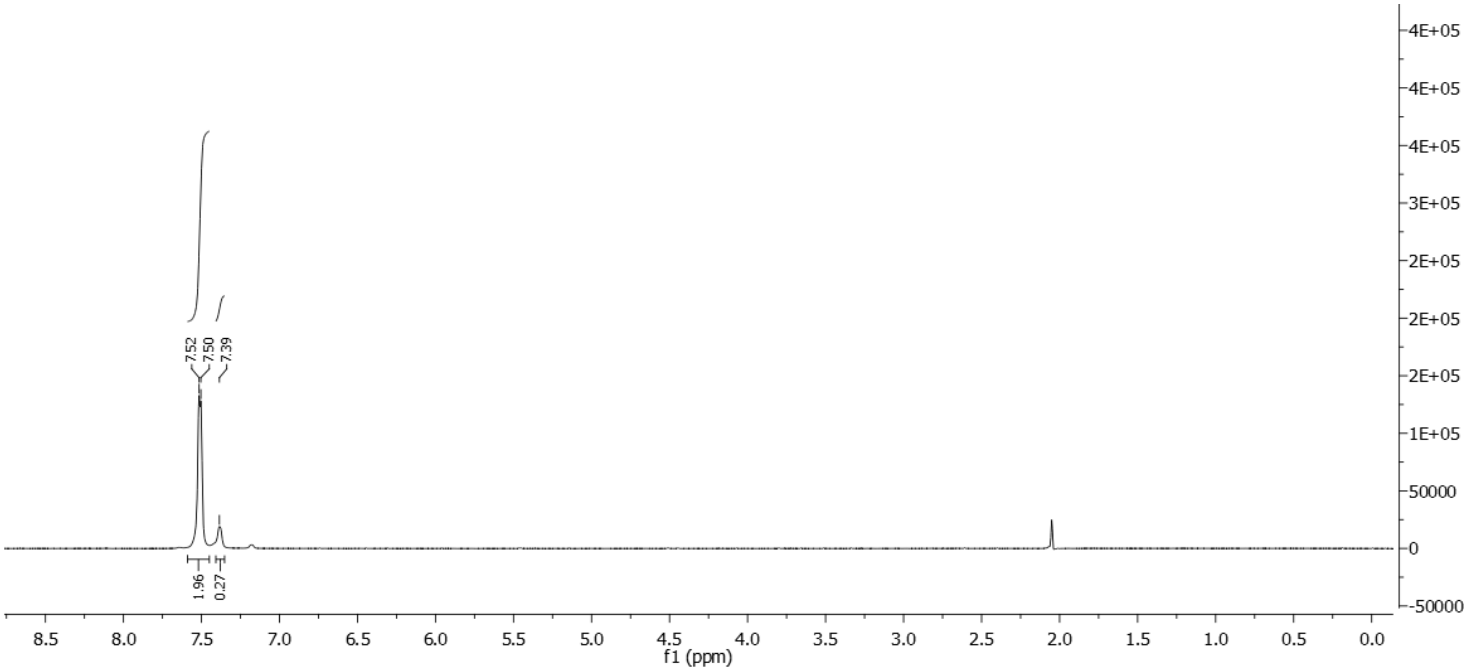

^{2}H-NMR spectrum of **20'**

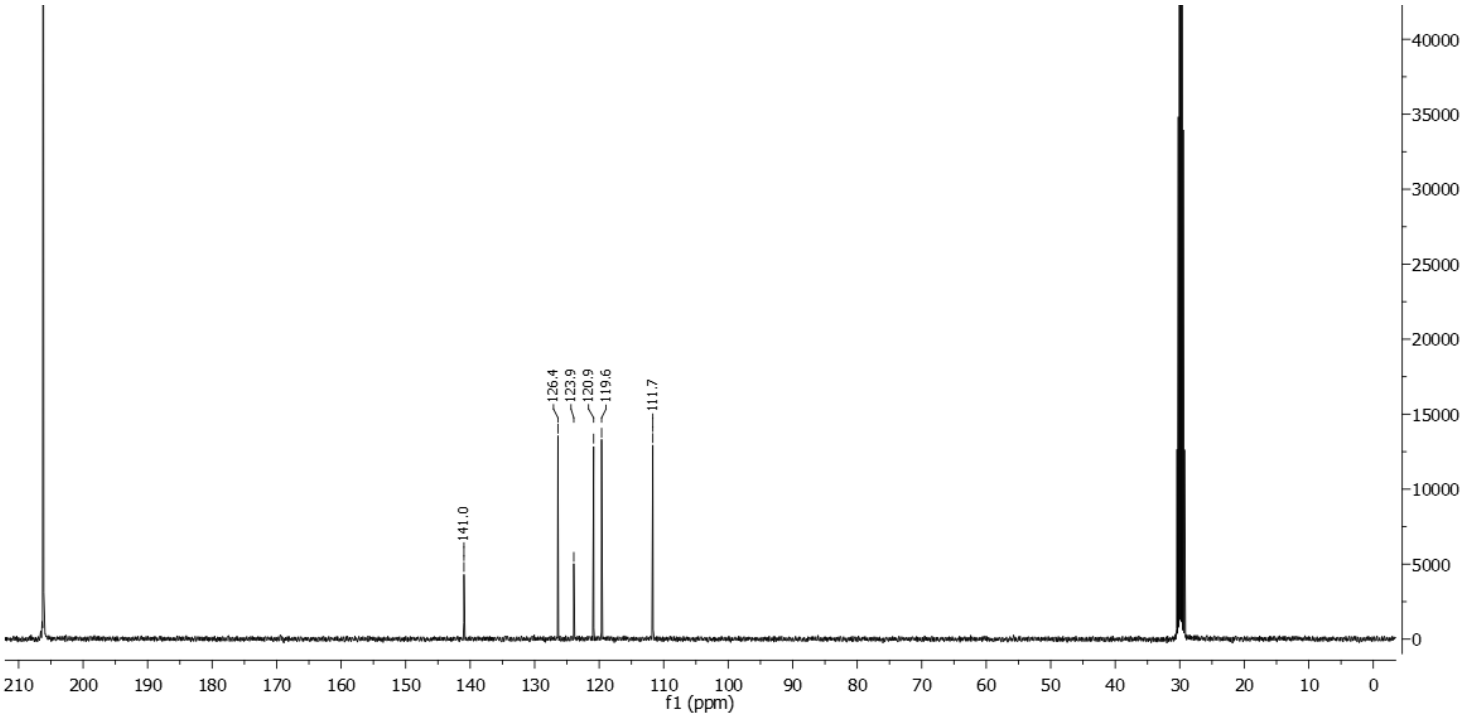

^{13}C-NMR spectrum of the non-deuterated starting material

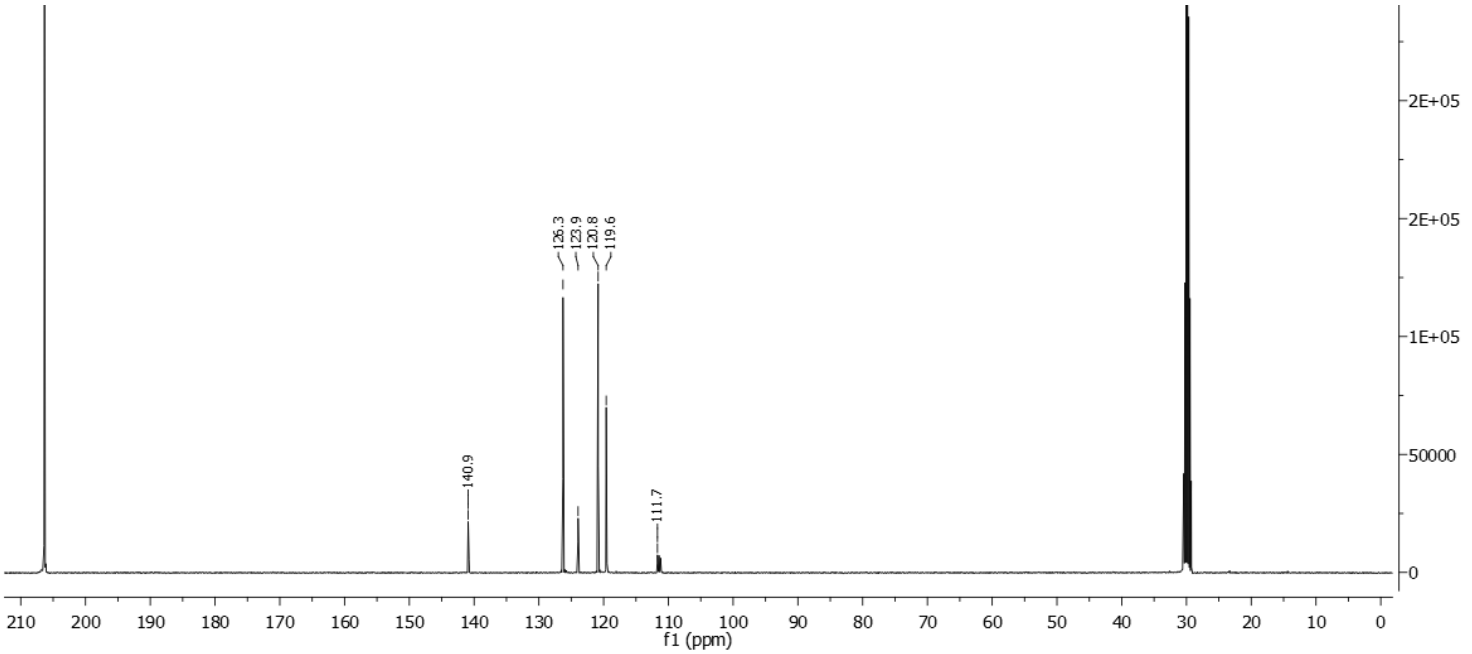

^{13}C-NMR spectrum of **20'**

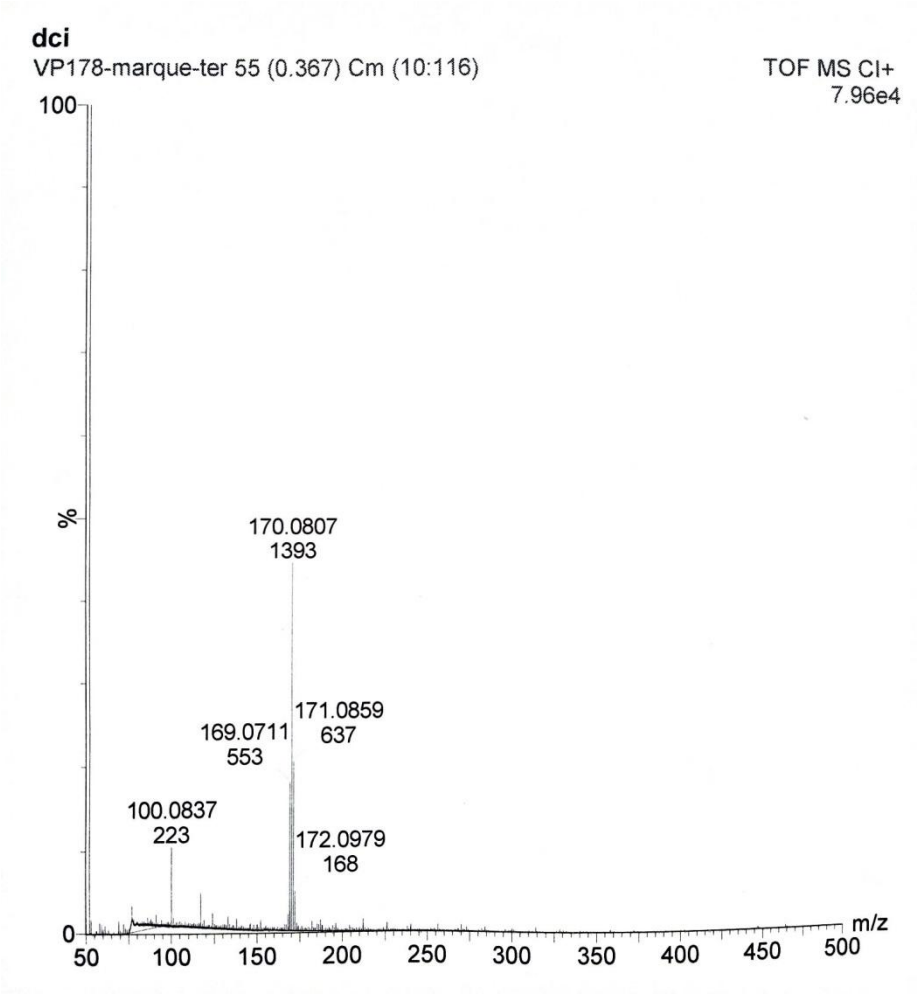

TOF-spectrum of **20'** after GC-MS analysis

3,6-Di-tert-butylcarbazole **21'**

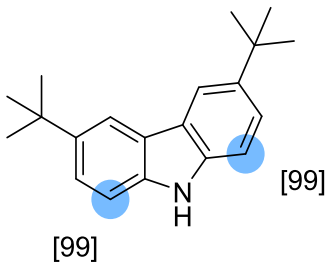

Chemical Formula: $C_{20}H_{25}N$

Substrate	Cs_2CO_3	Solvent (Volume)	RuNp@PVP cat.
22.9mg, 0.1mmol	32.6mg, 0.1mmol	THF (2mL)	7.22mg, 5mol%

Workup and purification:

After cooling down to room temperature the reaction mixture was poured on a 5mM solution of acetic acid in H_2O dist. (100mL). The aqueous phase was extracted three times with EtOAc (3 x 50mL) in a separation funnel. The solvent was removed under vacuum.

Yield: 23mg, 99%, white solid

^{1}H NMR (400 MHz, Acetone-*d*$_6$): δ 10.04 (bs, NH), 8.23 – 8.15 (m, 2H), 7.51 – 7.42 (m, 2H), 7.41 – 7.36 (m, 0.03H), 1.43 (s, 18H).

Deuterium incorporation was expected at δ 7.41 – 7.36. Isotopic enrichment values were determined against the integral at δ 8.23 – 8.15.

^{2}H-{^{1}H}NMR (92 MHz, Acetone): δ 7.40 (s).

^{13}C-{^{1}H}NMR (100 MHz, Acetone-*d*$_6$): δ 142.1, 139.5, 139.3, 123.9, 116.9, 111.1 (m), 35.2, 32.4.

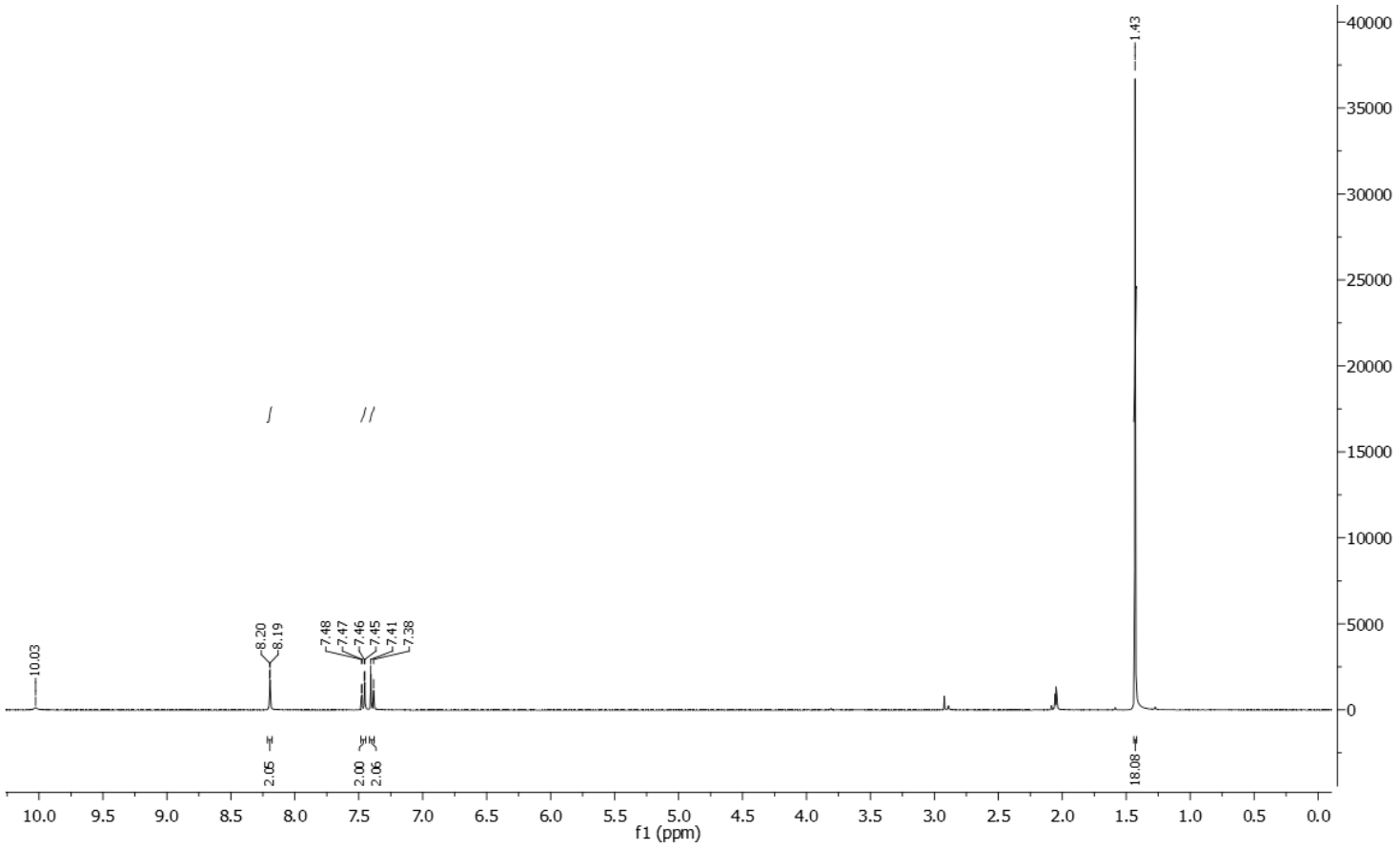

^{1}H-NMR spectrum of the non-deuterated starting material

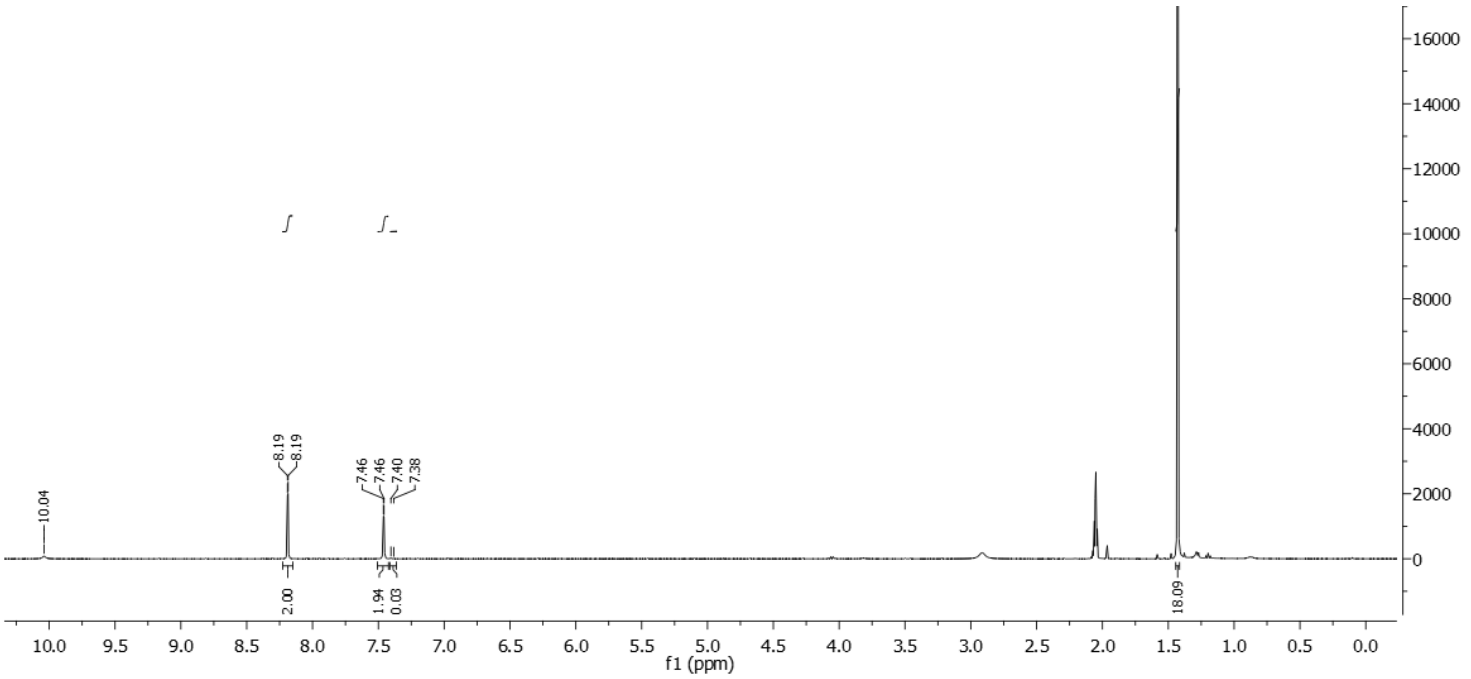

^{1}H-NMR spectrum of **21'**

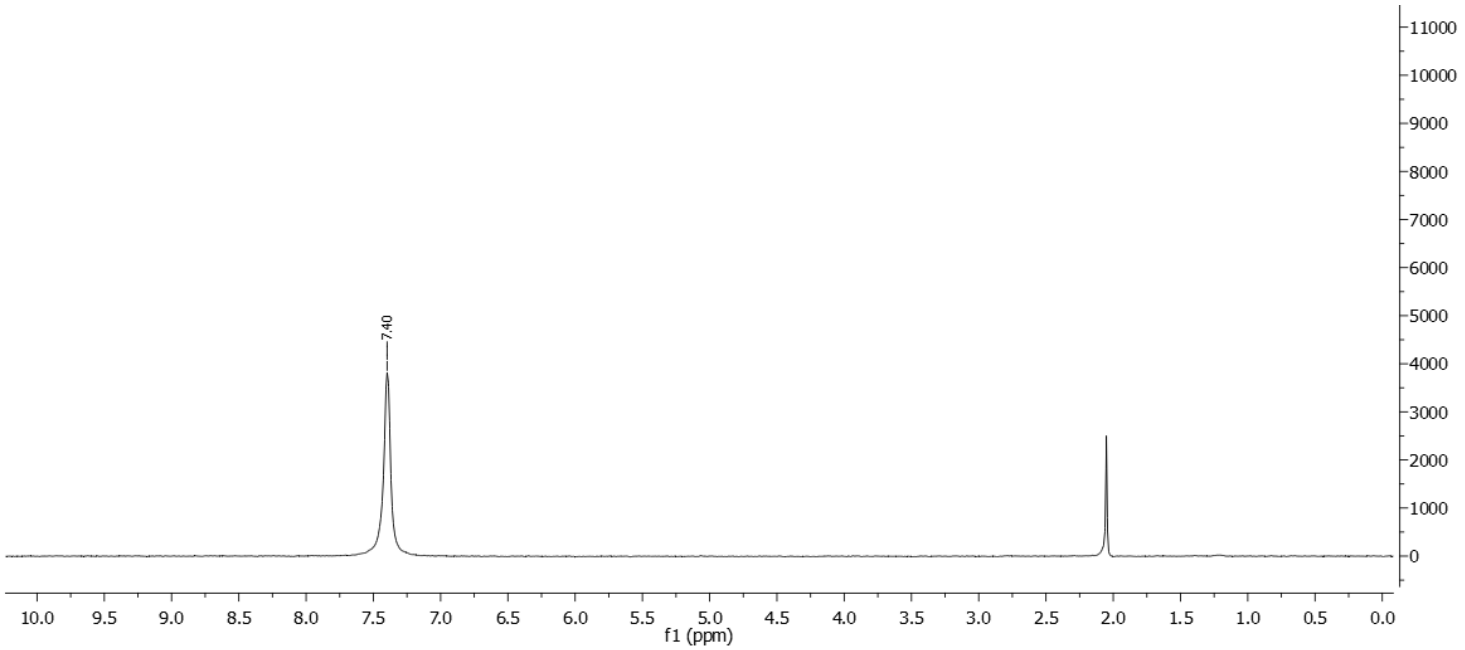

^{2}H-NMR spectrum of **21'**

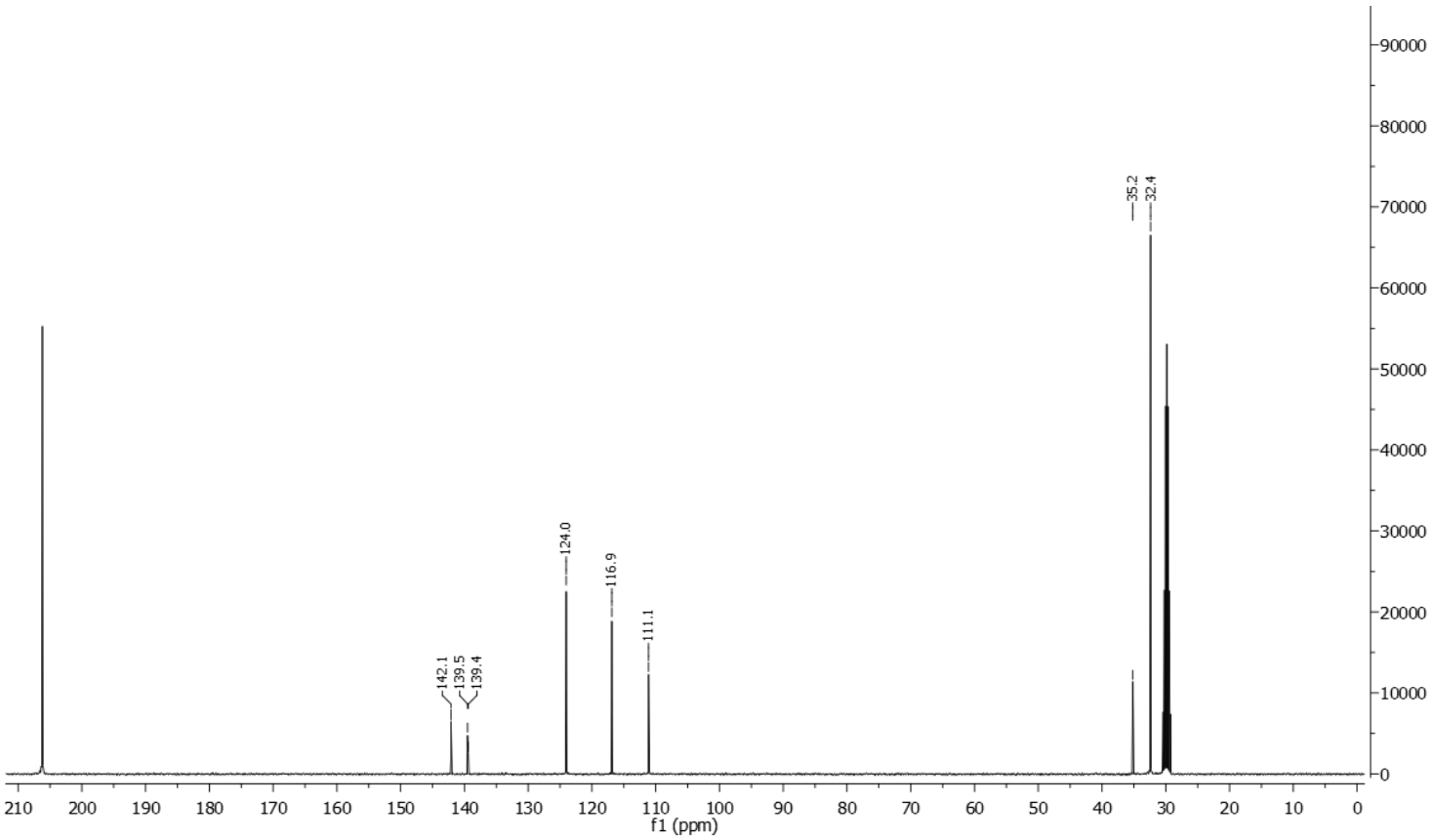

^{13}C-NMR spectrum of the non-deuterated starting material

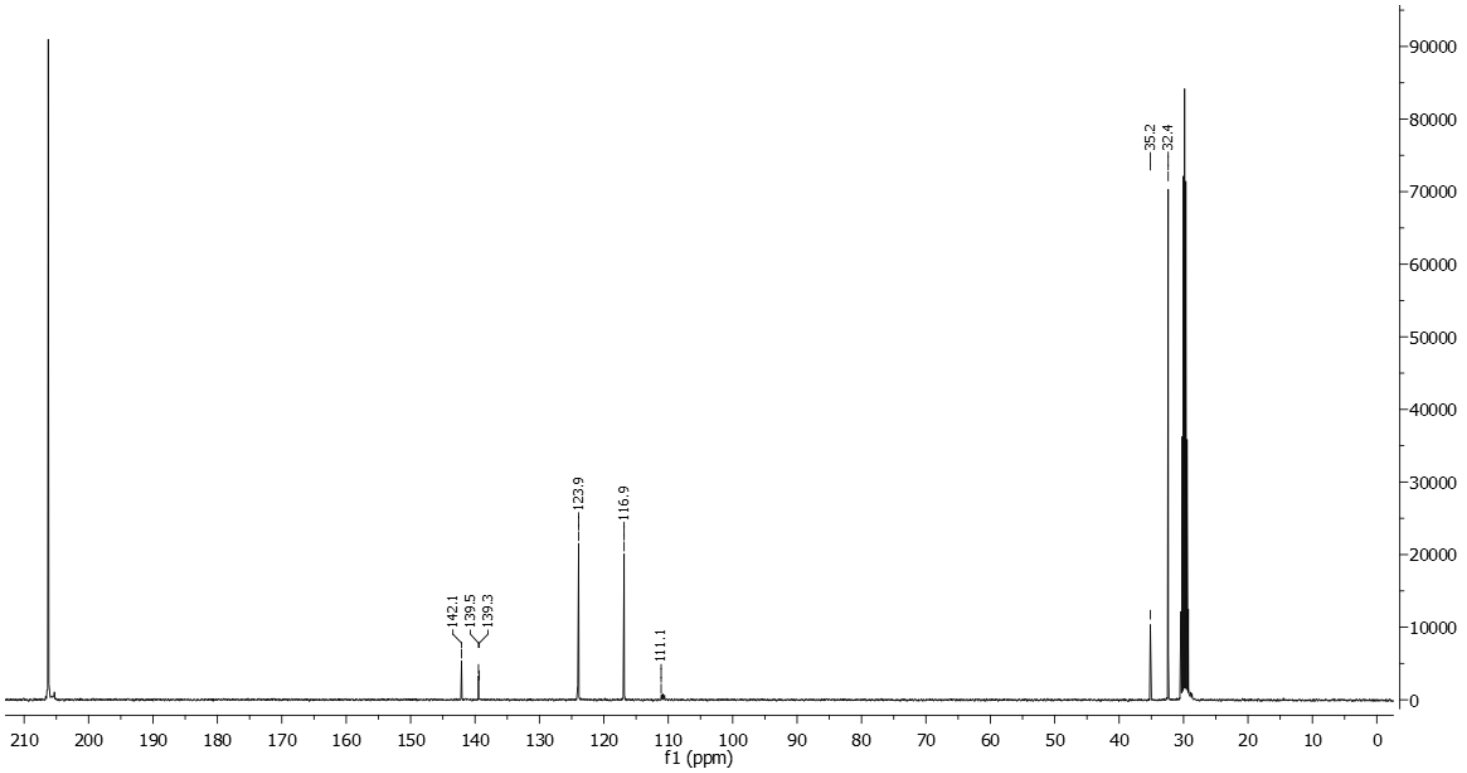

^{13}C-NMR spectrum of **21'**

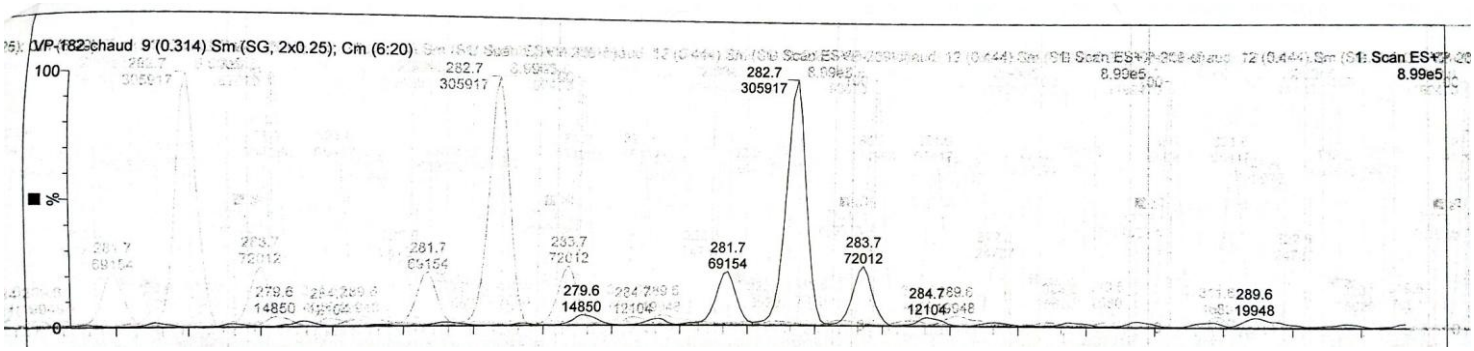

ESI-spectrum of **21'**

3,6-Diphenylcarbazole **22'**

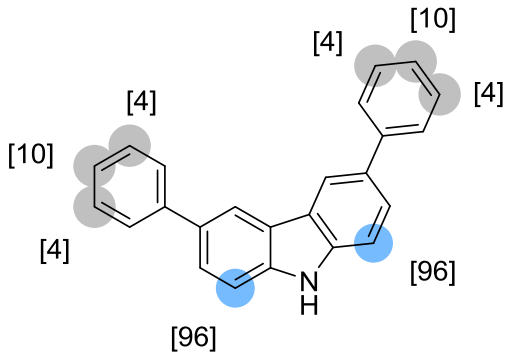

Chemical Formula: $C_{24}H_{17}N$

Substrate	Cs_2CO_3	Solvent (Volume)	RuNp@PVP cat.
63.8mg, 0.2mmol	65.2mg, 0.2mmol	THF (2mL)	14.4mg, 5mol%

Workup and purification:

After cooling down to room temperature the reaction mixture was poured on a 5mM solution of acetic acid in H_2O dist. (100mL). The aqueous phase was extracted three times with EtOAc (3 x 50mL) in a separation funnel. The solvent was removed under vacuum.

Yield: 68mg, 99%, white solid

^{1}H NMR (400 MHz, Acetone-d_6): δ 10.46 (bs, NH), 8.58 – 8.53 (m, 2H), 7.82 – 7.77 (m, 4H), 7.75 – 7.72 (m, 2H), 7.64 – 7.60 (m, 0.09H), 7.51 – 7.44 (m, 4H), 7.36 – 7.30 (m, 2H).

Deuterium incorporation was expected at δ 7.64 – 7.60. Isotopic enrichment values were determined against the integral at δ 8.58 – 8.53.

^{2}H-{^{1}H}NMR (92 MHz, Acetone): δ 7.62 (s, 1.91D), 7.48 (s, 0.17D). 7.33 (s, 0.20D)

^{13}C-{^{1}H}NMR (100 MHz, Acetone-d_6): δ 142.9, 141.0, 133.1, 129.6, 127.8, 127.2, 125.9, 124.9, 119.5, 112.2 (m).

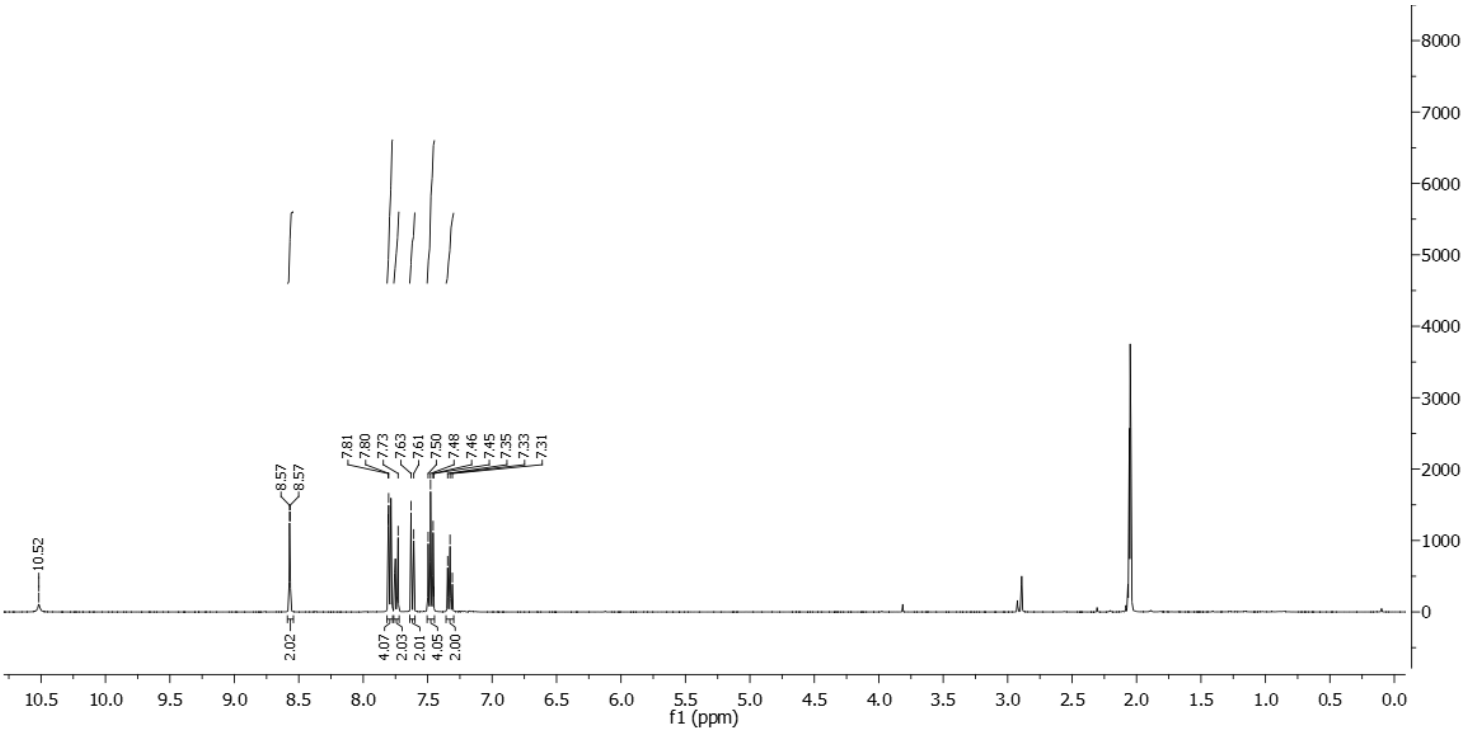

^{1}H-NMR spectrum of the non-deuterated starting material

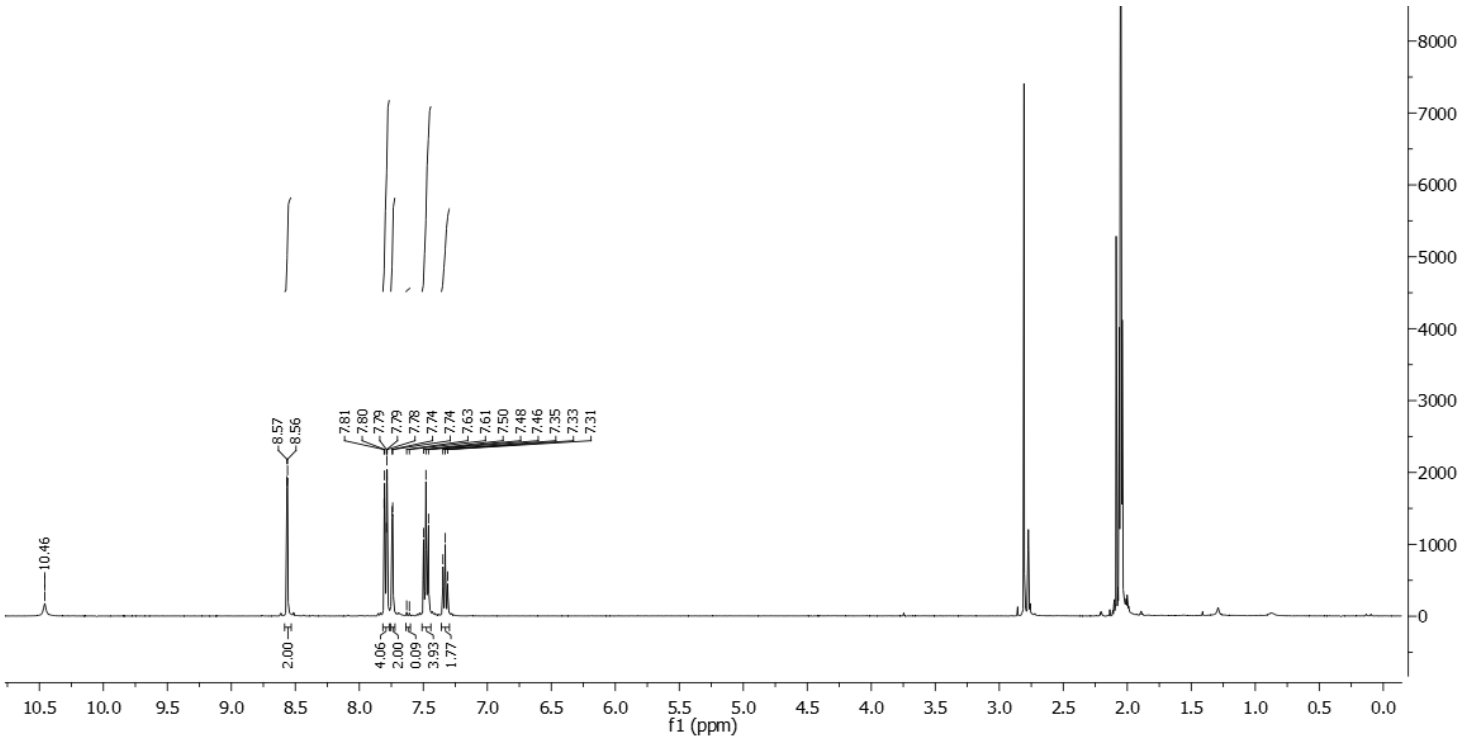

^{1}H-NMR spectrum of **22'**

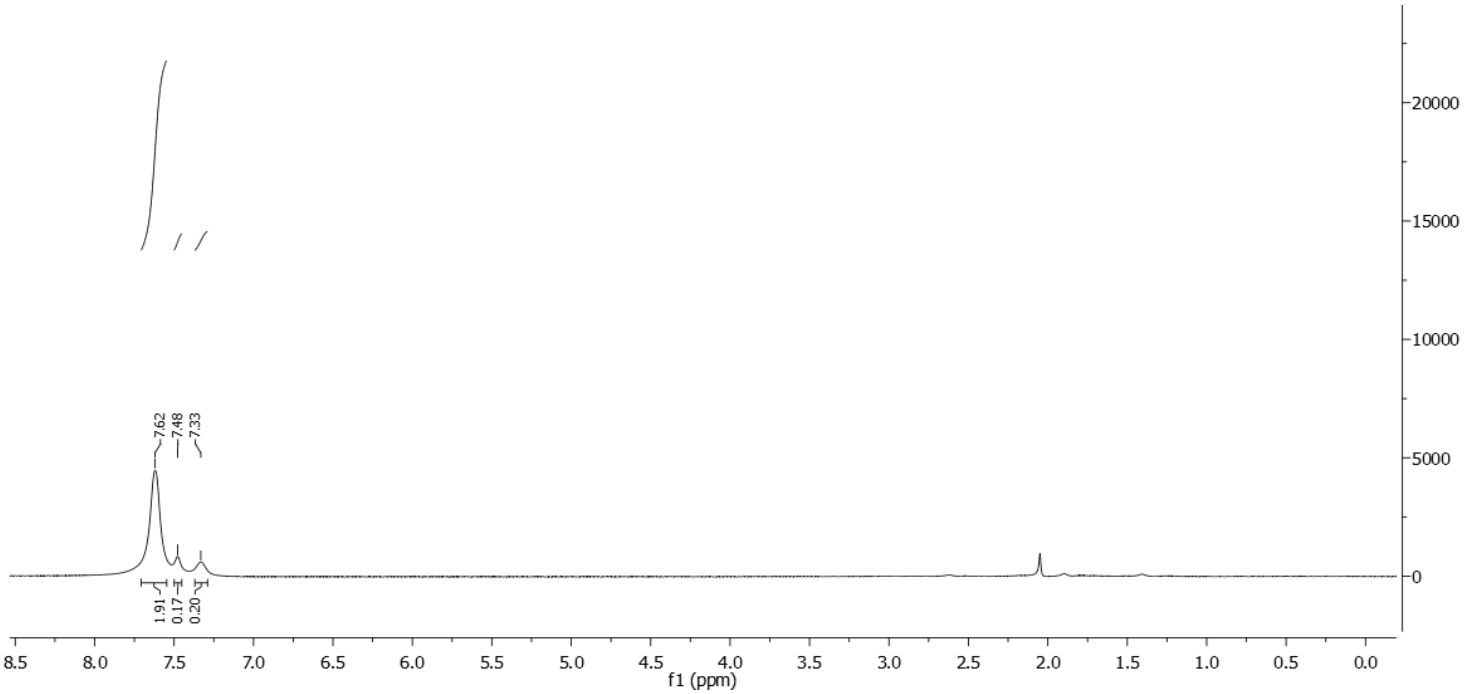

^{2}H-NMR spectrum of **22'**

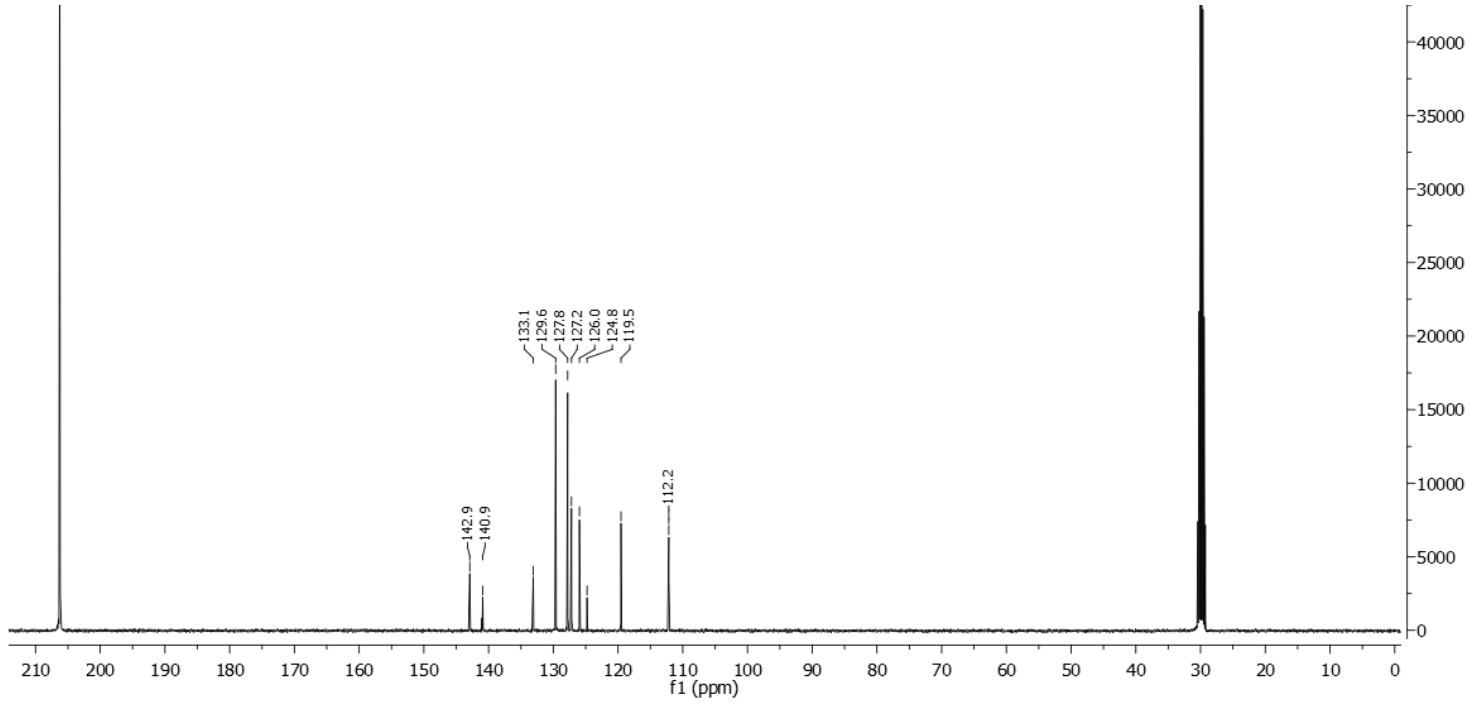

^{13}C-NMR spectrum of the non-deuterated starting material

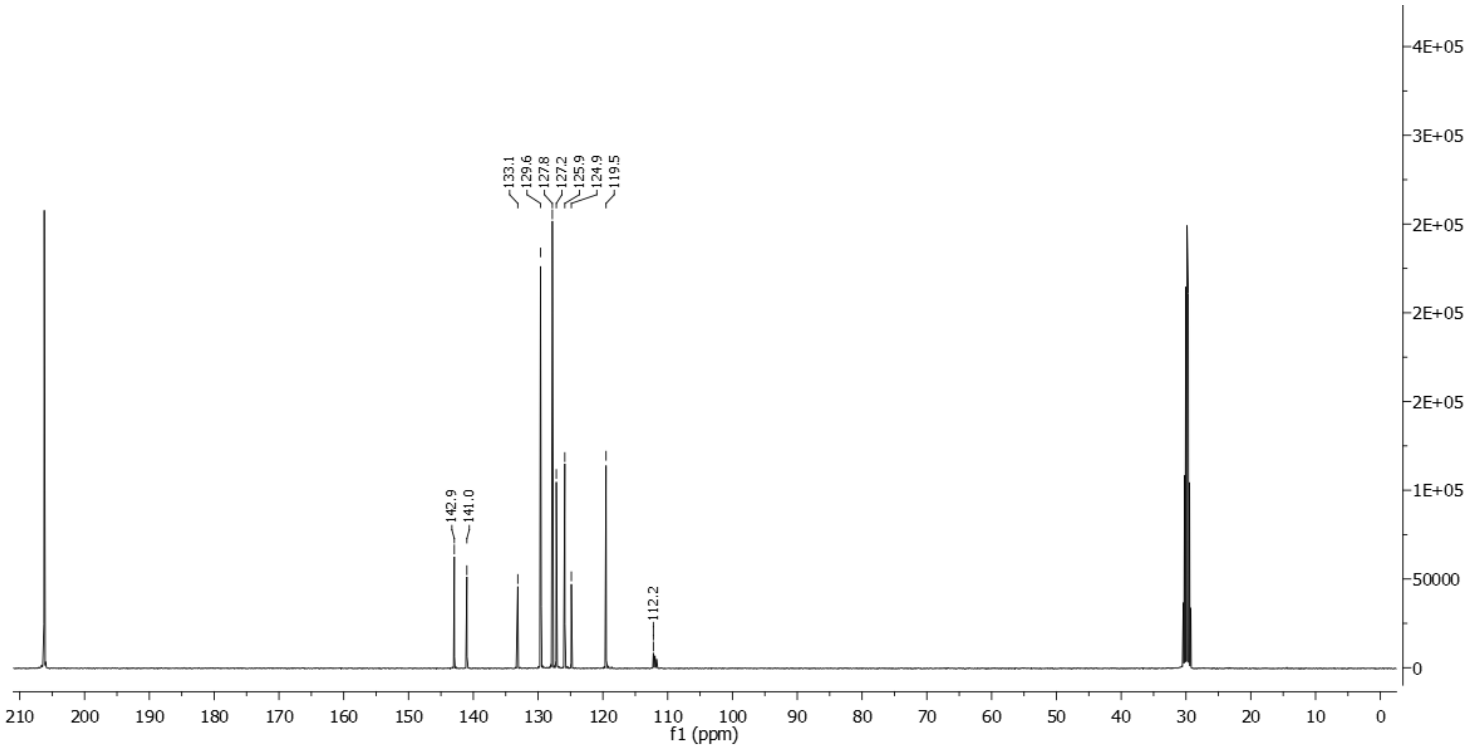

^{13}C-NMR spectrum of **22'**

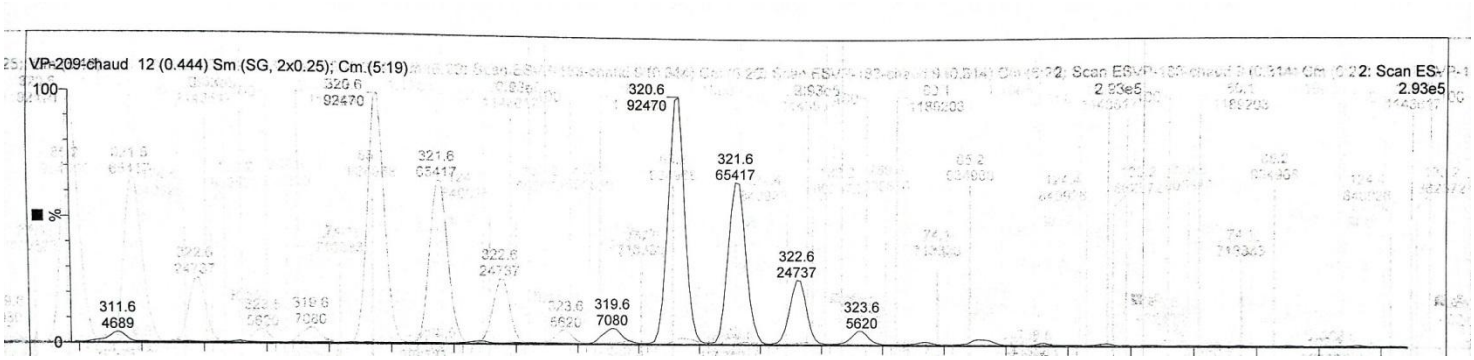

ESI-spectrum of **22'**

11,12-Dihydroindolo[2,3-a]carbazole **23'**

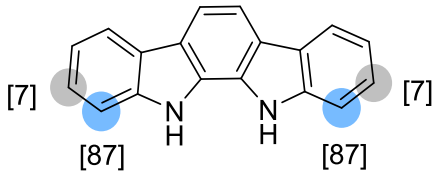

Chemical Formula: $C_{18}H_{12}N_2$

Substrate	Cs_2CO_3	Solvent (Volume)	RuNp@PVP cat.
25.6mg, 0.1mmol	65.2mg, 0.2mmol	THF (2mL)	7.22mg, 10mol%

Workup and purification:

After cooling down to room temperature the reaction mixture was poured on a 5mM solution of acetic acid in H_2O dist. (100mL). The aqueous phase was extracted three times with EtOAc (3 x 50mL) in a separation funnel. The solvent was removed under vacuum.

Yield: 26.0mg, 99%, white solid

^{1}H NMR (400 MHz, Acetone-d_6): δ 10.50 (bs, NH), 8.19 – 8.14 (m, 2H), 7.98 – 7.93 (m, 2H), 7.63 – 7.59 (m, 0.27H), 7.41 – 7.34 (m, 2H), 7.26 – 7.19 (m, 2H).

Deuterium incorporation was expected at δ 7.63 – 7.59. Isotopic enrichment values were determined against the integral at δ 8.19 – 8.14.

^{2}H-{^{1}H}NMR (92 MHz, Acetone): δ 7.62 (m, 1.74D), 7.39 (m, 0.15D).

^{13}C-{^{1}H}NMR (100 MHz, Acetone-d_6): δ 140.3, 126.8, 125.5, 125.3, 121.9, 120.5, 120.0, 112.6, 112.1 (m).

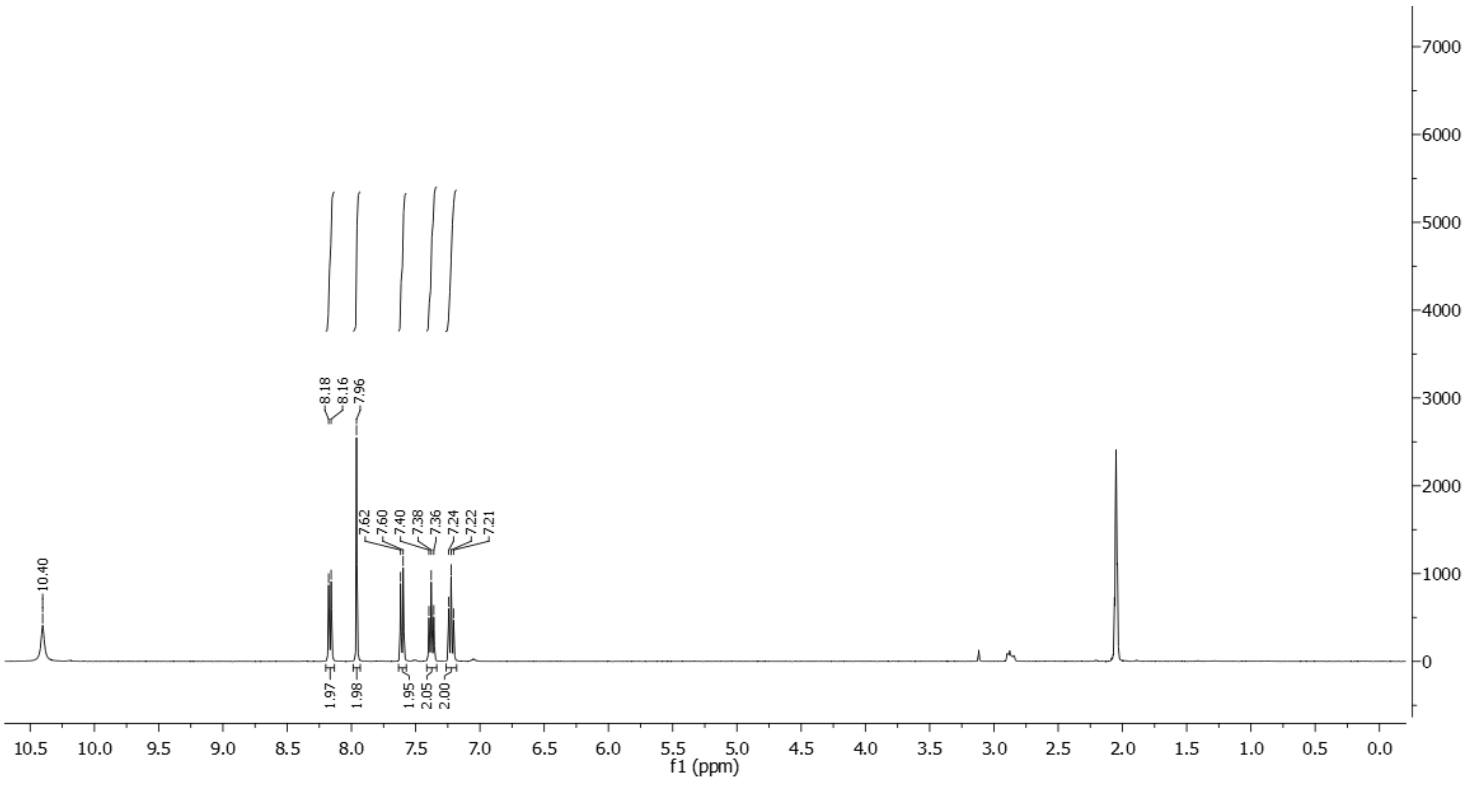

^{1}H-NMR spectrum of the non-deuterated starting material

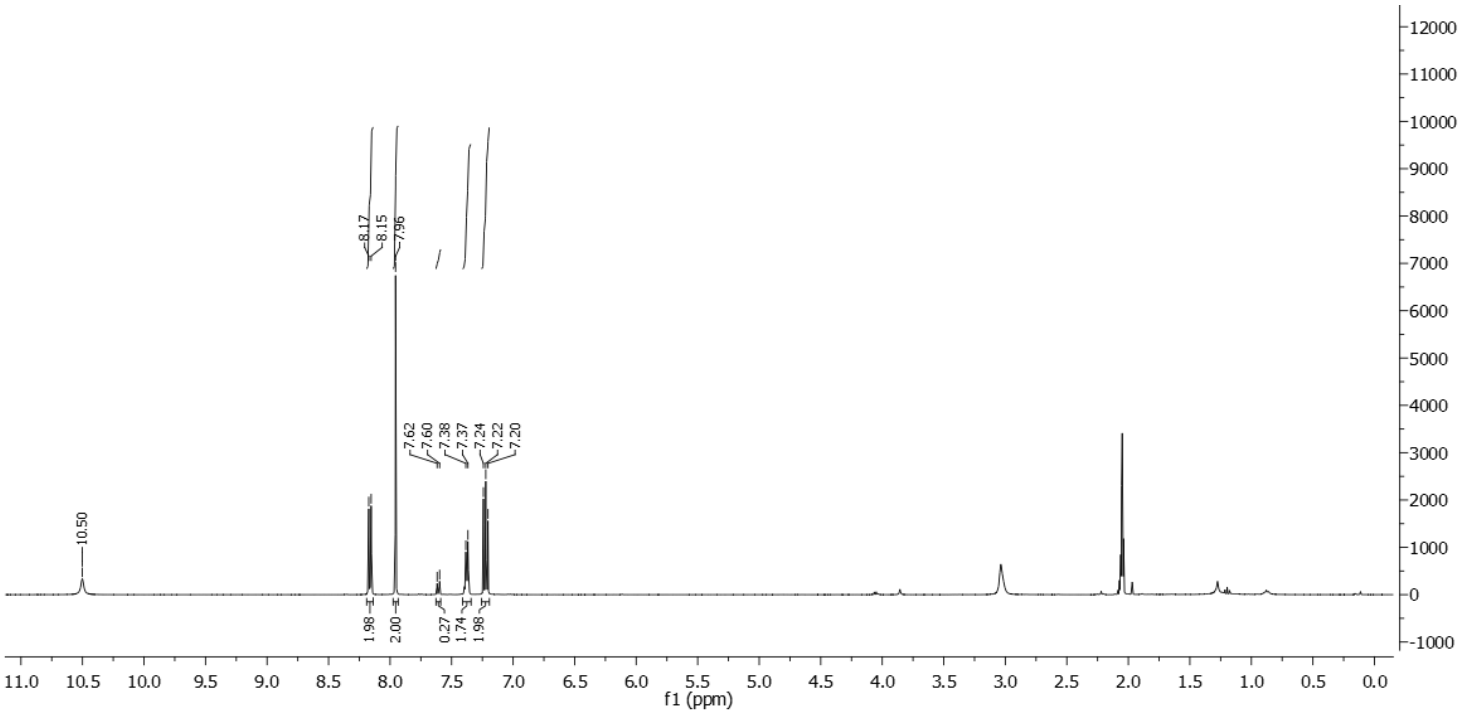

^{1}H-NMR spectrum of **23'**

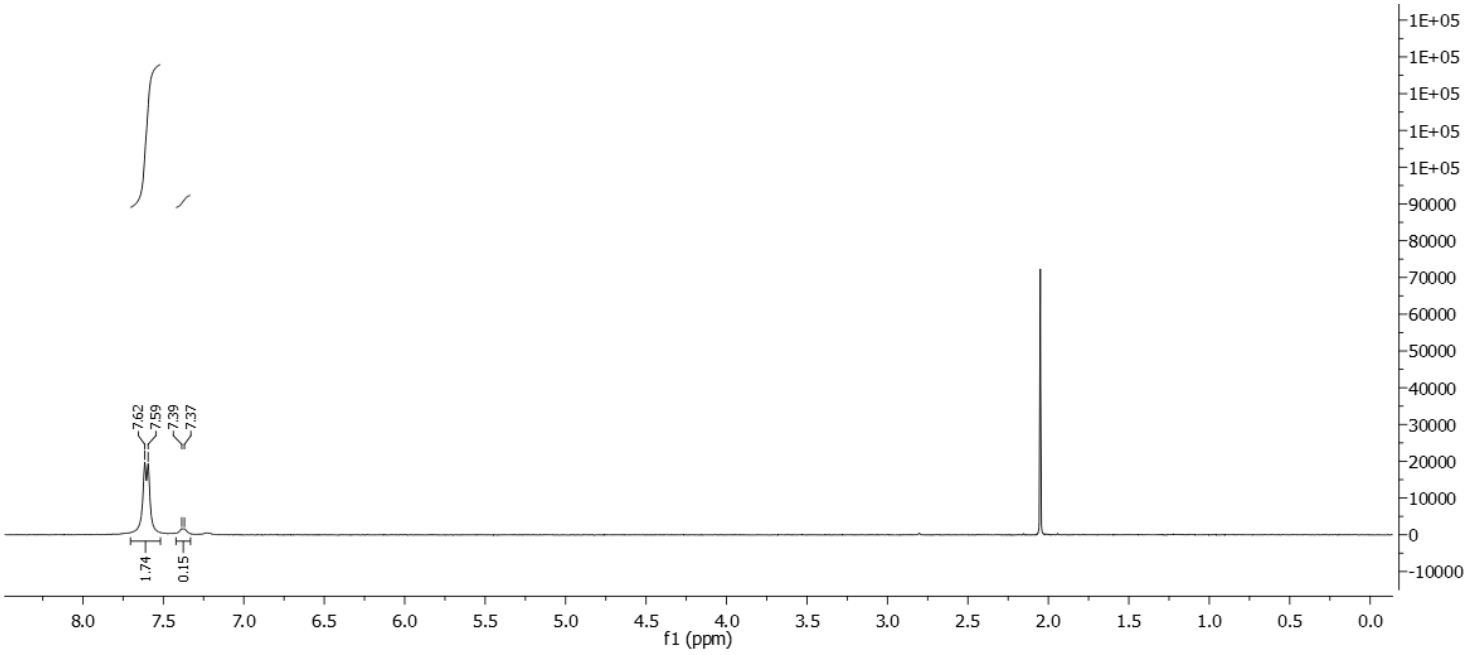

^{2}H-NMR spectrum of **23'**

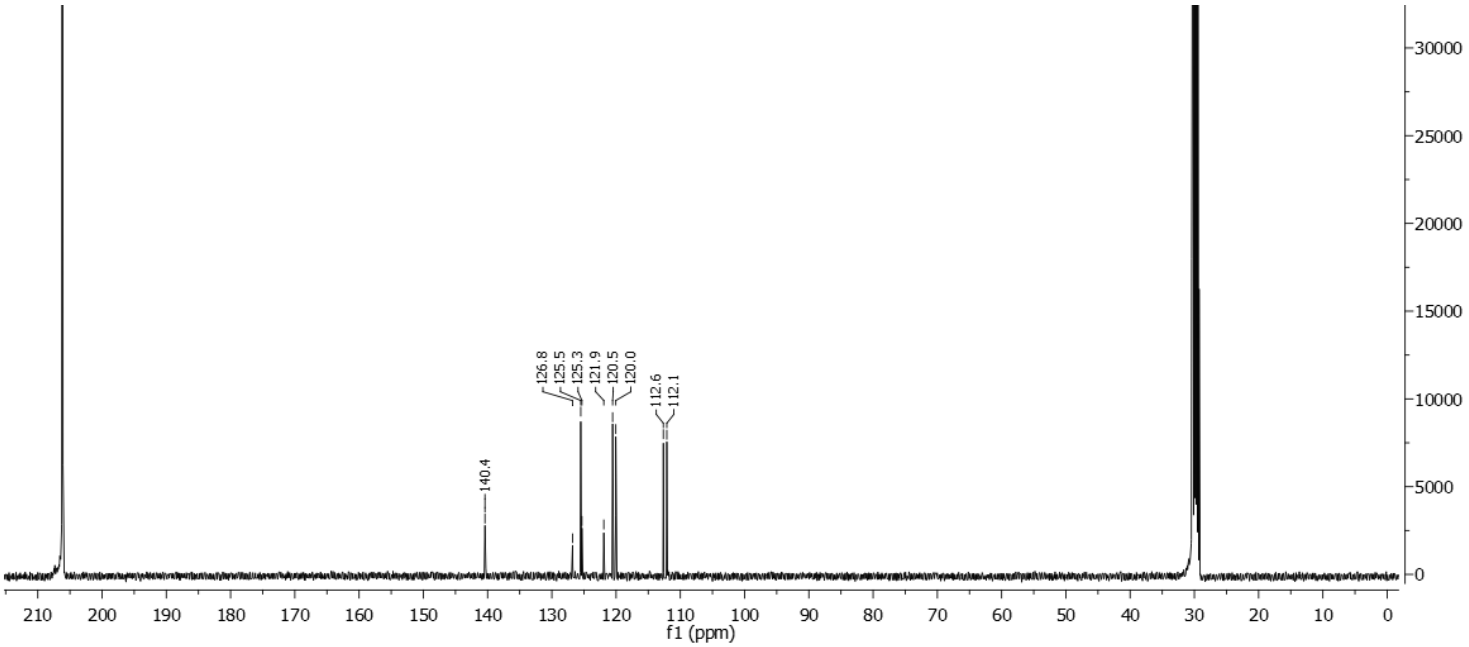

^{13}C-NMR spectrum of the non-deuterated starting material

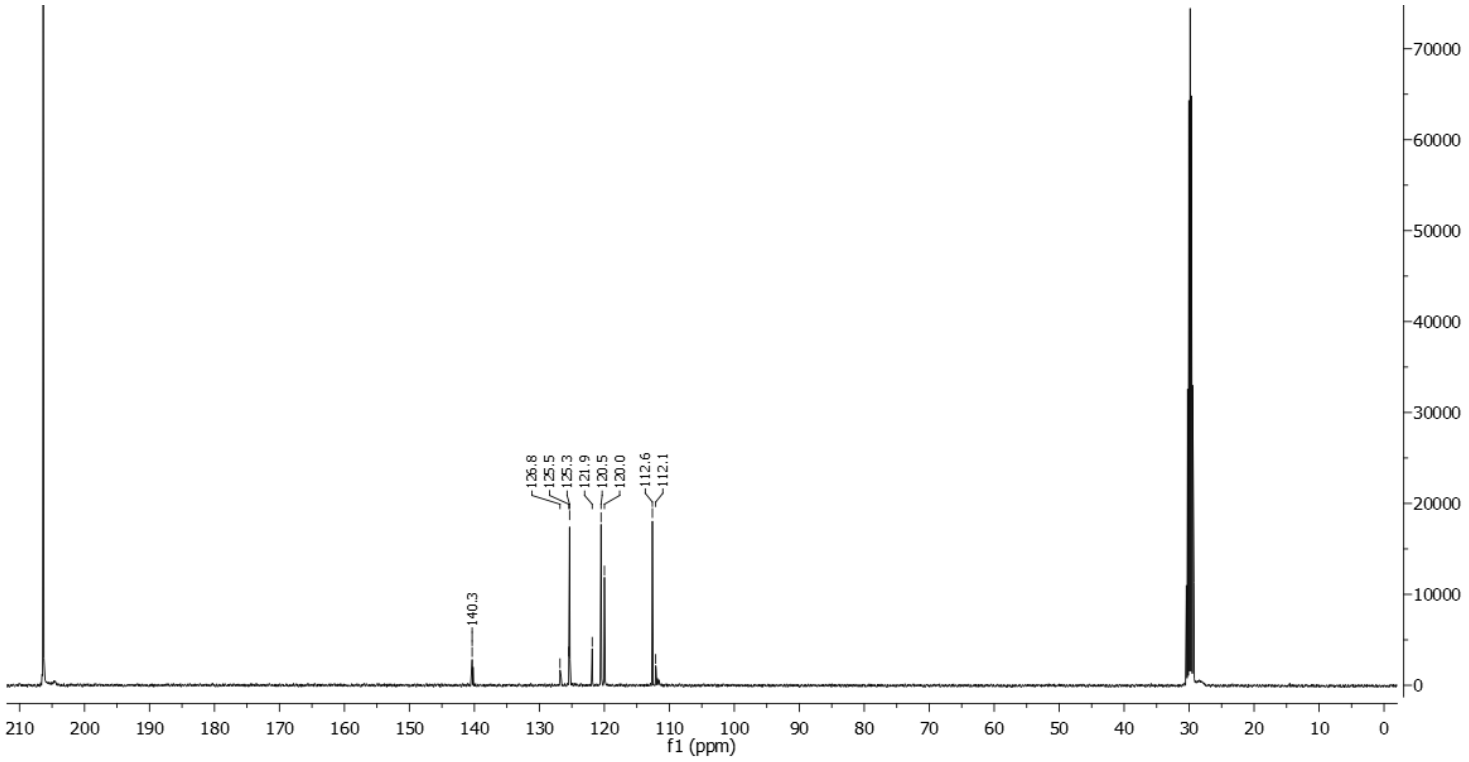

^{13}C-NMR spectrum of **23'**

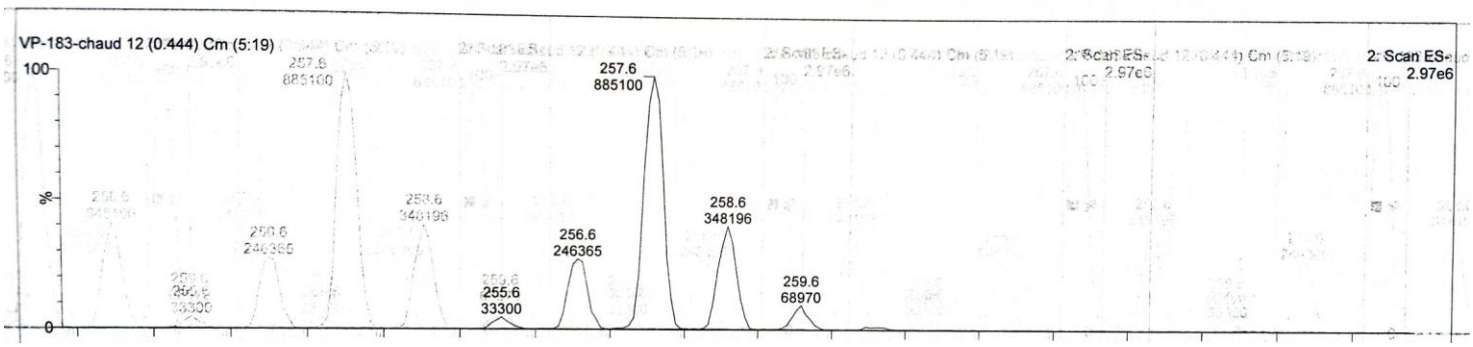

ESI-spectrum of **23'**

Deuterations of N-heterocyclic bioactive molecules

Pimprinine **25I** *(without base)*

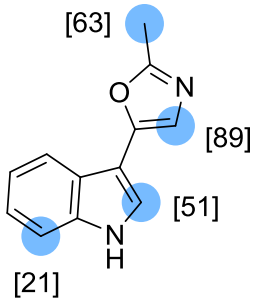

Chemical Formula: $C_{12}H_{10}N_2O$

Substrate	Solvent (Volume)	RuNp@PVP cat.
20.0mg, 0.1mmol	Methanol-d_4 (2mL)	28.9mg, 20mol%

Workup and purification:

After cooling down to room temperature the reaction mixture was poured on H_2O dist. (100mL) in a separation funnel. The aqueous phase was extracted three times with EtOAc (100mL). The solvent was removed under vacuum at room temperature and the crude product was recrystallized from acetone and MeOH (acetone : MeOH, 3:1).

Yield: 4.0mg, 20%, white solid

^{1}H NMR (400 MHz, Methanol-d_4): δ 7.81 – 7.75 (m, 1H), 7.60 (s, 0.38H), 7.46 – 7.41 (m, 0.71H), 7.23 – 7.12 (m, 2.21H), 2.53 – 2.48 (m, 1.08H).

Deuterium incorporation was expected at δ 7.60, δ 7.46 – 7.41, δ 7.23 – 7.12 and at δ 2.53 – 2.48. Isotopic enrichment values were determined against the integral at δ 7.81 – 7.75.

^{2}H-{^{1}H}NMR (92 MHz, Methanol): δ 7.58 (s, 0.51D), 7.42 (s, 0.21D), 7.13 (s, 0.89D), 2.49 – 2.41 (m, 1.89D).

^{13}C-{^{1}H}NMR (100 MHz, Methanol-*d_4*): δ 160.8, 150.0, 138.2, 125.3, 123.6, 123.4 (m), 121.3, 120.4, 119.2 (m), 112.8, 105.5 (m), 13.5 (m).

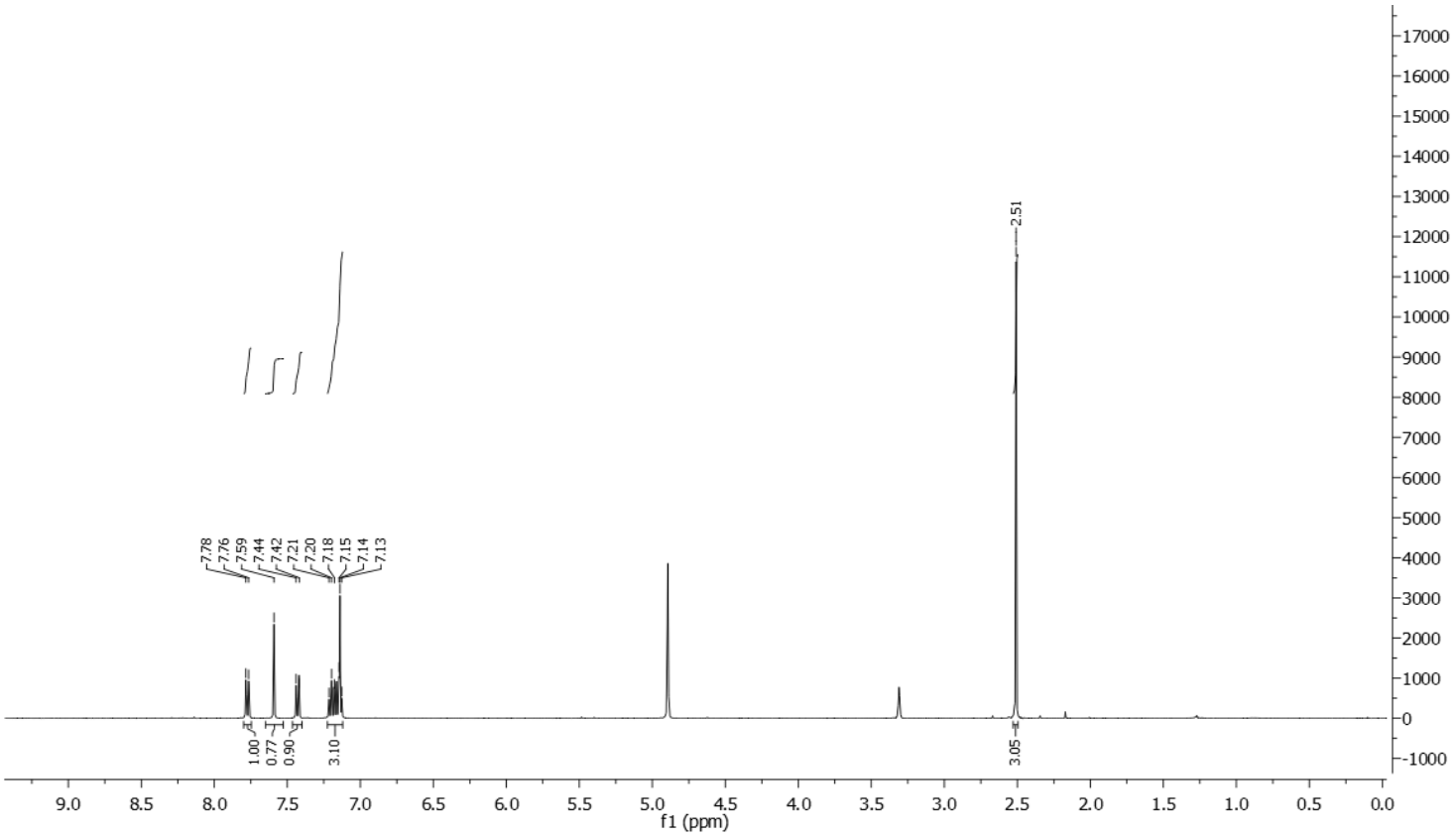

^{1}H-NMR spectrum of the non-deuterated starting material

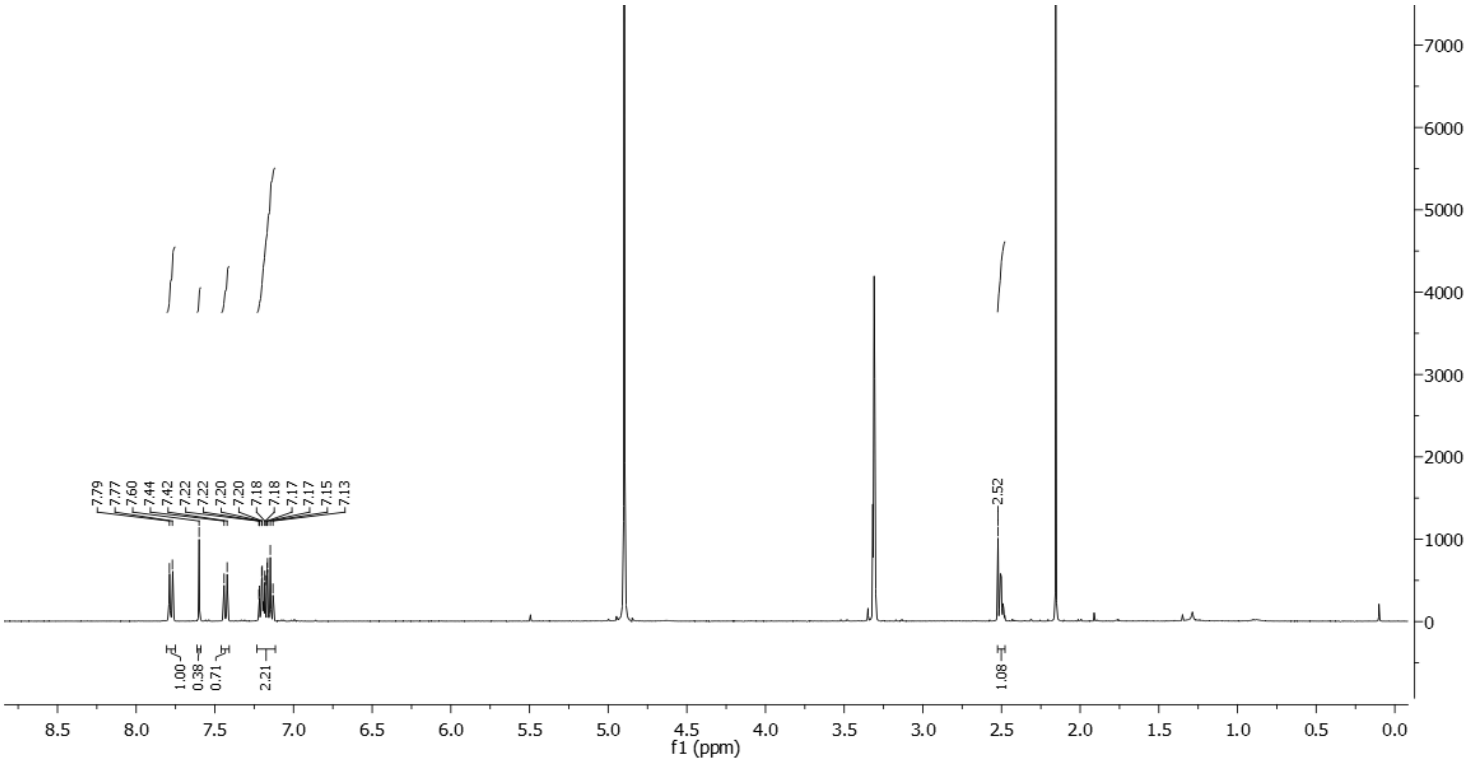

^{1}H-NMR spectrum of **25I**

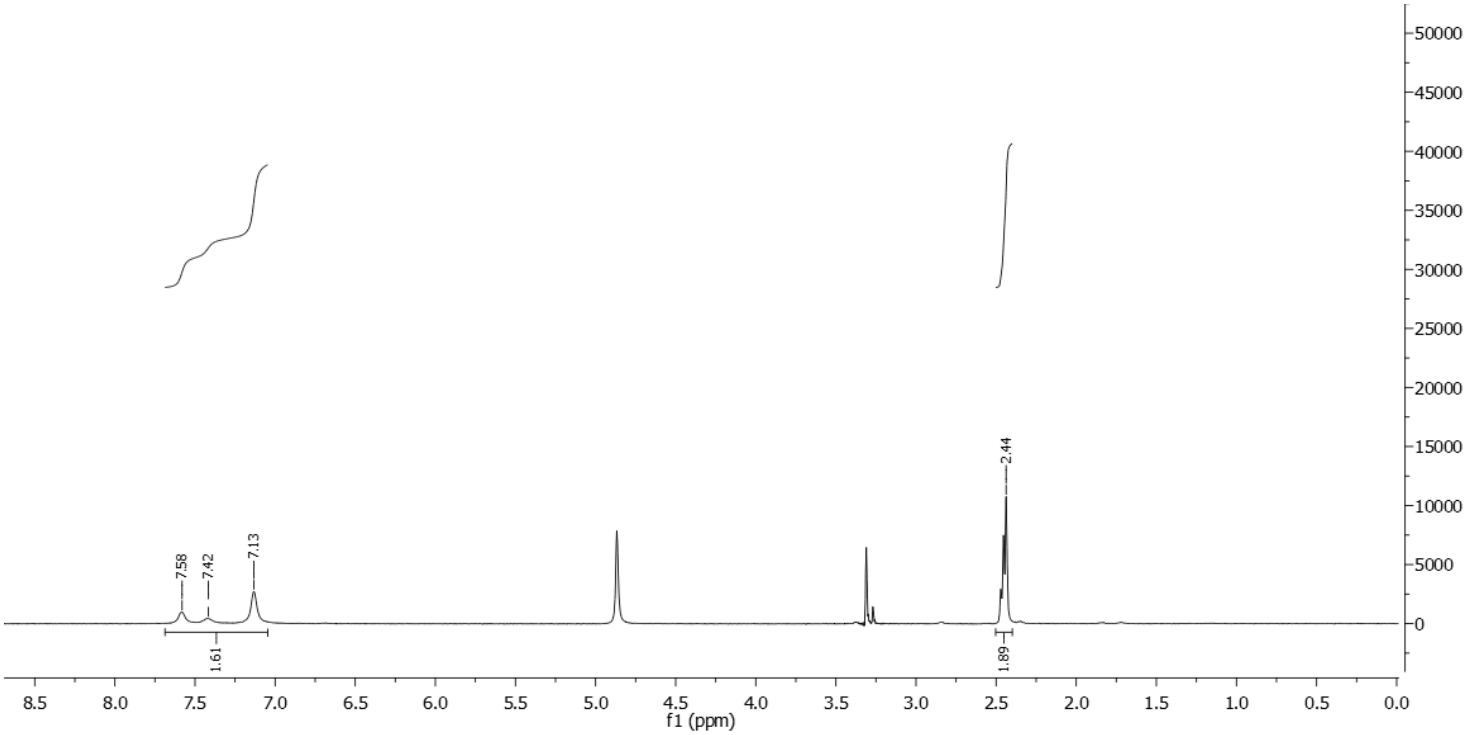

^{2}H-NMR spectrum of **25I**

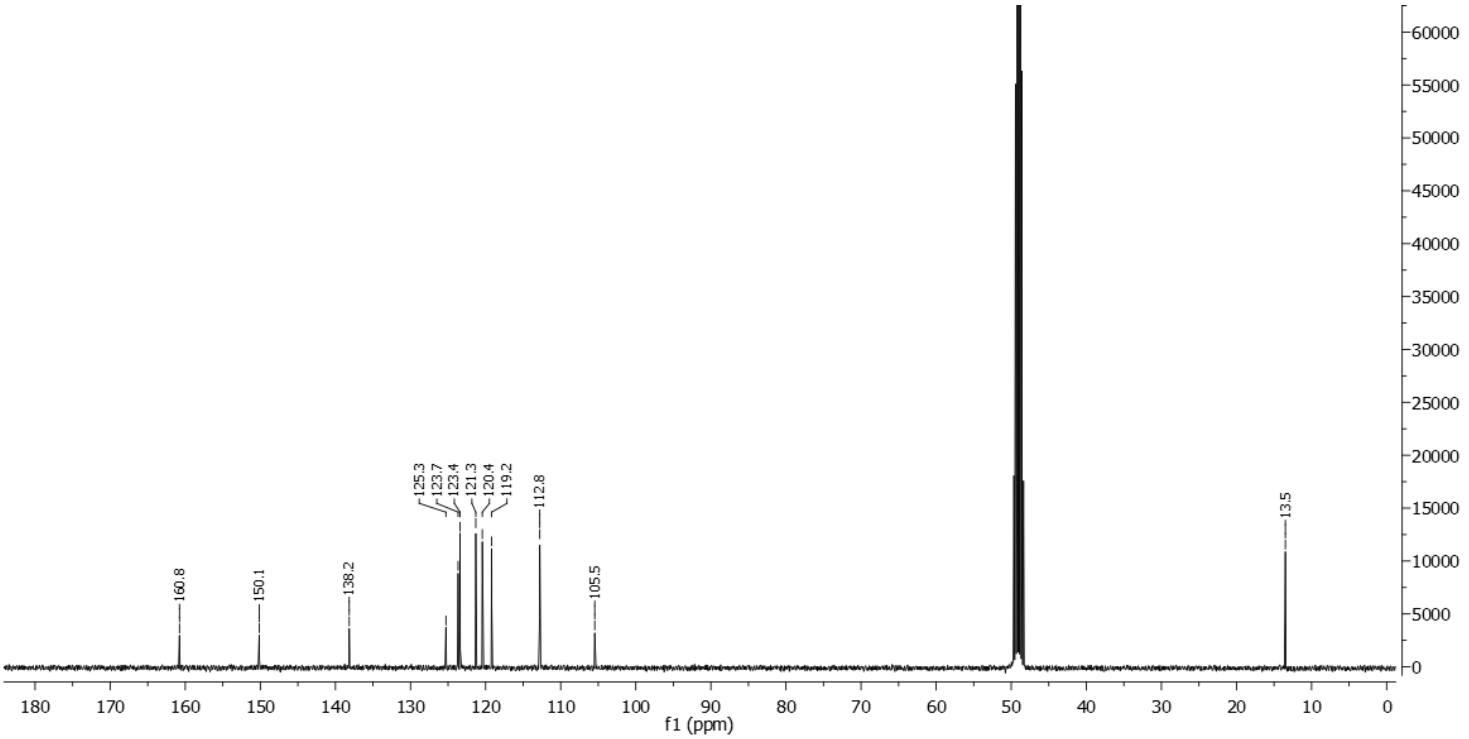

^{13}C-NMR spectrum of the non-deuterated starting material

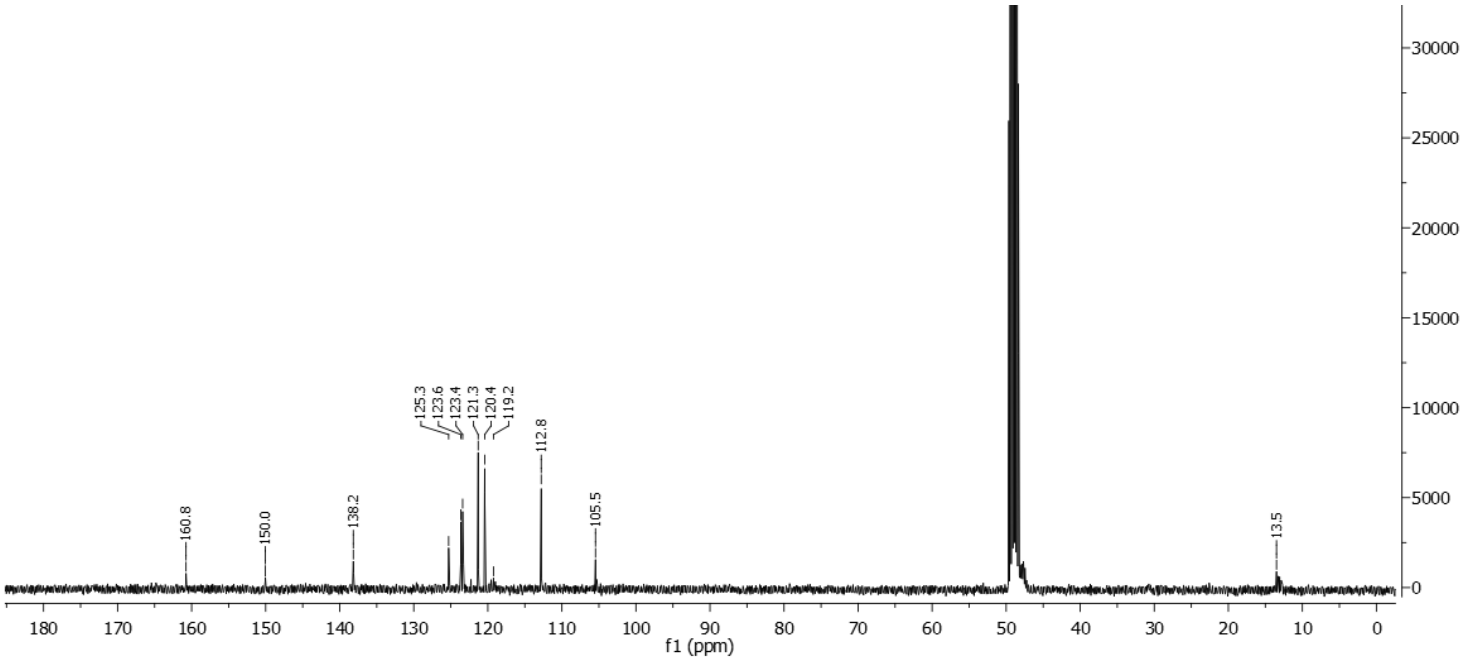

^{13}C-NMR spectrum of **25I**

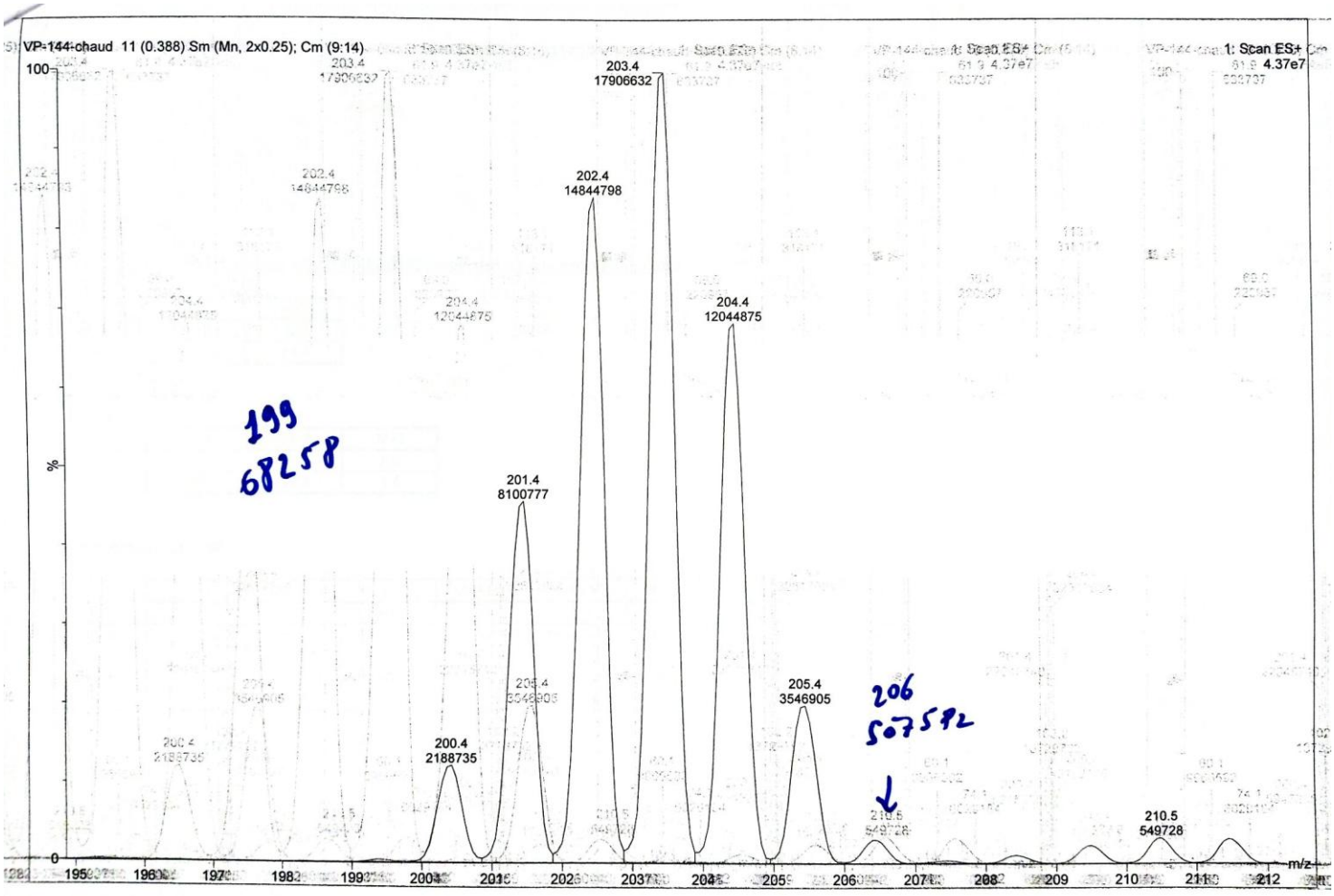

ESI-spectrum of **25I**

Pimprinine **25II** (with base)

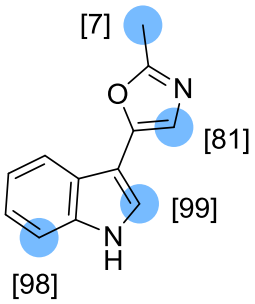

Chemical Formula: $C_{12}H_{10}N_2O$

Substrate	Cs_2CO_3	Solvent (Volume)	RuNp@PVP cat.
20.0mg, 0.1mmol	32.6mg, 0.1mmol	Methanol-d_4 (2mL)	28.9mg, 20mol%

Workup and purification:

After cooling down to room temperature the reaction mixture was poured on a 5mM solution of acetic acid in H_2O dist. (150mL). The aqueous phase was extracted three times with EtOAc (3 x 50mL) in a separation funnel. The solvent was removed under vacuum and the crude product was purified over SiO_2. Deuterium labelled pimprinine could be eluted at cyclohexane/EtOAc (1:4).

Yield: 3.0mg, 15%, white solid

^{1}H NMR (400 MHz, Methanol-*d_4*): δ 7.79 – 7.75 (m, 1H), 7.59 (s, 0.01H), 7.45 – 7.41 (m, 0.02H), 7.23 – 7.11 (m, 2.19H), 2.53 – 2.49 (m, 2.80H).

Deuterium incorporation was expected at *δ* 7.59, *δ* 7.45 – 7.41, *δ* 7.23 – 7.11 and at *δ* 2.53 – 2.49. Isotopic enrichment values were determined against the integral at *δ* 7.79 – 7.75.

^{2}H-{^{1}H}NMR (92 MHz, Methanol): δ 7.58 (s, 1D), 7.43 (s, 1D), 7.13 (s, 0.81D), 2.49 – 2.41 (m, 0.28D).

^{13}C-{^{1}H}NMR (100 MHz, Methanol-*d_4*): δ 160.8, 150.0, 138.1, 125.3, 123.5(m), 123.3, 121.3, 120.4, 119.0 (m), 112.8, 105.3 (m), 13.5 (m).

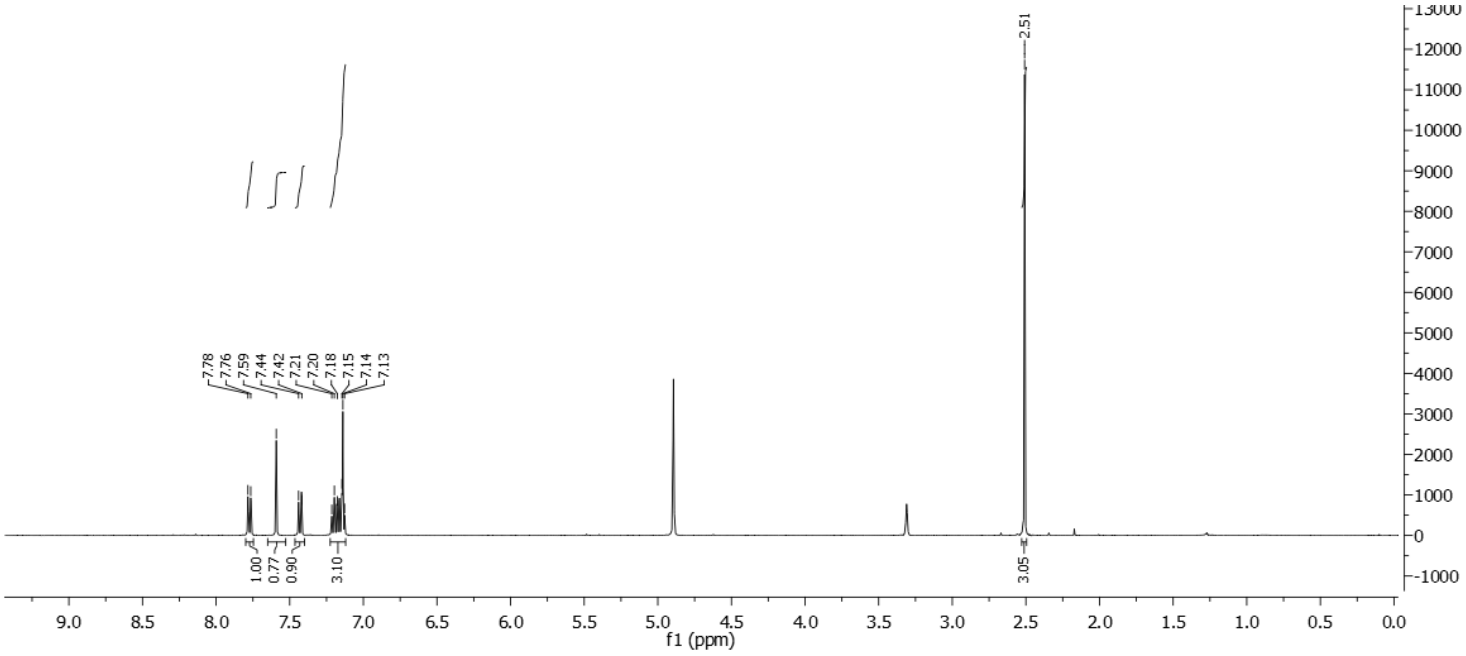

^{1}H-NMR spectrum of the non-deuterated starting material

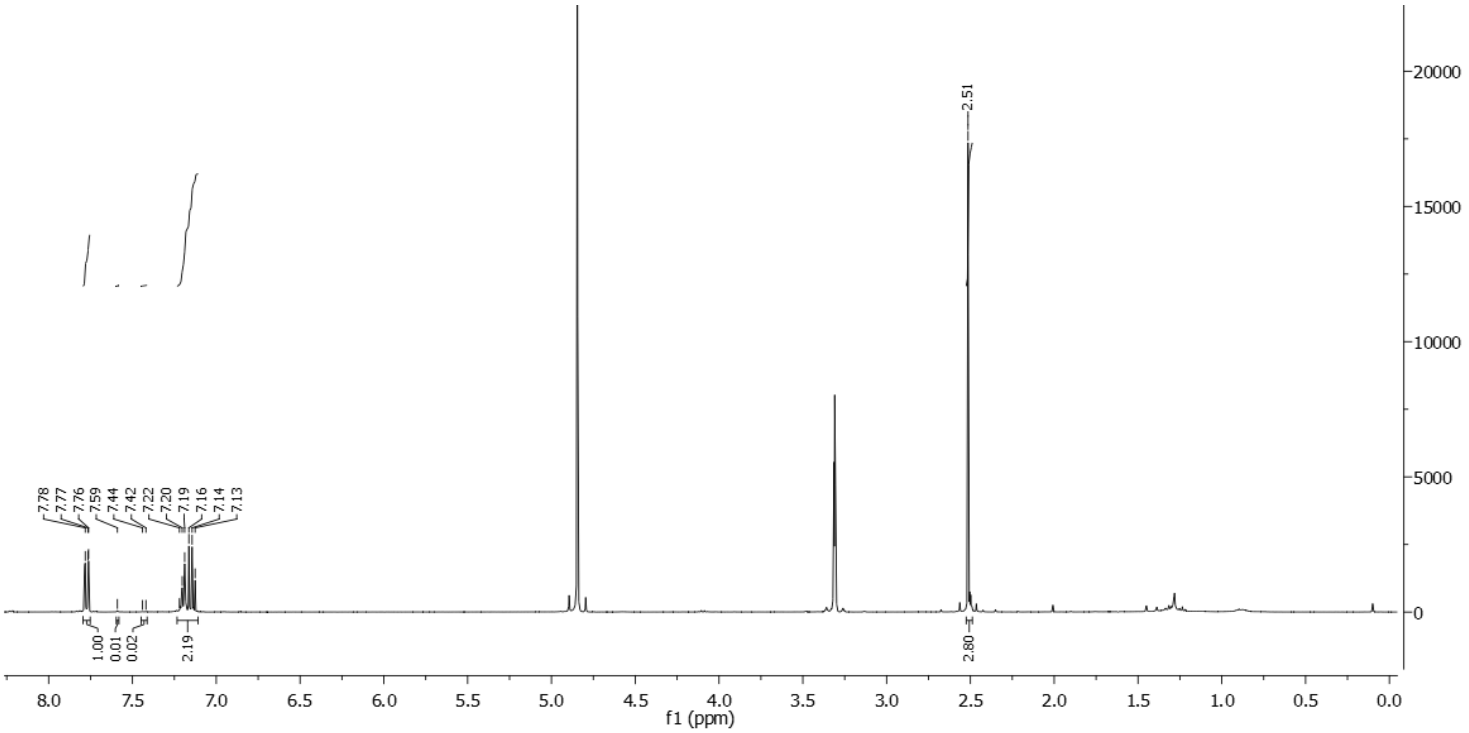

^{1}H-NMR spectrum of **25II**

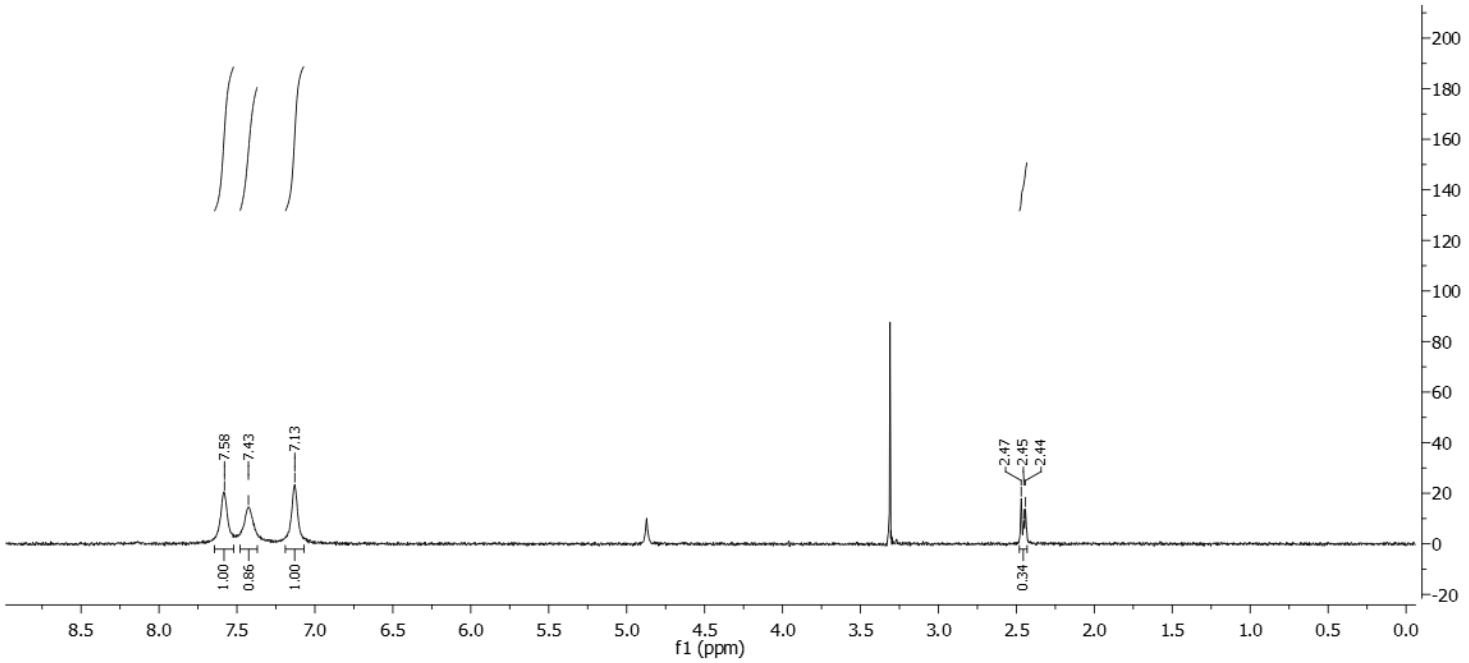

^{2}H-NMR spectrum of **25II**

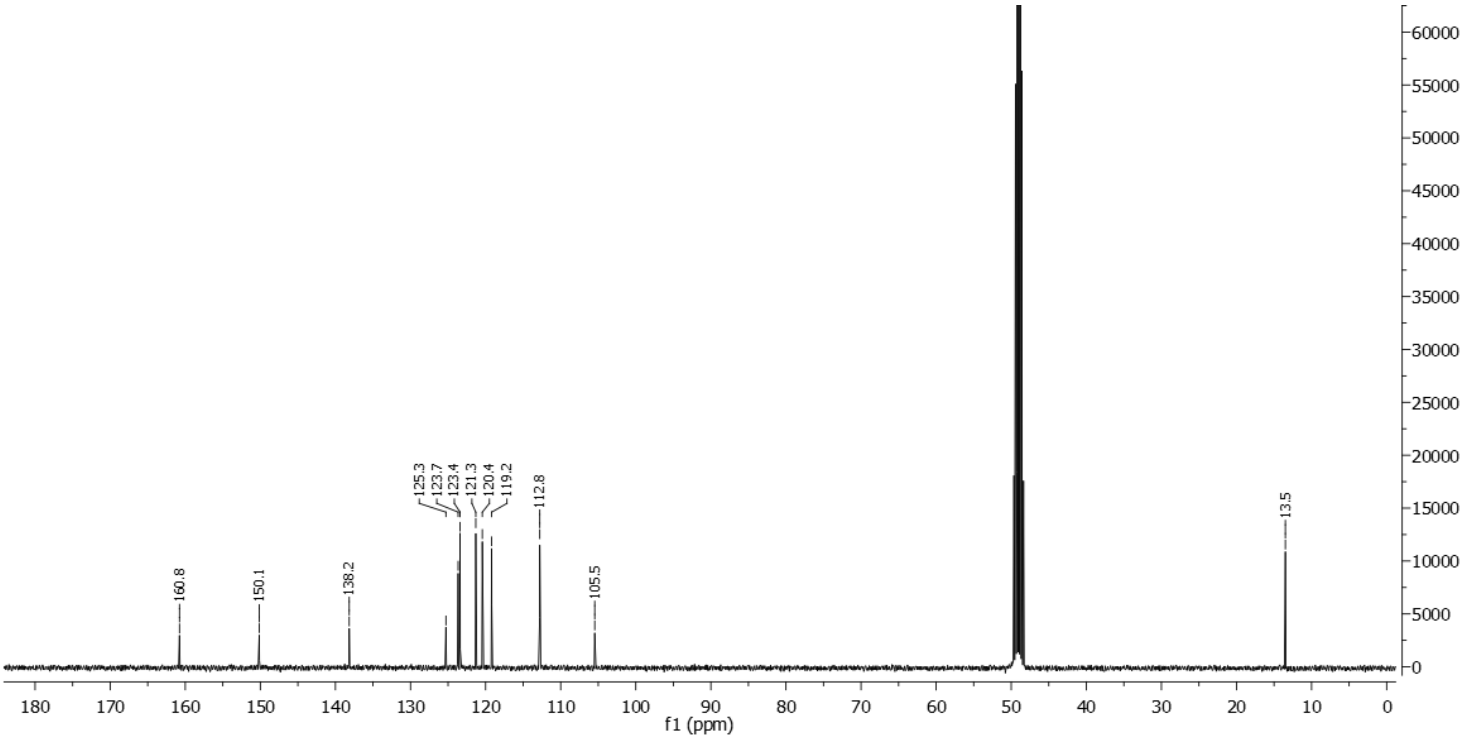

^{13}C-NMR spectrum of the non-deuterated starting material

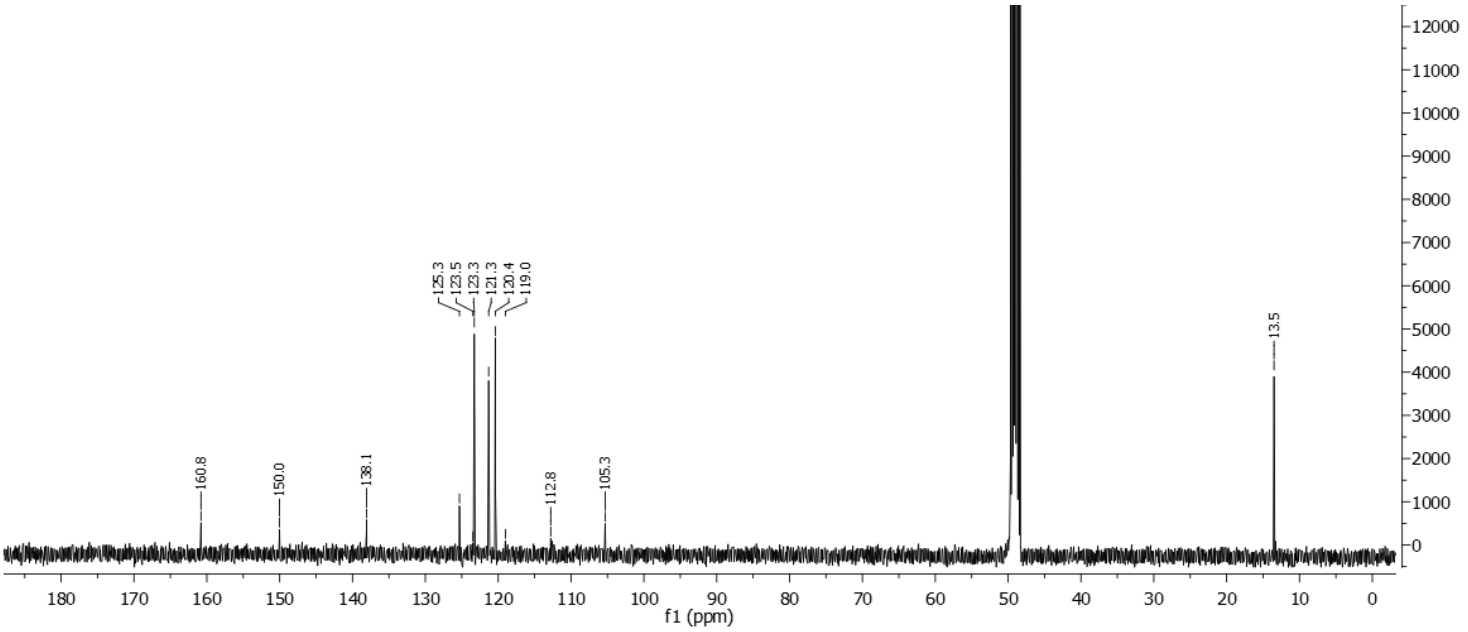

^{13}C-NMR spectrum of **25II**

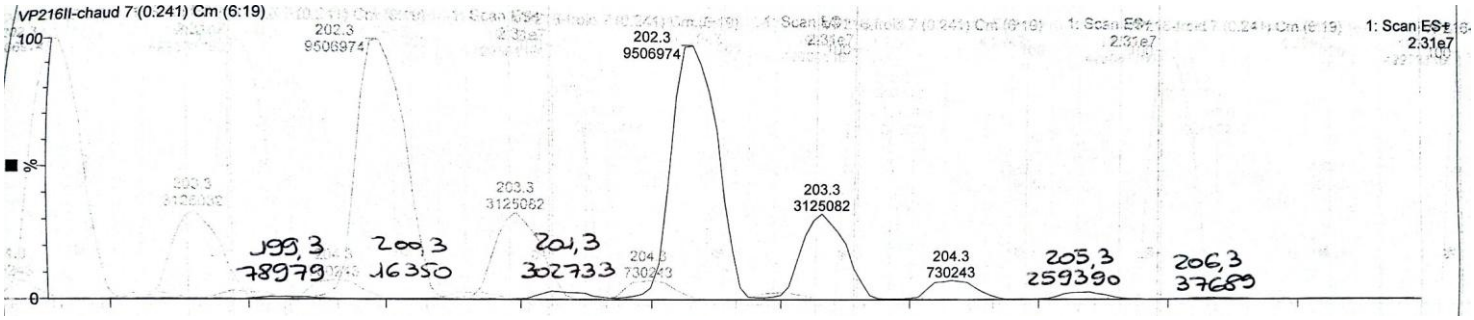

ESI-spectrum of **25II**

Carvedilol **26I**

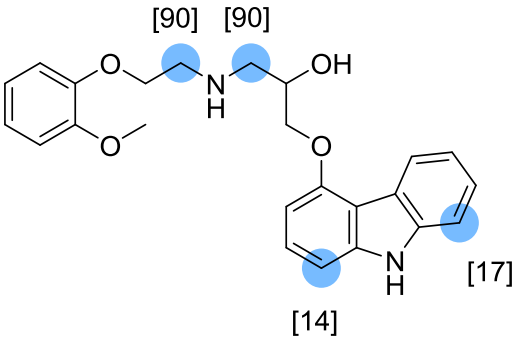

Chemical Formula: $C_{24}H_{26}N_2O_4$

Substrate	Solvent (Volume)	RuNp@PVP cat.
10.0mg, 25µmol	THF (1mL)	7.2mg, 20mol%

Workup and purification:

After cooling down to room temperature, EtOAc/cyclohexane (1:1, 3mL) was added to the reaction mixture and stirred for 10min to let precipitate RuNp@PVP. The suspension was passed through a Sep-Pak® C18 cartridge and then eluted with EtOAc (5mL). The solvent was removed under vacuum.

Yield: 10.0mg, 99%, white solid

^{1}H NMR (400 MHz, $CDCl_3$): δ 8.29 – 8.23 (m, 1H), 8.18 (bs, NH), 7.44 – 7.28 (m, 3H), 7.24 – 7.16 (m, 1H), 7.09 – 7.01 (m, 0.88H), 6.99 – 6.81 (m, 4H), 6.72 – 6.62 (m, 1H), 4.34 – 4.09 (m, 5H), 3.83 (s, 3H), 3.41 – 3.31 (m, 0.43H).

Deuterium incorporation was expected at δ 9.05 and at δ 7.97 – 7.88. Isotopic enrichment values were determined against the integral at δ 8.29 – 8.23.

^{2}H-{^{1}H}NMR (92 MHz, $CHCl_3$): δ 7.45 (s, 0.17D), 7.09 (s, 0.14D), 3.25 – 2.75 (m, 3.6D).

^{13}C-{^{1}H}NMR (100 MHz, $CDCl_3$): δ 155.3, 149.8, 148.4, 141.1, 138.9, 126.8, 125.1, 123.1, 122.7, 121.8, 121.1, 119.8, 114.2, 112.9, 112.0, 110.1, 104.0, 101.4, 70.4, 68.8, 68.5, 55.9, 52.1 (m), 48.8 (m).

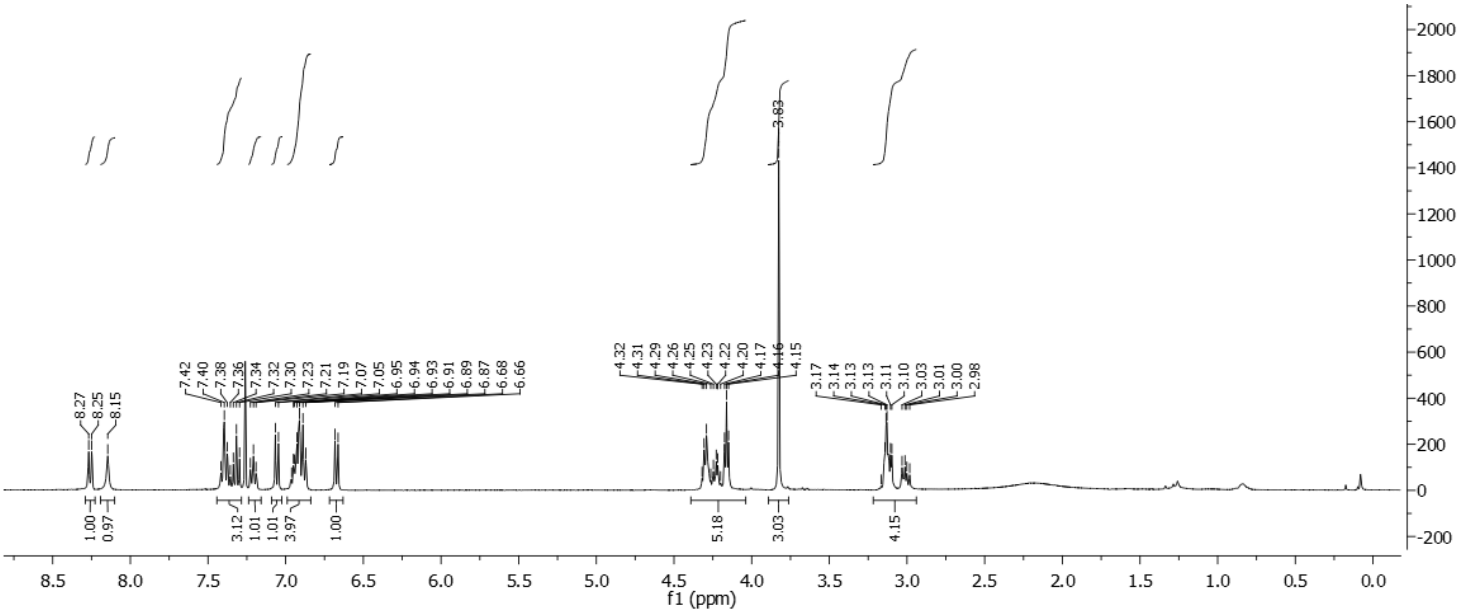

^{1}H-NMR spectrum of the non-deuterated starting material

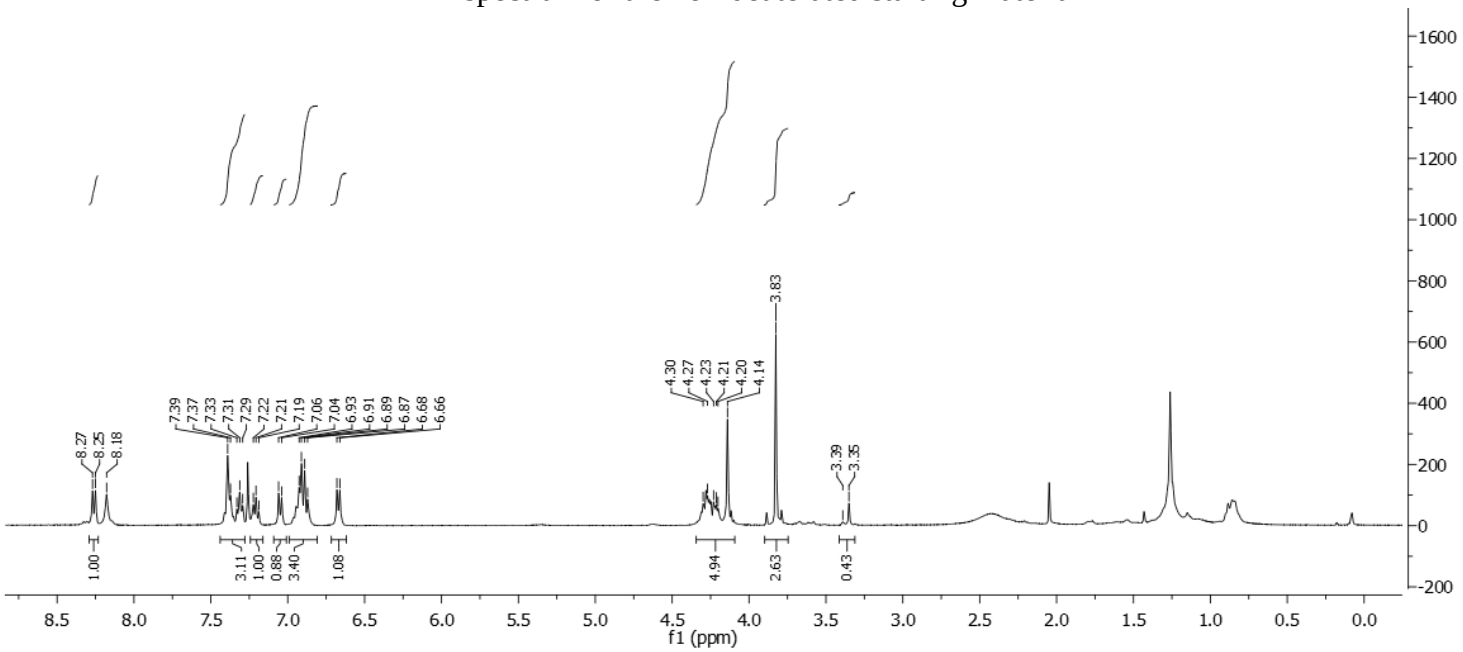

^{1}H-NMR spectrum of **26I**

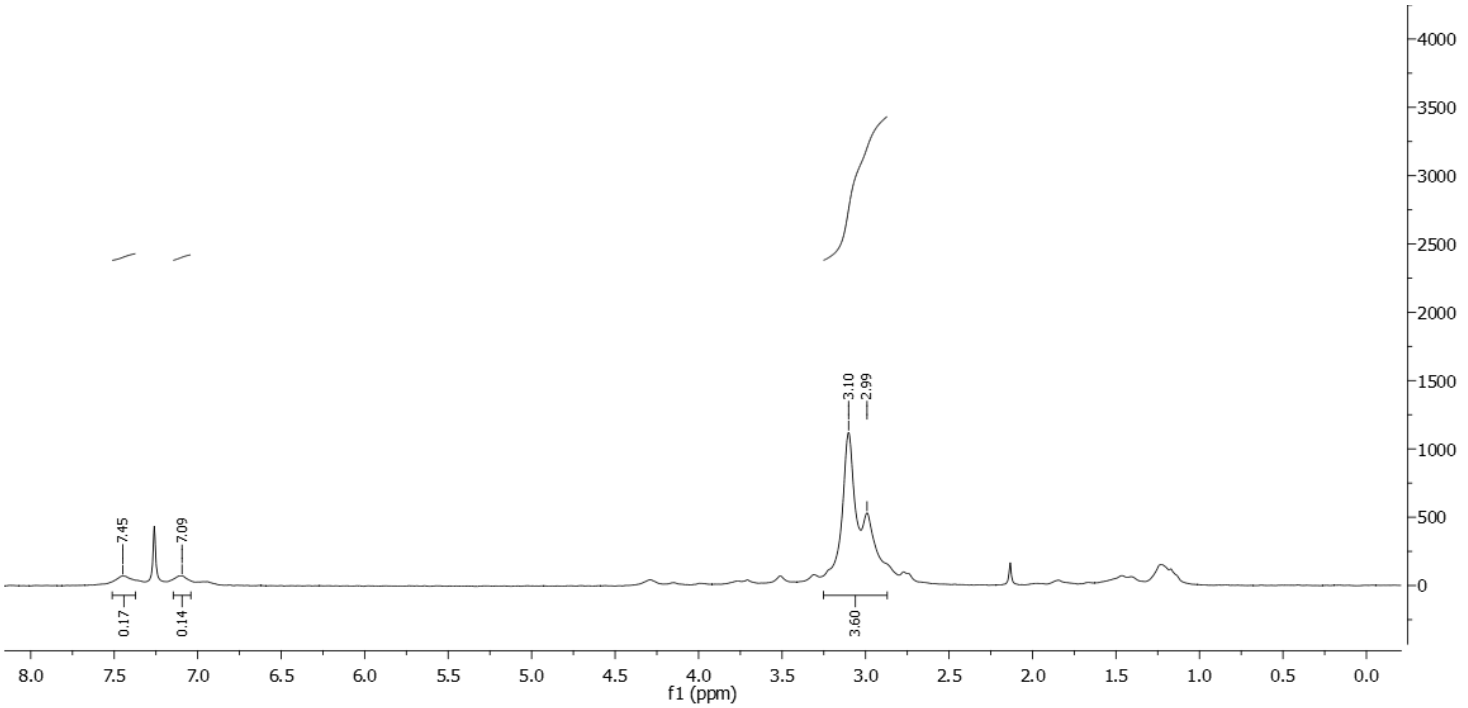

^{2}H-NMR spectrum of **26I**

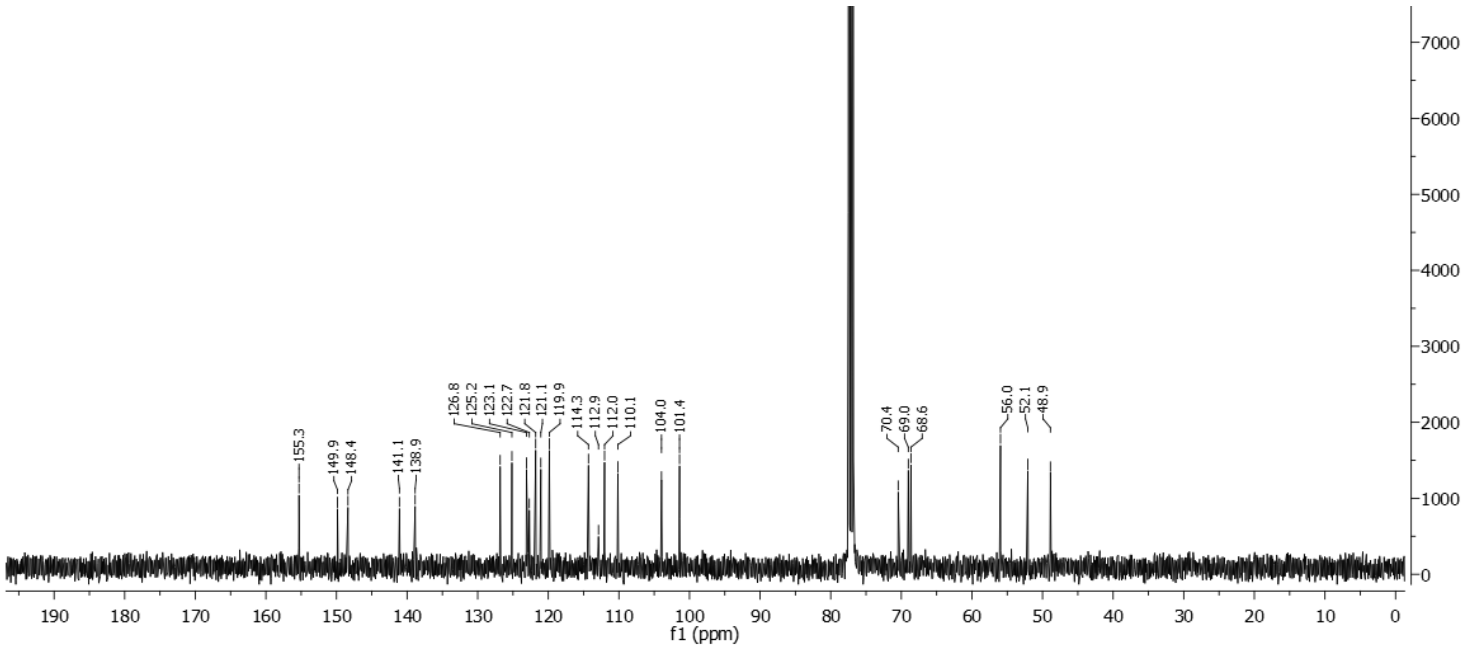

^{13}C-NMR spectrum of the non-deuterated starting material

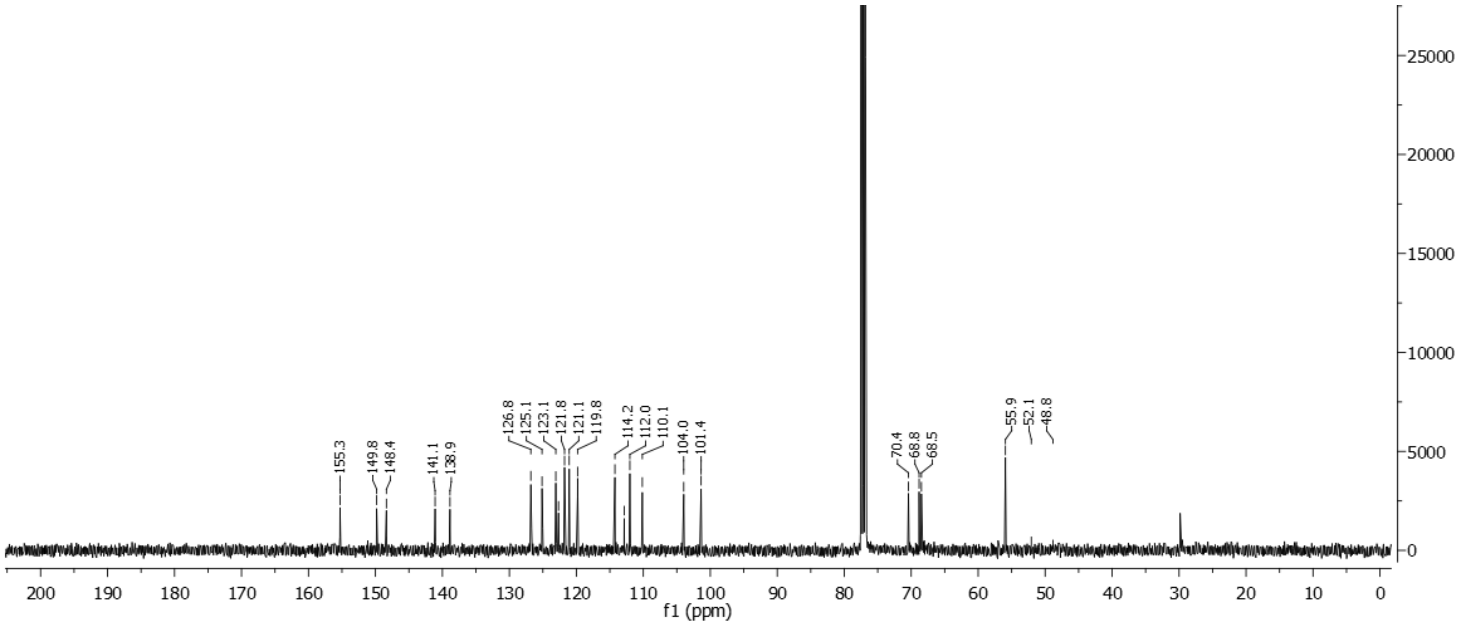

^{13}C-NMR spectrum of **26I**

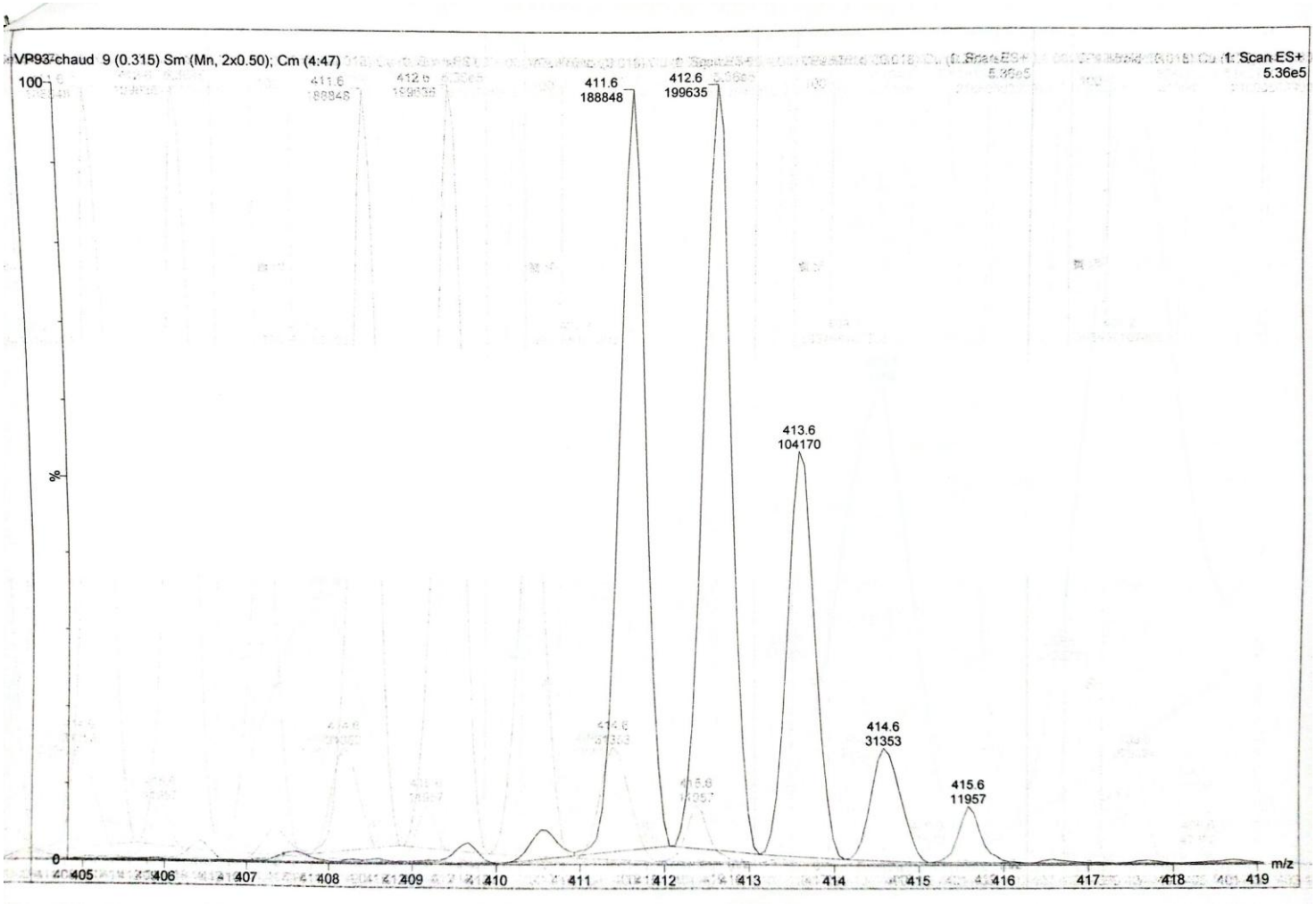

ESI spectrum of **26I**

N-Boc-carvedilol **26II**

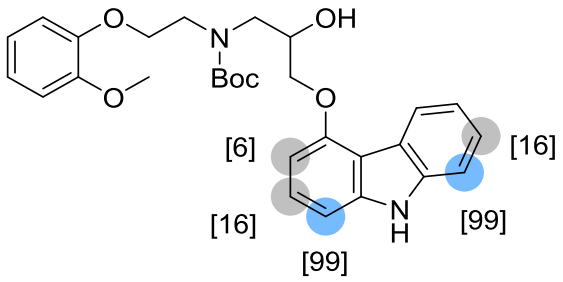

Chemical Formula: $C_{29}H_{34}N_2O_6$

Substrate	Cs_2CO_3	Solvent (Volume)	RuNp@PVP cat.
50.0mg, 0.1mmol	32.5mg, 0.1mmol	THF (1mL)	14.44mg, 10mol%

Workup and purification:

After cooling down to room temperature the reaction mixture was poured on a 5mM solution of acetic acid in H_2O dist. (100mL). The aqueous phase was extracted three times with EtOAc (3 x 50mL) in a separation funnel. The solvent was removed under vacuum and the crude product was purified over SiO_2. Deuterium labelled *N*-Boc-carvedilol could be eluted at cyclohexane/EtOAc (3:1).

Yield: 43.0mg, 86%, white solid

The complexity of the ^{1}H- and ^{13}C-spectrum is increased by the appearance of different rotamers. Signals are designated as multiplets (m) when they could not be nearer specified in the ^{1}H-spectrum. Just signals of the major rotamer are given in the ^{13}C-spectrum.

^{1}H NMR (400 MHz, Acetone-d_6): δ 10.31 (bs, NH), 8.54 – 8.30 (m, 1H), 7.50 – 7.44 (m, 0.01H), 7.41 – 7.23 (m, 2H), 7.18 – 7.07 (m, 1.01H), 7.02 – 6.80 (m, 4H), 6.76 – 6.68 (m, 1H), 4.72 – 4.43 (m, 2H), 4.32 – 4.15 (m, 4H), 3.98 – 3.88 (m, 1H), 3.83 – 3.78 (m, 2H), 3.75 (s, 3H), 3.74 – 3.64 (m, 1H), 1.52 – 1.41 (m, 9H).

Deuterium incorporation was expected at δ 7.50 – 7.44 and at δ 7.18 – 7.07. Isotopic enrichment values were determined against the integral at δ 8.54 – 8.30.

^{2}H-{^{1}H}NMR (92 MHz, Acetone): δ 7.45 (s), 7.29 (s), 7.10 (s), 6.87 (s).

^{13}C-{^{1}H}NMR (100 MHz, Acetone-d_6): δ 157.1, 156.3, 150.8, 149.5, 142.4, 140.1, 127.2, 125.3, 124.2, 123.4, 122.2, 121.6, 119.7, 114.7, 113.3, 110.9 (m), 104.8 (m), 101.4, 80.2, 71.3, 70.5, 68.4, 56.1, 53.2, 49.3, 28.6.

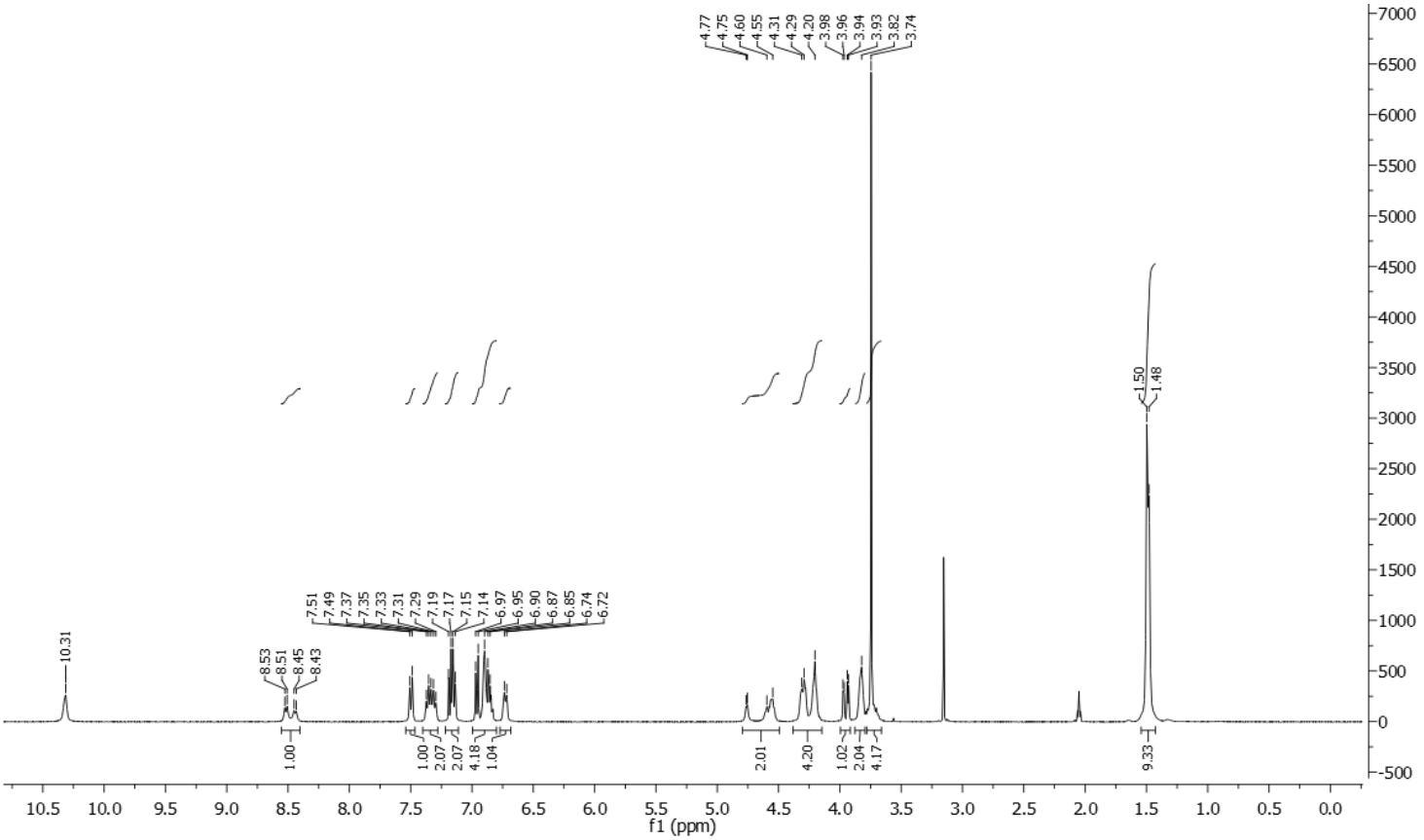

^{1}H-NMR spectrum of the non-deuterated starting material

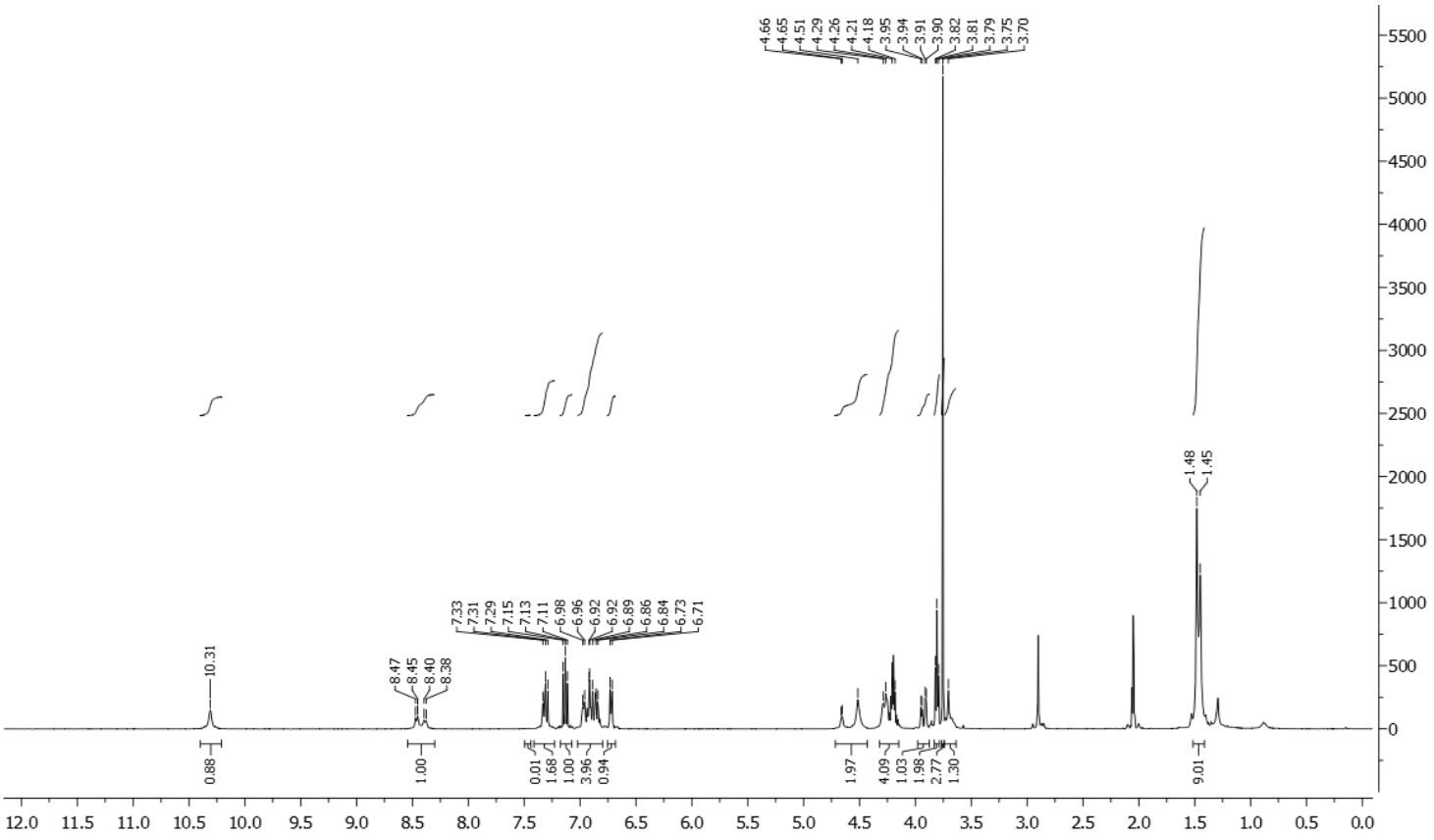

^{1}H-NMR spectrum of **26II**

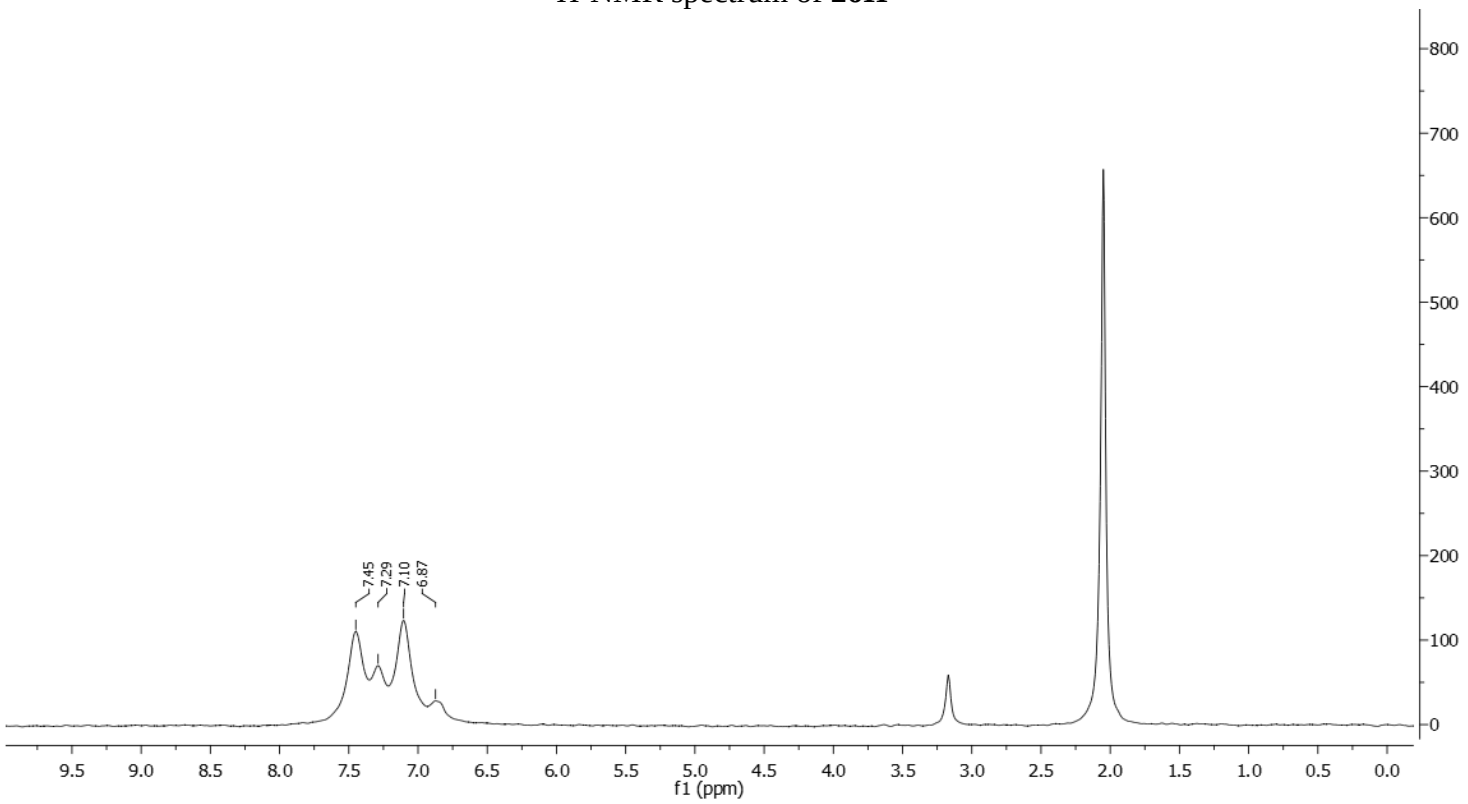

^{2}H-NMR spectrum of **26II**

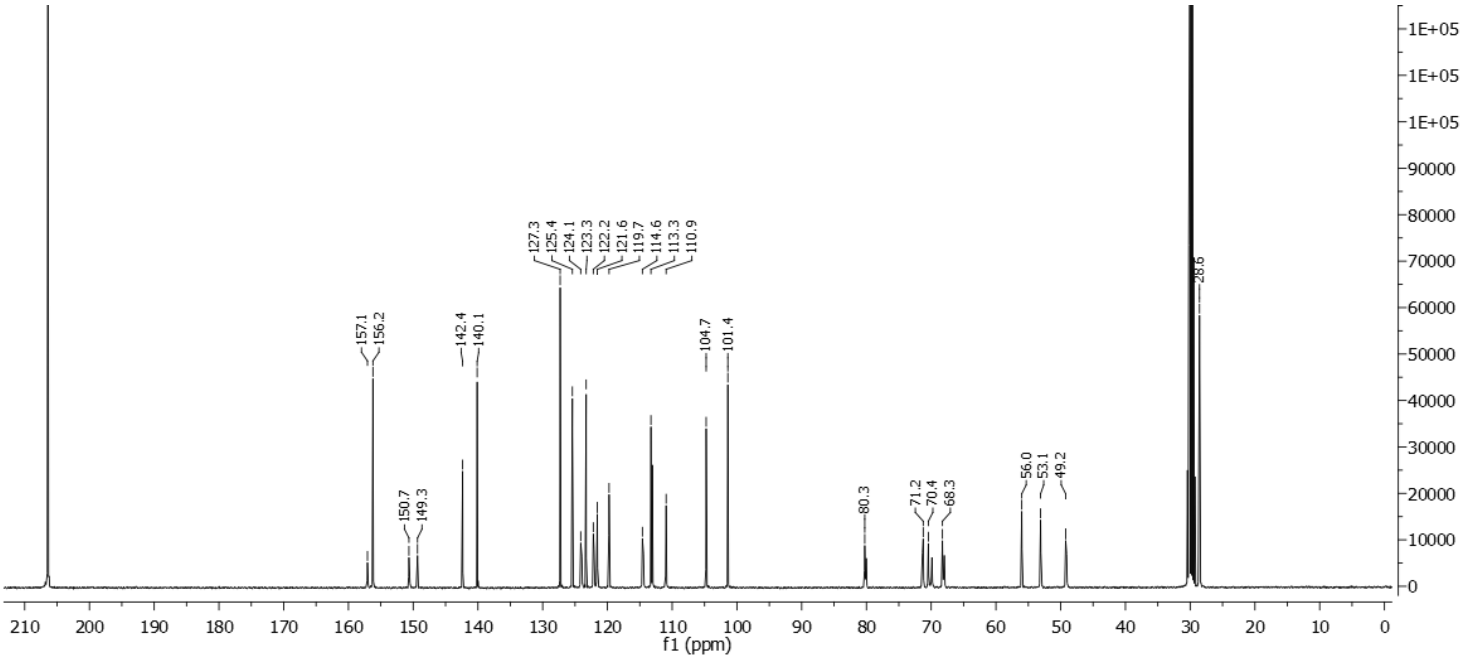

^{13}C-NMR spectrum of the non-deuterated starting material

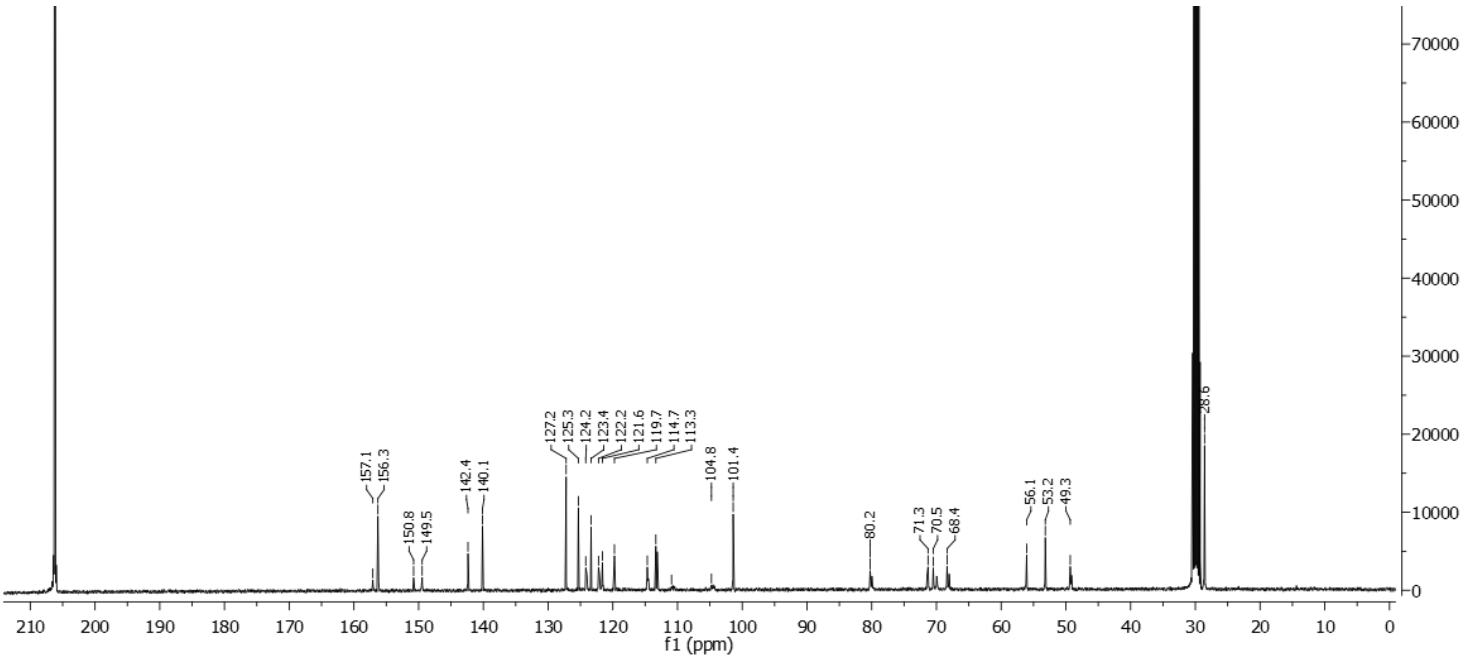

^{13}C-NMR spectrum of **26II**

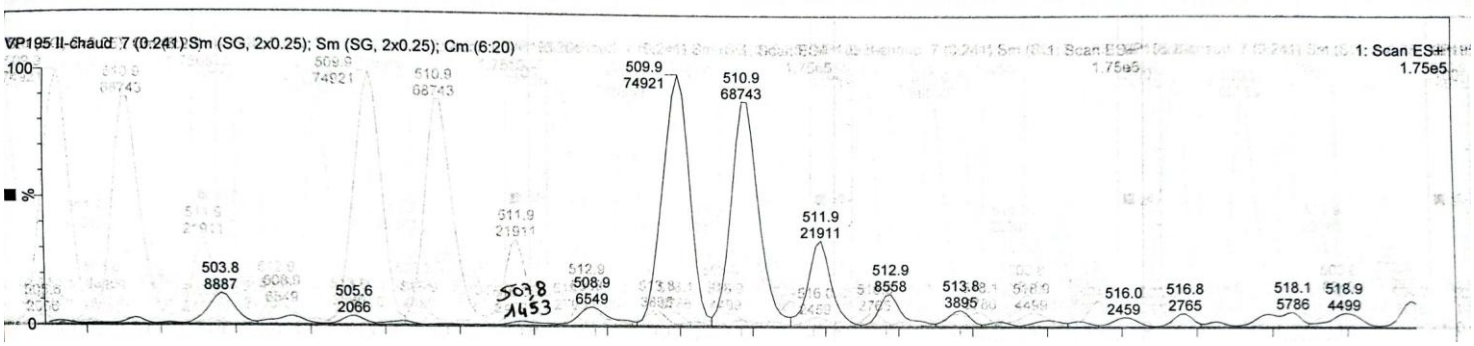

ESI spectrum of **26II**

Removal of the Boc-group to 7, 8-dideuterocarbazole-carvedilol **26III**

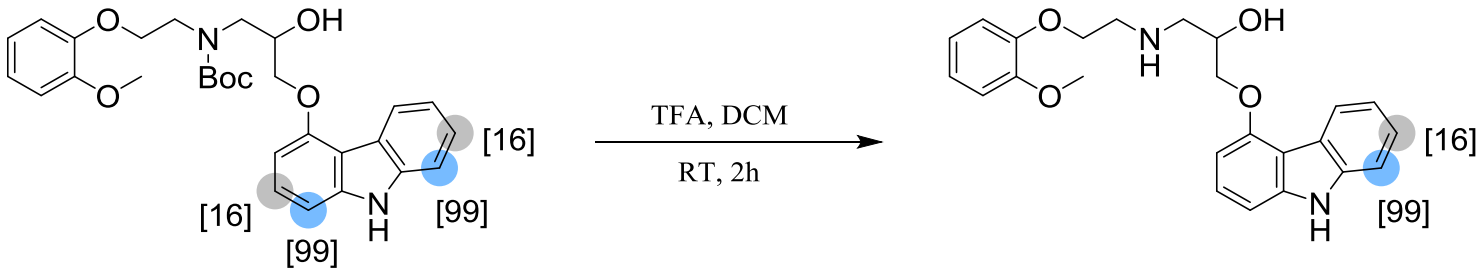

Chemical Formula: $C_{24}H_{26}N_2O_4$

7, 8-Dideuterocarbazole-*N*-boc-carvedilol **25** (20.0mg, 40µmol) was dissolved in DCM (1mL). TFA (74µL, 1.0mmol, 25eq) was added at 0°C and the mixture was stirred for 1h. Another amount of TFA (84µL, 1.1mmol, 28eq) was added at ambient temperature and stirring was continued for 1h more. The reaction mixture was poured on 150mL of an aqueous K_2CO_3 solution (0.03M). The aqueous phase was extracted three times with DCM (50mL). The solvent was removed under vacuum and the crude was purified over HPLC on a Waters XBridge C18 HPLC column (100x4,6 mm, 3.5 microns). Conditions: 1 ml/min, UV & mass detection, 25°C, Solvents & gradients: A: H_2O+1/1000 HCO_2H B: ACN+1/1000 HCO_2H

t (0)	95%A 5%B
t(24min)	50%A 50%B
t(25min)	0%A 100%B
t(30min)	0%A 100%B

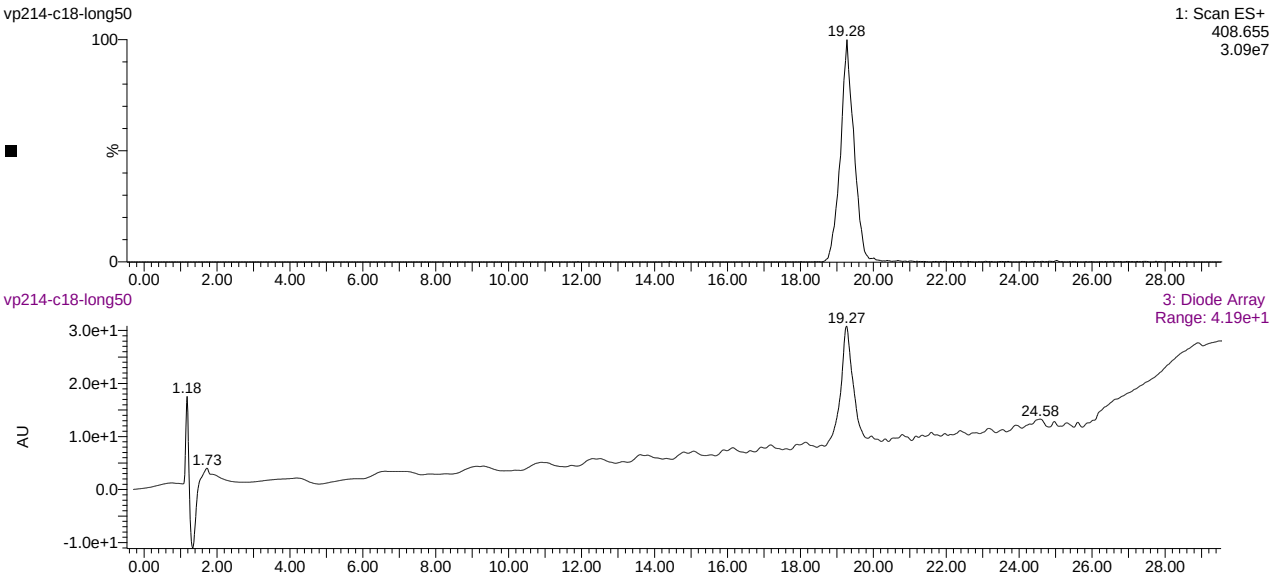

HPLC chromatogram of **26III**

Pure fractions were concentrated under reduced pressure and poured on 100mL of an aqueous K_2CO_3 solution (0.03M). The aqueous phase was extracted three times with EtOAc (50mL). The organic fractions were combined and the solvent was removed under vacuum.

Yield: 11.0mg, 66%, white solid

^{1}H NMR (400 MHz, $CDCl_3$): δ 8.28 – 8.22 (m, 1H), 8.18 (s, NH), 7.41 – 7.27 (m, 2H), 7.23 – 7.16 (m, 1H), 7.08 – 7.02 (m, 1H), 6.97 – 6.83 (m, 4H), 6.67 – 6.62 (m, 1H), 4.36 – 4.10 (m, 5H), 3.81 (s, 3H), 3.18 – 3.08 (m, 3H), 3.08 – 2.94 (m, 1H).

Deuterium incorporation was expected at δ 7.41 – 7.27. Isotopic enrichment values were determined against the integral at δ 8.28 – 8.22.

^{2}H NMR (92 MHz, $CHCl_3$): δ 7.44 (s)

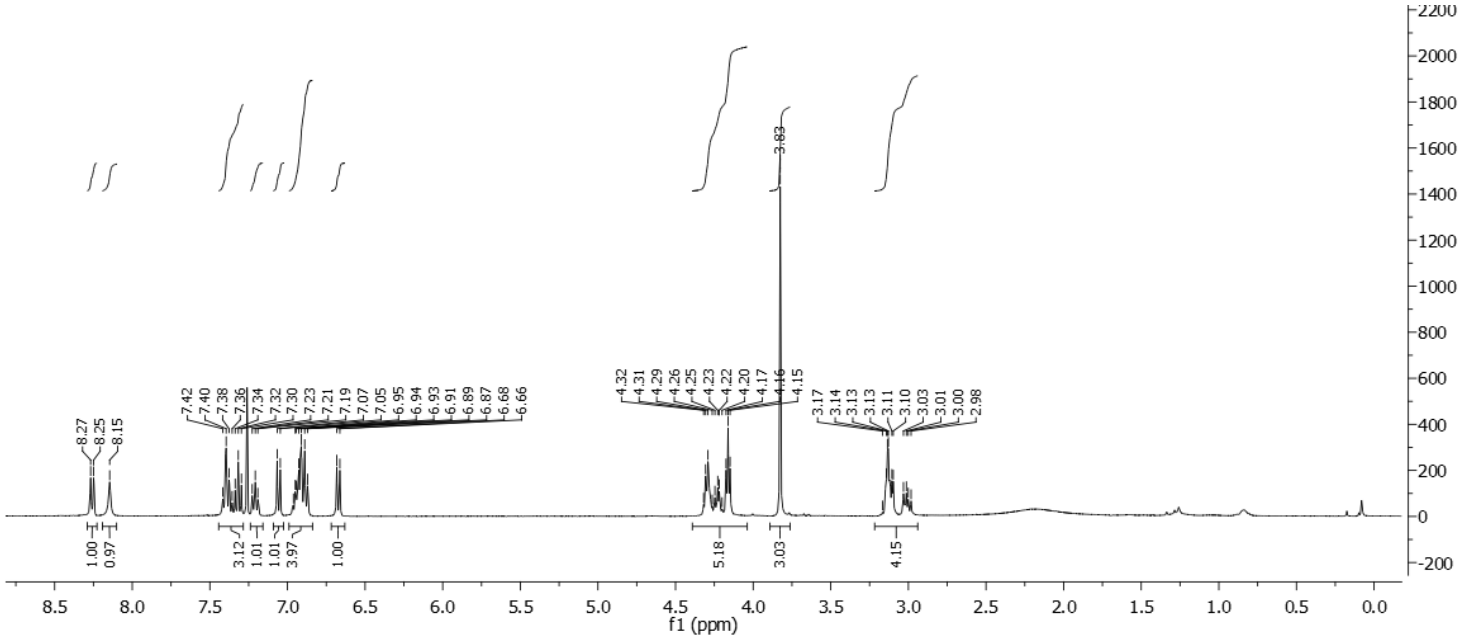

^{1}H-NMR spectrum of non-deuterated carvedilol

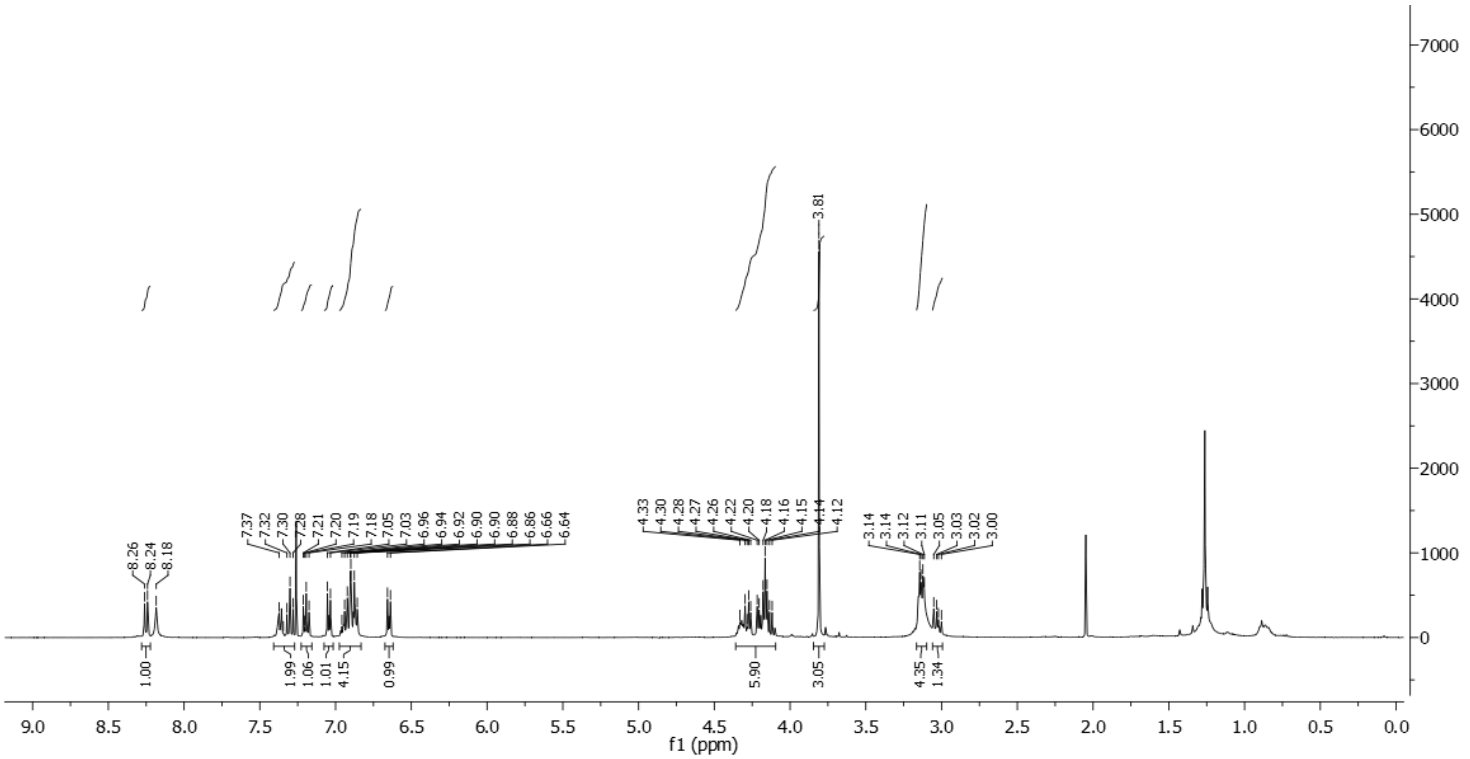

^{1}H-NMR spectrum of **26III**

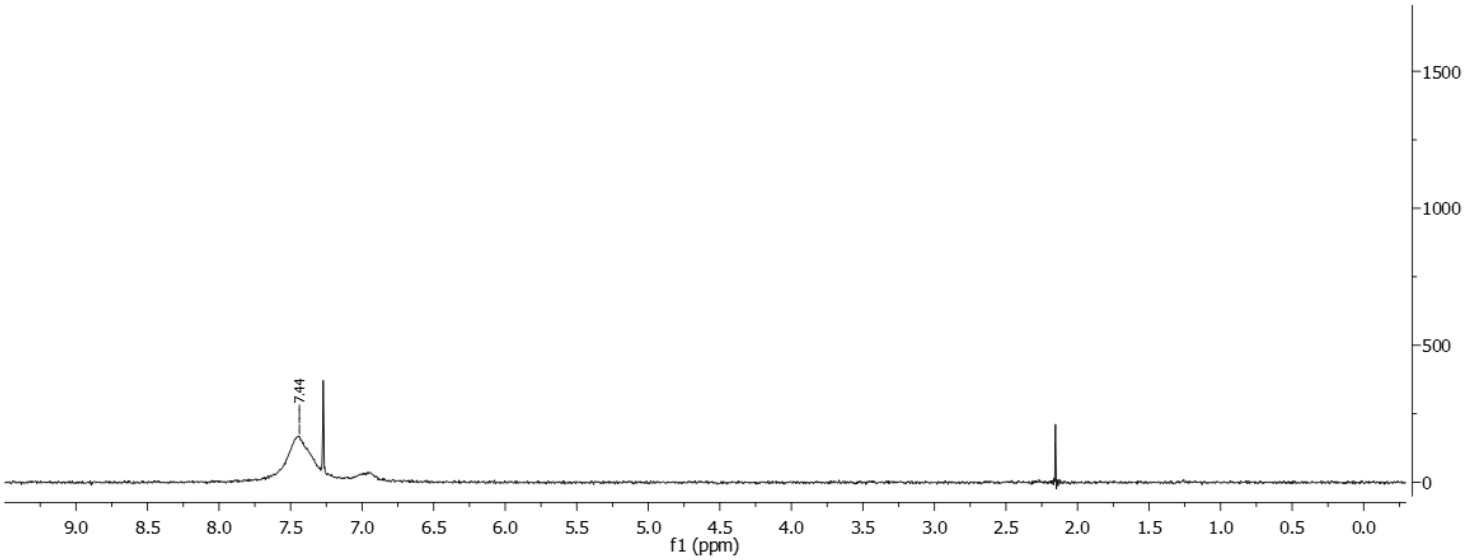

^{2}H-NMR spectrum of **26III**

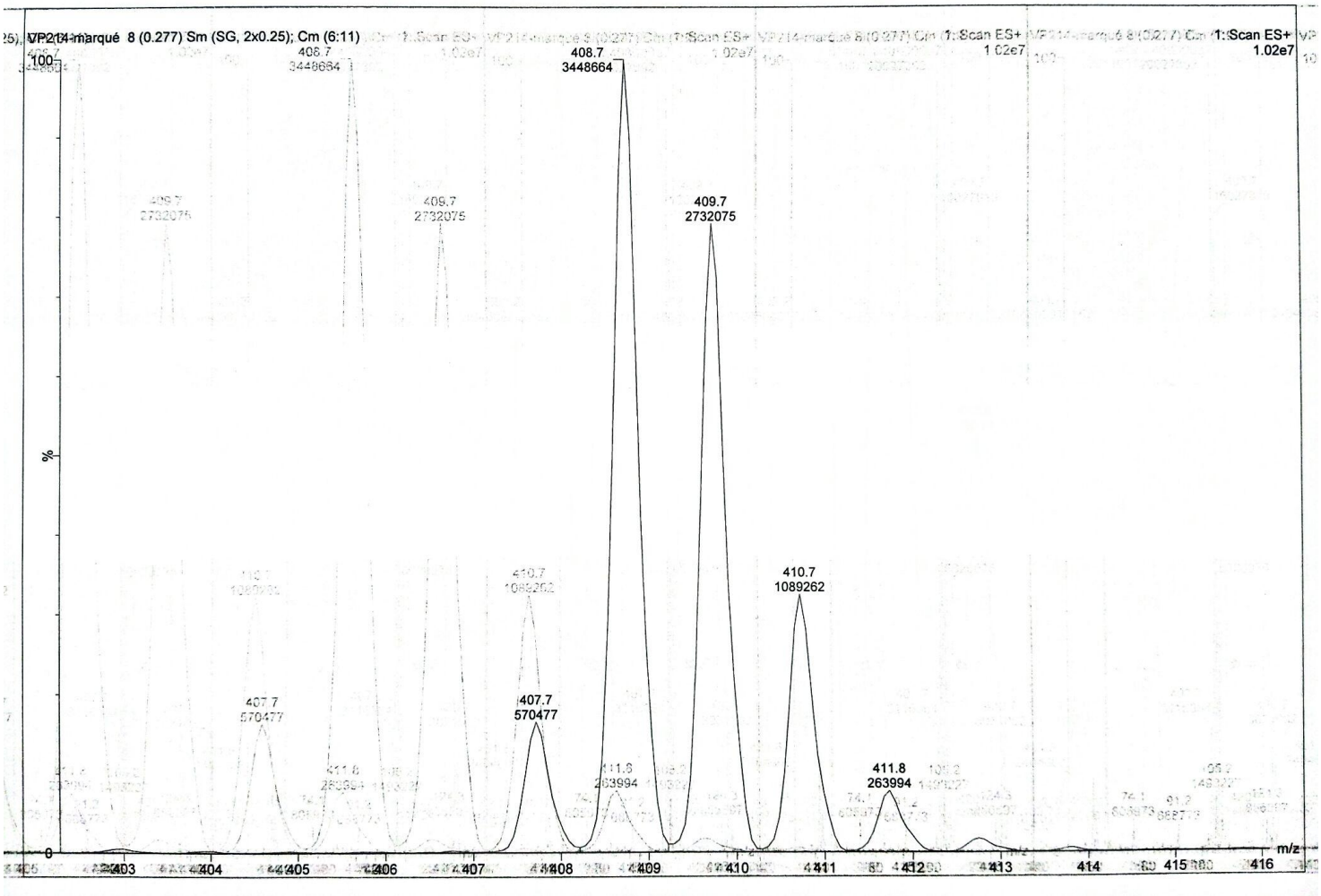

ESI spectrum of **26III**

Astemizole **27**

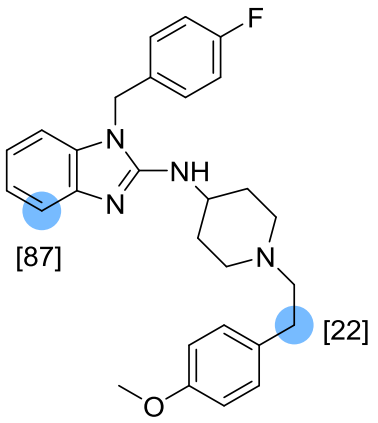

Chemical Formula: $C_{28}H_{31}FN_4O$

Substrate	Solvent (Volume)	RuNp@PVP cat.
45.9mg, 0.1mmol	THF (2mL)	28.9mg, 20mol%

Workup and purification:

After cooling down to room temperature, EtOAc/cyclohexane (1:1, 3mL) was added to the reaction mixture and stirred for 10min to let precipitate RuNp@PVP. The suspension was passed through a Sep-Pak® C18 cartridge and then eluted with EtOAc (5mL). The solvent was removed under vacuum to give 42mg of crude product. 10mg of the crude were purified over basic Al_2O_3. Elution started with cyclohexane/EtOAc (3:1). Pure product was eluted with THF/MeOH (1:1).

Yield: 6.0mg, 60%, white solid

^{1}H NMR (400 MHz, Acetone-*d_6*): δ 7.29 – 7.24 (m, 0.13H), 7.24 – 7.02 (m, 7H), 7.01 – 6.95 (m, 1H), 6.91 – 6.80 (m, 3H), 5.76 (d, J = 7.5 Hz, 1H), 5.28 (s, 2H), 3.97 – 3.85 (m, 1H), 3.75 (s, 3H), 2.97 – 2.90 (m, 2H), 2.73 – 2.66 (m, 1.84H), 2.54 – 2.49 (m, 1.54H), 2.20 – 2.06 (m, 4H), 1.62 – 1.50 (m, 2H).

Deuterium incorporation was expected at *δ* 7.29 – 7.24, *δ* 2.73 – 2.66 and at *δ* 2.54 – 2.49. Isotopic enrichment values were determined against the integral at *δ* 7.01 – 6.95.

^{2}H-{^{1}H}NMR (92 MHz, Acetone): δ 7.28 (s, 0.87D), 2.64 (s, 0.16D), 2.47 (s, 0.46D).

^{13}C-{^{1}H}NMR (100 MHz, Acetone-d_6): δ 158.9, 154.8, 144.2, 135.6, 134.1, 133.6, 130.4, 129.6, 121.5, 119.5, 116.5 (m), 116.3, 116.1, 114.4, 108.4, 61.4, 55.4, 53.4, 51.4, 44.9, 33.6 (m), 33.3.

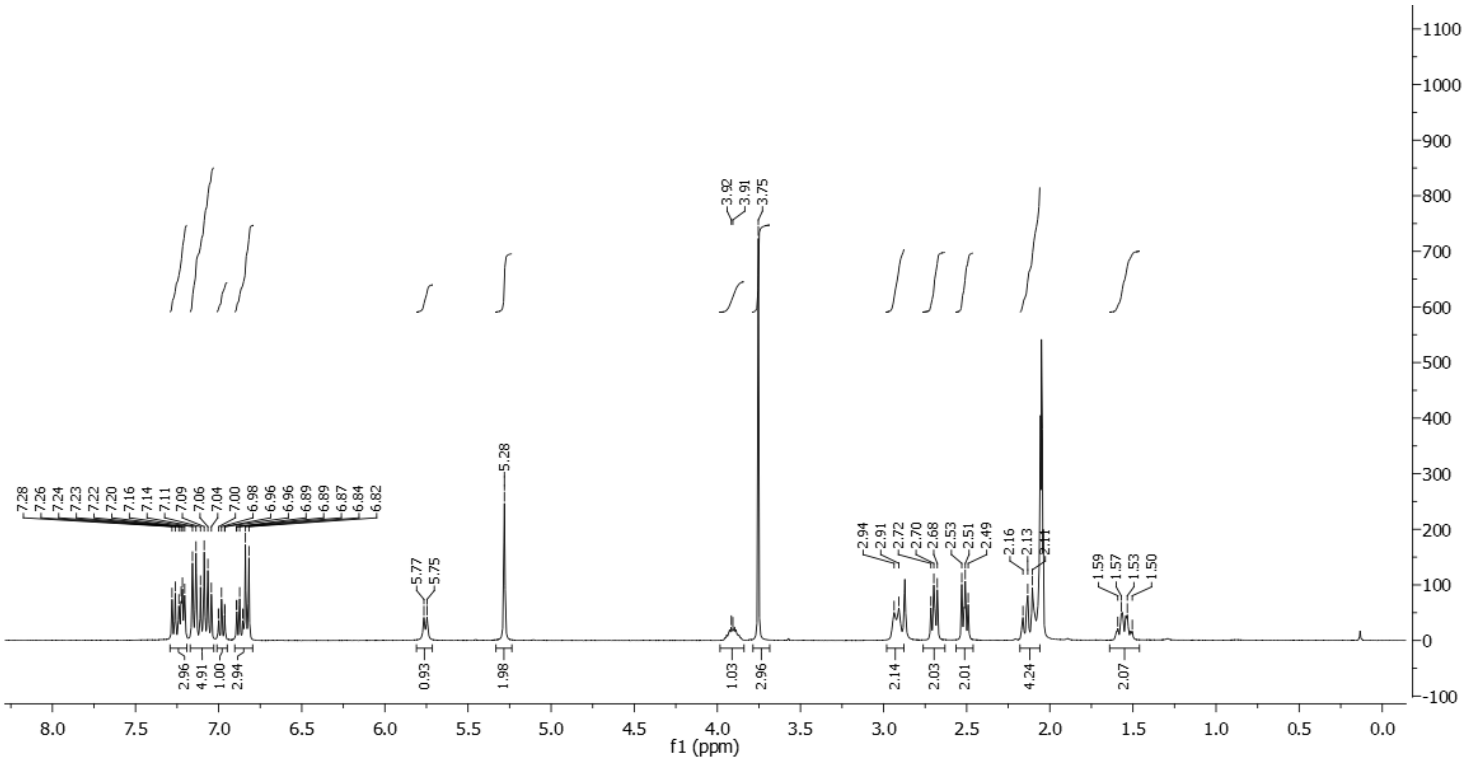

^{1}H-NMR spectrum of the non-deuterated starting material

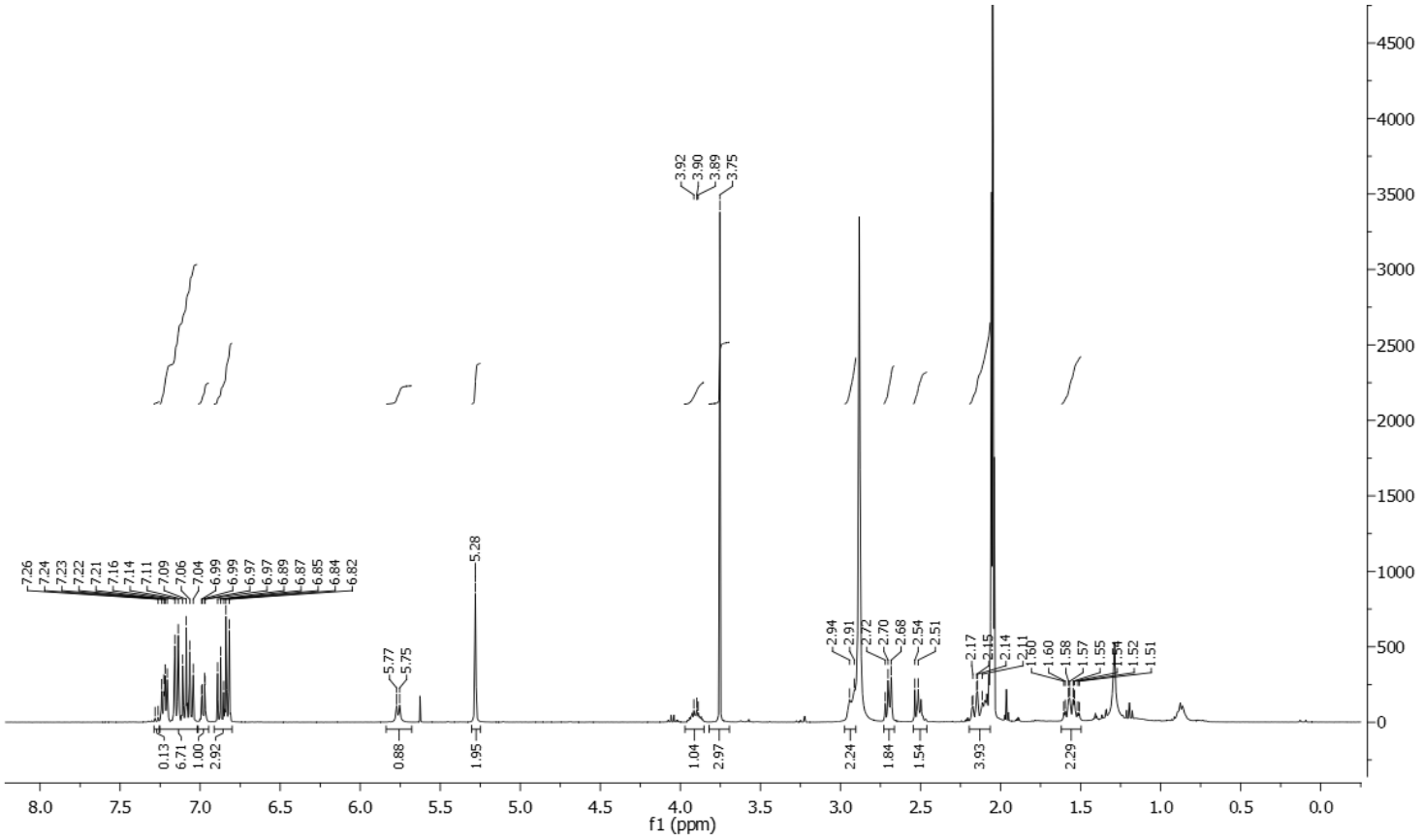

^{1}H-NMR spectrum of **27**

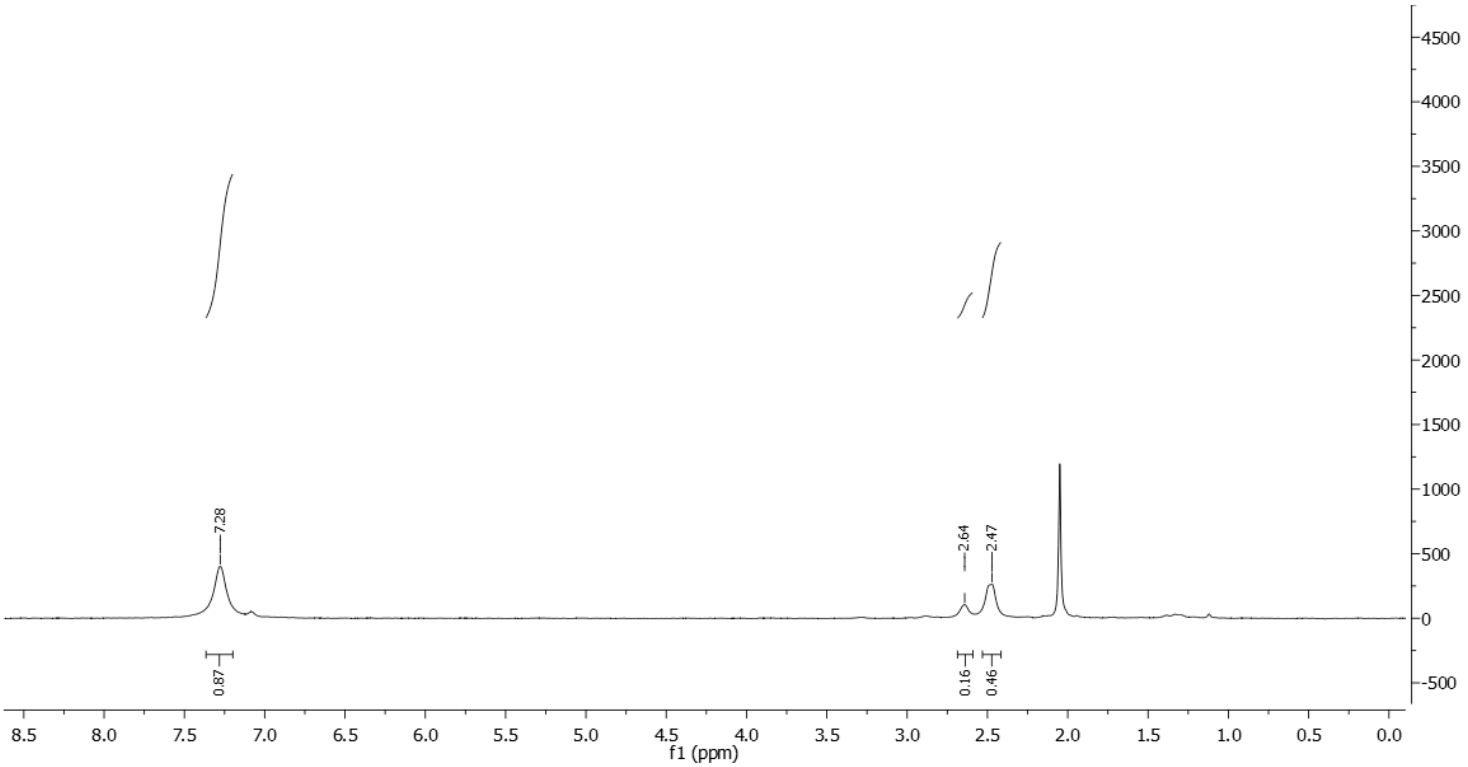

^{2}H-NMR spectrum of **27**

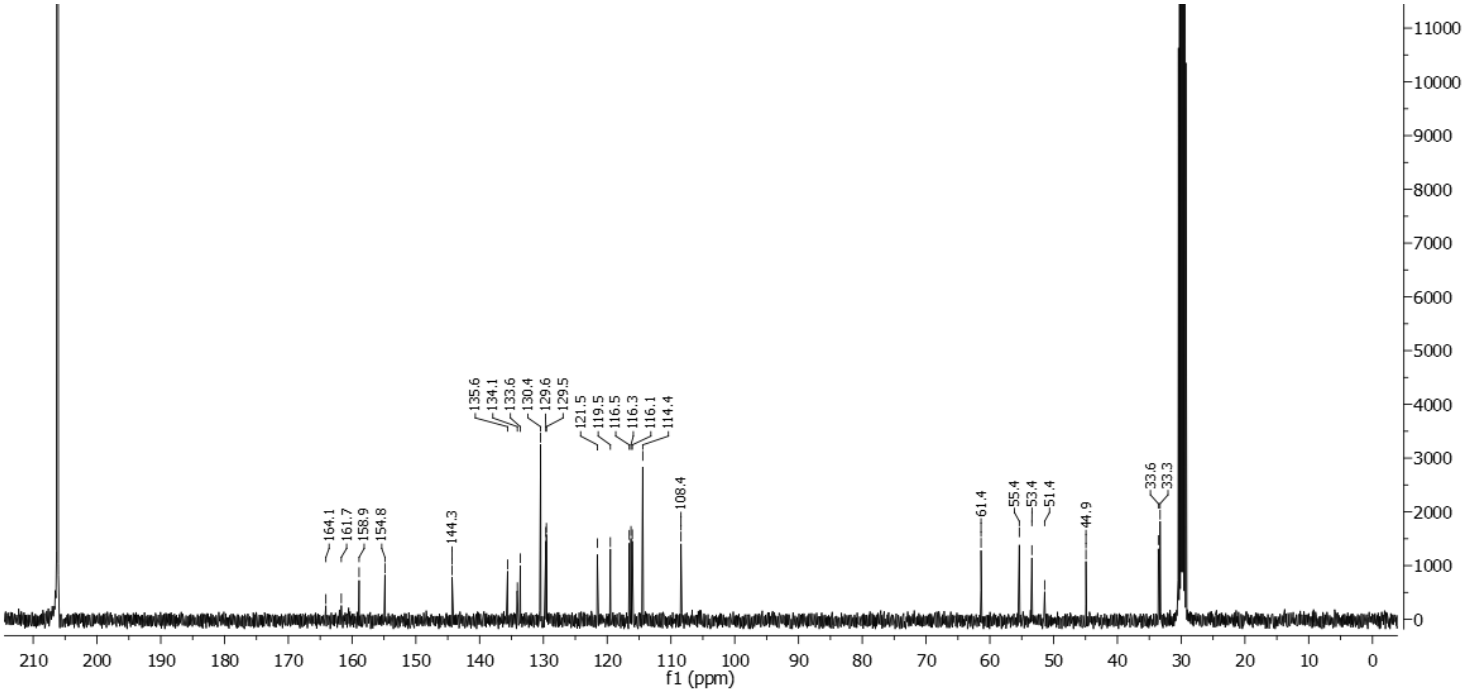

^{13}C-NMR spectrum of the non-deuterated starting material

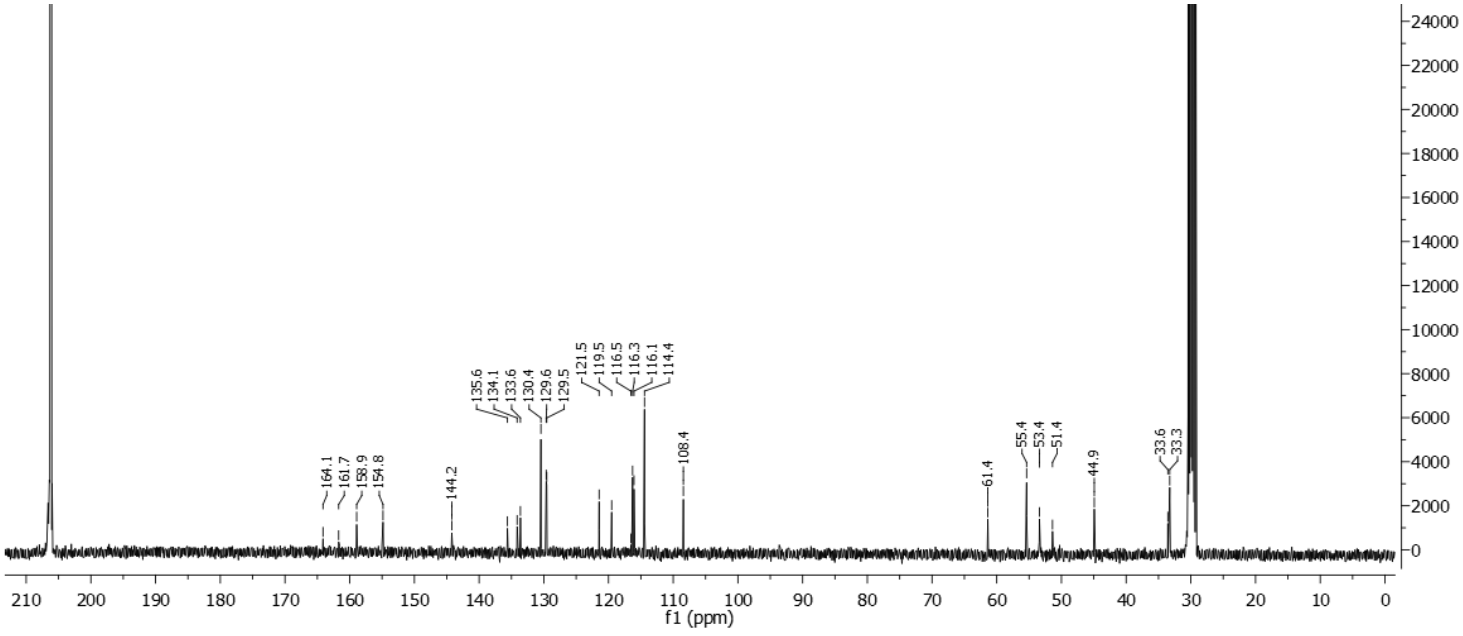

^{13}C-NMR spectrum of **27**

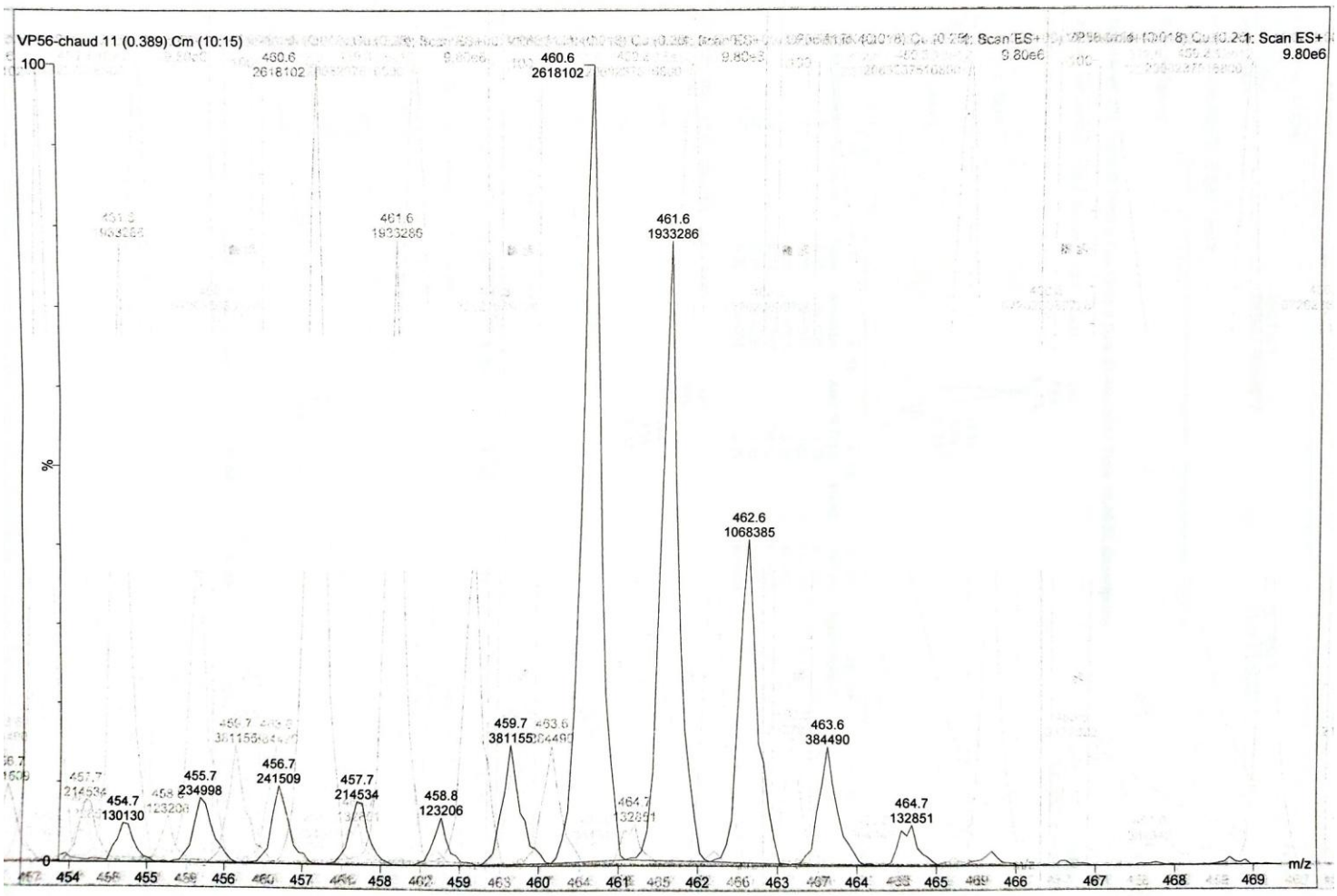

ESI-spectrum of **27**

Imiquimod **28**

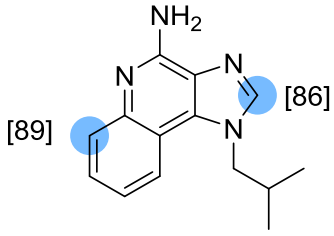

Chemical Formula: $C_{14}H_{16}N_4$

Substrate	Solvent (Volume)	RuNp@PVP cat.
10.0mg, 42µmol	DMA (2mL)	14.4mg, 24mol%

Workup and purification:

After cooling down to room temperature the reaction mixture was poured on H_2O dist. (100mL) in a separation funnel. The aqueous phase was extracted three times with EtOAc (50mL). The solvent was removed under vacuum at room temperature and the crude product was recrystallized from dichloromethane and methanol (DCM : MeOH, 4:1).

Yield: 8.0mg, 80%, white solid

^{1}H NMR (400 MHz, DMSO-d_6): δ 8.18 (s, 0.18H), 8.03 – 7.97 (m, 1H), 7.63 – 7.59 (m, 0.25H), 7.47 – 7.40 (m, 1H), 7.30 – 7.23 (m, 1H), 6.59 (s, 2H), 4.40 (d, *J* = 7.5 Hz, 2H), 2.21 – 2.13 (m, 1H), 0.91 (d, *J* = 6.6 Hz, 6H).

Deuterium incorporation was expected at δ 8.18 and at δ 7.63 – 7.59. Isotopic enrichment values were determined against the integral at δ 7.30 – 7.23.

^{2}H-{^{1}H}NMR (92 MHz, DMSO): δ 8.17 (s, 0.86D), 7.61 (s, 0.89D).

The low solubility of imiquimod did not allow to record ^{13}C-{^{1}H}NMR spectra.

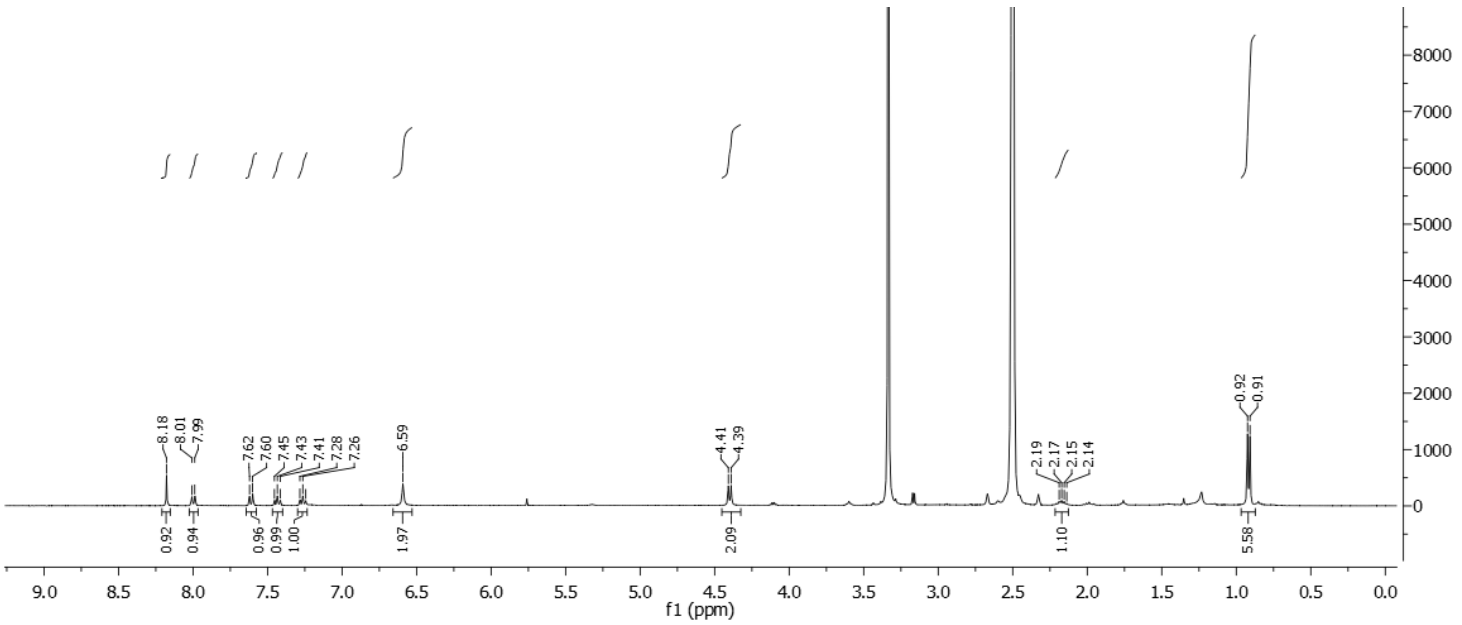

^{1}H-NMR spectrum of the non-deuterated starting material

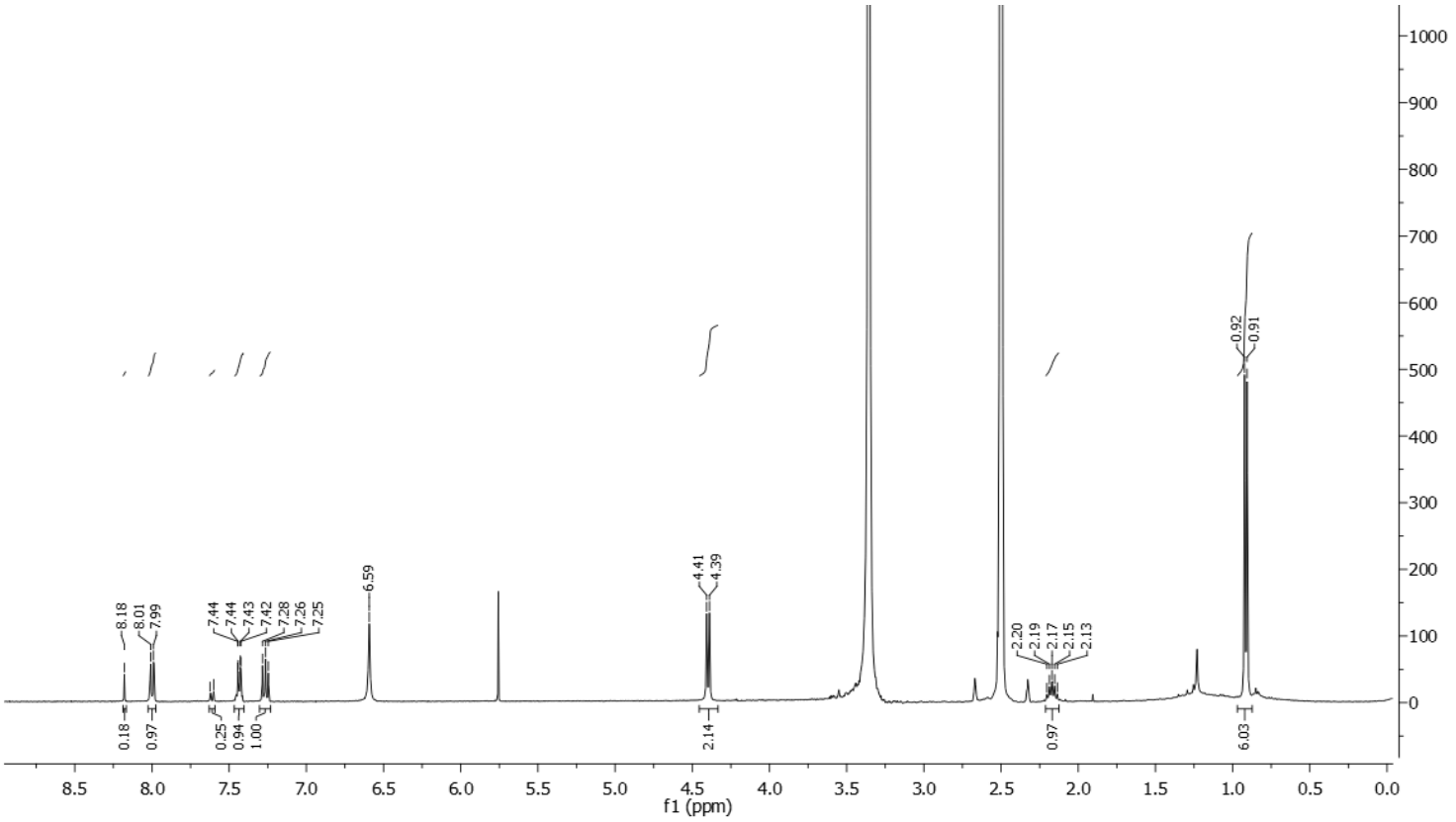

^{1}H-NMR spectrum of **28**

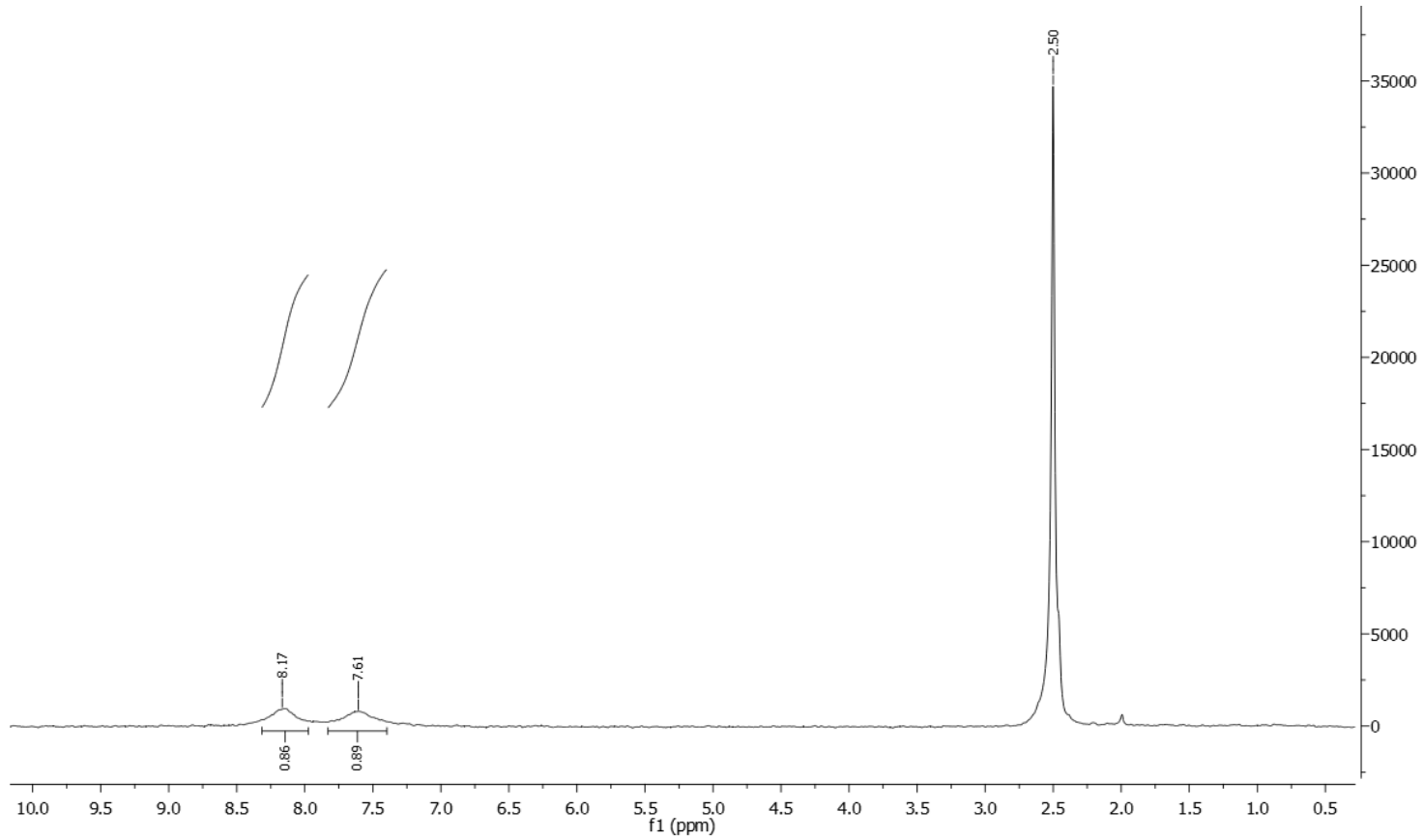

^{2}H-NMR spectrum of **28**

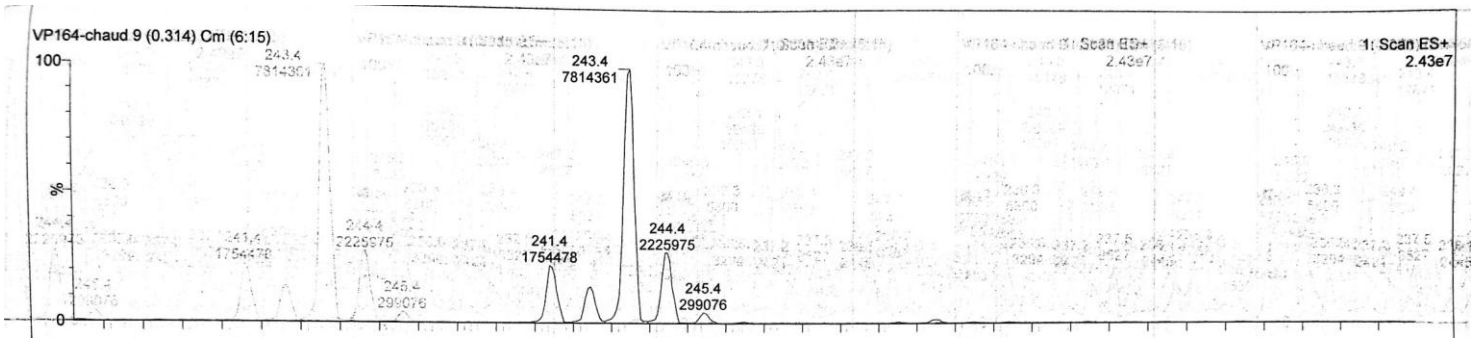

ESI-spectrum of **28**

Fluconazole **29**

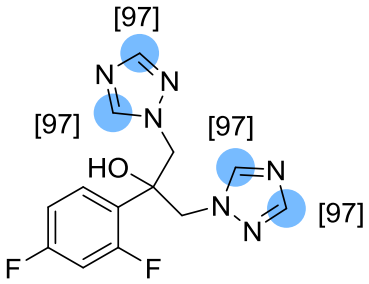

Chemical Formula: $C_{13}H_{12}F_2N_6O$

Substrate	Solvent (Volume)	RuNp@PVP cat.
61.2mg, 0.2mmol	THF (2mL)	28.9mg, 10mol%

Workup and purification:

After cooling down to room temperature, EtOAc/cyclohexane (1:1, 3mL) was added to the reaction mixture and stirred for 10min to let precipitate RuNp@PVP. The suspension was passed through a Sep-Pak® C18 cartridge and then eluted with EtOAc (5mL). The solvent was removed under vacuum.

Yield: 41.0mg, 67%, white solid

^{1}H NMR (400 MHz, Acetone-d_6): δ 8.28 (s, 0.07H), 7.76 (s, 0.07H), 7.42 – 7.33 (m, 1H), 7.08 – 6.98 (m, 1H), 6.89 – 6.81 (m, 1H), 5.63 (s, 1H), 4.90 (d, *J* = 15.0 Hz, 2H), 4.67 (d, *J* = 14.5 Hz, 2H).

Deuterium incorporation was expected at δ 8.28 and at δ 7.76. Isotopic enrichment values were determined against the integral at δ 6.89 – 6.81.

^{2}H-{^{1}H}NMR (92 MHz, Acetone): δ 8.26 (s, 0.97D), 7.75 (s, 0.97D).

^{13}C-{^{1}H}NMR (100 MHz, Acetone-d_6): δ 165.2 – 161.2 (m), 162.7 – 158.7 (m), 152.2 (m), 146.0 (m), 131.6 – 130.4 (m), 124.6 – 123.8 (m), 112.6 – 111.4 (m), 105.4 – 104.0 (m), 75.9 – 75.1 (m), 56.2 – 55.1 (m).

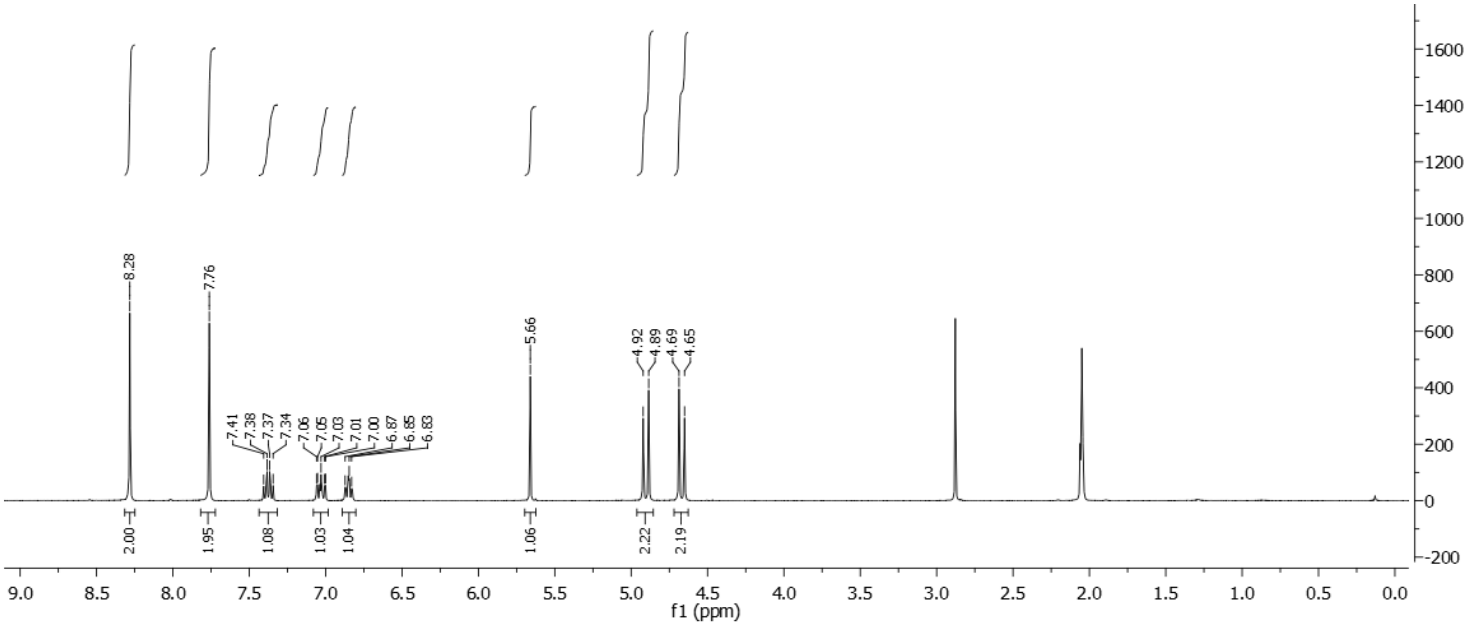

^{1}H-NMR spectrum of the non-deuterated starting material

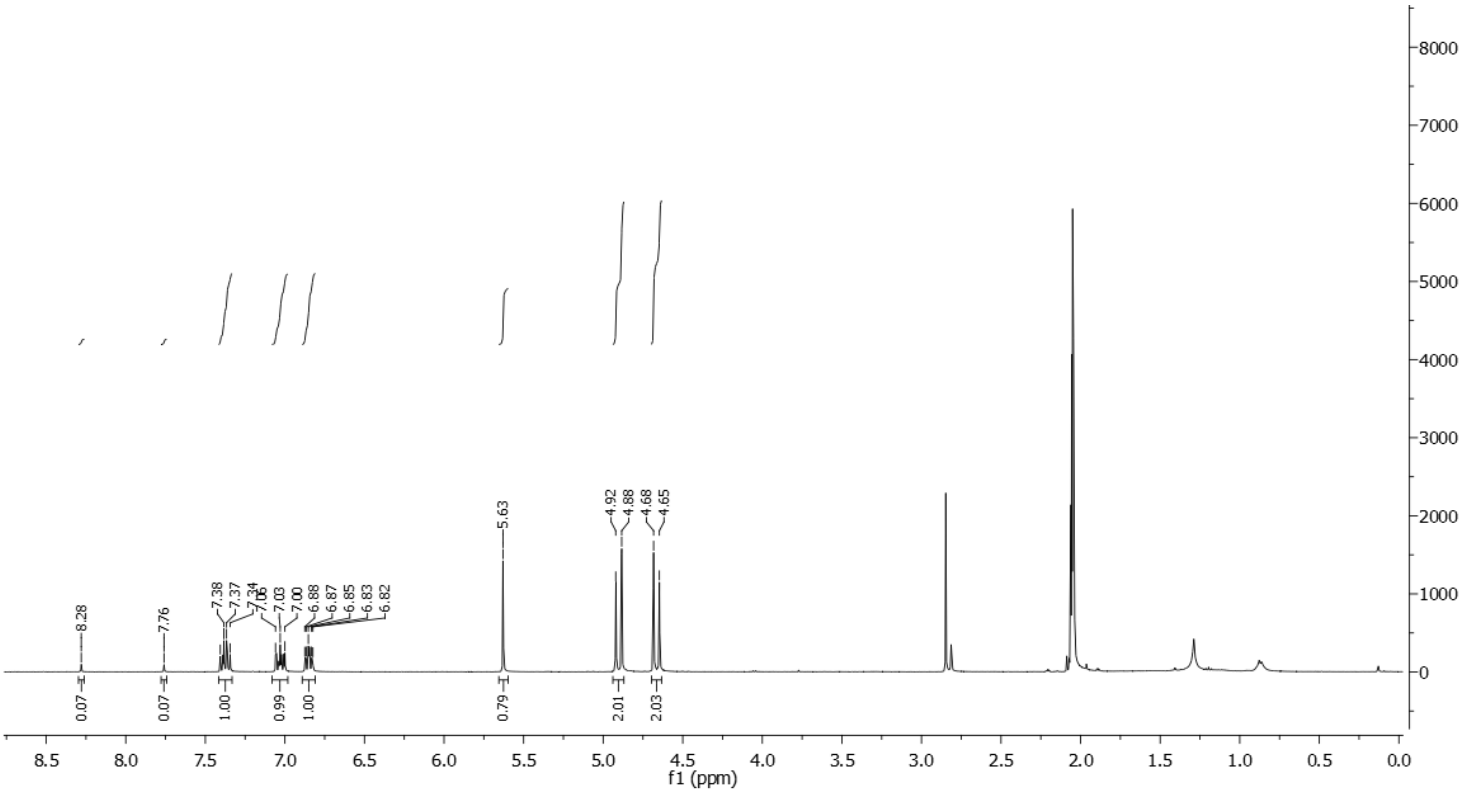

^{1}H-NMR spectrum of **29**

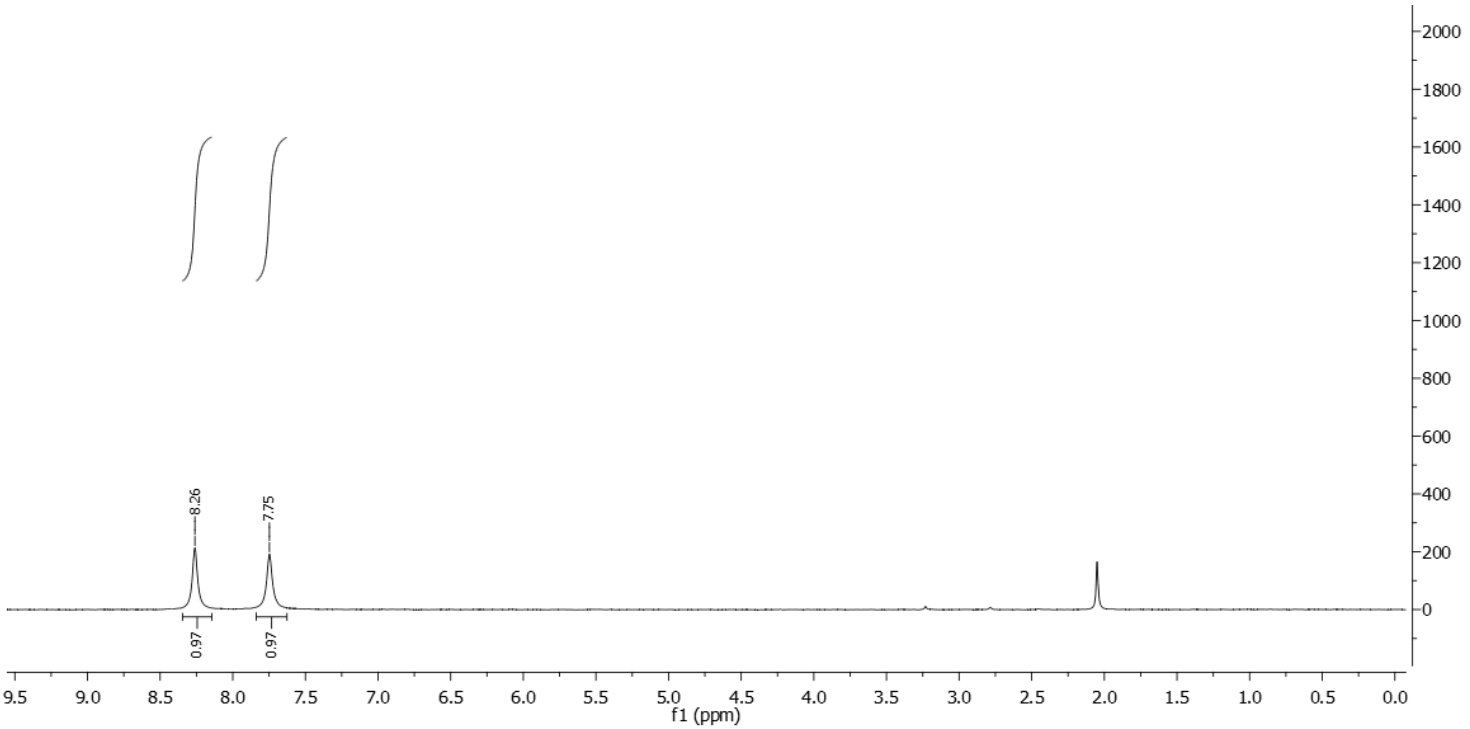

^{2}H-NMR spectrum of **29**

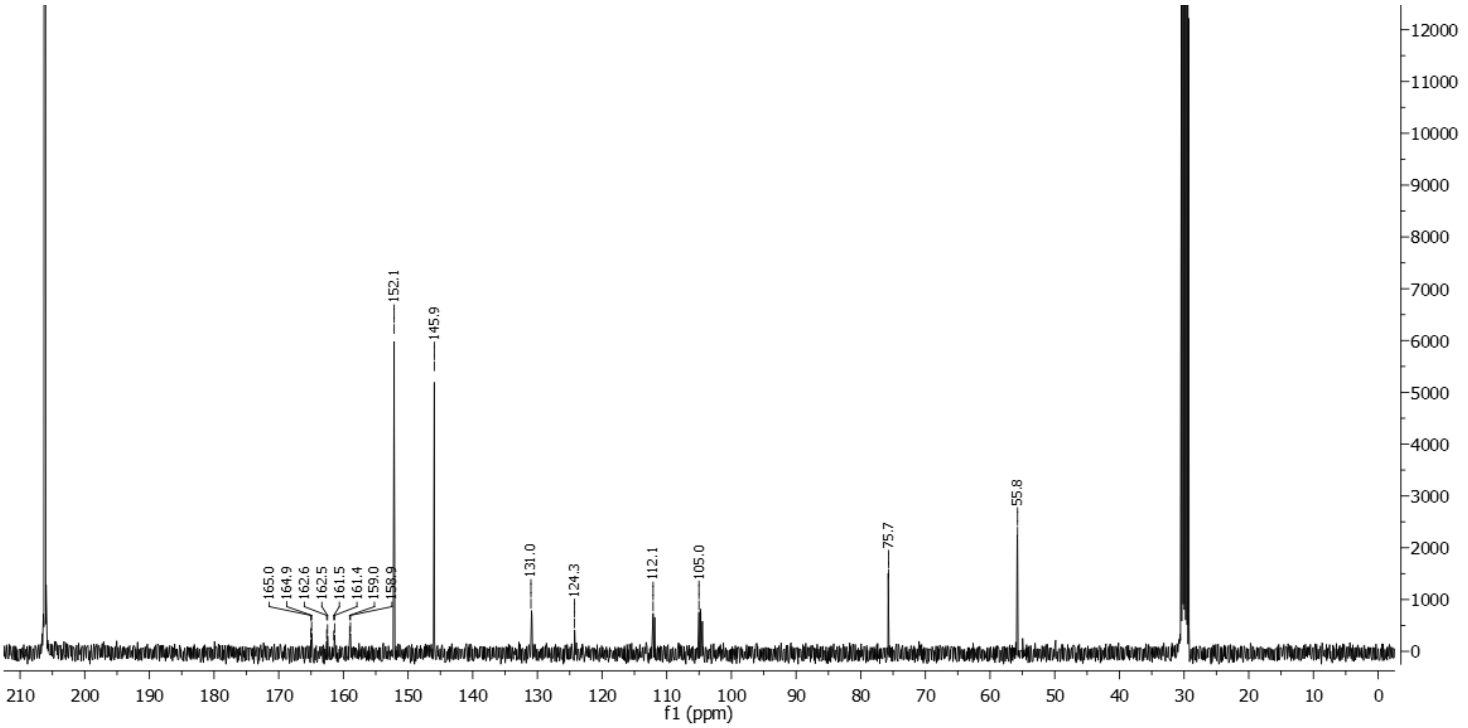

^{13}C-NMR spectrum of the non-deuterated starting material

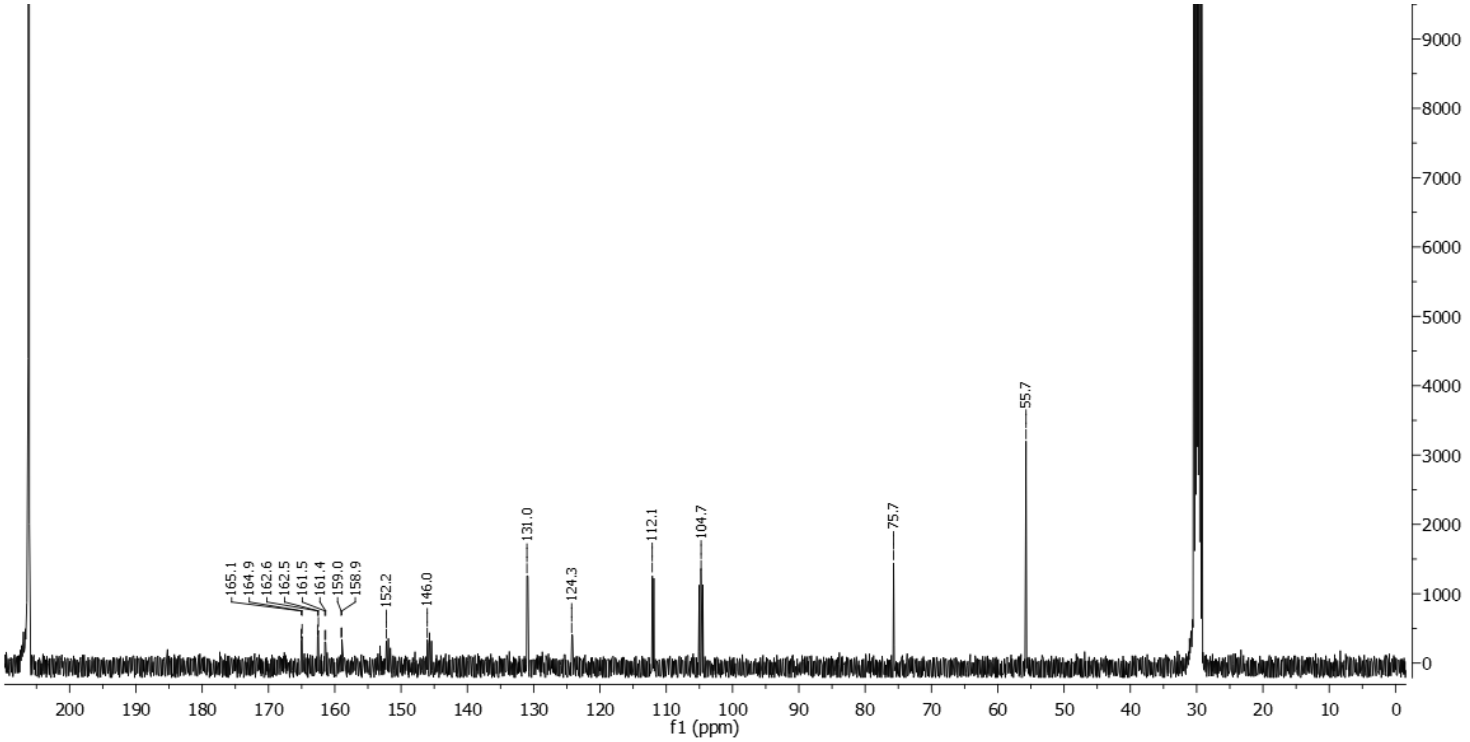

^{13}C-NMR spectrum of **29**

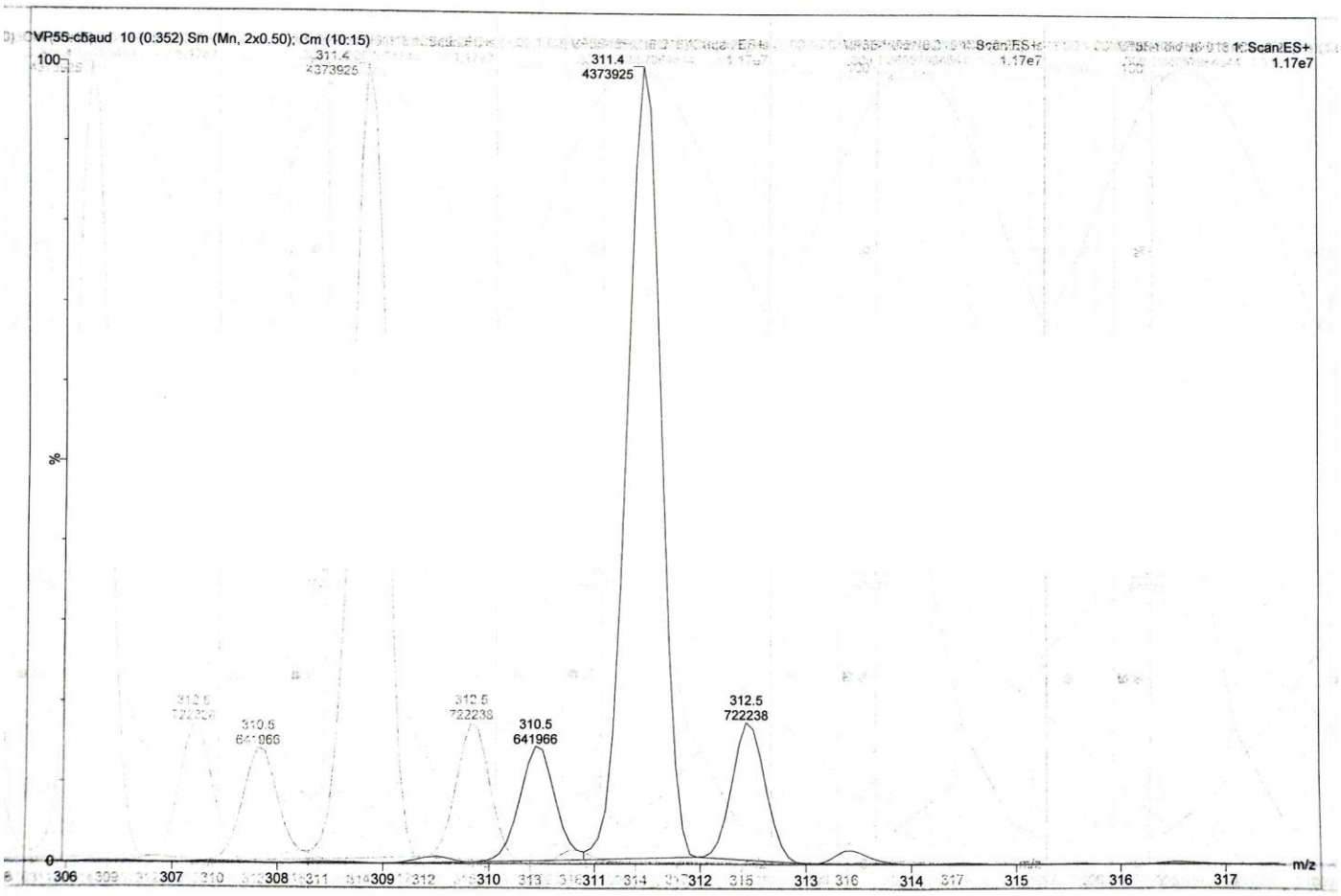

ESI-spectrum of **29**

Fluquinconazole **30**

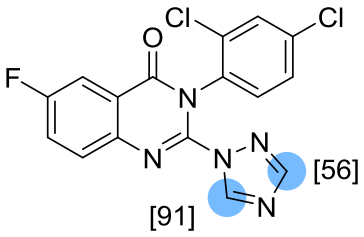

Chemical Formula: $C_{16}H_8Cl_2FN_5O$

Substrate	Solvent (Volume)	RuNp@PVP cat.
10.0mg, 27µmol	THF (2mL)	7.2mg, 19mol%

Workup and purification:

After cooling down to room temperature, EtOAc/cyclohexane (1:1, 3mL) was added to the reaction mixture and stirred for 10min to let precipitate RuNp@PVP. The suspension was passed through a Sep-Pak® C18 cartridge and then eluted with EtOAc (5mL). The solvent was removed under vacuum.

Yield: 7.0mg, 70%, white solid

^{1}H NMR (400 MHz, Acetone-*d*$_6$): δ 9.05 (s, 1H), 7.97 – 7.88 (m, 2.30H), 7.85 – 7.76 (m, 1H), 7.70 – 7.66 (m, 1H), 7.65 – 7.59 (m, 1H), 7.51 – 7.43 (m, 1H).

Deuterium incorporation was expected at δ 9.05 and at δ 7.97 – 7.88. Isotopic enrichment values were determined against the integral at δ 7.51 – 7.43.

^{2}H-{^{1}H}NMR (92 MHz, Acetone): δ 9.03 (s, 0.91D), 7.88 (s, 0.56D).

^{13}C-{^{1}H}NMR (100 MHz, Acetone-*d*$_6$): δ 164.0 – 160.8 (m), 161.3, 153.5, 146.9 (m), 143.6, 142.1, 136.4, 134.9, 133.8, 132.7, 131.7 – 131.3 (m), 130.2, 128.9, 125.2 – 124.5 (m), 123.4 – 123.2 (m), 113.4 – 112.7 (m).

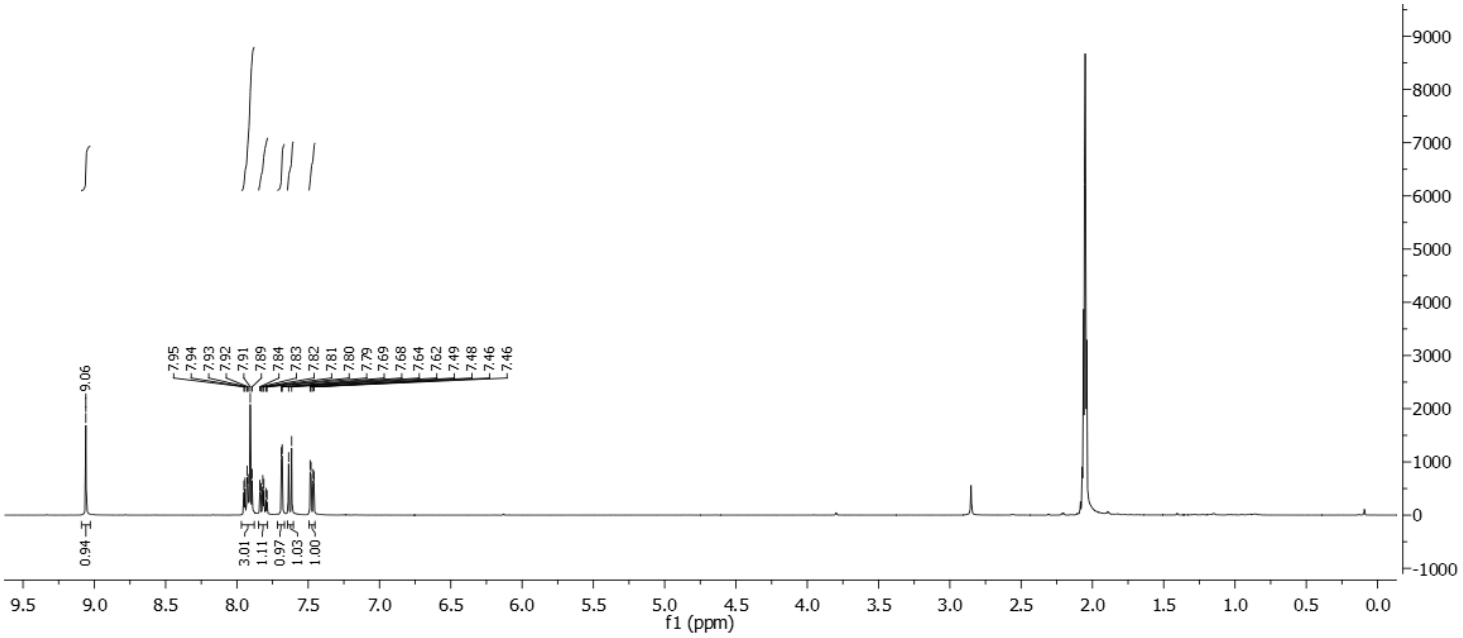

^{1}H-NMR spectrum of the non-deuterated starting material

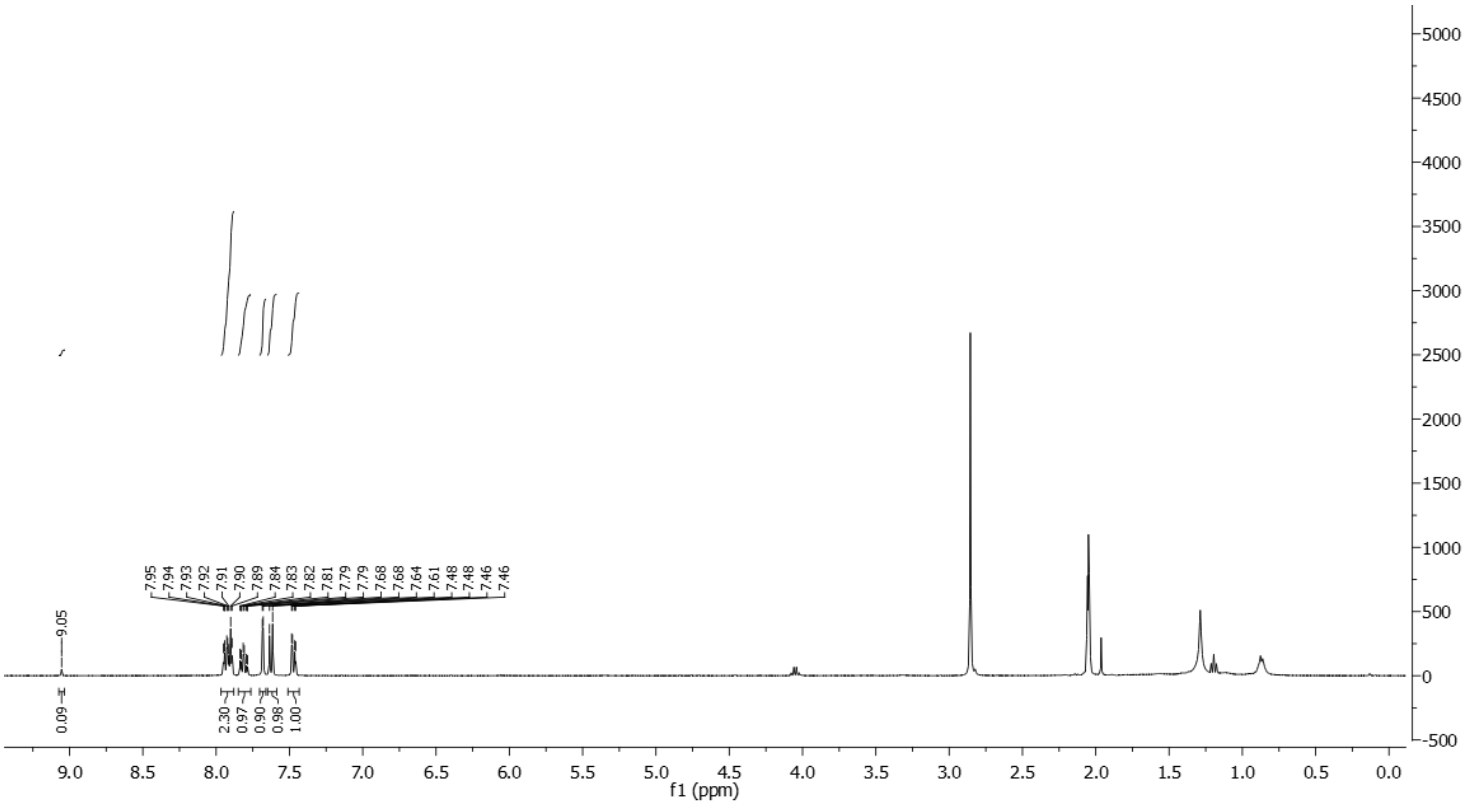

^{1}H-NMR spectrum of **30**

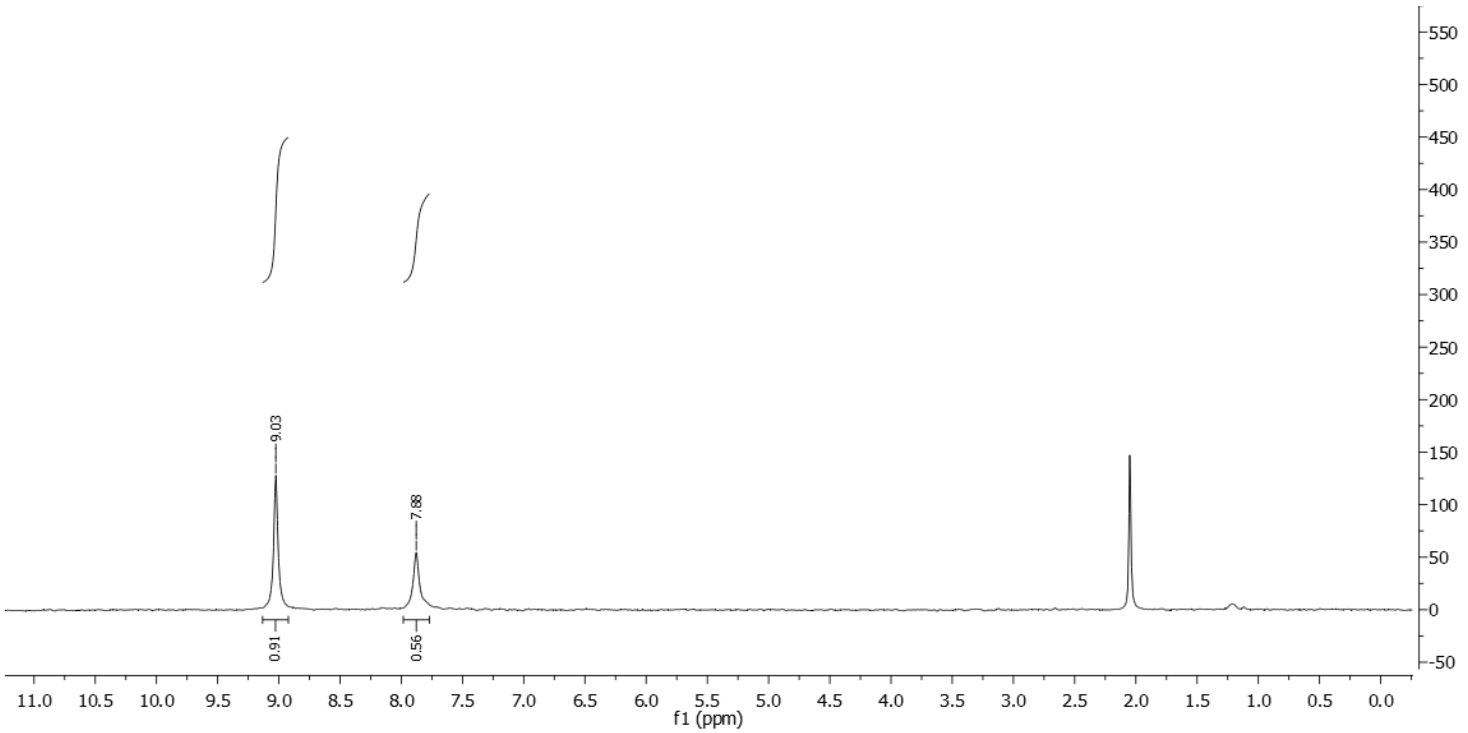

^{2}H-NMR spectrum of **30**

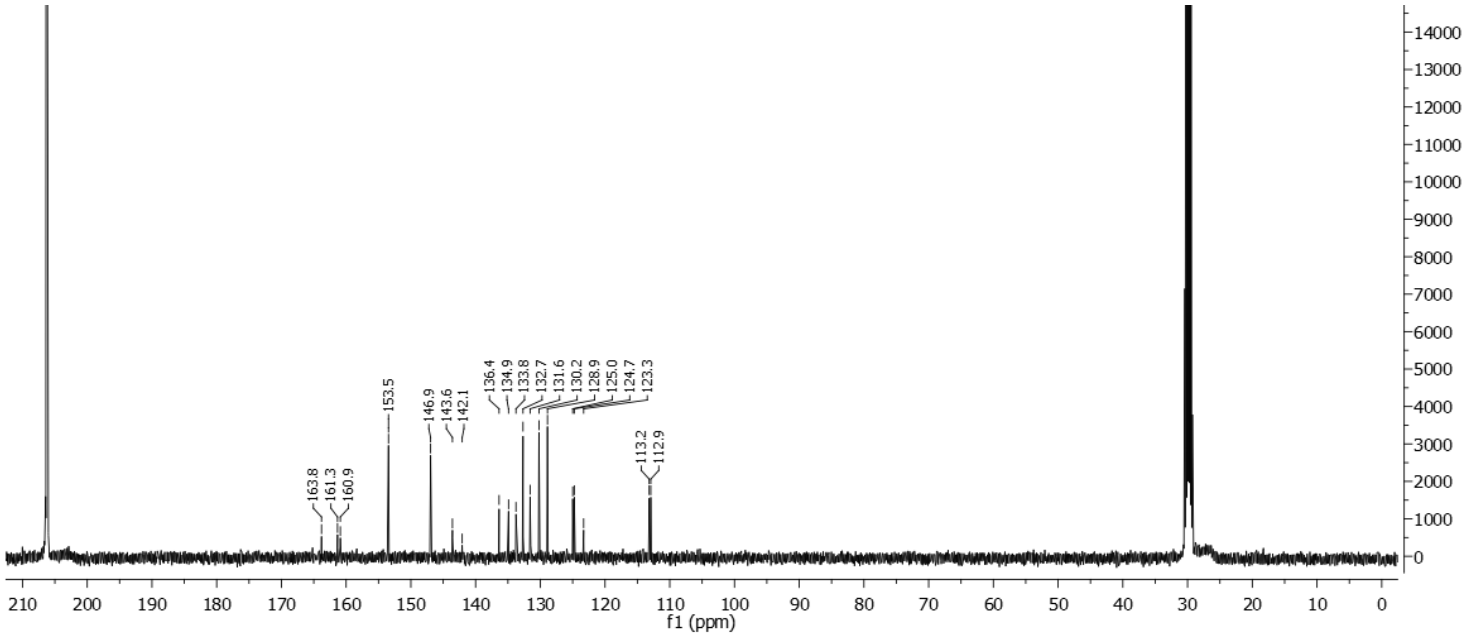

^{13}C-NMR spectrum of the non-deuterated starting material

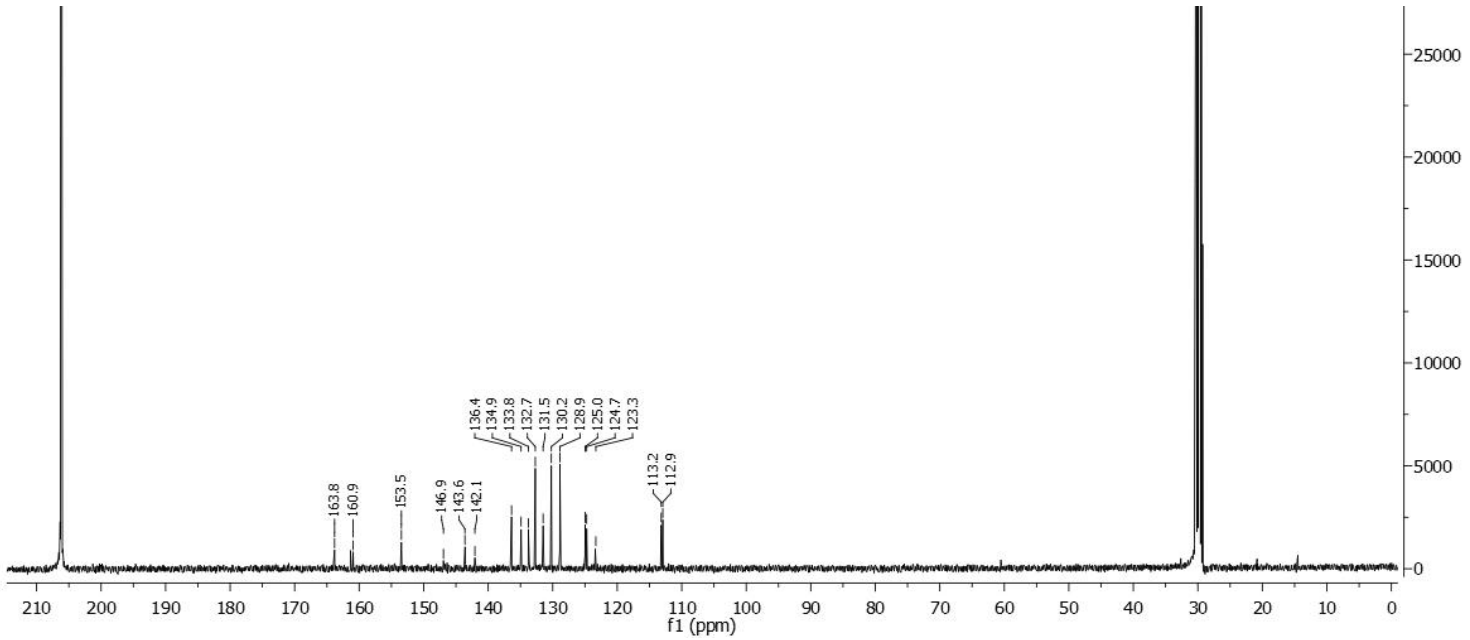

^{13}C-NMR spectrum of **30**

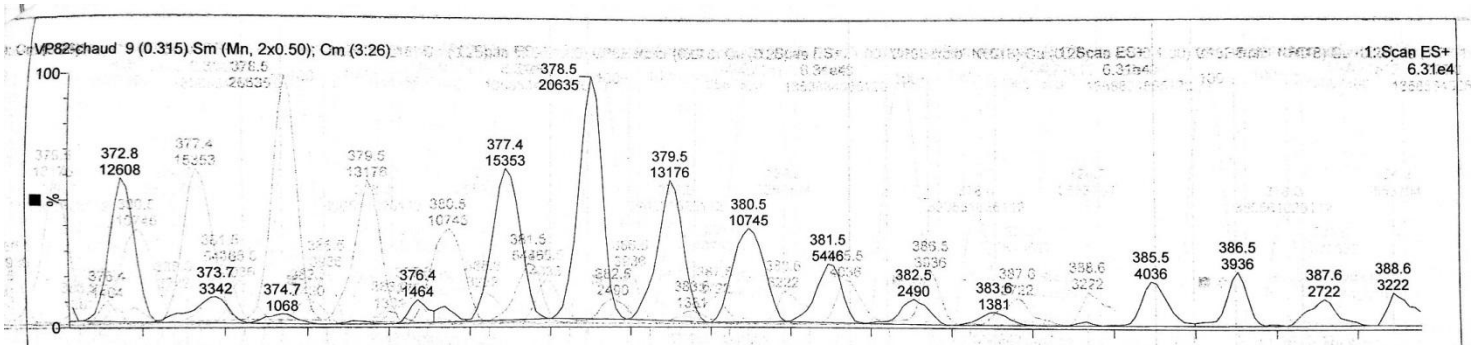

ESI spectrum of **30**

Suvorexant **31**

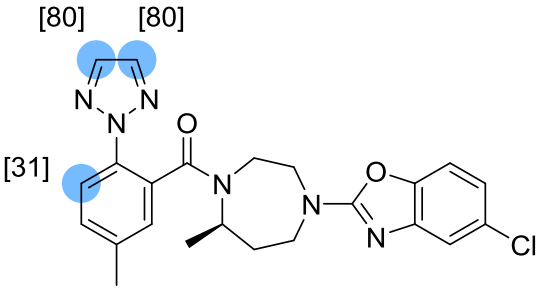

Chemical Formula: $C_{23}H_{23}ClN_6O_2$

Substrate	Solvent (Volume)	RuNp@PVP cat.	Reaction time
22.0mg, 50μmol	THF (0.5mL)	14.44mg, 20mol%	60h

Workup and purification:

After cooling down to room temperature, EtOAc (2mL) was added to the reaction mixture and stirred for 10min to let precipitate RuNp@PVP. The suspension was passed through a basic Al_2O_3 pad and then eluted with EtOAc (3mL). The solvent was removed under vacuum.

Yield: 23.0mg, 99%, white solid

The complexity of the recorded NMR spectra of suvorexant can be explained by the presence of several rotamers in solution (acetone-d_6) at room temperature.

^{1}H NMR (400 MHz, Acetone-d_6): δ 7.97 – 7.77 (m, 0.90H), 7.46 – 7.09 (m, 3.66H), 7.07 – 6.90 (m, 1H), 4.94 – 3.18 (m, 8H), 2.83 – 2.37 (m, 3H), 2.26 – 2.12 (m, 1H), 1.26 – 0.87 (m, 3H).

Deuterium incorporation was expected at δ 7.97 – 7.77 and at δ 7.46 – 7.09. Isotopic enrichment values were determined against the integral at δ 7.07 – 6.90.

^{2}H-{^{1}H}NMR (92 MHz, Acetone): δ 7.86 (s, 1.60D), 7.31 (s, 0.23D).

^{13}C-spectra were compared with spectra in literature. Just signals of the major rotamer are given.

^{13}C-{^{1}H}NMR (100 MHz, Acetone-d_6): δ 169.3, 164.3, 148.7, 146.5, 139.00, 136.6, 135.3, 131.6, 131.0, 129.6, 129.0, 123.4 (m), 120.5, 116.4, 110.3, 53.0, 47.7, 44.5, 41.3, 36.8, 20.9, 19.9.

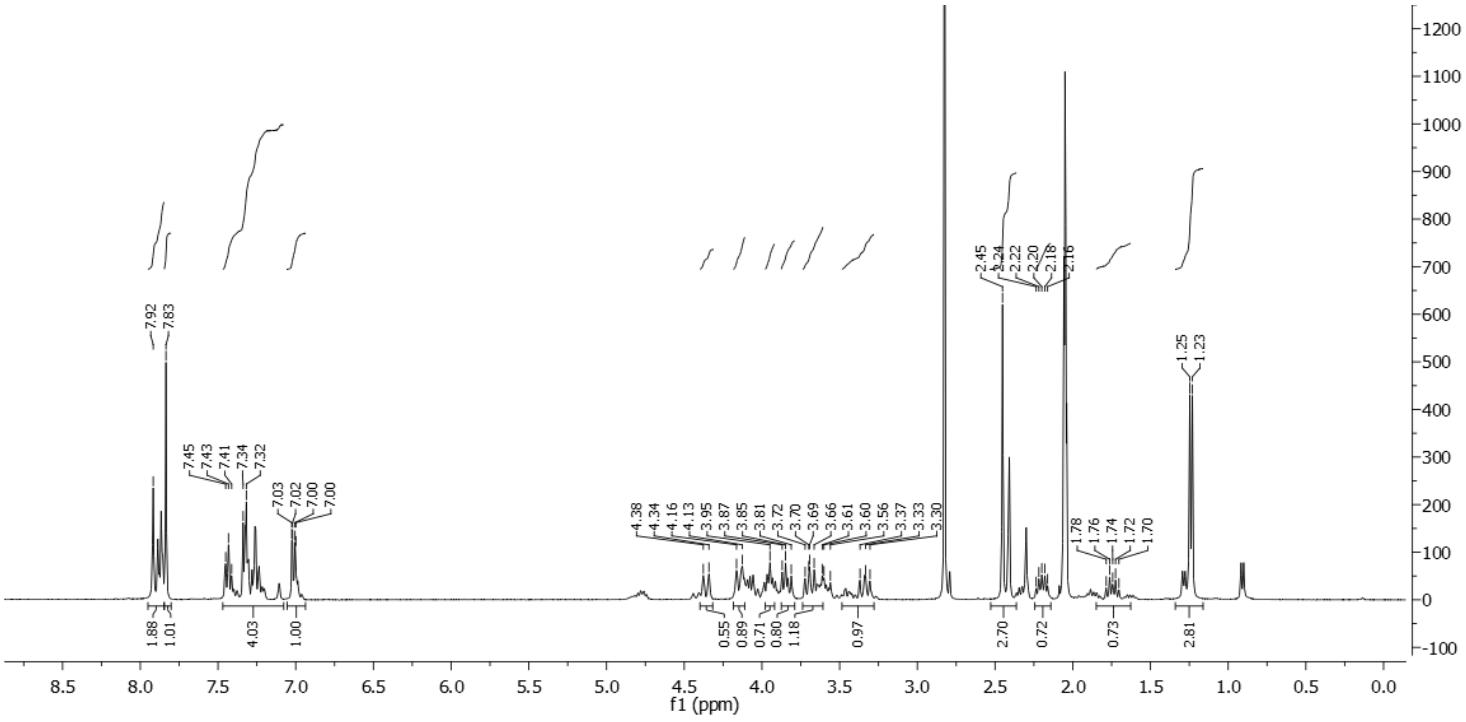

^{1}H-NMR spectrum of the non-deuterated starting material

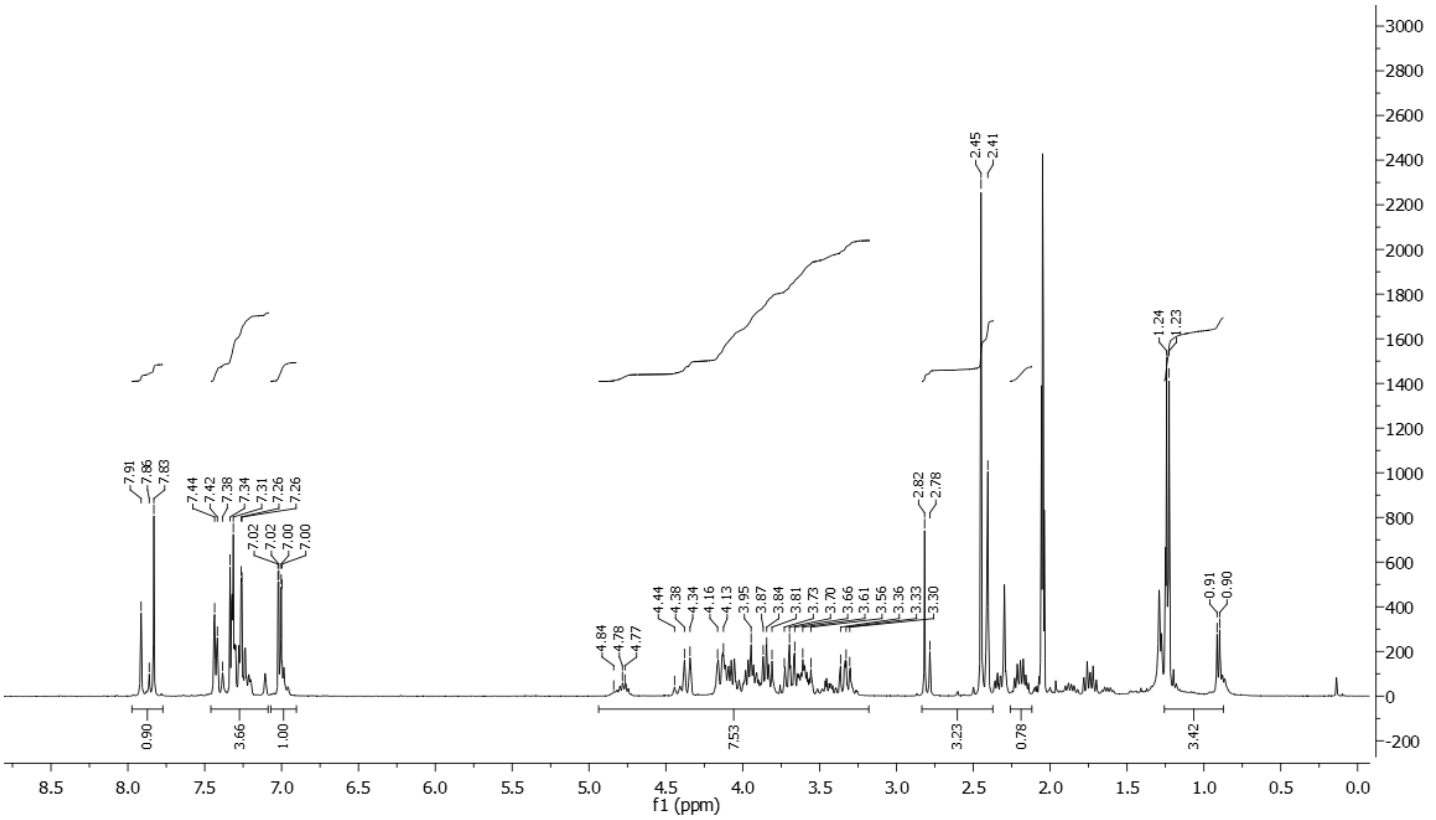

^{1}H-NMR spectrum of **31**

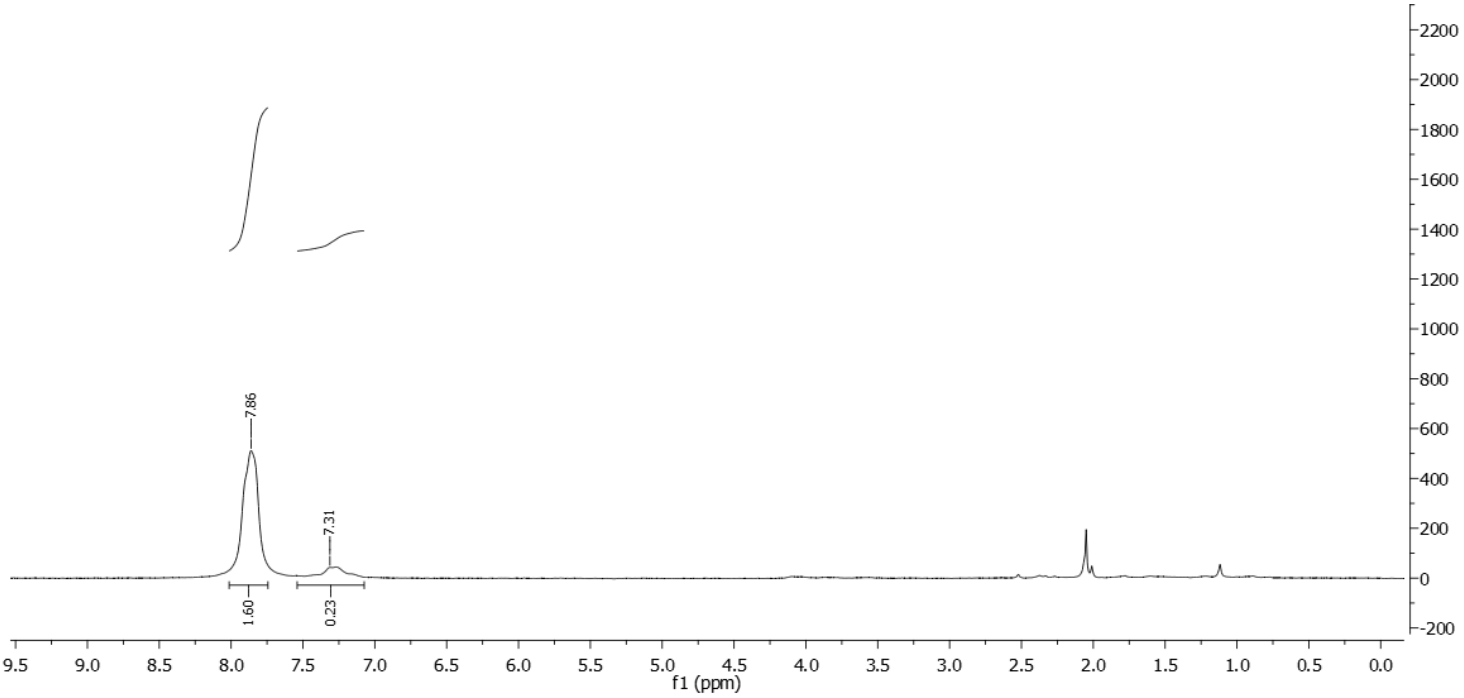

^{2}H-NMR spectrum of **31**

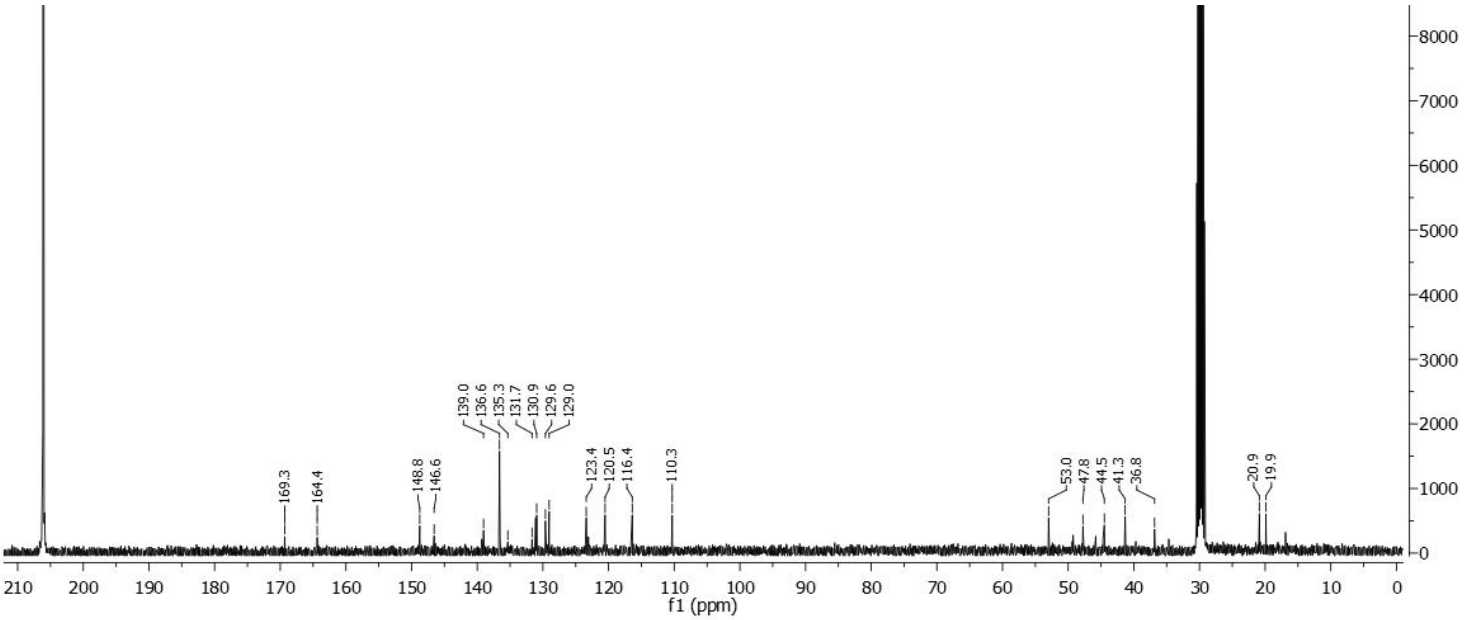

^{13}C-NMR spectrum of the non-deuterated starting material

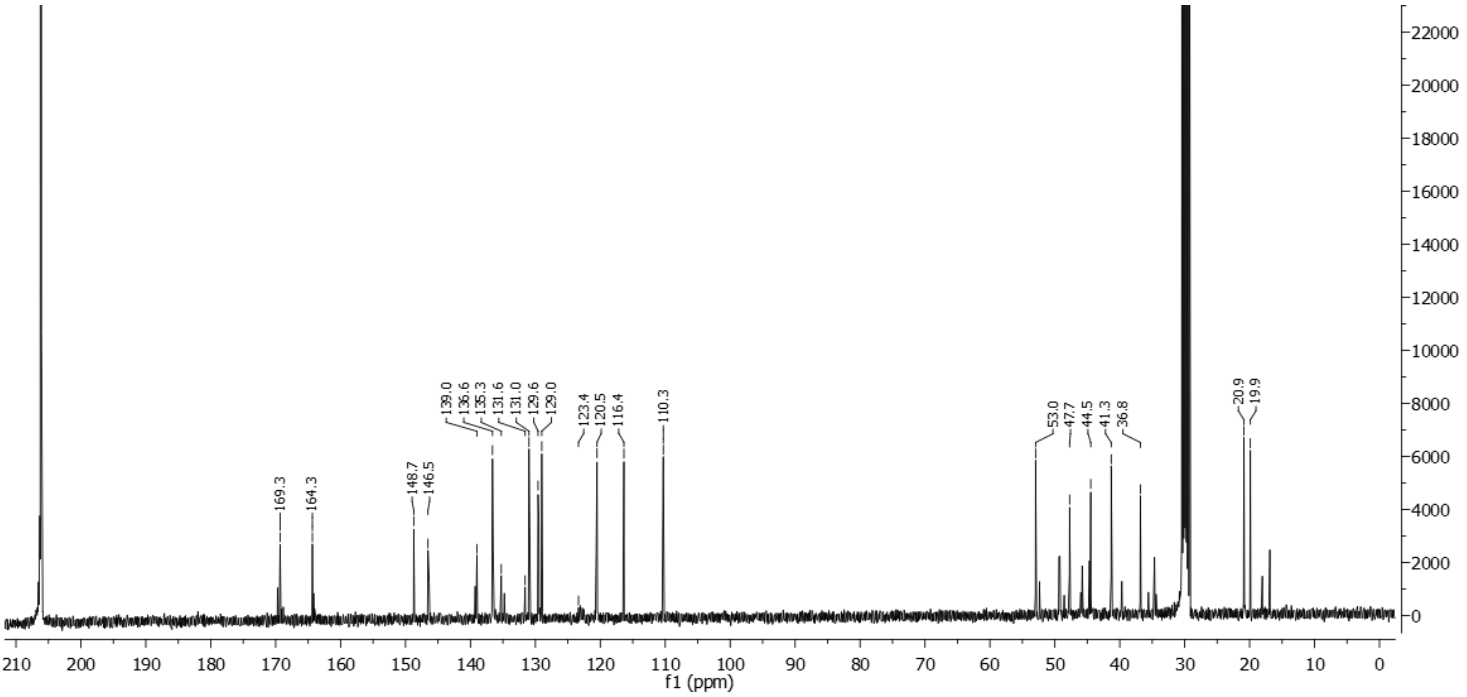

^{13}C-NMR spectrum of **31**

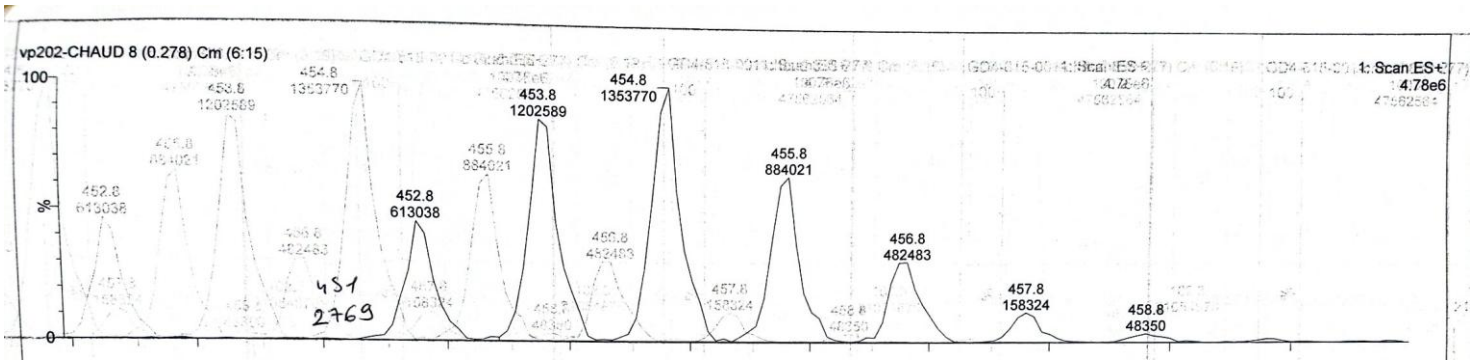

ESI spectrum of **31**

Deuterations of *N*-heterocycles by nickel nanoparticles

Preparation of the Ni-IMes Np stem solution:

A schlenk flask was charged with *IMes* (5.6mg, 18µmol, 0.25eq). THF (2mL) was added and stirred until the solid completely dissolved. $Ni(COD)_2$ (20mg, 74µmol, 1eq) was filled in a Fisher Porter flask. The organometallic precursor was dissolved in THF (5mL) and cooled down in a liquid nitrogen/acetone bath. The ligand solution was added to the $Ni(COD)_2$ solution. Upon warming to room temperature, argon was removed under reduced pressure and the Fisher Porter bottle flushed with D_2 gas (3bar). The reaction mixture was stirred for 3h at 70°C. The D_2 gas was removed and the F.P. bottle flushed with argon. The prepared nanoparticle stem solution was supposed to have a nickel concentration of 0.0148mmol/ml, and it was immediately used for H/D exchange reactions.

2,5-Diphenyloxazole **32**

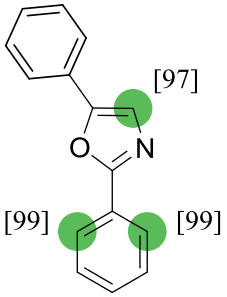

Chemical Formula: $C_{15}H_{11}NO$

Substrate	Solvent (Volume)	Ni-*IMes* Np solution
22.2mg, 0.1mmol	THF (1mL)	0.7mL, 10mol% Ni

Workup and purification:

After cooling down to room temperature ethylacetate (3mL) was added to the reaction mixture and stirred for 10min to let precipitate Ni-*IMes* Np. The suspension was passed through a celite pad and the product was eluted with ethylacetate (3mL). The solvent was removed under vacuum.

Yield: 23.0mg, 99%, white solid

^{1}H NMR (400 MHz, Acetone-d_6): δ 8.19 – 8.10 (m, 0.02H), 7.90 – 7.83 (m, 2H), 7.69 (s, 0.03H), 7.60 – 7.47 (m, 5H), 7.42 – 7.36 (m, 1H).

Deuterium incorporation was expected at δ 8.19 – 8.10 and at δ 7.69. Isotopic enrichment values were determined against the integral at δ 7.42 – 7.36.

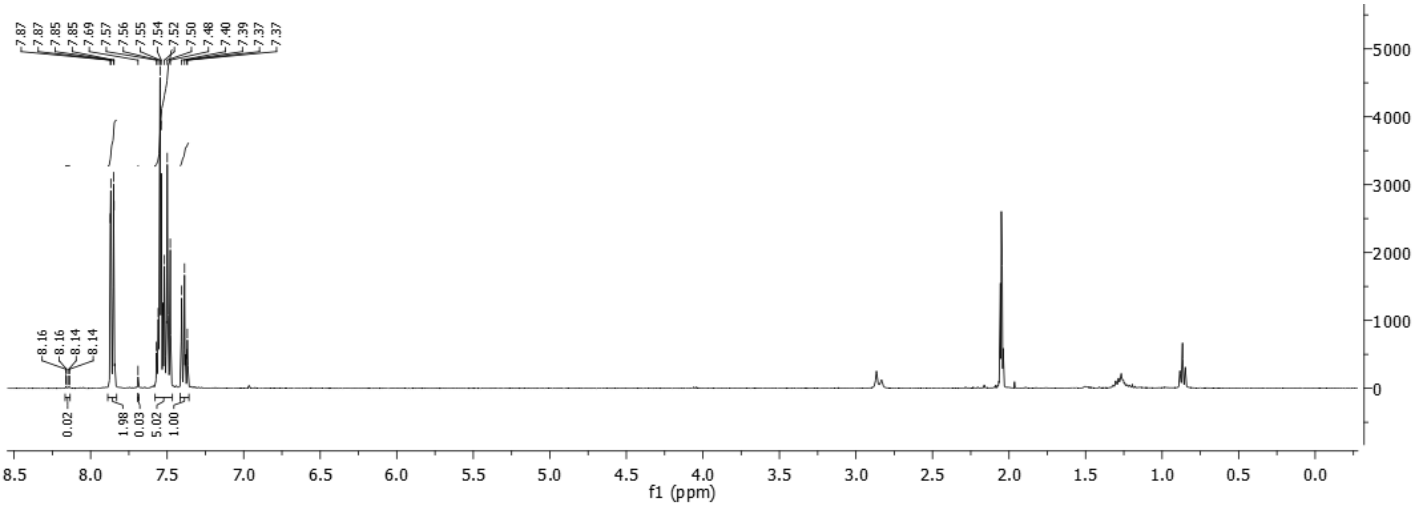

^{1}H-NMR spectrum of **32**

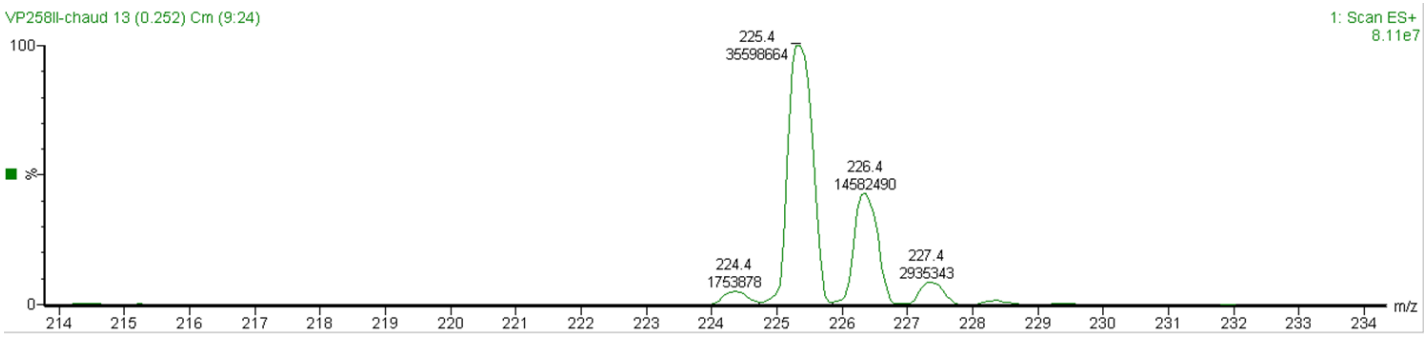

ESI spectrum of **32**

2-Phenylimidazole **33**

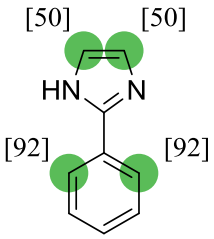

Chemical Formula: $C_9H_8N_2$

Substrate	Solvent (Volume)	Ni-*IMes* Np solution
28.8mg, 0.2mmol	THF (1mL)	0.7mL, 5mol% Ni

Workup and purification:

After cooling down to room temperature ethylacetate (3mL) was added to the reaction mixture and stirred for 10min to let precipitate Ni-*IMes* Np. The suspension was passed through a celite pad and the product was eluted with THF (3mL). The solvent was removed under vacuum.

Yield: 30.0mg, 99%, white solid

^{1}H NMR (400 MHz, acetone-d_6): δ 8.02 – 7.96 (m, 0.16H), 7.46 – 7.40 (m, 2H), 7.36 – 7.30 (m, 1H), 7.16 (s, 1H).

Deuterium incorporation was expected at δ 8.02 – 7.96 and δ 7.16. Isotopic enrichment values were determined against the integral at δ 7.36 – 7.30.

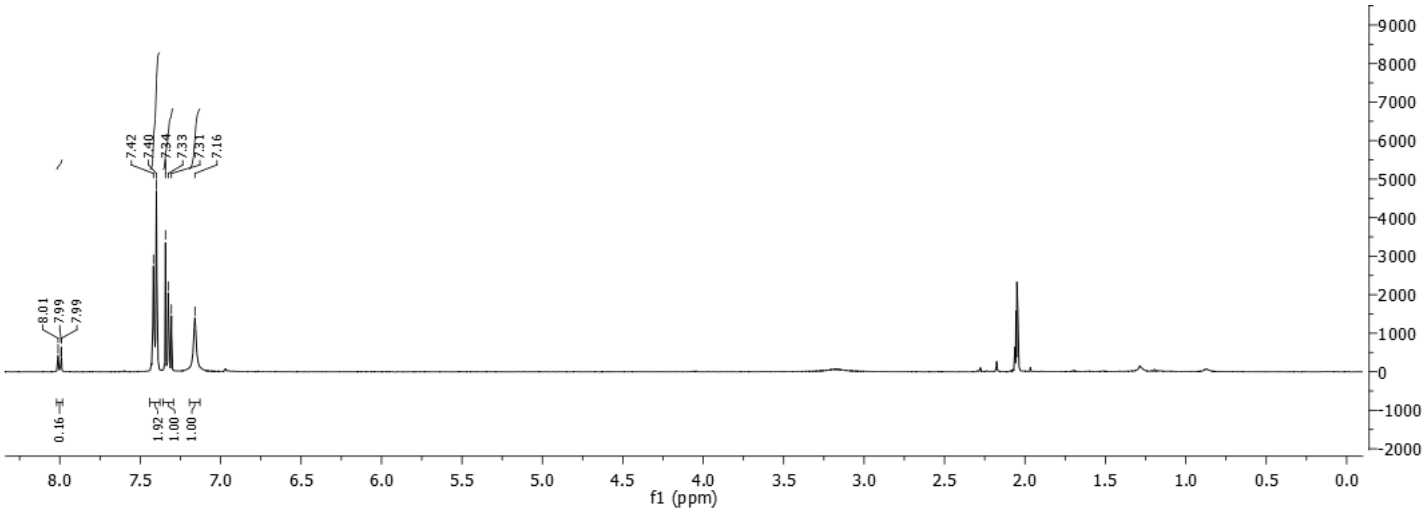

^{1}H-NMR spectrum of **33**

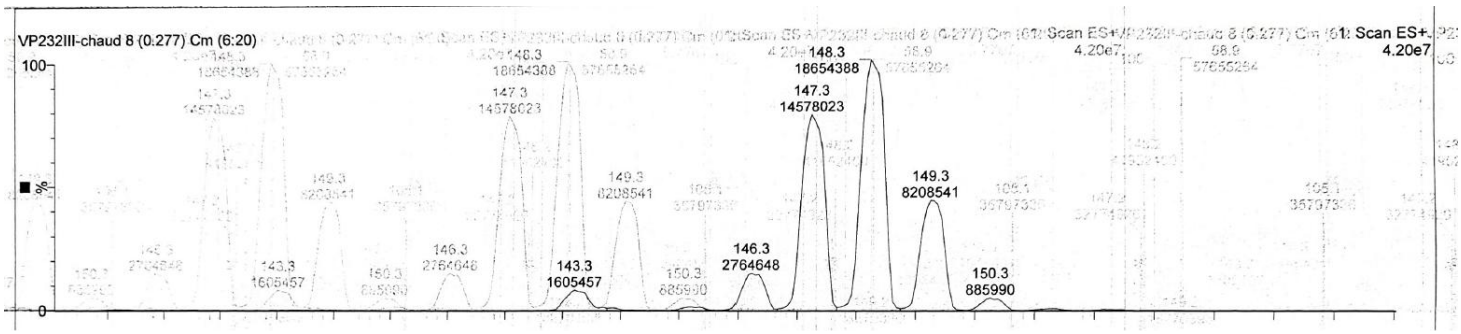

ESI spectrum of **33**

1-Phenyl-1H-1,2,4-triazole **34**

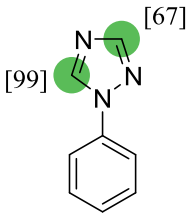

Chemical Formula:
$C_8H_7N_3$

Substrate	Solvent (Volume)	Ni-*IMes* Np solution
29.0mg, 0.2mmol	THF (1mL)	0.7mL, 5mol% Ni

Workup and purification:

After cooling down to room temperature ethylacetate (3mL) was added to the reaction mixture and stirred for 10min to let precipitate Ni-*IMes* Np. The suspension was passed through a celite pad and the product was eluted with THF (3mL). The solvent was removed under vacuum.

Yield: 30.0mg, 99%, white solid

^{1}H NMR (400 MHz, acetone-d_6): δ 9.05 (s, 0.01H), 8.12 (s, 0.33H), 7.91 – 7.84 (m, 2H), 7.62 – 7.50 (m, 2H), 7.46 – 7.38 (m, 1H).

Deuterium incorporation was expected at δ 9.03, δ 8.10 and at δ 7.91 – 7.84. Isotopic enrichment values were determined against the integral at δ 7.46 – 7.38.

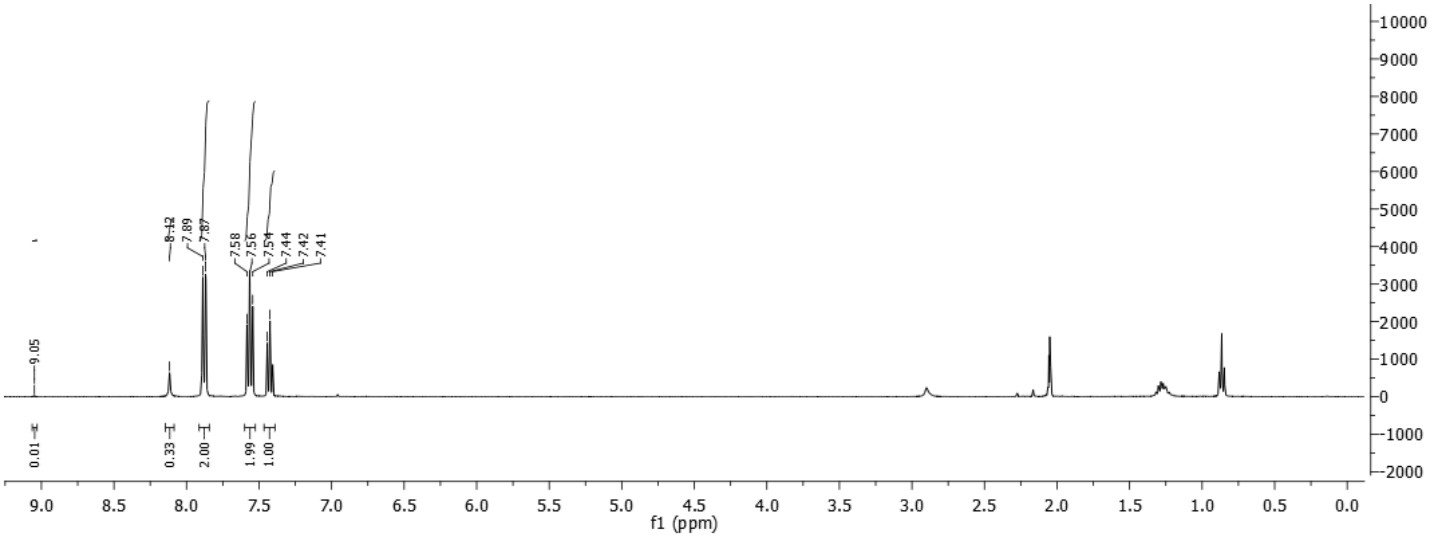

^{1}H-NMR spectrum of **34**

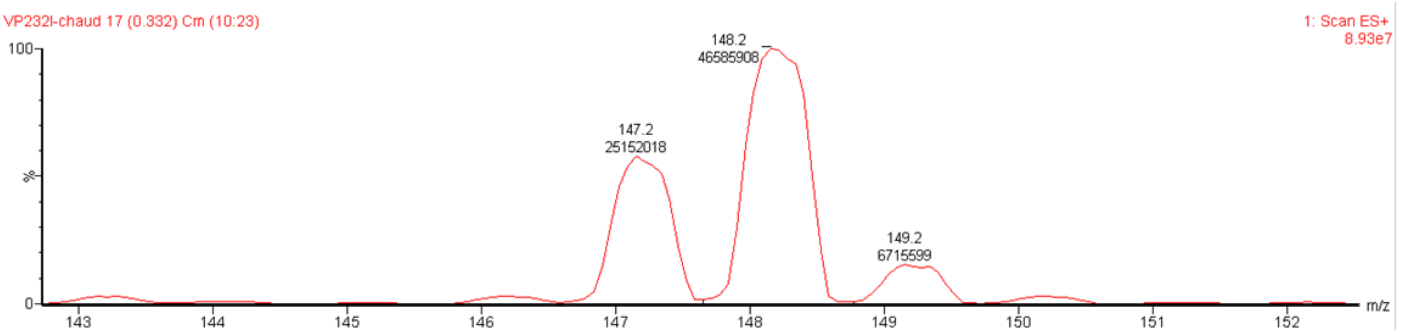

ESI spectrum of **34**

Benzothiazole **35**

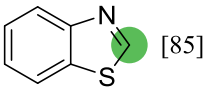

[85]

Chemical Formula:
C_7H_5NS

Substrate	Solvent (Volume)	Ni-*ICy* Np
27.0mg, 0.2mmol	THF (2mL)	5.0 mg, 29 mol% Ni

Workup and purification:

After cooling down to room temperature ethylacetate (3mL) was added to the reaction mixture and stirred for 10min to let precipitate Ni-*ICy* Np. The suspension was passed through a celite pad and the product was eluted with THF (3mL). The solvent was removed under vacuum.

Yield: 30.0mg, 99%, white solid

^{1}H NMR (400 MHz, acetone-d_6): δ 9.25 (s, 0.15H), 8.16 – 8.07 (m, 2H), 7.60 – 7.44 (m, 2H).

Deuterium incorporation was expected at δ 9.25. Isotopic enrichment values were determined against the integral at δ 7.60 – 7.44.

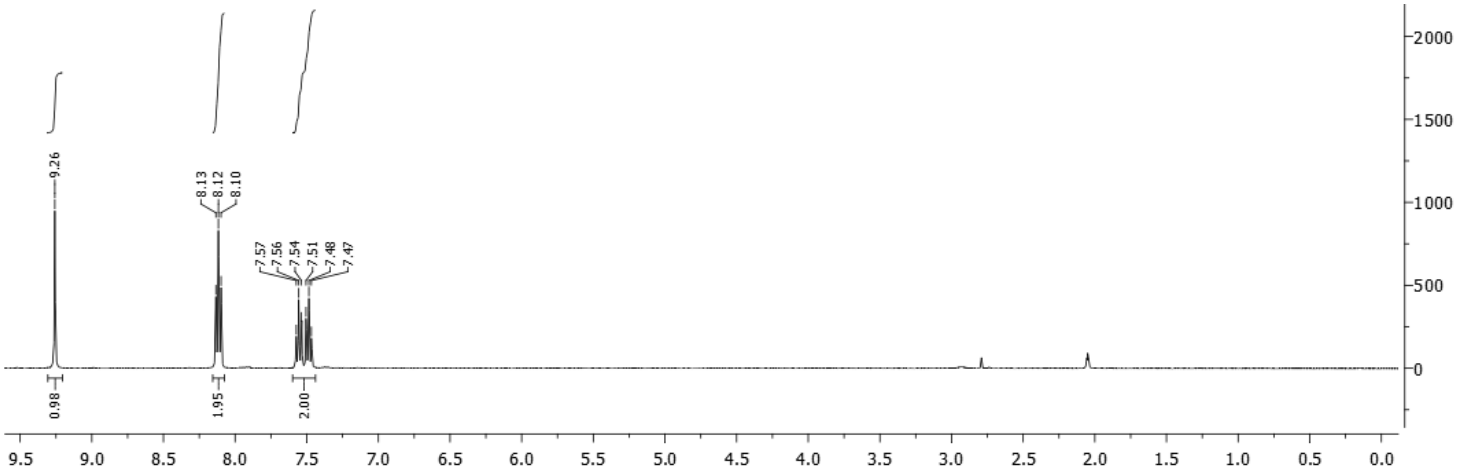

^{1}H-NMR spectrum of the non-deuterated starting material

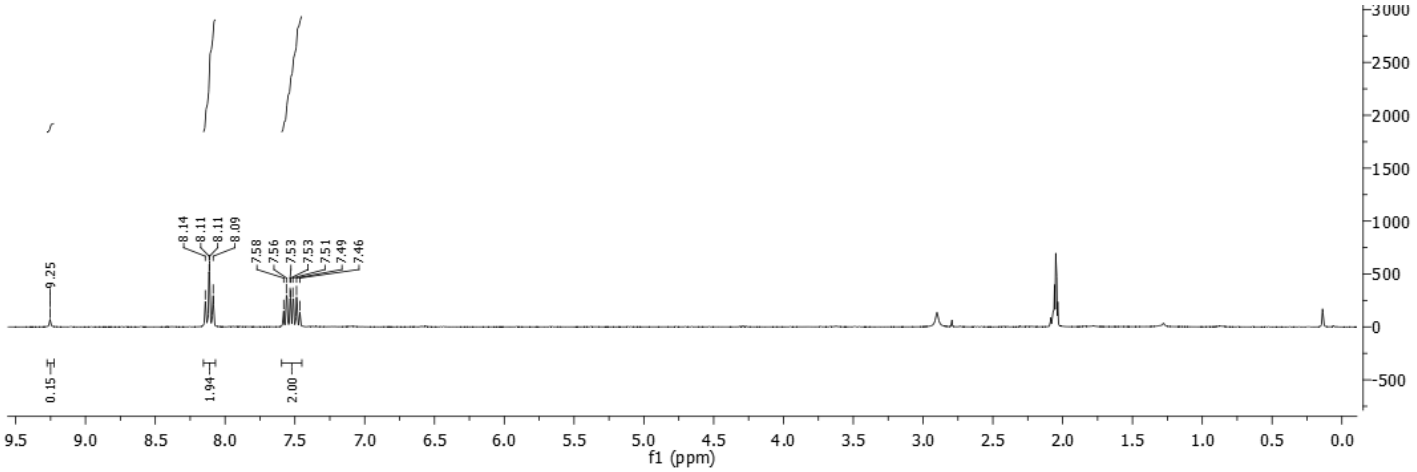

^{1}H-NMR spectrum of **35**

Compound	**M_0**	**M_{+1}**	**M_{+2}**	**M_{+3}**	**M_{+4}**	**M_{+5}**	**M_{+6}**	**M_{+7}**	**M_{+8}**	**Total D**
1	0%	6.6%	34.1%	53.8%	-0.4%	0.8%				2.4D
2	0%	79.5%	18.6%	0.9%						1.2D
3	13.4%	68.3%	17.1%	1.2%						1.1D
4	45.4%	54.3%	0.3%							0.6D
5	0.1%	2.1%	23.6%	26.5%	42.5%	4.0%	1.0%			3.2D
6	1.9%	74.1%	20.9%	3.2%						1.2D
7	32.3%	38.9%	22.5%	6.3%	2.5%	2.0%	0.6%			1.0D
8	7.8%	1.9%	49.3%	43.0%	1.8%					2.3D
9	1.5%	6.0%	32.2%	59.4%	0.9%					2.5D
10	5.3%	8.6%	29.9%	37.4%	18.7%	1.8%				2.6D
12	4.8%	21.5%	30.9%	25.1%	17.8%	4.5%				2.5D
13I	1.9%	1.0%	19.6%	21.4%	24.6%	32.4%	0.6%			3.7D
13II	0.0%	0.0%	4.2%	11.1%	25.3%	57.6%	1.8%			4.3D
14	0.4%	2.3%	12.3%	27.6%	57.3%					3.4D
15	0.9%	0.9%	11.4%	19.0%	67.8%	0.6%				3.5D
16	8.2%	12.3%	55.3%	19.9%	4.0%	0.4%				2.0D
17	19.9%	5.4%	57.1%	17.5%	18.0%	1.7%				2.4D
18	1.8%	0.6%	6.7%	19.7%	71.8%	0.9%				3.7D
19	12.7%	36.7%	35.1%	10.3%	5.1%	0.3%				1.6D
20	13.7%	20.4%	43.8%	22.1%	6.0%	1.1%	0.1%			2.0D
21	11.0%	35.9%	53.1%	1.4%						1.4D
22	7.7%	21.2%	56.0%	15.1%	4.3%	1.7%				2.0D

23	9.7%	30.5%	42.0%	13.5%	3.1%	1.2%				1.7D
24	73.4%	18.5%	6.4%	1.7%						0.3D
20'	4.8%	21.1%	52.0%	17.9%	4.1%					2.0D
21'	3.1%	18.1%	77.9%	0.9%	1.1%					1.7D
22'	8.1%	4.6%	60.4%	26.9%	6.9%	0.9%				2.4D
23'	1.6%	19.0%	66.3%	13.0%						1.9D
25I	0.3%	4.4%	15.7%	27.2%	31.0%	18.2%	3.2%	0.1%		3.5D
25II	0.7%	0.0%	2.6%	81.5%	15.2%					3.1D
26I	0.7%	0.1%	1.1%	1.4%	44.4%	35.2%	13.1%	2.3%	1.6%	4.7D
26II	1.1%	4.6%	55.5%	33.4%	1.7%	3.7%				2.2D
26III	9.2%	53.4%	29.4%	7.3%	0.7%					1.3D
27	8.1%	53.2%	23.5%	12.3%	2.9%					1.4D
28	16.1%	7.5%	68.6%	7.9%	0.3%					1.5D
29	0.2%	0.2%	0.6%	12.8%	85.9%	0.3%	0.1%			3.8D
30	6.8%	41.9%	46.5%	3.5%	-3.8%	1.3%	0.9%	2.8%		1.4D
31	0.1%	22.5%	37.8%	30.9%	7.9%	0.7%				1.9D
32	0,0%	0,0%	3,8%	76,5%	18,3%	2,0%				3.0D
33	0,7%	6,7%	34,8%	41,6%	16,2%					2.7D
34	1,8%	34,0%	59,9%	3,0%	1,5%	-0,2%				1.5D

RIS of deuterium labelled compounds determined by mass spectrometry

Tritiations of drugs

General Procedure for H/T exchanges:

A 2.5 mL Fischer–Porter bottle was equipped with a magnetic stir bar and charged with the substrate, (if not otherwise stated with Cs_2CO_3) & RuNp@PVP. THF was added to the Fischer–Porter bottle. The reaction medium was frozen in liquid nitrogen, set under vacuum & charged with T_2 gas. After reaching ambient temperature the pressure was noted. Then, the reaction mixture was stirred at 50°C (sand bath) for 24 hours. Activity and pressure of T_2 gas used, amounts of substrates, catalyst, solvent, work-up and purification procedures are individually indicated in all cases.

Tritiation of N-Boc-carvedilol **26***

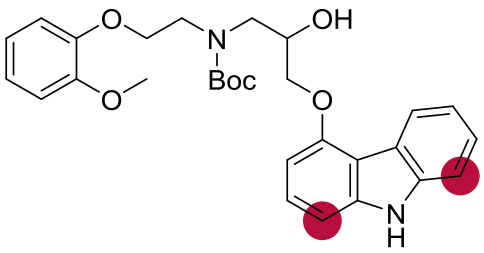

8.7 Ci/mmol

Chemical Formula: $C_{29}H_{34}N_2O_6$

Substrate	Cs_2CO_3	Solvent (Volume)	RuNp@PVP cat.	T_2 [21°C]
5.0mg, 10µmol	3.3mg, 10µmol	THF (0.3mL)	3mg, 20mol%	519mbar, 6.6Ci

Workup and purification:

After cooling down to room temperature, an acetic acid solution (1% in EtOAc, 0.5mL) was added to the reaction mixture and stirred for 3 minutes to let precipitate RuNp@PVP. The suspension was passed through a SiO_2 pad and then eluted with EtOAc (1.5mL). The solvent was removed under vacuum to give a white solid.

Analytical HPLC performed on an Waters XBridge C18 100mm x 4.6mm, 3.5µm, column. Condition: 1.0mL/min, UV & mass detection, 25°C, Solvents & gradients: Solvent A : H_2O + 0.1% HCOOH; Solvent B : ACN + 0.1% HCOOH

t (0min)	95%A 5%B
t(25min)	0%A 100%B
t(30min)	0%A 100%B

^{3}H-{^{1}H} NMR (427 MHz, Acetone-d_6): δ 7.59 (s, 0.15T), 7.25 (s, 0.15T).

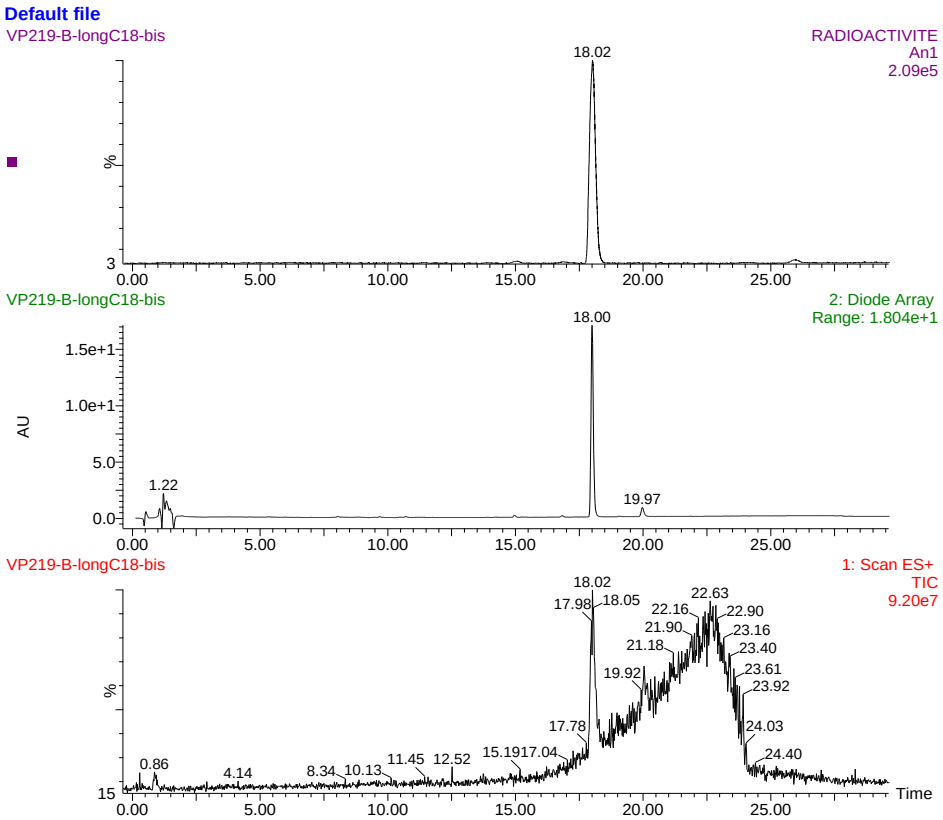

Chromatogram of **26***

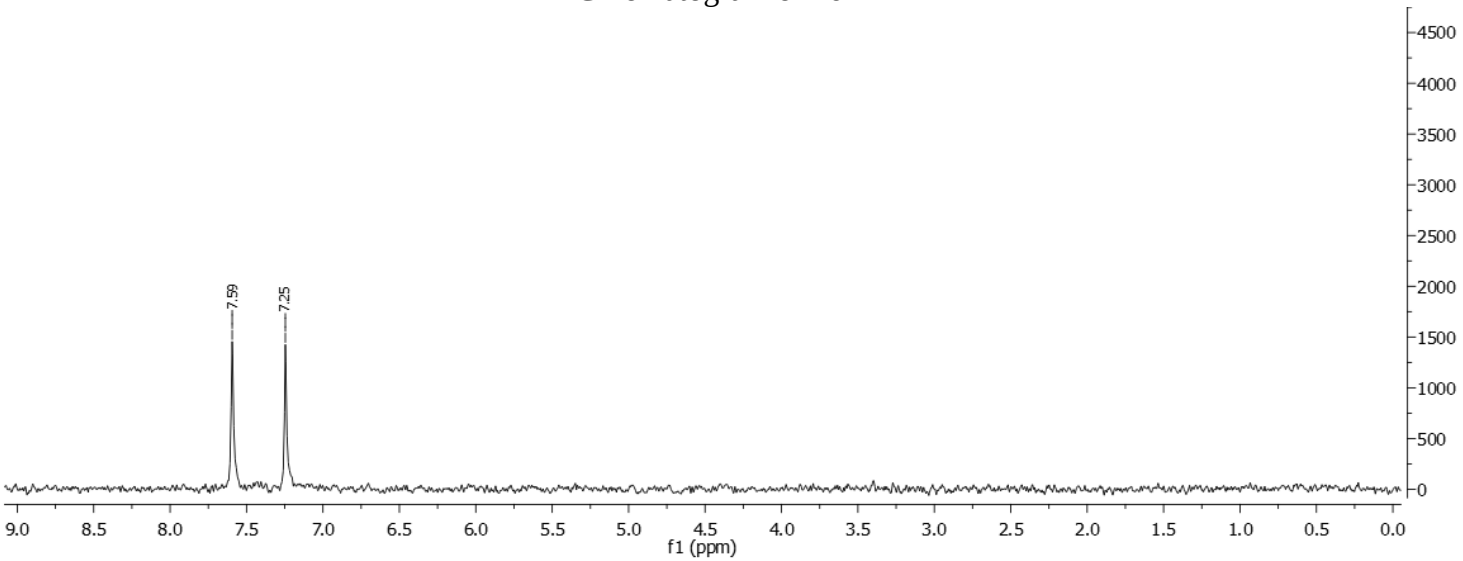

^{3}H-NMR spectrum of **26***

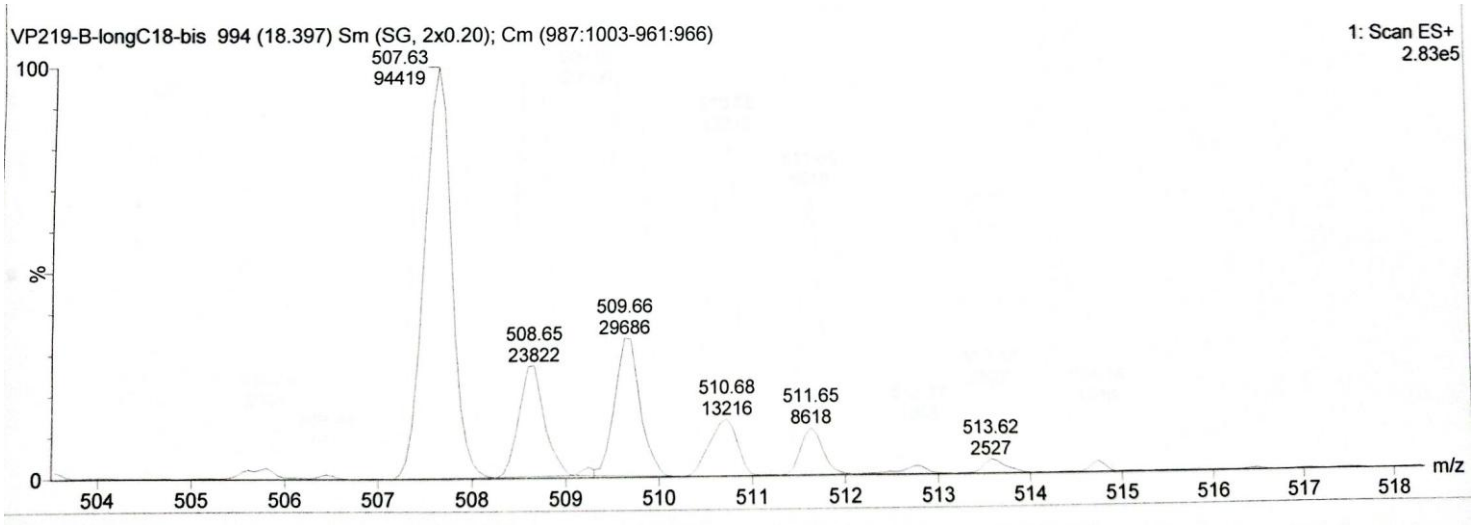

ESI spectrum of **26***

Tritiation of astemizole **27***

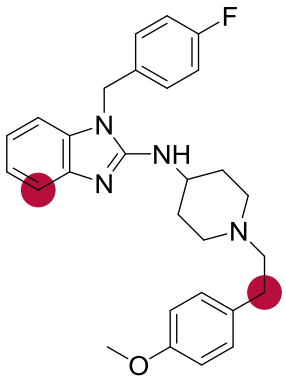

23.7 Ci/mmol

Chemical Formula: $C_{28}H_{31}FN_4O$

Substrate	Solvent (Volume)	RuNp@PVP cat.	T_2 [21°C]
5.0mg, 11µmol	THF (0.4mL)	14.0mg, 92mol%	970mbar, 12.4Ci

Workup and purification:

After cooling down to room temperature, EtOAc/cyclohexane (1:1, 1mL) was added to the reaction mixture and stirred for 3min to let precipitate RuNp@PVP. The suspension was passed through a C18-SiO_2 pad. The product was eluted with EtOAc (4.5mL). The solvent was removed under vacuum to give a white solid.

Analytical HPLC was performed on a Waters XBridge Prep Phenyl 150mm x 10mm, 5µm, column. Condition: 4.0mL/min, UV & mass detection, 25°C, Solvents & gradients: Solvent A : H_2O + 0.1% HCOOH; Solvent B : ACN + 0.1% HCOOH

t (0min)	95%A 5%B
t(25min)	0%A 100%B
t(30min)	0%A 100%B

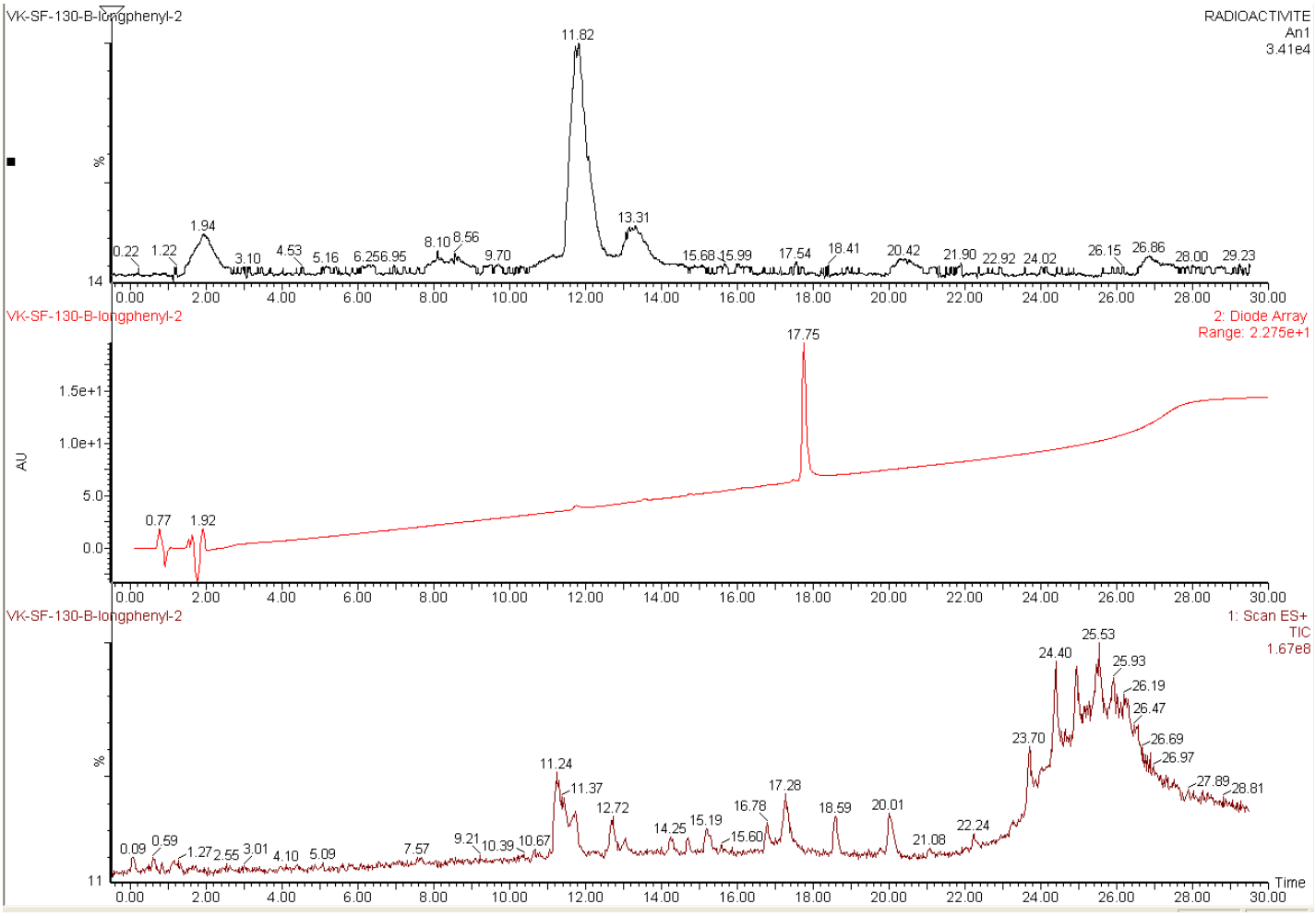

HPLC chromatogram

^{3}H-{^{1}H} NMR (427 MHz, Acetone-d_6): δ 7.31 (s, 0.42T), 2.60 – 2.45 (m, 0.33T).

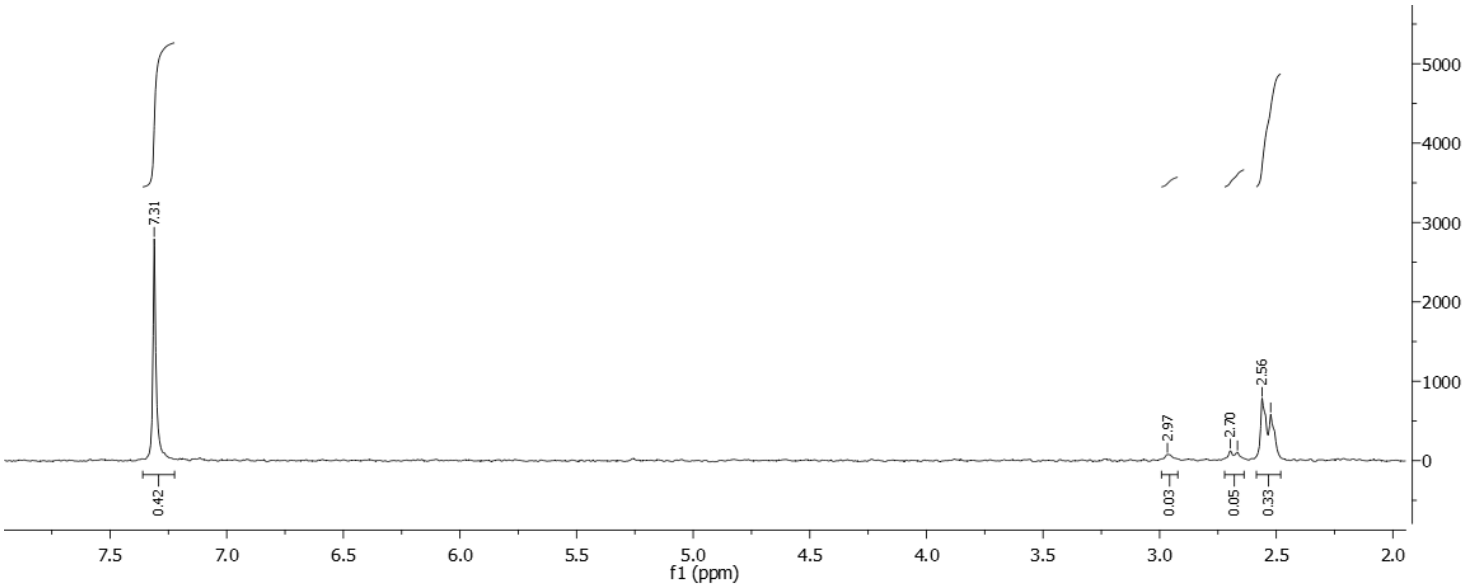

^{3}H-NMR spectrum of **27***

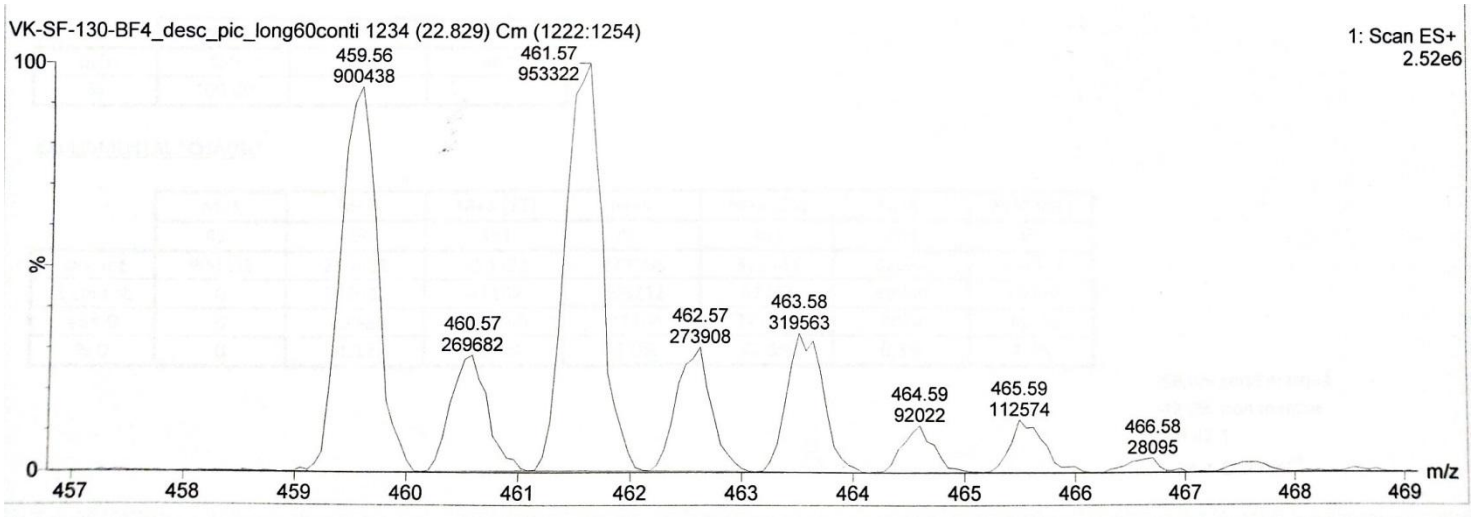

ESI-spectrum of **27***

Tritiation of fluconazole **29***

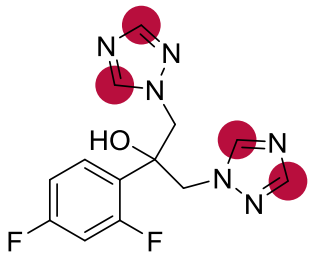

24.7 Ci/mmol

Chemical Formula: $C_{13}H_{12}F_2N_6O$

Substrate	Solvent (Volume)	RuNp@PVP cat.	T_2 gas [21°C]
5.0mg, 17µmol	THF (0.5mL)	3mg, 13mol%	869mbar, 11.1Ci

Workup and purification:

After cooling down to room temperature, EtOAc/cyclohexane (1:1, 1mL) was added to the reaction mixture and stirred for 3 minutes to let precipitate RuNp@PVP. The suspension was passed through a SiO_2 pad and then eluted with distilled THF (5mL). The solvent was removed under vacuum to give a white solid.

Analytical HPLC was performed on a Waters XBridge C18 250mm x 4.6mm, 3.5µm, column. Condition: 1.0mL/min, UV & mass detection, 25°C, Solvents & gradients: Solvent A: H_2O; Solvent B: MeOH

t (0min)	95%A 5%B
t(25min)	0%A 100%B
t(30min)	0%A 100%B

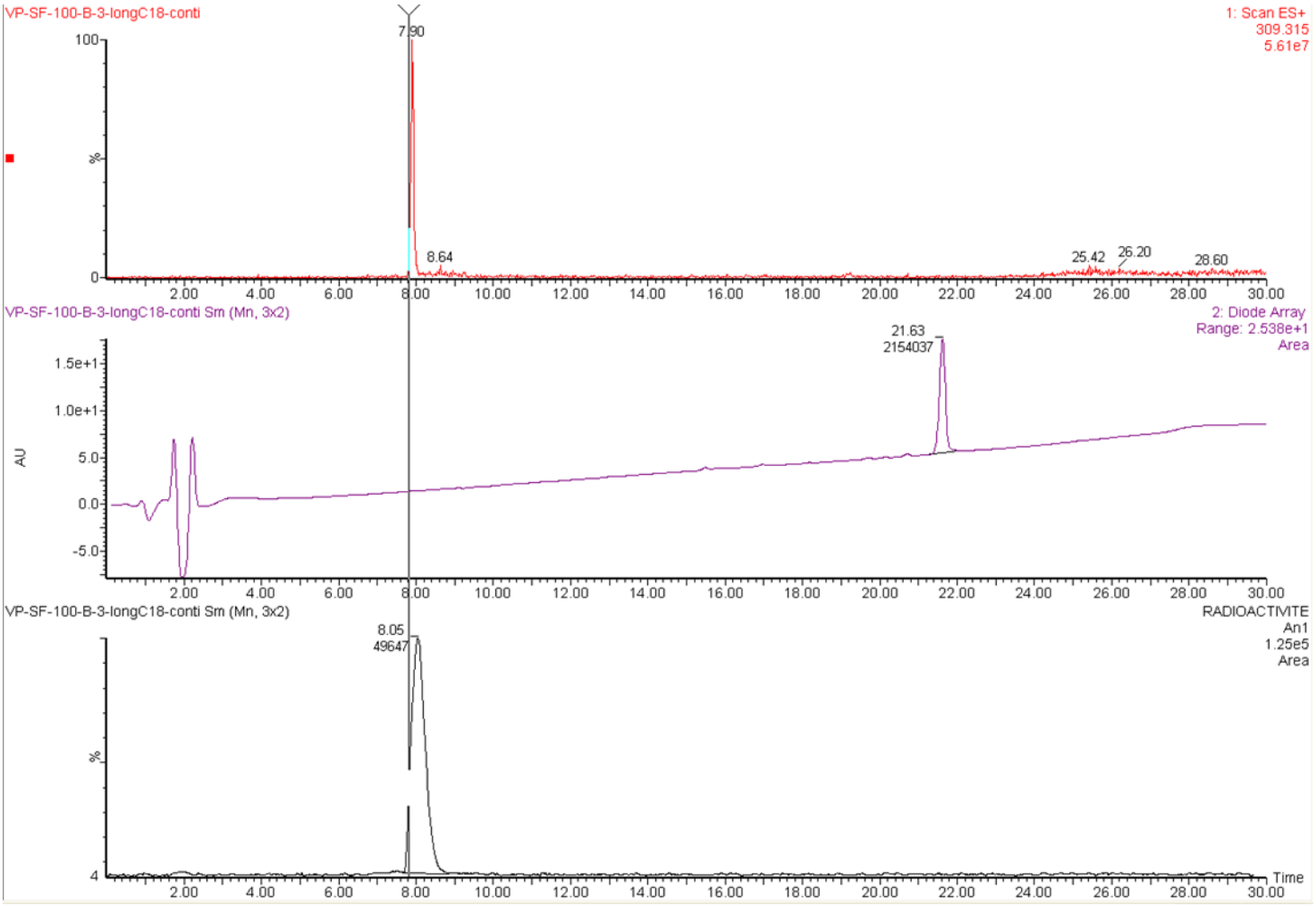

HPLC chromatogram

^{3}H-{^{1}H} NMR (427 MHz, Acetone-d_6): δ 8.33 (s, 0.66T), 7.79 (s, 0.24T).

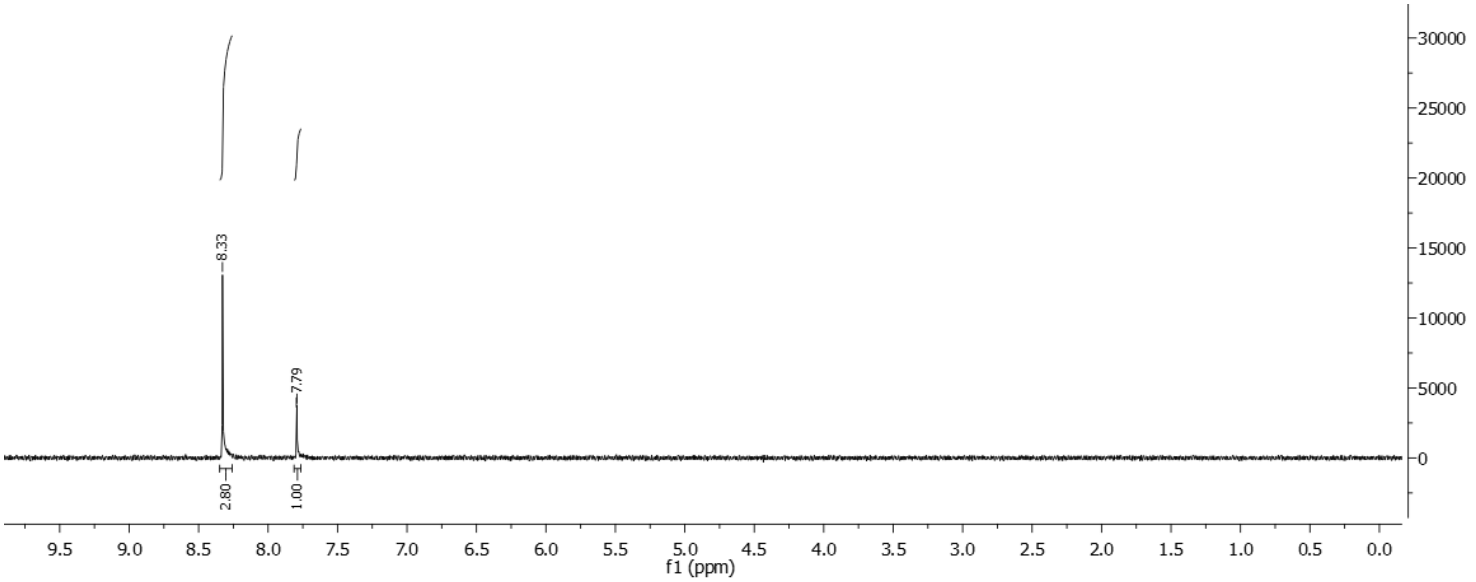

^{3}H-NMR spectrum of **29***

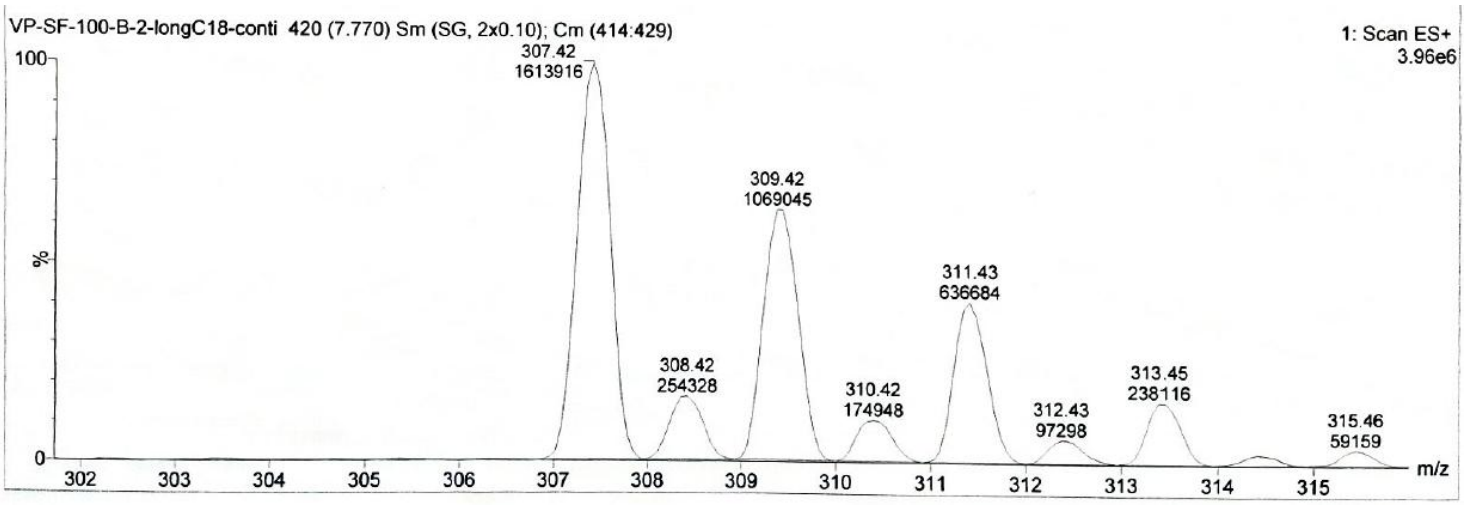

ESI-spectrum of **29***

Compound	M_0	M_{+1}	M_{+2} (1T)	M_{+3}	M_{+4} (2T)	M_{+5}	M_{+6} (3T)	M_{+7}	M_{+8} (4T)	Total T
26*	77.1%	-6.6%	21.3%	4.0%	4.2%					0.3T
27*	42.0%	-1.1%	42.5%	-1.0%	12.9%	0.1%	4.5%			0.8T
29*	46.1%	-0.3%	29.9%	0.1%	17.7%	-0.1%	6.6%			0.9T

RIS of tritium labelled compounds determined by mass spectrometry

References

(1) A. F. Holleman, E. Wiberg, N. Wiberg, *Inorganic Chemistry*, Academic Press, Berlin, **1995**, p. 247

(2) T. G. Gant, *J. Med. Chem.* **2014**, *57*, 3595-3611.

(3) J. Atzrodt, V. Derdau, W. J. Kerr, M. Reid, *Angew. Chem. Int. Ed.* **2018**, *57*, 1758-1784.

(4) D. J. Kushner, A. Baker, T. G. Dunstall, *Canadian Journal of Physiology and Pharmacology* **1999**, *77*, 79-88.

(5) N. A. Meanwell, *J. Med. Chem.* **2011**, *54*, 2529.

(6) C. Schmidt, *Nature Biotechnology* **2017**, *35*, 493 - 494.

(7) B. Halford, *C&EN Global Enterp* **2016**, *94*, 32-36.

(8) J. L. Koniarczyk, D. Hesk, A. Overgard, I. W. Davies, A. McNally, *J. Am. Chem. Soc.* **2018**, *140*, 1990-1993.

(9) J. Atzrodt, V. Derdau, *J. Label Compd. Radiopharm* **2010**, *53*, 674-685.

(10) R. Schoenheimer, D. Rittenberg, *Science* **1935**, *82*, 156-157.

(11) C. Birkemeyer, A. Luedemann, C. Wagner, A. Erban, J. Kopka, *Trends in Biotechnology* **2005**, *23*, 28-33.

(12) E. Heinzle, F. Matsuda, H. Miyagawa, K. Wakasa, T. Nishioka, *The Plant Journal* **2007**, *50*, 176-187.

(13) S. Lu, T. Jin, T. Yasuda, W. Si, K. Oniwa, K. A. Alamry, S. A. Kosa, A. M. Asiri, L. Han, Y. Yamamoto, *Org. Lett.* **2013**, *15*, 5674-5677.

(14) E. M. Simmons, J. F. Hartwig, *Angew. Chem. Int. Ed.* **2012**, *51*, 3066-3072.

(15) H. M. De Feyter, K. L. Behar, Z. A. Corbin, R. K. Fulbright, P. B. Brown, S. McIntyre, T. W. Nixon, D. L. Rothman, R. A. de Graaf, *Sci. Adv.* **2018**, *4*, eaat7314.

(16) R. M. Baldwin, *J Nucl Med.* **2005**, *46*, 1411-1413.

(17) R. Voges, J. R. Heys, T. Moenius, *Preparation of Compounds Labeled with Tritium and Carbon-14*, John Wiley & Sons, Chichester, **2009**, p. 4

(18) P. J. S. Chiu, K. F. Marcoe, S. E. Bounds, C.-H. Lin, J.-J. Feng, A. Lin, F.-C. Cheng, W. J. Crumb, R. Mitchell, *J Pharmacol Sci* **2004**, *95*, 311-319.

(19) P. Atkins, J. de Paula, *Physical Chemistry*, W. H. Freeman, New York, **2006**, p 652.

(20) J. M. Eiler, M. Clog, P. Magyar, A. Piasecki, A. Sessions, D. Stolper, M. Deerberg, H.-J. Schlueter, J. Schwieters, *International Journal of Mass Spectrometry* **2013**, *335*, 45-56.

(21) P. Atkins, J. de Paula, *Physical Chemistry*, W. H. Freeman, New York, **2006**, p 513.

(22) P. Lesot, *Encyclopedia of Analytical Science*, Elsevier, Orsay, **2019**, p 152-167.

(23) M.G. Kubinec, P.G. Williams, *Encyclopedia of Magnetic Resonance 10.1002/9780470034590.emrstm0576*, **2007**.

(24) A. Gomtsyan, *Heterocycles in drugs and drug discovery 10.1007/s10593-012-0960-z, Vol. 48*, **2012**.

(25) E. Vitaku, D. T. Smith, J. T. Njardarson, *J. Med. Chem.* **2014**, *57*, 10257-10274.

(26) J. A. Joule, K. Mills, *Heterocyclic Chemistry*, Wiley, Chichester, **2010**, p 1.

(27) J. A. Joule, K. Mills, *Heterocyclic Chemistry*, Wiley, Chichester, **2010**, p 557.

(28) R. R. Fraser, T. S. Mansour, S. Savard, *Can. J. Chem.* **1985**, *63*, 3505-3509.

(29) (a) C. R. Loomis, R. M. Bell, *J. Biol. Chem.* **1988**, *263*, 1682. (b) D. B. Longley, D. P. Harkin, P. G. Johnston, *Nat. Rev. Cancer* **2003**, *3*, 330.

(30) J. A. Joule, K. Mills, *Heterocyclic Chemistry*, Wiley, Chichester, **2010**, p 651.

(31) S. Joshi, A. S. Bisht, D. Juyal, *The Pharma Innovation Journal* **2017**, *6*, 109.

(32) R. Petrelli, P. Vita, I. Torquati, K. Felczak, D. J. Wilson, P. F. a. L. Cappellacci, *Recent Patents on Anti-Cancer Drug Discovery* **2013**, *8*, 103-125.

(33) G. C. Moraski, M. Chang, A. Villegas-Estrada, S. G. Franzblau, U. Möllmann, M. J. Miller, *European journal of medicinal chemistry* **2010**, *45*, 1703-1716.

(34) J. Xiang, J. Wang, M. Wang, X. Meng, A. Wu, *Tetrahedron* **2014**, *70*, 7470-7475.

(35) S. R. Naik, J. Harindran, A. B. Varde, *Journal of Biotechnology* **2001**, *88*, 1-10.

(36) Y. Wei, W. Fang, Z. Wan, K. Wang, Q. Yang, X. Cai, L. Shi, Z. Yang, *Virology Journal* **2014**, *11*, 195.

(37) J. Wood, K. Bonjean, S. Ruetz, A. Bellahcène, L. Devy, J. M. Foidart, V. Castronovo, J. R. Green, *Journal of Pharmacology and Experimental Therapeutics* **2002**, *302*, 1055-1061.

(38) A. Urayama, S. Yamada, R. Kimura, J. Zhang, Y. Watanabe, *Life Sciences* **2002**, *72*, 601-607.

(39) R. Gertler, H. C. Brown, D. H. Mitchell, E. N. Silvius, *BUMC Proceedings* **2001**, *14*, 13-21.

(40) K. Bourcier, R. Hyland, S. Kempshall, R. Jones, J. Maximilien, N. Irvine, B. Jones, *Drug Metabolism and Disposition* **2010**, *38*, 923-929.

(41) R. Kaur, A. R. Dwivedi, B. Kumar, V. Kumar, *Anti-Cancer Agents in Medicinal Chemistry* **2016**, *16*, 465-489.

(42) A. S. Bhatnagar, *Breast Cancer Research and Treatment* **2007**, *105*, 7-17.

(43) D. J. Williamson, S. L. Shepheard, R. G. Hill, R. J. Hargreaves, *European Journal of Pharmacology* **1997**, *328*, 61-64.

(44) S. Gottlieb, *BMJ* **1999**, *319*, 7.

(45) R. L. Wolen, R. H. Carmichael, A. S. Ridolfo, L. Thompkins, E. A. Ziege, *Biomedical Mass Spectrometry* **1979**, *6*, 173-178.

(46) A. W. Schmidt, K. R. Reddy, H.-J. Knölker, *Chem. Rev.* **2012**, *112*, 3193-3328.

(47) B. Wex, B. R. Kaafarani, *J. Mater. Chem. C* **2017**, *5*, 8622-8653.

(48) S. Wang, M. Cyronak, E. Yang, *Journal of Pharmaceutical and Biomedical Analysis* **2007**, *43*, 701-707.

(49) E. Crowe, F. Hossner, M. J. Hughes, *Tetrahedron* **1995**, *51*, 8889-8900.

(50) A.R. Katritzky, A. J. Boulton, *Advances in Heterocyclic Chemistry*, Academic Press, London, **1974**, p 175.

(51) A. W. Czarnik, *US Patent App. 12/195,956* **2009**.

(52) (a) J. B. A. Thijssen, A. G. Knaeps, J. J. P. Heykants, *J. Label Compd. Radiopharm* **1983**, *20*, 861-868. (b) S. G. Senderoff, A. J. Villani, S. W. Landvatter, K. T. Games, J. R. Heys, *J. Label Compd. Radiopharm* **1993**, *33*, 1091-1105.

(53) N. H. Werstiuk, C. Ju, *Can. J. Chem.* **1989**, *67*, 5 – 10.

(54) G. Heinkele, T. E. Mürdter, *J. Label Compd. Radiopharm* **2005**, *48*, 457-461.

(55) J. Atzrodt, V. Derdau, T. Fey, J. Zimmermann, *Angew. Chem. Int. Ed.* **2007**, *46*, 7744-7765.

(56) M. Yamamoto, K. Oshima, S. Matsubara, *Heterocycles* **2006**, *67*, 353-359.

(57) E. A. Cioffi, K. E. Alston, A. M. Patel, *Tetrahedron Letters* **2002**, *43*, 8985-8987.

(58) J. R. Heys, *J. Label Compd. Radiopharm* **2010**, *53*, 716-721.

(59) R. B. Moyes, P. B. Wells, *Journal of Catalysis* **1971**, *21*, 86-92.

(60) N. H. Sagert, R. M. L. Pouteau, *Can. J. Chem.* **1974**, *52*, 2960 - 2967.

(61) E. Alexakis, J. R. Jones, W. J. S. Lockley, *Tetrahedron Letters* **2006**, *47*, 5025-5028.

(62) A. M. Walji, E. D. Hostetler, H. Selnick, Z. Zeng, P. Miller, I. Bennacef, C. Salinas, B. Connolly, L. Gantert, M. Holahan, S. O'Malley, M. Purcell, K. Riffel, J. Li, J. Balsells, J. A. OBrien, S. Melquist, A. Soriano, X. Zhang, A. Ogawa, S. Xu, E. Joshi, J. Della Rocca, F. J. Hess, J. Schachter, D. Hesk, D. Schenk, A. Struyk, K. Babaoglu, T. G. Lohith, Y. Wang, K. Yang, J. Fu, J. L. Evelhoch, P. J. Coleman, *J. Med. Chem.* **2016**, *59*, 4778-4789.

(63) D. Hesk, C. F. Lavey, P. McNamara, *J. Label Compd. Radiopharm* **2010**, *53*, 722-730.

(64) R. Heys, *J. Chem. Soc., Chem. Commun.* **1992**, 680-681.

(65) D. Hesk, P. R. Das, B. Evans, *J. Label Compd. Radiopharm* **1995**, *36*, 497-502.

(66) J. Atzrodt, V. Derdau, W. J. Kerr, M. Reid, P. Rojahn, R. Weck, *Tetrahedron* **2015**, *71*, 1924-1929.

(67) J. A. Brown, A. R. Cochrane, S. Irvine, W. J. Kerr, B. Mondal, J. A. Parkinson, L. C. Paterson, M. Reid, T. Tuttle, S. Andersson, G. N. Nilsson, *Adv. Synth. Catal.* **2014**, *356*, 3551-3562.

(68) R. Pony Yu, D. Hesk, N. Rivera, I. Pelczer, P. J. Chirik, *Nature* **2016**, *529*, 195 - 199.

(69) A. A. Danopoulos, J. A. Wright, W. B. Motherwell, *Chem. Commun.* **2005**, 784-786.

(70) H. Yang, C. Zarate, W. N. Palmer, N. Rivera, D. Hesk, P. J. Chirik, *ACS Catal.* **2018**, *8*, 10210-10218.

(71) C. Zarate, H. Yang, M. J. Bezdek, D. Hesk, P. J. Chirik, *J. Am. Chem. Soc.* **2019**, *141*, 5034 - 5044.

(72) K. A. Guy, J. R. Shapley, *Organometallics* **2009**, *28*, 4020-4027.

(73) G. Pieters, C. Taglang, E. Bonnefille, T. Gutmann, C. Puente, J.-C. Berthet, C. Dugave, B. Chaudret, B. Rousseau, *Angew. Chem. Int. Ed.* **2014**, *53*, 230-234.

(74) A. Palazzolo, S. Feuillastre, V. Pfeifer, S. Garcia-Argote, D. Bouzouita, S. Tricard, C. Chollet, E. Marcon, D.-A. Buisson, S. Cholet, F. Fenaille, G. Lippens, B. Chaudret, G. Pieters, *Angew. Chem. Int. Ed.* **2019**, *58*, 4891-4895.

(75) S. Sun, C. B. Murray, D. Weller, L. Folks, A. Moser, *Science* **2000**, *287*, 1989-1992.

(76) O. Vidoni, K. Philippot, C. Amiens, B. Chaudret, O. Balmes, J.-O. Malm, J.-O. Bovin, F. Senocq, M.-J. Casanove, *Angew. Chem. Int. Ed.* **1999**, *38*, 3736-3738.

(77) A. Duteil, R. Queau, B. Chaudret, R. Mazel, C. Roucau, J. S. Bradley, *Chem. Mater.* **1993**, *5*, 341-347.

(78) C. Pan, K. Pelzer, K. Philippot, B. Chaudret, F. Dassenoy, P. Lecante, M.-J. Casanove, *J. Am. Chem. Soc.* **2001**, *123*, 7584-7593.

(79) T. Pery, K. Pelzer, G. Buntkowsky, K. Philippot, H.-H. Limbach, B. Chaudret, *ChemPhysChem* **2005**, *6*, 605-607.

(80) P. Lara, K. Philippot, B. Chaudret, *ChemCatChem* **2013**, *5*, 28-45.

(81) P. Lara, O. Rivada-Wheelaghan, S. Conejero, R. Poteau, K. Philippot, B. Chaudret, *Angew. Chem. Int. Ed.* **2011**, *50*, 12080-12084.

(82) P. Lara, T. Ayvali, M.-J. Casanove, P. Lecante, A. Mayoral, P.-F. Fazzini, K. Philippot, B. Chaudret, *Dalton Trans.* **2013**, *42*, 372-382.

(83) C. Taglang, L. M. Martínez-Prieto, I. del Rosal, L. Maron, R. Poteau, K. Philippot, B. Chaudret, S. Perato, A. Sam Lone, C. Puente, C. Dugave, B. Rousseau, G. Pieters, *Angew. Chem. Int. Ed.* **2015**, *54*, 10474-10477.

(84) L. M. Martíez-Prieto, B. Chaudret, *Acc. Chem. Res.* **2018**, *51*, 376-384.

(85) A. C. Giddens, H. I. M. Boshoff, S. G. Franzblau, C. E. Barry, B. R. Copp, *Tetrahedron Letters* **2005**, *46*, 7355-7357.

(86) J. R. Heys, *J. Label. Compd. Radiopharm.* **2007**, *50*, 770-778.

(87) N. Rothermel, D. Bouzouita, T. Röther, I. del Rosal, S. Tricard, R. Poteau, T. Gutmann, B. Chaudret, H.-H. Limbach, G. Buntkowsky, *ChemCatChem* **2018**, *10*, 4243-4247.

(88) W. J. Kerr, M. Reid, T. Tuttle, *Angew. Chem. Int. Ed.* **2017**, *56*, 7808-7812.

(89) H. H. Wasserman, M. B. Floyd, *Tetrahedron* **1966**, *22*, 441-448.

(90) (a) P. Howarth, M. Emanuel, S. Holgate, *British Journal of Clinical Pharmacology* **1984**, *18*, 1-8. (b) D. M. Richards, R. N. Brogden, R. C. Heel, T. M. Speight, G. S. Avery, *Drugs* **1984**, *28*, 38-61.

(91) M. P. Schön, M. Schön *British Journal of Dermatology* **2007**, *157*, 8-13.

(92) (a) G. Neugebauer, P. Neubert, *European Journal of Drug Metabolism and Pharmacokinetics* **1991**, *16*, 257-260. (b) P. M. Krstenansky, R. J. Cluxton, *Drug Intelligence & Clinical Pharmacy* **1987**, *21*, 947-953.

(93) J. A. Rodriguez, J. Hrbek, *Acc. Chem. Res.* **1999**, *32*, 719-728.

(94) P. Fouilloux, *Applied Catalysis* **1983**, *8*, 1-42.

(95) J. García-Antón, M. R. Axet, S. Jansat, K. Philippot, B. Chaudret, T. Pery, G. Buntkowsky, H. H. Limbach, *Angew. Chem. Int. Ed.* **2008**, *47*, 2074-2078.

(96) (a) G. Kresse, J. Fürthmuller, *Phys. Rev. B* **1996**, *54*, 11169–11186 (b) G. Kresse, J. Fürthmuller, *Comput. Mater. Sci*., **1996**, *6*, 15–50.

(97) J. P. Perdew, K. Burke, M. Ernzerhof, *Phys. Rev. Lett*. **1996**, *77*, 3865–3868.

(98) (a) P. E. Blöchl, *Phys. Rev. B*. **1994**, *50*, 17953–17979 (b) G. Kresse, *Phys. Rev. B*. **1999**, *59*, 1758–1775.

(99) J. D. Monkhorst, H. J. Pack, *Phys. Rev. B*. **1976**, *13*, 5188–5192.

(100) (a) G. Henkelman, B. P. Uberuaga, H. Jonsson, *J. Chem. Phys*. **2000**, *113*, 9901-9904 (b) G. Henkelman, H. Jonsson, *J. Chem. Phys.* **2000**, *113*, 9978-9985 (c) D. Sheppard, R. Terrell, G. Henkelman, *J. Chem. Phys*. **2008**, *128*, 134106-1-10.

Résumé rallongé : Cette thèse vise à développer de nouvelles méthodes de marquage efficaces permettant l'incorporation des isotopes de l'hydrogène dans les molécules organiques complexes. La méthode d'échange isotopique direct a été sélectionnée pour le marquage d'hétérocycles azotés. A l'heure actuelle, très peu de méthodes existent voire sont inexistantes pour certains types de composés et ce malgré la récurrence de ce type de sous-structures dans les molécules d'intérêt pharmacologique. Pour cette raison, la majeure partie de ce travail a consisté en le développement de nouvelles méthodes d'incorporation d'atomes de deutérium et de tritium sur des hétérocycles azotés catalysées par des nanoparticules métalliques. La première étape pour le marquage est la synthèse de nanoparticules de ruthénium stabilisées par le polymère polyvinylpyrrolidone (RuNp@PVP) et de nanoparticules de ruthénium stabilisées par un carbène hétérocyclique azoté (Ru-*ICy* Np). D'autres nanoparticules composées d'un métal non noble, abondant et peu cher ont également été synthétisées pour la première fois. Ainsi, des nanoparticules de nickel ont été synthétisées en les stabilisants par deux différents types de carbènes (Ni-*ICy* Np et Ni-*IMes* Np). Les nanoparticules de ruthénium ont ensuite été utilisées pour la mise au point des réactions de deutération des dérivés hétérocycliques azotés**.** RuNp@PVP s´est révélée être le nanocatalyseur le plus efficace et chimosélectif et a donc été employé pour la suite de ce projet pour étudier la deutération des oxazoles, des imidazoles, des benzimidazoles, des benzoxazoles, des triazoles et des carbazoles. En comparaison avec les travaux déjà décrits, RuNp@PVP s´est avéré un très bon catalyseur permettant des incorporations efficaces de deutérium en position alfa, beta et gamma de l'atome d'azote responsable de la coordination dans des conditions douces. En outre, la compatibilité du RuNp@PVP avec des substrats pourvus des différentes fonctionnalités protiques et polaires a mis en évidence son applicabilité large. Un autre résultat remarquable résidait dans le fait que l´ajout d´une base inorganique a permis d´empêcher la formation des sous-produits réduits et d´améliorer des enrichissements isotopiques en vicinité des liaisons N-H sur les carbazoles et les indoles. Par ailleurs, des calculs théoriques ont permis de rationaliser les regiosélectivités obtenues expérimentalement et d'identifier notamment des intermédiaires clefs inédites. D'un point de vue applicatif, l´échange isotopique catalysé par les nanoparticules de ruthénium a permis de synthétiser des standards internes deutérés de molécules bioactives et fragiles, comme par exemple la pimprinine, pour la quantification LC-MS. La tritiation des molécules complexes (le fluconazole, l'astémizole et le carvédilol) a pu être effectuée par cette méthode en seulement une étape de synthèse en utilisant des pressions du gaz de tritium inférieures à un bar. En dépit des résultats positifs obtenus, la catalyse par les nanoparticules de ruthénium ne permet pas toujours le marquage des molécules portant certaines groupements (thiazole, thioéthers), d´où l´intérêt de développer des nanocatalyseurs métalliques contenant d´autres métaux et d´autres ligands. Dû à ces limitations, la réactivité de nouveaux nanocatalyseurs de nickel pour l´échange H/D sur les hétérocycles azotés était aussi discutée. Après une optimisation de conditions réactionnelles, le catalyseur Ni-*IMes* Np s'est trouvé être le plus efficace pour nos réactions. La régiosélectivité de l´échange isotopique par cette méthode sur certains substrats modèles était comparable à celle obtenue avec les nanocatalyseurs de ruthénium dans le chapitre précédent. Néanmoins, l´absence des sous-produits réduits s´est avérée comme un avantage considérable de la méthode utilisant les nanoparticules de nickel, à l´inverse des résultats obtenus avec des nanocatalyseurs de ruthénium. Un autre point positif était la deutération du benzothiazole, qui ne pouvait pas être deutéré par les nanoparticules de ruthénium. Un inconvénient des deutérations catalysées par les nanoparticules de nickel résidait dans leur instabilité en présence des groupements polaires, comme par exemple les amines et les alcools, ce qui a limité leur applicabilité pour le marquage des substrats plus complexes. Le développement des nouvelles méthodes de stabilisation des nanoparticules de nickel fera l'objet des futurs travaux dans ce domaine.

Titre : Marquage des molécules d'intérêt biologique au deutérium et tritium par la catalyse des nanoparticules métalliques

Mots clés : marquage isotopique, radiochimie, nanoparticules, hétérocycles azotés, DFT

Résumé : Cette thèse vise à développer de nouvelles méthodes efficaces pour incorporer des isotopes de l'hydrogène dans les molécules organiques complexes, après une introduction portant sur les applications et la synthèse des molécules marquées par le deutérium et tritium. Les méthodes permettant le marquage, par échange isotopique direct, d'hétérocycles azotés par des isotopes de l'hydrogène restent perfectibles, voire inexistantes dans certains cas, malgré la récurrence de ce type de sous-structures dans les molécules d'intérêt pharmacologique. Pour cette raison, la majeure partie de ce travail a consisté au développement de nouvelles méthodes d'incorporation d'atomes de deutérium et de tritium sur des hétérocycles azotés catalysées par des nanoparticules métalliques. Dans un premier chapitre, la mise au point, le champ d'application d'une méthode de marquage mettant en jeu l'utilisation de nanocatalyseurs de ruthénium seront discutés. Dans ce cadre, des calculs théoriques ont permis de rationaliser les regiosélectivités obtenues expérimentalement et d'identifier notamment des intermédiaires clefs inédits. D'un point de vue applicatif, cette méthode a permis de synthétiser des étalons internes deutérés pour la quantification LC-MS mais aussi des molécules complexes tritiées ayant des activités spécifiques élevées en une étape de synthèse. Dans un autre chapitre, la synthèse et la réactivité de nouveaux nanocatalyseurs de nickel permettant de réaliser des échanges isotopiques sélectifs seront discutés.

Title : Tritium and Deuterium Labelling of Bioactive Molecules Catalyzed by Metallic Nanoparticles

Keywords : isotopic labelling, radiochemistry, nanoparticles, *N*-heterocycles, DFT

Abstract: This PhD thesis deals with the development of new efficient methods for the incorporation of hydrogen isotopes into organic molecules, which represents a serious issue and a field of tremendous importance for drug discovery and drug development processes. After giving an introduction about hydrogen isotopes and their applications in organic molecules, the course will proceed to an overview of different chemical transformations for establishing deuterium or tritium labels on molecular frameworks. The possibilities to label *N*-heterocycles by hydrogen isotopes through hydrogen isotope exchange (HIE) are still very restricted and even impossible for some representatives despite the strong recurrence of these substructures in numerous biologically active molecules. For this reason, the emphasis of the practical part will lie on the development of new methods for the incorporation of deuterium and tritium on *N*-heterocycles through metal nanoparticle catalysis. In the first chapter, HIE through ruthenium nanocatalysts will be optimized and the application range will be demonstrated. In this context, DFT-based calculations allowed to explain experimental regioselectivities and to identify new key-intermediates. In terms of application, it was shown that the ruthenium-catalyzed method is useful for the synthesis of deuterium labelled internal standards for LC-MS quantifications and for the tritiation of complex molecules displaying satisfying specific activities. In the next chapter, the synthesis of new nickel nanoparticles and their potential to catalyze selective HIE on *N*-heterocyclic derivatives will be discussed.

Université Paris-Saclay
Espace Technologique / Immeuble Discovery
Route de l'Orme aux Merisiers RD 128 / 91190 Saint-Aubin, France